4407

Winglets on Wings at Numbers

NASA Contractor Report 4407

The Effects of Winglets on Low Aspect Ratio Wings at Supersonic Mach Numbers

James A. Keenan and John M. Kuhlman
West Virginia University
Mechanical and Aerospace Engineering Department
Morgantown, West Virginia

Prepared for
Langley Research Center
under Grant NAG1-951

National Aeronautics and
Space Administration
Office of Management
Scientific and Technical
Information Program
1991

[redacted] INTERNATIONAL [redacted]

THE EFFECTS OF WINGLETS ON LOW ASPECT RATIO WINGS AT SUPERSONIC MACH NUMBERS

The following final report has been prepared under the sponsorship of the NASA Langley Research Center under Grant NAG-1-951, Mr. Steven X.S. Bauer and Mr. Peter F. Covell, technical monitors. This reports consists of the Master's thesis prepared by the first author, under the direction of the second author.

ACKNOWLEDGEMENTS

I would like to thank my family and friends for their support and encouragement in completing this work and for their support throughout the years. I also wish to thank my thesis committee, Dr. J. B. Fanucci, Dr. G. J. Morris, and Dr. J. M. Kuhlman (my advisor), for their advice and support on matters ranging from education, research, and life in general. Their advice has been very valuable and I hope to continue to use what I have learned from each of them for quite some time.

A special thanks to John Moody, Larry "Chip" Peal Jr., and Bret Bledsoe for their help in allowing this work to be completed.

This work was supported in part by NASA Langley Research Center, Hampton, Virginia under grant NAG-1-951, Mr. Steven X. S. Bauer and Mr. Peter F. Covell, technical monitors. NASA Langley also provided use of their computer facilities via TELNET as well as the required computer run time.

ABSTRACT

A computational study has been conducted on two wings, of aspect ratios 1.244 and 1.865, each having 65° leading edge sweep angles, to determine the effects of nonplanar winglets at supersonic Mach numbers. A Mach number of 1.62 was selected as the design value. The winglets studied were parametrically varied in alignment, length, sweep, camber, thickness, and dihedral angle to determine which geometry had the best predicted performance. For the computational analysis, an available Euler marching technique was used.

The results indicated that the possibility existed for wing-winglet geometries to equal the performance of wing-alone bodies in supersonic flows with both bodies having the same semispan . The performance parameters of main interest were the lift-to-pressure drag ratio and the pressure drag coefficient as functions of lift coefficient. The lift coefficient range was from -0.20 to 0.70 with particular emphasis on the range of 0.10 to 0.22. In the range of interest, the first base wing with winglet used NACA 1402 airfoils for the base wing and was shown to have lift-to-pressure drag ratios within 0.136% to 0.360% of the NACA 1402 wing-alone. The differences in total drag coefficients were within 0.111% to 0.480% for these two geometries.

The other base wing was a "natural" flow wing which was previously designed specifically for a Mach number of 1.62. Solutions for the "natural" flow wing with winglets may not have been valid. However, the results obtained showed that the "natural" wing-alone had a slightly higher lift-to-pressure drag than the "natural" wing with winglets.

TABLE OF CONTENTS

LIST OF FIGURES

LIST OF TABLES

NOMENCLATURE

ENGLISH

b/2	= wing semispan.
$\bar{c}$	= chord length.
$\bar{c}_f$	= mean skin friction drag coefficient.
c_r	= root chord length.
C_D	= drag coefficient.
ΔC_D	= incremental drag coefficient
C_{DP}	= pressure drag coefficient.
C_L	= lift coefficient.
ΔC_L	= incremental lift coefficient
C_M	= pitching moment coefficient.
C_P	= surface pressure coefficient.
e	= energy.
h	= enthalpy.
INU	= surface, circumferential grid points at which THTU angles are specified.
J	= Jacobian matrix.
L/D	= lift-to-drag ratio.
m	= maximum ordinate of the mean line expressed as a fraction of chord.
M	= Mach number.
n	= normal vector.
NPT	= number of grid points per patch for SIMP and EMTAC.
p	= pressure.
Q, E, F, G	= vector columns from conservation equations.
$\underline{Q}$, $\underline{E}$, $\underline{F}$, $\underline{G}$	= fluxes of Q,E,F,G.
Q', E', F', G'	= numerical flux vectors of Q,E,F,G.
Re_L	= Reynolds number.

S	= wing reference area
t	= time.
THTU	= angle of grid line at INU grid point for SIMP or EMTAC.
u, v, w	= component velocities in cartesian coordinates.
U	= contravariant velocity.
V	= volume.
x, y, z	= Cartesian axes or geometric coordinates.
Δx	= incremental step size.
x/c, y/c, z/c	= fractional geometric coordinates in terms of chord.
x/l	= non-dimensional location in axial direction.
XEND	= final axial marching plane location for SIMP or EMTAC.
XSTART	= first axial location for SIMP or EMTAC.

GREEK

α	= angle of attack (in degrees).
γ	= ratio of specific heats.
δ_{ij}	= Kronecker delta.
λ	= taper ratio or eigenvalue.
ρ	= density.
τ,ξ,η,ζ	= transformed cartesian coordinates.

CHAPTER 1

INTRODUCTION

1.1 Induced Drag and Winglets

One of the most dominant parameters in determining aircraft flight performance, aerodynamics, and economics is drag. Drag consists of several different components; three of these components being profile drag, induced drag, and wave drag. For low subsonic Mach number flows, profile and induced drag are the only two forms of interest, with induced drag being the larger of the two as higher amounts of lift are generated. As transonic and supersonic Mach numbers are encountered, wave drag becomes a significant factor in the total drag component. To improve performance and aerodynamics, many methods and attempts have been made to reduce each component of the total drag.

One of the more common ways to reduce total drag has been to attempt to lower the induced drag, which is also called drag due to lift. One method which has been used to reduce induced drag is that of altering the flow of air around the wing-tip of an aircraft. To prevent or reduce this wing-tip airflow or leakage, winglets have been and are being used for induced drag reduction. Winglets are small, nearly vertical, winglike surfaces mounted at the tips of a wing [1]. For the winglets to be fully effective, they must efficiently produce significant side forces. These side forces reduce lift-induced flow above and below the wing-tip . Physically, the effect of winglets is to vertically diffuse the tip vortex at the tip and just downstream of the tip. Since the tip vortex is altered, the tilting of the lift vector is reduced thus decreasing the lift induced drag [2] . Because of the beneficial effects of winglets, they are presently being used on aircraft such as the Gulfstream IV and the Boeing 747-400 series [3] .

1.2 Previous Research

Although winglets are presently being used to reduce induced drag, they did not simply appear in the present form of nearly vertical surfaces resembling wings.

Researchers have long acknowledged that a non-planar lifting system should have lower levels of induced drag than a planar wing. For example, Lanchester in 1897 patented an idea for vertical surfaces at the tips of wings. Theoretical analyses have also shown the potential for non-planar systems to reduce drag. However, early experimental studies typically showed that these plates or surfaces had little effect in reducing drag until high angles of attack were obtained. At lower angles of attack, any reduction of induced drag was typically more than offset by friction drag associated with the increased surface area of the vertical surfaces. These surfaces also tended to cause an increase in structural weight due to increased loads and moments. Because of the added weight penalty, a greater induced drag reduction could be obtained by simply increasing the span of the wing or adding wing-tip extensions while maintaining the same weight penalty.

However, Whitcomb [1] showed in 1976 that earlier experimenters had not generated significant side forces with their vertical endplates. As stated before, these side forces were needed to reduce the outflow beneath the wing and inflow above the wing. Whitcomb also pointed out that in previous work the end plate had a low aspect ratio and therefore was not an efficient lifting surface. To generate the necessary side forces, Whitcomb used design philosophies typical for the design of wings; thus the vertical surfaces were termed "winglets".

Whitcomb conducted an investigation of the tip mounted winglets which employed his new design strategy on a second-generation, wide-body, jet transport wing as reported in reference 1. The configuration studied consisted of the base wing, an upper winglet and a lower winglet. The upper winglet was placed rearward so that the increased velocity over the inner surface of the winglet and the higher velocity of the wing-tip leading edge were not superimposed. Also, the winglet had a dihedral of 75°, i.e., a 15° cant from the vertical, which allowed reduced effects of mutual interference. The height of the winglet was 15% of the semispan, although an optimum height for each application must be a tradeoff between aerodynamic and structural considerations. Whitcomb stated

that the leading edge sweep should be roughly that of the wing for effectiveness at supercritical design conditions. Winglet effectiveness was also best when the winglet trailing edge sweep was near that of the wing.

The design conditions for Whitcomb's test were for a Mach number of 0.78 and a lift coefficient of 0.44. However, multiple angles of attack were investigated for the configuration. The results of the test indicated that the lower winglet had little effect at the design conditions. The overall results showed for the subsonic Mach number of 0.78 and lift coefficient of 0.44 that winglets reduced induced drag by about 20% and increased wing lift to drag ratio by approximately 9%. Also, the negative increments in pitching moments associated with winglets were less than those created by an equivalent wing-tip extension. Finally, the winglet improvement in the lift-to-drag ratio was more than twice as great as that generated by the wing-tip extension [1] with the same wing root bending moment.

In a similar test, Flechner, Jacobs, and Whitcomb [4] tested a second generation transport wing with an aspect ratio of 7.13 at Mach numbers of 0.70, 0.80, and 0.83 for lift coefficients of up to 0.65. The winglet in this test had a cant angle of 18° and was toed out 2° relative to the fuselage centerline. In this case, toe out indicated that if the winglet had a dihedral of 0°, the airfoils would be rotated -2 ° about their trailing edge. This test showed again that the induced drag was significantly reduced, by 13%, which also resulted in the total drag being lowered. The winglets once again caused small negative increments in the pitching moment coefficients at near design conditions. Winglets were found to produce substantially greater reductions in drag coefficient at near design conditions than a wing-tip extension based on equal effects on wing root bending moment coefficient. Also noted was the fact that the added skin friction and form drag of the winglets dominated at low lift coefficients. However, as the lift coefficient increased, the favorable effects of the winglets increased.

After winglets had been demonstrated to reduce induced drag on high aspect ratio wings at high subsonic Mach numbers, Heyson, Reibe, and Fulton [5] conducted a theoretical parametric study on winglets and wing-tip extensions using linearized subsonic potential flow theory. In their study, a number of aspect ratios, linear washouts, and taper ratios were examined for the base wing. For the tip extensions, a simple linear extrapolation of characteristics of the base wing was used. Finally, the winglets studied had no geometric twist and no taper. The winglet lengths were 15% of the base wing semispan and were canted out 15°. The leading edge sweep of the winglet was kept at 45 ° as compared to the leading edge sweep of 30° for the wing. The results of this parametric study showed that it was possible for a properly designed winglet to develop an induced efficiency increment ranging from two to five times as large as that for a wing-tip extension with the same increment in wing root bending moment coefficient.

Also, several points were made about beneficial effects and harmful effects of winglets. First, the efficiency factor and wing root bending moment both went up as the winglet length increased. Thus, aerodynamic benefits would have to be weighed against structural penalties. Next, leading edge sweeps and subsonic Mach number effects were examined. Unsweeping the winglet tended to be undesirable since this would have reduced the critical Mach number of the geometry, while sweeping the winglet forward would have created aeroelastic divergence problems. Because of these facts, rearward sweep was recommended to minimize interference and compressibility drag in the juncture. Increasing Mach number was found to have an adverse effect on winglet performance. The lowest aspect ratio wing fitted with a winglet, however, was least affected by the increase in Mach number. The researchers noted that "there was more opportunity for Mach number to create adverse interference effects of profile and compressibility drag with the winglet than with a wing-tip extension." The main emphasis, however, showed that winglets were effective on low aspect ratio wings as

well as on high aspect ratio wings. All of these trends were predicted by the linear theory potential flow analytical method, and were consistent with the experimental results of Whitcomb[1].

In Heyson, Reibe, and Fulton, the lowest aspect ratio studied was 4.0. However, highly swept wings such as those used in fighter configurations can have even lower aspect ratios. Kuhlman and Liaw [6] conducted a preliminary numerical design study of wing-winglets where the aspect ratio of the base wing ranged from 1.75 through 2.67. These wing planforms typically had a taper ratio of 0.2 and leading edge sweeps of 45° to 60°, while the winglet length was held at 15% of the wing semispan. For this study, a lift coefficient of approximately 0.3 was the design point for a Mach number of 0.8. This examination of lower aspect ratio wings versus corresponding wing-winglet geometries at transonic speeds indicated that the wing-winglet configurations had decreases in pressure drag of 15% at the design point as compared to wing-alone geometries. Total drag for wing-winglet shapes were 12% less than the corresponding wing-alone geometries. These predicted drag reductions were similar to those obtained by winglets on higher aspect ratio wings.

Kuhlman, Liaw, and Cerney [7] also investigated those geometries in reference 6 at off design conditions, as well as winglets with lengths of approximately 25% of the base wing semispan. For this study, increases in the lift to pressure drag ratio of 14.6% to 15.8% were predicted for wing-winglets as compared to corresponding wing-alone configurations at the same lift. For the longer winglet, 25%(b/2), the lift to pressure drag ratio was increased 19.4% relative to the wing-alone case. The lift-to-total drag ratio was increased by 15.4%. One of the final conclusions of this study stated that the predicted percentages were mainly independent of the base wing aspect ratio or leading edge sweep. However, as the Mach number was increased above 0.9, the onset of drag rise was evident. From the results obtained, winglets were seen to have the potential to reduce drag on low aspect ratio wings, significantly more so than on high aspect ratio

wings. This was due to the fact that the percentage of reduction for the drag coefficients was the same for high or low aspect ratio wings. However, the lift to drag ratio was lower for a low aspect ratio wing and a reduction in the drag coefficient for a low aspect ratio wing would have a larger effect in improving performance, i.e. lift-to-drag ratio.

Cerney [8] investigated the same low aspect ratio planforms as in reference 7, but used supercritical airfoils instead of conventional airfoils. The results of this study showed that at a lift coefficient of 0.39 and at a Mach number of 0.9, the supercritical wing-winglet design produced 2.8% less pressure drag than the conventional airfoil design. However, benefits were not obtained at lower Mach numbers in this case.

All of the previous work discussed to this point was for either high or low aspect ratio wings at flow speeds which were typically high subsonic or transonic Mach numbers. Brown [9] conducted a numerical study to enhance performance of low aspect ratio wing-winglet geometries at transonic velocities. However, once the transonic designs were finished, the configurations were evaluated numerically at a supersonic Mach number of 1.6. For this study, two separate computer codes were used. The first code, SIMP [10], solved the conservative form of the full potential equations to obtain the supersonic results. The other code, called EMTAC [11], solved the Euler equations to obtain solutions for wing and wing-winglet geometries. For the transonic Mach numbers, a pressure drag reduction of 16.3% was obtained for two wing-winglet geometries as compared to similar base wings. Another geometry of a wing with winglet was shown to decrease the total drag by 9.5% over the comparable wing. These results were typical of results demonstrated earlier for low aspect ratio wing-winglet configurations. The study then focused on the supersonic Mach number of 1.6. In this instance, the two cropped delta wings with winglets that had showed a drag decrease transonically had the reverse effect at supersonic speeds. The drag coefficients increased as much as 8.3% at a lift coefficient of 0.13 as compared to the wing-alone configuration drag. The conclusions reached were that winglets were still capable of reducing drag at transonic

Mach numbers, but at supersonic speeds, the winglets would have to be designed for that flight regime. Thus, the transonically designed winglets were not expected to be a fair test of the effects of winglets for supersonic Mach numbers.

In the previous studies and investigations presented, the majority of the emphasis has been the effect of winglets on pressure drag or on induced drag. However, other viewpoints do exist. Asai [12] in particular has stated that the main reason that a winglet was more effective than a tip extension in drag reduction was not due to the fact that a winglet was non-planar, but that a winglet has such a narrow chord length that the relative friction drag penalty was small compared to the friction penalty of a tip extension.

In the present review, winglets have been shown to be effective in reducing pressure drag and total drag for both high aspect ratio and low aspect ratio wings. However, these works have focused on subsonic or transonic Mach numbers. Recent papers have begun to place emphasis on the need for drag reduction at supersonic speeds [13]. In Bushnell's paper, an assertion was made that there is a very real need for improved supersonic aerodynamic performance, and that even a 10% improvement in L/D would be significant. With growing interest in a high speed civil transport and high speed business type transports [14], the importance of methods to reduce drag at supersonic speed is steadily growing.

1.3 Objective of Present Study

The objective of the present work was to determine the effects of winglets on low aspect ratio wings in supersonic flows. In particular, the design range of interest was for a Mach number of 1.62 and lift coefficients approximately from 0.10 to 0.22 [15,16]. This design range was established as desirable by the previous research in references 15 and 16. Performance was also of interest at higher Mach numbers and lift coefficients. To determine these effects, the study was purely numerical, using codes that employed the unsteady Euler equations and the full potential equations. A generic and arbitrary wing

was selected and used as a base wing. Also, wing-tip extensions were used for comparison purposes to establish the winglets effectiveness or lack thereof. These extensions would allow wing-winglet geometries to have approximately equal surface areas and semispan lengths as compared to wings with extensions. Although subsonic design analysis emphasized root bending coefficients, this study was intended only to determine if any aerodynamic benefit could be found from the winglets.

A secondary goal of this study was to determine the effect of winglets designed for the "natural" flow wing of references 15 and 16. Only the outer 10% of the semispan of the "natural" flow wing was allowed to be altered in this study. If improvements could be shown in performance and in drag reductions for the "natural" flow wing, then the "natural" flow wing model presently being built at NASA-Langley would be altered at the tip and the winglet designed by this study would be mounted for testing.

CHAPTER 2

METHOD OF ANALYSIS

2.1 Euler Marching Code Description

An Euler method was chosen for the aerodynamic simulations in the present work. The code selected was called EMTAC [11], for Euler Marching Technique for Accurate Computation. This particular code numerically solved the unsteady Euler equations which, in turn, governed the exact nonlinear inviscid gas dynamics of the flow. By using an Euler method, strong shocks should be captured by the code as well as weaker shocks. Also, the use of Euler equations would allow rotational and vortex effects to be represented in the flow around the geometry of interest. Because of the nonlinearity of the method and its potential for predicting vortex effects, EMTAC should have yielded a realistic representation of the flows considered.

The EMTAC code was used on the voyager CRAY-2S supercomputer at NASA-Langley, accessed from West Virginia University via WVNET and then TELNET. In general, the code was developed to solve the unsteady Euler equations in three dimensions at supersonic speeds with subsonic pockets. To solve the equations, the calculations were done in a marching direction aligned with the axial direction of the given aerodynamic body. At each marching step, the flow quantities were solved for in the cross flow plane. Upon obtaining these results, the marching procedure continued axially. However, this continuous marching was for supersonic regions only. For subsonic regions or subsonic pockets, the marching swept back and forth axially across the region to reach a converged solution. In this manner, the solution for the entire flow field around a particular geometry was generated. A summary of the EMTAC code, governing equations, and solution method has been given in Appendix A.

Since the EMTAC method used a finite volume scheme, several steps of importance were essential for the calculation method previously described. The first step was for the configuration geometry to be described at a limited number of discrete points.

The geometry of interest was represented by a series of cross flow plane cuts as shown in figure 2.1.1. For each cross flow plane, the cut consisted of several patches which were described by 2 to 30 points in the y-z plane. Another restriction to the cross flow plane geometry was that its description should begin at the centerline of the upper surface and proceed outboard. Once the maximum outboard point was encountered, the points were then ordered from outboard to the lower surface centerline. This surface geometry, once generated, was used by EMTAC to set up a body fitted coordinate system so that the boundary conditions could be enforced at the body surface. When calculations were necessary between described cross sectional geometries, EMTAC established a key point system that was generated using cubic splines. These key points were then joined from one prescribed geometry station to the next. The intermediate axial cuts were linearly interpolated from the two closest user prescribed cuts. This system allowed geometries to be established and boundary conditions to be enforced wherever flow field calculations were required.

The second step was that of grid generation. Numerical methods, especially finite difference schemes, need the flow region discretized into grids. This particular code used an elliptic grid generator in the cross flow planes. For the grid generation to start, the gridding routine placed a grid around the already established cross flow body surface geometry. The users control of this grid generator was limited to specifying the number of radial and circumferential points around the geometry. Also, the user was allowed to control certain radial lines and what angles these lines would have as referenced to the horizontal axis. This permitted some control of the grid and helped in preventing the grid from overlapping itself at complex geometric regions.

A third essential area of the code was solving the discretized governing equations. A description of the equation manipulations and solution process has been given in Appendix A.

The last topic for the code description was the output of relevant information. Once the EMTAC program finished solving at a marching plane, a subroutine would compute axial force, vertical force, and side force by numerically integrating the pressure acting on the elemental surface areas. After obtaining the forces, lift, pressure drag, and moment coefficients were calculated based upon user prescribed reference areas and lengths. These coefficients, forces, and pressures as well as other flow field data were presented in line printer form. Flow field and surface variables were also written to a separate pair of files for graphical display. Further details of EMTAC were given in Appendix A and reference 11.

2.2 Full Potential Code Description

To attempt to verify the results from the EMTAC code, another numerical code was used. This code was named SIMP, for Supersonic Implicit Marching Potential [10]. SIMP was very similar in its mode of operation compared to EMTAC except that the SIMP code numerically solved the exact nonlinear potential equations. The code also had a marching procedure that proceeded from the apex to the trailing edge of the geometries studied. As in the case for EMTAC, the SIMP code could sweep back and forth through subsonic pockets or bubbles. The exact same methods were used for this code for defining the geometry and gridding around the geometry as were used for EMTAC. This similarity was one of the major reasons why SIMP was chosen to verify some results. For a more complete description of the SIMP code, the reader is referred to reference 10.

2.3 Friction Drag Analysis

Although the codes used were able to give flow field properties, non-dimensional coefficients, and forces, they did not calculate forces due to friction or friction drag coefficients. To determine the total drag on any particular geometry, the coefficient of friction needed to be calculated and added to the pressure drag coefficient determined by either program. Also, note that the pressure drag given by the codes was a combination

of wave drag and induced drag. To find an approximate skin friction coefficient, an assumption was made that the flow over any of the geometries, wing-winglet or wing with tip extension, would have turbulent flow. Another simplification was made that the geometries would be thin enough to allow use of a frictional coefficient for a flat plate to estimate the frictional drag. The equation finally selected was given as:

$$\bar{c}_f = \frac{0.523}{\ln^2 (0.06\ Re_L)} \qquad (2.3.1)$$

which was valid for a flat, smooth plate at any turbulent Reynolds number [17]. Because this equation was based on a Reynolds number with characteristic length, L, the length was selected to be the mean aerodynamic chord of the geometric body of interest. The mean aerodynamic chord was found by using one of the following equations[18] :

$$\bar{c} = \frac{2}{S} \int_0^{b/2} c^2 (y)\, dy \qquad (2.3.2), \text{ or}$$

$$\bar{c} = \frac{2\, c_r}{3} \frac{1 + \lambda + \lambda^2}{1 + \lambda} \qquad (2.3.3).$$

The value of Re_L was obtained by multiplying the Reynolds number per foot times the mean aerodynamic chord. The Reynolds number per foot was listed in reference 19 as 2 x 10^6 per foot. This was the nominal operating Reynolds number in the Langley Unitary Plan Wind Tunnel. To change the configuration in this study from nondimensional units to English units, the scale factor of 3 feet per 100 units was used. This value was obtained by knowing that the root chord length in this study was 100 units and that a typical model length for the Langley Unitary Plan Wind Tunnel was approximately 3 feet. Thus from equations 2.3.1 through 2.3.3, a skin friction coefficient could be found and in turn, a total drag coefficient calculated.

From the previous discussion, a method has been given that would find the predicted aerodynamic performance of any geometries that should be of interest. The next topic to be addressed is the selection of the geometries which have been numerically studied.

CHAPTER 3

DESIGN AND ALTERATION OF GEOMETRIES

3.1 Base Wing Geometries and Alteration

In general, the base wing was selected to be of a generic nature. The wing selected was a cropped, or clipped, delta wing. The leading and trailing edge sweeps were 65° and 0°, respectively. Also, a taper ratio of 0.2 was chosen and an arbitrary root chord length of 100 units was established. Because of the taper ratio, the root chord choice and the leading edge sweep, the tip chord was automatically set at 20 units, the semispan of the base wing was 37.305 units and the aspect ratio was 1.244 (Fig 3.1.1). The parameters listed gave the essential details of the base wing planform.

Several considerations went into determining the planform and its dimensions. One reason for selecting a sweep angle of 65° was to contain the geometry entirely behind the shock wave created by the apex of the wing. This large sweep angle would allow larger Mach numbers to be studied without the leading edge becoming supersonic. The second reason that the leading edge was fixed at 65° was that the "natural" flow wing [16] to be studied also had a 65 degree leading edge sweep. The trailing edge sweep angle value was also set to mimic that of the "natural" flow wing trailing edge, and to provide simplicity for using the EMTAC and SIMP codes. In either of the codes, swept trailing edges could have been modeled, but the user had to supply the analytical definition of the trailing edge. By keeping the trailing edge sweep set at zero degrees, the edge could simply be defined once, and the codes would not have to be altered continuously.

The root chord was set at a non-dimensional value that would help in avoiding computer errors due to round-off in the geometric description. Also, the selection of a 0.2 taper ratio allowed a wing-tip chord length which would be large enough for winglets to easily be attached. With a large tip chord, a winglet large enough to affect the flow could be defined. The previous considerations were the main factors in determining the development of the base wing planform.

Once the general dimensions of the planform had been established, the next detail of the base wing design was to determine its aerodynamic shape. In this case, the NACA four digit airfoil series[20] was selected to represent the streamwise geometric design. The four digit series was chosen due to the airfoils ease in being analytically defined and the fact that no one airfoil series was obviously better than another for the purpose of this study. Due to a lack of obvious choice, the NACA 1402 was the final airfoil chosen to use for the base wing. For more detail of the NACA four digit series nomenclature and analytical equations see Appendix B or reference 20. The selection of the airfoil shape completed the simple base wing design since no geometric or aerodynamic twist was used.

Although the base wing definition process was completed, the geometry still needed to be converted from its defined form into a usable format for EMTAC and SIMP. To conduct this conversion, a simple FORTRAN program was written (Appendix C). The conversion program started with the wing being described by a series of streamwise airfoils (Fig 3.1.2), NACA 1402 in this case, which were in turn defined by a set of discrete points. Each of these airfoils could have had a different amount of twist about the trailing edge and/or could have had a different airfoil shape from the others.

Once the geometry was adequately defined, cross sectional cuts were needed in order that the SIMP and EMTAC codes could be used. The previously mentioned FORTRAN program was used to perform this manipulation. This program allowed the user to specify the number and location of cross sectional cuts desired. After the location of the cross sectional cut was determined, an interpolation process began. Interpolation was performed first on the upper surface of the wing. At each airfoil location a new thickness and span location were found at the desired axial location and written to an output file. Next, span distances and upper surface locations were found between the present airfoil and the next outboard airfoil. Once the points located between the two airfoils were calculated, the next outboard airfoil was considered, then in between airfoils, and so on until the leading edge or the tip of the wing was encountered. Afterwards a similar

interpolation procedure was used on the lower surface of the wing. However, this marching process was performed from outboard to inboard until the root chord of the wing was encountered. Upon completing one cross section, the program calculated the next downstream cross-sectional cut until the trailing edge was reached.

The cross sectional geometric cuts obtained in this fashion were still not useable for EMTAC or SIMP, since the cuts did not contain the same number of points per axial cut. A final program, EXPCONX, was written to take the previously described output and interpolate spanwise on each cut such that there would be an identical number of points per cross sectional cut (Appendix D). To do so, the upper surface coordinates of a cut were read from a file. This surface was separated into two lengths along the local half span. The lengths were defined by the user in terms of a percentage of the local semispan. This allowed a sudden change in geometry or more complex regions to be modelled more accurately with a greater number points. Interpolations were performed until the two patches had an equal number of points, where in this particular instance 30 points per patch were selected. The new coordinates were written to a file in the EMTAC and SIMP format. The lower surface coordinates were next read by EXPCONX and treated in a manner similar to the upper surface. Examples of the final results of conversion from streamwise airfoils to cross sectional cuts can be seen in figures 3.1.2 and 3.1.3, respectively.

The other base wing considered in the present study was the "natural" flow wing described in references 15 and 16. The "natural" flow wing was designed with a leading edge sweep of 65° and a trailing edge sweep of 0° for a Mach number of 1.62. The design lift coefficients ranged from approximately 0.0 to 0.4 with special emphasis placed on coefficients of 0.1 and 0.3. To design the "natural" flow wing, the codes described in references 10 and 11 were used. These are the same codes used in the present study. The final dimensions of the planform were a root chord of 100 units and a semispan of 46.63 units.

The "natural" flow wing design differed from previous supersonic designs in several ways. First, the typical thickness distributions of uncambered delta wings result in a geometry which is conical about the wing-tip. However, for supersonic flow, the flow field is nearly conical about the apex of the wing. Also, the supersonic flow tends to have a recompression line which is independent of the geometry of the wing and exists along a ray that starts at the wing apex (figure 3.1.4). In figure 3.1.4, the recompression line as well as the maximum thickness line have been indicated. Outboard of the recompression line, the pressure tends to be lower for the flow and thus creates a suction. Inboard of the recompression line, pressure increases. From geometric and flow considerations, adverse drag effects were present in regions A and C while beneficial effects were gained from zones B and D. The "natural" flow wing was designed to take these effects into account. In doing so, the maximum thickness line was swept back so as to take advantage of the recompression line (Fig 3.1.5). When the trailing edge was encountered, the particular airfoil was stopped and a base area along the trailing edge was produced.

For the airfoil definitions in references 15 and 16, the modified NACA four digit series was used. The "natural" flow wing was analytically altered in a parametric study to find the best thickness, leading edge bluntness, and camber[16]. Another parametric variation was a "shearing" process that was used to alter the thickness of the airfoils as they changed spanwise. In this manner, the "natural" flow wing design process was completed. The final combination of the items previously listed for the "natural" flow wing gave a 10% drag reduction as compared to near conical wings at a lift coefficient of 0.1 and a 14% drag reduction at a lift coefficient of 0.3 as also compared to a near conical wings. To attach winglets to this geometry in the present study, the outer 10% of the semispan was allowed to be altered.

3.2 Wing-tip Extensions

For comparison purposes, wing-tip extensions have been used so that wing geometries would have approximately the same semispan as wing-winglet geometries. Since the base wing had no geometric or aerodynamic twist, the tip extension was simply selected to consist of NACA 1402 airfoils and stopped at a semispan of 40 units. The "natural" flow wing did not have a wing-tip extension and was compared to the wing-winglet configurations as it was originally designed.

3.3 Winglet Design and Configurations for the NACA 1402 Wing

Since no known numerical or experimental study had been conducted specifically on winglets at supersonic speeds, the design philosophy which has been successful for transonic designs has also been used as a starting point in the present study. The general planform of the winglet had a trailing edge sweep of 0° where the winglet trailing edge coincided with the trailing edge of the base wing. The length of most of the winglets studied was approximately 15% of the base wing semispan. The winglet leading edge sweep was parametrically altered and should be noted for each winglet or group of winglets. The root chord of the winglet was typically 65% of the tip chord of the base wing except where noted. This winglet root chord length allowed the leading edge of the winglet to be placed in the approximate location of the maximum thickness of the wing-tip airfoil. The airfoil shapes that describe the winglets were essentially divided into two groups. The first group had zero thickness and was described by mean lines of the NACA four digit series. The second group of airfoil shapes was described by the NACA four digit series and typically had a maximum thickness of 4 percent of chord length. To attach the winglet to the base wing, a FORTRAN program (Appendix E) was used to linearly interpolate a series of four airfoils between the base wing tip airfoil and the winglet root airfoil. These four airfoils were used to define a curved juncture between the winglet and wing.

Since the winglets were described by airfoils consisting of discrete points, they were also manipulated by the programs listed in Appendices C and D. These programs set the geometries into appropriate EMTAC and SIMP format. Once again, the first program described operated by interpolating on the upper surface from inboard to outboard. However, the geometry was no longer of a planar nature. To compensate for this fact, the winglet airfoil coordinates were first calculated in the plane of the wing and then the winglet was rotated about the trailing edge of the tip chord and span location. Each airfoil in the juncture was rotated about the trailing edge of the wing-tip airfoil. Once the proper rotations had been performed, the program listed in Appendix C shifted the juncture and winglet such that the geometry did not overlap itself in the spanwise direction. The process of obtaining cross-sectional cuts was carried out in the same fashion as for the wing-alone. The program that gave the same number of points per patch also ran exactly as described earlier for the wing-alone.

Although a general planform for the winglet geometries had been established, several parametric alterations were conducted on both the zero thickness winglets as well as the 4% thick winglets. Also, some special cases were investigated to help provide insight or to attempt to lower the pressure drag results. The first geometries which will be discussed are the zero thickness winglets. These winglets were studied over a geometric angle of attack range from -5° to 15°. The basic zero-thickness winglets had a winglet leading edge sweep of 65°, and a dihedral or an anhedral of 75°. This allowed a comparison to be made of the effects of having a winglet pointing up relative to a comparable winglet case pointing down. A wide range of winglet incidence was investigated for both up and down winglet cases. For both dihedrals, the 0% thick winglet was toed out 0, 2, 4, and 6 degrees. These winglets were toed in as well at angles of 2, 4, and 6 degrees. The terms "toed in" and "toed out" reflect the direction that the winglet was rotated about its trailing edge. Toed out indicated that for a winglet with dihedral, the airfoils of the winglet, if they were in the plane of the wing, were rotated to a negative geometric incidence. This

could also be viewed as shifting leading edge outboard from the geometric centerline of the body if the winglet was perpendicular to the wing. For toed in, a winglet with dihedral would have positive incidence in the plane of the wing. When a winglet had anhedral, negative dihedral, the incidences were reversed as compared to the positive dihedral case. These geometries were studied using the EMTAC code and the wing-winglet case with the highest predicted lift-to-drag ratio was selected as compared to all the other cases, with a particular emphasis in the lift coefficient range of 0.10 to approximately 0.22.

After selecting the best geometric alignment and winglet dihedral, up or down from the wing plane, the next parametric test was conducted on the leading edge sweep of the winglet. This parametric variation was conducted on the sweep angles of 0°, 22°, and 44° where 65° was already completed due to the initial parametric study. Again, the leading edge that produced the lowest pressure drag or best lift-to-pressure drag ratio in the lift coefficient range of 0.10 to 0.22 was selected as most desirable. The geometric alignment or parameter that resulted in better performance was set as a fixed value in the remaining parametric variations.

Initially, the zero thickness winglets were merely flat plates. Because of that fact, another parameter that was altered was the camber of the winglets. The camber selections were for m equal to -0.02, -0.01, 0.00, 0.01, and 0.02 ,where "m" is the maximum ordinate of the mean line expressed as a fraction of chord, as has been defined for the NACA four digit series in Appendix B. Of course, the 0.00 case had already been investigated since it was the planar case. Finally, the last parameter to be investigated was the winglet length. Since the winglet length had been held to 15% of the base wing semispan, two more cases were studied for winglet lengths of 10% and 12.5% of the semispan. Once the effects of length variation had been examined, the study of zero thickness winglets was concluded.

Although a zero thickness winglet gave an indication of the effectiveness of winglets on altering the supersonic flow around the NACA 1402 base wing, they were not reasonable

for a real design. Because of this fact, the performance of winglets with thickness was also examined. A similar strategy was applied to the winglets with thickness as was applied to the winglets without thickness. Once again the winglet planform was selected to be similar to that of the flat plate winglet except the leading edge sweep was set at 50° which was the sweep typical of the transonic designs. The same angle of attack range was run for each geometry, -5° through 15°. As before, both 75° and -75° dihedral was studied for a series of toe in and toe out angles. The airfoil selected for the winglet in this case was a 2404. This somewhat highly cambered airfoil was selected due to the fact that large amounts of camber had been found to be helpful transonically. The toe out angles for the 75° dihedral winglet were 2°, 3°, and 4°. For the anhedral winglet, the toe in angles were 1°, 2°, 3°, and 4° while the toe out angles were 0° and 1°. After these selected geometries were studied using the EMTAC code, the geometry that had the best lift-to-pressure drag ratio and pressure drag polar as compared to the other cases was the one selected to continue with other parametric variations.

With the dihedral fixed as well as the toe in or toe out angle, the camber of the winglet airfoils with thickness was varied. Using NACA four digit series notation again, "m", the maximum ordinate of mean line expressed as a fraction of chord, was selected to be -0.01, 0.00, 0.01, and 0.03 while the 0.02 case had been tested using the NACA 2404 airfoils. After the camber series had been compared, three parameters of interest were left to be studied. These parameters were leading edge sweep, winglet length, and dihedral effects. For the variation of the winglet leading edge sweep, the angles of 60°, 65°, and 68° were chosen. One of the final parameters was the winglet length. Since the winglet length had been 15% of the semispan for the initial studies, the other lengths were selected as 7.5%, 10.0%, and 12.5% of the base wing semispan. The final parameter studied was the effect of anhedral. For this alteration, angles of 30° and 50° anhedral were selected. Upon completing the test cases of length, sweep, and dihedral, the remaining

studies were the special case winglets and the winglets applied to the "natural" flow wing.

The special case which was studied in most detail was that of winglets with a root chord equal in length to that of the tip chord of the base wing. Again, winglets with 75° dihedral and 75° anhedral were studied. The planform of these winglets had a 0° trailing edge sweep continuous with the base wing trailing edge and a leading edge sweep of 50°. A NACA 2404 airfoil was used in the study of toe in and toe out. For winglets rotated above the plane of the wing, the toe out angles were limited to 2°, 3°, 4°, and 6°. The toe in angles for the winglets below the plane of the wing were 2°, 3°, and 4°. The best case was found from these geometries by mutual comparison of the predicted performance. The other parameter varied for the full tip chord winglets was the location of the maximum camber. The three locations tested for the maximum camber were at 20%, 40%, and 60% of the local chord length. Both upward orientated and downward orientated winglets were tested for a toe out angle of 0°. These two parameters discussed were the only two variations conducted for winglets whose root chord length equalled the base wing tip chord.

Another parametric study was done to examine the effects of decreasing winglet thickness with different amounts of camber. In this instance, the airfoils selected for the winglet were 2% thick relative to the local chord and had maximum camber values,"m", of -0.01, 0.00, 0.01, 0.03, and 0.04 The winglets had a planform identical to that of the flat plate winglets except the leading edge sweep was 50° and all winglets had a dihedral of -75°. The toe angle for these geometries was kept at a 2° toe in angle.

3.4 Winglet Design for the "Natural" Flow Wing

The final winglet studies involved the "natural" flow wing of references 15 and 16. As stated before, only the outer 10% of the semispan of this wing could be altered which meant that the earliest that the winglet or juncture could begin to appear would be at a root

chord position of 90 units. Therefore, the maximum tip chord could only be 10 units, or half the tip chord length of the previously studied NACA 1402 base wing. This restriction posed constraints in the free development of the winglet geometry. Another problem encountered for the "natural" flow wing was the fact that the streamwise contours were no longer complete NACA airfoils in the outer 10% of the wing semispan. The contours present were truncated at the trailing edge. However, continuity of the wing and winglet geometry was desirable. To keep geometric continuity, a span location was selected for the tip of the base "natural" wing. The streamwise contour of this span location was found and used as the "airfoil" contour for the winglets to be studied. This decision allowed the trailing edge of the winglet to have a base area similar to that of the "natural" flow wing. For the juncture definition between the wing and winglet, a third order polynomial was used instead of airfoils due to the fact that the truncated airfoils tended to be too thick for this region.

For placing the "natural" wing with winglet into EMTAC format, another program was required (Appendix F). The geometric definition of the "natural" wing was given in 100 cross sectional cuts with each cut consisting of three patches. However, in order to define a geometry with a winglet attached, cross sectional cuts with four patches were preferred. Thus the program, CHANGE, listed in Appendix F had two purposes. The first purpose was to take the unaltered "natural" wing and change all three patch cuts into four patch sections. The same number of points per cross section was maintained when a winglet was not present. The second purpose of CHANGE was to take the prescribed definition of the "natural" wing, already in EMTAC format, and the output results of the FORTRAN program listed in Appendix C then "splice" the two bodies together into a wing-winglet combination. For more details of that procedure, refer to Appendix F.

Because of the geometric constraints, fewer parameters were varied for the "natural" winglets. For the dihedral angles, only 65° and -65° were run due to the thickness in the juncture of the wing-winglet. The toe angles for these configurations were 0° and 2° toe

out and 2° and 4° toe in for the downward winglet. The 65° dihedral winglet was run at 2° toe in and 0°, 2°, and 4° toe out angles. These geometries were run at angles of attack of -5°, 0°, 2.5°, 7°, and 9.5° for a Mach number of 1.62

The planform of the winglet was identical in all cases. The root chord length of the winglet was 10 units while the tip chord length of the winglet was 1.01 units. The trailing edge sweep was fixed at 0° and the leading edge sweep was 55°. These planform parameters and restrictions fixed the winglet length at 6.29 units, or 15% of 41.97 units which is the altered wing semispan length.

With the geometries selected and properly converted to EMTAC form, the next step in this study was to obtain the predicted performance coefficients and associated forces for each geometry.

CHAPTER 4

RESULTS AND COMPARISONS

4.1 Presentation and Convergence of Results

The focus of this chapter is to present the results obtained from the EMTAC code. To understand the results, a series of comparisons will be conducted between winglets for each parametric variation, and the best performing wing-winglet would be compared to the relevant base wing. The two base wings were the NACA 1402 base wing and the "natural" flow wing. Some results that will be presented are incremental force build up along the geometries; total force build up along the geometries; predicted performance plots; and in a limited number of cases, off-body contour plots were used. The presented information was useful in showing the relative performance of each of the geometries as well as judging the accuracy of the solutions.

For output from the computer codes used in the present study to be of use, the solutions that they generated must be independent of the particular grid used. A previous study by McGrath, Covell, and Walker [21] has shown that a minimum cross flow plane grid density was necessary for convergence of solutions using the EMTAC code. Grid density was defined to be the number of grid points along the surface circumference times the number of grid points normal to the surface of the body being studied. The maximum grid density for EMTAC was 2400, 80 by 30 points. The study of McGrath, et. al., demonstrated that a grid density of 1220 cross sectional grid points could be used to insure convergence for wing-body configurations. Because of that study, the grid densities for the geometries developed in the present work were restricted to a 59 by 25 grid or higher. With a minimum grid density of 1475, all solutions obtained should have had results that were independent of the grid used.

Other factors in assuring convergence were the values of NCON and GLOBIT listed in the EMTAC headers. NCON stipulated the number of marching steps to the XSTART

location of region one. This value was selected at first to be 30 units. However, NCON was later changed to 300 units but had no effect on the solutions obtained from EMTAC. GLOBIT was a variable that controlled the number of global iterations that EMTAC did for each marching step. This value was initially set at 2 when the study began and was changed to 5 for the "natural" flow winglet cases and the final NACA 1402 winglet design. The alteration of GLOBIT affected the results in the fourth significant digit and was assumed non-critical except in run time. For a GLOBIT value of 2, the typical run time was approximately 1200 cpu seconds. However, increasing GLOBIT to 5 increased the run time approximately to 3000 cpu seconds.

4.2 The NACA 1402 Base Wing with Extension

For all of the present wing-winglet designs, only a limited range of projected semispans were used. This semispan range was from 39.6532 units to 40.796741 units. Because a consistent comparison between wing-winglet designs and a wing-alone design was wanted, an extension was added to the NACA 1402 base wing. This extension fixed the semispan of the wing to 40 units. With a semispan of 40 units, the maximum difference between semispan ranged between 0.87% to 1.97% for all wing-winglets to be studied.

To obtain a solution from the EMTAC program, grids were specified for four axial regions. These regions were from the wing apex to a specified axial location, followed by three restarts. Although the wing alone geometry could have been calculated with one grid description and one region, several regions were used to develop an understanding of the EMTAC restart option. A typical grid for a wing-alone has been given in figure A.3.1. Table 4.2.1. lists the relevant values of grid parameters and restart locations for the wing-alone case. In this table, XSTART indicated where the code began to calculate three-dimensional flow field values for the configuration for a particular region. The XEND value determined the axial ending location of the calculation. The values, NPT, INU, and THTU, were used to control the grid in the cross flow plane. NPT values

determined the number of points in each patch in the circumferential direction. The variable INU specified which line or lines extending radially from the body surface would have slopes controlled in the grid, while the THTU value indicated the angle or angles between the controlled radial line(s) and the horizontal plane. Also, the axial size for the marching solutions for each region was given by Δx.

For the base wing with extension, the angles of attack of -5°, 0°, 2.5°, 5°, 9° and 15° were run for a Mach number of 1.62. The lift coefficients, pressure drag coefficients, and pitching moment coefficients have been listed in Table 4.2.2. To check for valid, converged solutions, two items were routinely checked for this, and all subsequent geometries. The first item checked was the densities in the flow field output. In particular, the appearance of negative density values was monitored. Although density cannot be negative in physical situations, the EMTAC code could calculate negative densities in the flow field. The possible source of the negative densities could be related to the fact that the solution of the flowfield was for the discretized equations instead of the exact analytical functions. Also, the code did not restrict or alter the results obtained by the volume differencing technique. Typically, negative densities would appear on the surface of the body at the outermost part of the semispan. In other words, the leading edge was the physical location for any non-physical negative densities. The results of a run at an angle of attack were dismissed if negative densities were observed more than two radial grid points out from the surface. Also, if negative densities were observed on the body surface for a large portion, e.g. 5 to 10, of the circumferential grid points, the result was discarded as an unreliable solution. The wing-alone configuration would usually have no more than one or two negative densities at 4 or 5 marching planes. At lower angles of attack, negative densities were totally absent while at higher angles of attack, 9° or 15°, a greater number of negative densities appeared.

The second item checked to insure accurate realistic solutions was the smoothness of the incremental force build up distributions, as shown in figure 4.2.1. The incremental force

build ups in figure 4.2.1 appear to have a "bucket" or discontinuity at approximately axial locations of 0.80 through 0.85. However, this drop appeared not as a result of a solution error, but due to the plotting method in the software provided by NASA-Langley where the actual incremental force coefficient was plotted. For the region of 0.8 to 0.85, approximately, the axial step size for the solution was 0.1 units. This step size was one-half the step size of region one or region four. Thus, it should be noted that the vertical height of the "bucket" was one-half that of regions 1 and 4 because of the smaller axial step size. The incremental force plots for lift and pressure drag were also examined for discontinuities. If discontinuities or large spikes were evident in either the lift or drag plots, the solution was considered diverged or unrealistic. Although these two checks were done independently, it was observed that solutions which contained a large number of negative densities were usually divergent as well, as judged by the axial force build up plots. However, solutions that were divergent did not always have a considerable number of negative densities. The total lift and pressure drag force build ups have also been given for this wing-alone configuration in figure 4.2.2.

4.3 Toe In and Toe Out for 0% Thick Winglets with Dihedral

Once again, the first step in obtaining a solution for a geometry was to generate an appropriate grid. For 0% thick winglets with 75° dihedral and a winglet leading edge sweep of 65°, the parameters for the best grids established have been given in Table 4.3.1. The wing-winglet geometries differed from the wing-alone not only in geometric make-up, but also required at least four separate axial regions to allow proper grids to be placed around the geometry. Examples of the grids used for the 0% winglets at 75° dihedral have been given in figure 4.3.1. As in the wing-alone case, the same checks were used to test for physically believable solutions for the wing-winglet geometries. Typical examples of incremental and total lift build up and pressure drag build up distributions for an angle of attack of 5° are shown in figures 4.3.2 and 4.3.3 for this winglet geometry. In figures

4.3.2 and 4.3.3, results are for the geometry of the winglet case with 2° toe out. The other 75° dihedral cases tested were 0, 2, 4, and 6 degrees toe out and 2, 4, and 6 degrees toe in. Incremental force build up distributions appeared quite similar to those of figure 4.3.2 for all of these cases.

To select the best performance of a winglet, several factors were examined. Among these factors were lift-to-pressure drag ratio, pressure drag coefficient, and moment coefficient as functions of lift coefficient. The main factors however were lift-to-pressure drag ratio versus lift coefficient and pressure drag coefficient versus lift coefficient, with emphasis on performance in the lift coefficient range of 0.10 to 0.22. Once the best winglet performance was selected, the particular geometric parameter being parametrically studied was fixed during the remaining studies.

The first parameter varied was toe in and toe out for winglets with positive dihedral. As previously stated, a limited range of coefficients and lift-to-drag ratios were used to determine which winglet performed better in a parameter study. The lift-to-pressure drag ratio performance plot was considered physically reliable due to the trend of the plot. As the lift coefficient became larger, the lift-to-pressure drag ratio decreased, while at lower lift coefficients, the lift-to-pressure drag ratio was essentially linear in nature. This trend was typical of lift-to-drag plots from theoretical and experimental considerations. Figures 4.3.4 through 4.3.11 show the plots of coefficients and ratios of interest versus lift coefficients. The exact values of angle of attack, lift coefficient, pressure drag coefficient, and moment coefficient have been given in Table 4.3.2, as obtained from the EMTAC code. Figures 4.3.4 through 4.3.7 were for the toe out angles of 2°, 4°, and 6° as well as 0° toe out. The angle of attack as a function of lift coefficient and moment coefficient as a function of C_L revealed that the four winglets were close to one another in their behavior and in affecting the flow field. By examining the lift-to-pressure drag ratio and pressure drag polar, with emphasis in the lift coefficient range of 0.10 to 0.22, a difference was observed between the four winglets under consideration. Of the four, the winglet with 0° toe out

can be seen to have a lift-to-pressure drag performance (figure 4.3.5) that would be a penalty compared to the other three. As for the other three cases, an identical performance prediction was obtained over most of the global lift coefficient range. However, for the C_L range of interest, the geometries with 2° and 4° of toe out performed better than both the 0° and 6° toe out geometries. Also, the 6° toe out had questionable results based on the incremental drag build up. A closer inspection of figure 4.3.5 showed that the 2° toe out geometry outperformed the 4 degree toe out configuration out of the specified lift coefficient range. Because of this off design performance, the winglet with 2° toe out was chosen as the best of the four cases for those inspected.

Toe in angles of 2°, 4°, and 6° and 0° toe out have also been presented in figures 4.3.8 through 4.3.11 for the same winglet planform and dihedral angle. Although the toe in angles of 2°, 4°, and 6° performed similarly through the lift coefficient range, a significant difference was obvious in the lift coefficient range of 0.10 to 0.22. The 0° toe out winglet is seen to outperform the other three alignments in figures 4.3.9 and 4.3.10. However, it has previously been shown that the winglet with a 2° toe out had a better performance than the 0° toe out winglet. From this comparison, the winglet with 2° toe out was determined to be the best for this parametric variation.

4.4 Toe In and Toe Out for 0% Thick Winglets with Anhedral

For winglets with anhedral, i.e., negative dihedral, grids similar to those for winglets with positive dihedral were used, but with the plane of the wing being the plane of symmetry. The grids required by the 0% thick, -75° dihedral winglets have previously been listed in Table 4.3.1 with the variables, INU, NPT, and THTU, being the same as discussed in 4.2. Also, examples of the grids were given in figure 4.4.1. As with the upward winglets discussed in section 4.3, the predicted performance levels of the downward winglets were compared against one another, with the best performance determining the optimal value of the parameter under study. The predicted performance

was determined by the EMTAC code results listed in Table 4.4.1. Figures 4.4.2 through 4.4.9 give the performance plots for the toe in angles of 2°, 4°, and 6° and the toe out angles of 2°, 4°, and 6° as well as 0° toe out. The first figures considered were 4.4.2 through 4.4.5. These plots were for the toe in angles and the 0° toe out angle. The plots of angle of attack and moment coefficient as functions of lift coefficient indicated little difference among the winglets. However, studying the lift-to-pressure drag ratio plot, the 2° toe in winglet was able to outperform the 4° and 6° toe in winglets at a lift coefficient of approximately 0.05. In the C_L range of interest, the 2° and 4° toe in winglets outperformed the 6° in and 0° toe out winglet alignments. From these considerations, the 2° toe in was selected as the best alignment for the downward winglet.

Results for the remaining winglets with anhedral, toed out 2°, 4°, and 6° are presented and compared with 0° toe out in figures 4.4.6 through 4.4.9. An immediate distinction is evident for lift coefficients ranging from 0.10 to 0.22. The winglet with 0° toe out had a better lift-to-pressure drag performance and a better or equal drag polar. However, the 2° toe in winglet configuration was already demonstrated to be more effective than the 0° toe out winglet. From these facts, the best performance was given by the winglet when it was toed in 2°. The incremental lift and drag build ups for this configuration have been given in figure 4.4.10 for an angle of attack equal to 5° while the total lift and drag build ups have been given in figure 4.4.11. The smoothness of these axial force distributions is similar to the distributions obtained for the other geometries.

After determining the best winglet cases for 75° and -75° dihedral winglets with no thickness, a comparison was made between the 2° toe out, 75° dihedral wing-winglet; the 2° toe in, 75° anhedral wing-winglet; and the wing with extension at a semispan of 40 units. This comparison has been presented in figures 4.4.12 through 4.4.15. For the total lift coefficient range of -0.2 to approximately 0.7, a trend was apparent that the wing-alone and 2° toed in, downward winglet slightly outperformed the 75° dihedral winglet toed out 2°. In the C_L range of interest, the 75° dihedral winglet with 2° toe out was outperformed

by the two other configurations in both drag polar and lift-to-pressure drag ratio. The -75° dihedral winglet was also slightly outperformed by the NACA 1402 wing with extension in some instances. However, the -75° dihedral winglet generally duplicated the wing-alone performance. Due to this comparison, future zero thickness winglet studies were fixed to have anhedral and the winglet had a toe in of 2°.

4.5 Camber Effects on the 0% Thick Winglet

After setting the winglet geometry to an anhedral of 75° and to a 2° toe in, the next parametric variation was for camber. The values of "m" investigated were -0.02, -0.01, 0.00, 0.01, and 0.02 where m is the maximum ordinate of the mean line as a fraction of the chord, see Appendix B. The location of the maximum ordinate was at 40% chord for the winglets studied. The grids used in this study have been listed in Table 4.3.1. The force and moment coefficient results from EMTAC for these configurations have been listed in Table 4.5.1. For the five configurations which were run, the results differed negligibly. This may be seen in figures 4.5.1 through 4.5.4 where only results for the two extreme cases of 0.02 and -0.02 were represented on the plots. These two configurations, as well as those not shown, plotted exactly on top of one another. Because of no alteration or improvement could be found from this parametric study, the winglet was to remain uncambered for the rest of the parametric variations.

4.6 Leading Edge Sweep of Winglets with No Thickness

For the previous parametric studies, the winglet leading edge sweep had been set at 65°. The next alterations were made on the winglet leading edge sweep. The leading edge sweeps selected were 0°, 22°, 44°, along with the previous sweep of 65°. As usual for wing-winglet geometries, four axial regions of grids were needed. The grids specified for each winglet have been given in Table 4.3.1. Although the EMTAC code had been reliable for computing results in the earlier parametric variations, the program had trouble obtaining

solutions for the 0° and 22° leading edge sweeps. Because of discontinuities in the incremental force build ups and the program terminating its operation, the parameter of 0° leading edge sweep could not be included in this variation. Results for the leading edge sweeps of 22° and 44° were also questionable as judged by oscillations in the incremental force build ups. A possible explanation to the problems encountered by the 0° and 22° leading edge sweep winglets might be related to the fact that for a Mach number of 1.62 these angles caused the winglet leading edge to be supersonic. As for the 44° leading edge sweep, its close proximity to a leading edge shock may have been the problem. For a Mach number of 1.62, a minimum leading edge sweep of 38.11° could be used and be able to retain a subsonic leading edge. The leading edge sweep of 65° was maintained throughout the last parametric variation due to the other sweeps having questionable solutions.

The values of the calculated coefficients (Table 4.6.1) have been plotted for performance even though the believability of the solutions was questioned, see figures 4.6.1 through 4.6.4. If the solutions to the winglet with a leading edge sweep of 44° were to be considered as converged, then this winglet would have been the one taken as best. The winglet with a leading edge of 44° had a better lift-to-pressure drag ratio performance (figure 4.6.2) than the 65° leading edge sweep or the wing-alone configuration. However, this conclusion is uncertain because of the questionable validity of solutions for the 44° sweep winglet.

4.7 Length Variation of the Winglet with No Thickness

The last variational study conducted for zero thickness winglets was for the effects of winglet length. All winglets to this point had a length equal to 15% of the base wing semispan. To determine the effect of winglet length on performance, two other winglet lengths were selected at 10% and 12.5% of the length of the base wing semispan. The grids and related specifiers for these configurations have been given in Table 4.3.1 and

are the same as those for the -75° dihedral winglet. The coefficients generated by EMTAC have been listed in Table 4.7.1. As before, the performance of the geometries and the wing-alone have been plotted in figures 4.7.1 through 4.7.4. The wing-alone outperformed or equalled the performance of all three wing-winglet configurations. Also of note was the fact that the three wing-winglet geometries had the same predicted performance even though the winglets were of different lengths. The best case could not be selected due to the fact that all three cases had the same performance.

4.8 Toe Out for Winglets with Thickness and Dihedral

Once winglets with zero thickness had been parametrically tested, the next phase of the study was to test winglets with thickness. The winglet airfoil thickness selected was 4% of the local chord length and the camber value of "m" was 0.02. The first parametric study conducted was for winglets with 75° dihedral and a leading edge sweep of 50°. Due to the results of winglets without thickness, only positive toe out angles were tested. The angles tested were 2°, 3°, and 4°, as well as 0° toe out. The grid parameters used on these geometries have been listed in Table 4.8.1, while example grids are shown in figure 4.8.1. The calculated EMTAC code force and moment coefficients values have been given in Table 4.8.2. The procedure used to determine the best winglet alignment was the same as that used for winglets without thickness. Several performance criteria were compared between the four winglet geometries tested.

The performance data are plotted in figures 4.8.2 through 4.8.5. The four winglets under consideration performed identically except for the lift-to-pressure drag ratio versus lift coefficient (figure 4.8.3). In the specific range of interest, the 3° and 4° toe out winglets perform the same as the 2° toe out winglet around the C_L value of 0.2. However, winglets with 3° and 4° toe out outperform the 2° toe out near the 0.105 value of lift coefficient. The 0° toe out alignment was worse in performance than the other three winglets in the lift coefficient range of interest. Over the total range of C_L's covered, the

2° toe out was a better configuration than the 3° and the 4° toe out alignments near a lift coefficient of 0.05. Based upon off design performance plus the close or equal performance in the design range, the 2° toe out angle was selected for further study.

The incremental lift and pressure drag force build up plots have been shown in figure 4.8.6 for 5° angle of attack to indicate the validity of the solutions. The total force build up plots have been also given in figure 4.8.7.

4.9 Toe In and Toe Out for the Winglet with Thickness and Anhedral

The parametric alteration of toe out and toe in has also been conducted on a cambered winglet with anhedral. The winglet had a leading edge sweep of 50°, a length of 15% of the semispan and an anhedral of 75°. The mean camber value used was for "m" equal to 0.02. The grids needed for computation around this body have been given in Table 4.8.1 while examples of these grids have been given in figure 4.9.1. Since the zero thickness winglets performed better with negative dihedral, more toe in and out angles were studied for the 4% thick downward winglet than the winglet with thickness and positive dihedral. The toe in angles attempted were 1°, 2°, 3°, and 4° while the toe out angles were 0° and 1°. The calculated EMTAC performance results for this parametric variation have been given in Table 4.9.1.

To select the best alignment of the winglet, performance plots were again used to compare the various toe angles against one another. The toe in angles of 1° through 4° have been compared against one another in figure 4.9.2 through 4.9.5. Once the best alignment was found among those four, it would be compared with 0° and 1° toe out alignments. Examining figures 4.9.2 through 4.9.5, the toed in winglets were almost identical in performance. However, in the lift-to-pressure drag ratio plot, the 1° and 2° toe in angles showed better performance at a lift coefficient of approximately 0.05. As for the lift coefficient range of interest, the 2° toe in angle was better than the 1° toe in angle and equaled the performance of the 3° and 4° toe in angles. Due to this performance, the 2°

toe in angle was selected to be compared with the 0° and the 1° toe out angles in figures 4.9.6 through 4.9.9.

For the lift coefficient range of approximately 0.0 to 0.7, all winglets performed nearly identical to one another. In the lift coefficient range of 0.10 to 0.22, a noticeable difference could be observed especially in the pressure drag polar and the lift-to-pressure drag ratio plots (figures 4.9.7 and 4.9.8). The 2° toe in angle had a lower drag polar and a higher lift-to-drag ratio which indicated that the 2° toe in was the best alignment of the three.

The best alignment for winglets with dihedral and anhedral have been found. For the remaining parametric variations, the winglet position that obtained the best performance was used. To determine the best alignment, the 75° dihedral winglet with 2° toe out was compared with the -75° dihedral winglet that was toed in 2°. The wing-alone configuration has also been plotted in the performance plots (figures 4.9.10 through 4.9.13). By examining figures 4.9.10 through 4.9.13, the best wing-winglet performance was found to be the -75° dihedral winglet with a 2° toe in. The 2° toe in, downward winglet had a lower pressure drag polar and a higher lift -to-pressure drag ratio especially in the lift coefficient range of 0.10 to 0.22. However, the wing with a semispan of 40 units was able to slightly outperform the best winglet case throughout the lift coefficient range. The incremental lift and drag forces have been given in figures 4.9.14 for the winglet that was toed in 2° and had a -75° dihedral at 5° angle of attack. The total forces for this winglet alignment have also been given in figure 4.9.15.

4.10 Camber Effectiveness for the 4% Thick Winglet

The winglet chosen to proceed with in the parametric study was toed in 2° and had a dihedral of -75°. The leading edge sweep of the winglet was still fixed at 50°. In this parametric study, the maximum ordinates of mean line expressed as a fraction of chord, "m", were studied at values of -0.01, 0.00, 0.01, 0.02, and 0.03. The EMTAC grids

used have been listed in Table 4.8.1 which were the same grids that had previously been used. The corresponding performance coefficients were given in Table 4.10.1.

To help in presenting the performance results, results for various values of camber have been divided into two groups. The first group was for the camber values of 0.01, 0.02, and 0.03 (figures 4.10.1 through 4.10.4). The second group consisted of -0.01, 0.00 and the geometry with the best drag reduction or lift-to-drag increase in the first group (figures 4.10.5 through 4.10.8). The first set of plots had only one obvious difference for the three configurations. This difference was in figure 4.10.2 which was a plot of lift-to-pressure drag for lift coefficients ranging from 0.10 to 0.22. The highest lift-to-drag ratio was obtained by the winglet with "m" equal to 0.01 at a C_L of approximately 0.105. Since there were no other differences apparent, the winglet with a camber value of 0.01 was taken as giving the best performance. This winglet was then compared to an uncambered winglet, 0.00, and a winglet with negative camber, -0.01 (Figures 4.10.5 through 4.10.8). In this comparison, no difference was noticeable except in figure 4.10.6. However, the difference was so small no distinction could be made between the three cases. Due to the lack of any difference, the uncambered winglet was chosen for future parametric studies. The validity of the solutions for the uncambered winglet with -75° dihedral and 2° toe in at an angle of attack equal to 5°was shown by the incremental force build up results in figure 4.10.9. The total force results were given in figure 4.10.10.

4.11 Effect of 4% Thick Winglet Length Alteration

With the parameters studied to this point, the best performance of a wing-winglet geometry was found to be for a winglet that was uncambered, toed in 2°, and had a dihedral of -75°. The leading edge sweep of the winglet was still fixed at 50°. The next parametric variation involved the length of the winglet. All 4% thick winglets that had been studied so far had a length of 15% of the base wing semispan. To investigate the effect of

winglet length, three other lengths have been used. These lengths were 7.5%, 10%, and 12.5% of the base wing semispan. The same grid information was used as for the 15%, winglet , given in Table 4.8.1. The predicted performance coefficients for these geometries have been listed in Table 4.11.1. Again, predicted performance results have been shown in figures 4.11.1 through 4.11.4. By examining these figures, no difference was observable between the performance of winglets of various lengths. This lack of difference between the cases was extremely similar to that observed for the winglets with zero thickness. Due to the fact that no difference was observed, the winglet with a length equal to 15% of the semispan length was selected for use with additional parametric alterations. This selection allowed a better comparison between future parametric changes and those parameters already studied.

4.12 Leading Edge Sweep Variation for the 4% Thick Winglets

One of the last parameters to be changed on the 4% thick winglets was the leading edge sweep of the winglet. Since the EMTAC code had difficulty with low winglet leading edge sweep angles, only sweep angles of 50° and greater were considered. In particular, the leading edge sweeps were selected to be 50°, 60°, 65°, and 68°. The sweep angle of 68° was the highest chosen due to the geometric limitation that the tip chord length of the winglet was approximately zero. Any sweeps higher than 68° would have reduced the winglet length. The grid specifiers for these geometries have been given in Table 4.8.1. The resulting force and moment coefficients from EMTAC have been given in Table 4.12.1.

Once again, the performance predictions have been presented in figures 4.12.1 through 4.12.4. As in the length comparison, very little difference can be observed between the different configurations. The only result that could be seen to have a difference from one geometry to another was the lift-to-pressure drag ratio (figure 4.12.2). No difference was observable between the geometries for C_L's greater than 0.3. However, for a lift

coefficient equal to 0.05, the more highly swept winglets outperformed the 50° sweep winglet. Because of this fact, the leading edge sweep was selected to be 60°. This geometry would allow equal or better performance as compared to the other winglet configurations. The incremental and total forces have been given in figures 4.12.5 and 4.12.6 for this geometry.

4.13 Dihedral Changes for the 4% Thick Winglet

The last parameter to be changed was the dihedral angle. The dihedral angles chosen were -30° and -50°. Although these cases were of interest, no valid solutions could be obtained. Without convergent solutions for other dihedral angles, the geometric configuration with -75° dihedral was the last winglet case to be parametrically studied for the NACA 1402 base wing.

4.14 Comparison of the NACA 1402 Base Wing to Best Wing-Winglet

Upon completion of the winglet parametric variation, the best overall performance was observed for an uncambered winglet with a 60° leading edge sweep, -75° dihedral, 2° toe in and a length equal to 15% of the base wing semispan length. To indicate the performance level of this wing-winglet configuration, a comparison was made to the NACA 1402 base wing with an extension. The grid configurations surrounding the two bodies have been given in Table 4.14.1 while the predicted aerodynamic coefficients have been listed in Table 4.14.2.

The grid parameters were changed for the wing-winglet case due to a problem with the outer boundary conditions in the EMTAC code. Although previous warnings had been given about the appearance of negative densities being possible, the EMTAC manual gave no such warnings about violations of the outer boundary conditions. For the wing-winglet case, the line output file listed boundary condition violations for the second axial region. However, adjusting the grid, as listed in Table 4.14.1, corrected the problem. An

examination with previous performance coefficients indicated that the coefficient values were typically changed in the fourth significant figure. Since the variation had been at the outer boundary of the grid and the performance coefficients were not severely affected, the parameters studied previously were not re-run.

With the new grid and results, the base wing and wing-winglet cases were compared in several ways. The performance predictions have again been given in figures 4.14.1 through 4.14.4. Two extra values for lift coefficient were included in this figures. The values were approximately 0.1 and 0.2. Little difference was observable between these two configurations for predicted performance plots, especially in figures 4.14.1,4.14.3, and 4.14.4.

The performance plots were not particularly useful in this instance in determining which geometry had the better performance. Therefore a numerical comparison was used to examine the exact size of the difference in lift-to-drag ratio and drag coefficient. In this case, a friction drag estimate was obtained for each geometry as has been described in Chapter 2, Section 3. The mean aerodynamic chord for the wing with extension was calculated to be 69.244 units. The mean aerodynamic chord of the base wing with winglet was 69.017 units. The skin friction estimates for the base wing and wing-winglet were 0.006796 and .006778, respectively. The two points of comparison were selected to be at lift coefficients of approximately 0.1 and 0.2 (Table 4.14.3). For a C_L of approximately 0.1, the base wing with an extension had a higher total drag than the wing-winglet case, by 0.1108%, but due to a slightly higher lift coefficient, the lift-to-drag ratio was higher than the wing-winglet case. For the lift coefficient of approximately 0.2, the wing-winglet geometry had a lower drag, by 0.4801%, and a higher lift-to-drag ratio than the base wing. The percent difference in lift-to-drag ratio was 0.3586% for the lift coefficient approximately equal to 0.1 and 0.1355% for a lift coefficient of approximately equal to 0.2. These differences were obtained by subtracting the wing value from the wing-winglet value and then dividing by the wing value. Due to some differences in C_L and the slight

fluctuation in results due to alterations in the grid, the overall conclusion was that these two geometries had nearly identical performance in the range of interest.

Another method of comparing these two configurations was to examine the surface pressure coefficients, the local crossflow Mach number contours, and the local static pressure to freestream static pressure ratio contours around the geometries. This comparison has been made for an angle of attack of 5° and at three axial locations for each geometry. The first axial location was at 59.7 units (figure 4.14.5). Only one set of plots have been given since both geometries were identical at this axial location. The geometries remained identical through the first 80 units. In figure 4.14.5, the surface pressure coefficient was essentially smooth which was another indication that the solution was valid at this axial location. The contours of the static pressure ratios have also been given. The pressure contours demonstrated the effect of decreasing pressure around the wing-tip and the amount of change in the flow field at the wing-tip. Finally, the local Mach contours were given. Again, the majority of the flow field activity was at the wing-tip. From the Mach contours, the flowfield was seen to have relatively low crossflow velocities especially toward the centerline of the geometry. The next axial locations for the base wing at 88.8 and 99.6 units have been presented in figures 4.14.6 and 4.14.7. The surface pressure contours, static pressure ratio contours and local crossflow Mach number contours indicated limited change had taken place, and these contours were very similar to the contours for axial location 59.7.

Similar figures have been given for the wing-winglet case at axial locations of 88.2 and 99.6 units (figures 4.14.8 and 4.14.9). For the axial location of 88.2 units, the surface pressure coefficient shows a difference as compared to the wing-alone at x=88.8 units. The surface C_p for the wing- winglet had a increase in the C_p values on the lower outboard surface as compared to the base wing. This effect was related to the winglet being orientated in a downward direction, i.e., anhedral. The static pressure ratio contours also demonstrated this effect as the ratios increased at the winglet. The crossflow Mach number

contours have also been given. From these contours, a shift can be seen in the crossflow velocities. For the wing-alone, increasing Mach number contours were primarily on the upper outboard surface while for the wing-winglet case , the increasing Mach number contours were shifted farther out and downwards. At an axial location of 99.6 units in figure 4.14.9, a more profound difference in C_p's and contours was evident between the base wing and the wing-winglet geometry. The surface pressure coefficients for the wing-winglet were essentially the same as the wing-alone values for the inboard 80% of the semispan. However, for the winglet case, a large increase in pressure was evident on the lower outboard surface near the winglet. By examining the pressure ratio contours and Mach number contours, the effect of the winglet was seen to be to shift or rotate the flowfield downward. This can be seen by selecting contours of equivalent values around the wing and the wing-winglet geometries and following them to the surface of the body. The smoothness of these contours was another way in which the validity of the solution could be checked.

A final comparison between the two geometries, the wing-alone and the best wing-winglet, was to alter the freestream Mach number and examine the effects. The Mach numbers investigated were 1.4, 1.62, 2.0, 2.5, 3.0, and 3.5. The calculated performance coefficients have been listed in Table 4.14.4. The predicted performance results for the Mach numbers have been presented in figures 4.14.10 through 4.14.21. In figure 4.14.10 through 4.14.13, the Mach numbers of 1.4 and 1.62 have been shown. At these relatively low Mach numbers, the difference in performance between these geometries was greatest for C_L values of approximately 0.05. For example, the difference in the lift-to-pressure drag ratio was 3.97% at a Mach number of 1.4 and a C_L of 0.05 with the wing performing better than the winglet case As Mach number was increased, the difference in the predicted performance for the geometries lessened. Also, as Mach number was increased, the EMTAC code did not typically give valid solutions for angles of attack at or above 15°. The essential result of this Mach number study was that the effects demonstrated at M=1.62

were the same as for higher Mach numbers. This concluded the comparison between the NACA 1402 base wing with extension and this particular wing-winglet case.

4.15 Investigation of the Special Cases with Thickness

As mentioned in Chapter 3, investigations of several other geometries were conducted. The first of these studies was for full tip winglets. Full tip winglets were winglets whose root chord length was the same length as the tip chord of the base wing. Both upward and downward rotated winglets were examined at various toe out and toe in angles. The angles of attack of that have been investigated were -5°, 0°, 2.5°, 5°, 9°, and 15° for a Mach number of 1.62. The grids used have been listed in Table 4.15.1. For the winglets with 75° dihedral and a leading edge sweep of 50°, four toe out angles have been studied. These angles were 2°, 3°, 4° and 6°. The predicted performance coefficients have been listed in Table 4.15.2 and the predicted performance results have been given in figures 4.15.1 through 4.15.4. In this study, the winglet toed out 3° had the best performance in the lift coefficient range of interest. The next geometries considered were the full tip winglets with 75° anhedral at a Mach number of 1.62. The toe in angles for these geometries were 2°, 3°, and 4°. The computational grids used have been given in Table 4.15.1 and the performance coefficients have been listed in Table 4.15.3. Figures 4.15.5 through 4.15.8 show the predicted performance results. No distinction could be made between the three geometries studied. Finally the best winglets from these two groups were compared to the NACA 1402 base wing with extension. These geometries were the 75° dihedral, 3° toe out winglet and the -75° dihedral, 2° toe in winglet. The performance comparison has been given in figures 4.15.9 through 4.15.12. The main result was that the wing-alone was able to equal or outperform the geometries with winglets in the lift coefficient range of interest.

The next special case study was that of maximum camber location. Since the NACA four digit series was used for airfoil description, the maximum camber location could be easily shifted analytically. For this study, the same computational grids were used as listed

in Table 4.15.1. The toe out angles for both the 75° dihedral and 75° anhedral winglets were fixed at zero degrees and the winglets were full tip chord winglets. For the maximum camber location, three values were arbitrarily selected. The locations for maximum camber have been chosen to be 20%, 40%, and 60% of the local chord length from the winglet leading edge. The predicted coefficients have been listed in Table 4.15.4 for a Mach number of 1.62. The predicted performance of the 75° dihedral winglets has been presented in figures 4.15.13 through 4.15.16. Some difference was evident between the geometries in the lift coefficient range of interest. However, this difference was not very large. Similar results were obtained for the 75° anhedral winglets in figures 4.15.17 through 4.15.20. The best performance overall was typically given by the base wing.

The next special case study involved decreasing the winglet thickness from 4% to 2% and varying the camber of the airfoils. The winglet anhedral was fixed at 75°, and the winglet had a leading edge sweep of 50°. The toe in angle had been set at 2°. The length of the root chord was chosen to be 65% the length of the base wing tip chord. The computational grid parameters used have been listed in Table 4.15.5. The various "m" values used were -0.01, 0.0, 0.01, 0.03, and 0.04. The predicted performance coefficients have been listed in Table 4.15.6. The performance results for -0.01, 0.01 and 0.0 have been given in figures 4.15.21 through 4.15.24. The performance of all three cases were indistinguishable except for the case of -0.01 at a C_L of 0.1. However, even the difference here was slight. The "m" values of 0.01, 0.03, and 0.04 have been presented in figures 4.15.25 through 4.15.28. In this comparison, an obvious difference existed between the three configurations in their lift-to-pressure drag performance (figure 4.15.26). The higher lift-to-pressure drag values were achieved by the 0.01 case.

To examine the effectiveness of some of these special cases, they have been compared to the NACA 1402 base wing and the wing-winglet discussed at the beginning of this section. The four geometries compared in figures 4.15.29 through 4.15.32 were the base wing; the 4% thick, uncambered, 75° anhedral winglet; the 2% thick, uncambered 75°

anhedral winglet; and the full tip winglet with a -75° dihedral. All three winglet cases were toed in 2°. In figure 4.15.30, the full tip winglet does not perform as well as the other two winglet cases or the base wing for lift coefficients near 0.05. For the two remaining winglet cases their performance was equivalent to the base wing performance.

From the parametric variations and the limited number of special case studied, it has been possible to show that geometries with winglets can equal the supersonic performance of a wing-alone geometry.

4.16 The "Natural" Flow Wing and "Natural" Flow Wing with Winglets

After concluding the parametric study of the NACA 1402 base wing with winglets, the next investigation focused on the "natural" flow wing described in references 15 and 16, and the effects of winglets on this wing. The grid parameters used for the "natural" flow wing have been given in Table 4.16.1. Four typical grids have been shown in figure 4.16.1. For this geometry, the angles of attack of -5°, 0°, 2.5°, 5°, and 9° were studied at a Mach number of 1.62. The predicted performance coefficients have been listed in Table 4.16.2 for the "natural" flow wing. The incremental and total force plots were given in figures 4.16.2 and 4.16.3. Both upward and downward orientated winglets were investigated. In particular, the winglets had 65° of dihedral or anhedral and a leading edge sweep of 55°.

For the 65° anhedral winglets, several toe out and toe in angles have been studied. The toe in angles were 2° and 4° while the toe out angles were 0° and 2°. The grid parameters necessary for these geometries have been listed in Table 4.16.1. Typical grids for the 2° toe out winglet have been given in figure 4.16.4 and the EMTAC generated performance coefficients have been presented in Table 4.16.3. For the winglets, the angles of attack studied were -5°, 0°, 2.5°, 5°, 7°, and 9.5°. The incremental force plots for the 2° toe out case at an angle of attack of 5° have been given in figure 4.16.5. The total force build ups at 5° have been plotted in figure 4.16.6. For the incremental lift, the solution was not

entirely smooth but appeared stable. However, the incremental drag had a large discontinuity at a distance of 90% root chord. This indicated that the solution was probably not valid. All the winglets tested had similar spikes in the same general axial location. Different grids, marching step sizes, and boundary conditions were attempted in an effort to eliminate this discontinuity. However, all attempts failed to do so; therefore the results with the smallest discontinuities have been presented. These results were for geometries that had no outer boundary condition violations and no negative densities at lower angles of attack, i.e., 0° to 5° angle of attack.

For comparison purposes between the various 65° anhedral winglets, the predicted performance coefficients have been plotted in figures 4.16.7 through 4.16.10. The most noticeable difference occurred in the lift-to-pressure drag ratio (figure 4.16.8). In this case, the winglet with a 2° toe out had a higher lift-to-pressure drag ratio. This trend was opposite that of the NACA 1402 case studies where the downward winglets performed better toed in than toed out. A difference was also observed in the pressure drag polar for C_L's ranging from 0.05 to 0.20 (figure 4.16.9) where the 4° toe in winglet had the highest drag.

The next study investigated the winglets with 65° dihedral. The toe out angles for this winglet were 0°, 2°, and 4° while the toe in angle was 2°. The grid parameters used have been listed in Table 4.16.1 while the predicted performance coefficients have been given in Table 4.16.4. Again, a comparison between the four alignments was desirable. The predicted performance coefficients have been plotted in figure 4.16.11 through 4.16.14. In figure 4.16.12, the lift-to-pressure drag ratio of the 2° toe in winglet was most desirable since it gave the highest values of performance in the range of interest.

Although the validity of the winglet cases was suspect, a comparison was made between the 2° toe in upward winglet, the 2° toe out downward winglet, and the original "natural" flow wing. This performance comparison has been shown in figures 4.16.15 through 4.16.18. In these figures, a large difference was noticeable between the three

configurations, especially in the lift-to-pressure drag ratio (figure 4.16.16). The "natural" flow wing had the best performance based on these predicted coefficients.

To further compare the "natural" flow wing to wing-winglets, the 65° anhedral winglet with 2° toe out was selected. The effect of adding a winglet to the base wing was more easily seen by examining surface pressure coefficients, local crossflow Mach number contours, and the contours of local static pressure to freestream static pressure ratio. Three axial locations will be presented for an angle of attack of 5° at a freestream Mach number of 1.62. These axial locations were at 59.7, 92.8, and 99.6 units. For the axial location of 59.7 units, only one set of figures will be given (figure 4.16.19) since the plots were the same for both geometries. Note that the plots would be identical for both geometries before the axial location of 90 units due to the fact that the geometry of the "natural" flow wing was unaltered until after x= 90 units. At the axial location of 59.7 units, the pressure ratio contours, the cross flow Mach number contours, and the surface pressure coefficients were smooth. This was a further indication that the solution was valid up to this point. The next axial location for the "natural" flow wing was at 92.8 units (figure 4.16.20). The surface pressure coefficients do not appear as smooth as they did for the axial location of 59.7 units. However, this difference could be due to the changing shape of the body. The body was altered spanwise such that two pockets of lower pressure existed on the upper surface. This can be seen by observing the pressure ratio contours. Although the contours presented in figure 4.16.20 were smooth, this was not the case for the wing-winglet geometry at 92.8 units (figure 4.16.21). The surface pressure coefficients were much larger than those of the wing-alone on the outer lower surface, approximately 7.5 times as large. This strongly indicated that the solution might not be valid. Also, the pressure ratio contours indicated that the solution was invalid. As compared to the wing, the maximum pressure ratios for the winglet case were twice as large as the maximum pressure ratios for the wing. The final axial location examined was at 99.6 units. For the "natural" flow wing, the contours were smooth which indicated a valid solution (figure 4.16.22). When

comparing these plots to those of the wing-winglet case (figure 4.16.23), the solution of the wing-winglet case appears to be valid. This could indicate that any non-physical disturbances may have damped out. Also note, that the magnitudes of the pressure ratios and crossflow Mach numbers are essentially the same. However, further comparisons were not done since totally valid solutions were not obtainable.

4.17 SIMP Verification

Although the SIMP code was originally planned to be used in verifying the predicted values from the EMTAC code, this was not possible. For wing-winglet geometries, valid solutions were not be obtained by the full potential code. However, SIMP was able to obtain results for the wing-alone[9] using one region and no restarts. For wing-winglet geometries, the restart option was necessary. But, the restart option could not be manipulated to run the wing-winglets geometries.

CHAPTER 5

CONCLUSIONS AND RECOMMENDATIONS

5.1 Conclusions

From the parametric studies conducted for the winglets on the NACA 1402 base wing, several conclusions can be drawn. First, winglets can be designed and aligned in supersonic flow such that little or no performance penalty will be incurred relative to a wing of equal projected span. Another conclusion that can be drawn is that alteration of winglet length, sweep, and camber may not be as critical as the toe angle or the orientation of the winglet relative to the wing. This, however, would not hold if length, sweep, or camber were taken to an extreme. These conclusions differ from trends which have been documented for winglets in subsonic or transonic applications, where winglets result in a drag reduction. This subsonic drag reduction increases with increasing winglet length.

In the present study, winglets with negative dihedral and toe in were found to typically outperform similar winglets with positive dihedral. A possible explanation of this could be that the downward winglet provides a rounded smooth juncture on the upper surface. This smooth upper surface juncture appears to allow an acceleration of the flow in the crossflow plane and therefore a suction in the direction of lift. A similar juncture was created by the winglets with positive dihedral but the suction surface would provide force in the negative lift direction. In conclusion, the overall aerodynamic effects of winglets in supersonic flow are minimal and they show no improvement over wing-alone geometries. This could be due to the fact that the winglets have a small zone of influence. For a Mach number of 1.62, the zone of influence is 38° inboard and outboard from the leading edge of the winglet. Inboard of the Mach line, the span essentially behaves as a two dimensional or infinite span. As Mach number was increased, the zone of influence became even smaller as exhibited in the results of chapter 4, section 14.

For the " natural" flow wing with and without winglets, conclusions can be made but the accuracy of the solutions for these winglet cases is probably poor. However, the one note of interest was that the best alignment for the "natural" flow winglets appears to be opposite of the NACA four digit airfoil winglets. Essentially, the toe angles were equal and opposite for the two sets of cases. Unlike the NACA four digit airfoil series winglets, the "natural" winglets were never able to equal the "natural" flow wing performance in the C_L range of interest, but this may have been due to the "spikes" which were observed in the incremental drag build up for the winglet case.

5.2 Recommendations

With this study of winglets in supersonic flows completed, several recommendations for future study can be suggested. The first recommendation is to find another code, preferably a supersonic one, that could easily confirm the performance results obtained from the EMTAC code. One possible way to do this might be to use EMTAC-MZ[22] which has the capability to perform calculations for subsonic flow and is based upon the EMTAC code. EMTAC-MZ would also allow a better defined grid around the winglet due to its multi-zone capability. With results from subsonic flows, EMTAC-MZ[22] solutions could be compared with results from other codes as well as experimental results from transonic designs. This would indirectly help confirm the accuracy of the results obtained by the EMTAC code for supersonic Mach numbers. In this study, only NACA airfoils were examined for winglet shapes. A different definition of geometry could be beneficial such as that the "shearing" process used to develop the "natural" flow wing. A supersonic wind tunnel study of one wing-winglet would be beneficial in verifying the EMTAC results. This wing-winglet case could have an uncambered winglet with adjustable toe in or out and fittings for anhedral or dihedral alignment.

The final recommendations involve geometric alterations that may actually reduce the induced drag on wings at supersonic speeds or have control possibilities. Since the trailing

edge sweep was set at 0° for the EMTAC code, another code or a modified EMTAC code could be used that would be capable of handling non-planar wakes with non-zero trailing edge sweep. This swept winglet trailing edge would allow extra surface to be present on the winglet which could act as a lifting surface. The other geometric recommendation would be to alter the leading edge of the wing in supersonic flows. In the present study, it was found that changing the length of the winglet had little effect on predicted performance values, and that anhedral was better than dihedral. Because of these facts, it is felt that a detailed design of a rounded and drooped leading edge might increase lift and/or thrust without a drag penalty. Although winglets for the NACA 1402 base wing demonstrated no improvement in aerodynamic performance, no other advantages were examined such as improvement in stability or in structural loading. These topics could be considered for further winglet studies in supersonic flow. One such possibility for winglets supersonically could be their usefulness in acting as control surfaces for yaw. By allowing the toe angles to be different on each semispan, an effective yaw moment might be created. These recommendations could be useful in further verifying the predicted performance values found in this study, or improving wing performance supersonically.

REFERENCES

1. Whitcomb, Richard T., "A Design Approach and Selected Wind-Tunnel Results at High Subsonic Speeds for Wing-Tip Mounted Winglets," NASA TN D-8260, July 1976.

2. Henderson, William P., and Holmes, Bruce J., "Induced Drag-Historical Perspective," SAE Aerotech '89 Conference, Anaheim California, Sept. 25-28, 1989.

3. Mackerodt, Fred, "Big Bird," Popular Mechanics, vol. 166, No. 3, March 1989.

4. Flechner, Stuart G., Jacobs, P. F., and Whitcomb, R. T., "A High Subsonic Speed Wind-Tunnel Investigation of Winglets on a Representative Second-Generation Jet Transport Wing," NASA TN D-8264, July 1976.

5. Heyson, Harry H., Riebe, G. D., and Fulton, C. L., "Theoretical Parametric Study of the Relative Advantages of Winglets and Wing-Tip Extensions," NASA TP-1020, 1977.

6. Kuhlman, J. M. and Liaw, P., "Winglets on Low-Aspect Ratio Wings," Journal of Aircraft, Vol. 25, No. 10, October 1988, pp.932-941.

7. Kuhlman, J. M., Liaw, P., and Cerney, M. J., "Theoretical/Numerical Study of Feasibility of Use of Winglets on Low Aspect Ratio Wings at Subsonic and Transonic Mach Numbers To Reduce Drag," NASA CR-4174, August 1988.

8. Cerney, M. J., "Numerical Design Study of Winglets on Low Aspect Ratio Wings Using Supercritical Airfoil Technology," Master's Thesis, Engineering, WVU, 1988.

9. Brown, Christopher K., "Computational Study of Induced Drag Reduction Due to Winglets on Low Aspect Ratio Wings at Transonic and Supersonic Speeds," Master's Thesis, Engineering, WVU, 1990.

10. Shanker, Vijaya, Szema, K-Y., and Bonner, Ellwood, "Full Potential Methods for Analysis/ Design of Complex Aerospace Configurations," NASA CR-3982, May 1986.

11. Szema, K-Y., Chakravarthy, S., and Shankar, Vijaya, "Supersonic Flow Computations Over Aerospace Configurations Using a Euler Marching Solver," NASA CR-4085, July 1987.

12. Asai, Keisuke, 'Theoretical Considerations in the Aerodynamic Effectiveness of Winglets," Journal of Aircraft, Vol. 22, No. 7, July 1985, pp.635-637.

13. Bushnell, D., "Supersonic Aircraft Drag Reduction," Paper AIAA 90-1596, Presented at AIAA 21st Fluid Dynamics, Plasma Dynamics and Lasers Conference, Seattle WA, June 18-20, 1990.

14. Demeis, R., "Sukhoi and Gulfstream Go Supersonic," Aerospace America, Vol. 28, No. 4, April 1990, pp 40-42.

15. Wood, R. M., and Bauer, S. X. S., "Evaluation of a Three-Dimensional Empirically Derived Wing at Supersonic Speeds," Paper AIAA-88-0481, Presented at AIAA 26th Aerospace Sciences Meeting, Reno, NV, Jan. 11-14, 1988.

16. Bauer, S. X. S., Wood, R. M., and Brown, S. M., "A Natural Flow Wing Design Employing 3-D Nonlinear Analysis Applied at Supersonic Speeds," Paper AIAA-89-2167, Presented at AIAA 7th Applied Aerodynamics Conference, Seattle, WA, July 31- Aug. 2, 1989.

17. White, Frank M., Heat Transfer, Addison-Wesley Publishing Inc.,Reading, Mass., 1984, p 260.

18. Etkin, B., Dynamics of Flight, Wiley, New York, 1959, pp 500-503.

19. Jackson, Charlie, Jr., Corlett, W. A., and Monta, W. J., "Description and Calibration of the Langley Unitary Plan Wind Tunnel," NASA TP-1905, Nov. 1981.

20. Abbott, Ira H., and Von Doenhoff, A. E., Theory of Wing Sections, Dover Publications, Inc., New York, 1959, pp 111-114.

21. McGrath, B. E., Covell, P. F., and Walker, I. J., "Euler Code Evaluation of a Conical Vehicle at Supersonic Speeds," Paper AIAA-89-2193, Presented at AIAA 7th Applied Aerodynamics Conference, Seattle, WA, July 31-Aug. 2, 1989.

22. Szema, K-Y. and Chakravarthy, S. R., "A User Guide for the EMTAC-MZ CFD Code," NASA CR-4283, May 1990.

23. Davis, S. F., "A Simplified TVD Finite Difference Scheme via Artificial Viscosity," NASA CR-172373, June 1984.

24. Harten, A., "High Resolution Schemes for Hyperbolic Conservation Laws," Journal of Computational Physics, 1983, pp 357-393.

25. Sweby, P. K., "High Resolution Schemes Using Flux Limiters for Hyperbolic Conservation Laws," Siam Journal of Numerical Analysis, Vol. 21, No. 5, October 1984, pp. 995-1011.

26. Boppe, Charles W., "Transonic Flow Field Analysis for Wing-Fuselage Configurations," NASA CR-3243, May 1980.

27. Boppe, Charles W., "Aerodynamic Analysis for Aircraft with Nacelles, Pylons, and Winglets at Transonic Speeds," NASA CR-4066, 1987.

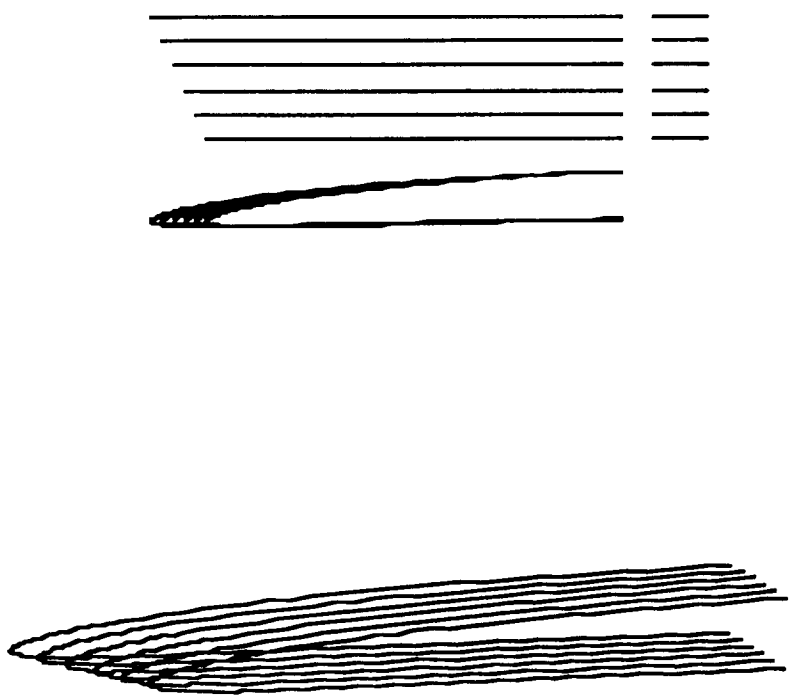

Figure 2.1.1: Typical example of cross flow geometric cuts of the NACA 1402 base wing to be used by EMTAC or SIMP, three orthographic views and an isometric projection.

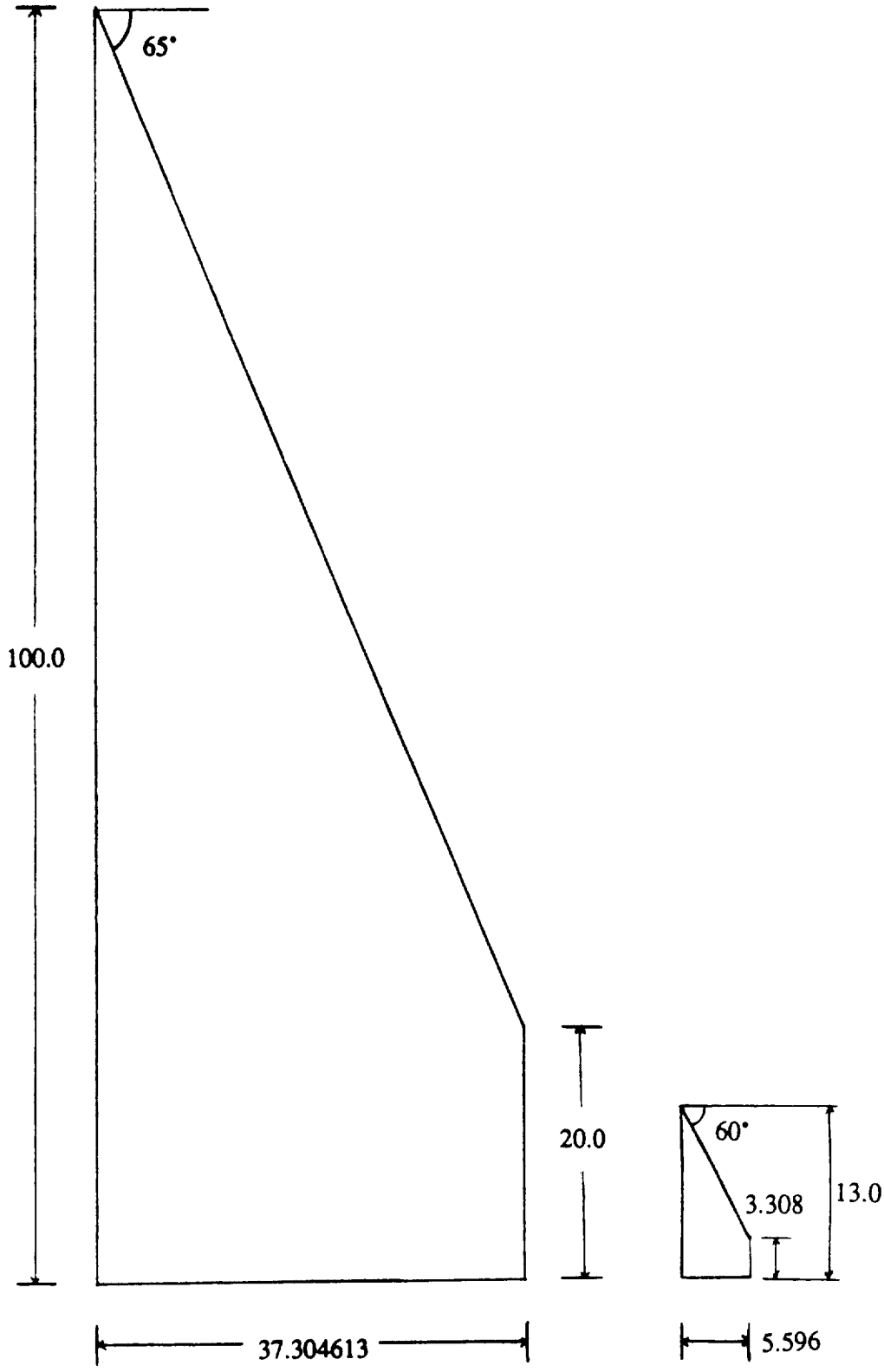

Figure 3.1.1: Planforms of the NACA 1402 base wing and best winglet with non-dimensional units.

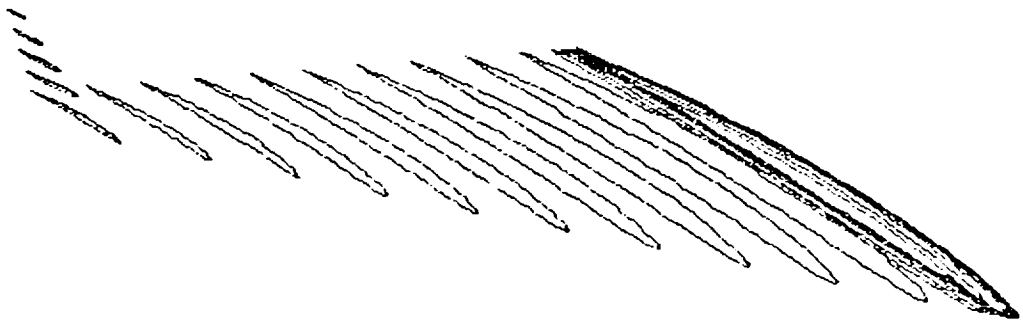

Figure 3.1.2: Streamwise NACA 1402 airfoils of the NACA 1402 base wing and dihedral winglet.

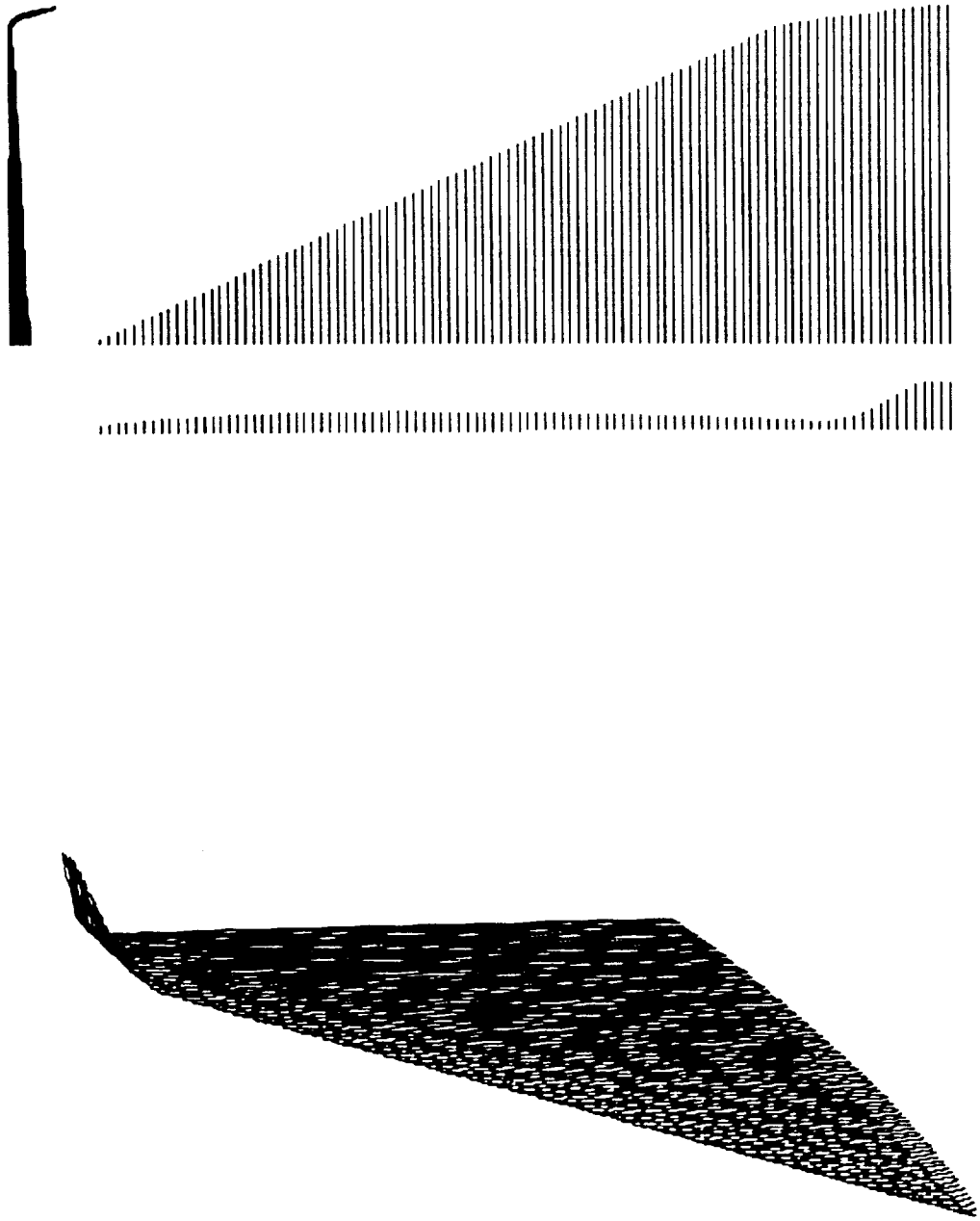

Figure 3.1.3: Cross flow geometric cuts for the NACA 1402 base wing with dihedral winglet, three orthographic views and an isometric projection.

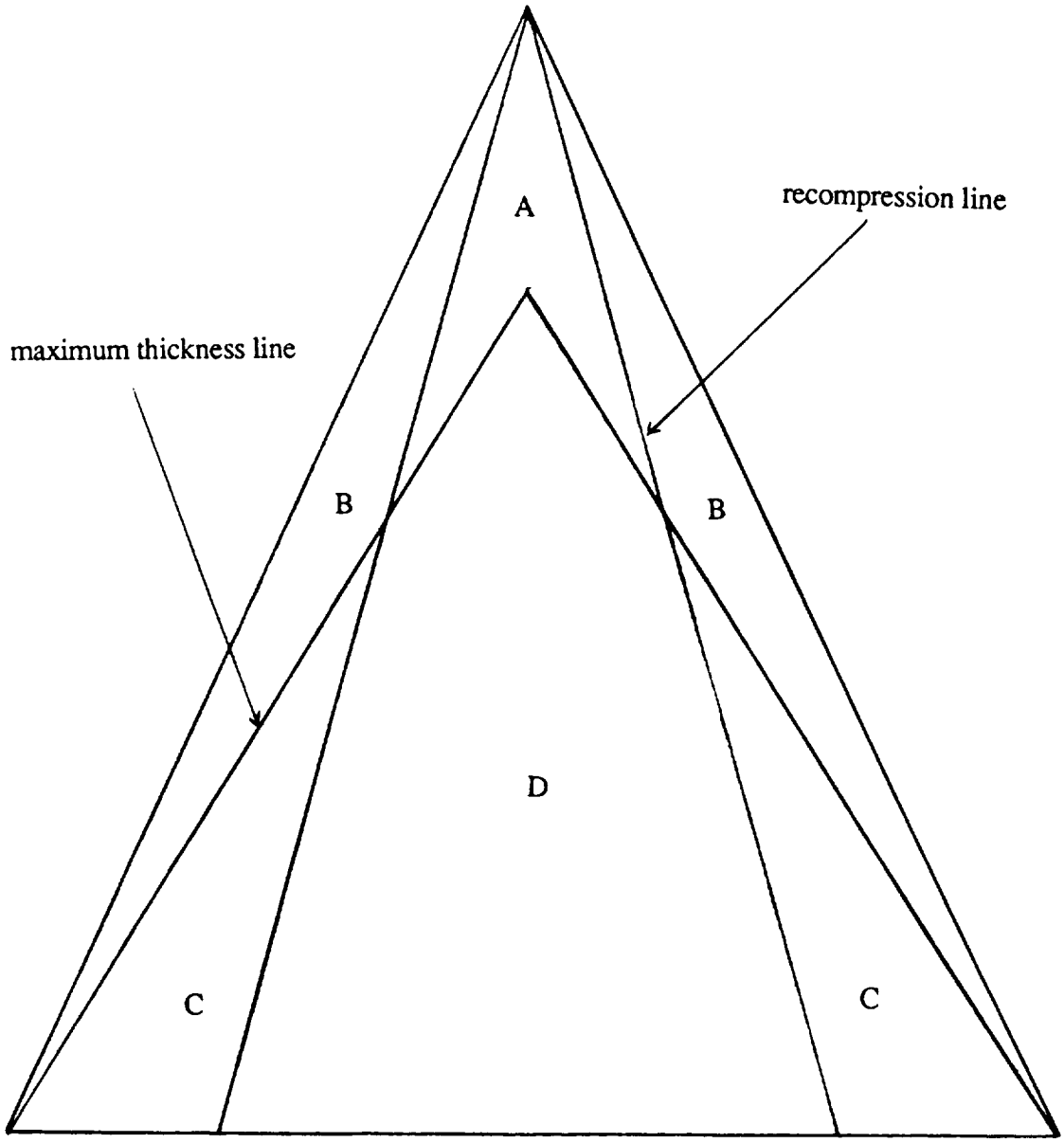

Figure 3.1.4: Schematic of a delta wing planform showing a recompression line as well as a maximum thickness line.

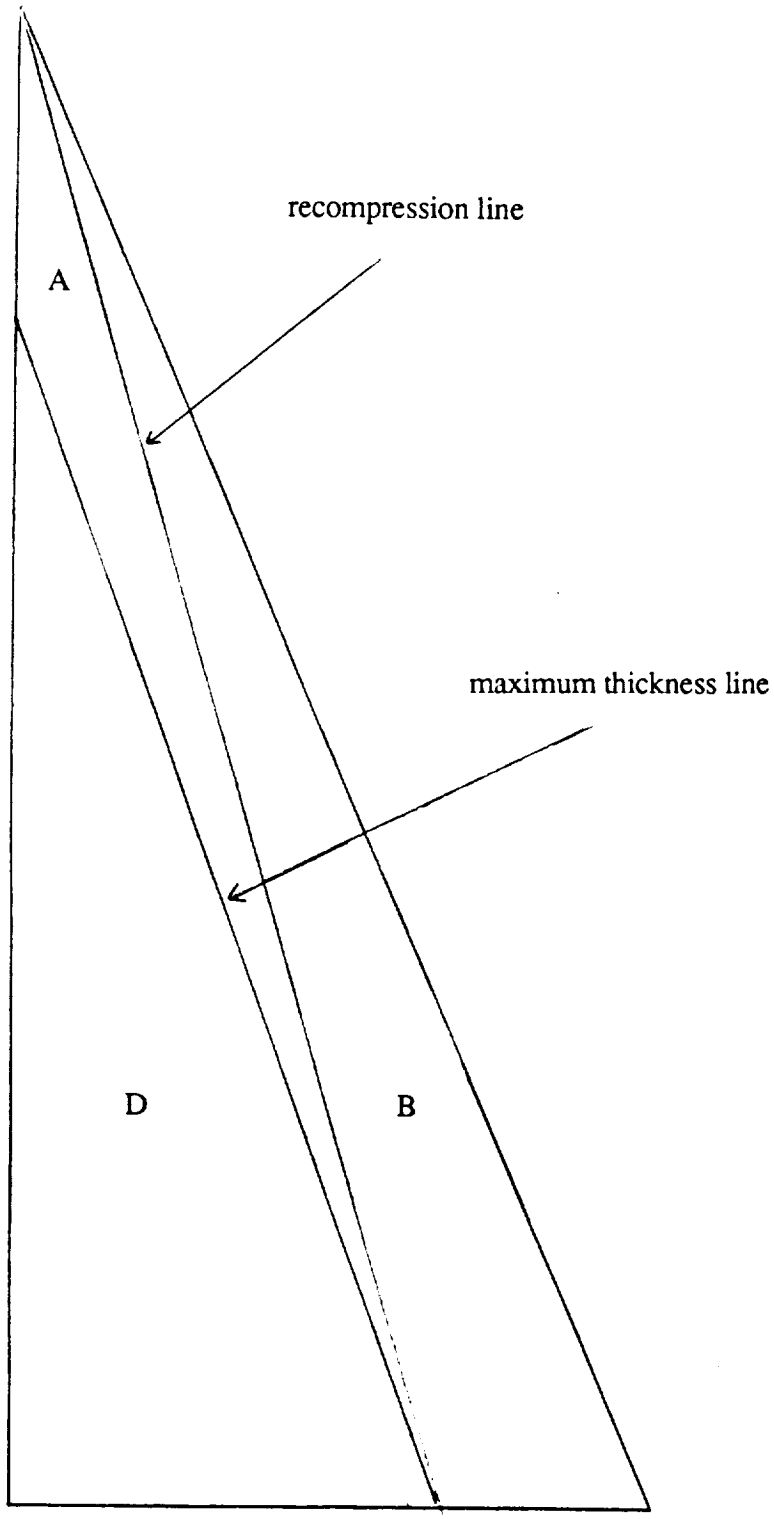

Figure 3.1.5: "Natural" flow wing planform with maximum thickness line and recompression line.

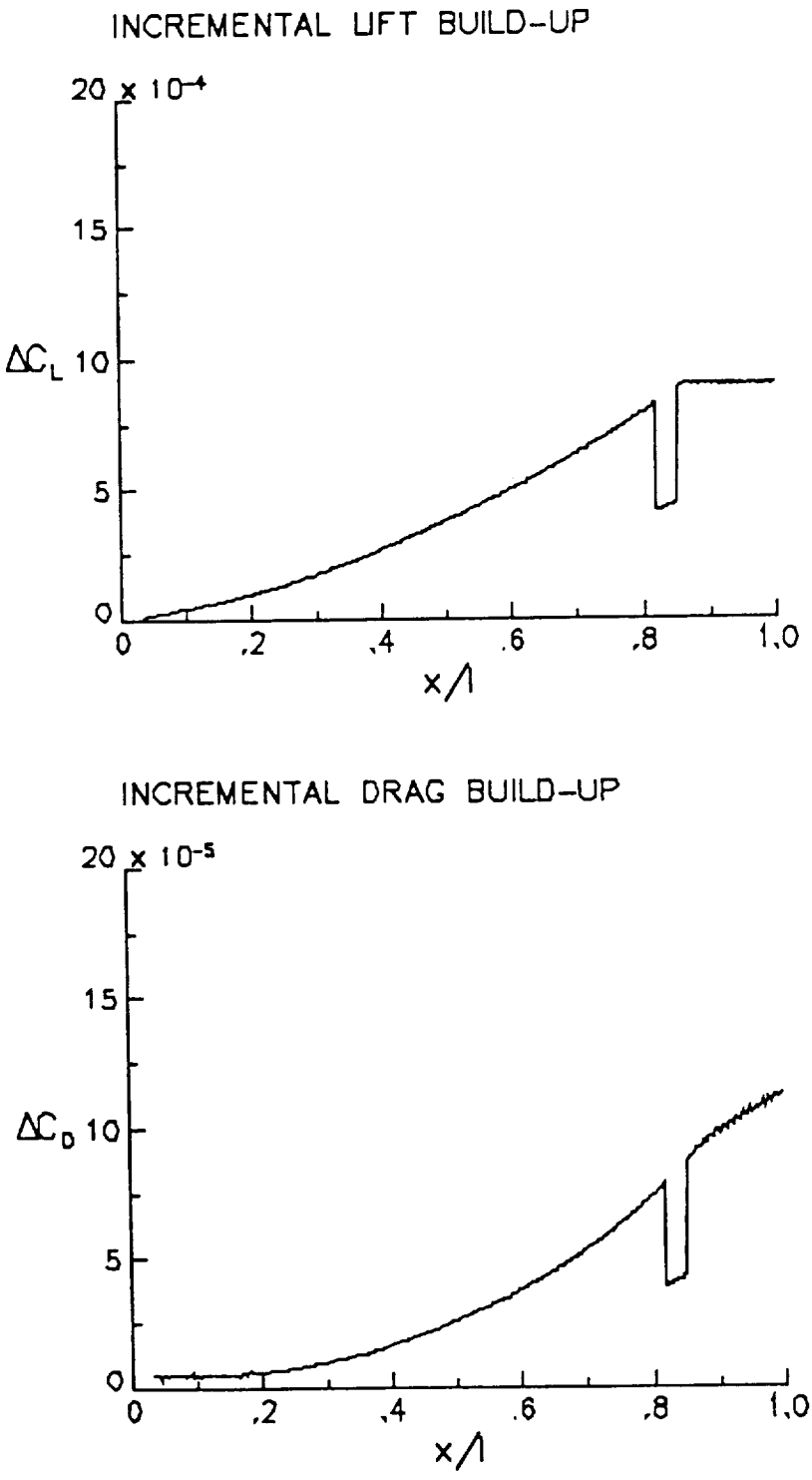

Figure 4.2.1: Incremental lift and pressure drag build ups for the NACA 1402 base wing at 5° angle of attack, M=1.62.

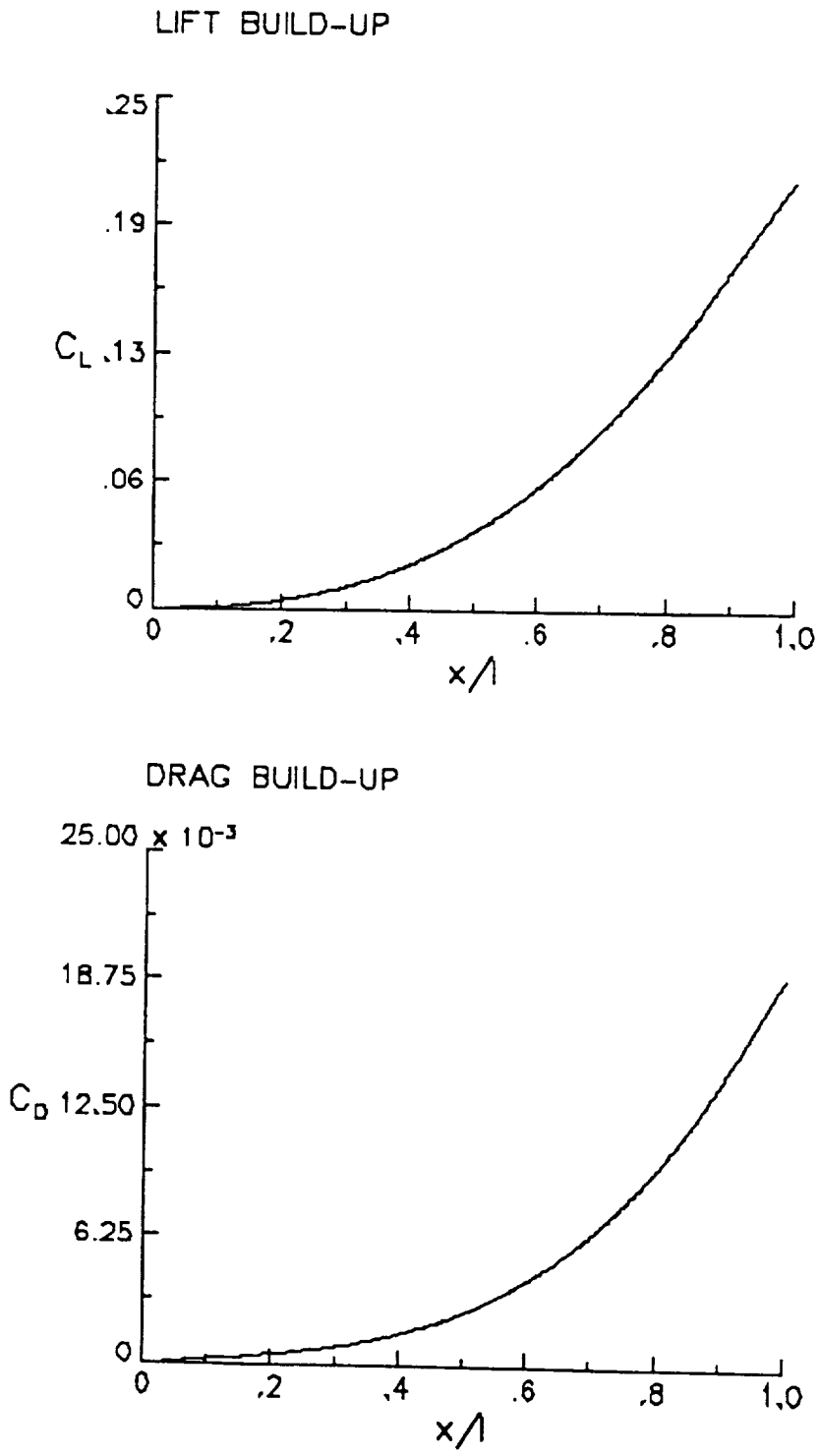

Figure 4.2.2: Total lift and pressure drag plots for the NACA 1402 base wing at 5° angle of attack, M=1.62.

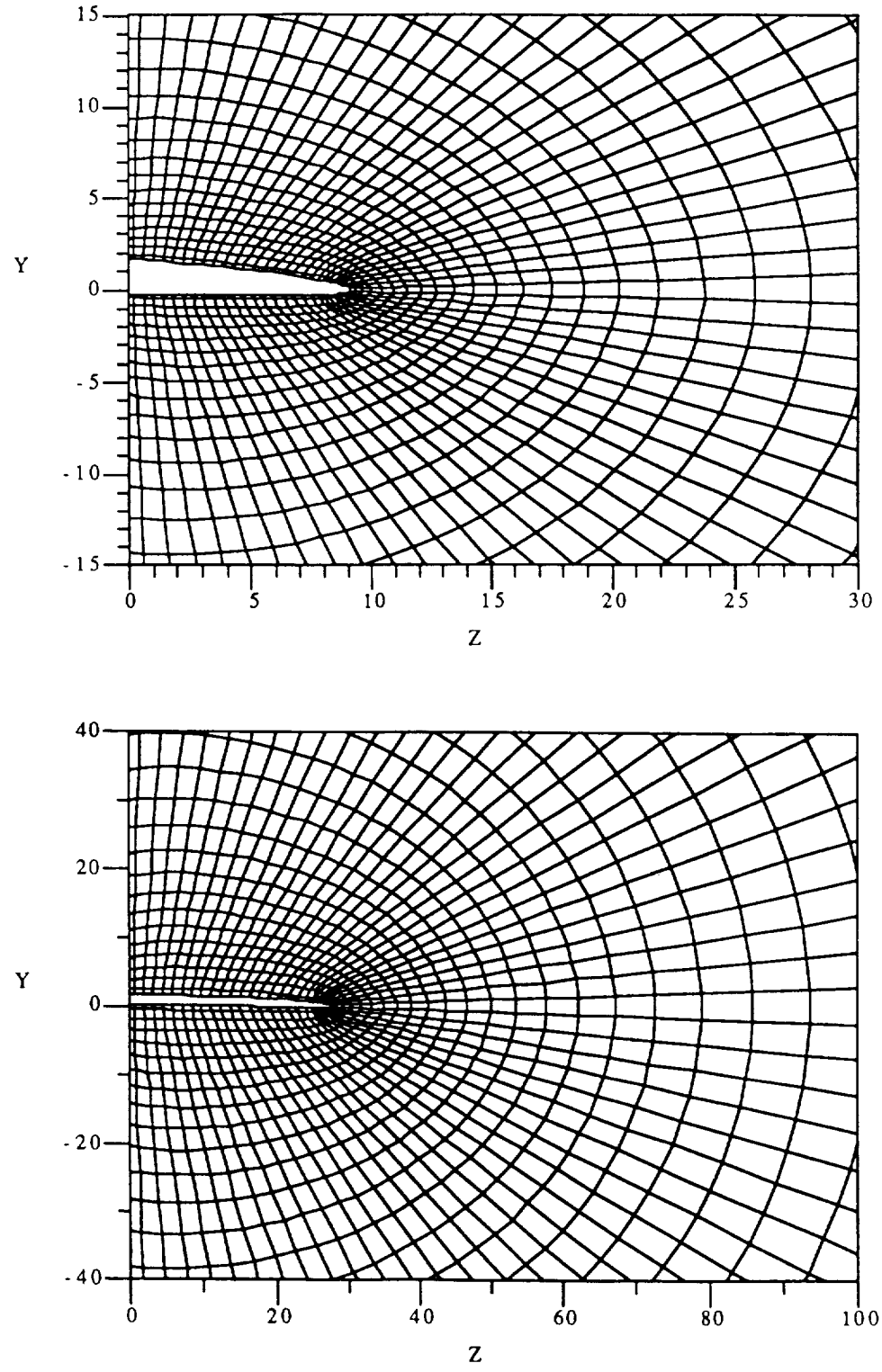

Figure 4.3.1: Computational grid surrounding the NACA 1402 base wing and 0% thick, 75° dihedral winglet at x=19.7, 59.7, 88.15, and 99.6.

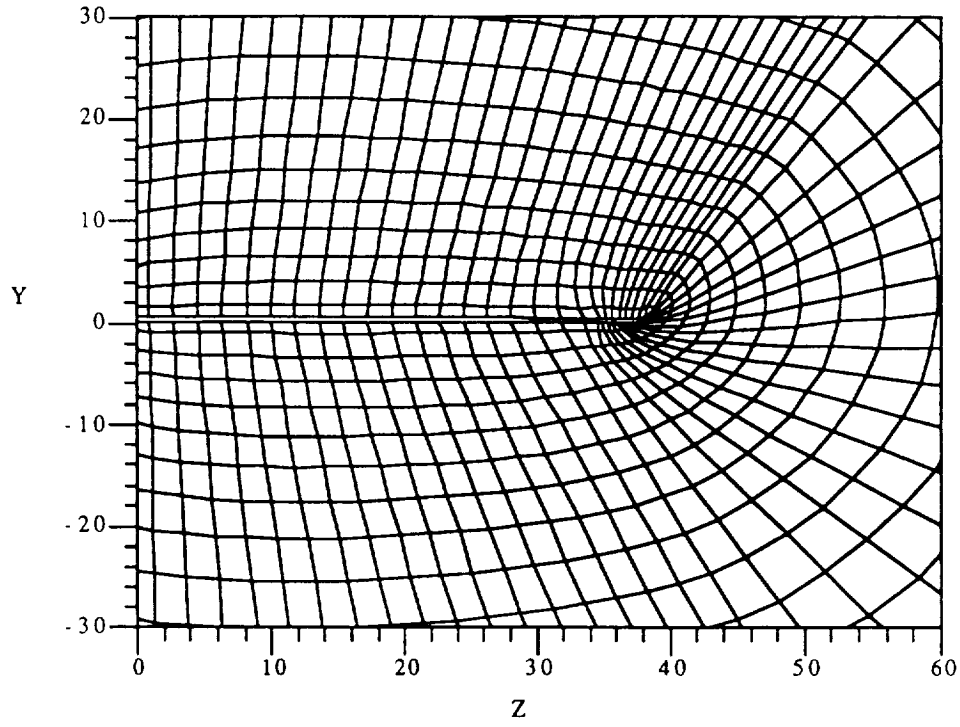

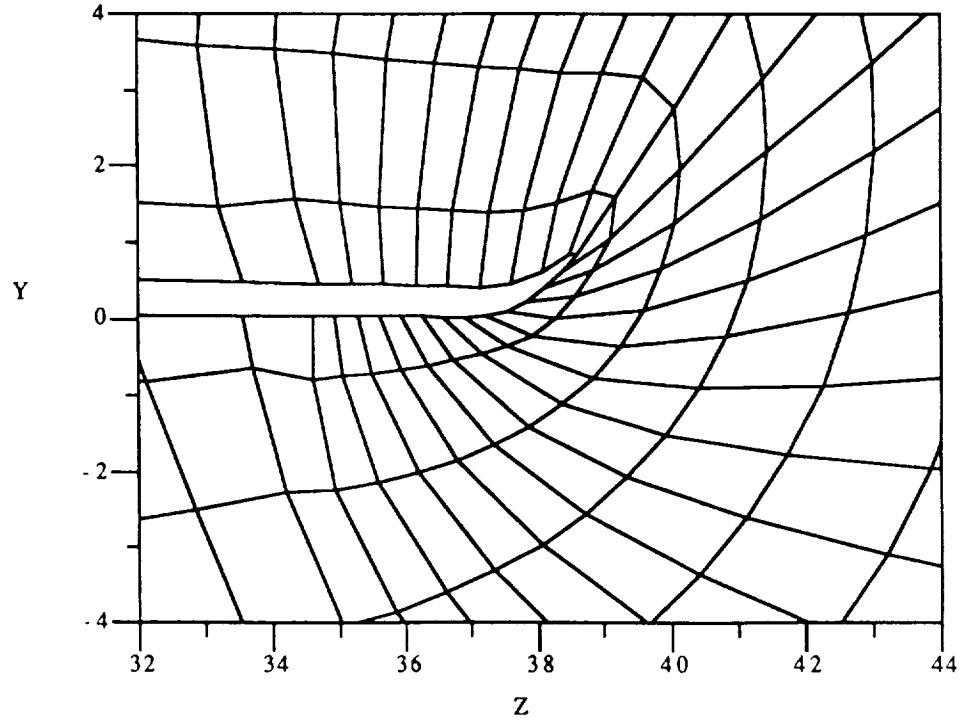

Figure 4.3.1: Continued, x=88.15.

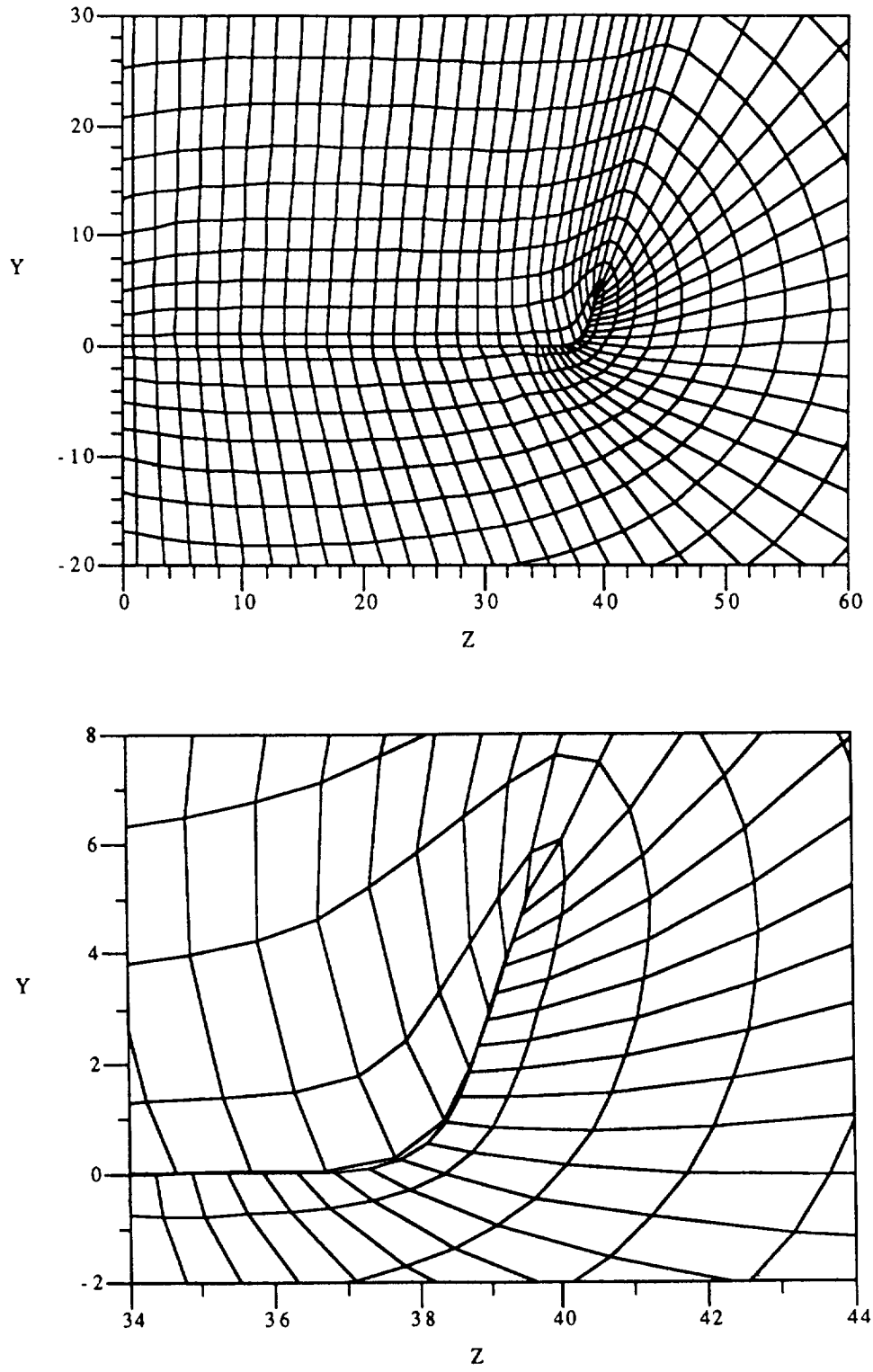

Figure 4.3.1: Continued, x=99.6.

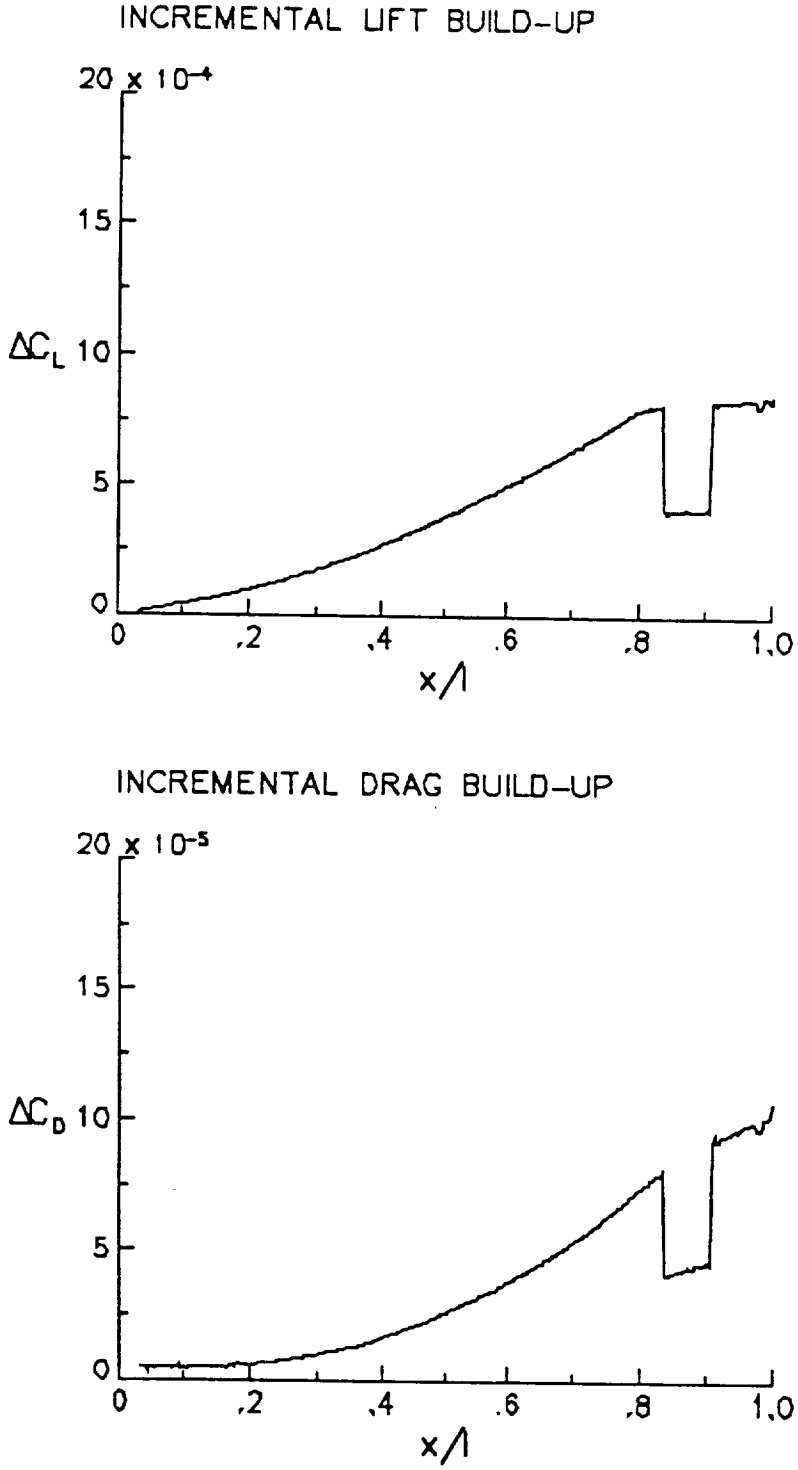

Figure 4.3.2: Incremental lift and pressure drag build up for the NACA 1402 base wing with a 0% thick, 2° toe out, 75° dihedral winglet at 5° angle of attack, M=1.62.

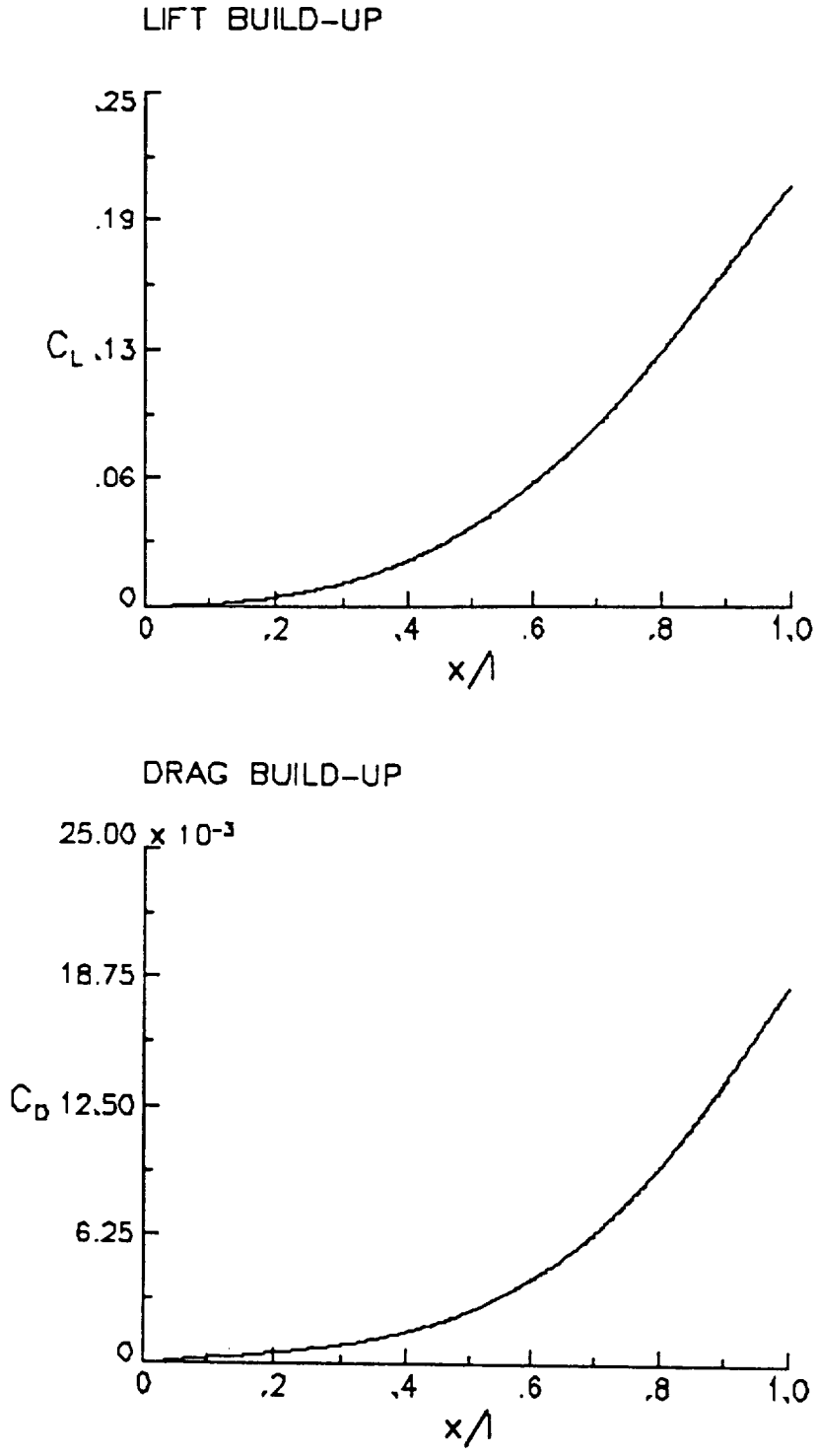

Figure 4.3.3: Total lift and pressure drag build up for the NACA 1402 base wing with a 0% thick, 2° toe out, 75° dihedral winglet at 5° angle of attack, M=1.62.

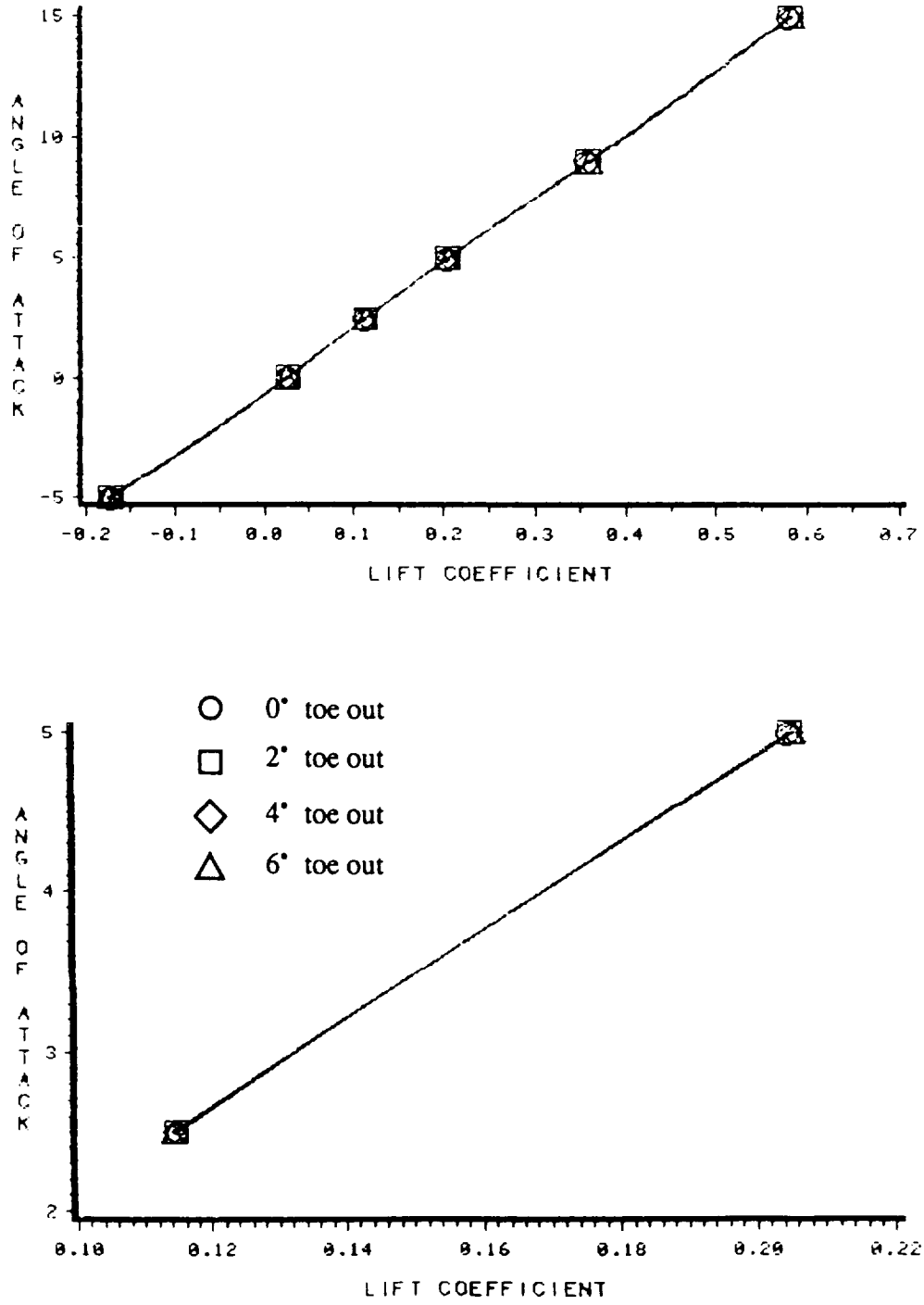

Figure 4.3.4: Predicted performance of the NACA 1402 base wing with 0% thick, 75° dihedral winglets; M=1.62; angle of attack versus lift coefficient.

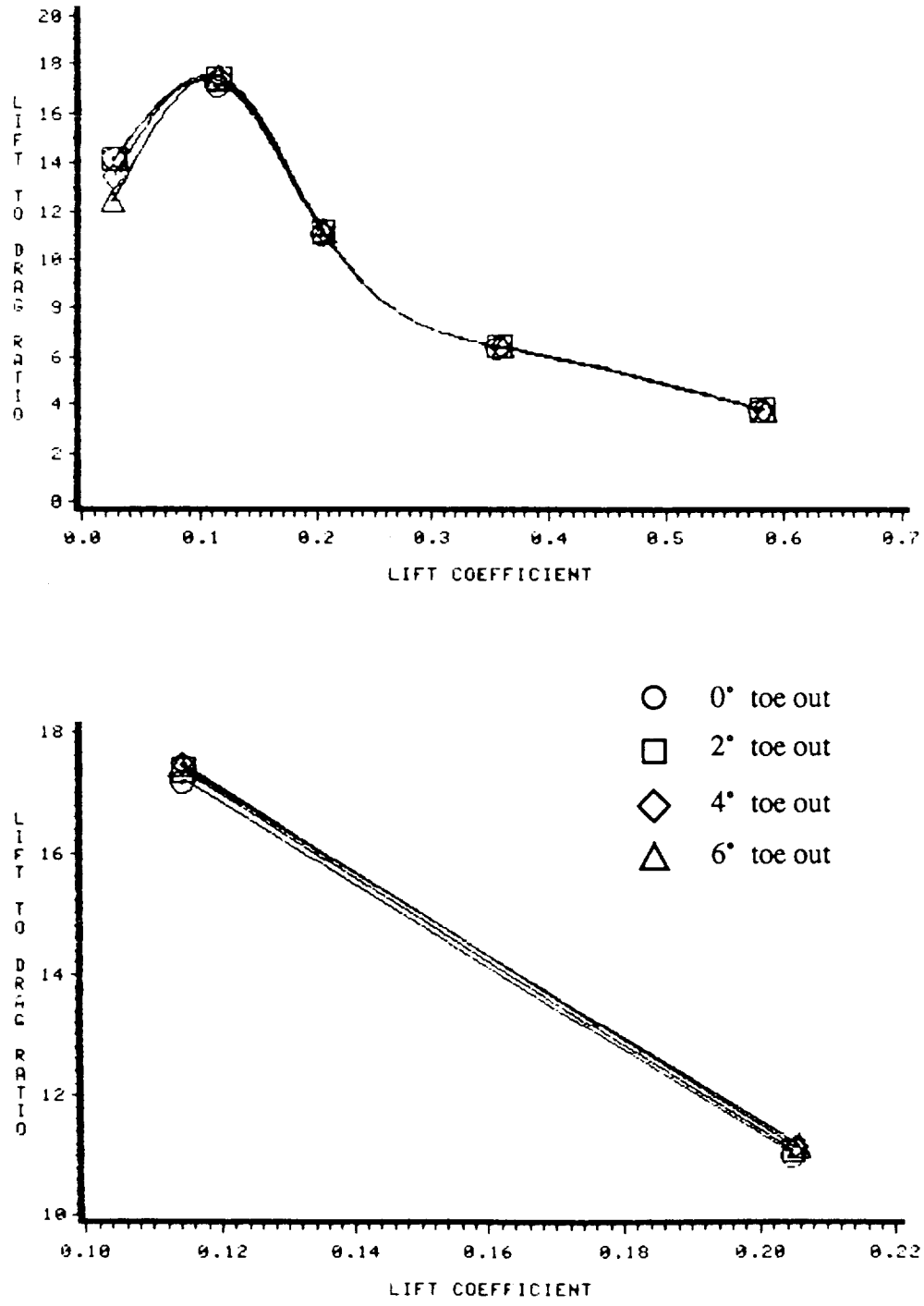

Figure 4.3.5: Predicted performance of the NACA 1402 base wing with 0% thick, 75° dihedral winglets; M=1.62; lift-to-pressure drag ratio versus lift coefficient.

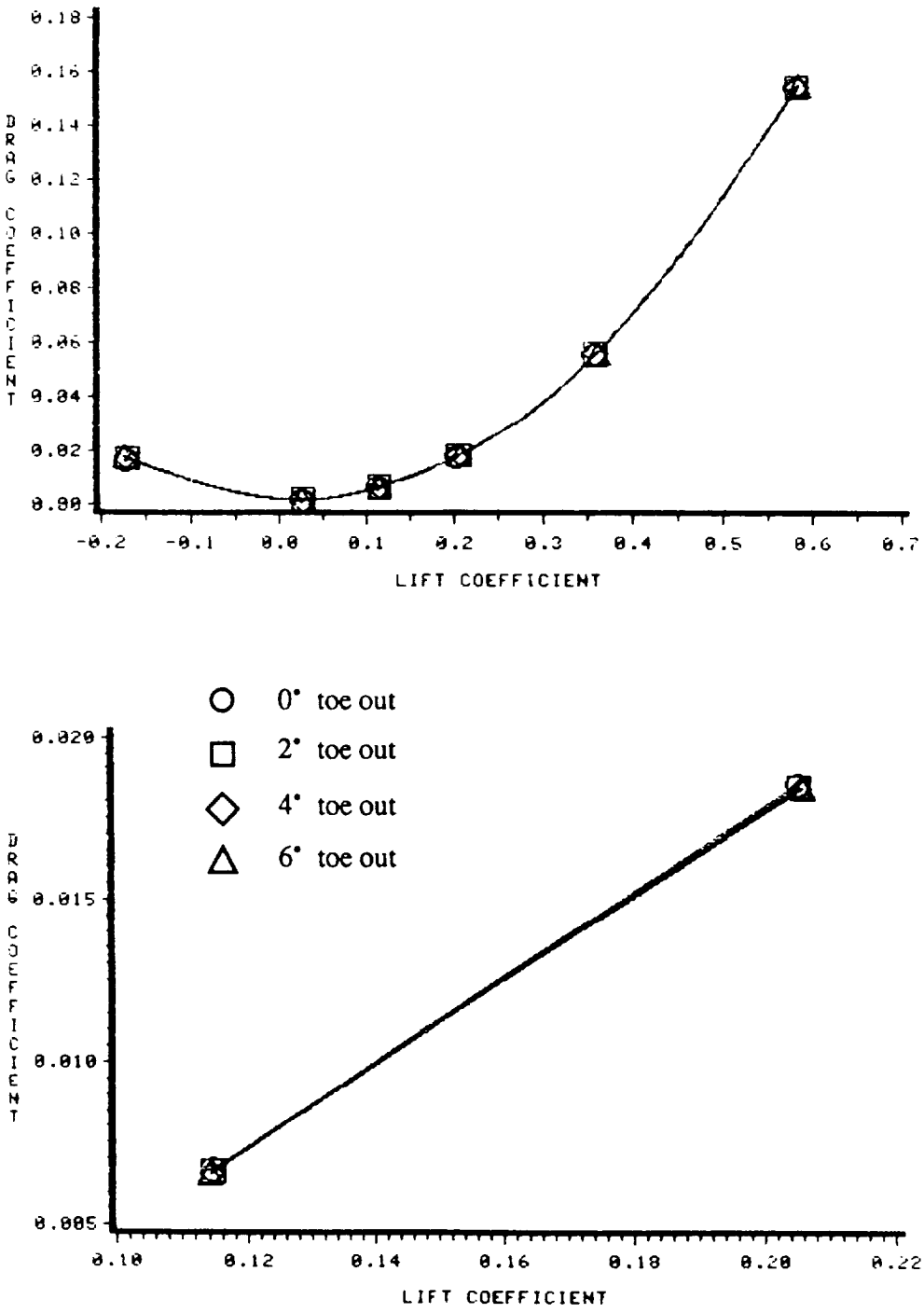

Figure 4.3.6: Predicted performance of the NACA 1402 base wing with 0% thick, 75° dihedral winglets; M=1.62; pressure drag coefficient versus lift coefficient.

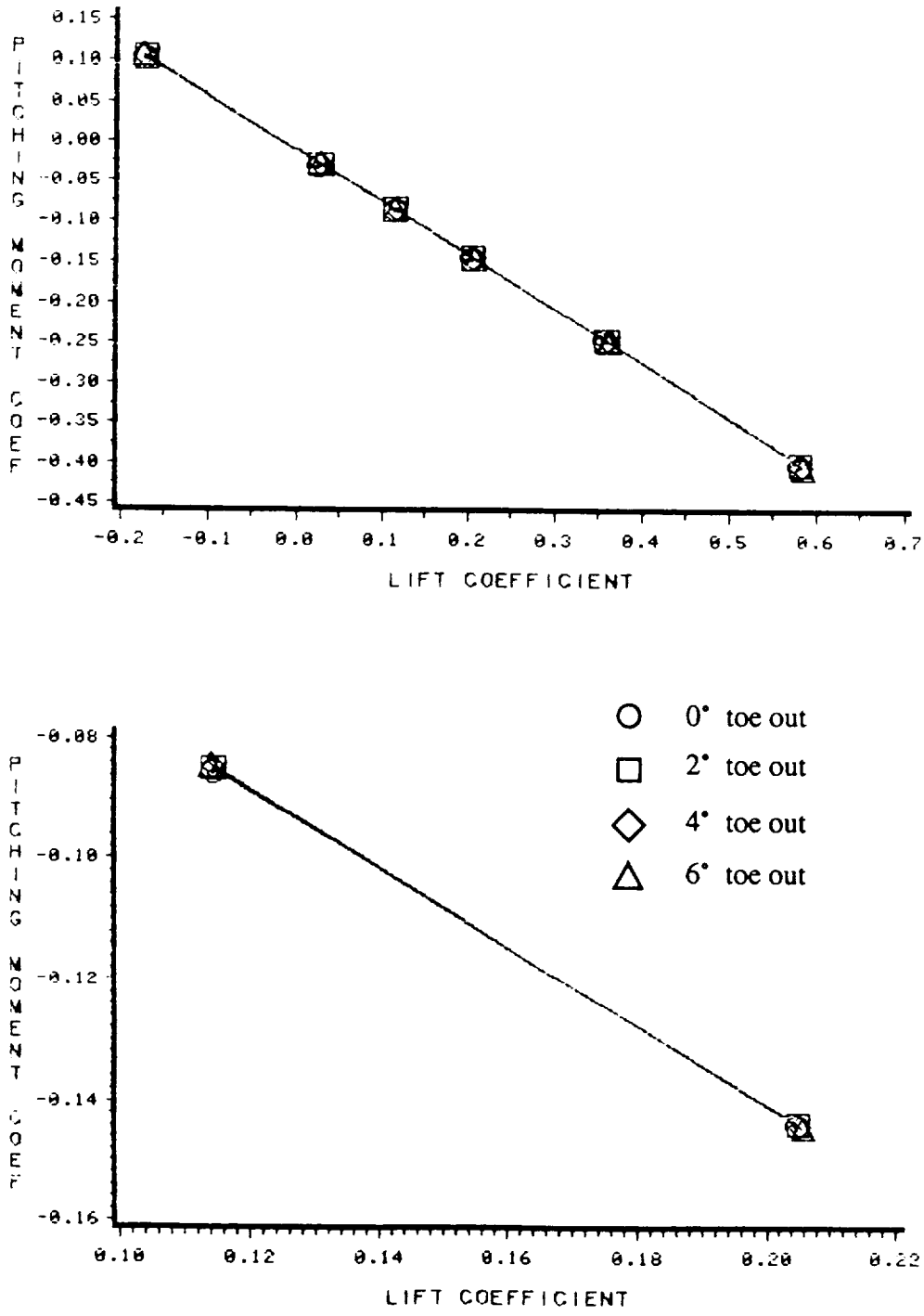

Figure 4.3.7: Predicted performance of the NACA 1402 base wing with 0% thick, 75° dihedral winglets; M=1.62; pitching moment coefficient versus lift coefficient.

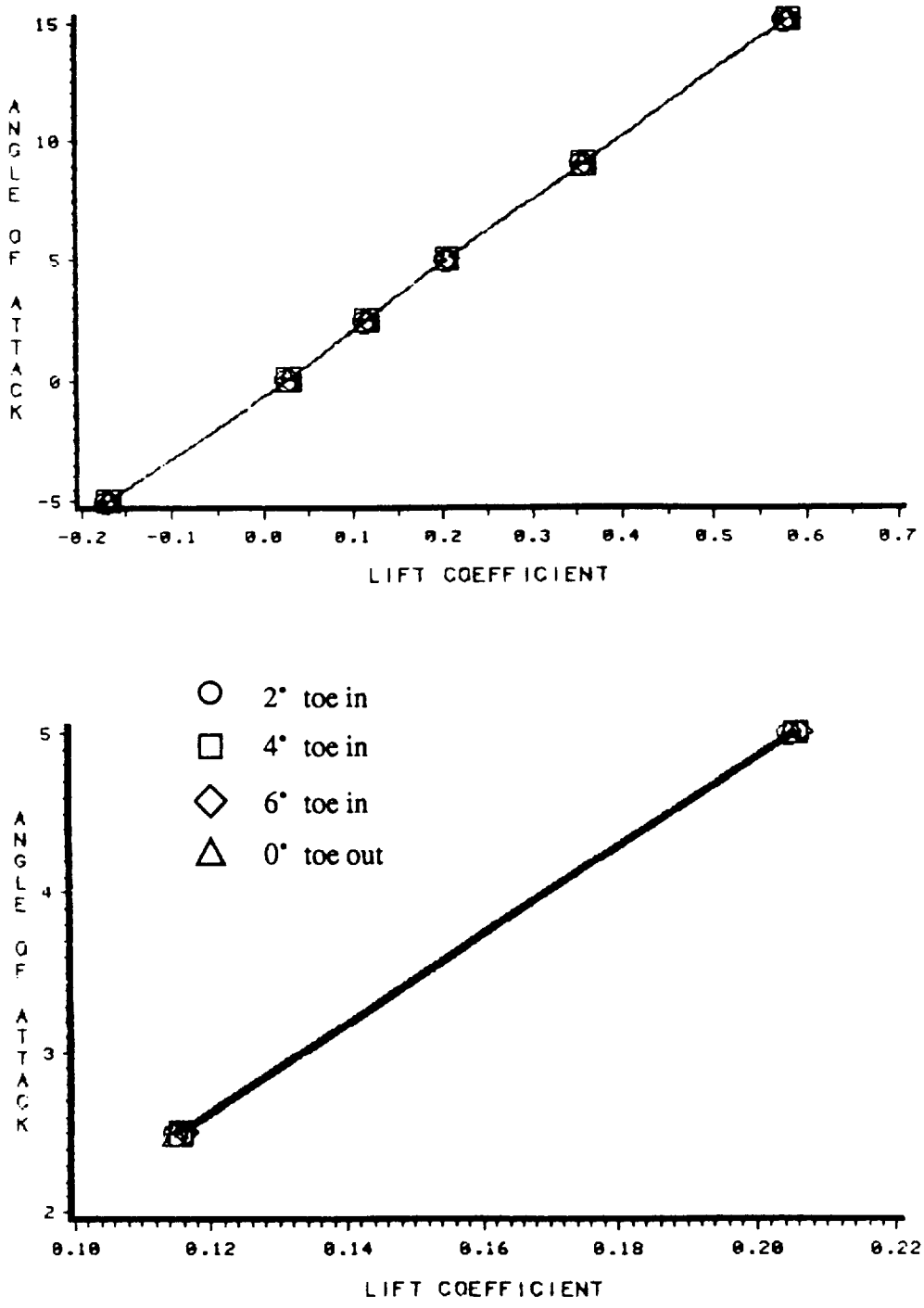

Figure 4.3.8: Predicted performance of the NACA 1402 base wing with 0% thick, 75° dihedral winglets; M=1.62; angle of attack versus lift coefficient.

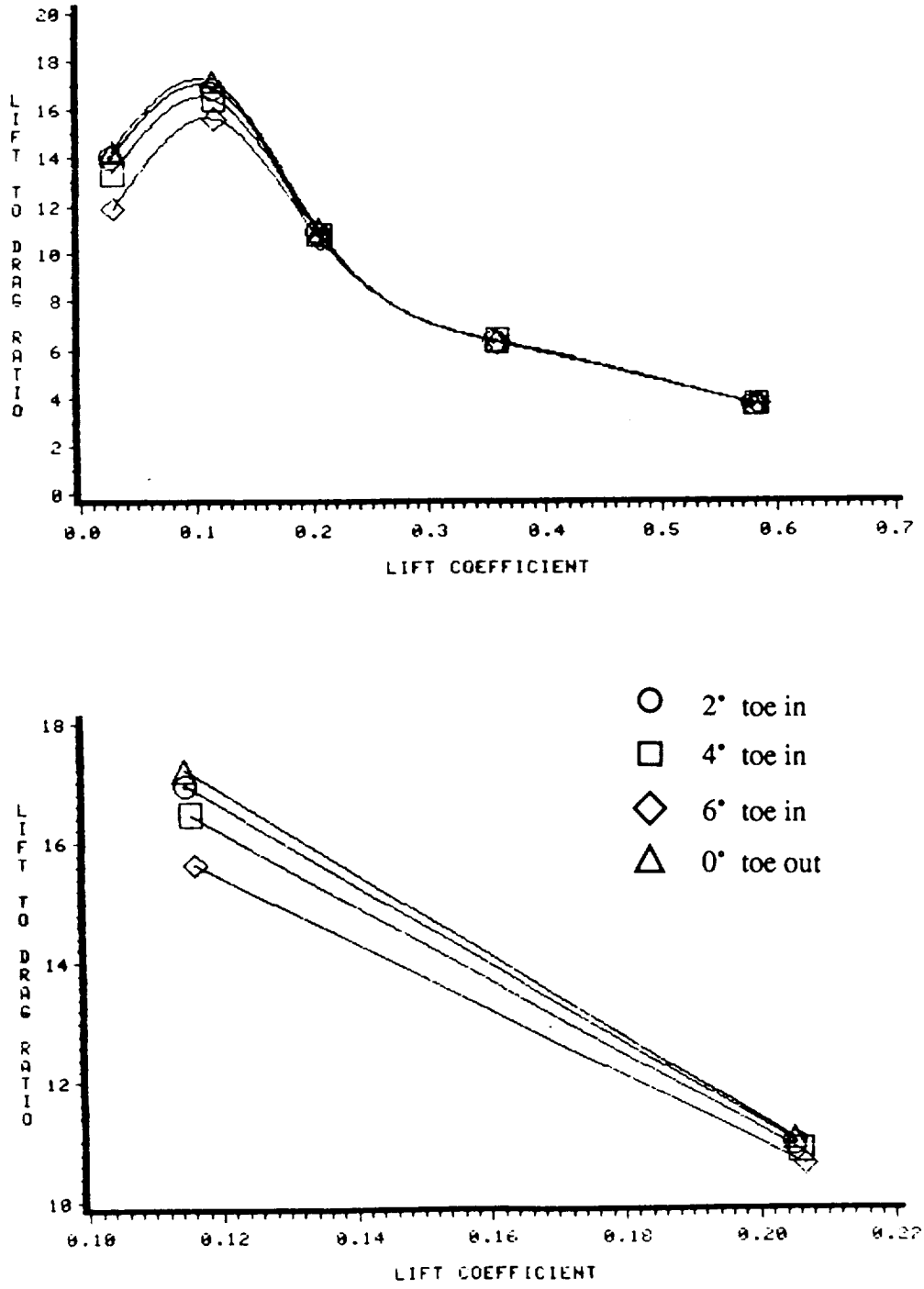

Figure 4.3.9: Predicted performance of the NACA 1402 base wing with 0% thick, 75° dihedral winglets; M=1.62; lift-to-pressure drag ratio versus lift coefficient.

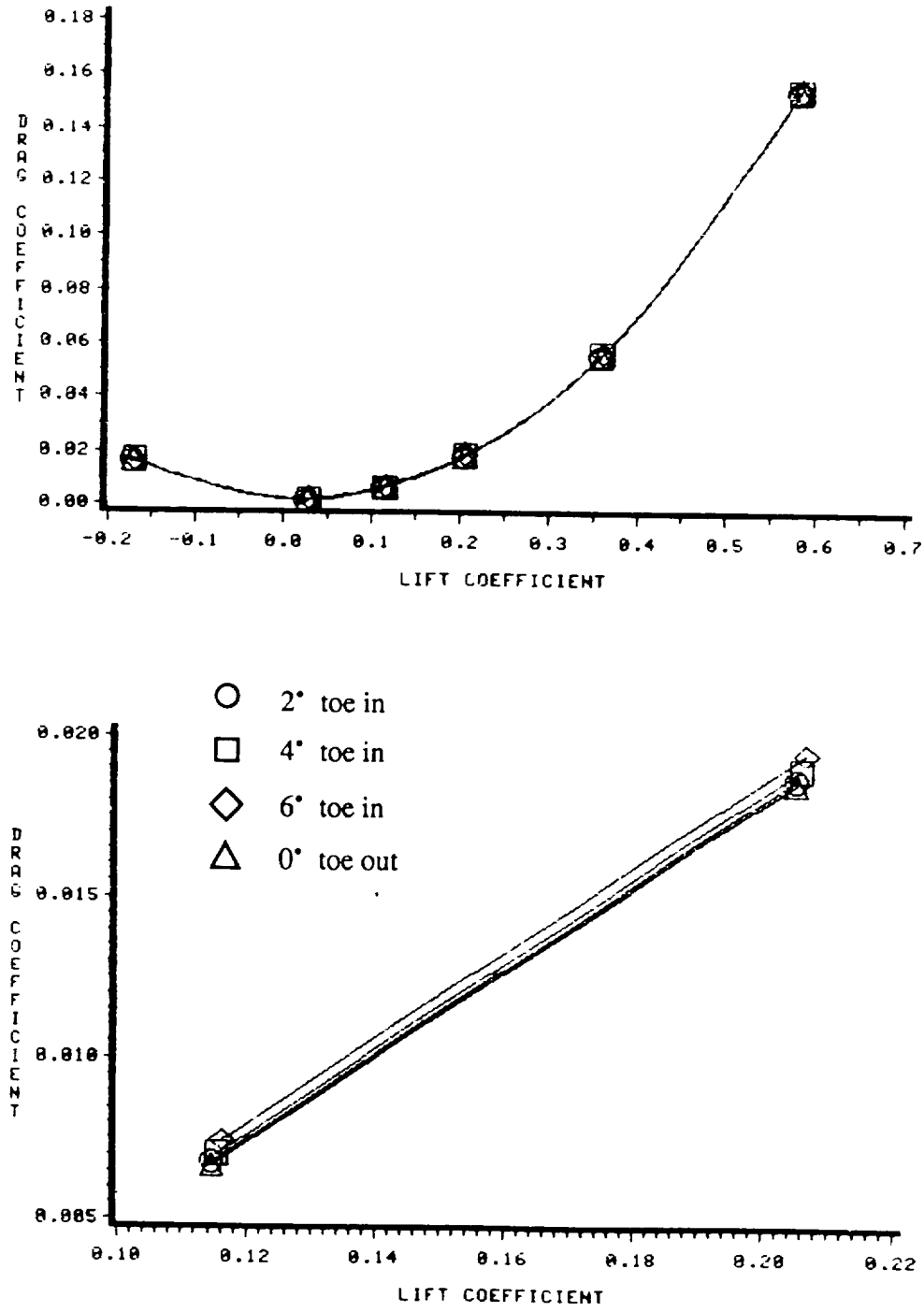

Figure 4.3.10: Predicted performance of the NACA 1402 base wing with 0% thick, 75° dihedral winglets; M=1.62; pressure drag coefficient versus lift coefficient.

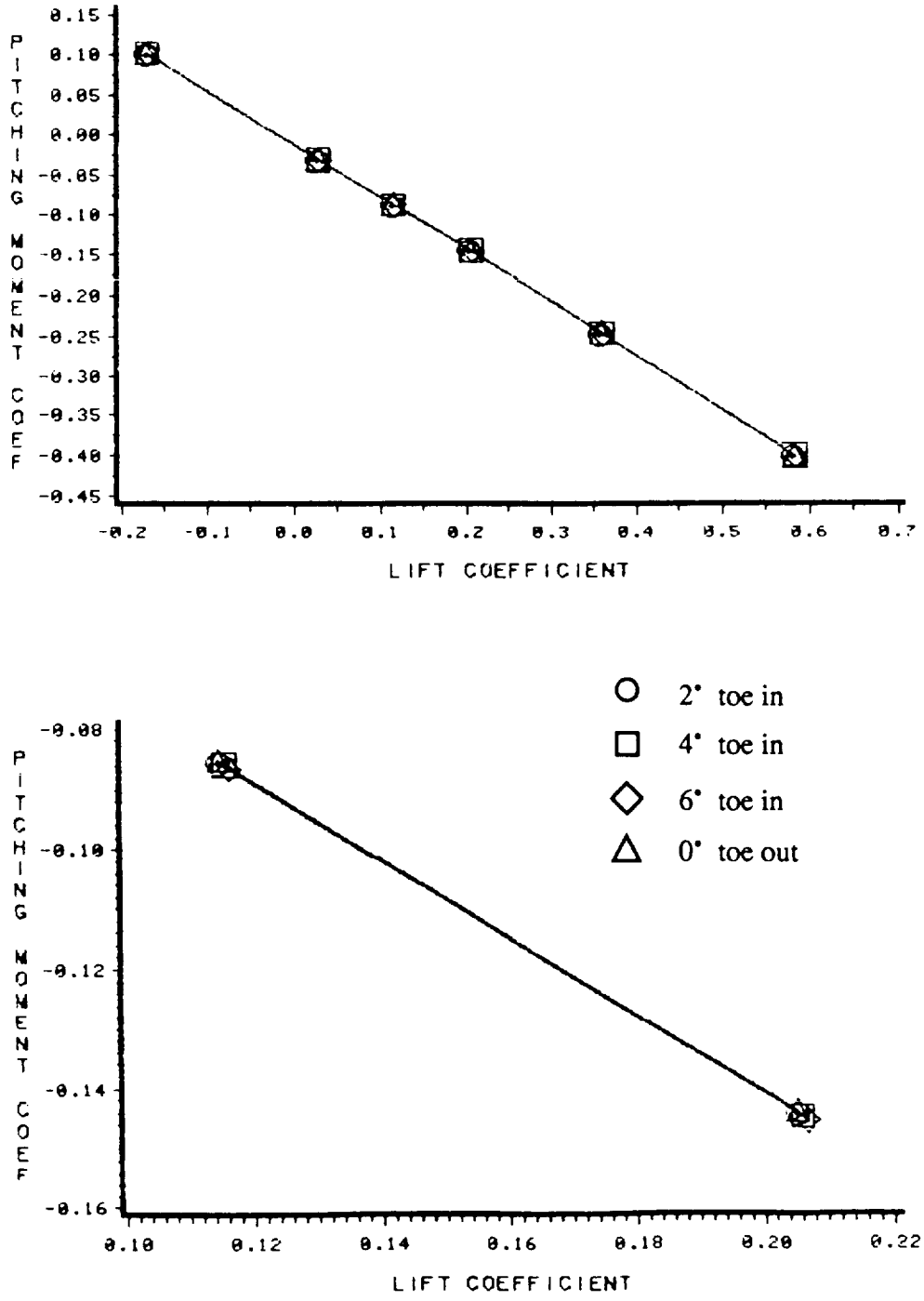

Figure 4.3.11: Predicted performance of the NACA 1402 base wing with 0% thick, 75° dihedral winglets; M=1.62; pitching moment coefficient versus lift coefficient.

C-2

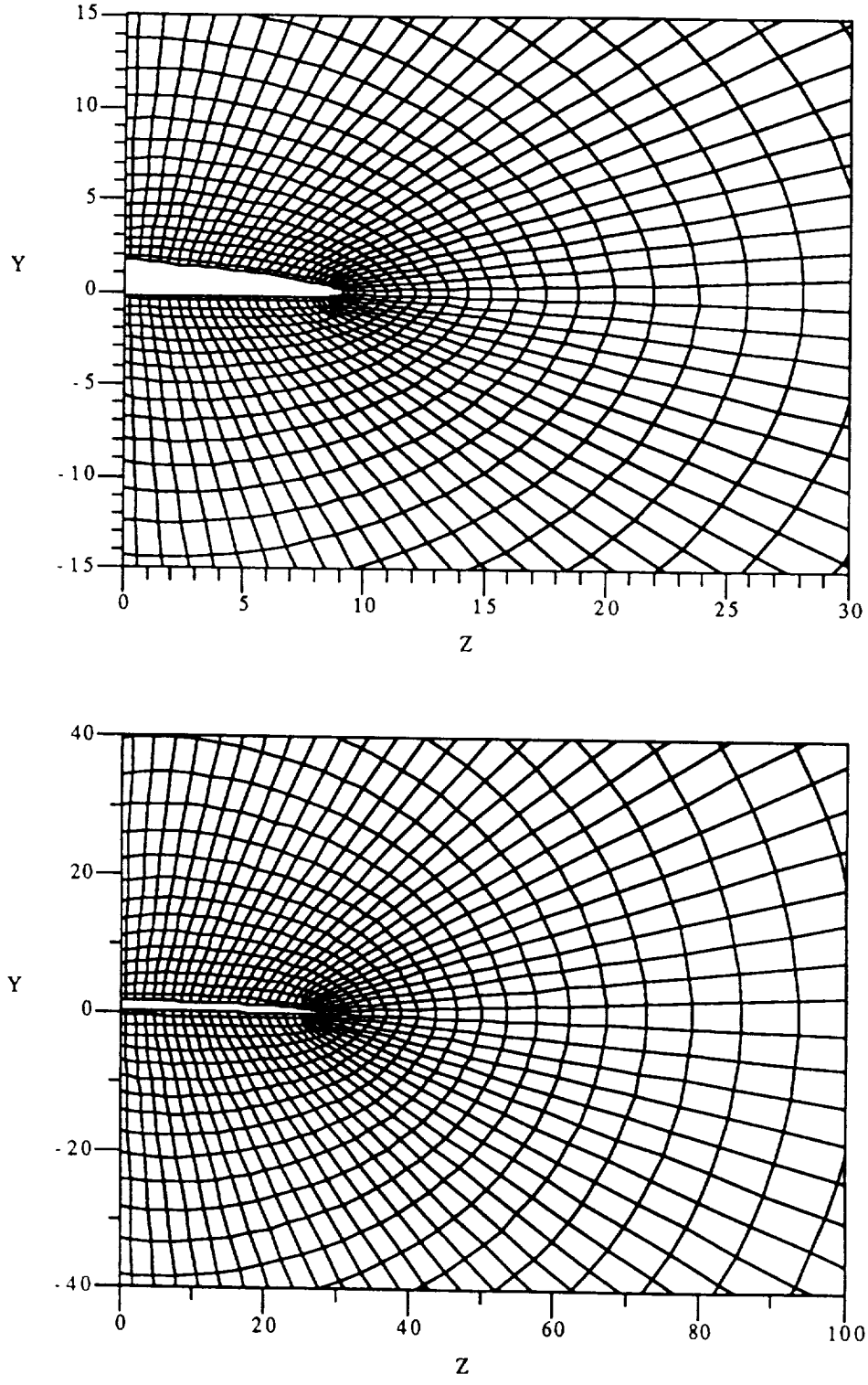

Figure 4.4.1: Computational grid surrounding the NACA 1402 base wing with a 0% thick, 75° anhedral winglet at x= 19.7,59.7.89.8, 99.4.

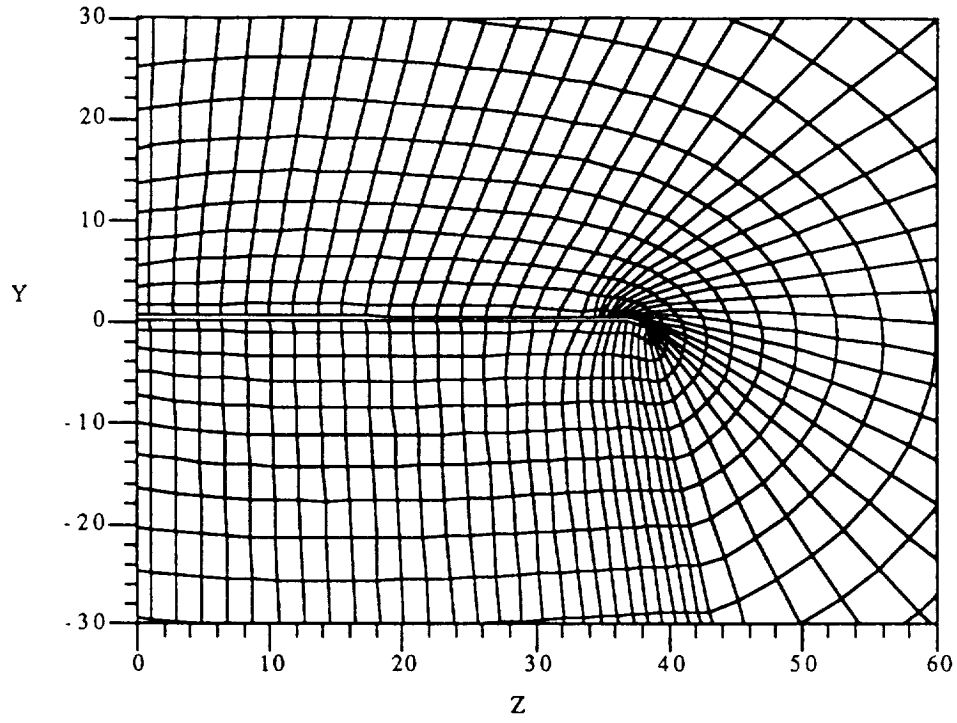

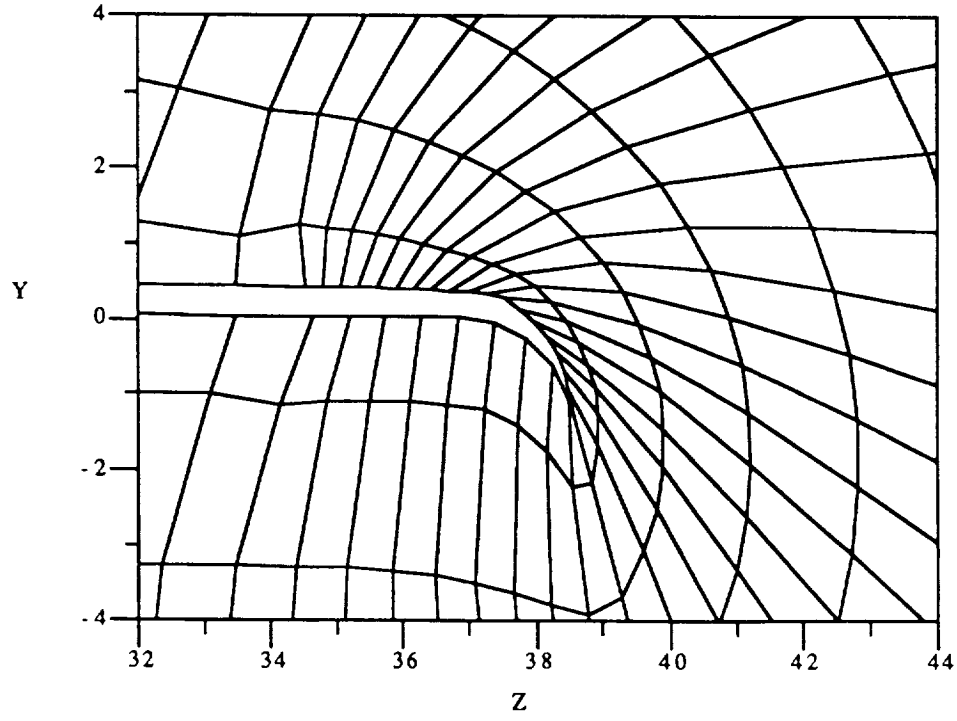

Figure 4.4.1: Continued, x=89.8

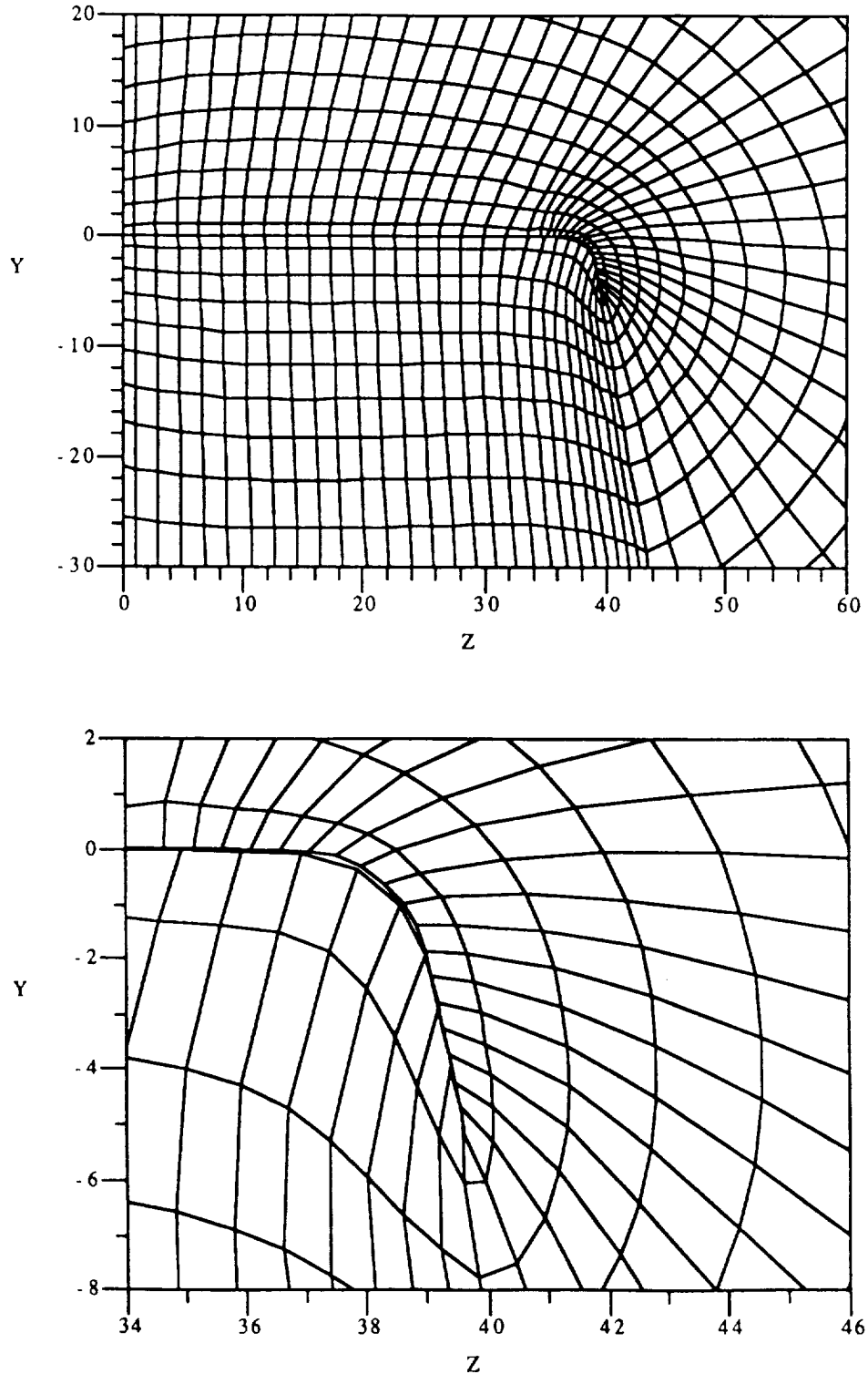

Figure 4.4.1: Continued, x= 99.6

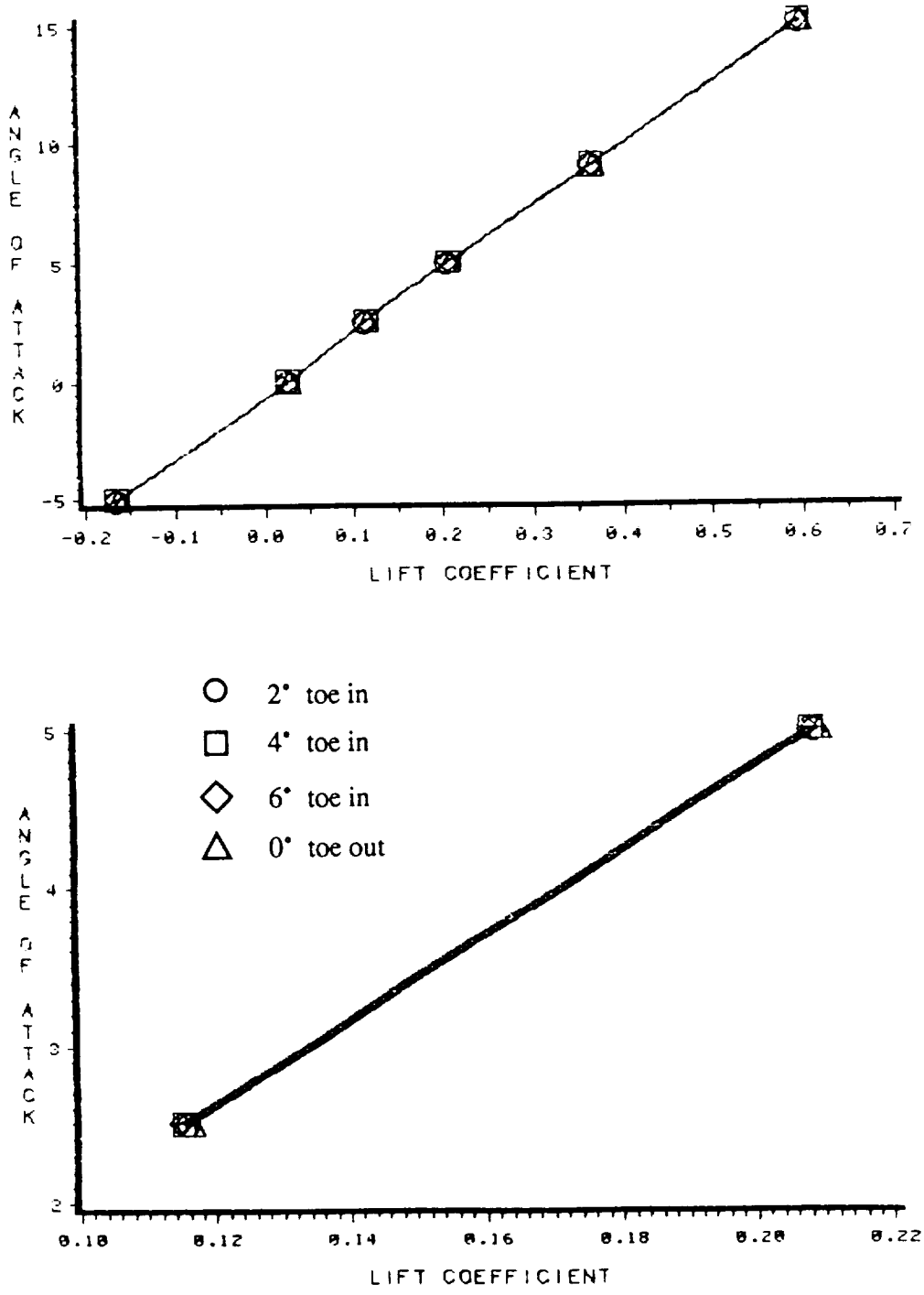

Figure 4.4.2: Predicted performance of the NACA 1402 base wing with 0% thick, 75° anhedral winglets; M=1.62; angle of attack versus lift coefficient.

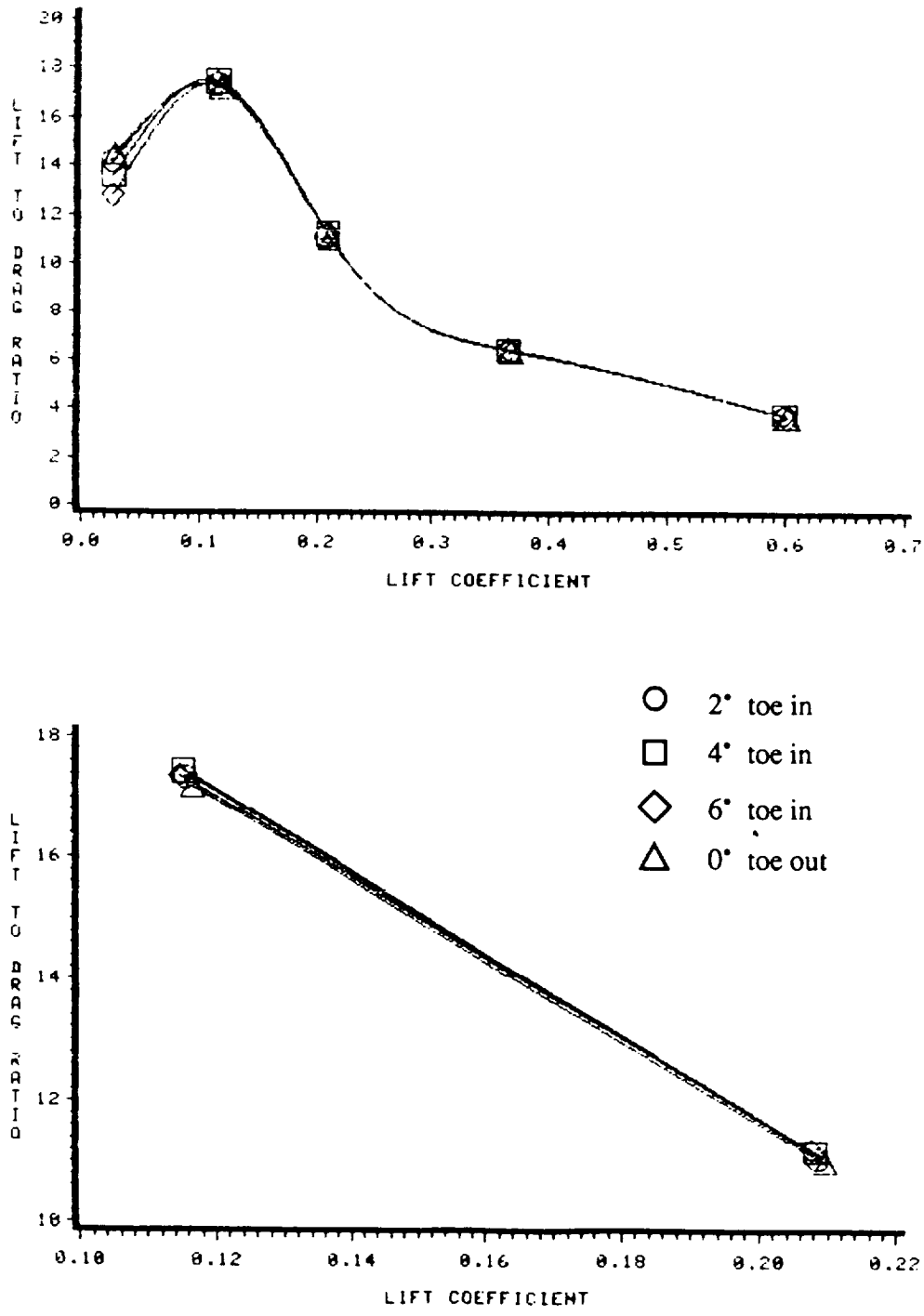

Figure 4.4.3: Predicted performance of the NACA 1402 base wing with 0% thick, 75° anhedral winglets; M=1.62; lift-to-pressure drag ratio versus lift coefficient.

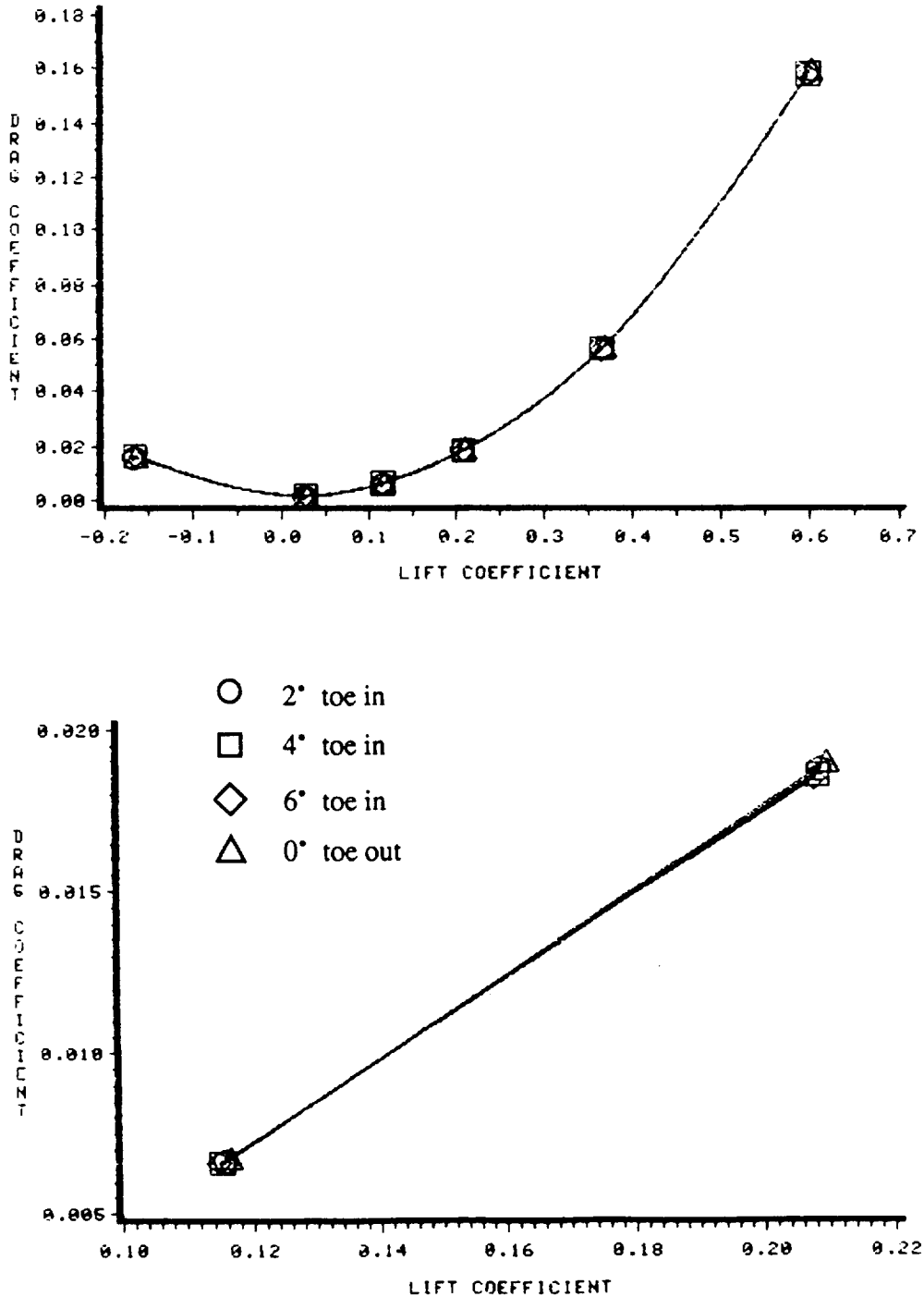

Figure 4.4.4: Predicted performance of the NACA 1402 base wing with 0% thick, 75° anhedral winglets; M=1.62; pressure drag coefficient versus lift coefficient.

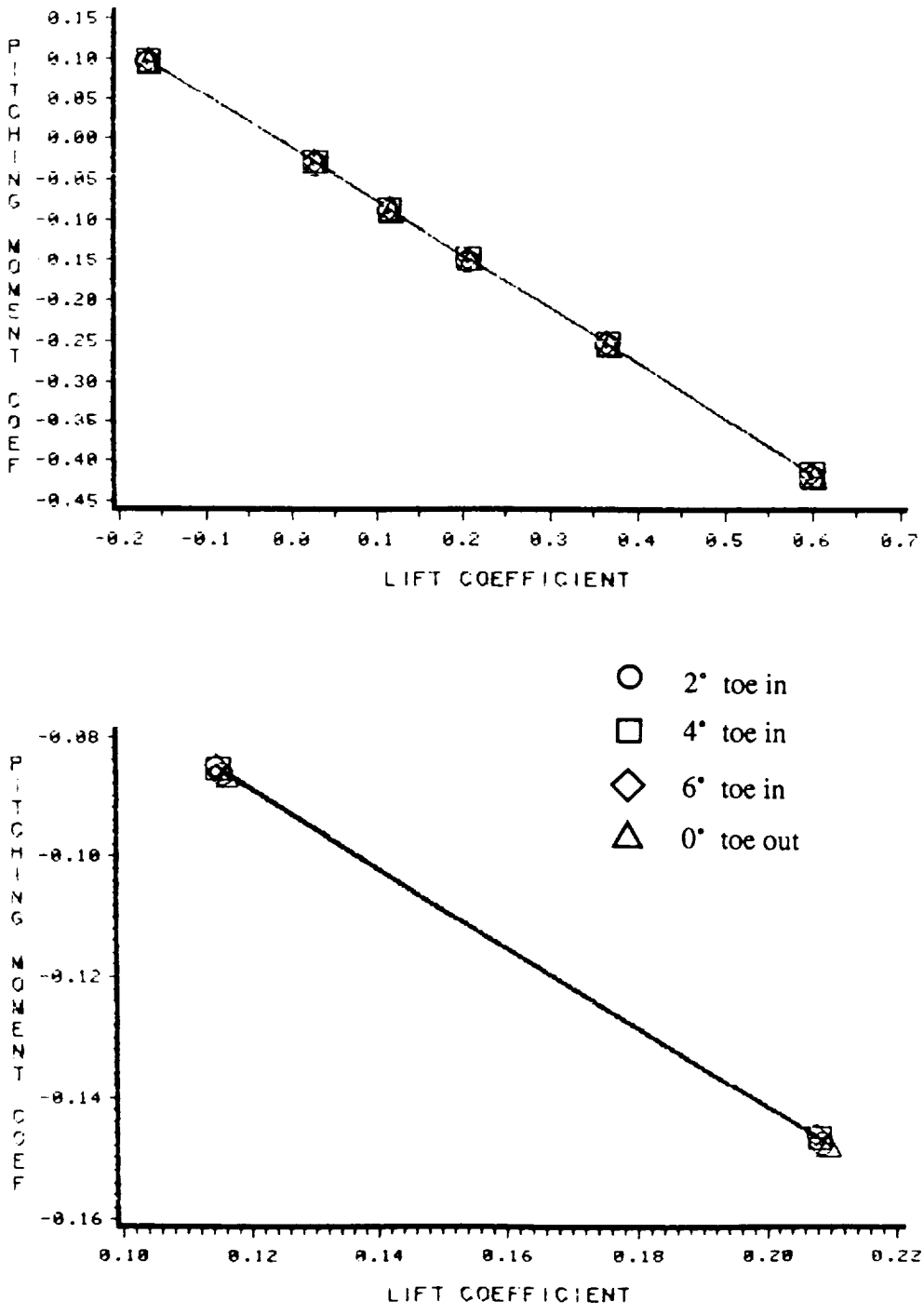

Figure 4.4.5: Predicted performance of the NACA 1402 base wing with 0% thick, 75° anhedral winglets; M=1.62; pitching moment coefficient versus lift coefficient.

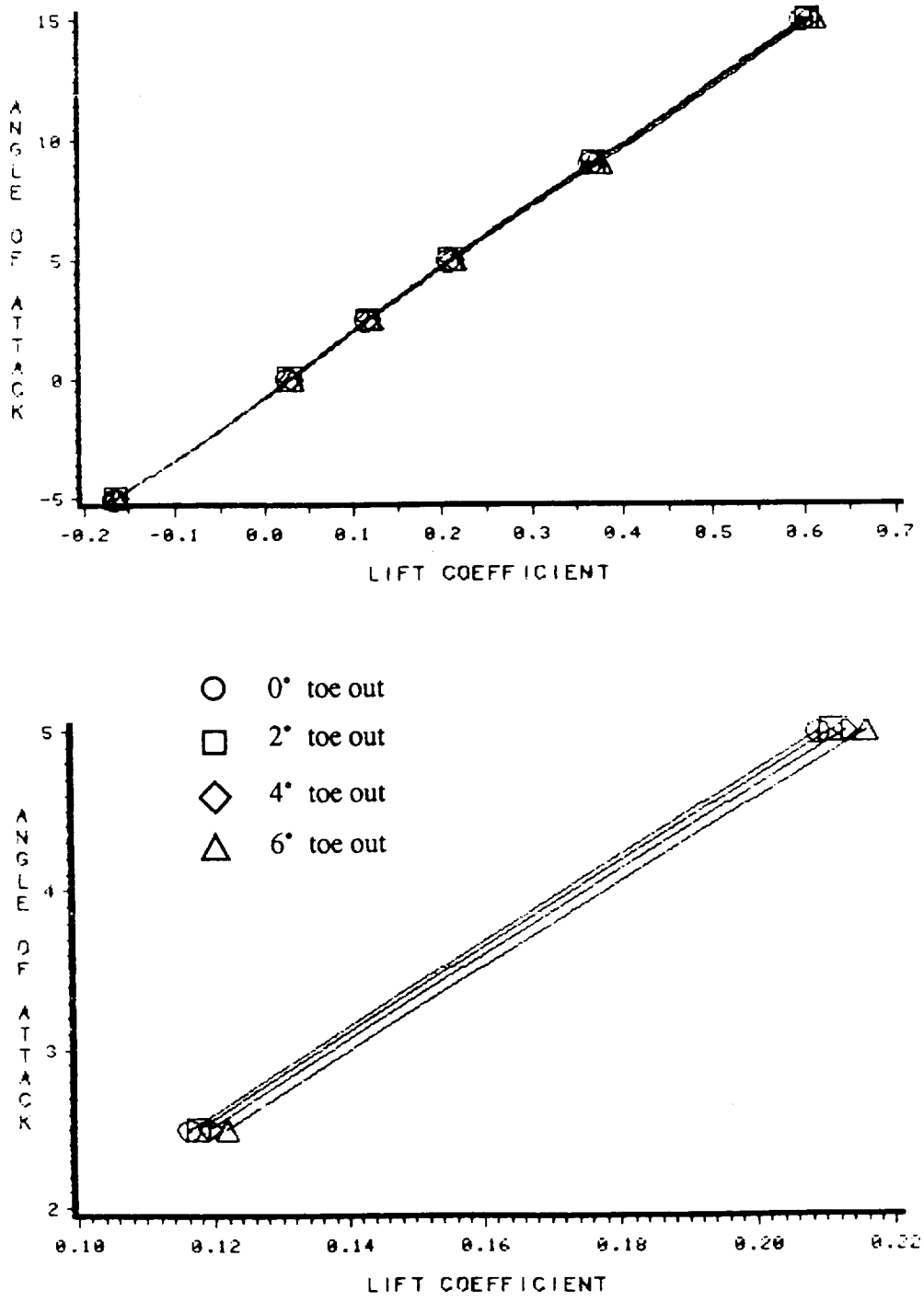

Figure 4.4.6: Predicted performance of the NACA 1402 base wing with 0% thick, 75° anhedral winglets; M=1.62; angle of attack versus lift coefficient.

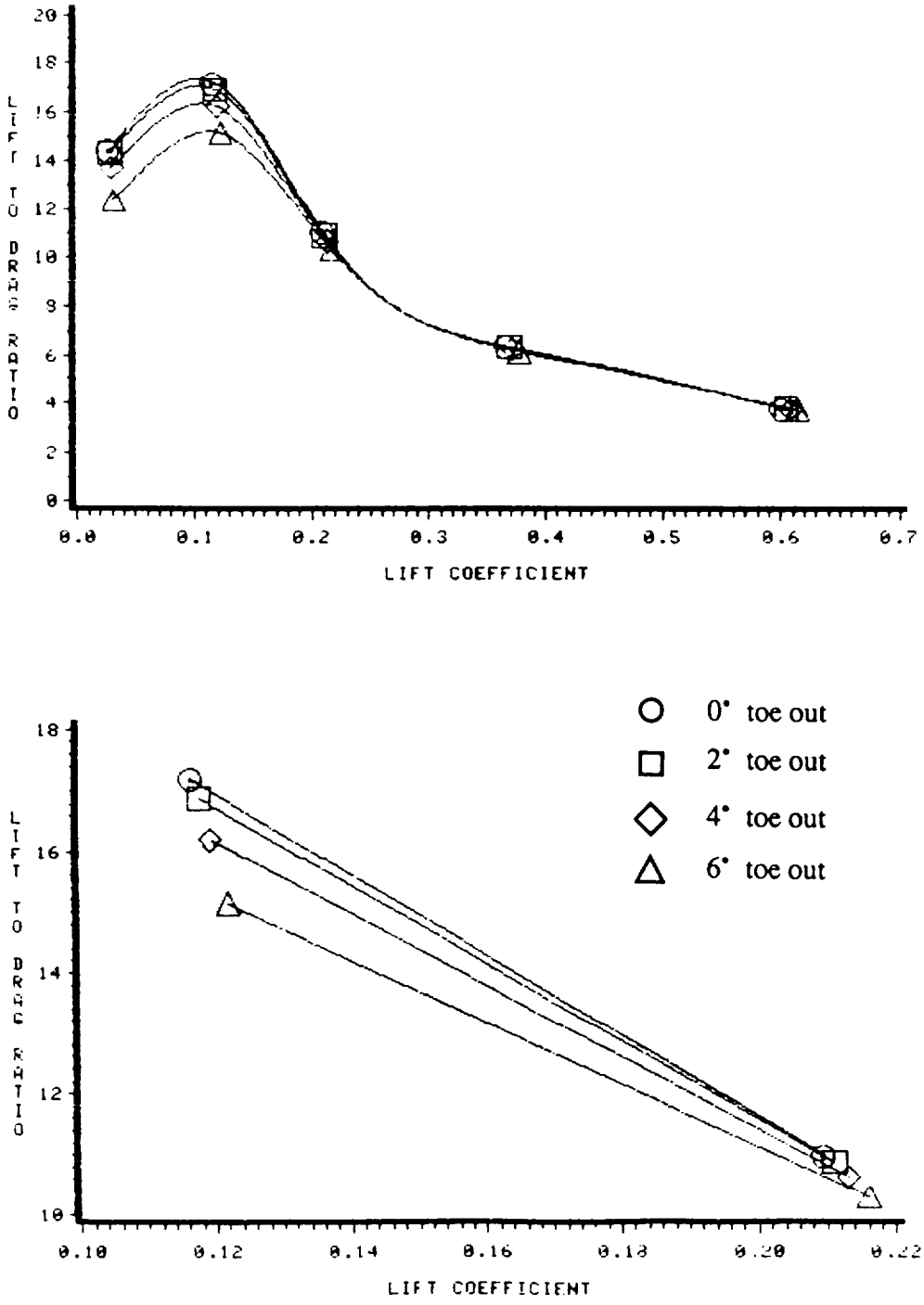

Figure 4.4.7: Predicted performance of the NACA 1402 base wing with 0% thick, 75° anhedral winglets; M=1.62; lift-to-pressure drag versus lift coefficient.

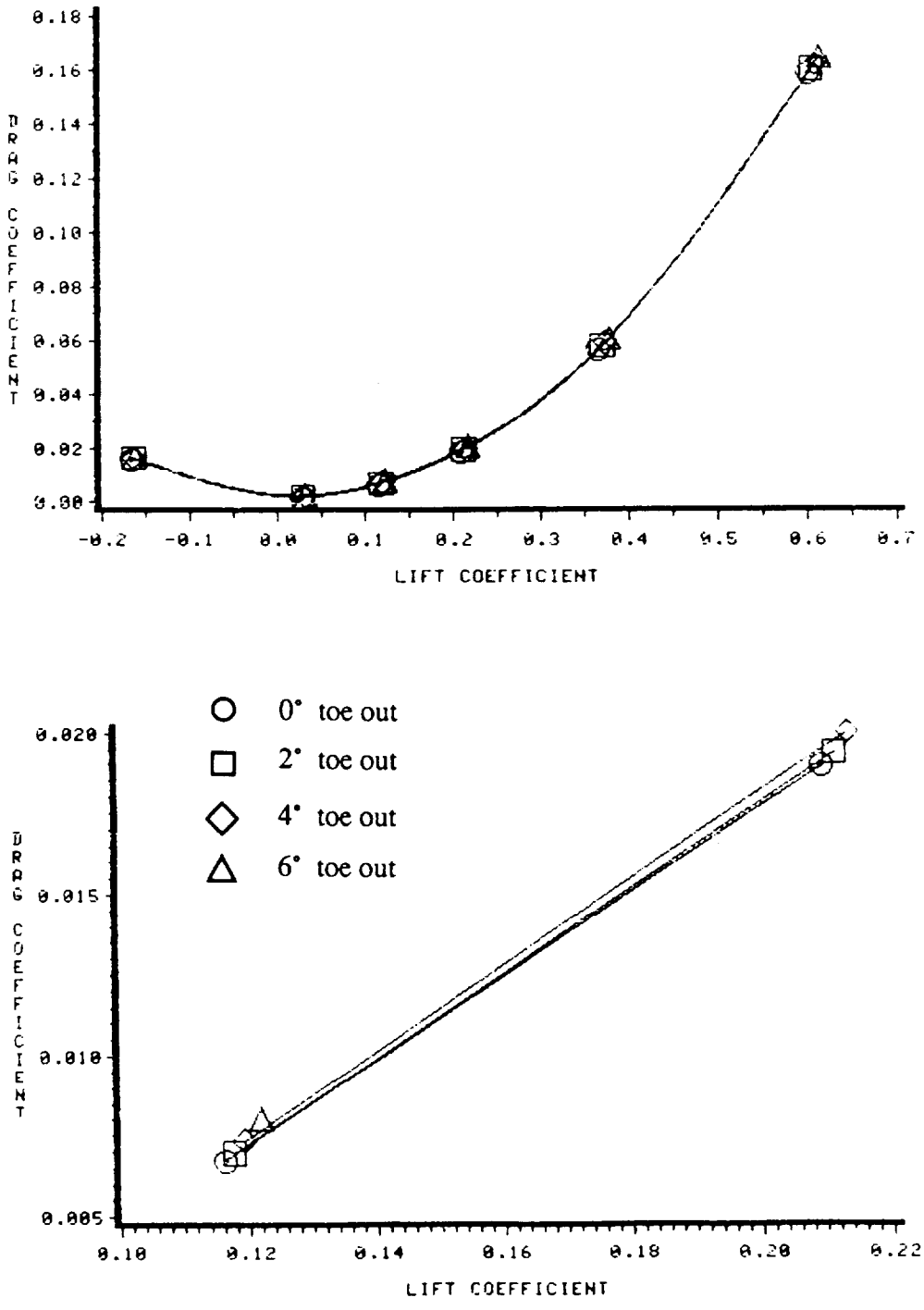

Figure 4.4.8: Predicted performance of the NACA 1402 base wing with 0% thick, 75° anhedral winglets; M=1.62; pressure drag coefficient versus lift coefficient.

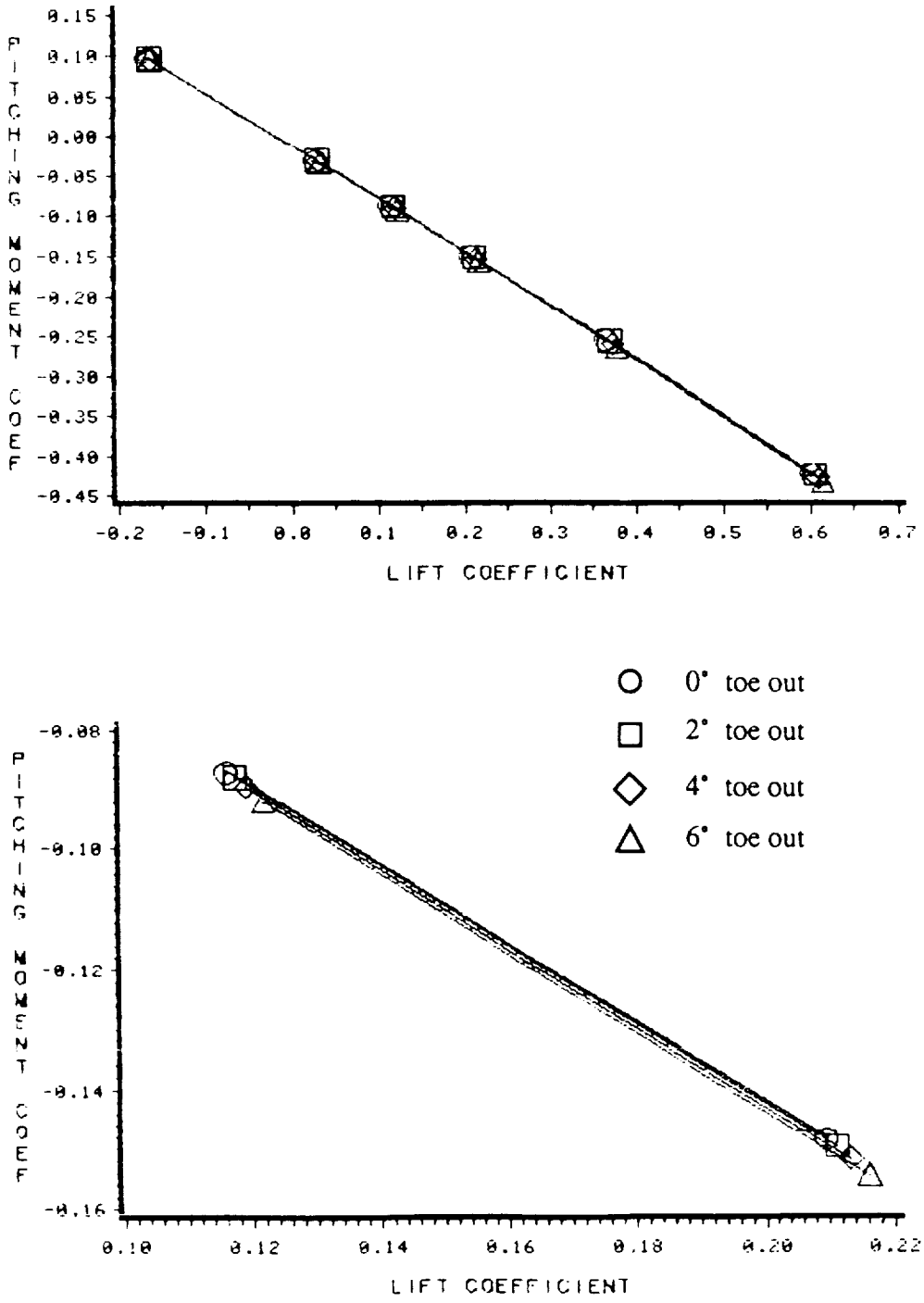

Figure 4.4.9: Predicted performance of the NACA 1402 base wing with 0% thick, 75° anhedral winglets; M=1.62; pitching moment coefficient versus lift coefficient.

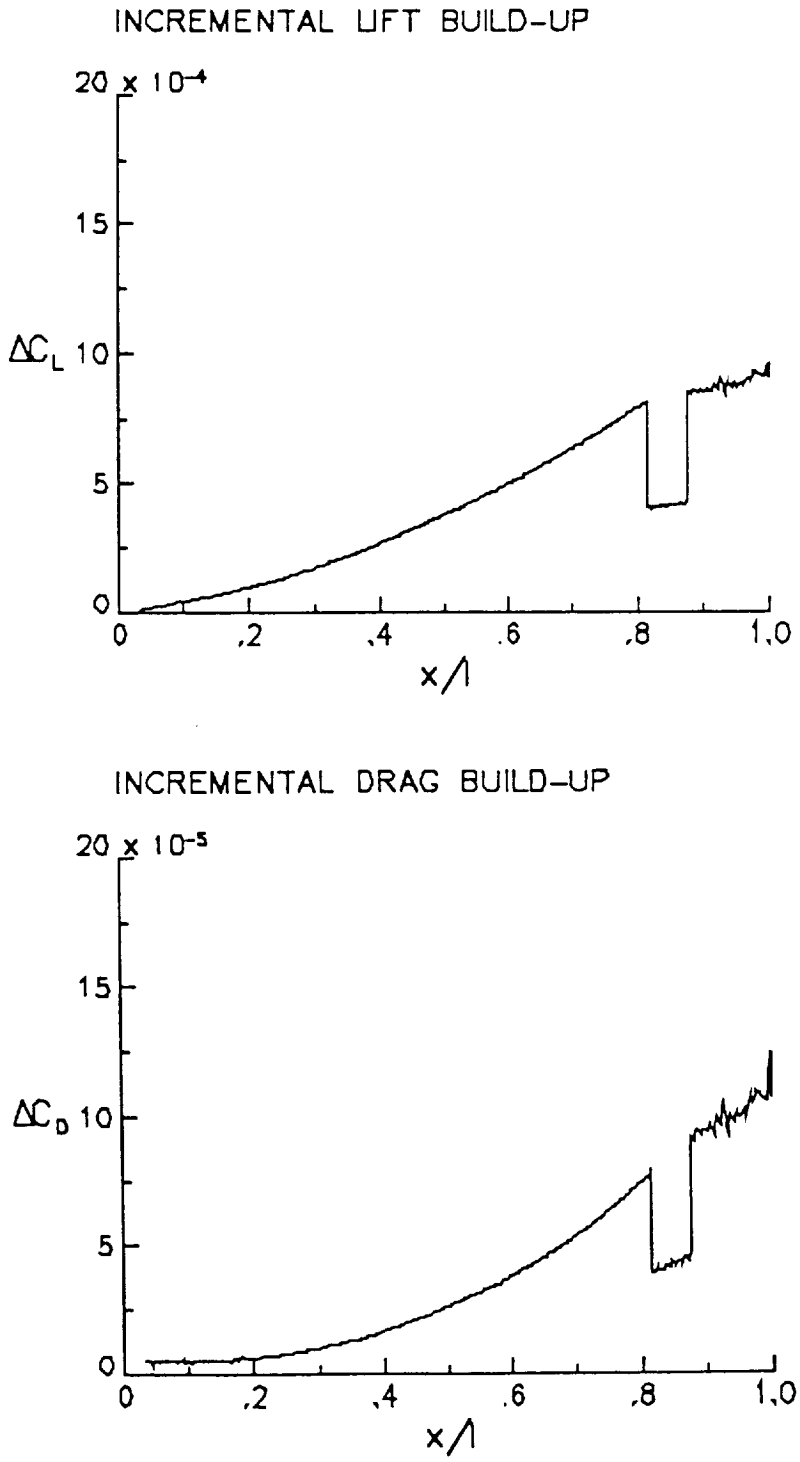

Figure 4.4.10: Incremental lift and pressure drag build up for the NACA 1402 base wing with a 0% thick, 2° toe in, 75° anhedral winglet at 5° angle of attack, M=1.62.

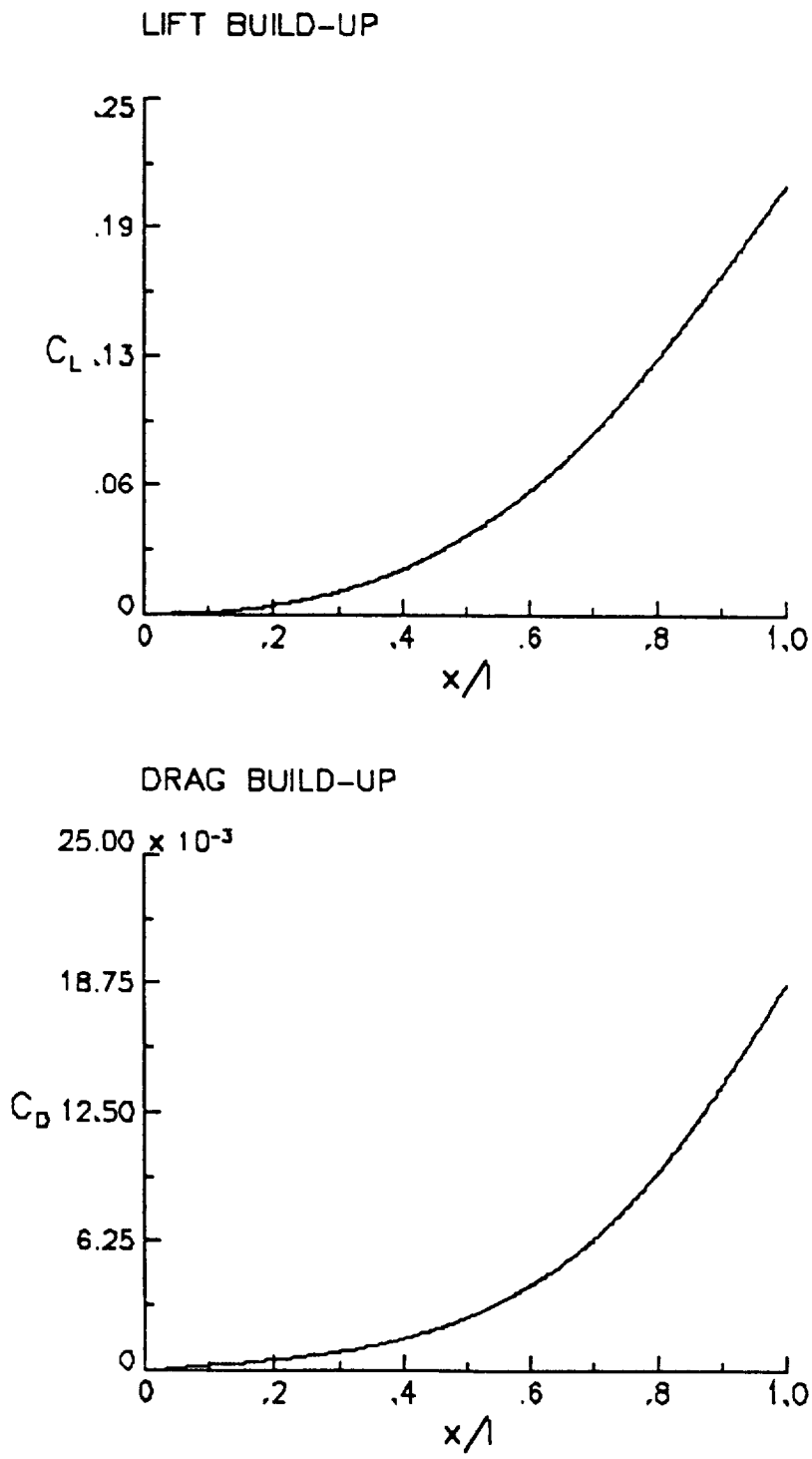

Figure 4.4.11: Total lift and pressure drag build up for the NACA 1402 base wing with a 0% thick, 2° toe in, 75° anhedral winglet at 5° angle of attack, M=1.62.

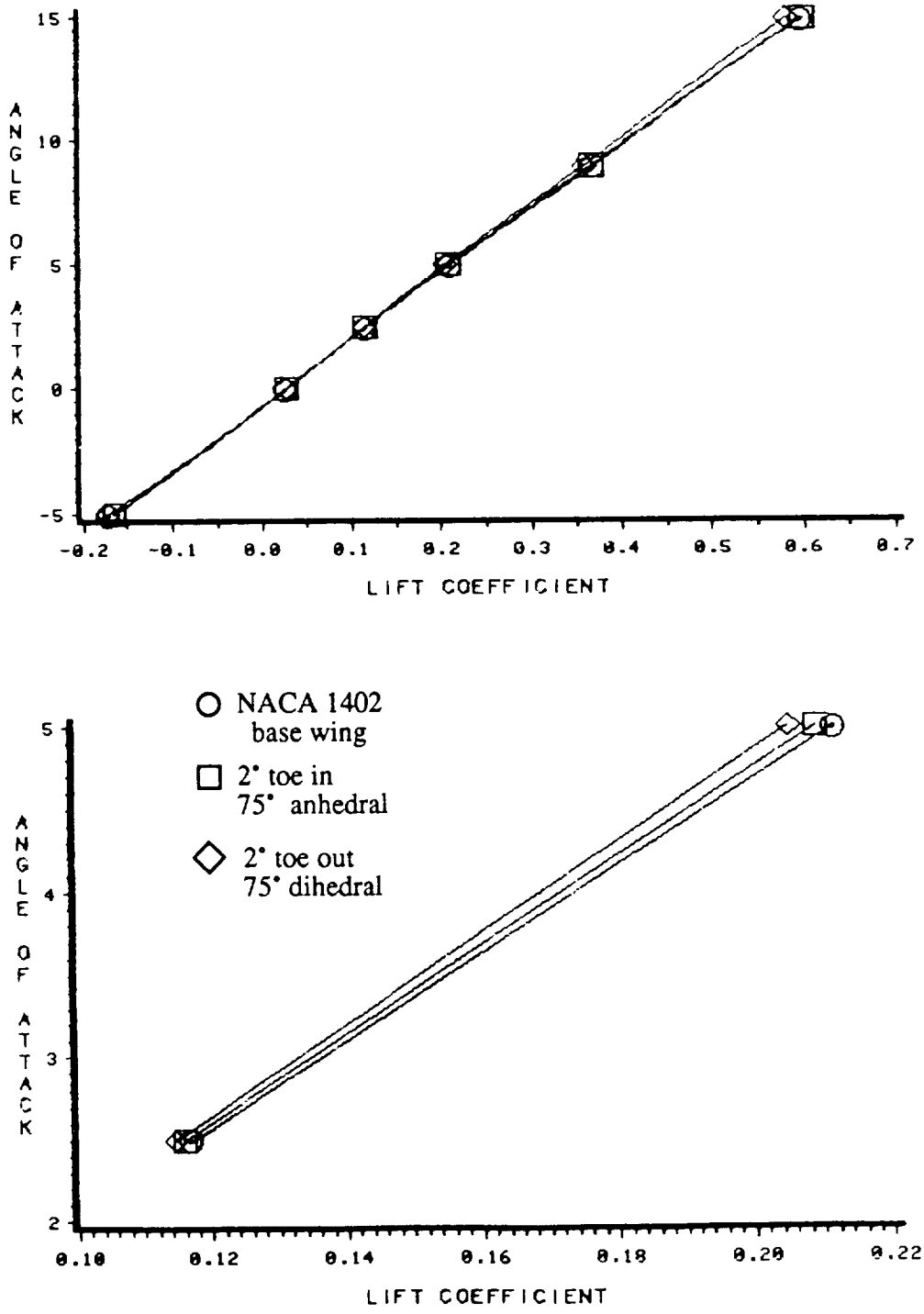

Figure 4.4.12: Comparison of the predicted performance between the NACA 1402 base wing with extension; the 2° toe out, 75° dihedral wing-winglet; and the 2° toe in, 75° anhedral wing-winglet; M=1.62; angle of attack versus lift coefficient.

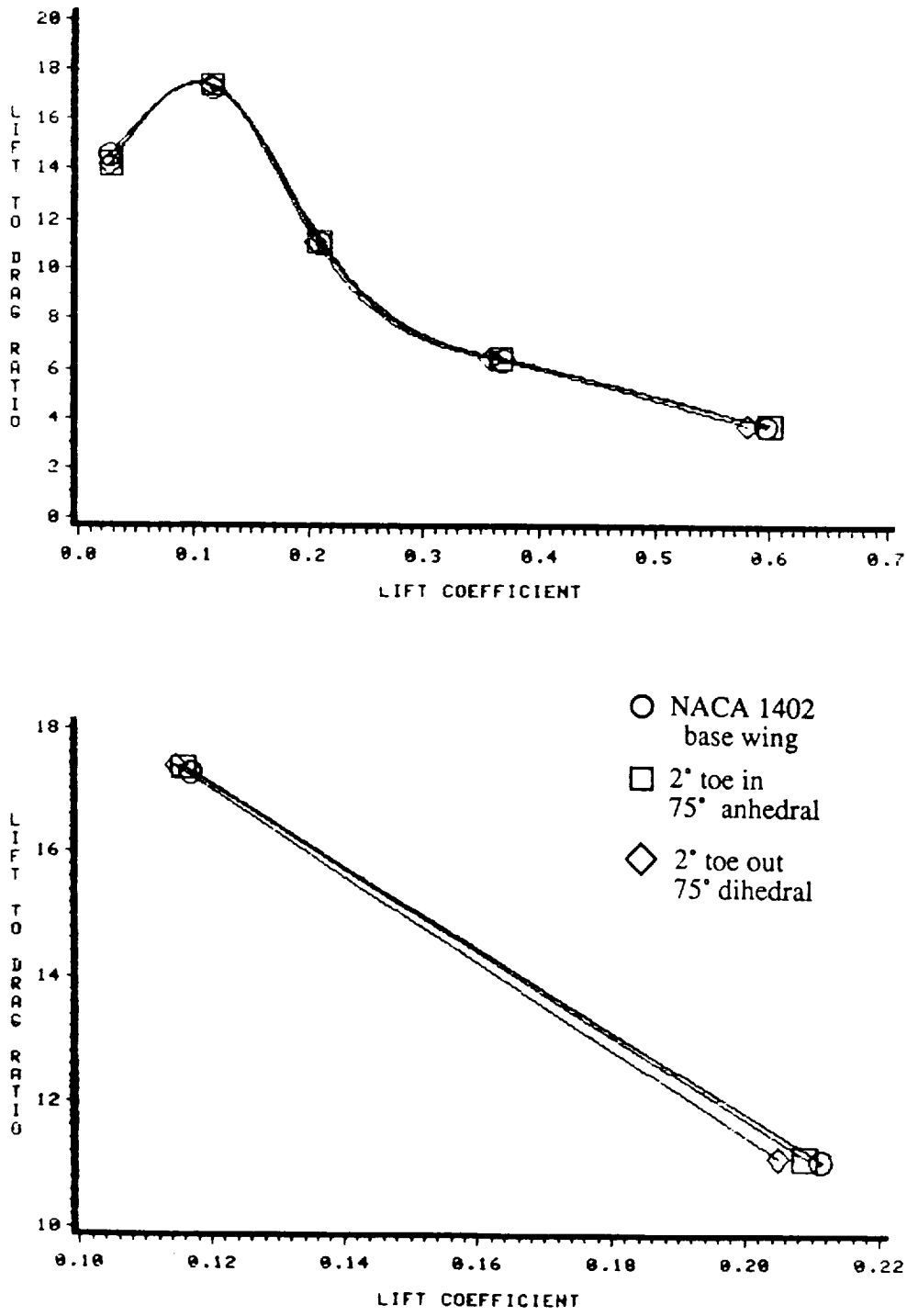

Figure 4.4.13: Comparison of the predicted performance between the NACA 1402 base wing with extension; the 2° toe out, 75° dihedral wing-winglet; and the 2° toe in, 75° anhedral wing-winglet; M=1.62; lift-to-pressure drag ratio versus lift coefficient.

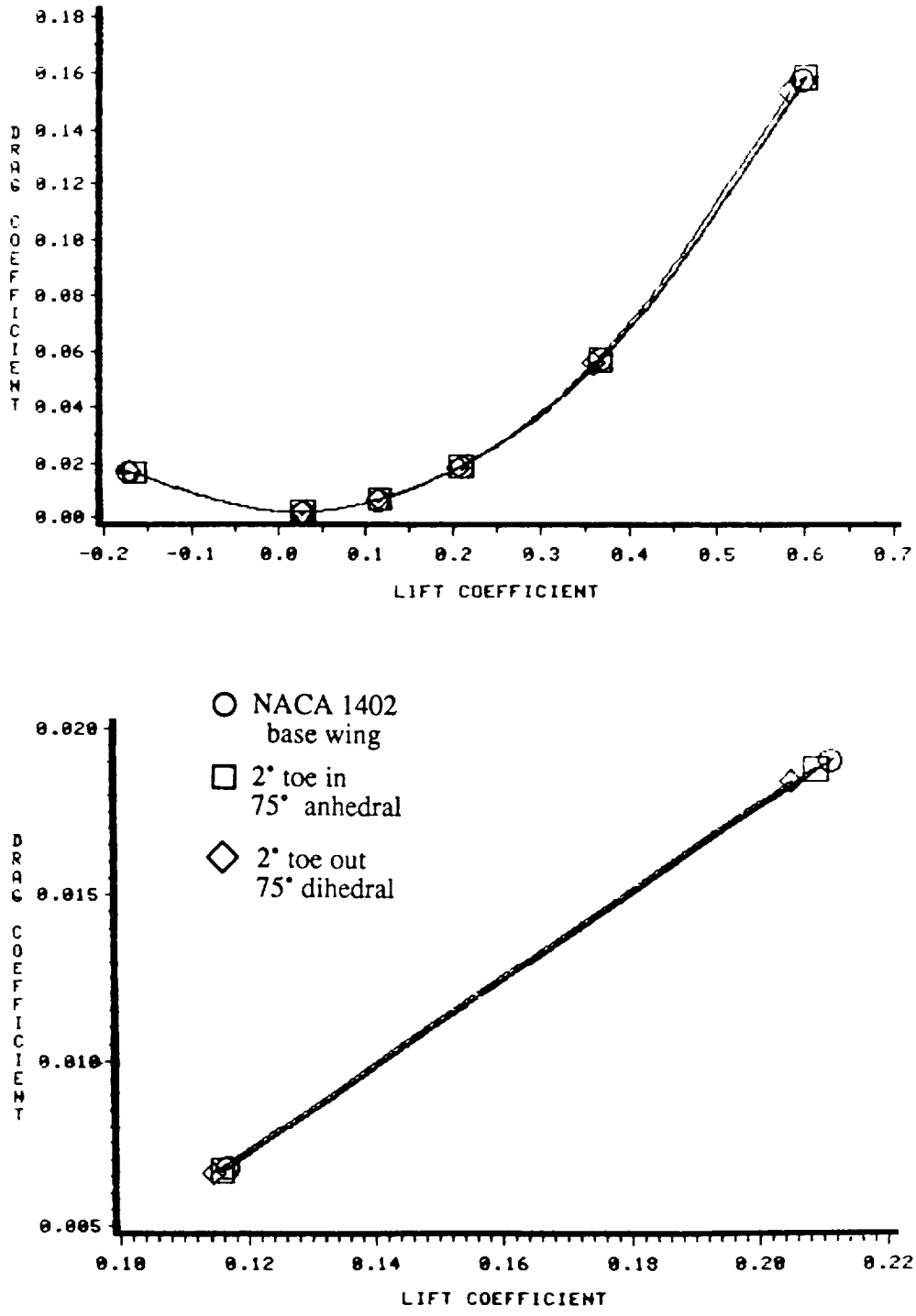

Figure 4.4.14: Comparison of the predicted performance between the NACA 1402 base wing with extension; the 2° toe out, 75° dihedral wing-winglet; and the 2° toe in, 75° anhedral wing-winglet; M=1.62; pressure drag coefficient versus lift coefficient.

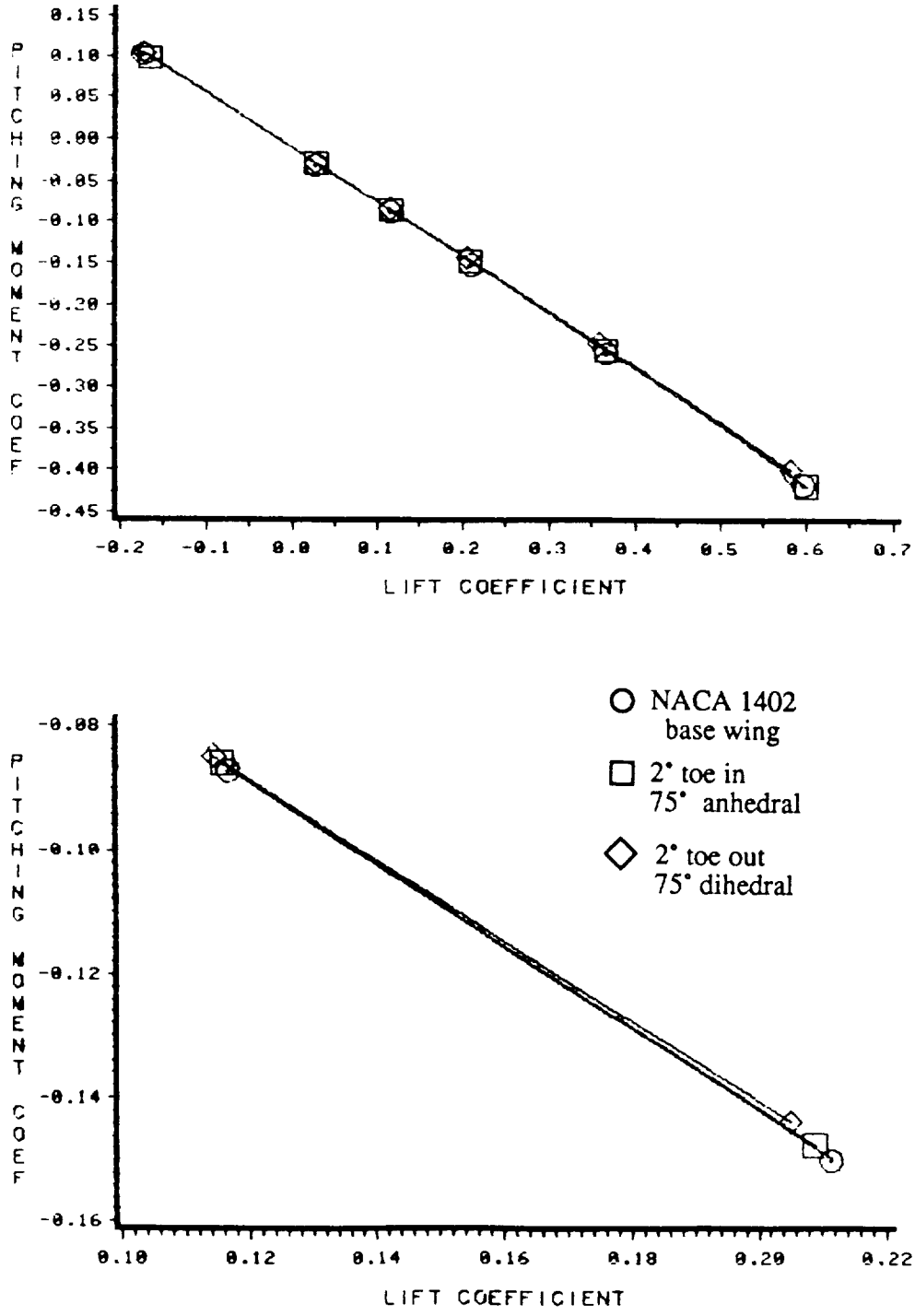

Figure 4.4.15: Comparison of the predicted performance between the NACA 1402 base wing with extension; the 2° toe out, 75° dihedral wing-winglet; and the 2° toe in, 75° anhedral wing-winglet; M=1.62; pitching moment coefficient versus lift coefficient.

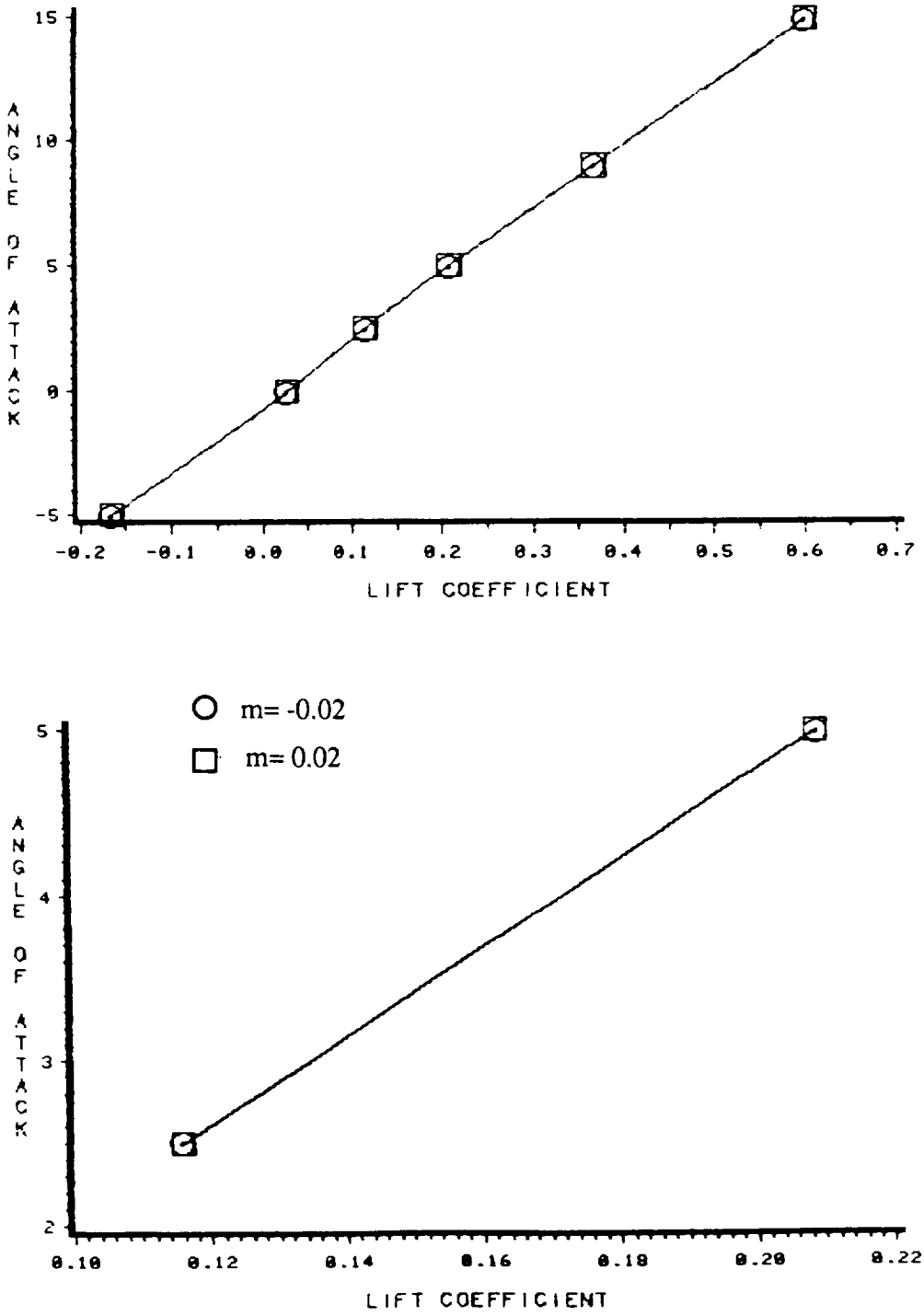

Figure 4.5.1: Predicted performance of the NACA 1402 base wing with 0% thick, 75° anhedral winglets with variable camber; M=1.62; angle of attack versus lift coefficient.

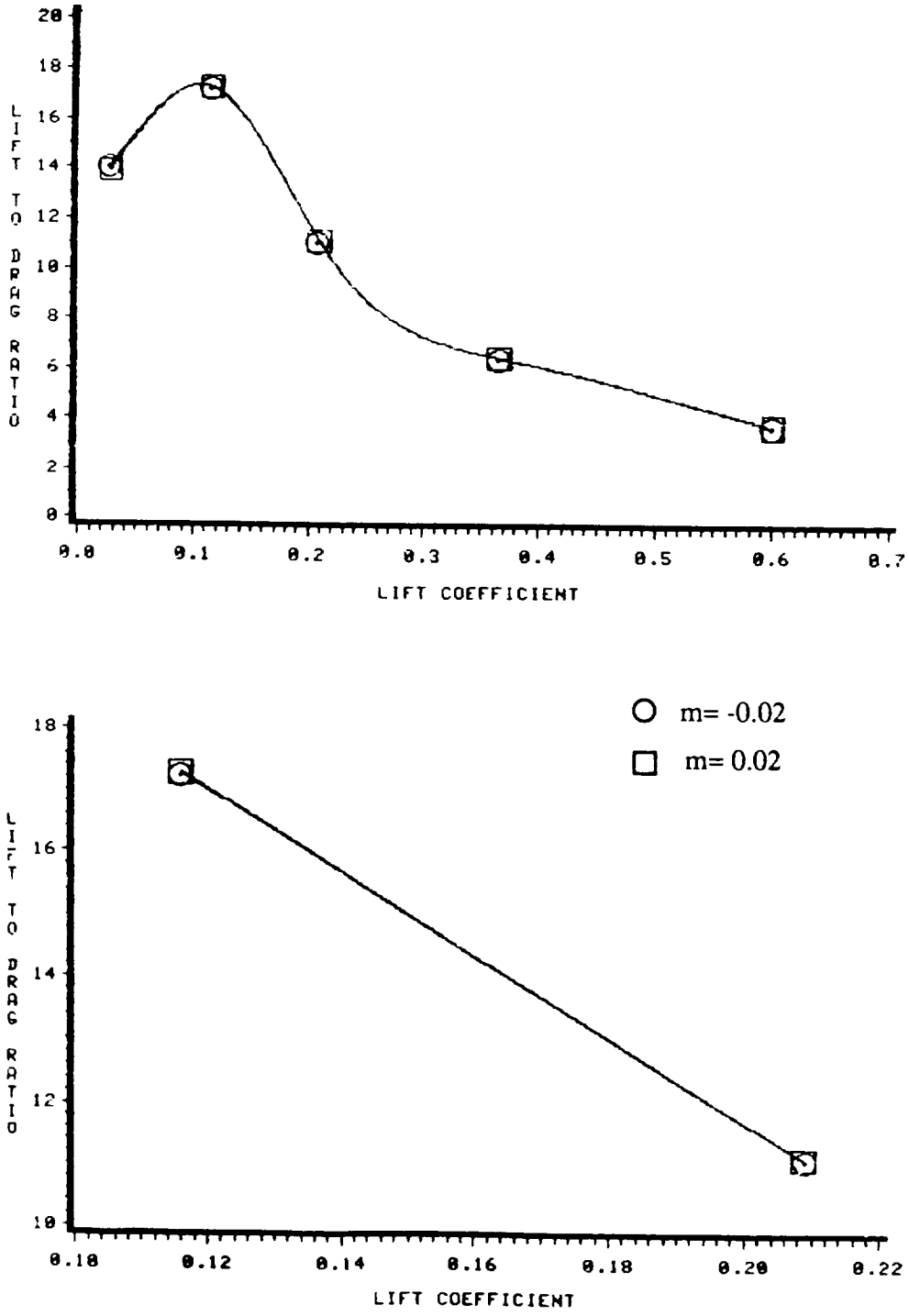

Figure 4.5.2: Predicted performance of the NACA 1402 base wing with 0% thick, 75° anhedral winglets with variable camber; M=1.62; lift-to-pressure drag ratio versus lift coefficient.

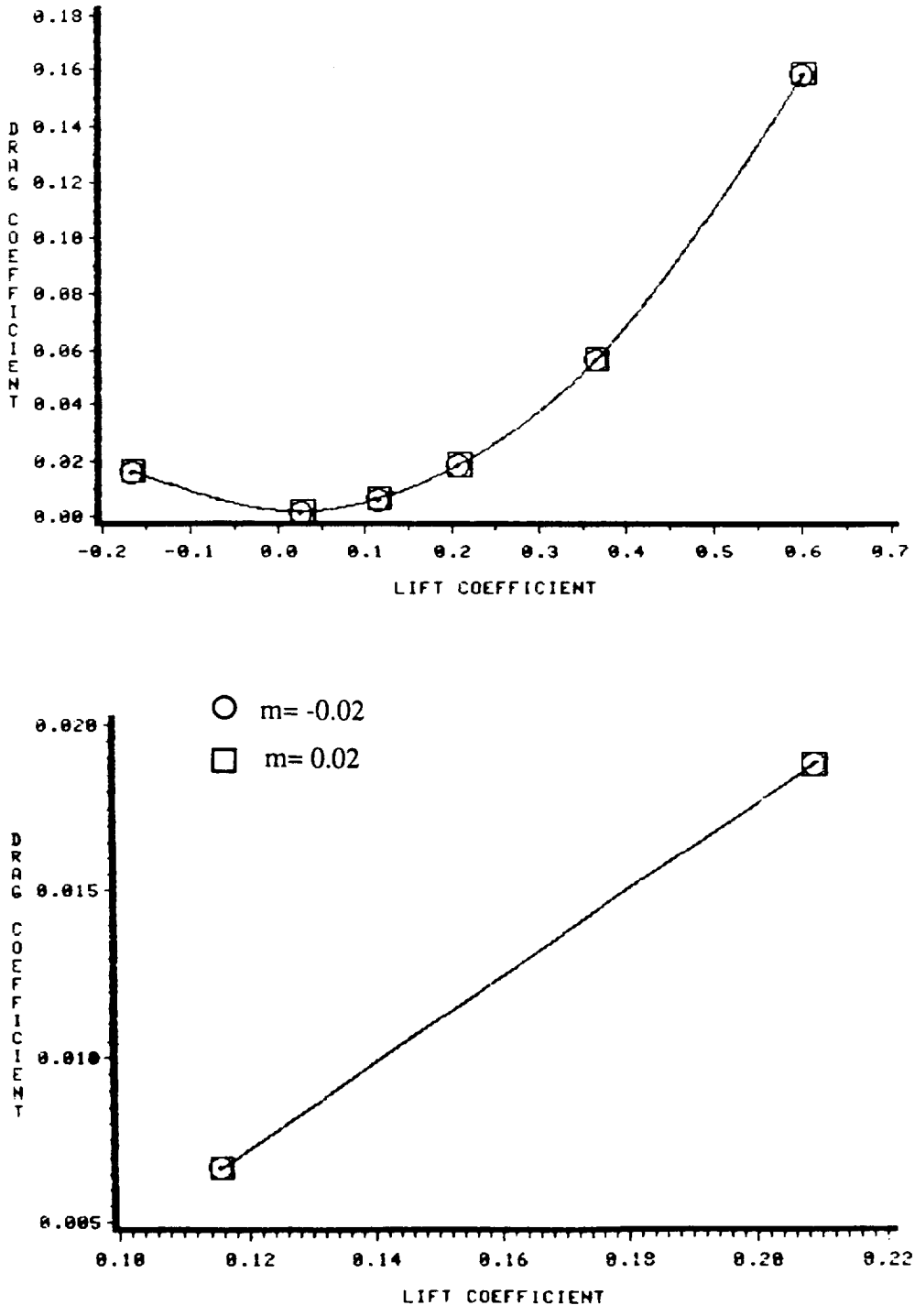

Figure 4.5.3: Predicted performance of the NACA 1402 base wing with 0% thick, 75° anhedral winglets with variable camber; M=1.62; pressure drag coefficient versus lift coefficient.

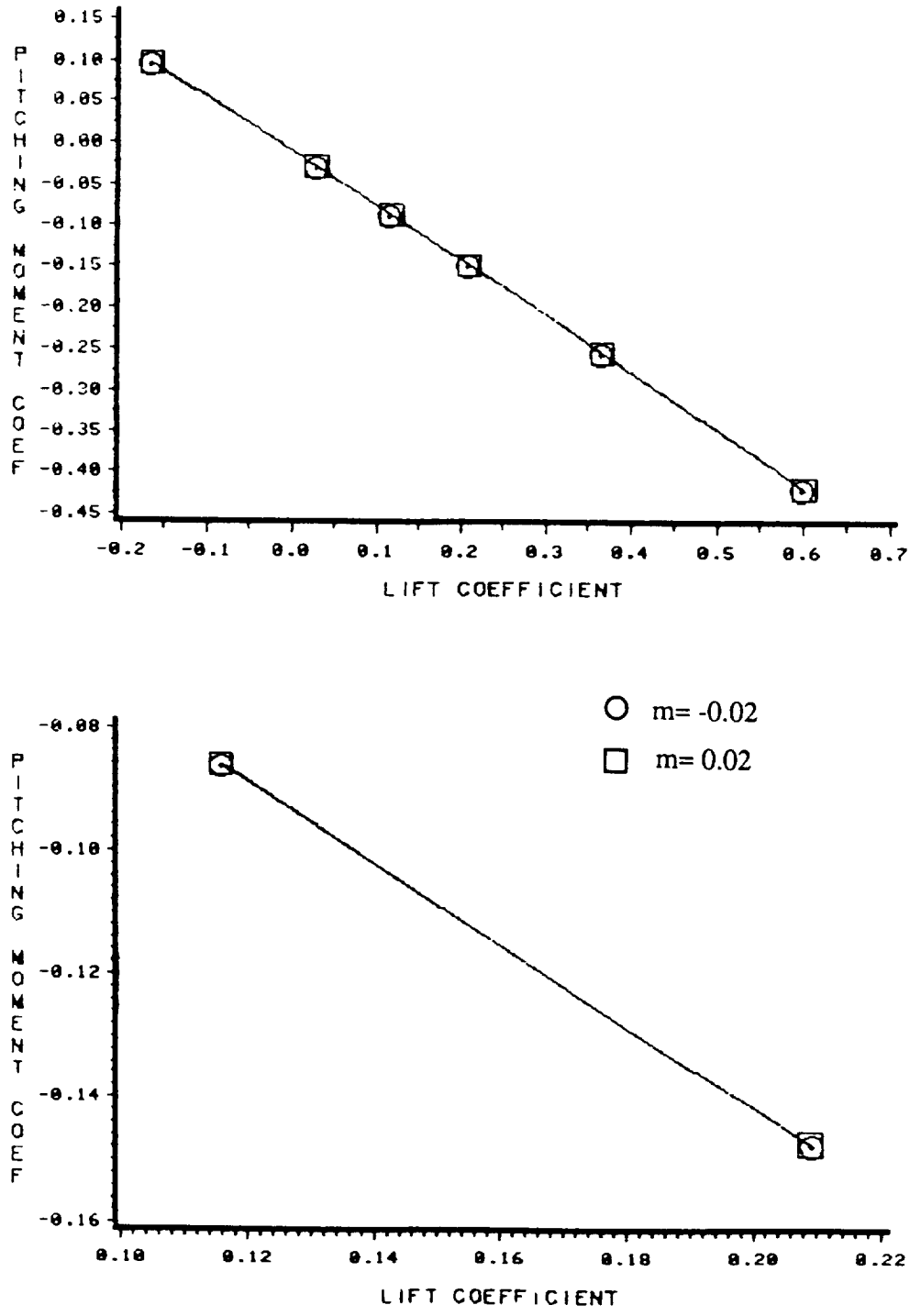

Figure 4.5.4: Predicted performance of the NACA 1402 base wing with 0% thick, 75° anhedral winglets with variable camber; M=1.62; pitching moment coefficient versus lift coefficient.

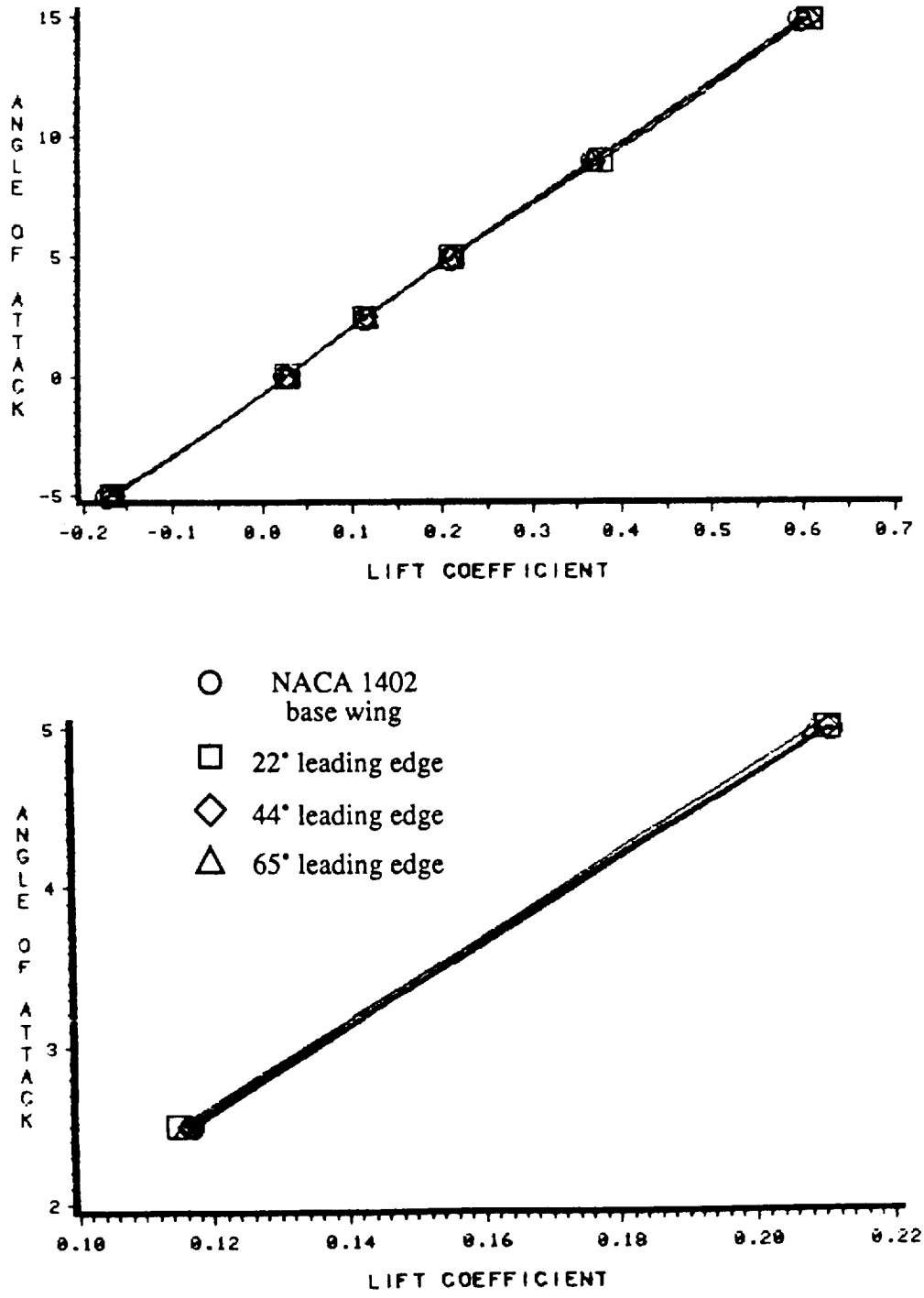

Figure 4.6.1: Predicted performance of the NACA 1402 base wing with 0% thick, 75° anhedral winglets with variable leading edge sweep; M=1.62; angle of attack versus lift coefficient.

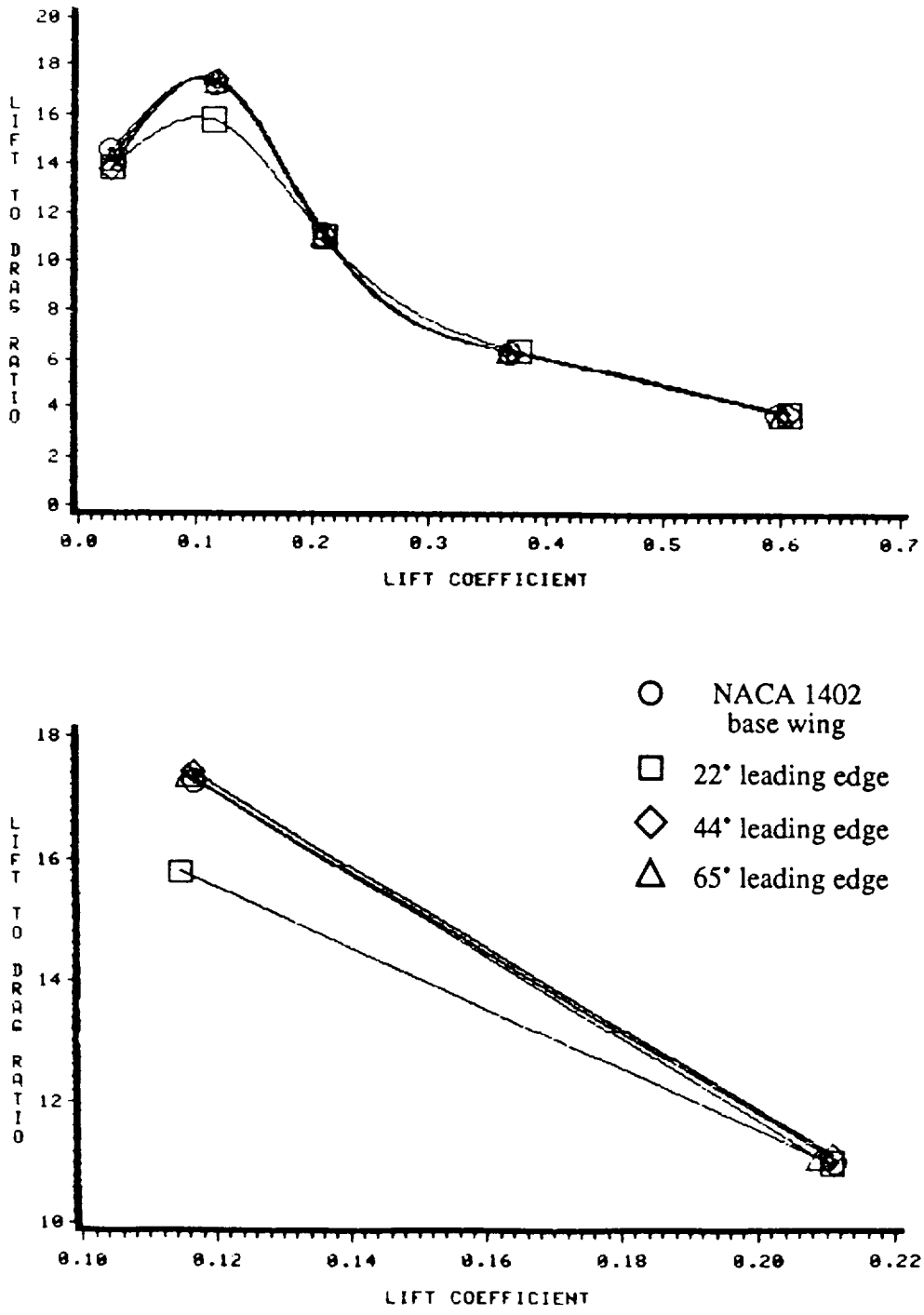

Figure 4.6.2: Predicted performance of the NACA 1402 base wing with 0% thick, 75° anhedral winglets with variable leading edge sweep; M=1.62; lift-to-pressure drag ratio versus lift coefficient.

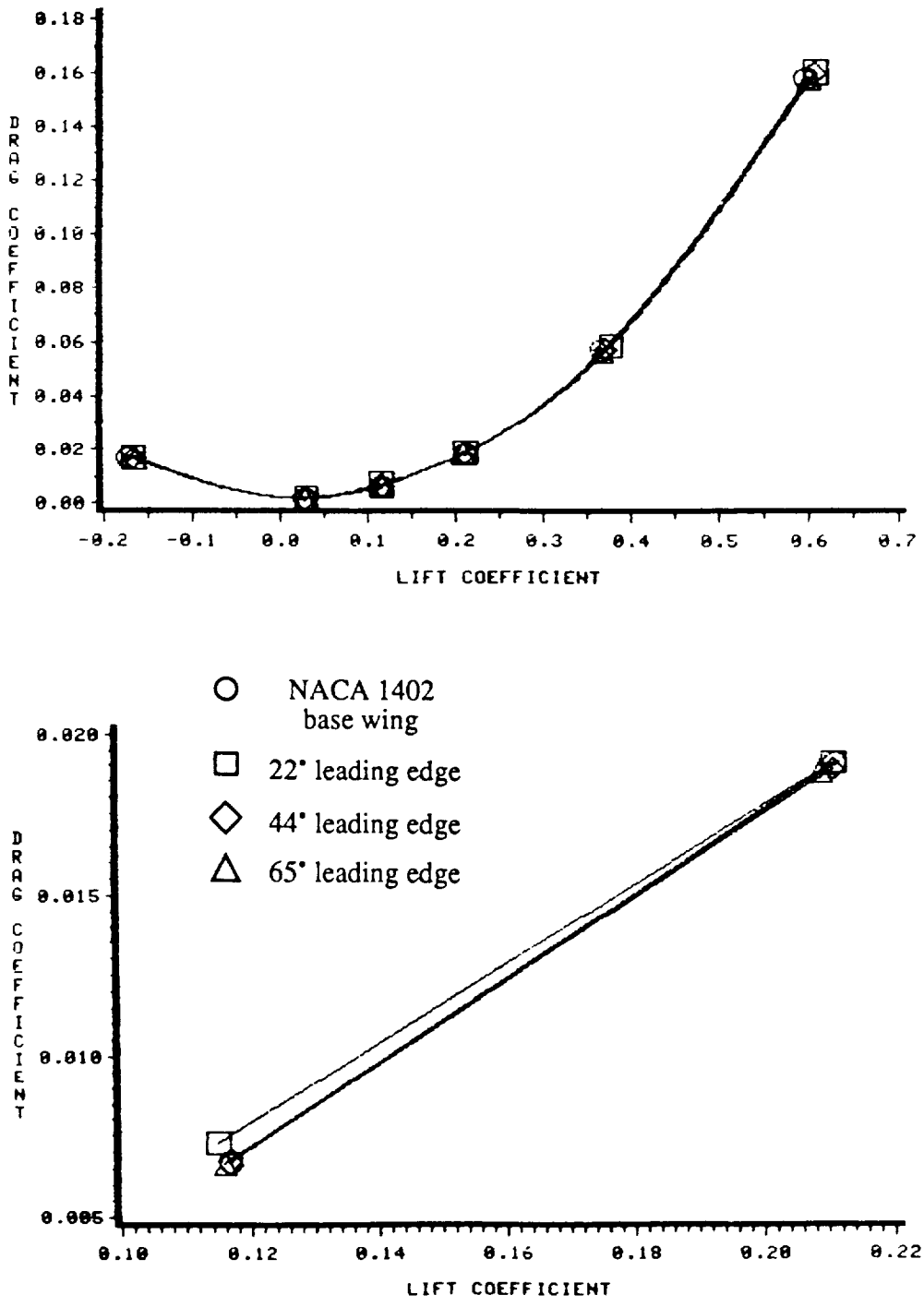

Figure 4.6.3: Predicted performance of the NACA 1402 base wing with 0% thick, 75° anhedral winglets with variable leading edge sweep; M=1.62; pressure drag coefficient versus lift coefficient.

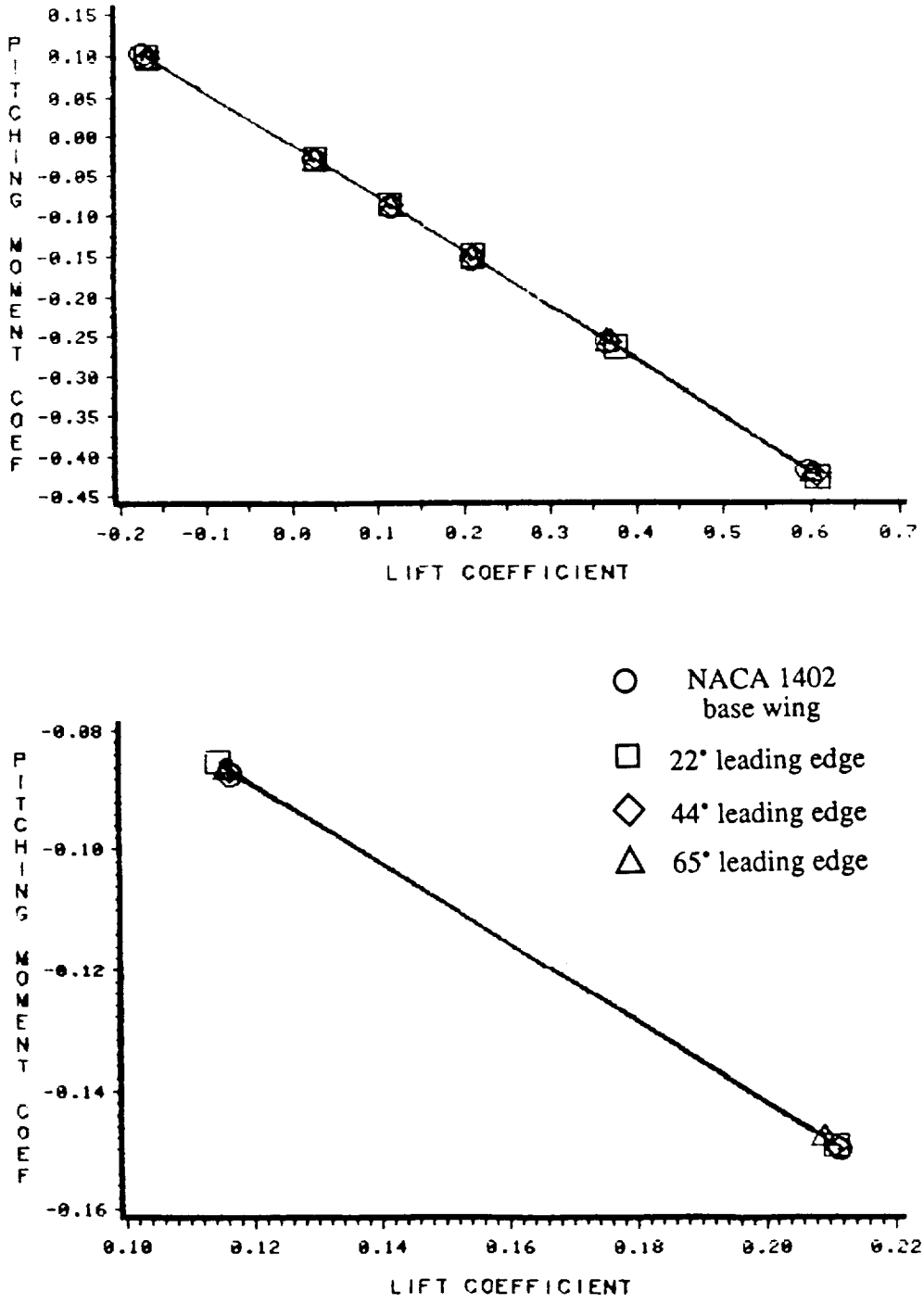

Figure 4.6.4: Predicted performance of the NACA 1402 base wing with 0% thick, 75° anhedral winglets with variable leading edge sweep; M=1.62; pitching moment coefficient versus lift coefficient.

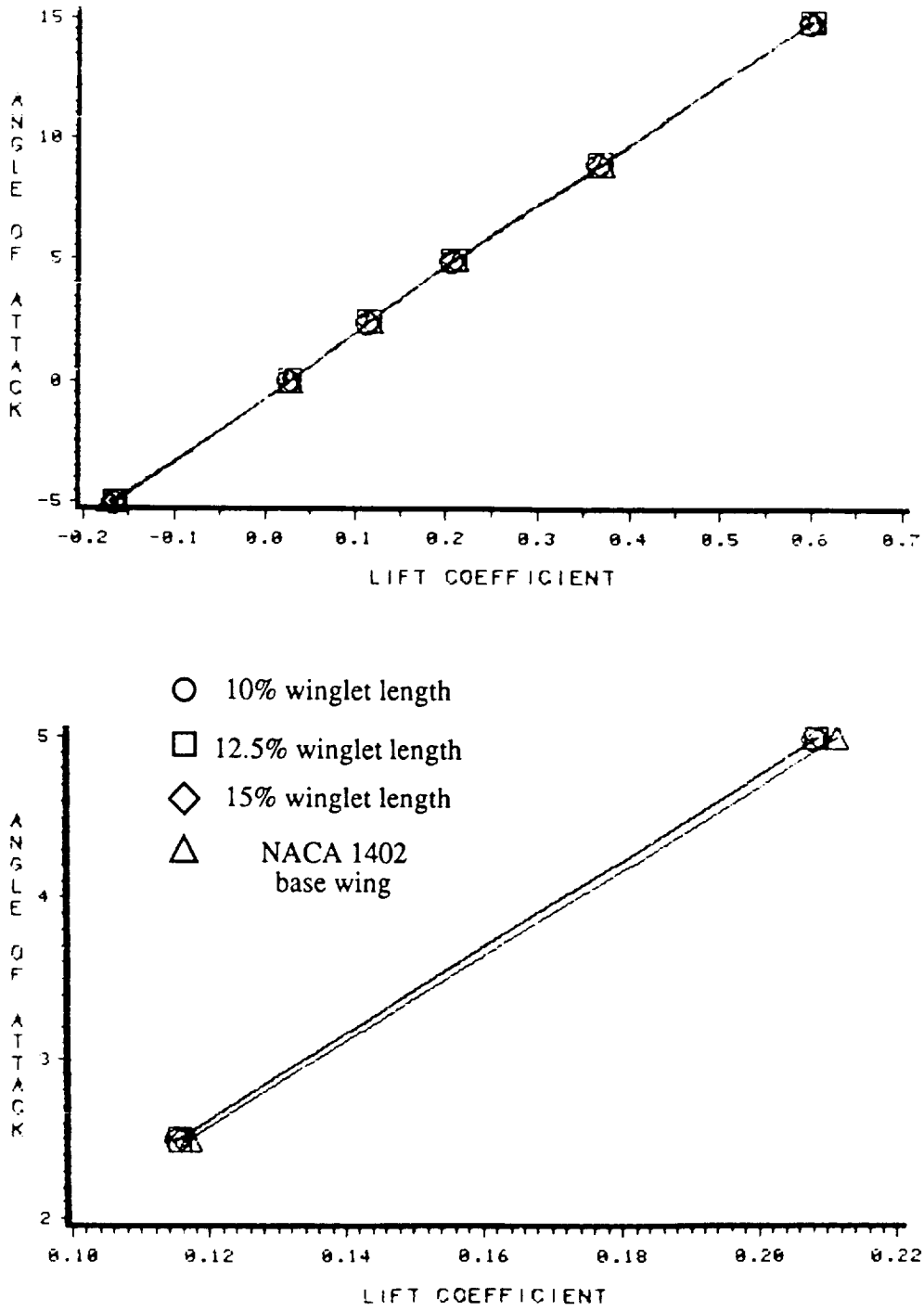

Figure 4.7.1: Predicted performance of the NACA 1402 base wing with 0% thick, 75° anhedral winglets with variable length; M=1.62; angle of attack versus lift coefficient.

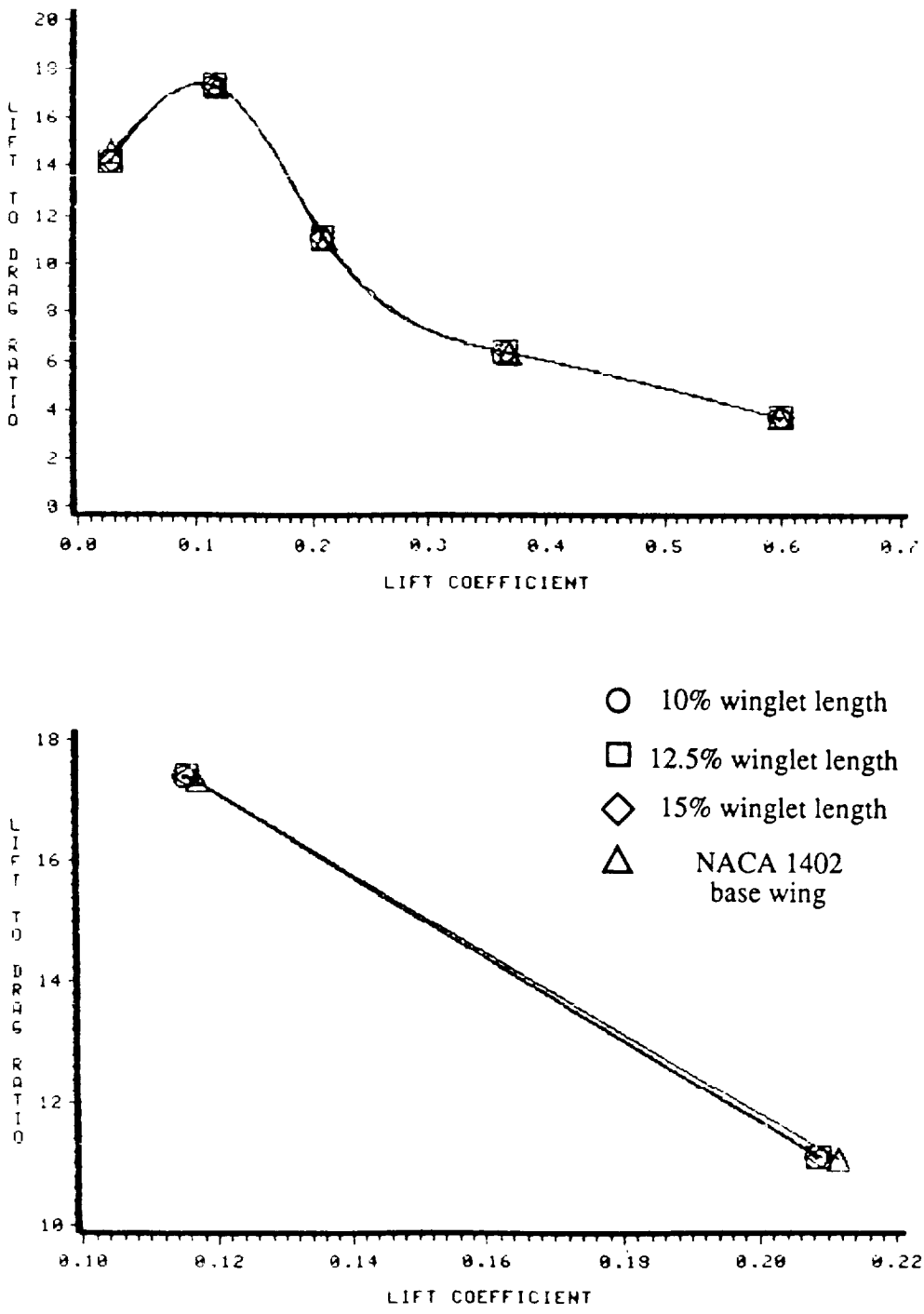

Figure 4.7.2: Predicted performance of the NACA 1402 base wing with 0% thick, 75° anhedral winglets with variable length; M=1.62; lift-to-pressure drag ratio versus lift coefficient.

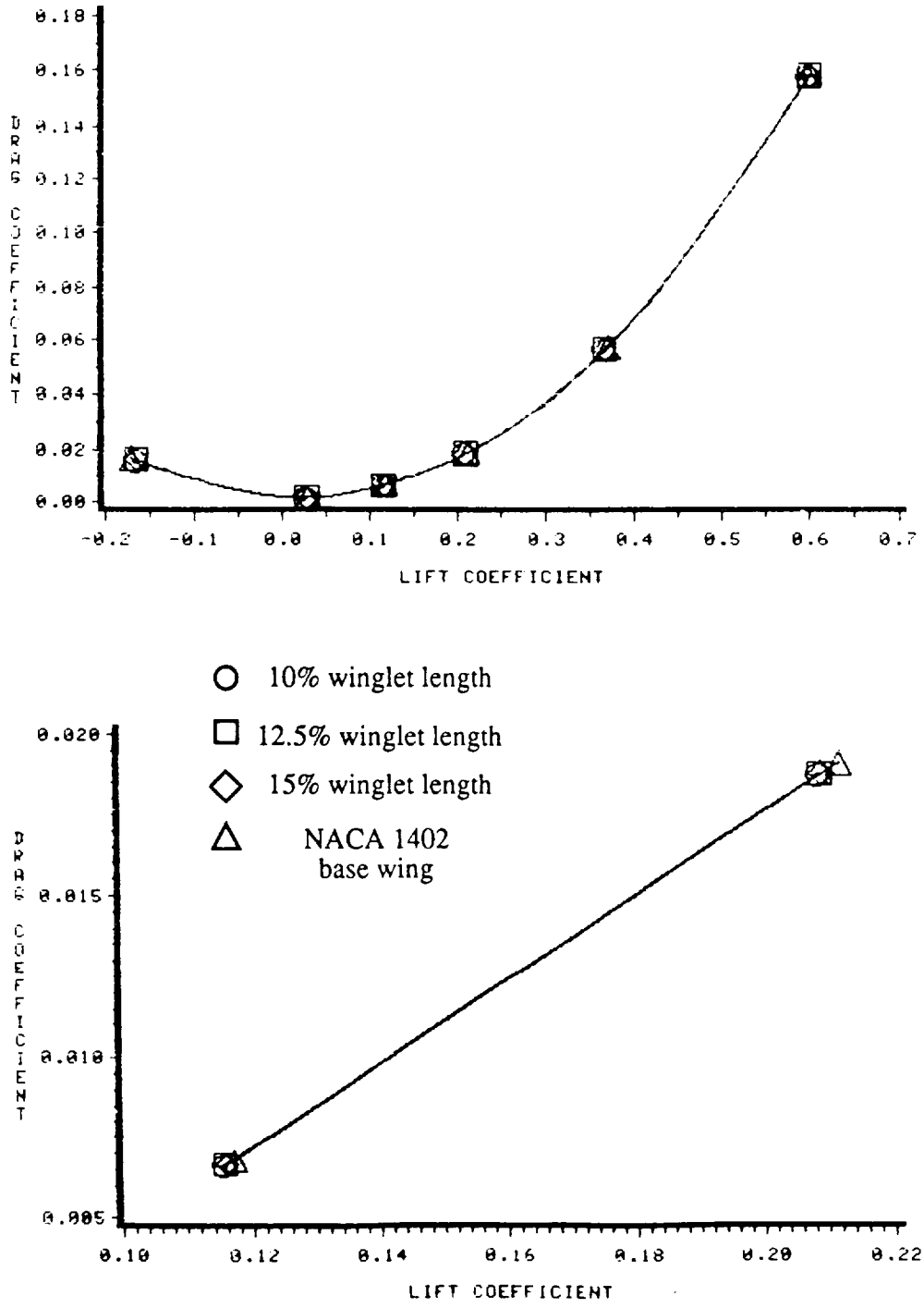

Figure 4.7.3: Predicted performance of the NACA 1402 base wing with 0% thick, 75° anhedral winglets with variable length; M=1.62; pressure drag coefficient versus lift coefficient.

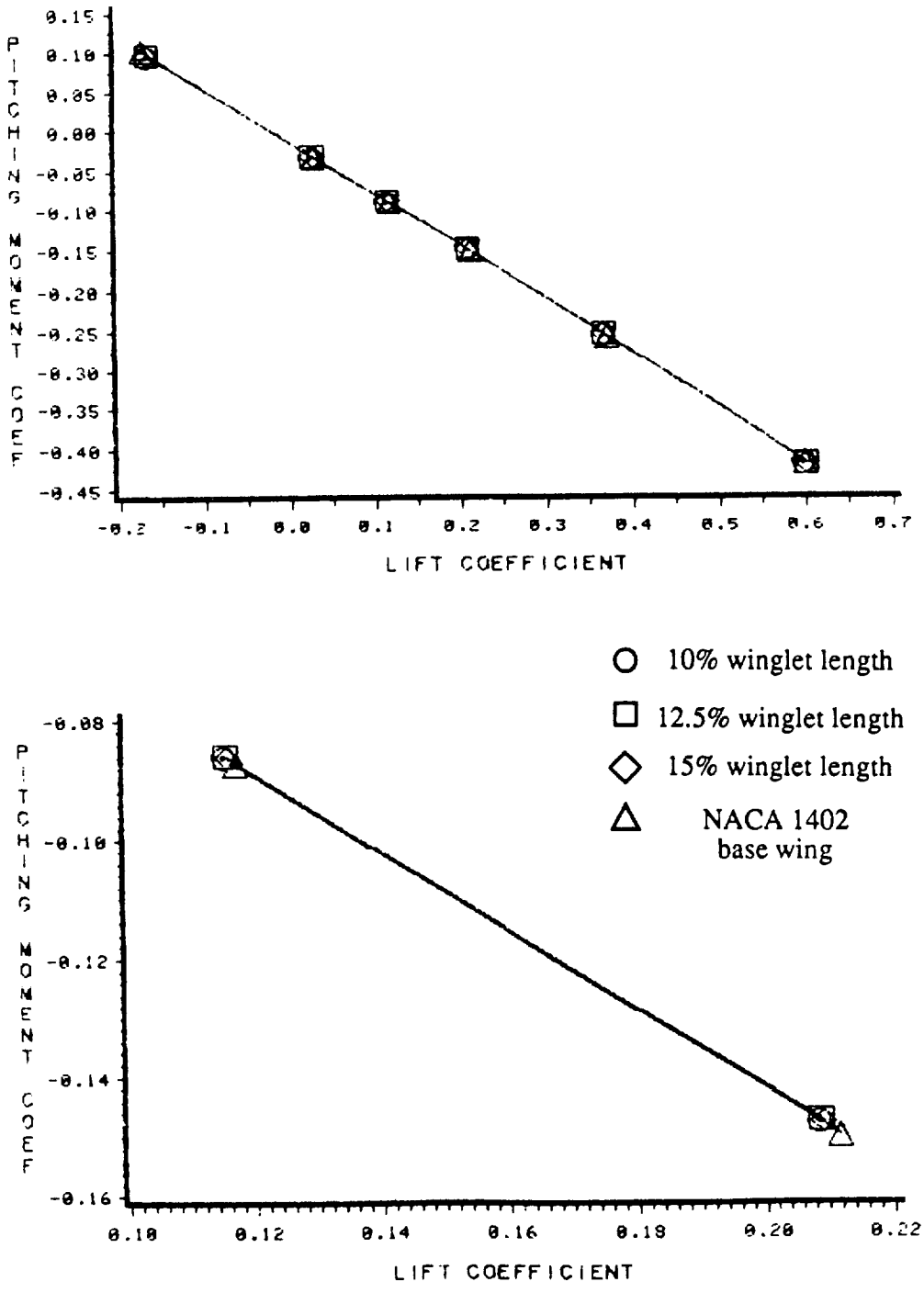

Figure 4.7.4: Predicted performance of the NACA 1402 base wing with 0% thick, 75° anhedral winglets with variable length; M=1.62; pitching moment coefficient versus lift coefficient.

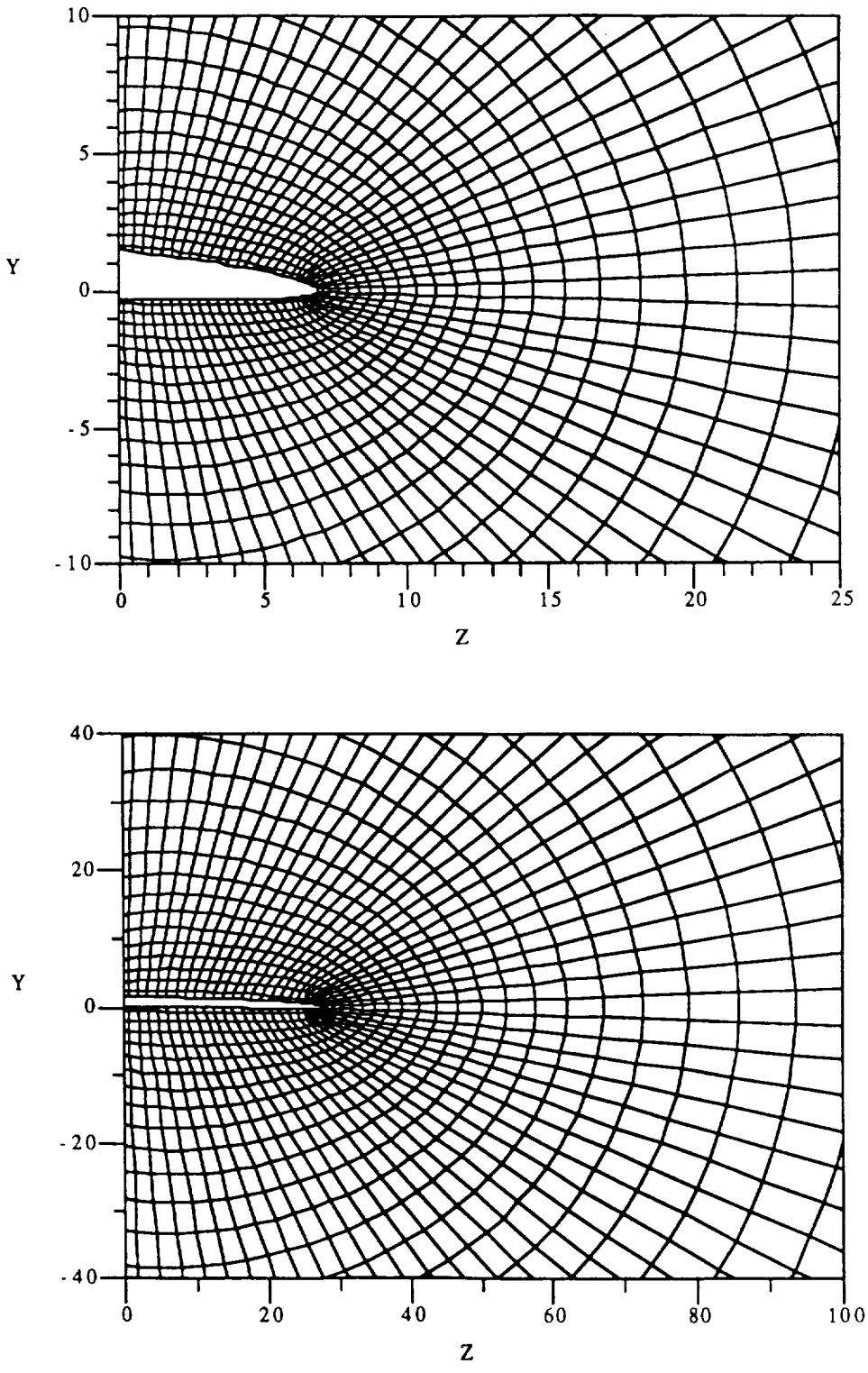

Figure 4.8.1: Computational grids for the NACA 1402 base wing with a 4% thick, 75° dihedral at x= 14.9, 59.7, 88.5, and 99.6.

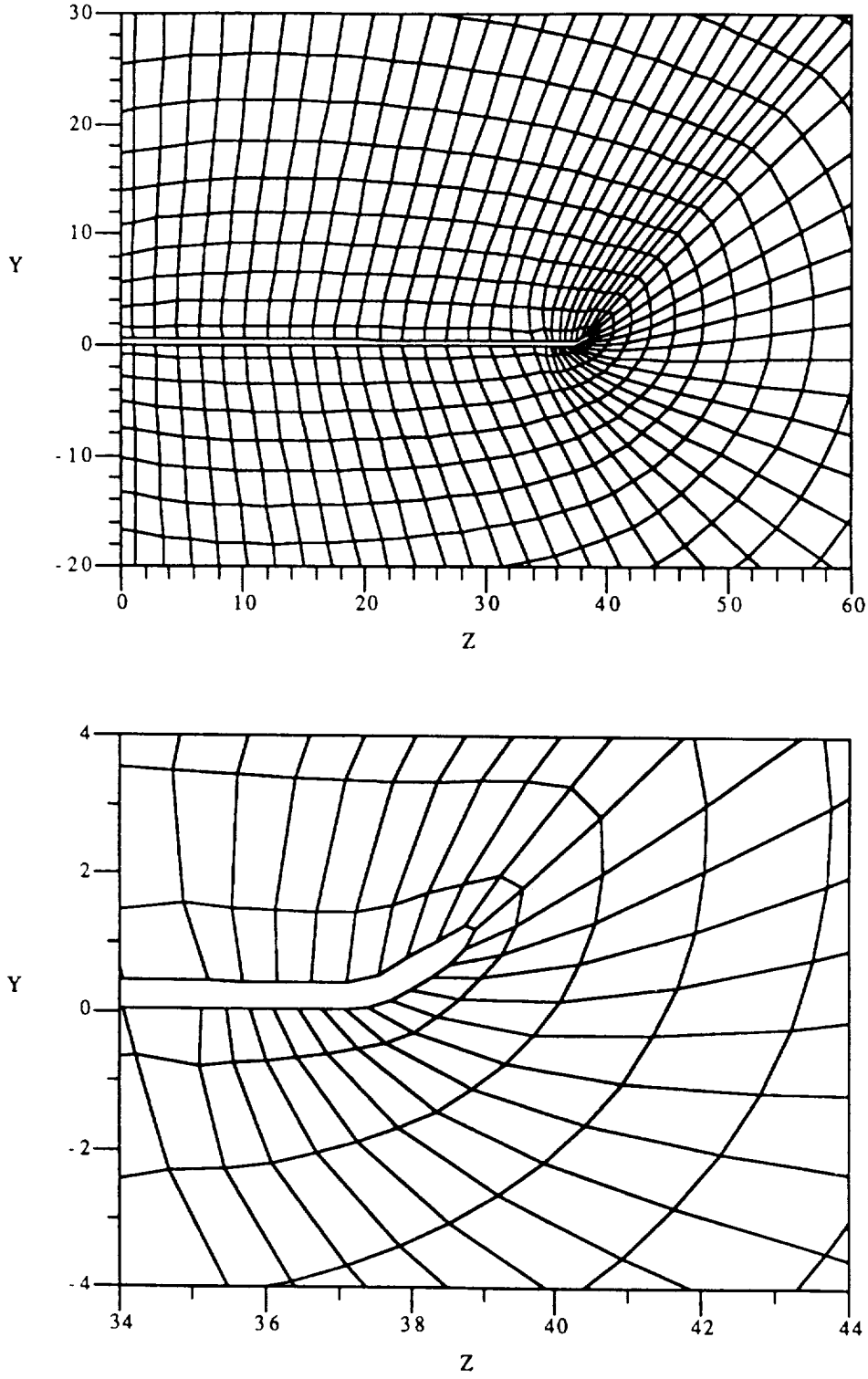

Figure 4.8.1: Continued, x= 88.5.

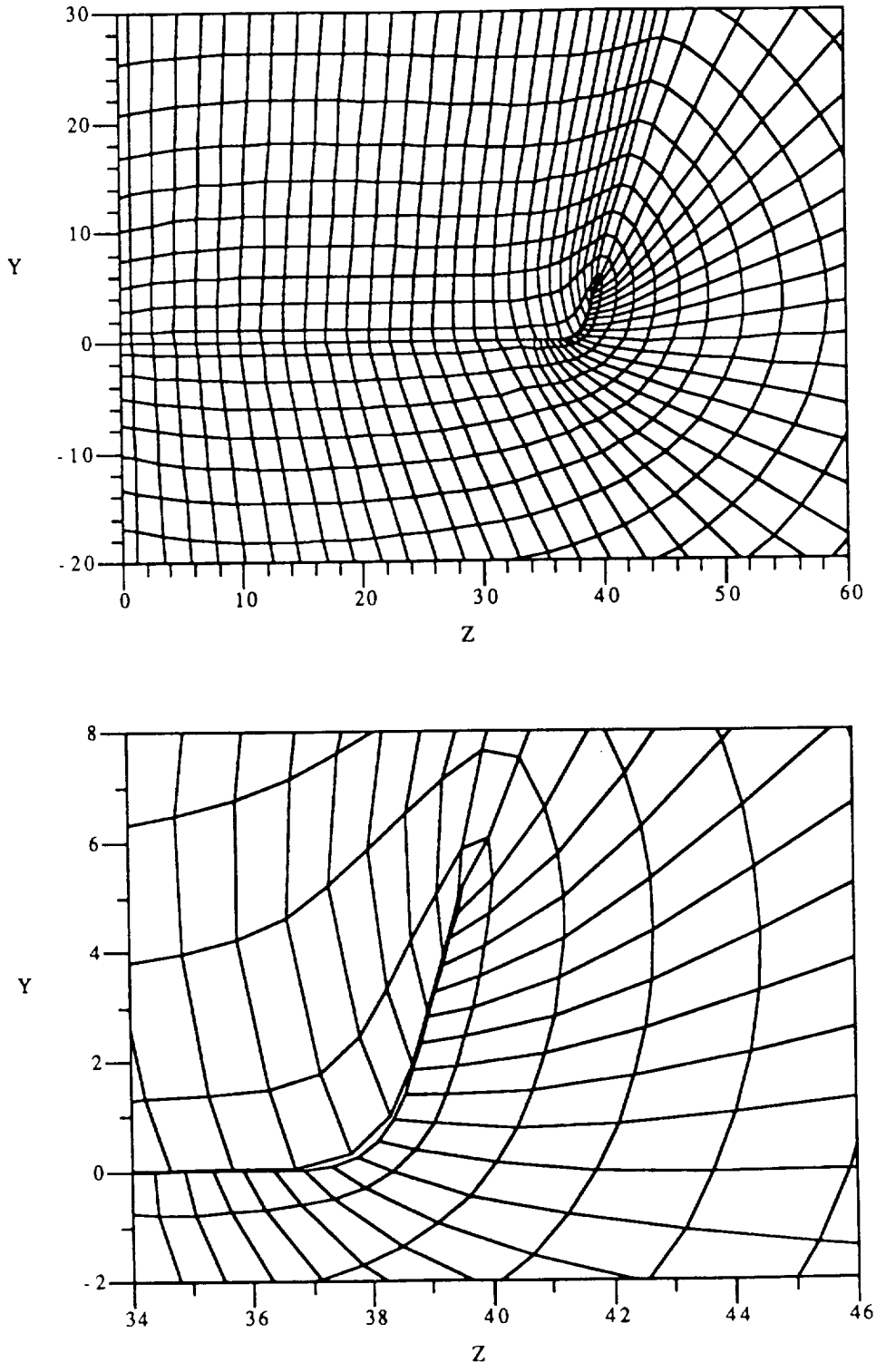

Figure 4.8.1: Continued, x= 99.6.

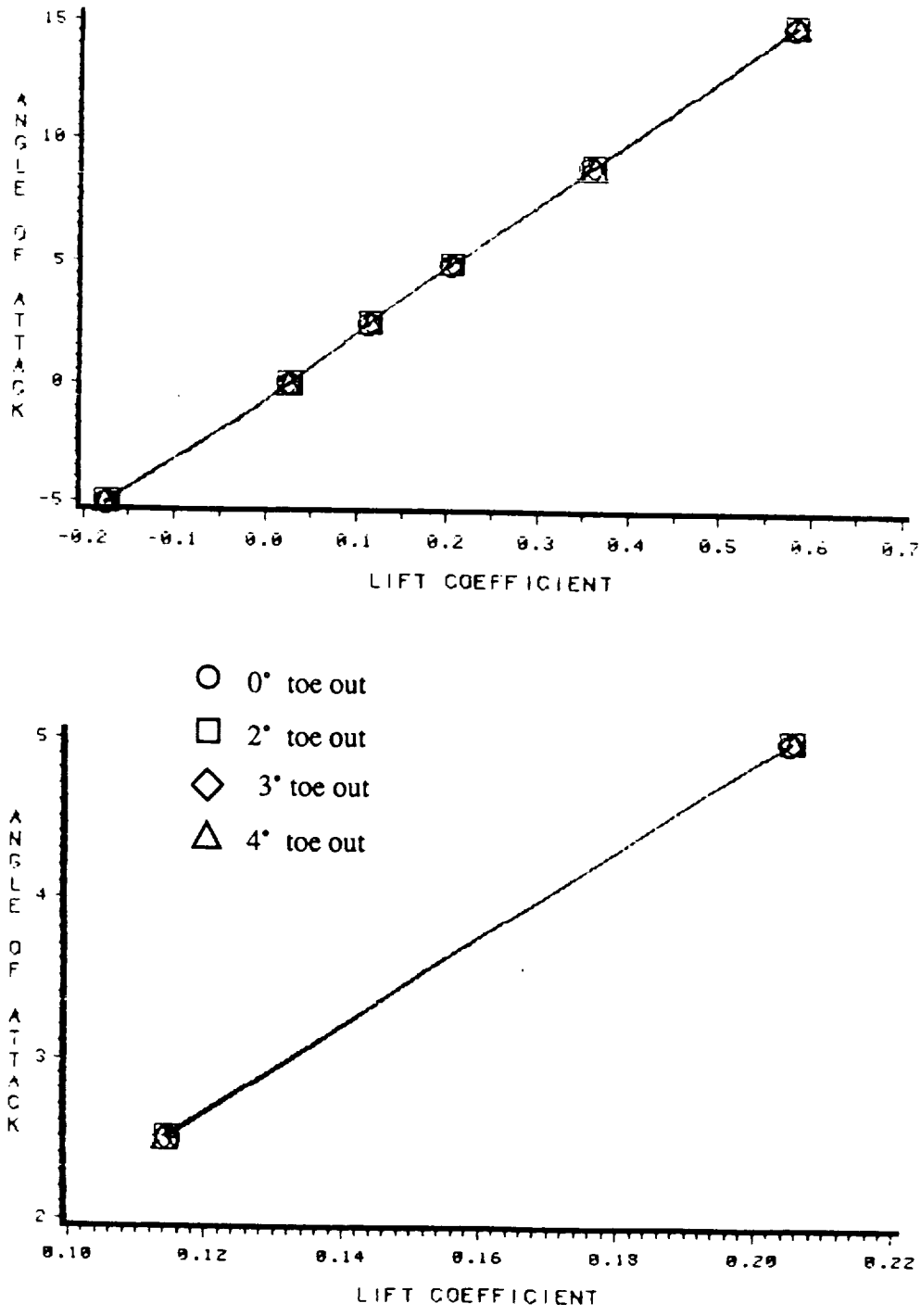

Figure 4.8.2: Predicted performance of the NACA 1402 base wing with 4% thick, 75° dihedral winglets; M=1.62; angle of attack versus lift coefficient.

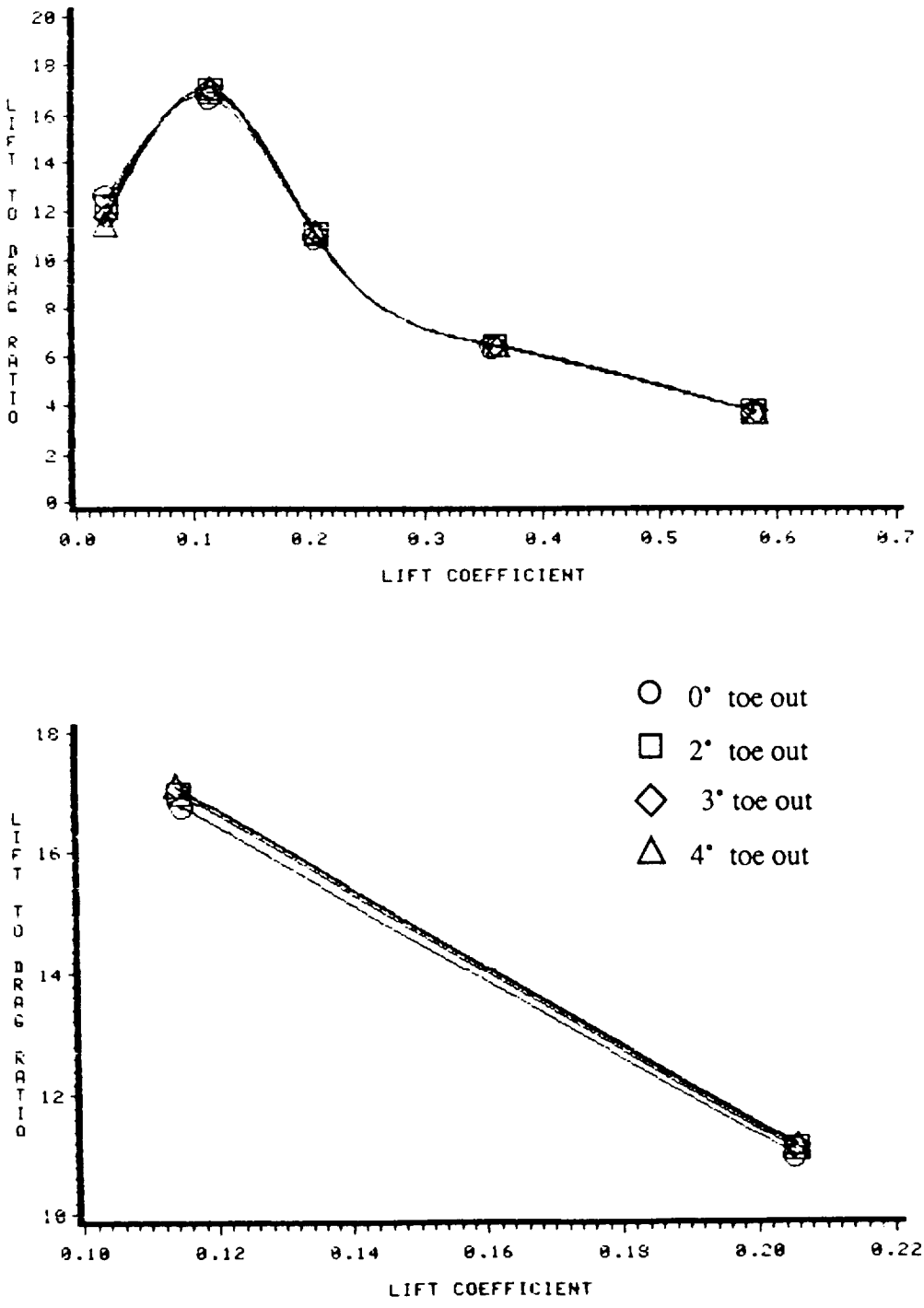

Figure 4.8.3: Predicted performance of the NACA 1402 base wing with 4% thick, 75° dihedral winglets; M=1.62; lift-to-pressure drag ratio versus lift coefficient.

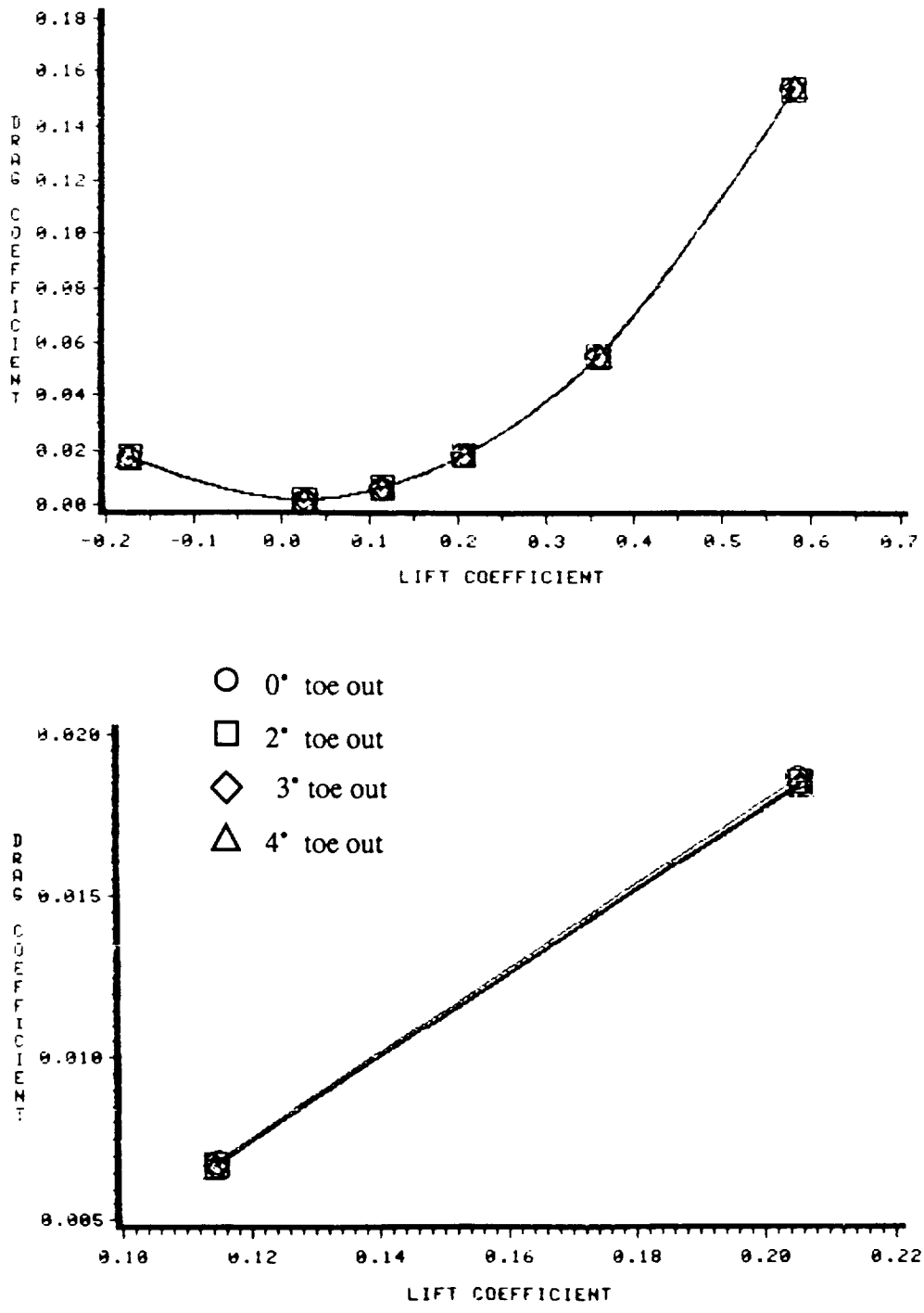

Figure 4.8.4: Predicted performance of the NACA 1402 base wing with 4% thick, 75° dihedral winglets; M=1.62; pressure drag coefficient versus lift coefficient.

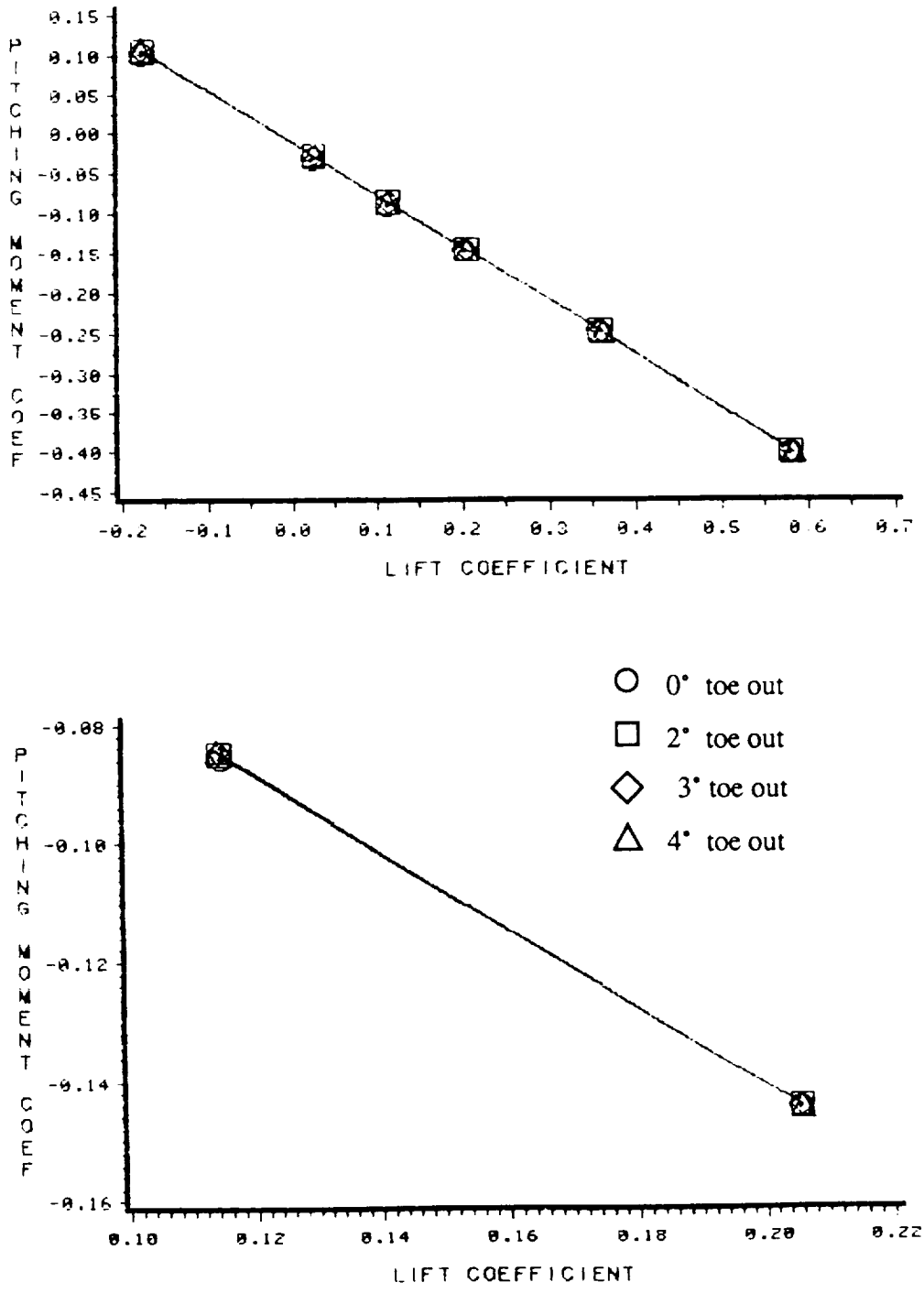

Figure 4.8.5: Predicted performance of the NACA 1402 base wing with 4% thick, 75° dihedral winglets; M=1.62; pitching moment coefficient versus lift coefficient.

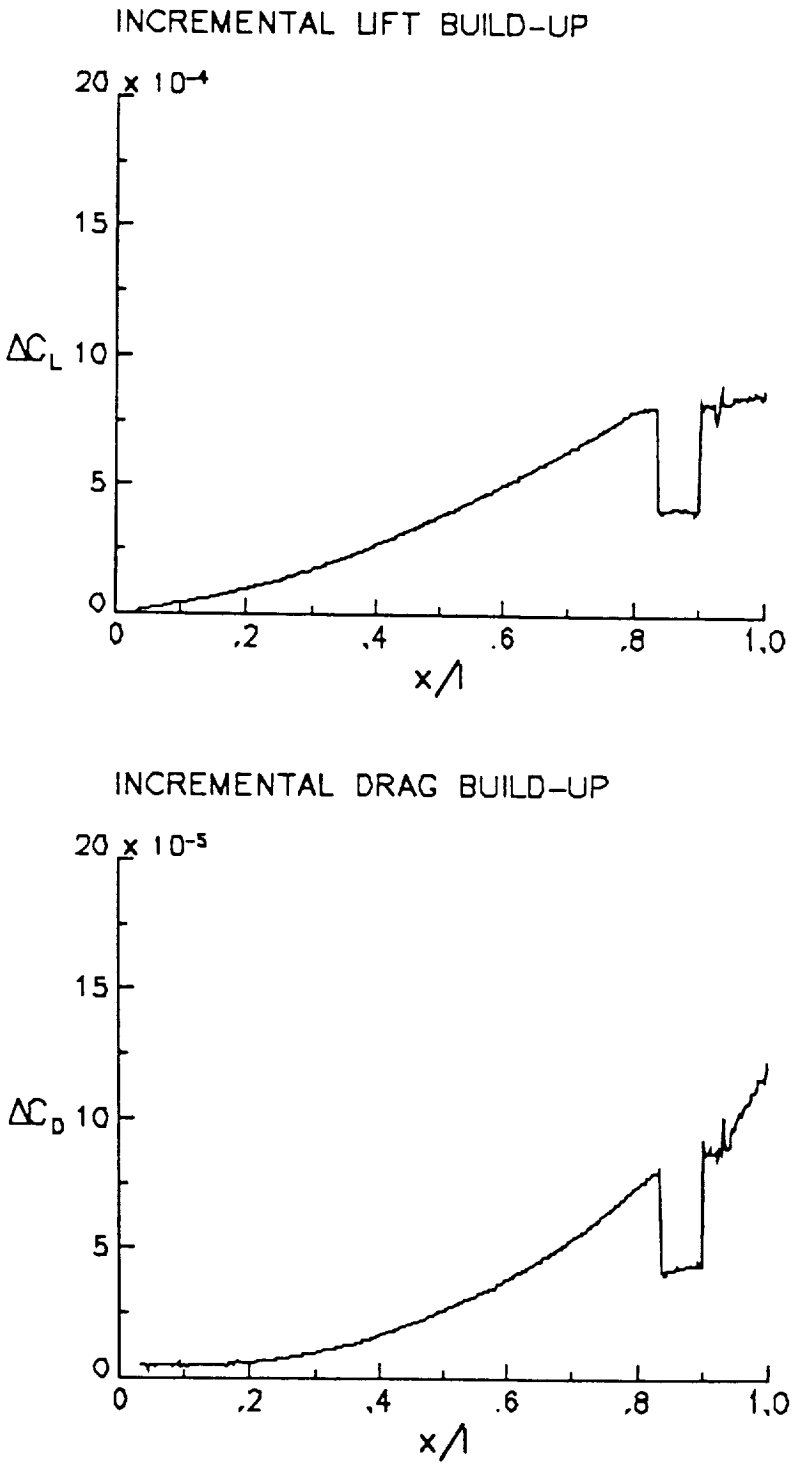

Figure 4.8.6: Incremental lift and pressure drag build up for the NACA 1402 base wing with a 4% thick, 2° toe out, 75° dihedral winglet at 5° angle of attack, M=1.62.

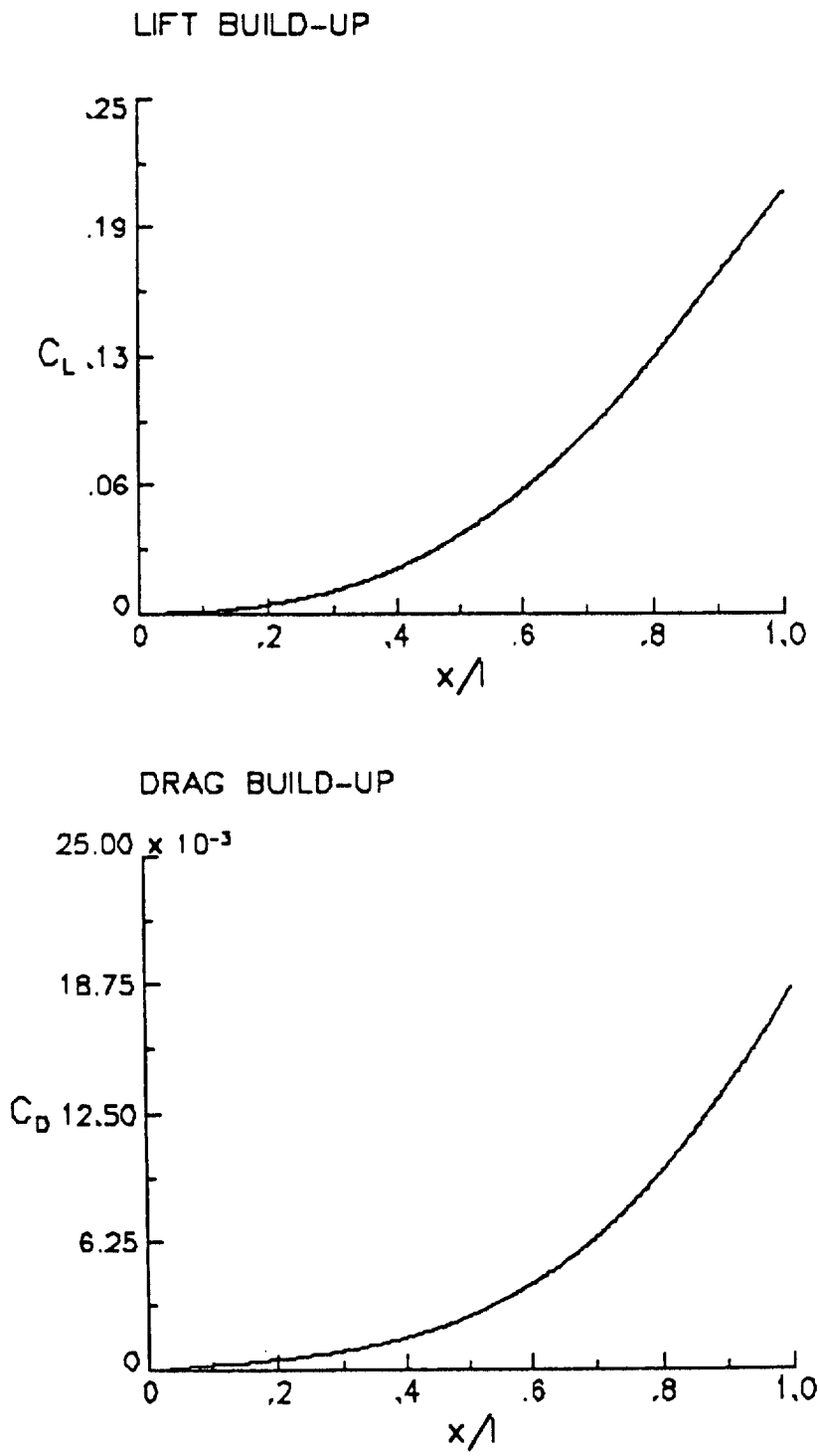

Figure 4.8.7: Total lift and pressure drag build up for the NACA 1402 base wing with a 4% thick, 2° toe out, 75° dihedral winglet at 5° angle of attack, M=1.62.

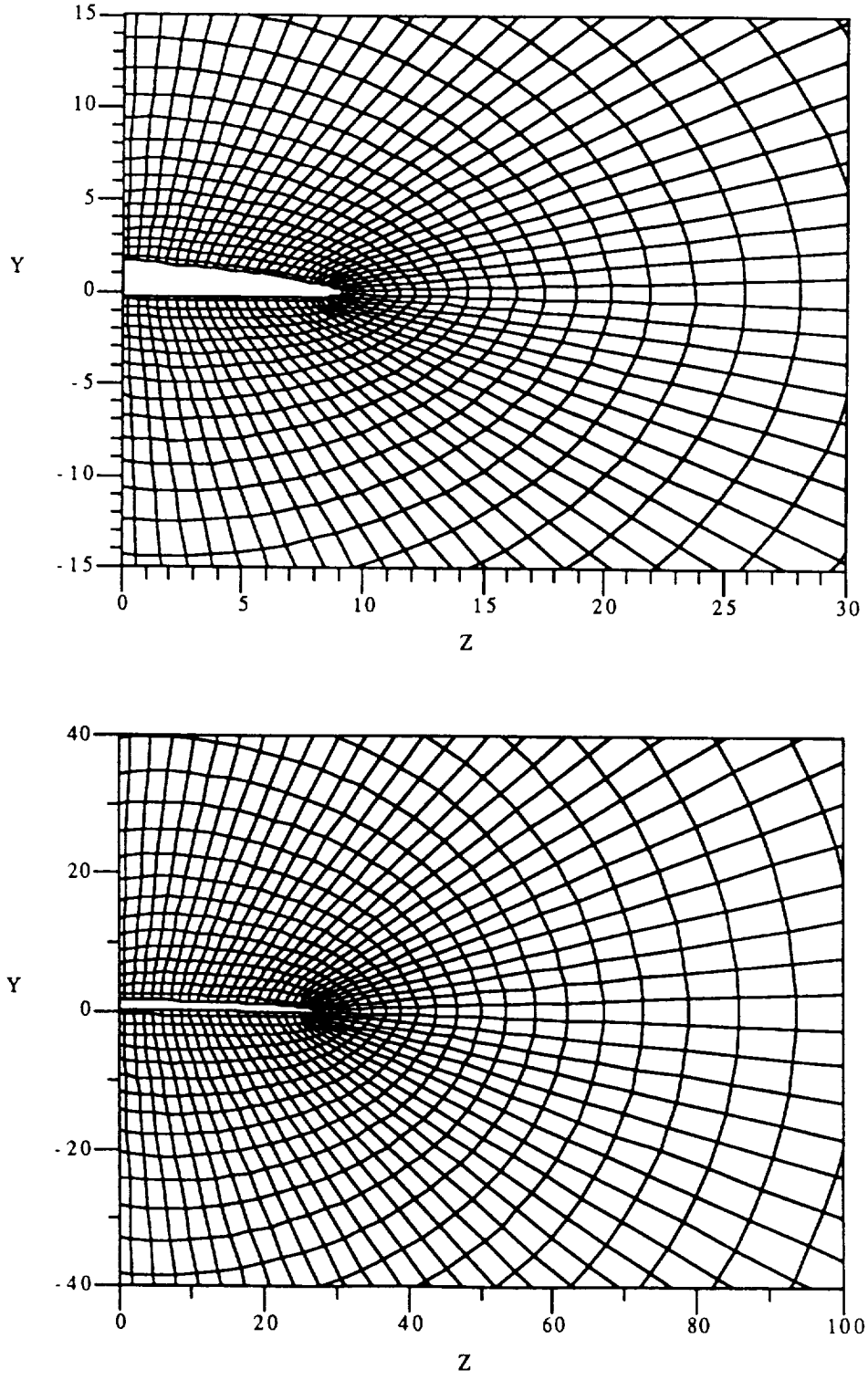

Figure 4.9.1: Computational grids for the NACA 1402 base wing with a 4% thick, 75° anhedral winglet at x= 19.7, 59.7, 89.8, and 99.4.

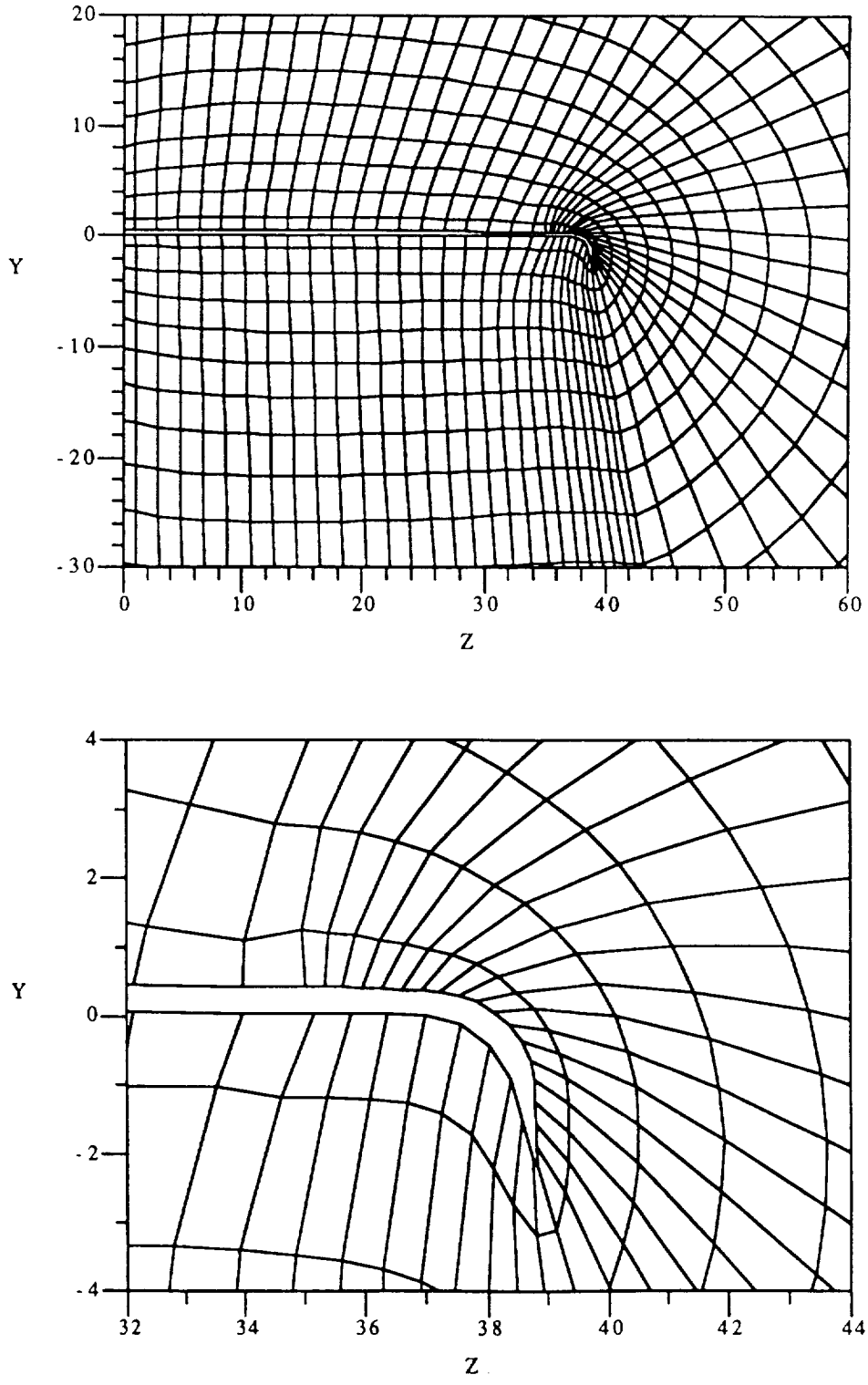

Figure 4.9.1: Continued, x=89.8.

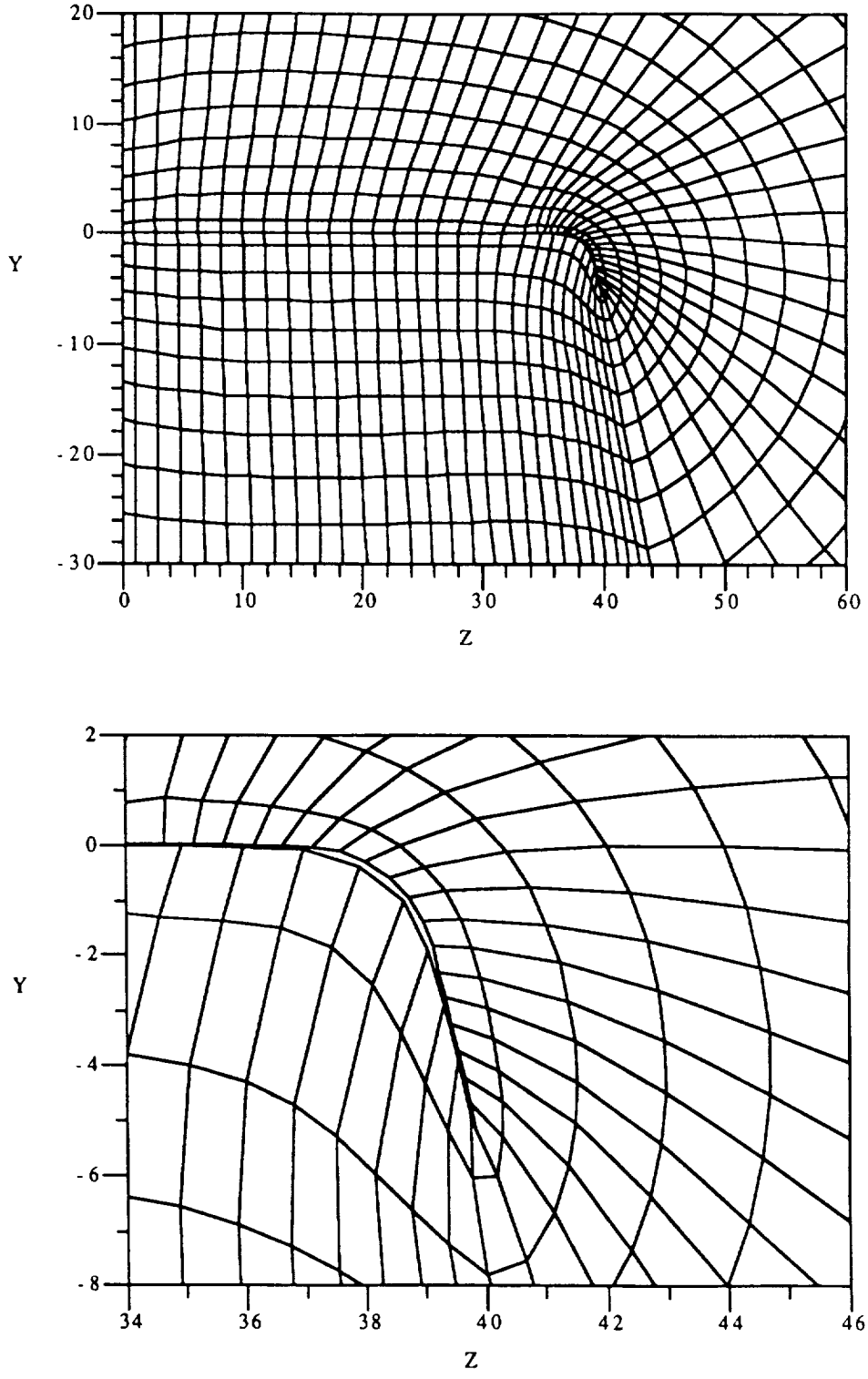

Figure 4.9.1: Continued, x=99.4.

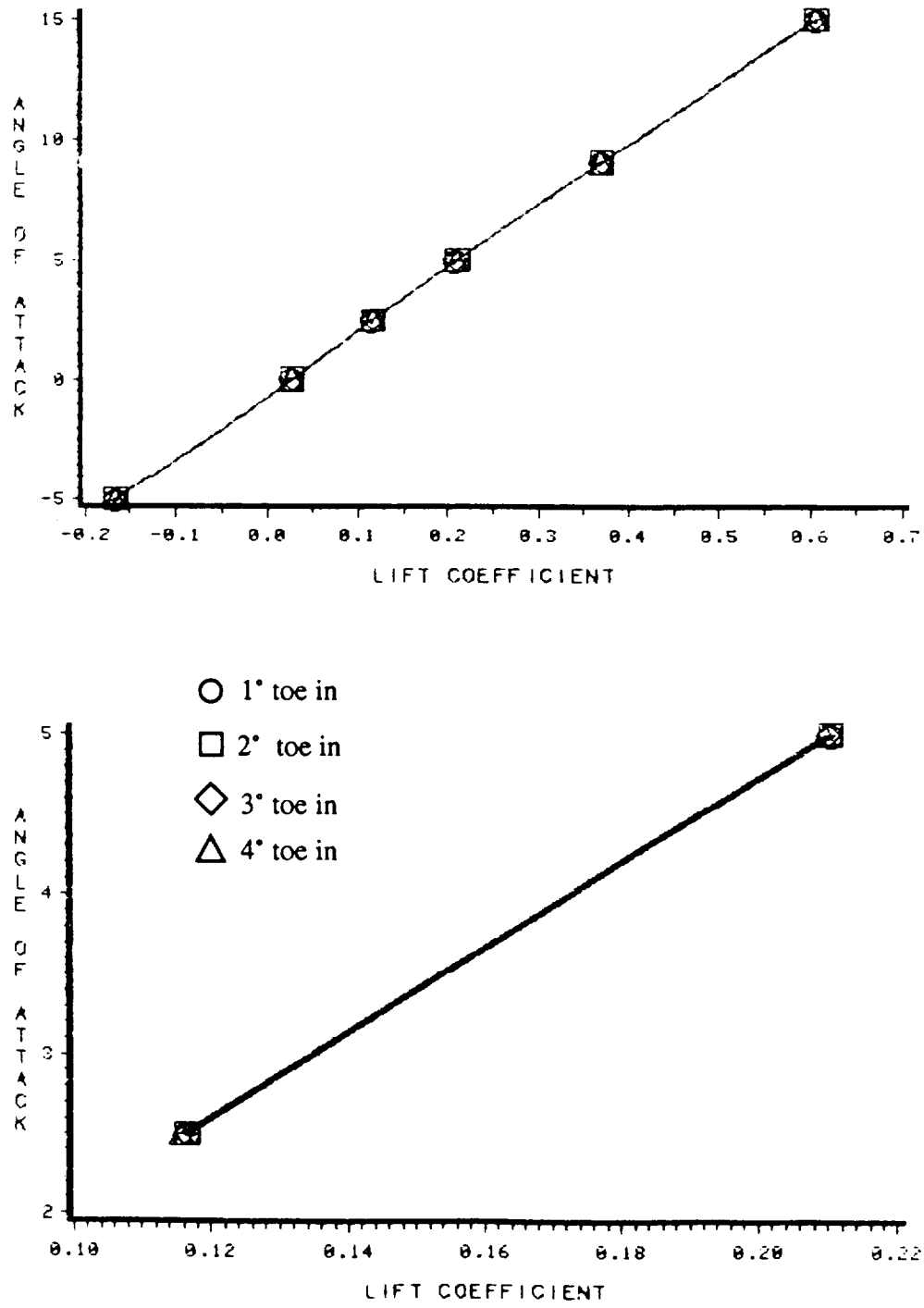

Figure 4.9.2: Predicted performance of the NACA 1402 base wing with 4% thick, 75° anhedral winglets; M=1.62; angle of attack versus lift coefficient.

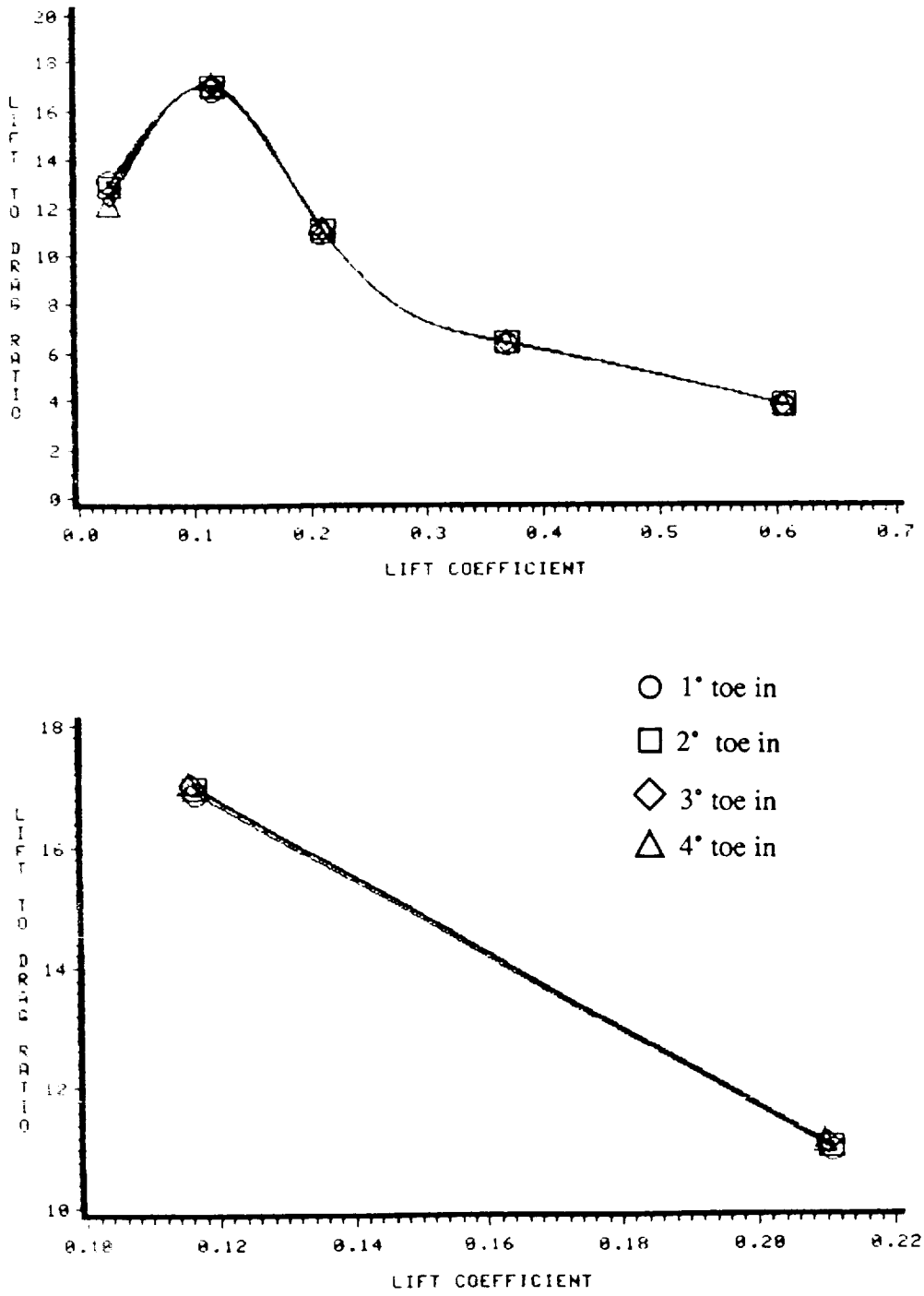

Figure 4.9.3: Predicted performance of the NACA 1402 base wing with 4% thick, 75° anhedral winglets; M=1.62; lift-to-pressure drag coefficient versus lift coefficient.

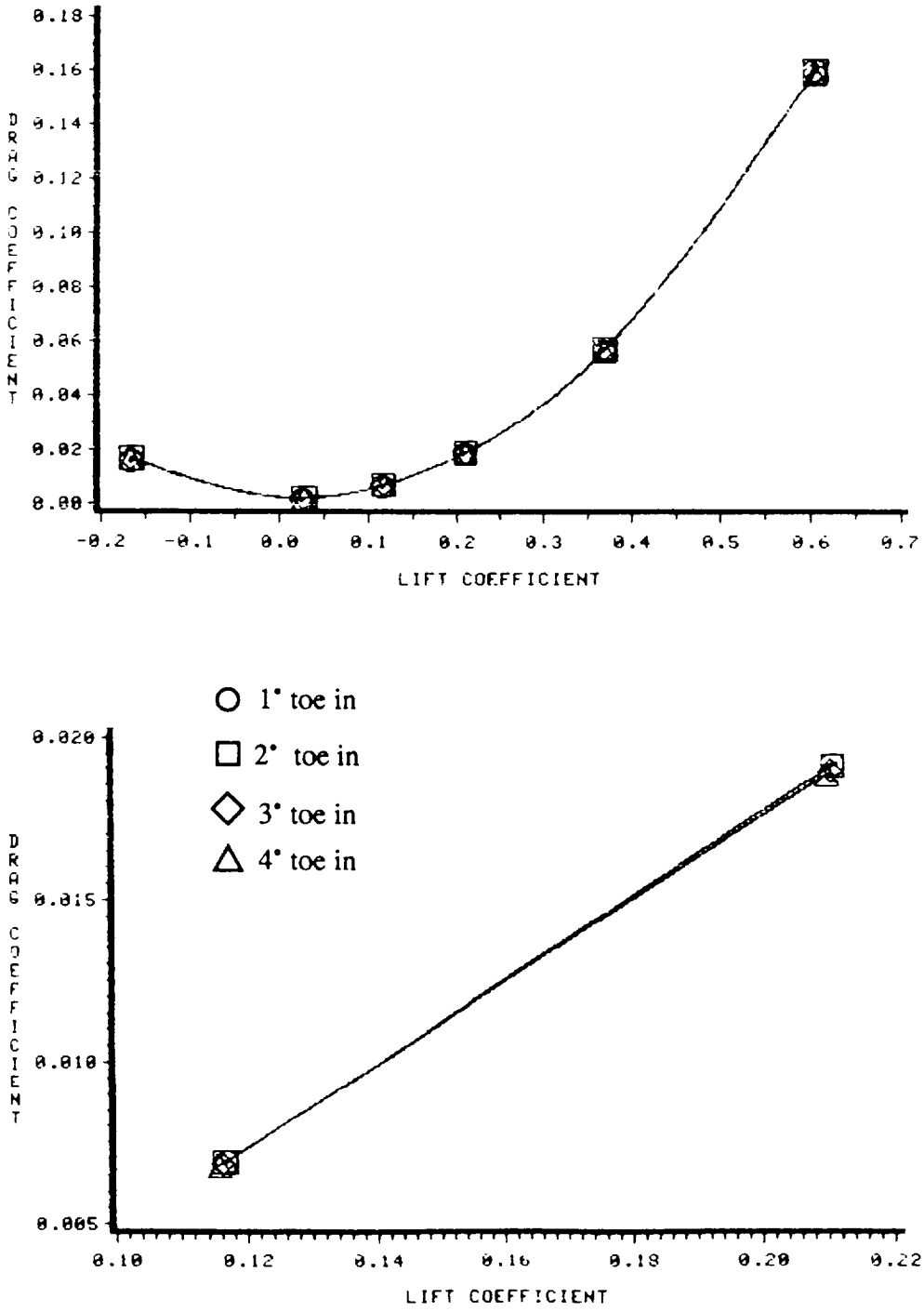

Figure 4.9.4: Predicted performance of the NACA 1402 base wing with 4% thick, 75° anhedral winglets; M=1.62; pressure drag coeffient versus lift coefficient.

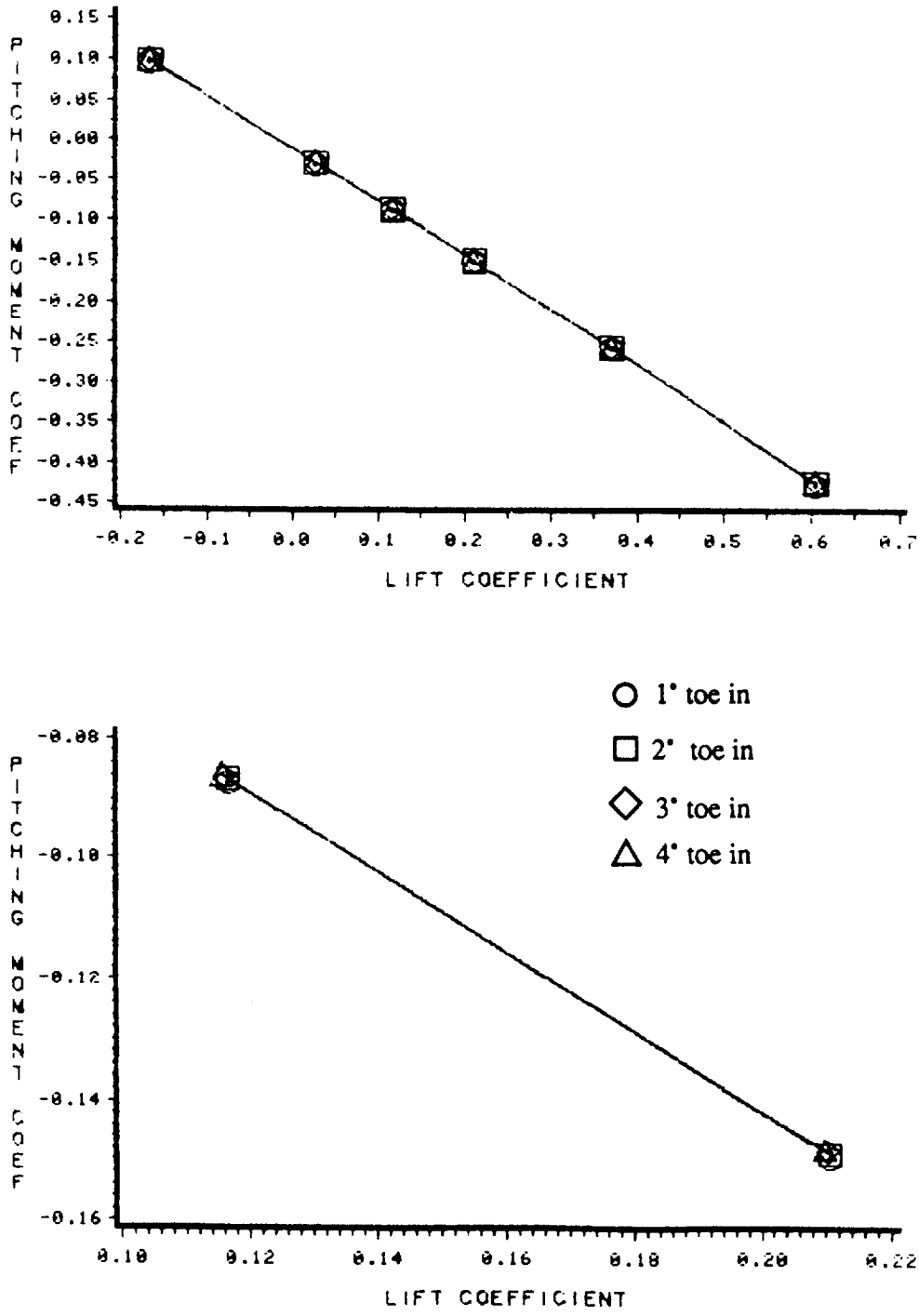

Figure 4.9.5: Predicted performance of the NACA 1402 base wing with 4% thick, 75° anhedral winglets; M=1.62; pitching moment coefficient versus lift coefficient.

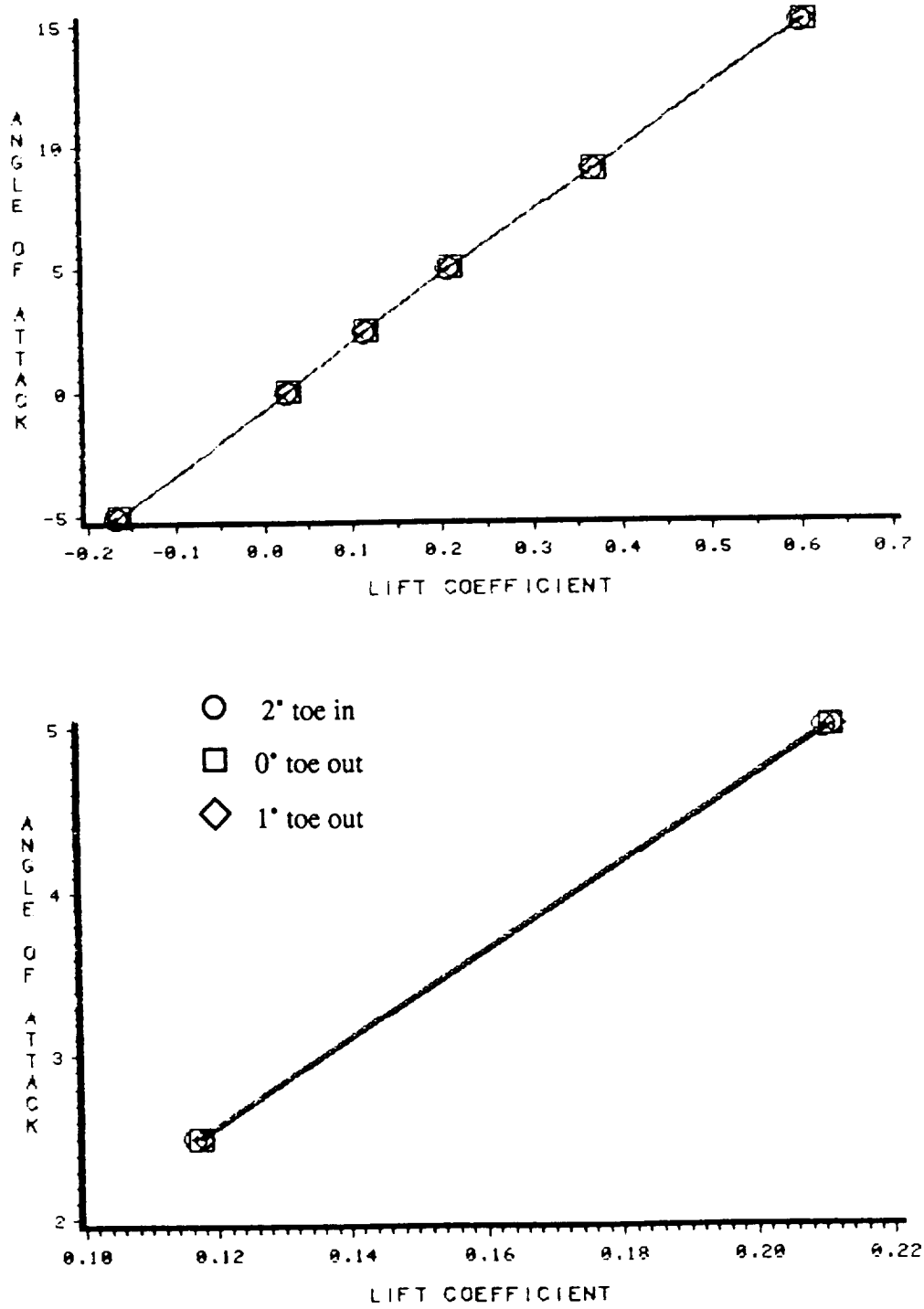

Figure 4.9.6: Predicted performance of the NACA 1402 base wing with 4% thick, 75° anhedral winglets; M=1.62; angle of attack versus lift coefficient.

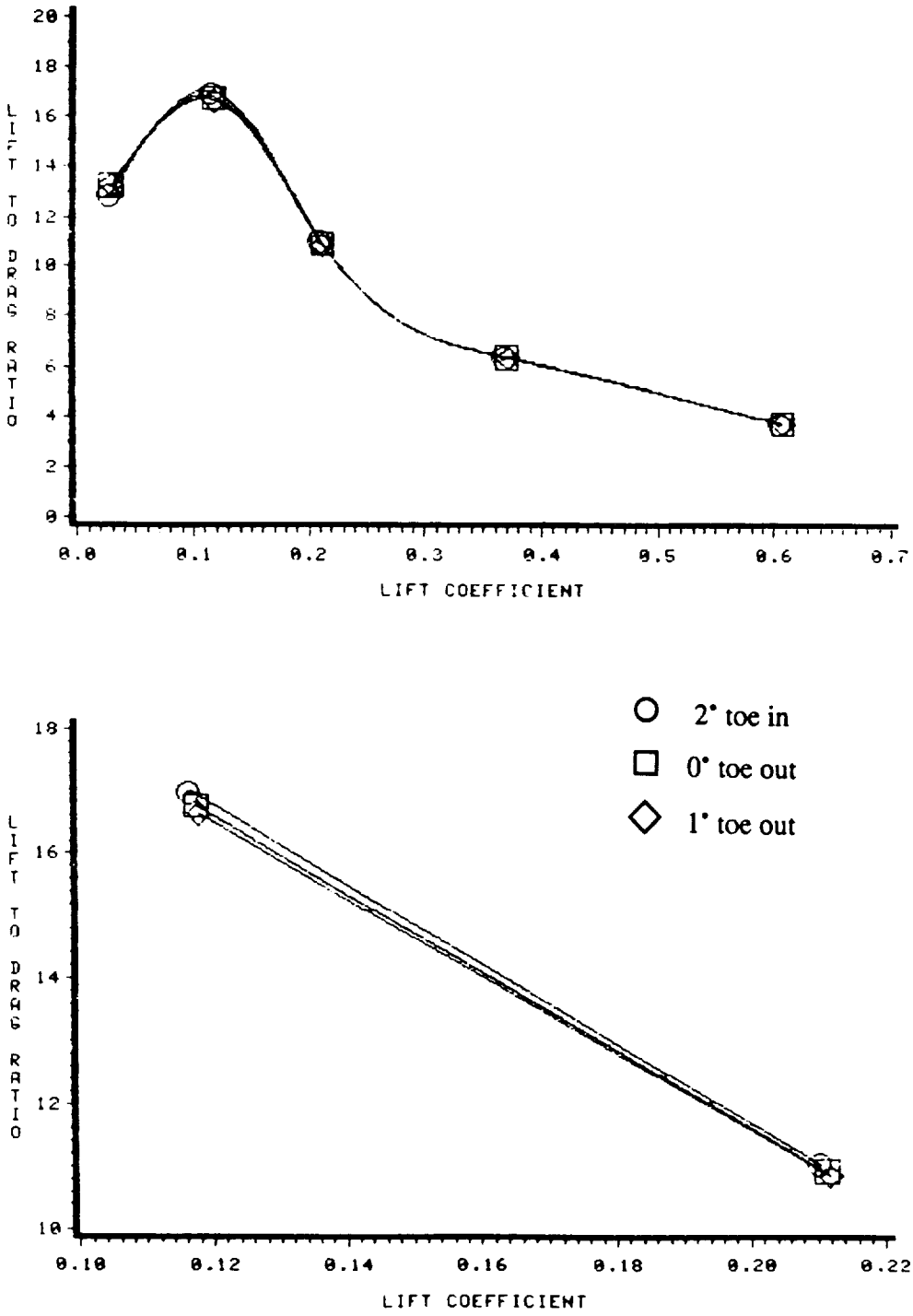

Figure 4.9.7: Predicted performance of the NACA 1402 base wing with 4% thick, 75° anhedral winglets; M=1.62; lift-to-pressure drag ratio versus lift coefficient.

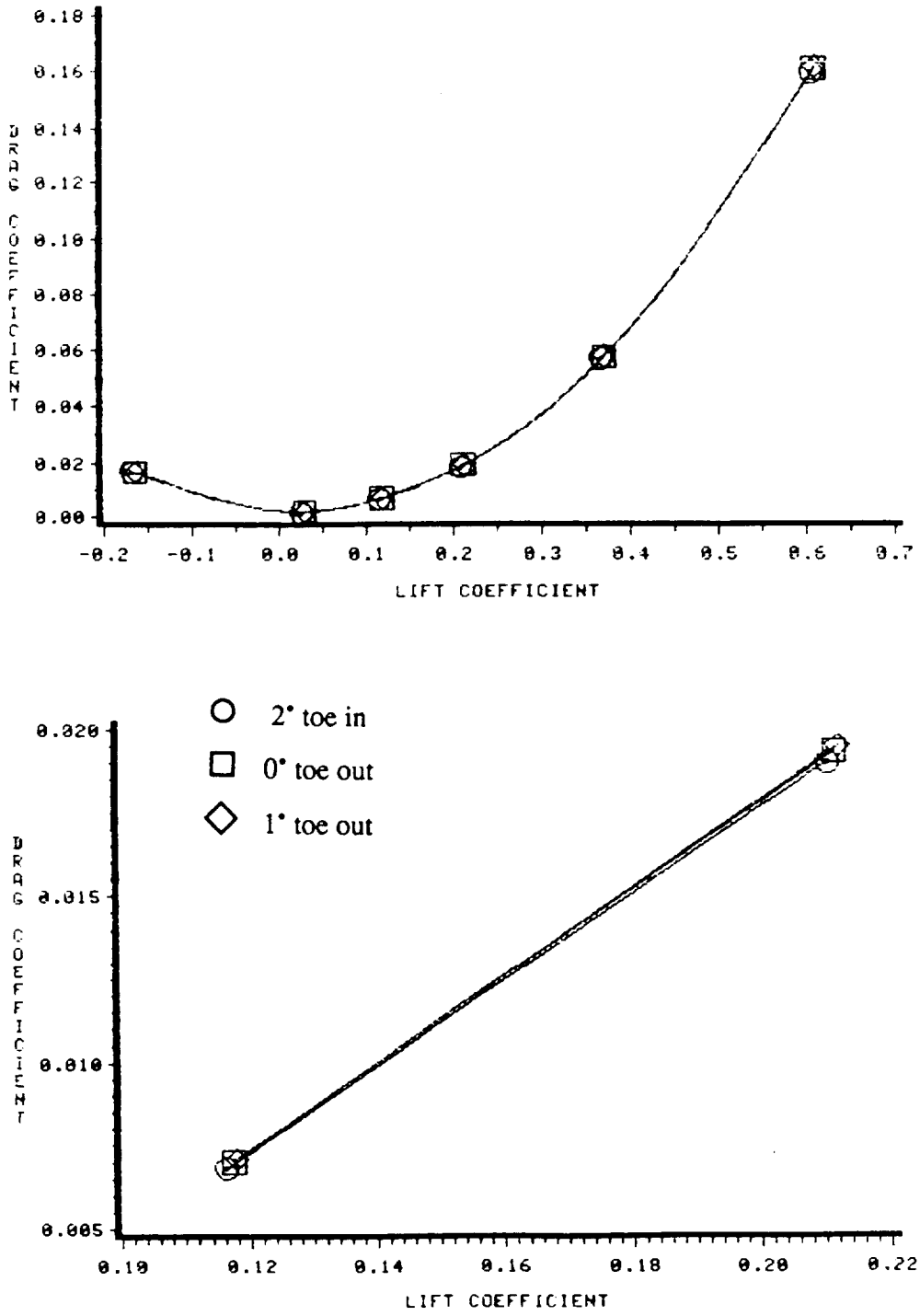

Figure 4.9.8: Predicted performance of the NACA 1402 base wing with 4% thick, 75° anhedral winglets; M=1.62; pressure drag coefficient versus lift coefficient.

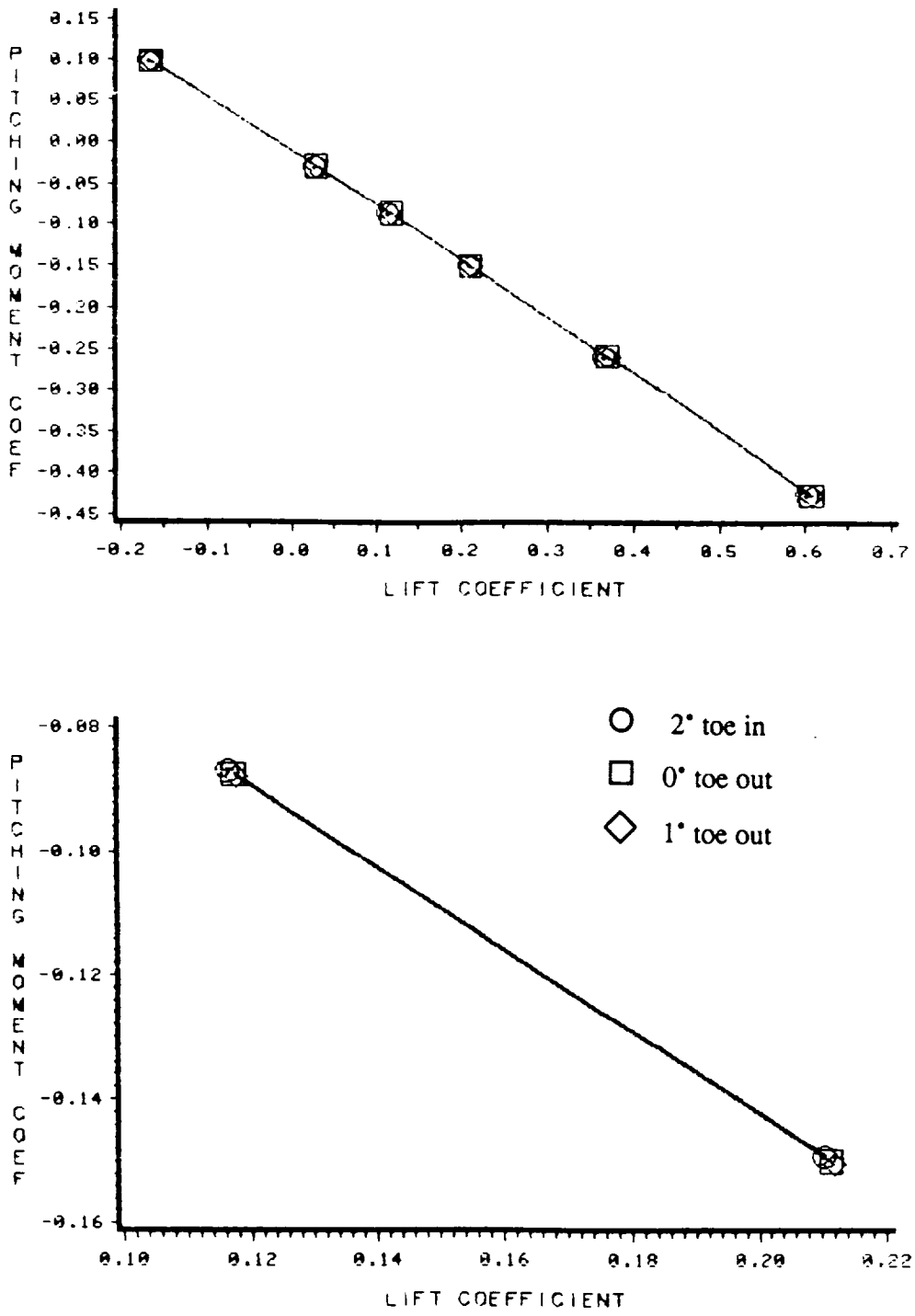

Figure 4.9.9: Predicted performance of the NACA 1402 base wing with 4% thick, 75° anhedral winglets; M=1.62; pitching moment coefficient versus lift coefficient.

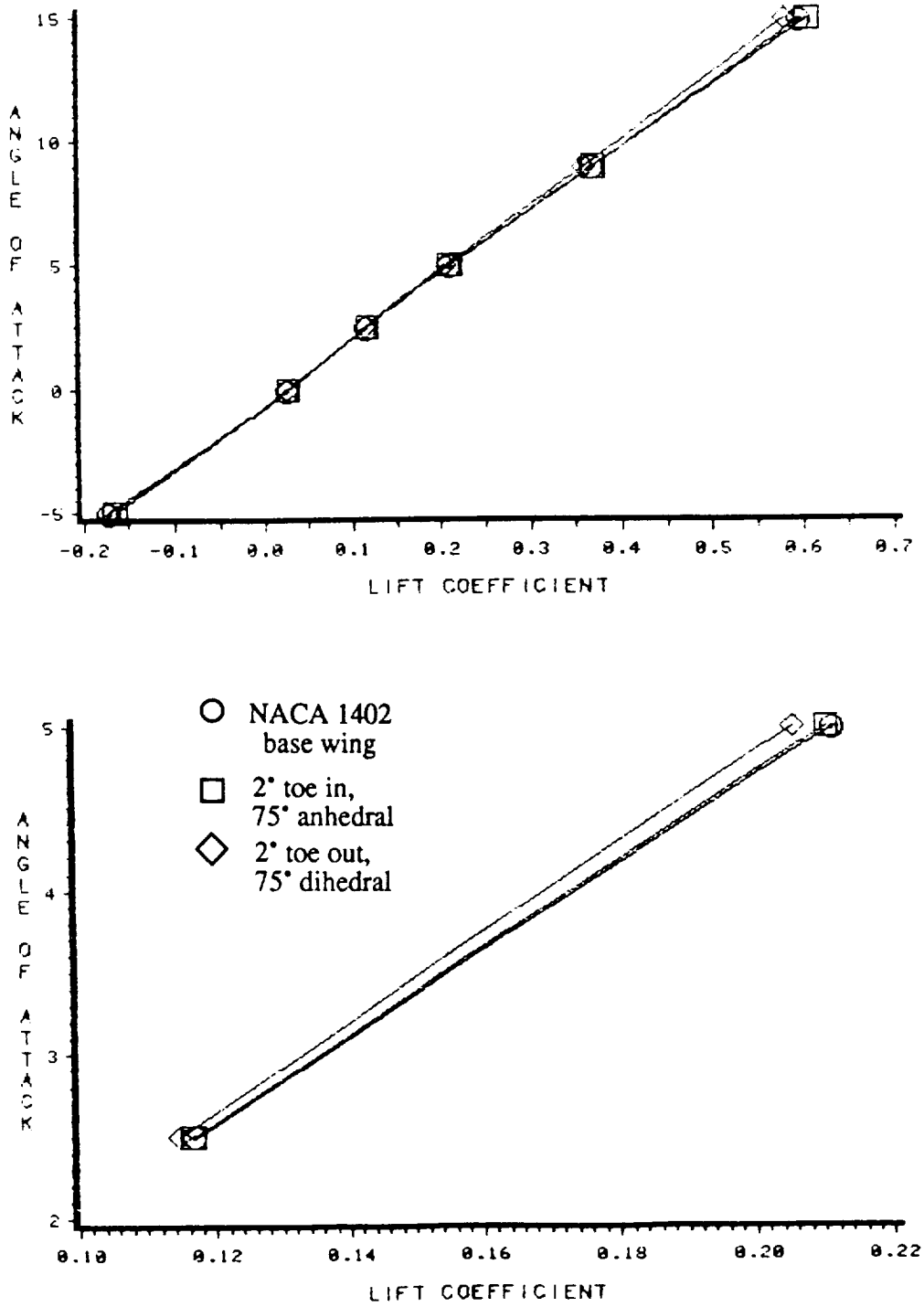

Figure 4.9.10: Comparison of the predicted performance of the NACA 1402 base wing with extension; the 4% thick, 2° toe in, 75° anhedral wing-winglet; and the 4% thick, 2° toe out, 75° dihedral wing-winglet; M=1.62; angle of attack versus lift coefficient.

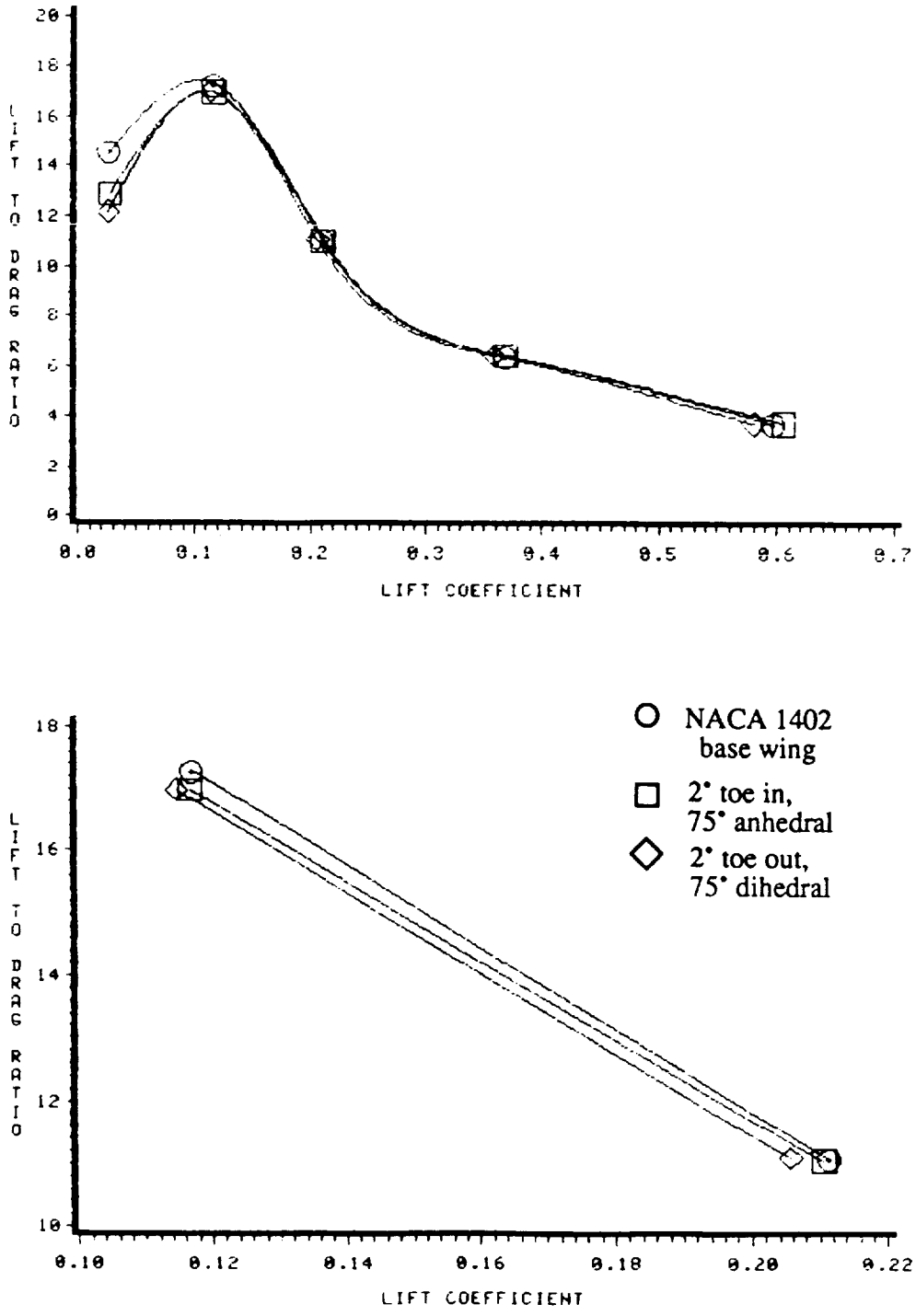

Figure 4.9.11: Comparison of the predicted performance of the NACA 1402 base wing with extension; the 4% thick, 2° toe in, 75° anhedral wing-winglet; and the 4% thick, 2° toe out; 75° dihedral wing-winglet; M=1.62; lift-to-pressure drag ratio versus lift coefficient.

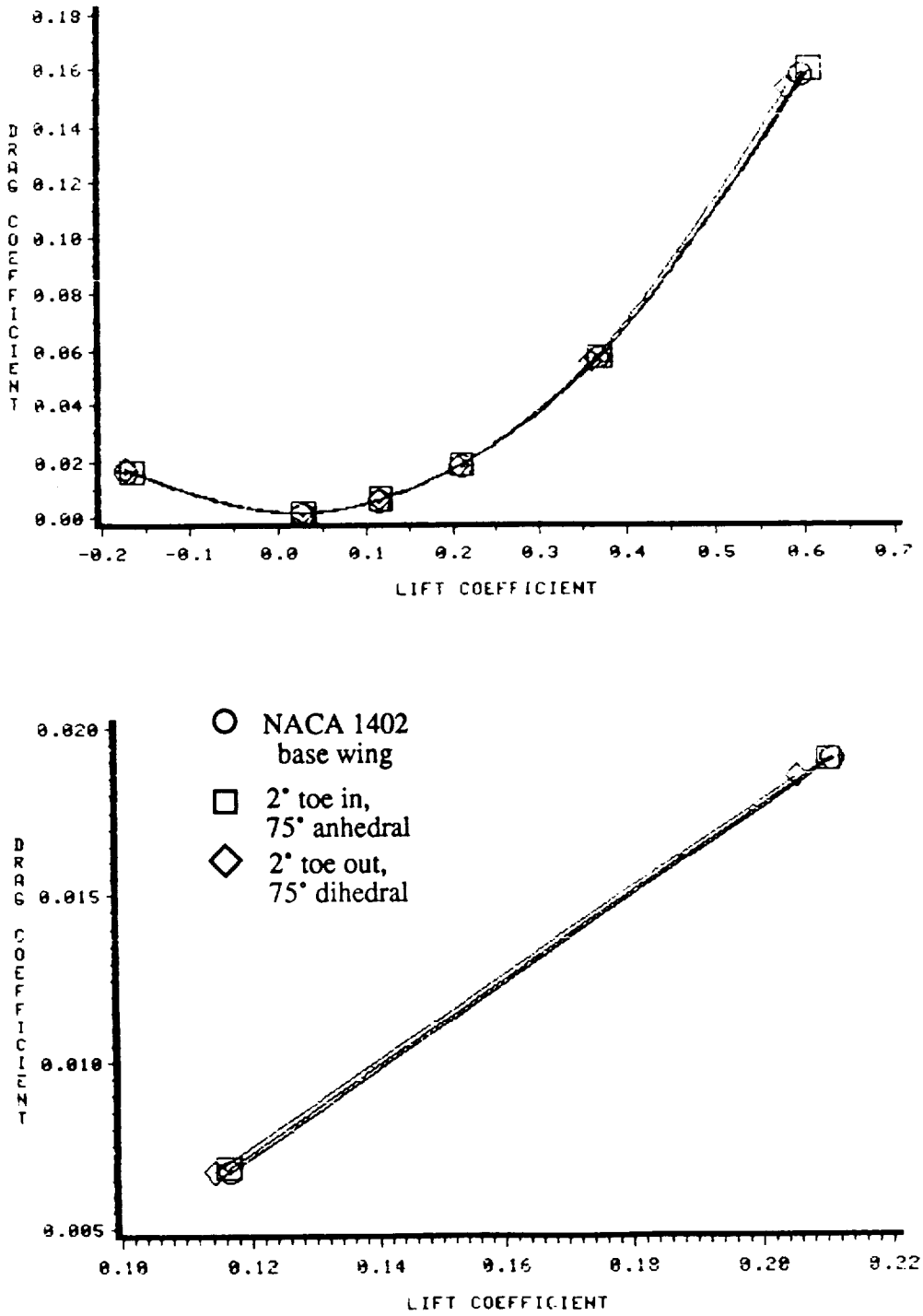

Figure 4.9.12: Comparison of the predicted performance of the NACA 1402 base wing with extension; the 4% thick, 2° toe in, 75° anhedral wing-winglet; and the 4% thick, 2° toe out; 75° dihedral wing-winglet; M=1.62; pressure drag coefficient versus lift coefficient.

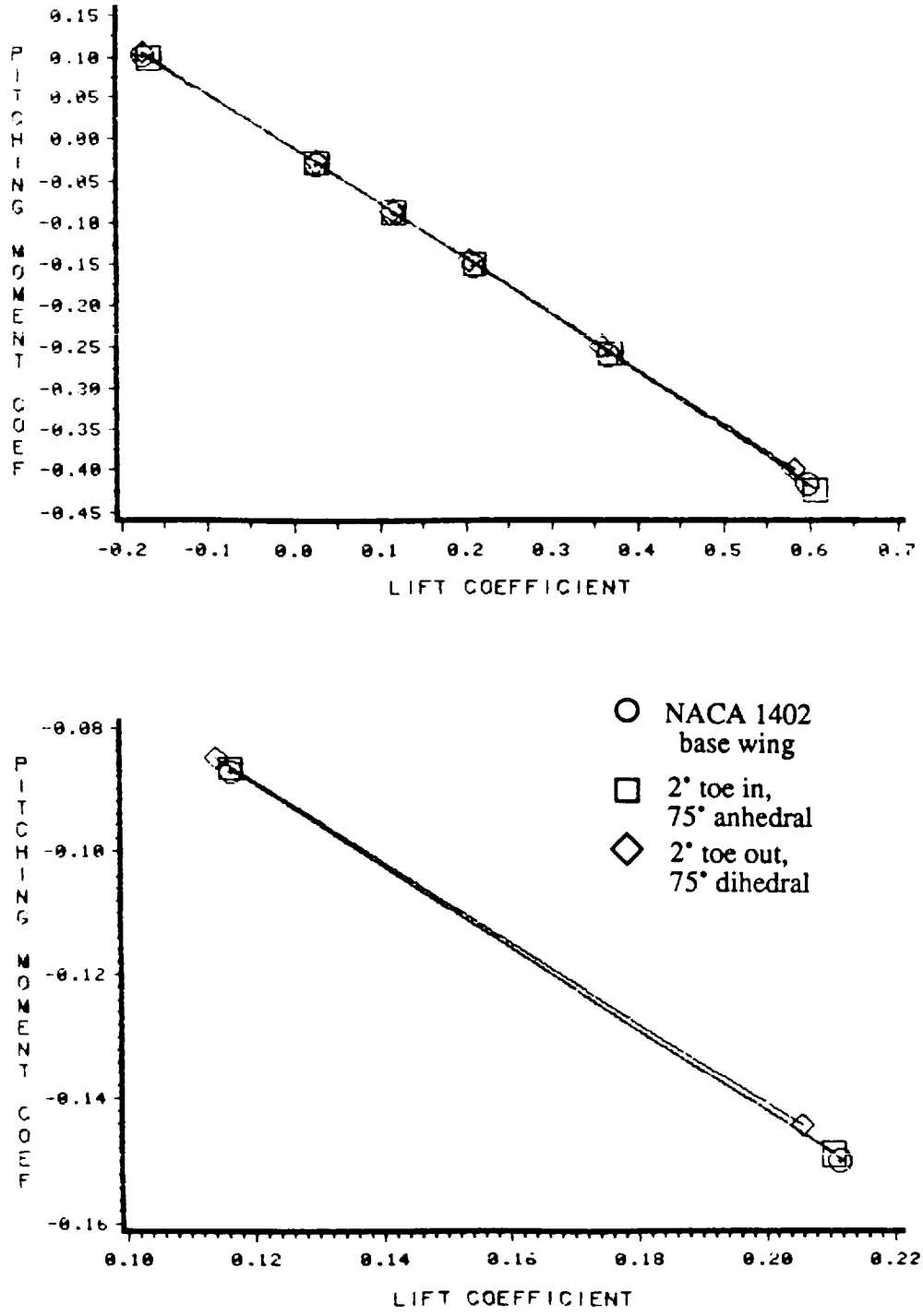

Figure 4.9.13: Comparison of the predicted performance of the NACA 1402 base wing with extension; the 4% thick, 2° toe in, 75° anhedral wing-winglet; and the 4% thick, 2° toe out; 75° dihedral wing-winglet; M=1.62; pitching moment coefficient versus lift coefficient.

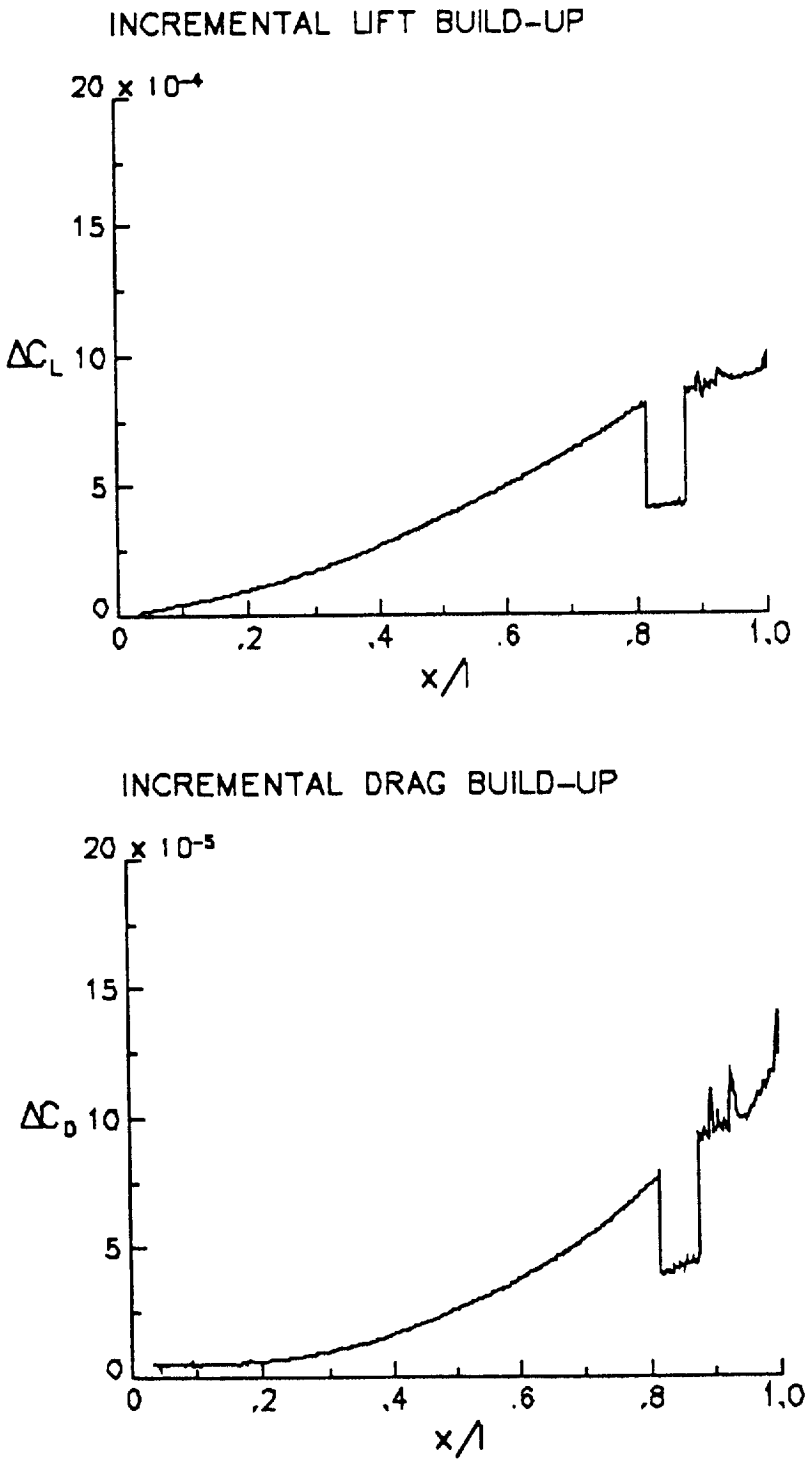

Figure 4.9.14: Incremental lift and pressure drag build up for the NACA 1402 base wing with a 4% thick, 2° toe in, 75° anhedral winglet at 5° angle of attack, M=1.62.

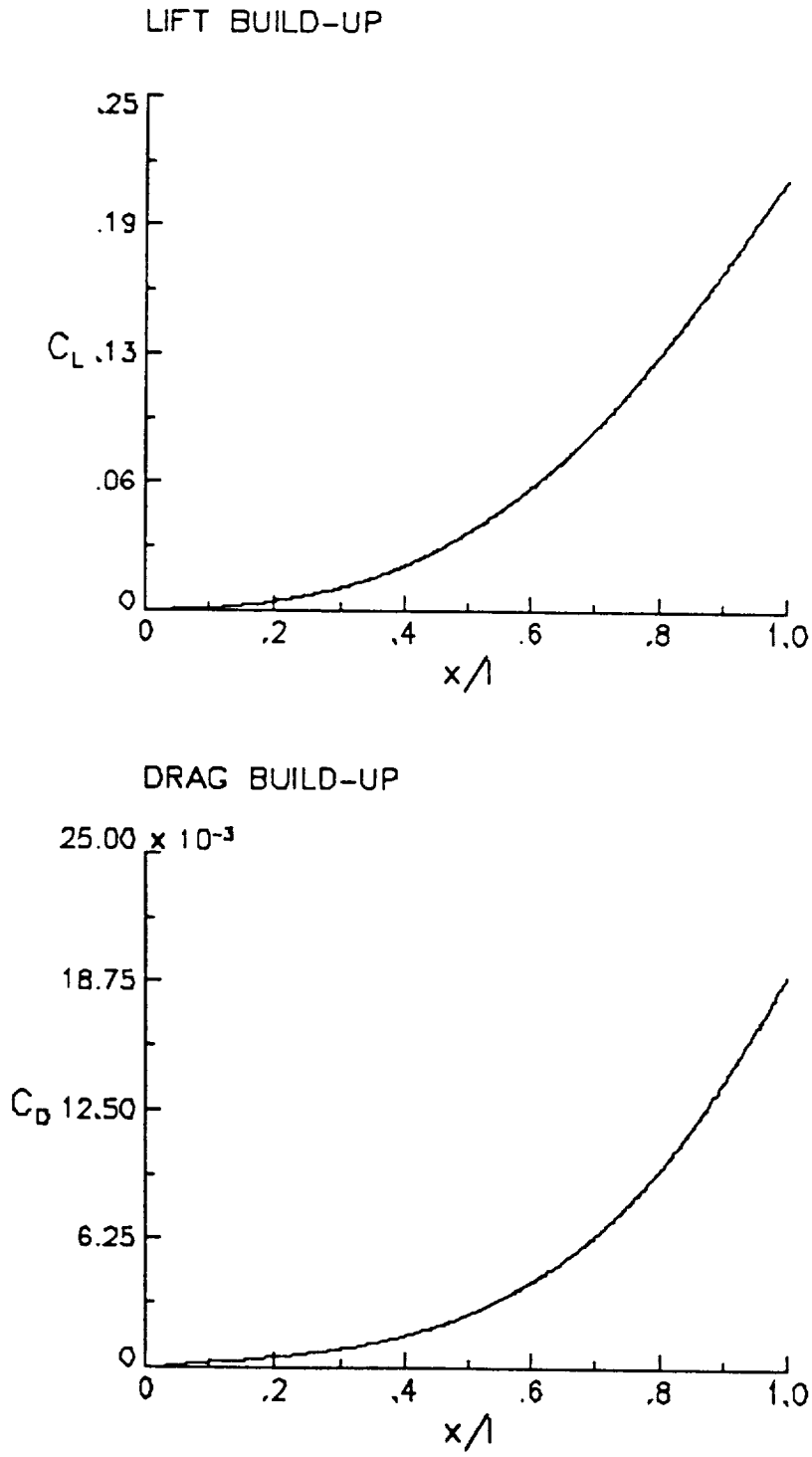

Figure 4.9.15: Total lift and pressure drag build up for the NACA 1402 base wing with a 4% thick, 2° toe in, 75° anhedral winglet at 5° angle of attack, M=1.62.

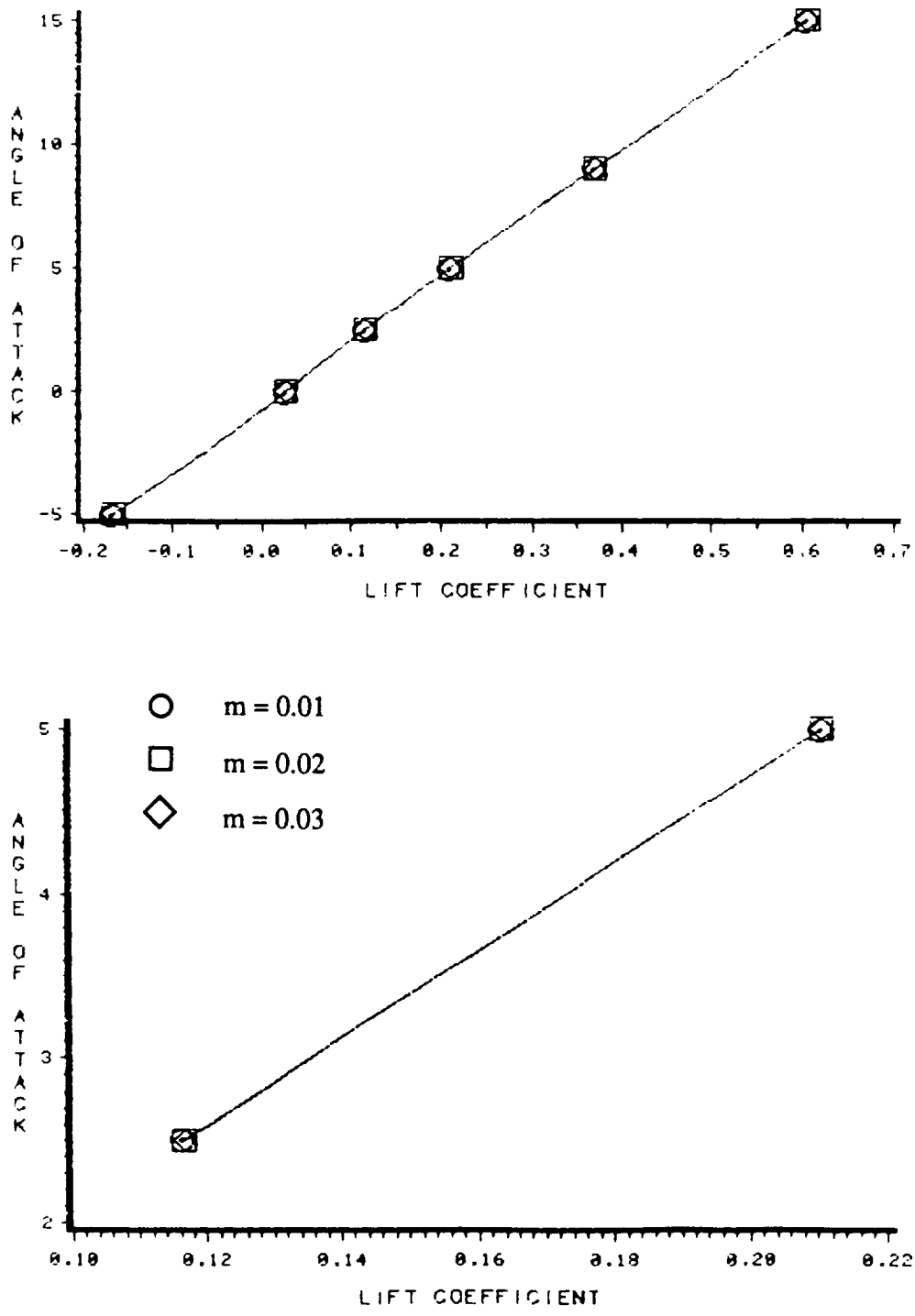

Figure 4.10.1: Predicted performance of the NACA 1402 base wing with 4% thick, 75° anhedral winglets with variable camber; M=1.62; angle of attack versus lift coefficient.

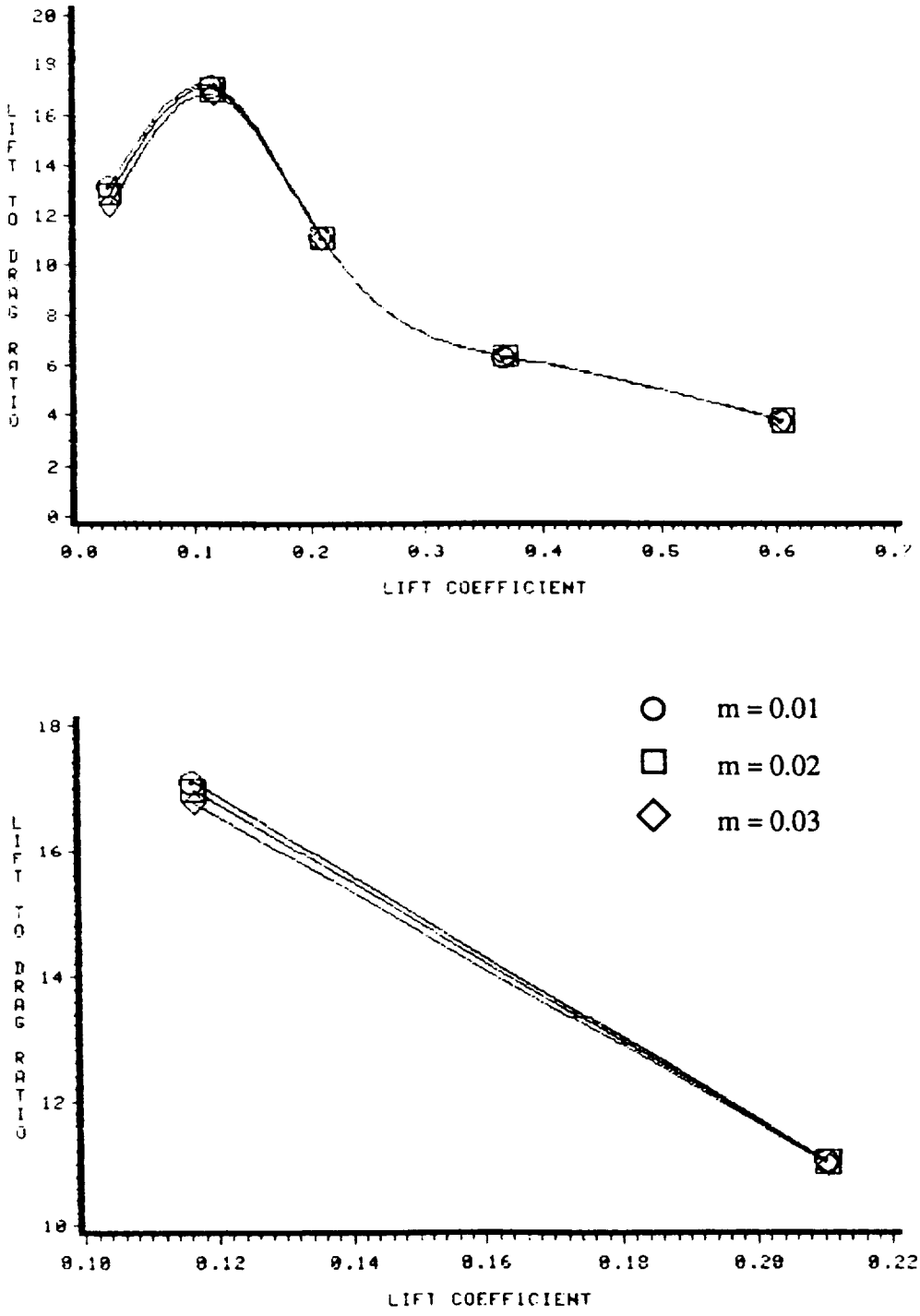

Figure 4.10.2: Predicted performance of the NACA 1402 base wing with 4% thick, 75° anhedral winglets with variable camber; M=1.62; lift-to-pressure drag ratio versus lift coefficient.

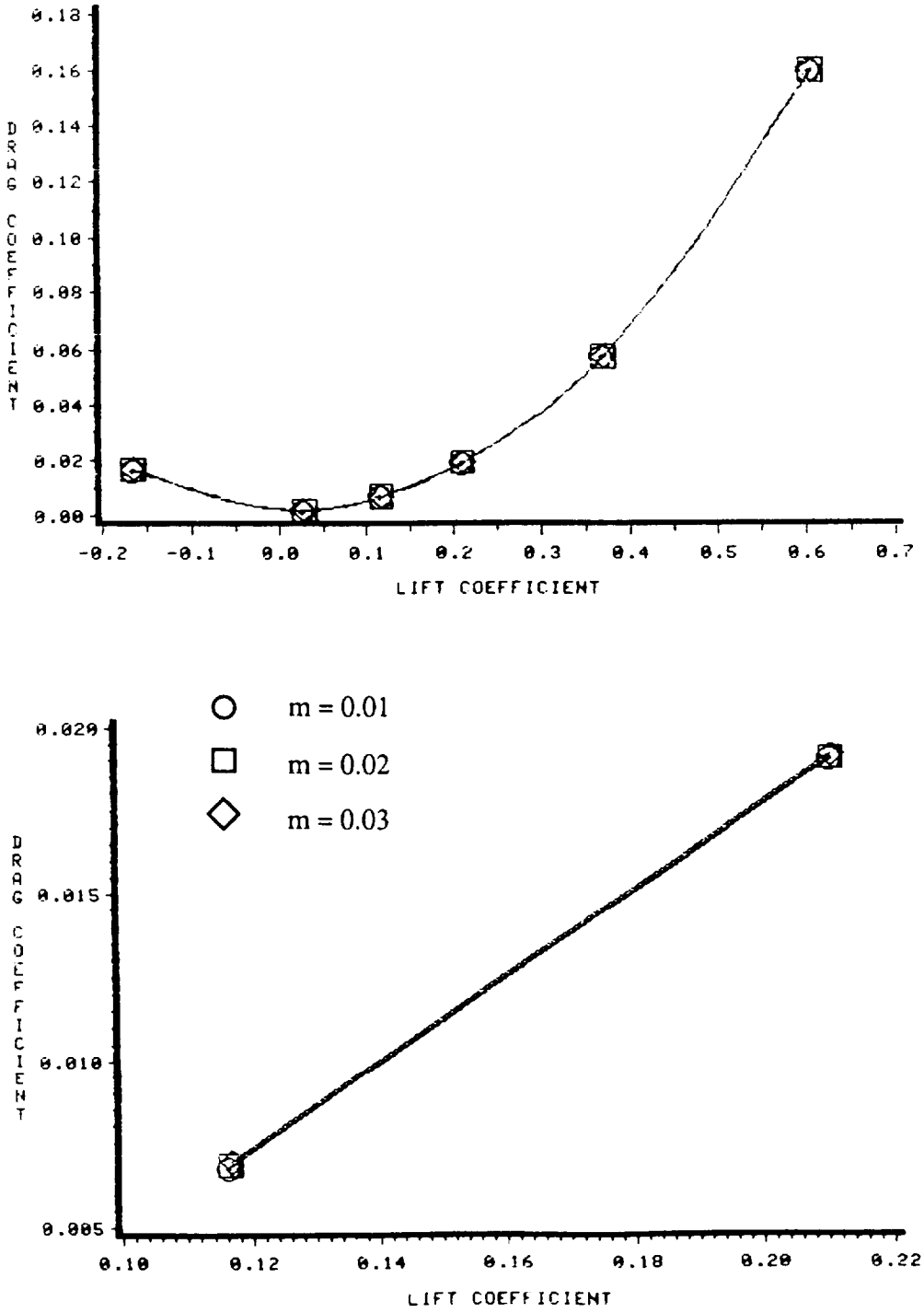

Figure 4.10.3: Predicted performance of the NACA 1402 base wing with 4% thick, 75° anhedral winglets with variable camber; M=1.62; pressure drag coefficient versus lift coefficient.

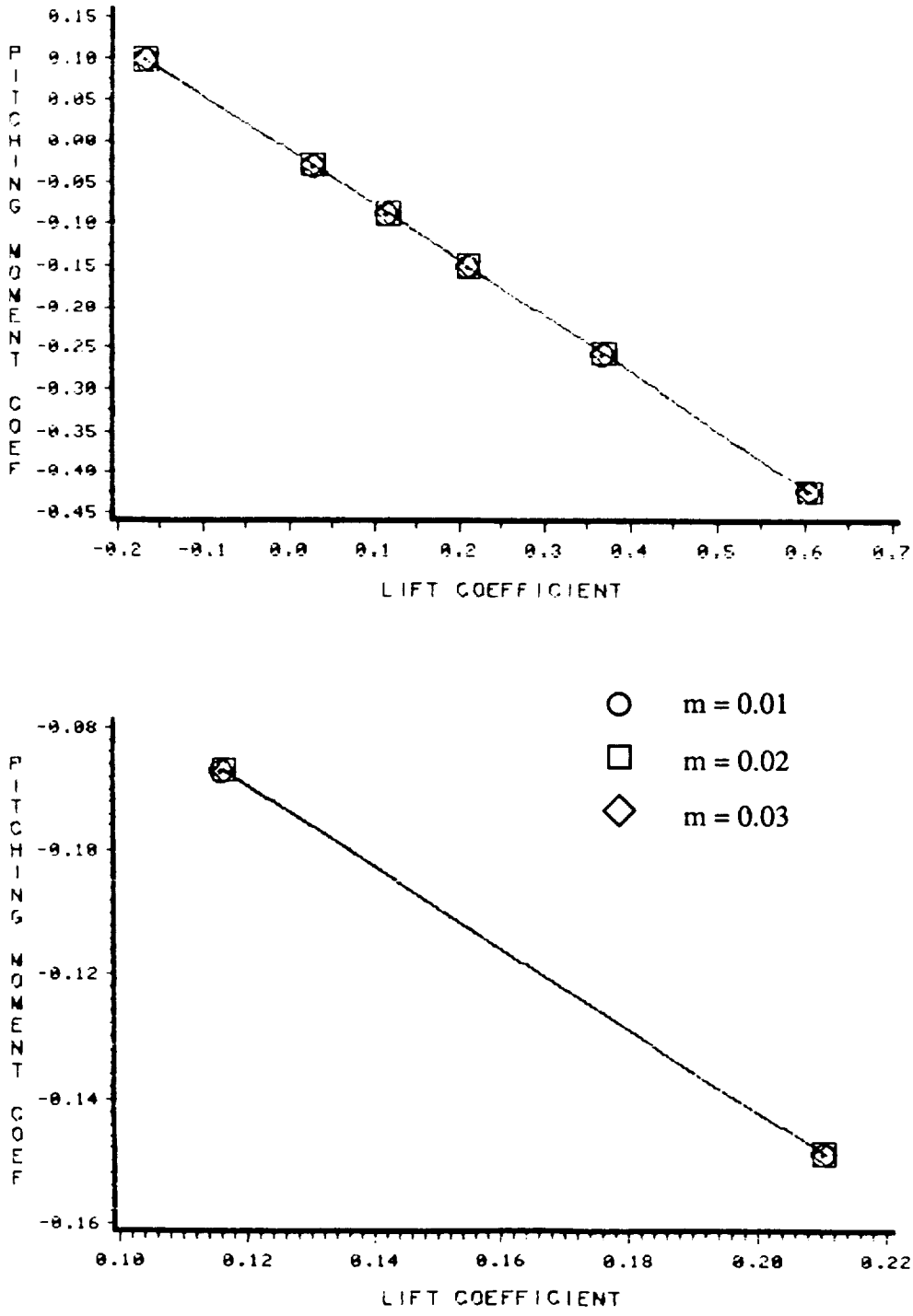

Figure 4.10.4: Predicted performance of the NACA 1402 base wing with 4% thick, 75° anhedral winglets with variable camber; M=1.62; pitching moment coefficient versus lift coefficient.

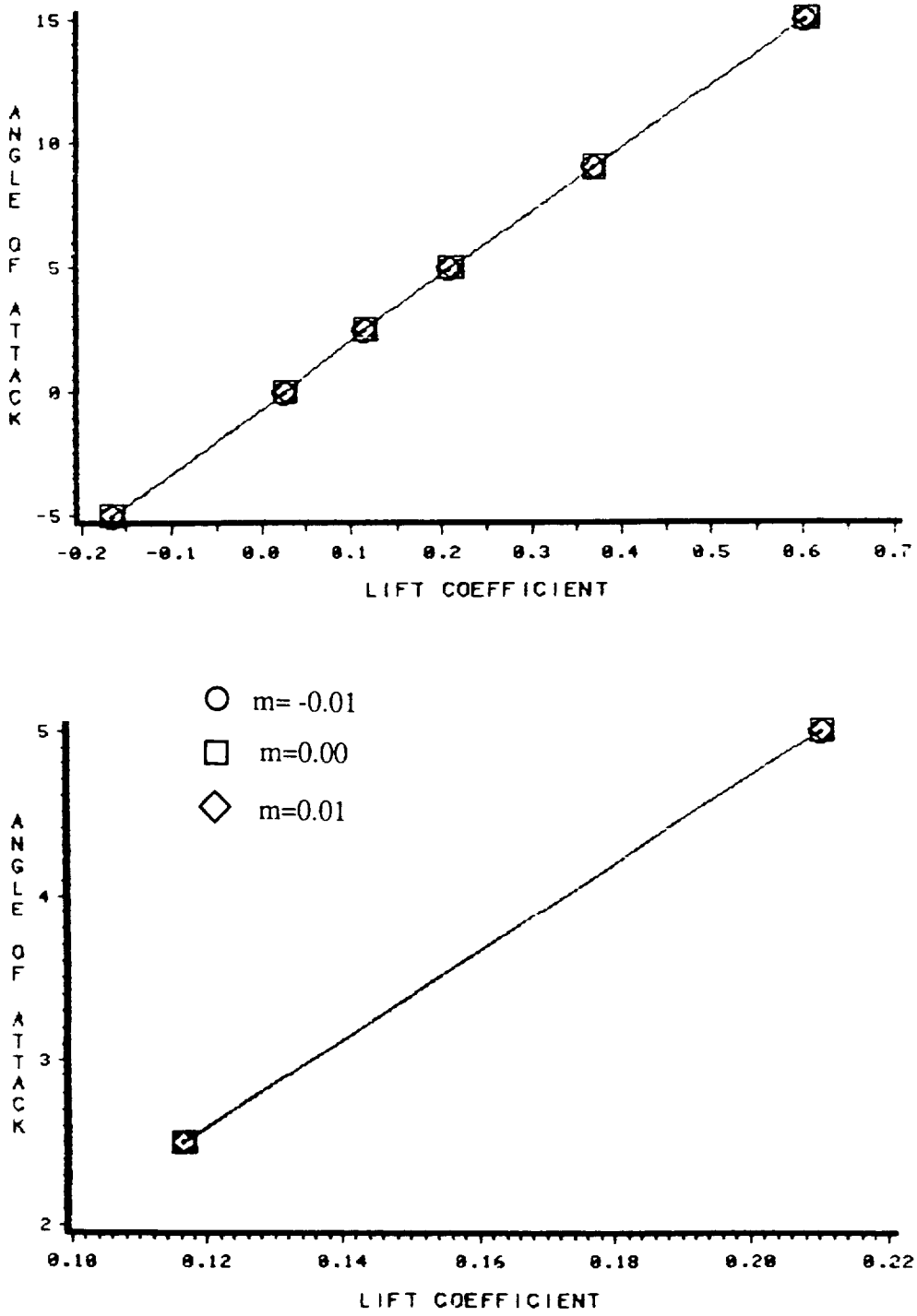

Figure 4.10.5: Predicted performance of the NACA 1402 base wing with 4% thick, 75° anhedral winglets with variable camber; M=1.62; angle of attack versus lift coefficient.

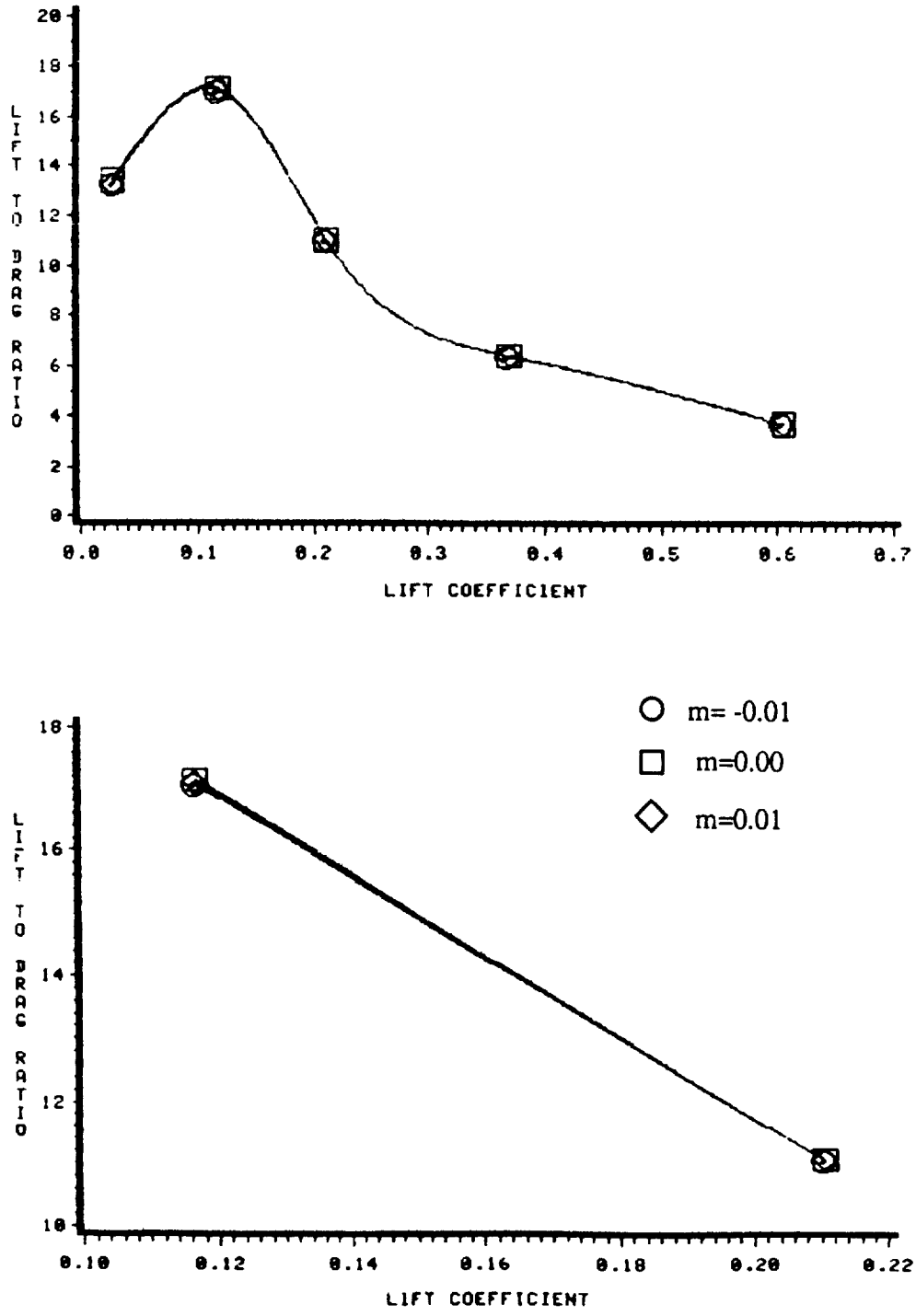

Figure 4.10.6: Predicted performance of the NACA 1402 base wing with 4% thick, 75° anhedral winglets with variable camber; M=1.62; lift-to-pressure drag ratio versus lift coefficient.

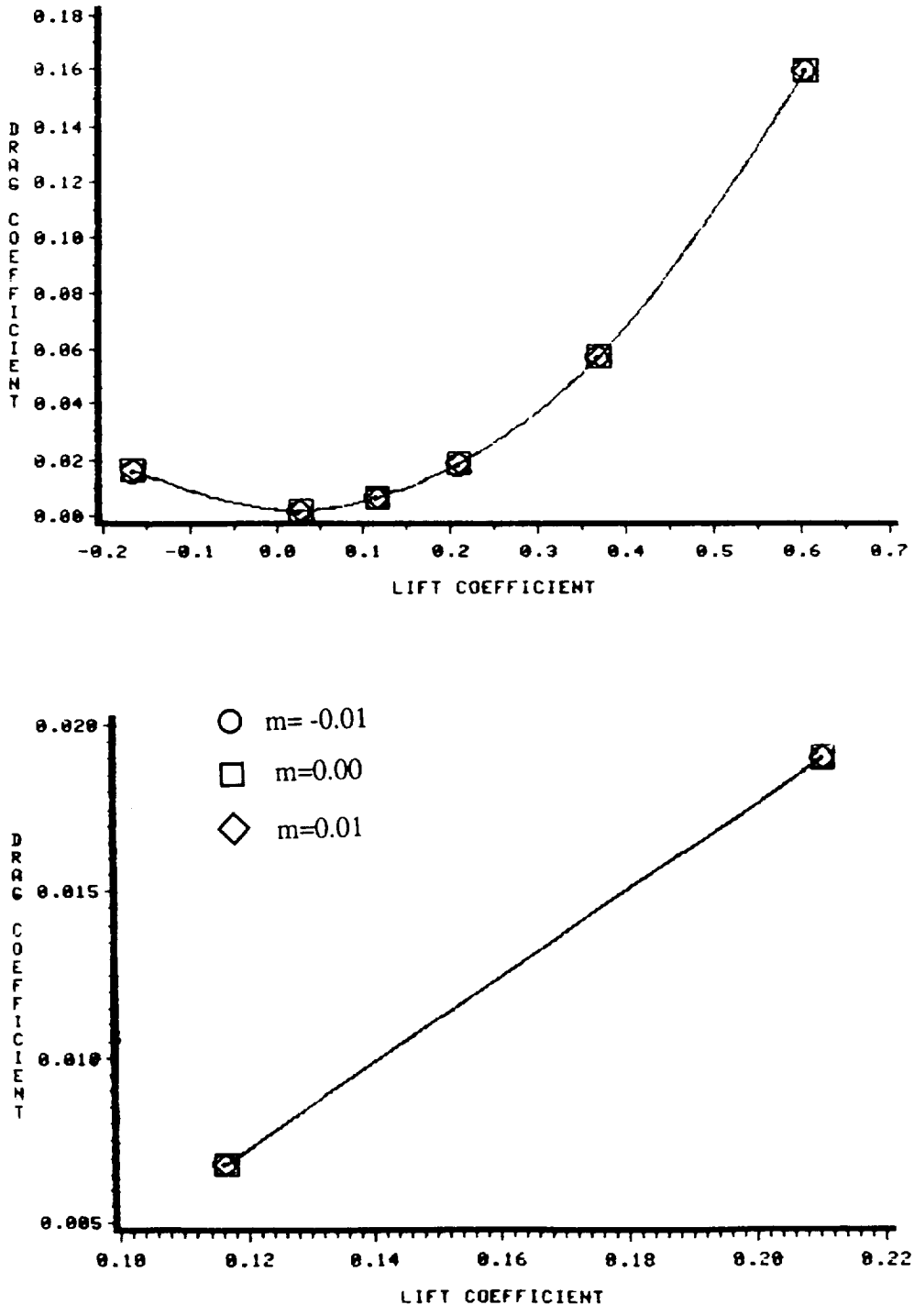

Figure 4.10.7: Predicted performance of the NACA 1402 base wing with 4% thick, 75° anhedral winglets with variable camber; M=1.62; pressure drag coefficient versus lift coefficient.

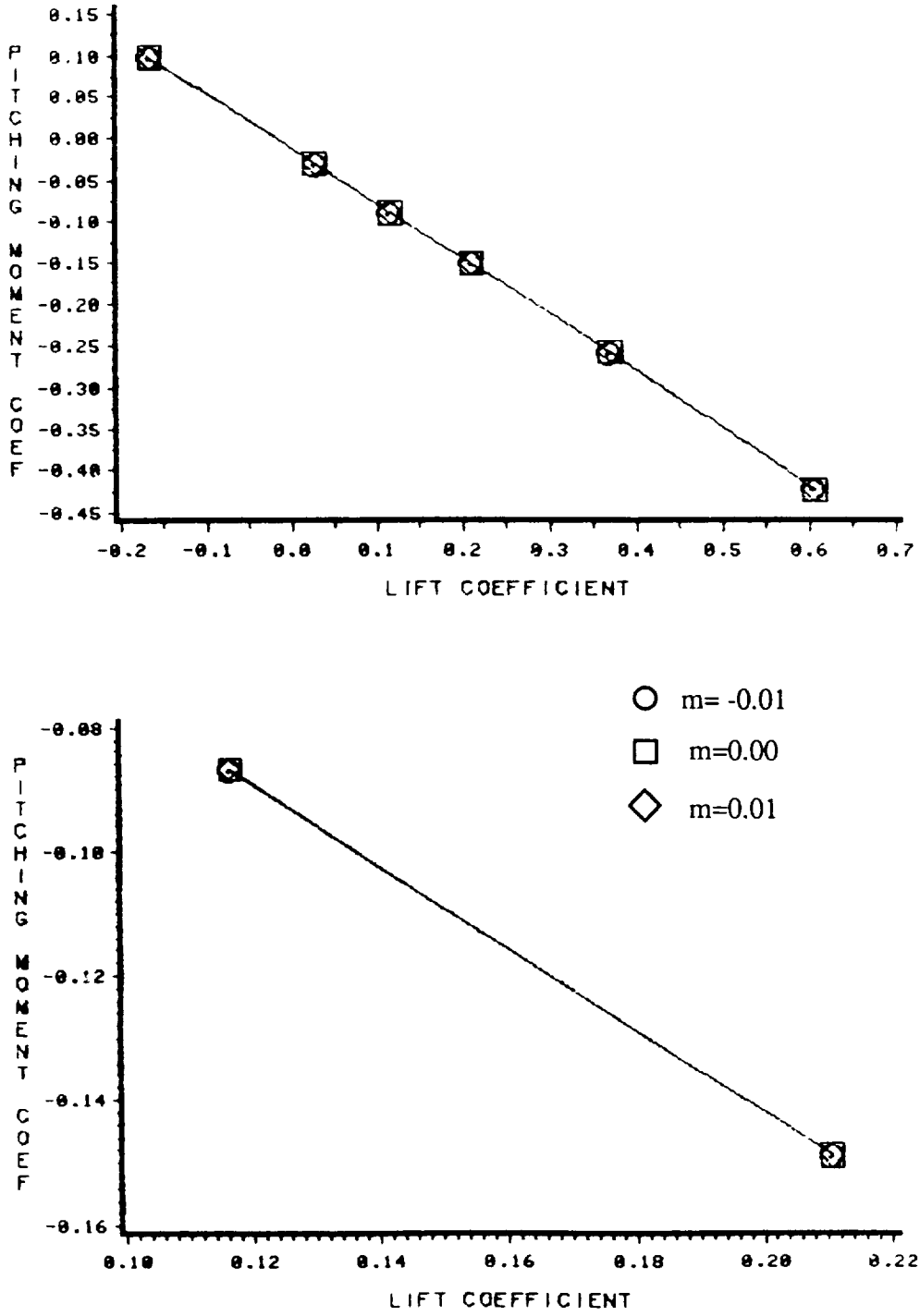

Figure 4.10.8: Predicted performance of the NACA 1402 base wing with 4% thick, 75° anhedral winglets with variable camber; M=1.62; pitching moment coefficient versus lift coefficient.

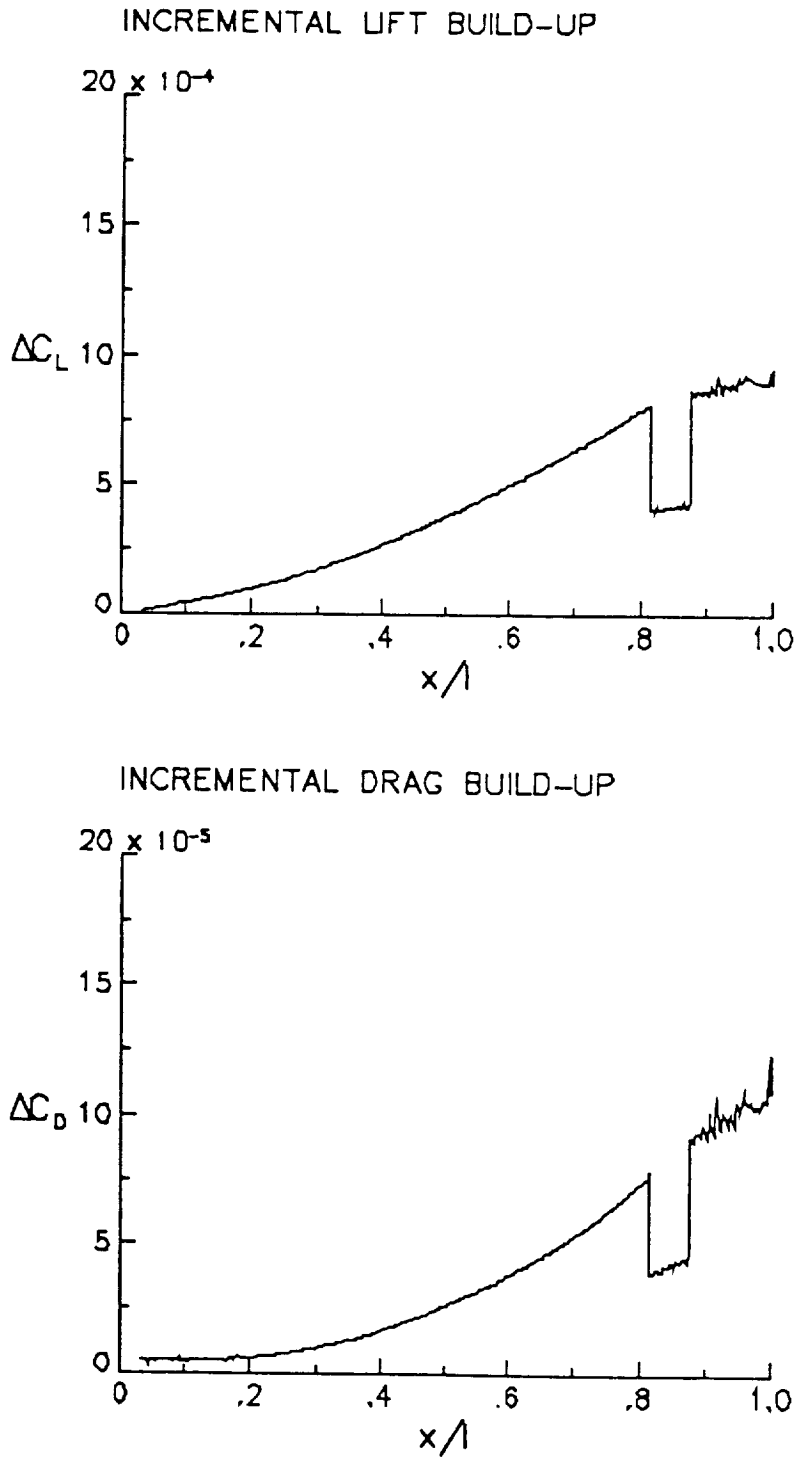

Figure 4.10.9: Incremental lift and pressure drag build up for the NACA 1402 base wing with a 4% thick, 2° toe in, uncambered, 75° anhedral winglet at 5° angle of attack, M=1.62.

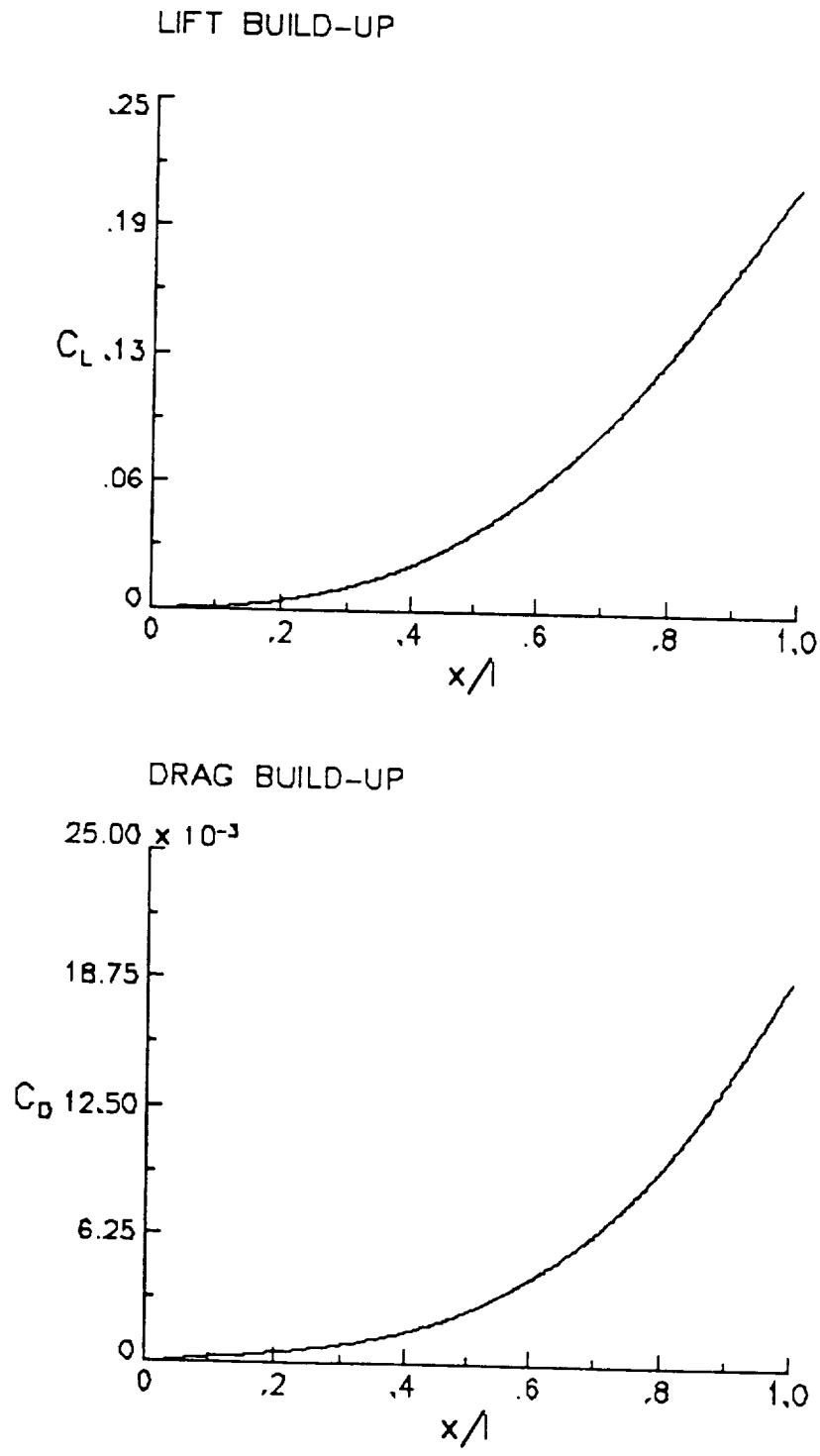

Figure 4.10.10: Total lift and pressure drag build up for the NACA 1402 base wing with a 4% thick, 2° toe in, uncambered, 75° anhedral winglet at 5° angle of attack, M=1.62.

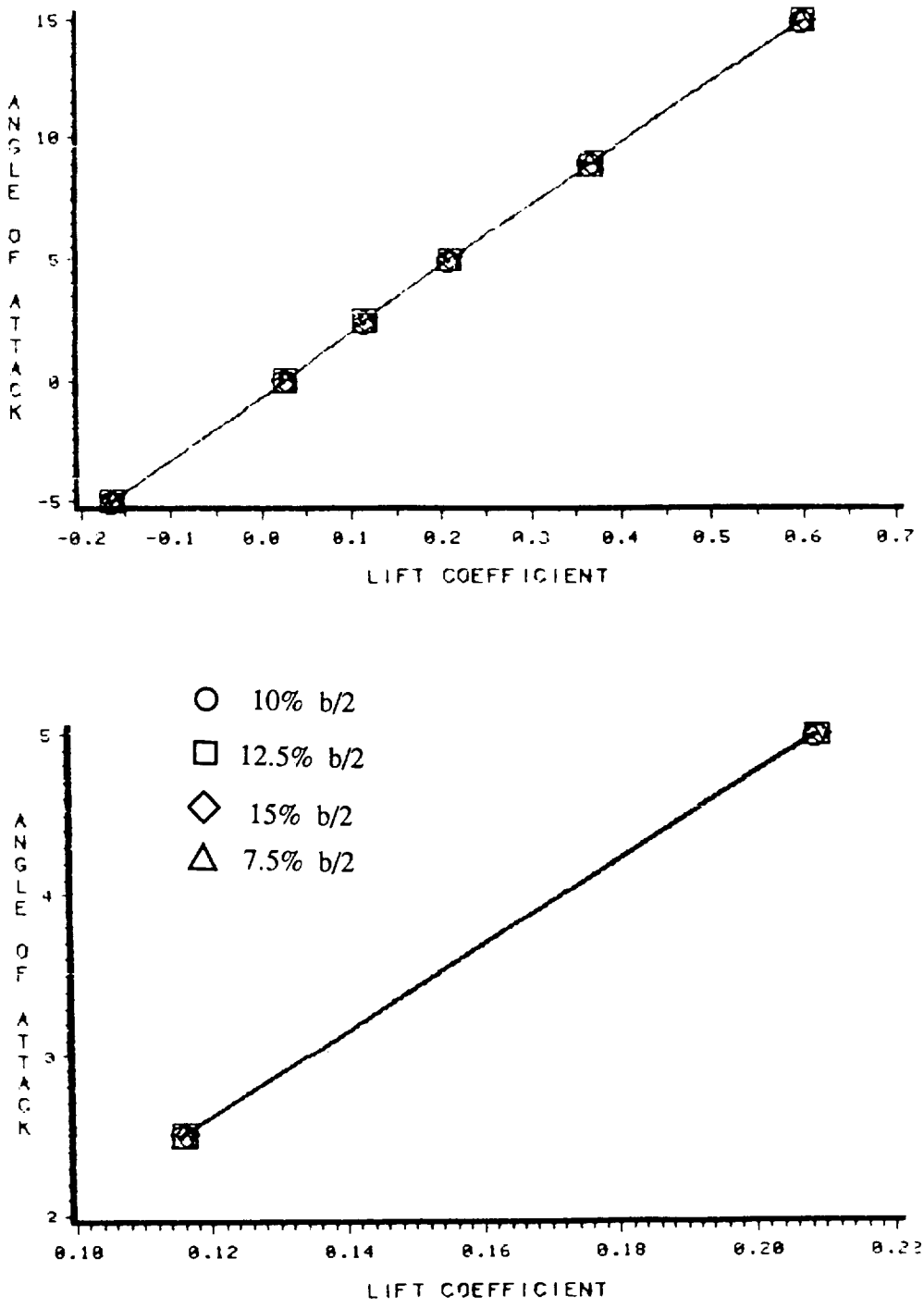

Figure 4.11.1: Predicted performance of the NACA 1402 base wing with 4% thick, 75° anhedral winglets with variable length; M=1.62; angle of attack versus lift coefficient.

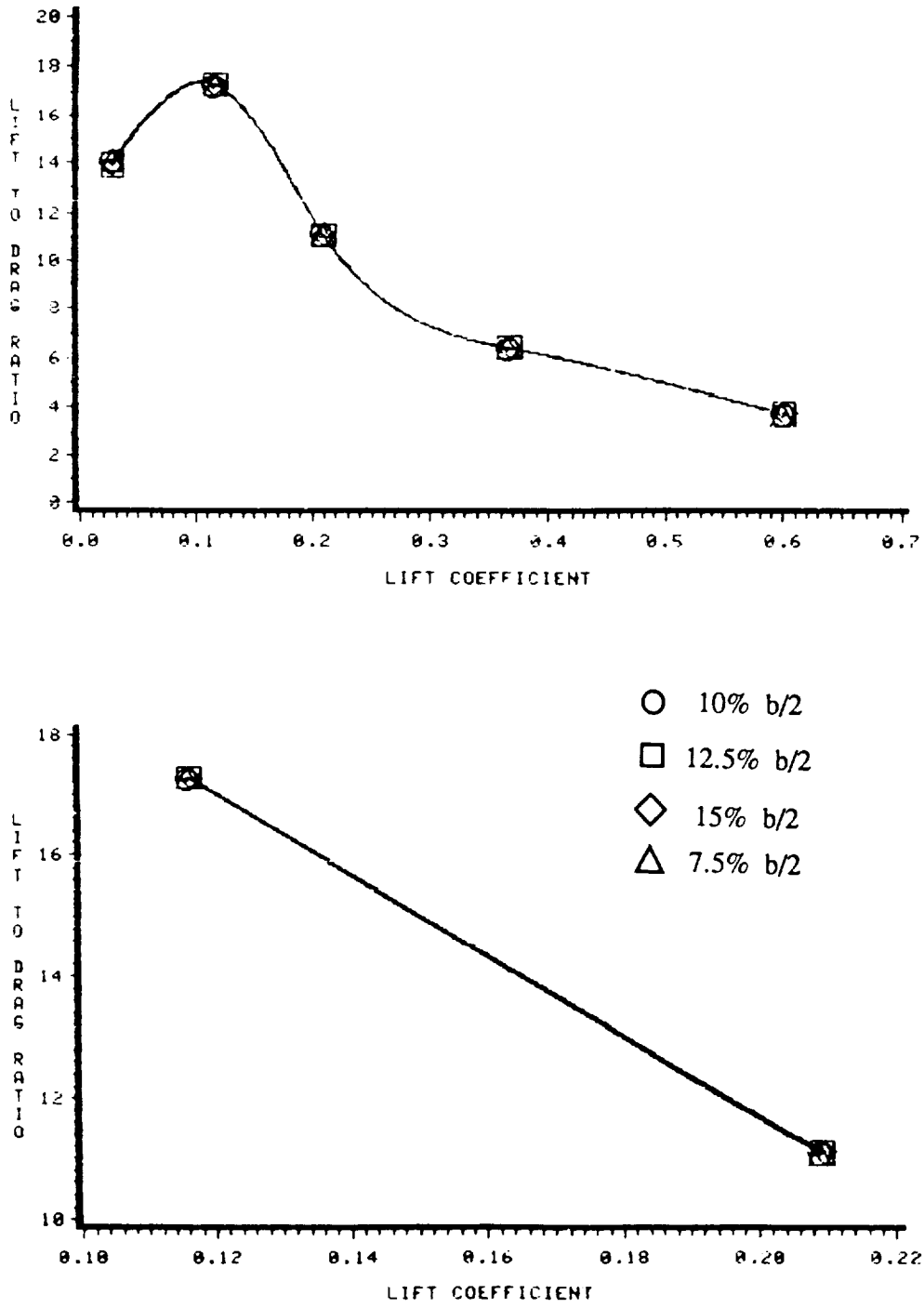

Figure 4.11.2: Predicted performance of the NACA 1402 base wing with 4% thick, 75° anhedral winglets with variable length; M=1.62; lift-to-pressure drag ratio versus lift coefficient.

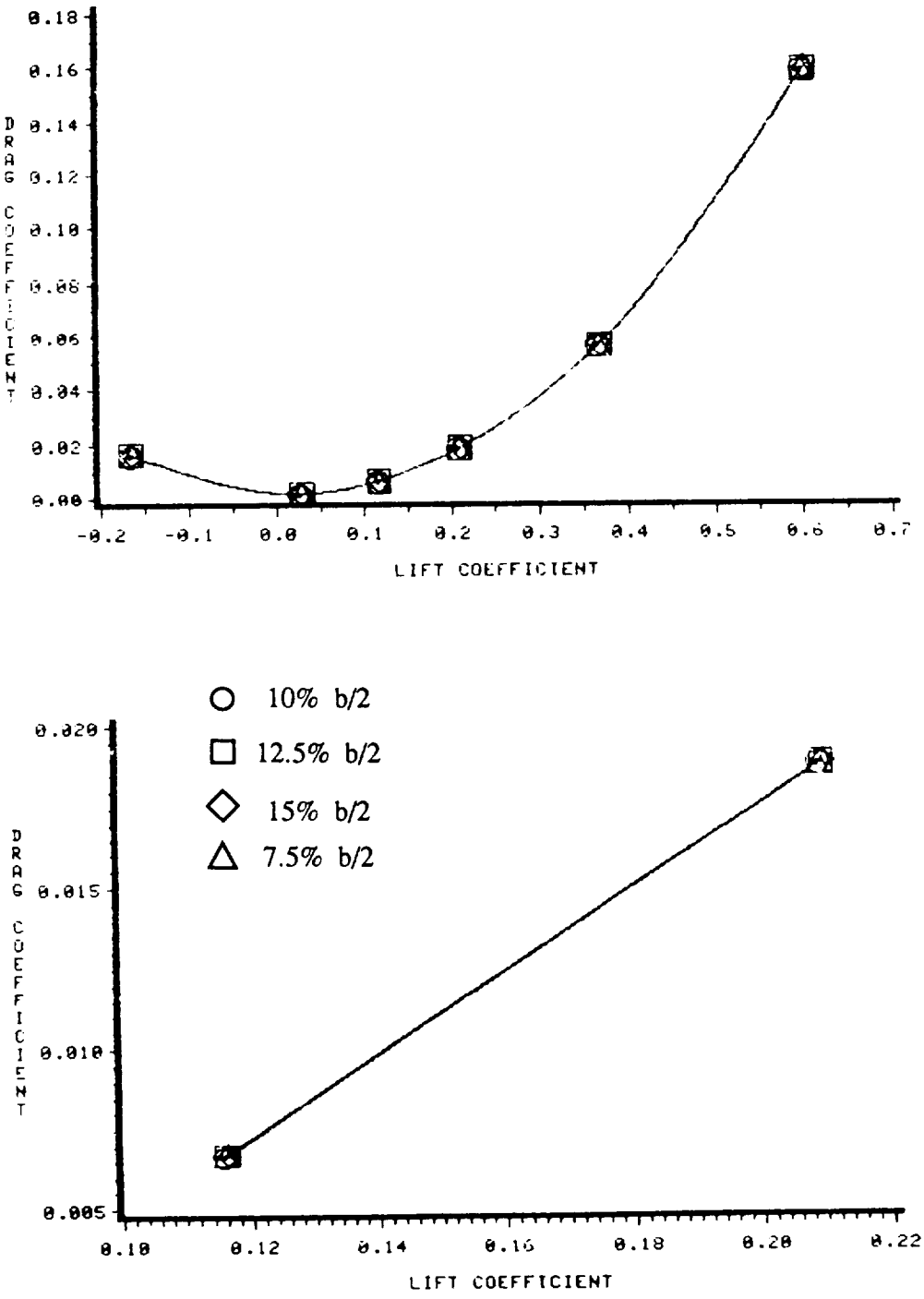

Figure 4.11.3: Predicted performance of the NACA 1402 base wing with 4% thick, 75° anhedral winglets with variable length; M=1.62; pressure drag coefficient versus lift coefficient.

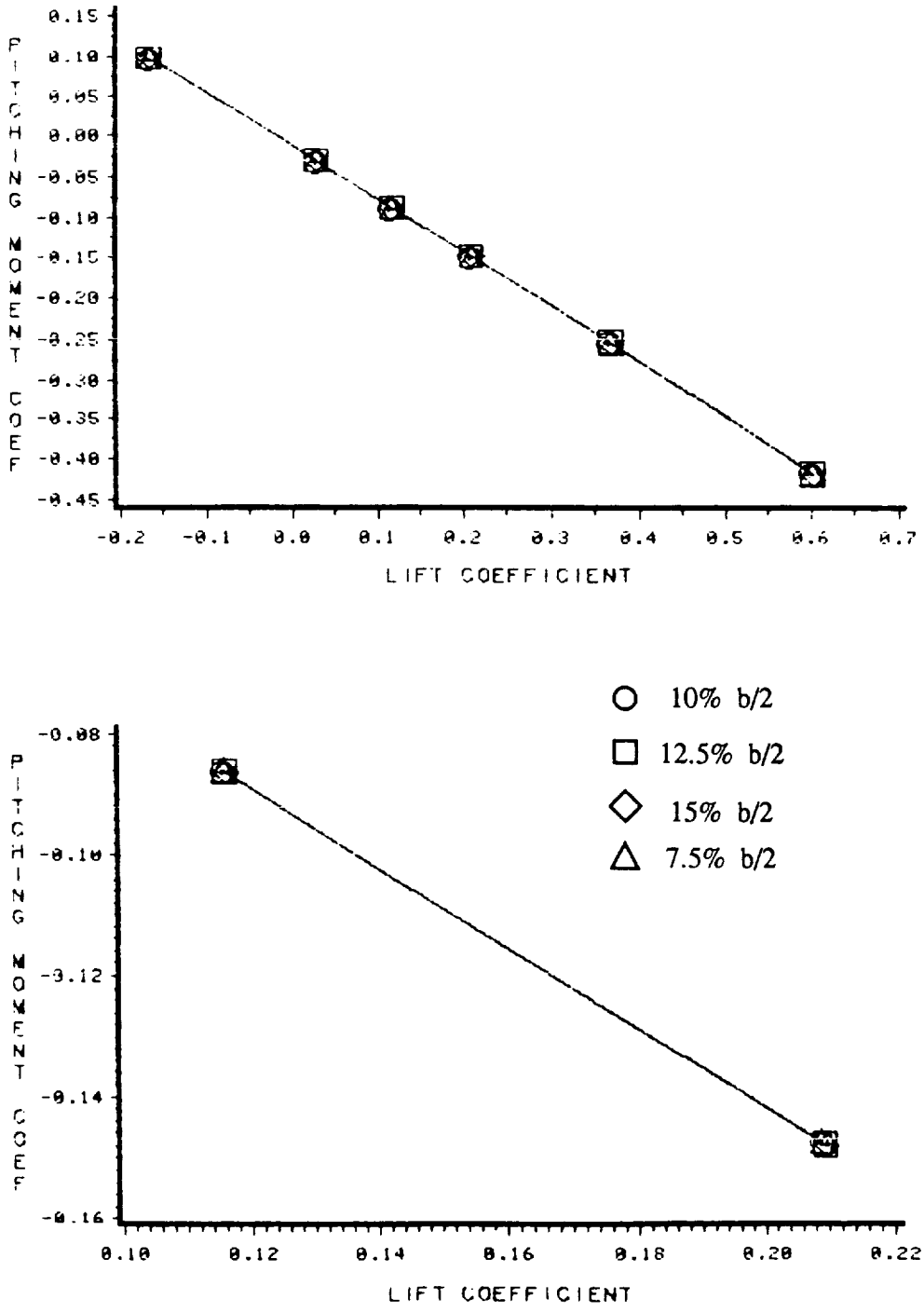

Figure 4.11.4: Predicted performance of the NACA 1402 base wing with 4% thick, 75° anhedral winglets with variable length; M=1.62; pitching moment coefficient versus lift coefficient.

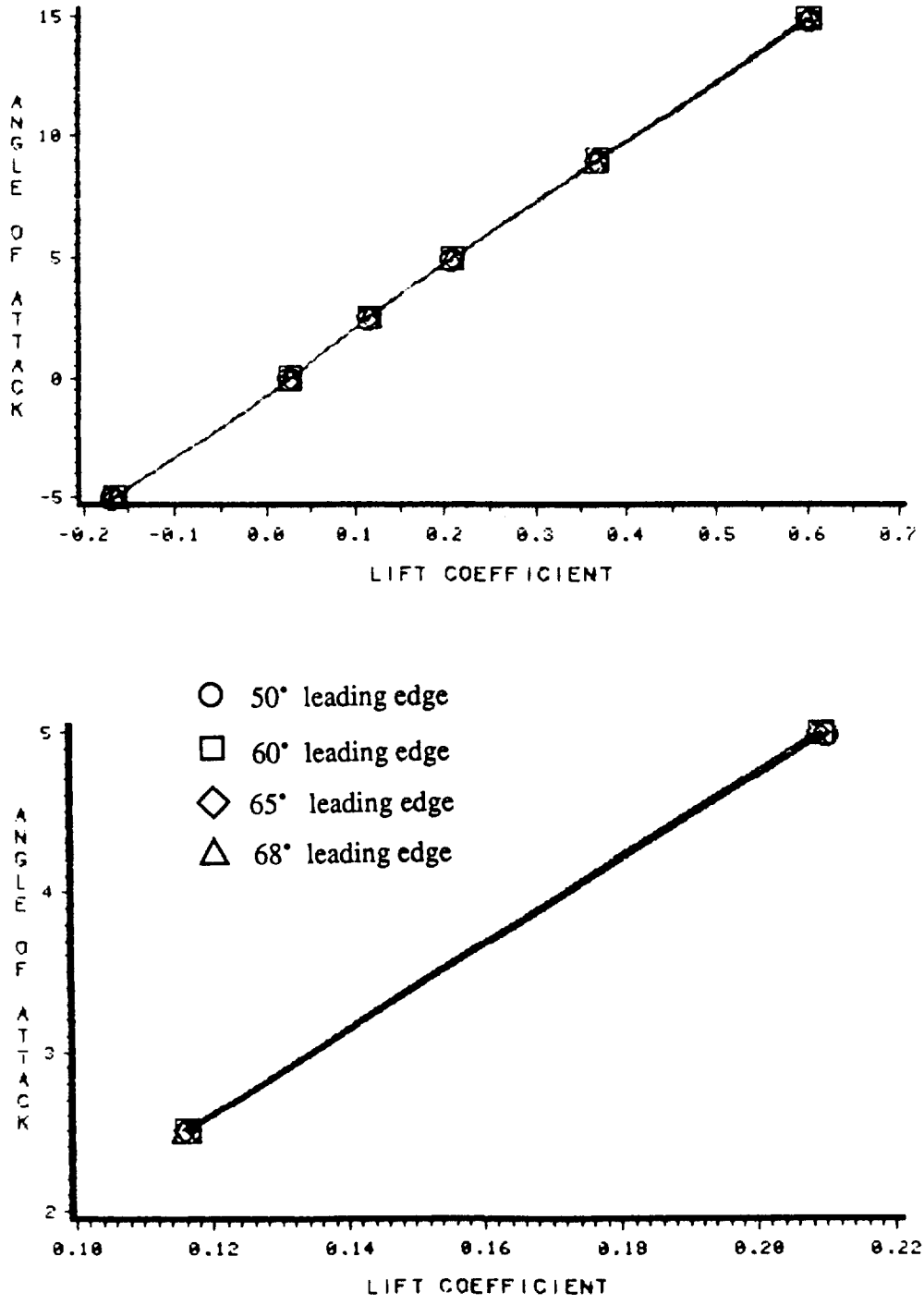

Figure 4.12.1: Predicted performance of the NACA 1402 base wing with 4% thick, 75° anhedral winglets with variable leading edge sweep; M=1.62; angle of attack versus lift coefficient.

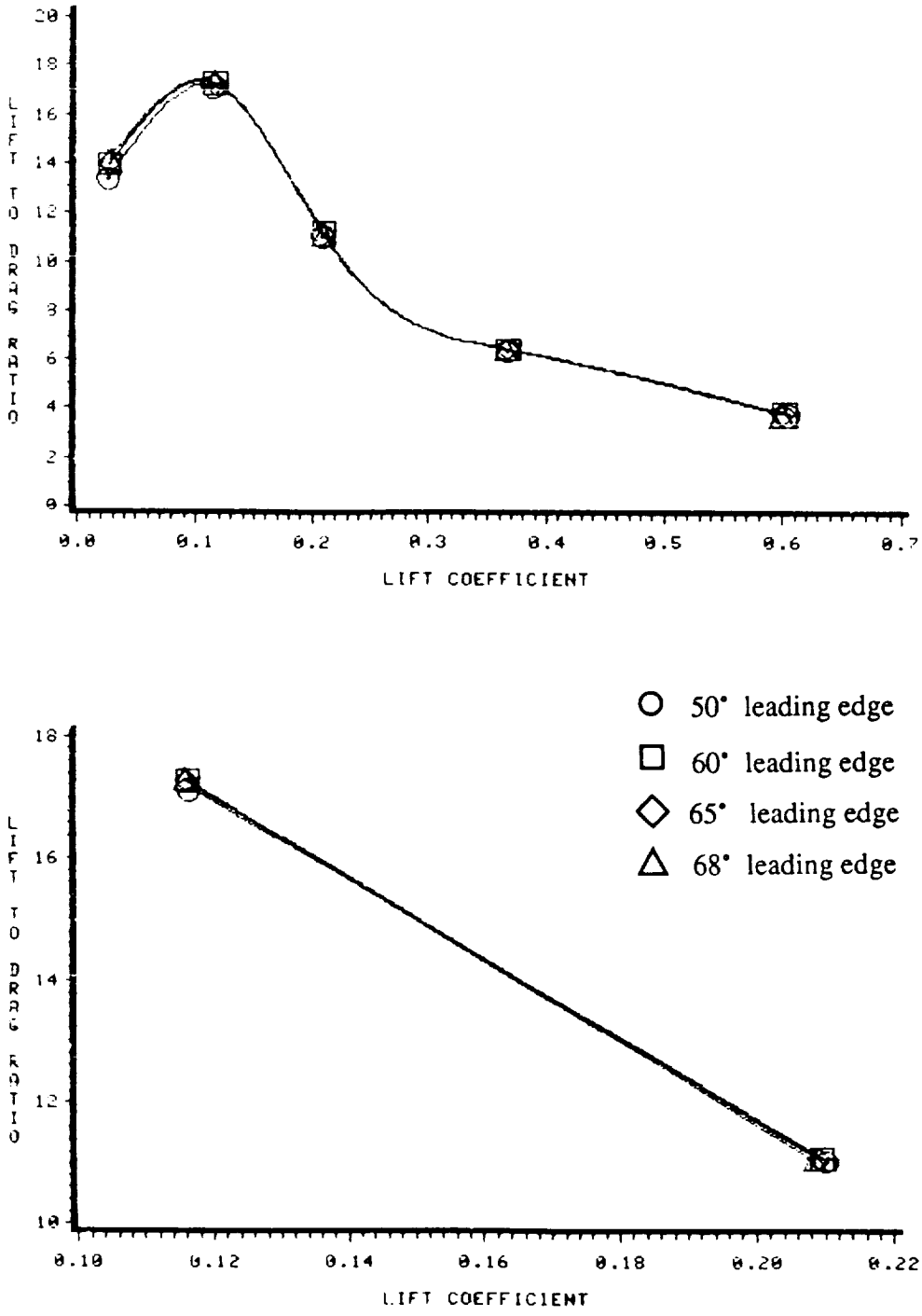

Figure 4.12.2: Predicted performance of the NACA 1402 base wing with 4% thick, 75° anhedral winglets with variable leading edge sweep; M=1.62; lift-to-pressure drag ratio versus lift coefficient.

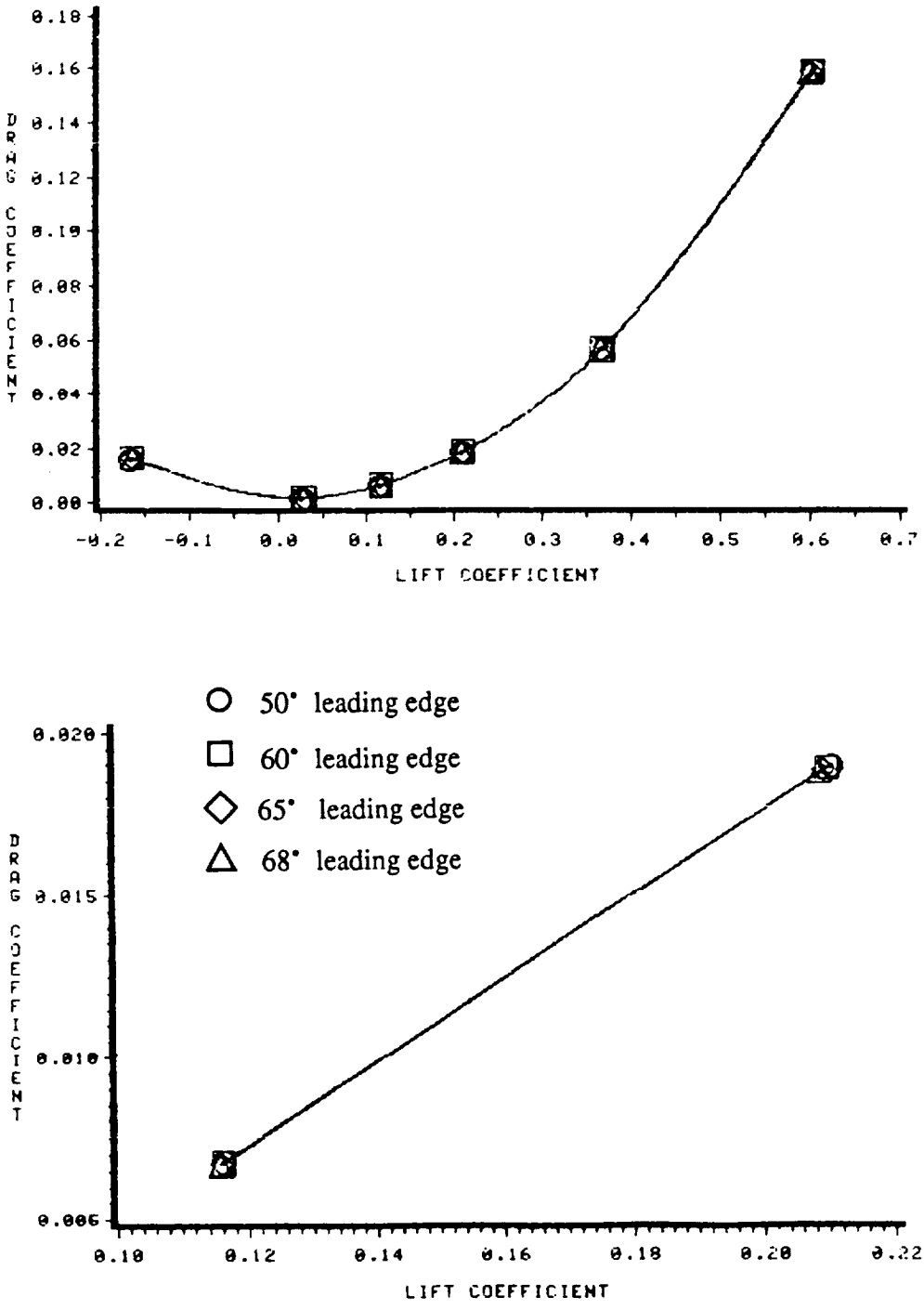

Figure 4.12.3: Predicted performance of the NACA 1402 base wing with 4% thick, 75° anhedral winglets with variable leading edge sweep; M=1.62; pressure drag coefficient versus lift coefficient.

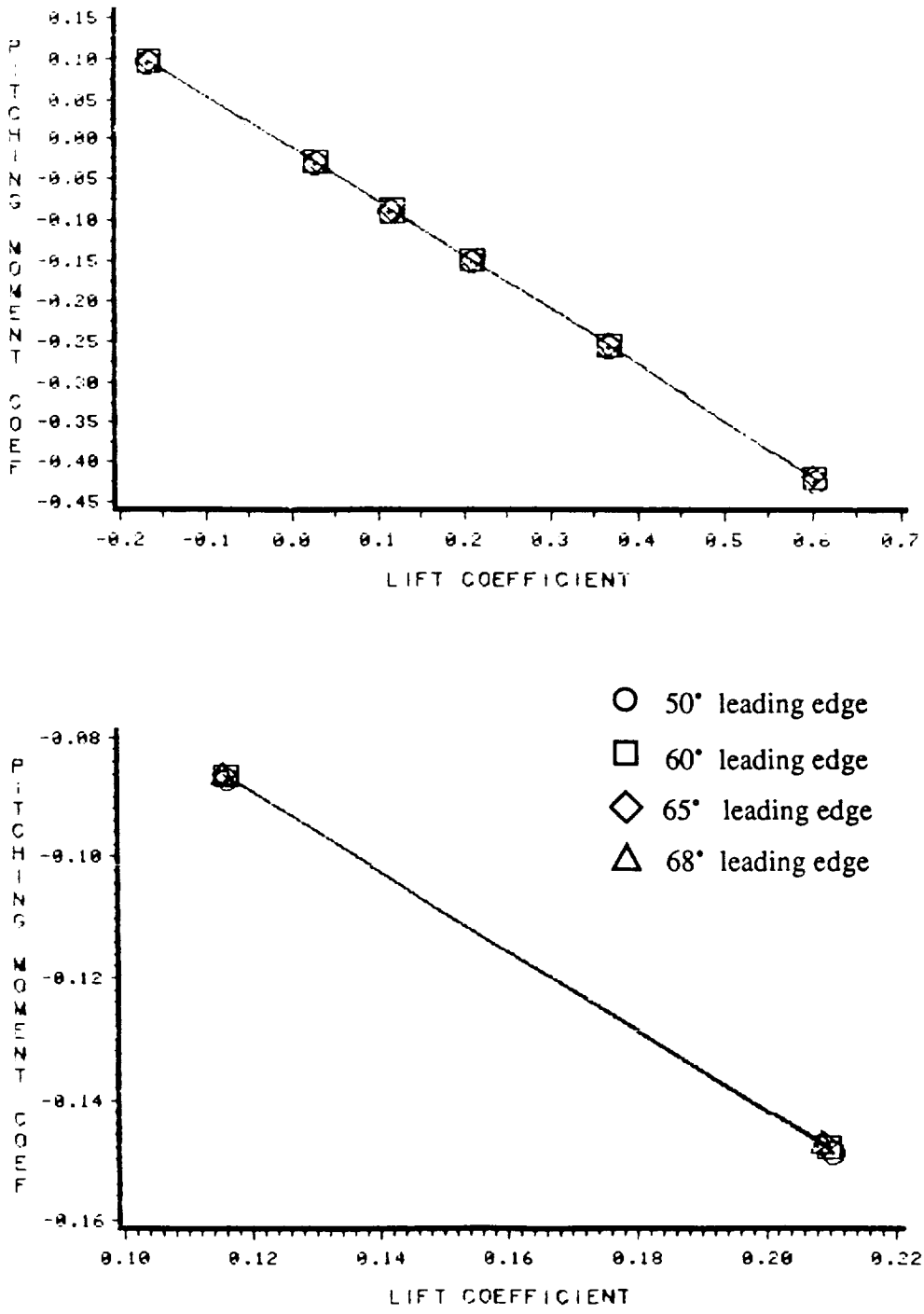

Figure 4.12.4: Predicted performance of the NACA 1402 base wing with 4% thick, 75° anhedral winglets with variable leading edge sweep; M=1.62; pitching moment coefficient versus lift coefficient.

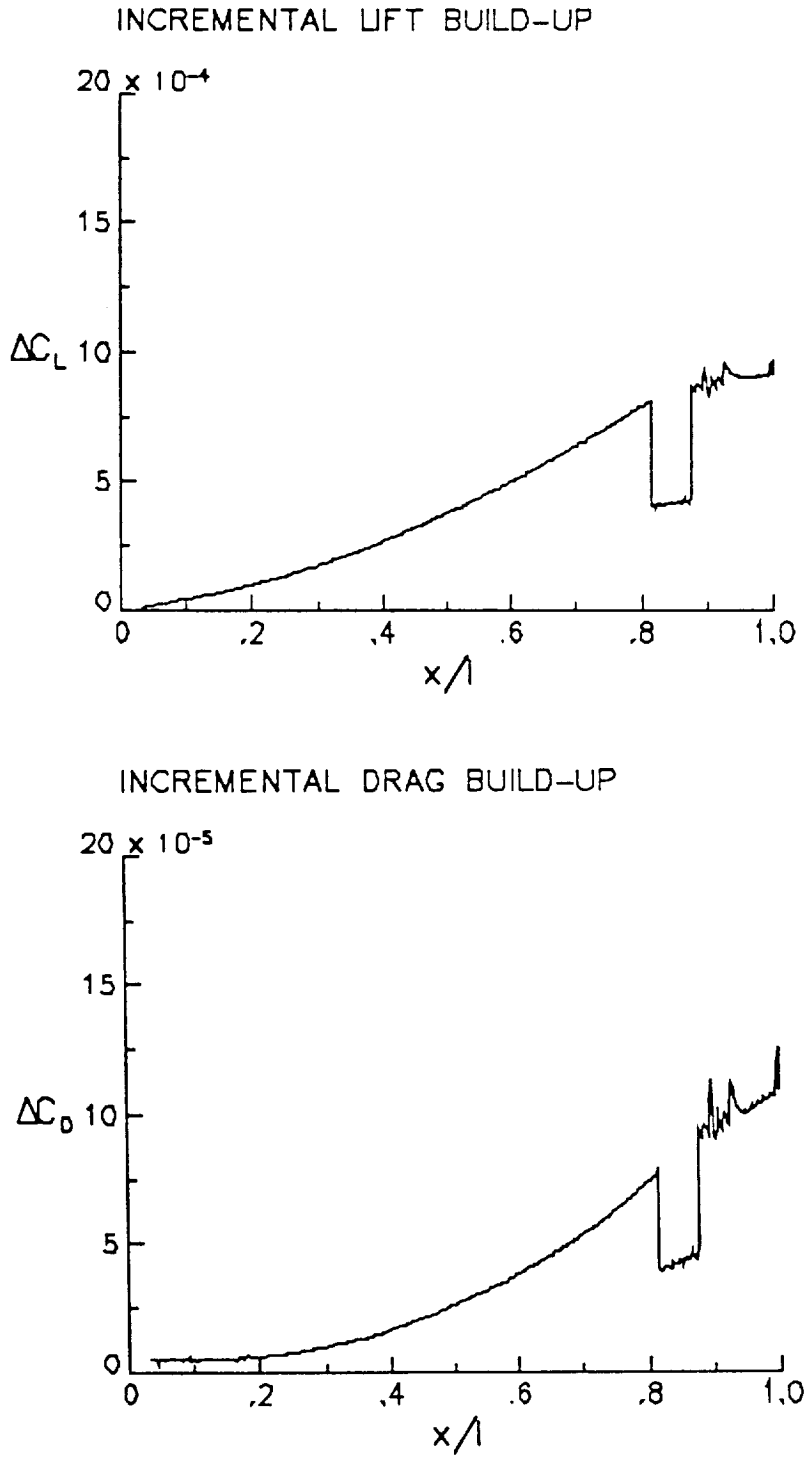

Figure 4.12.5: Incremental lift and pressure drag build up for the NACA 1402 base wing with a 4% thick, 2° toe in, 60° leading edge sweep, 75° anhedral winglet at 5° angle of attack, M=1.62.

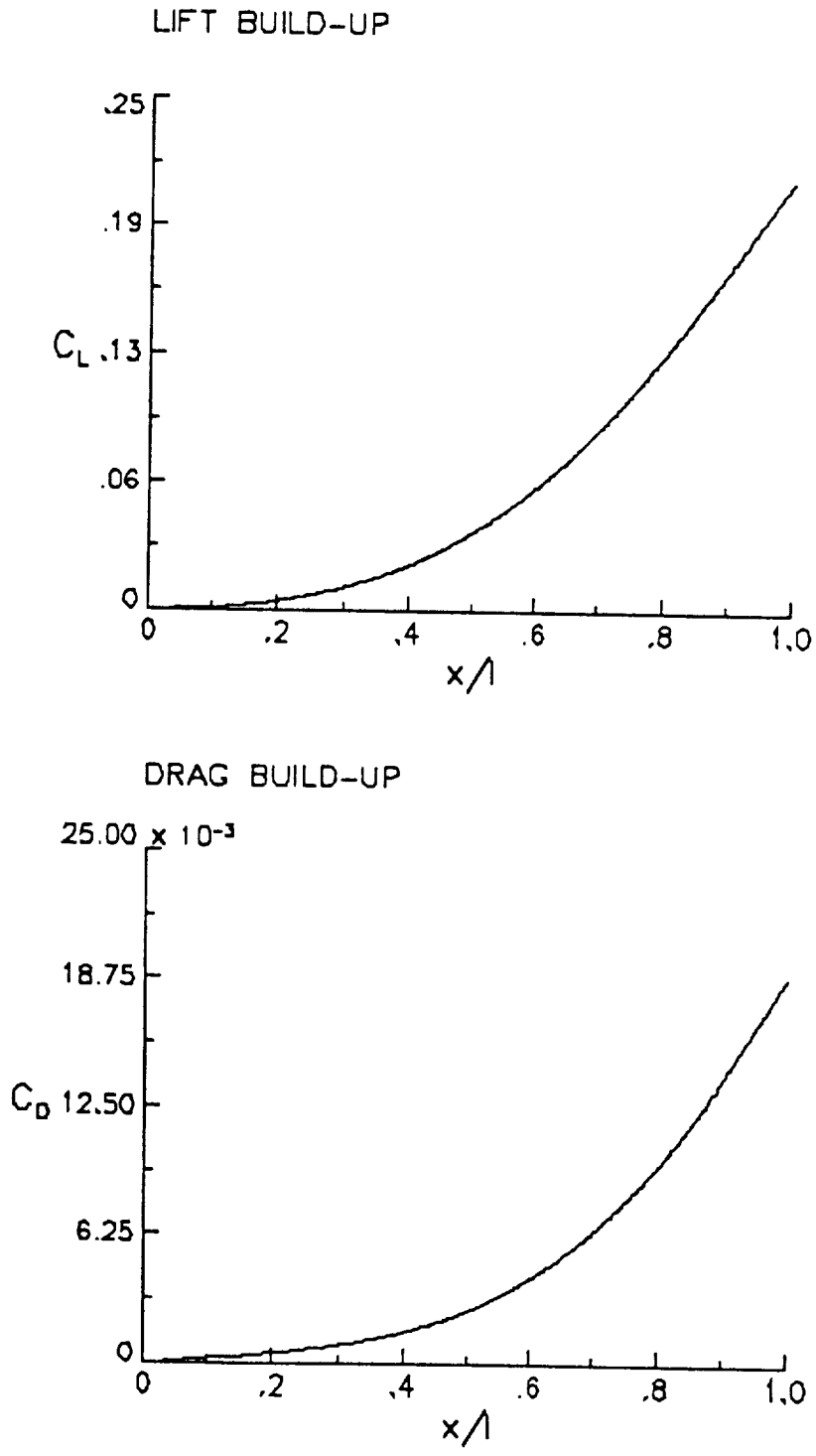

Figure 4.12.6: Total lift and pressure drag build up for the NACA 1402 base wing with a 4% thick, 2° toe in, 60° leading edge sweep, 75° anhedral winglet at 5° angle of attack, M=1.62.

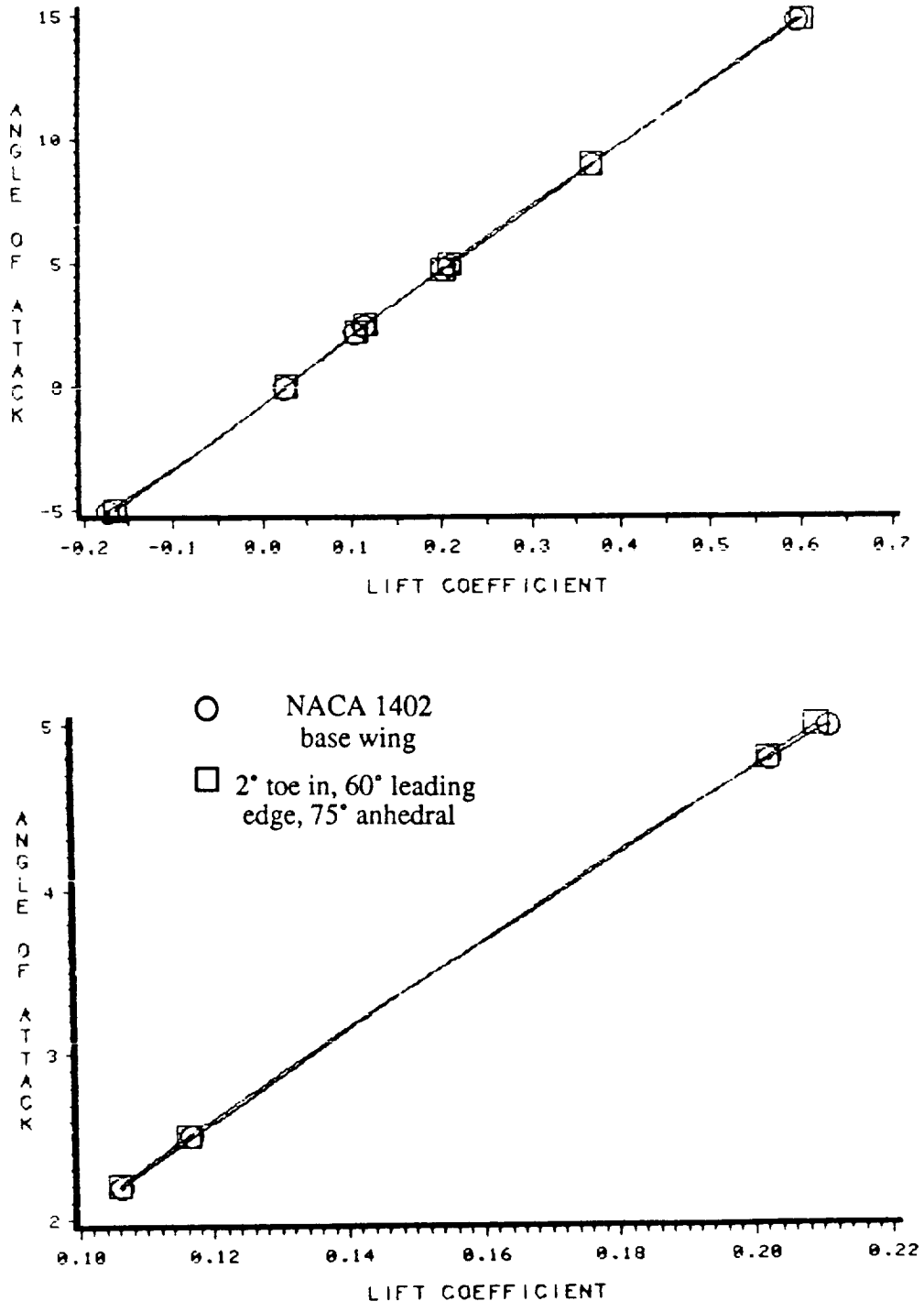

Figure 4.14.1: Comparison of the predicted performance between the NACA 1402 base wing with extension and the 4% thick, 2° toe in, uncambered, 60° leading edge sweep, 75° anhedral wing-winglet; M=1.62; angle of attack versus lift coefficient.

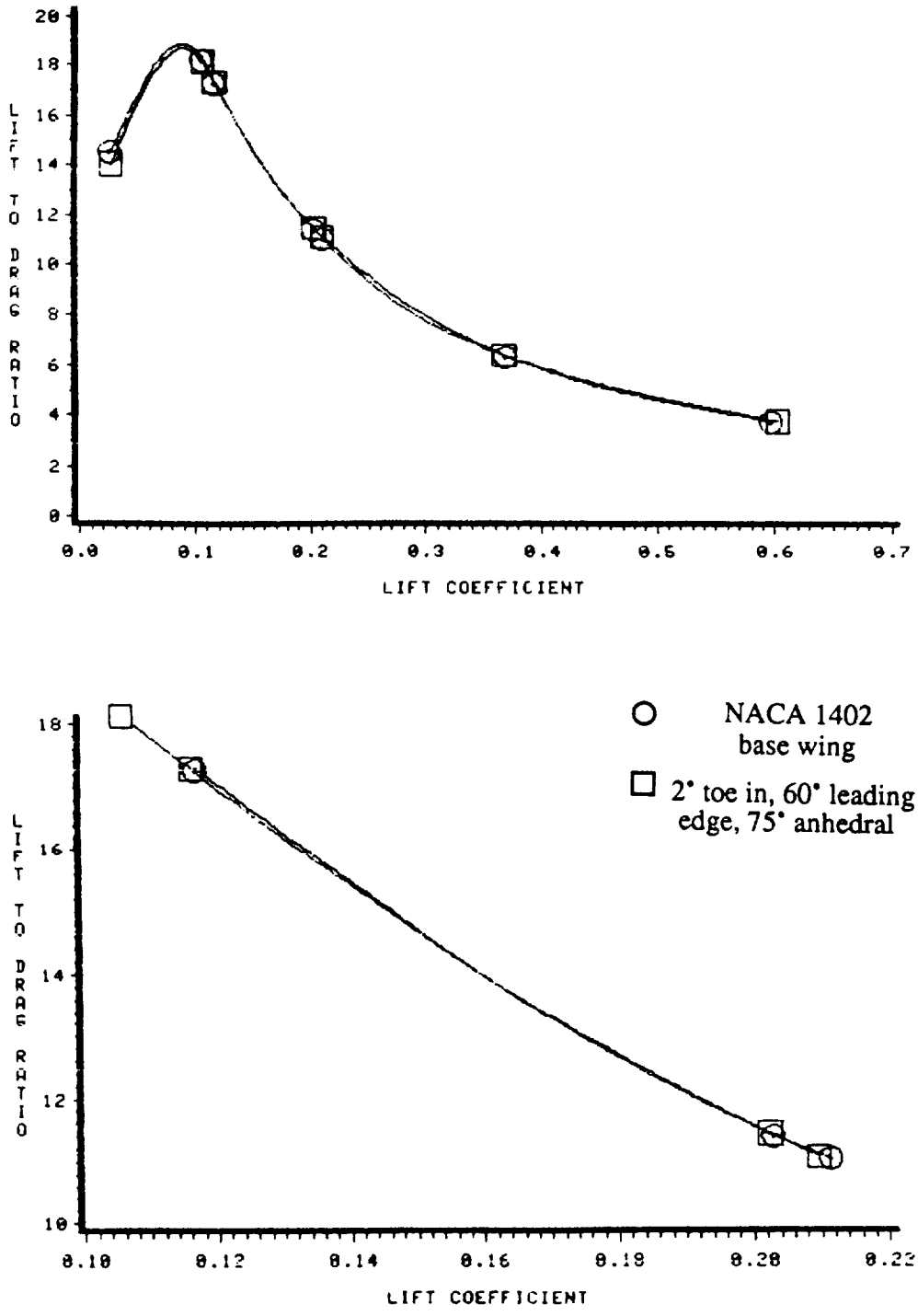

Figure 4.14.2: Comparison of the predicted performance between the NACA 1402 base wing with extension and the 4% thick, 2° toe in, uncambered, 60° leading edge sweep, 75° anhedral wing-winglet; M=1.62; lift-to-pressure drag ratio versus lift coefficient.

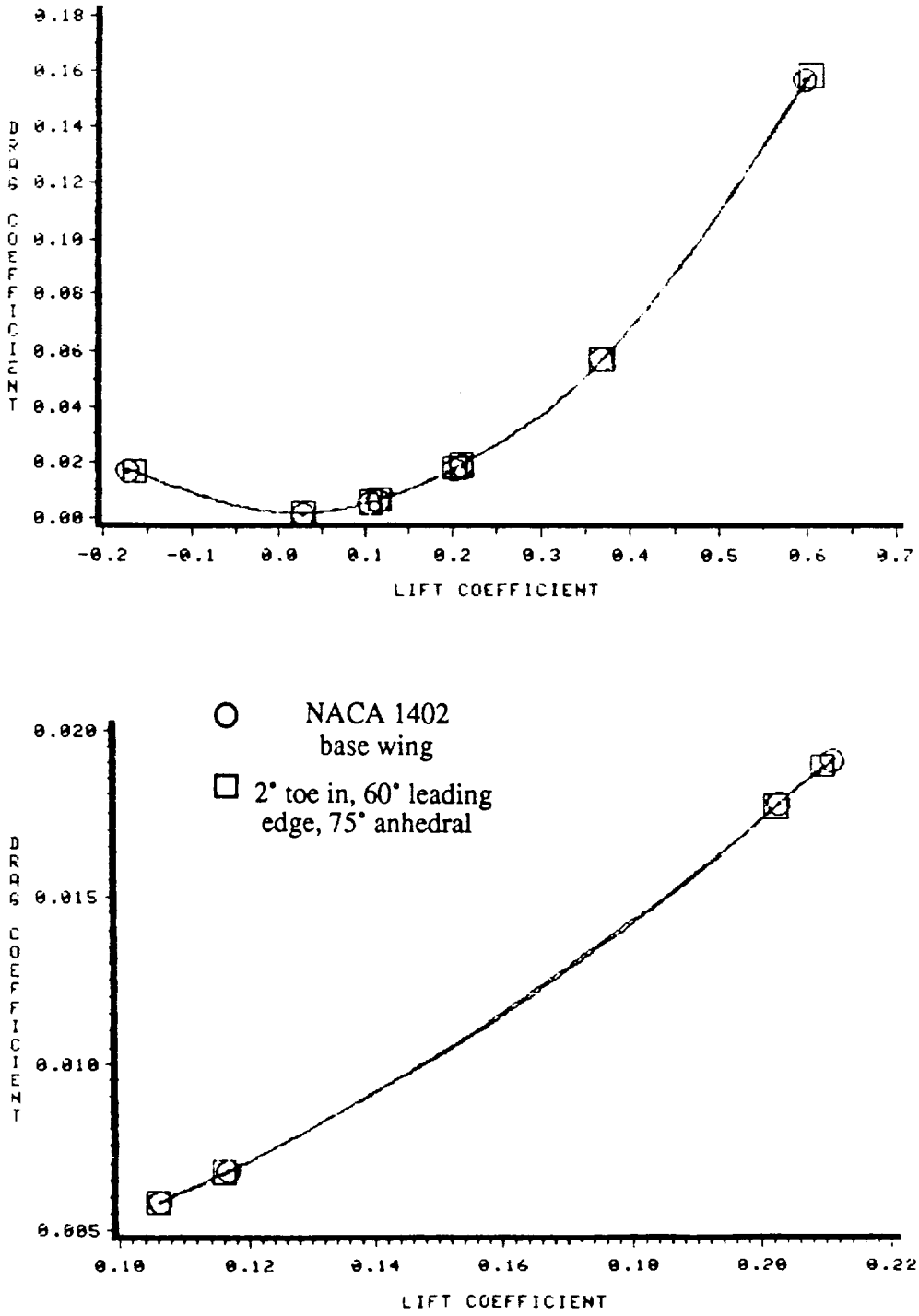

Figure 4.14.3: Comparison of the predicted performance between the NACA 1402 base wing with extension and the 4% thick, 2° toe in, uncambered, 60° leading edge sweep, 75° anhedral wing-winglet; M=1.62; pressure drag coefficient versus lift coefficient.

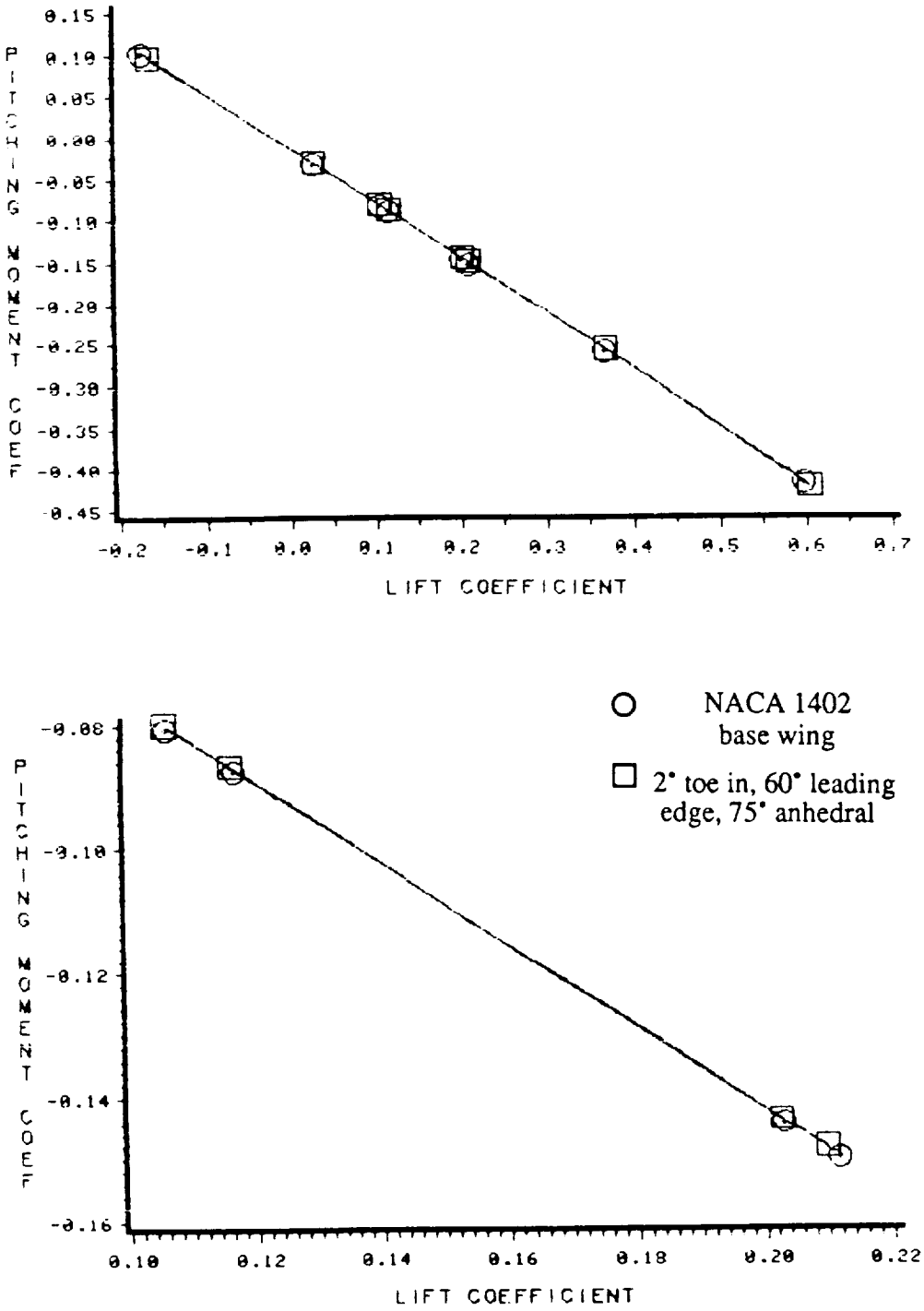

Figure 4.14.4: Comparison of the predicted performance between the NACA 1402 base wing with extension and the 4% thick, 2° toe in, uncambered, 60° leading edge sweep, 75° anhedral wing-winglet; M=1.62; pitching moment coefficient versus lift coefficient.

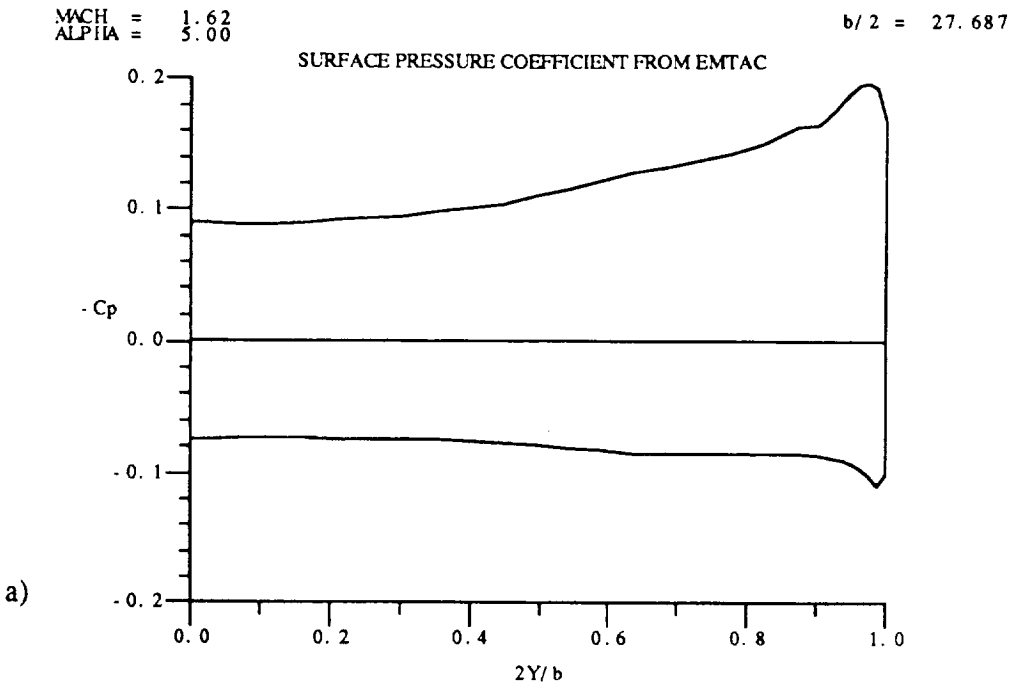

a)

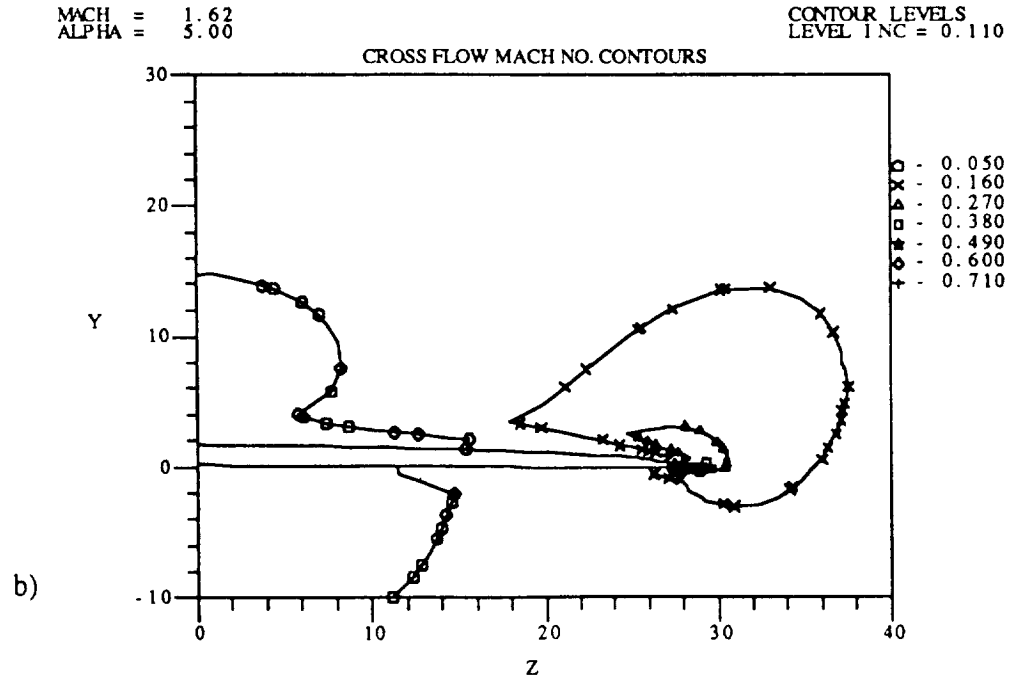

b)

Figure 4.14.5: NACA 1402 base wing at axial location 59.7 units and a 5° angle of attack, M=1.62, a) surface pressure coefficient; b) crossflow Mach number contours; c) static pressure ratio contours and d) enlarged scale static pressure ratio contours.

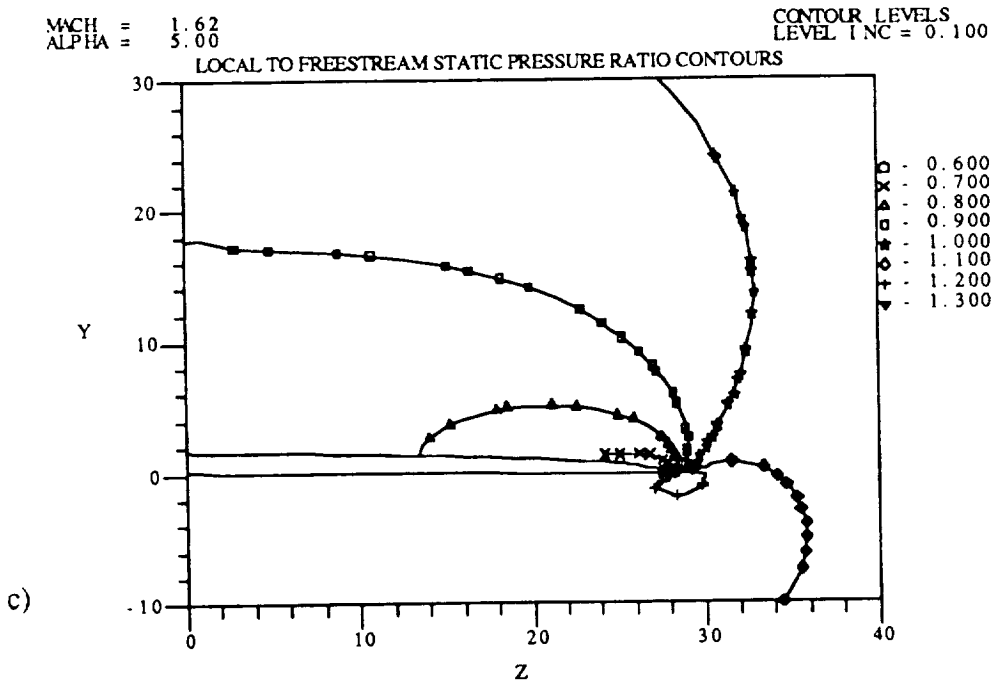

c)

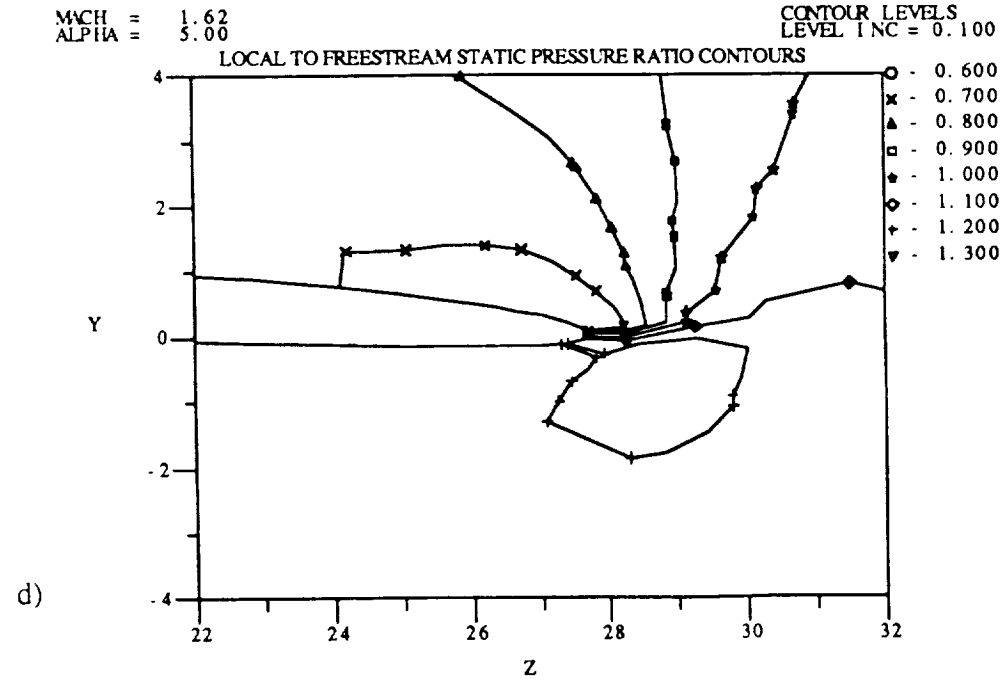

d)

Figure 4.14.5: Continued.

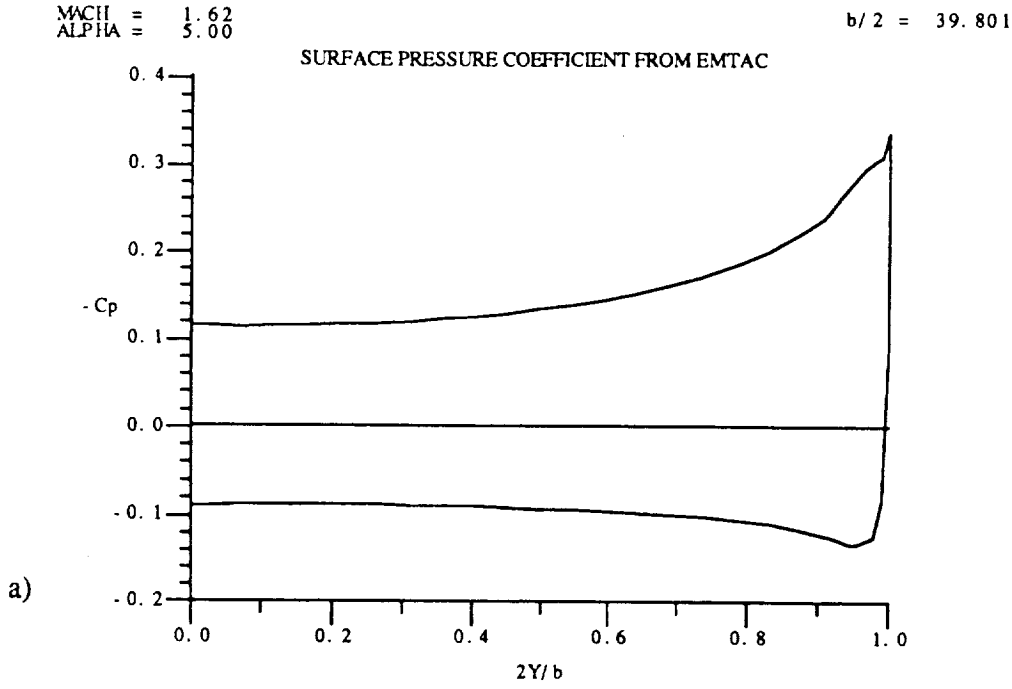

a)

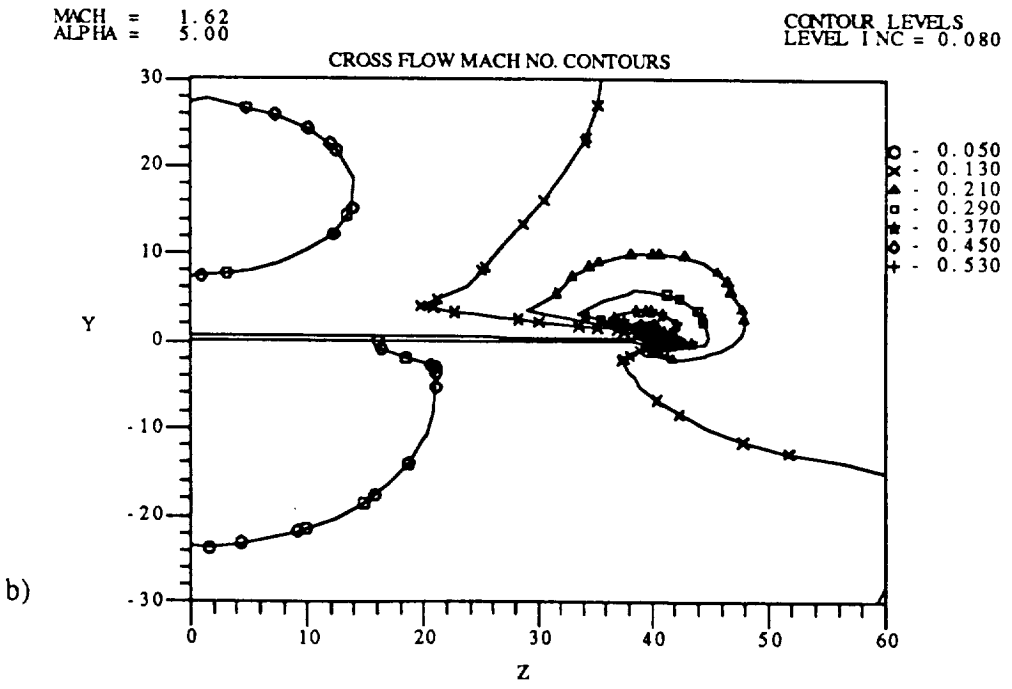

b)

Figure 4.14.6: NACA 1402 base wing at axial location 88.8 units and a 5° angle of attack, M=1.62, a) surface pressure coefficient; b) crossflow Mach number contours; c) static pressure ratio contours and d) enlarged scale static pressure ratio contours.

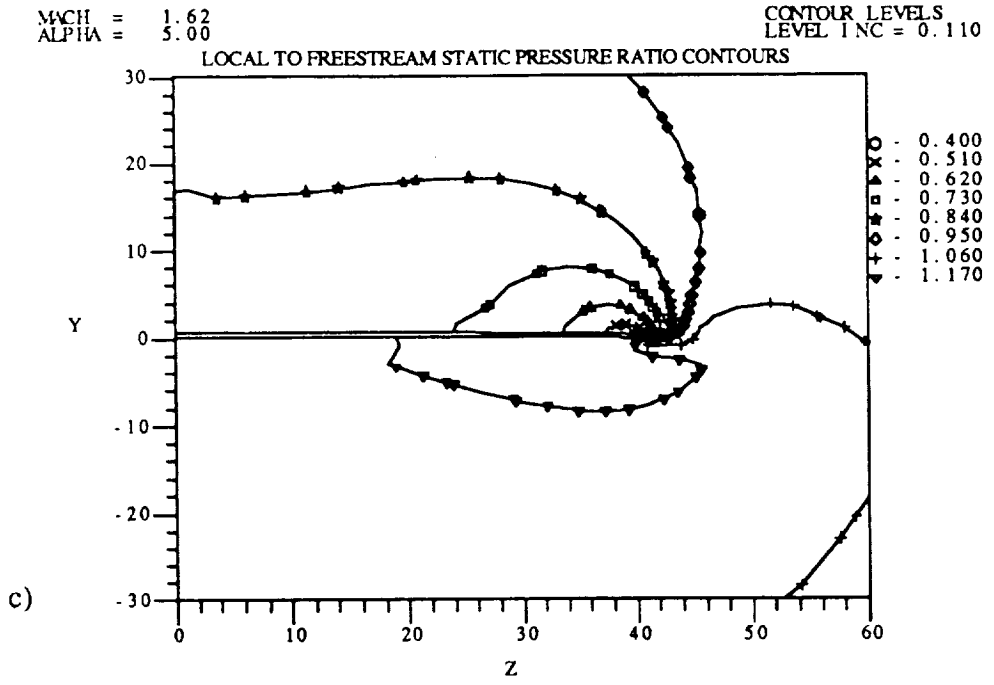

c)

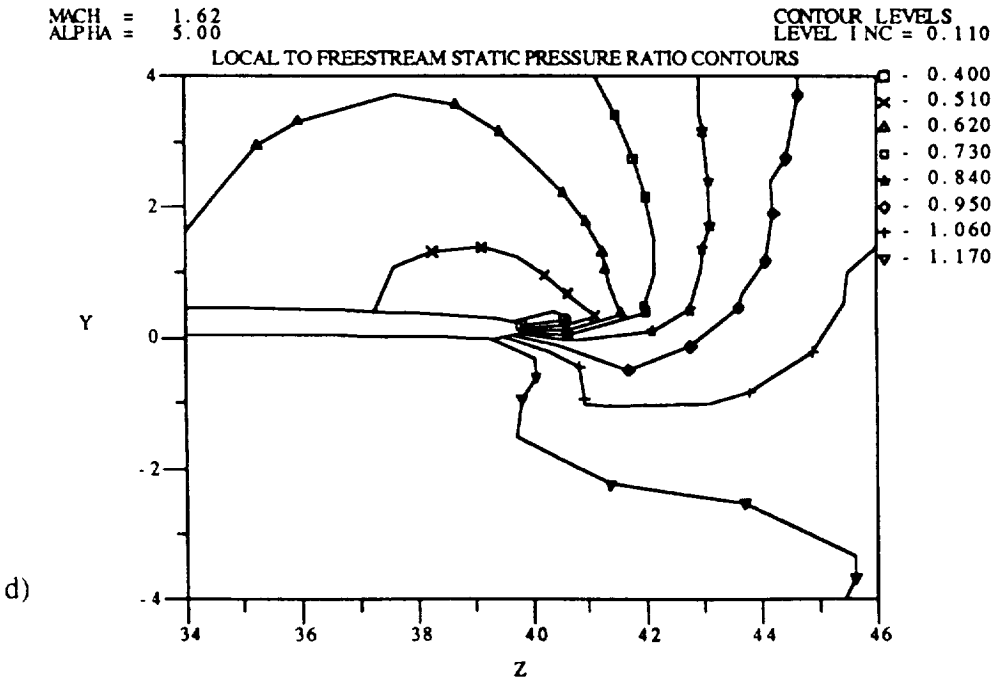

d)

Figure 4.14.6: Continued.

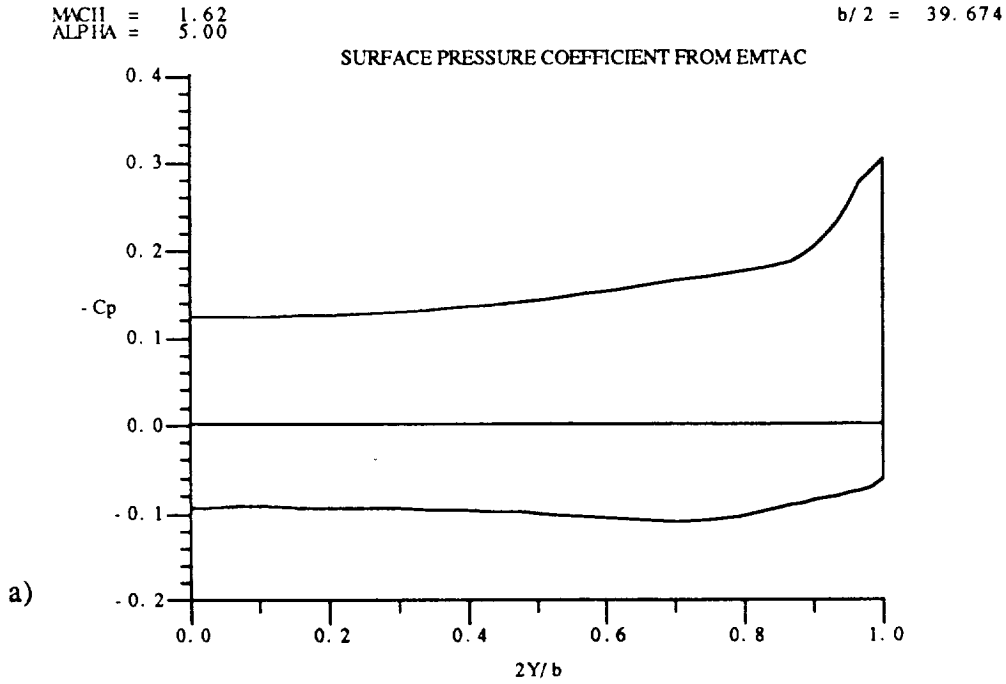

a)

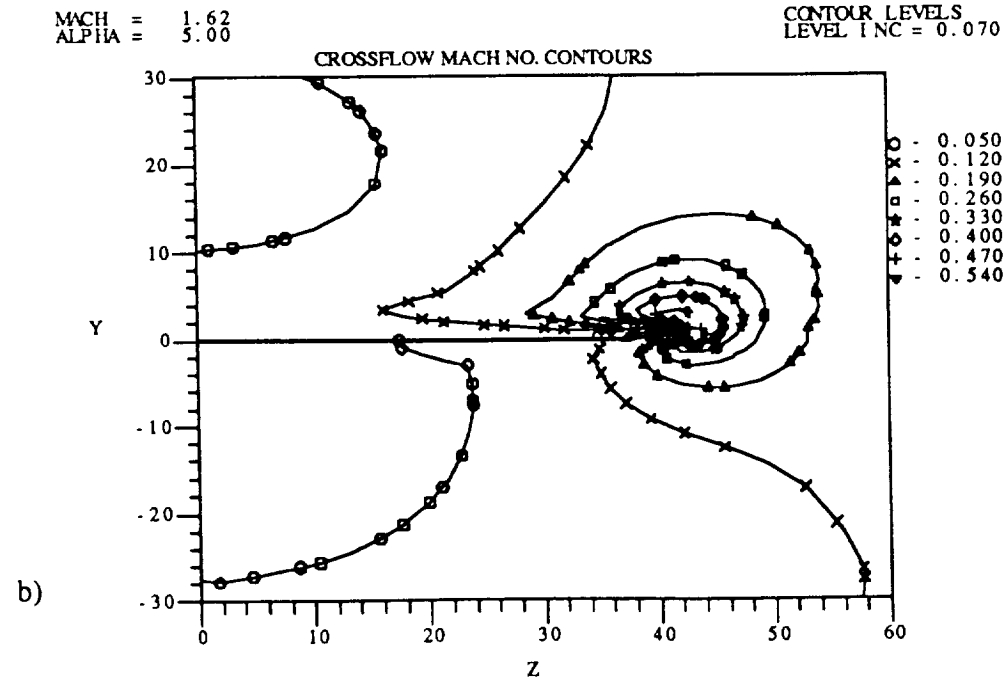

b)

Figure 4.14.7: NACA 1402 base wing at axial location 99.6 units and a 5° angle of attack, M=1.62, a) surface pressure coefficient; b) crossflow Mach number contours; c) static pressure ratio contours and d) enlarged scale static pressure ratio contours.

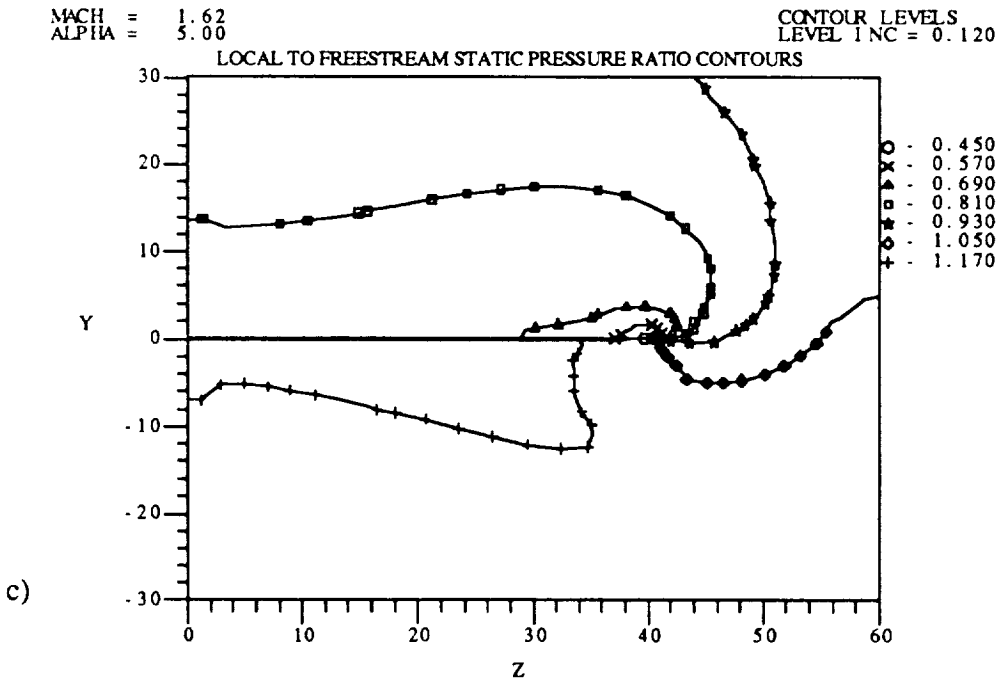

c)

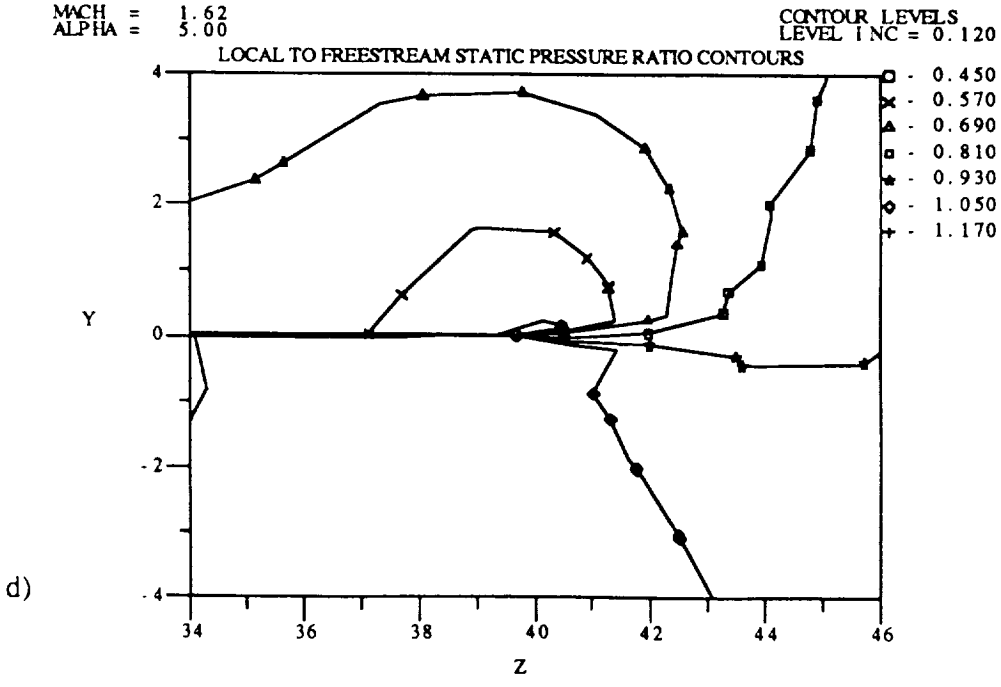

d)

Figure 4.14.7: Continued.

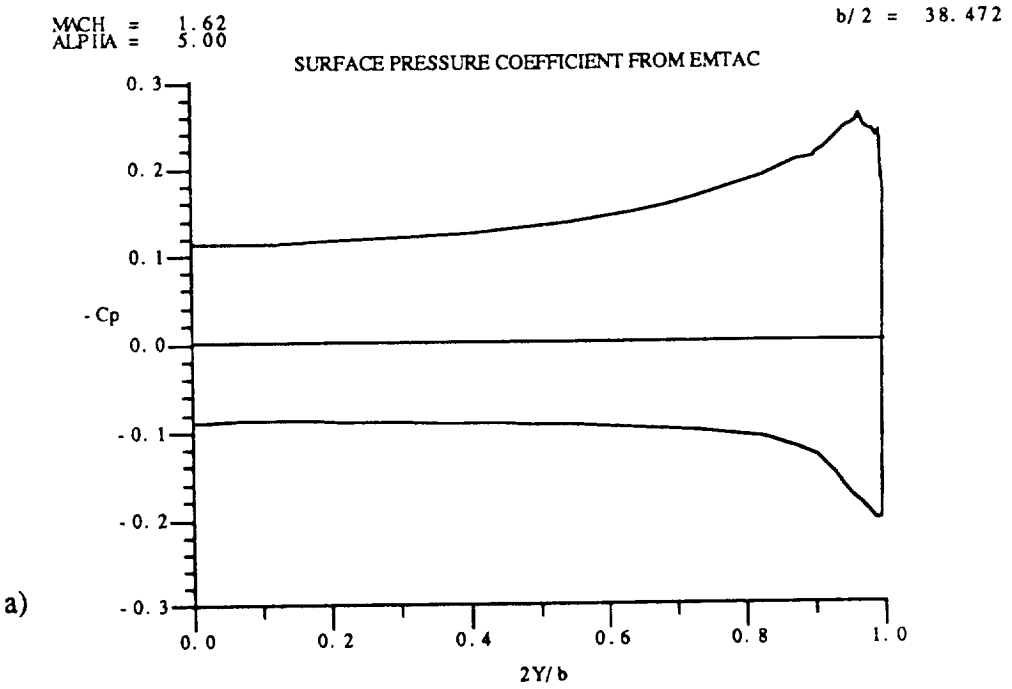

a)

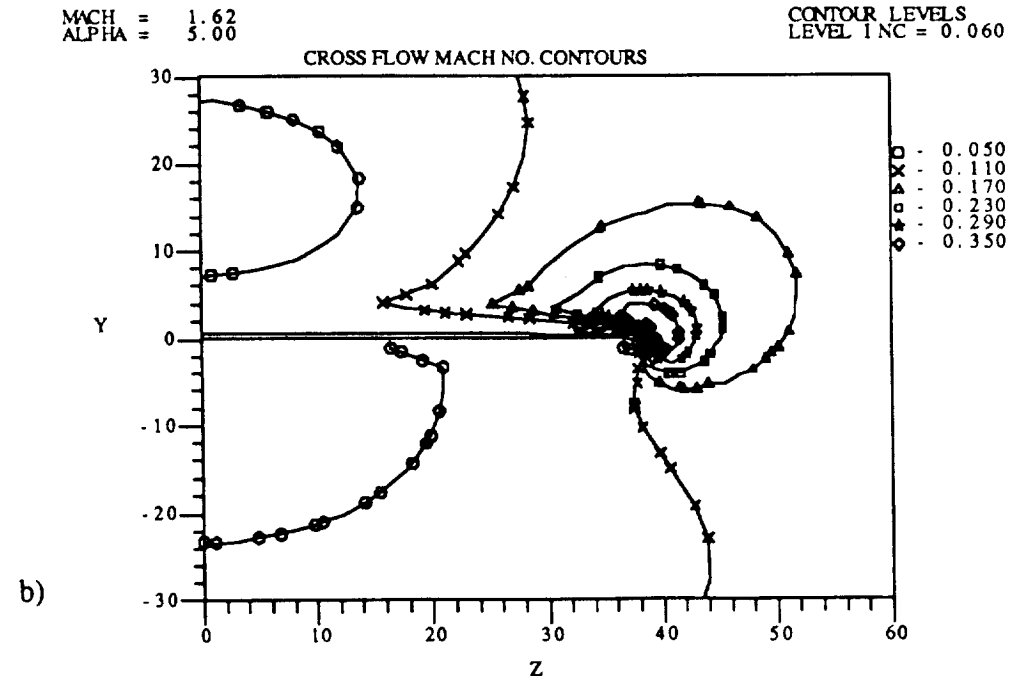

b)

Figure 4.14.8: NACA 1402 base wing-winglet at axial location 88.2 units and a 5° angle of attack, M=1.62, a) surface pressure coefficient; b) crossflow Mach number contours; c) static pressure ratio contours and d) enlarged scale static pressure ratio contours.

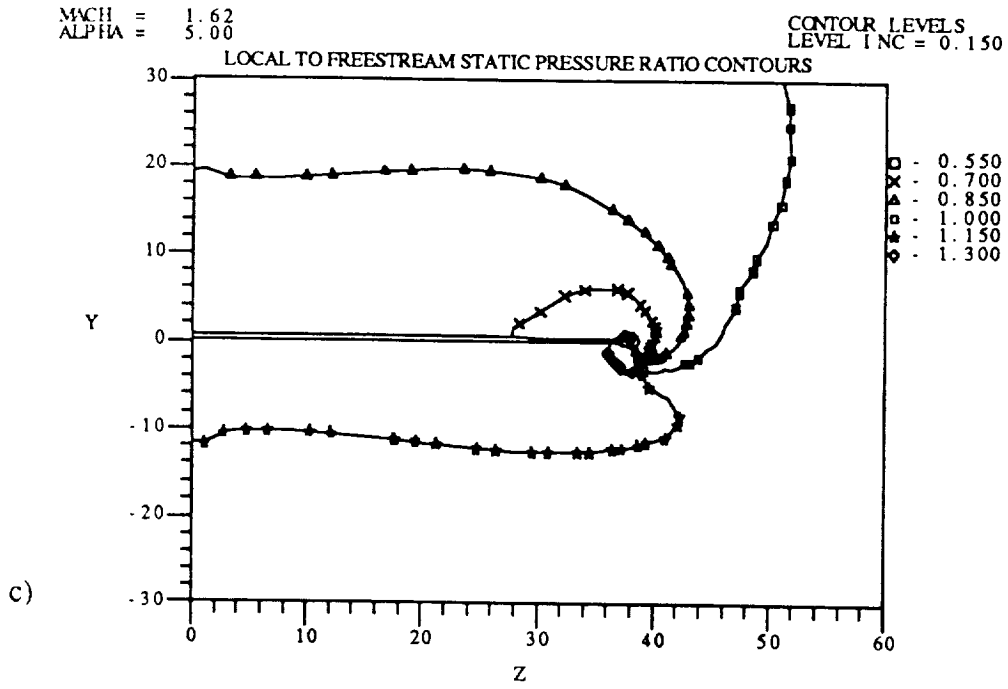

c)

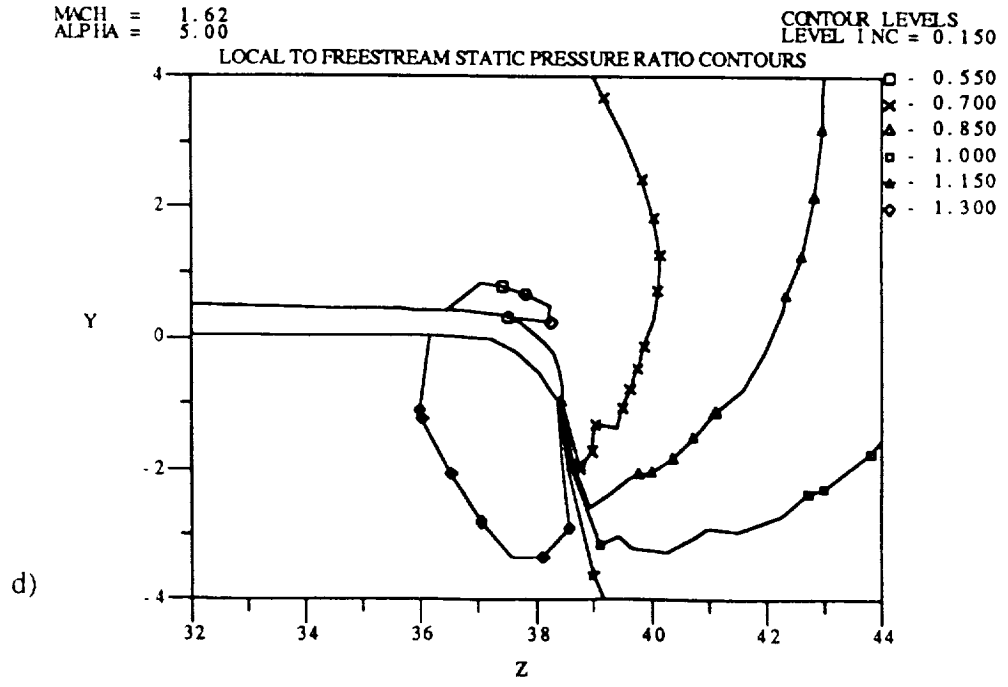

d)

Figure 4.14.8: Continued.

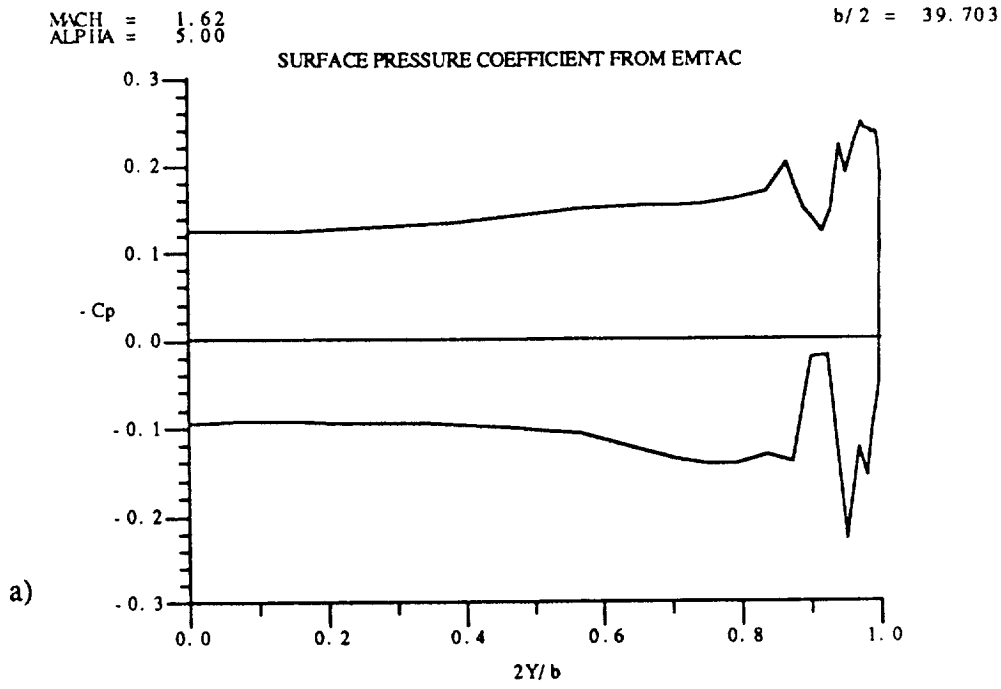

a)

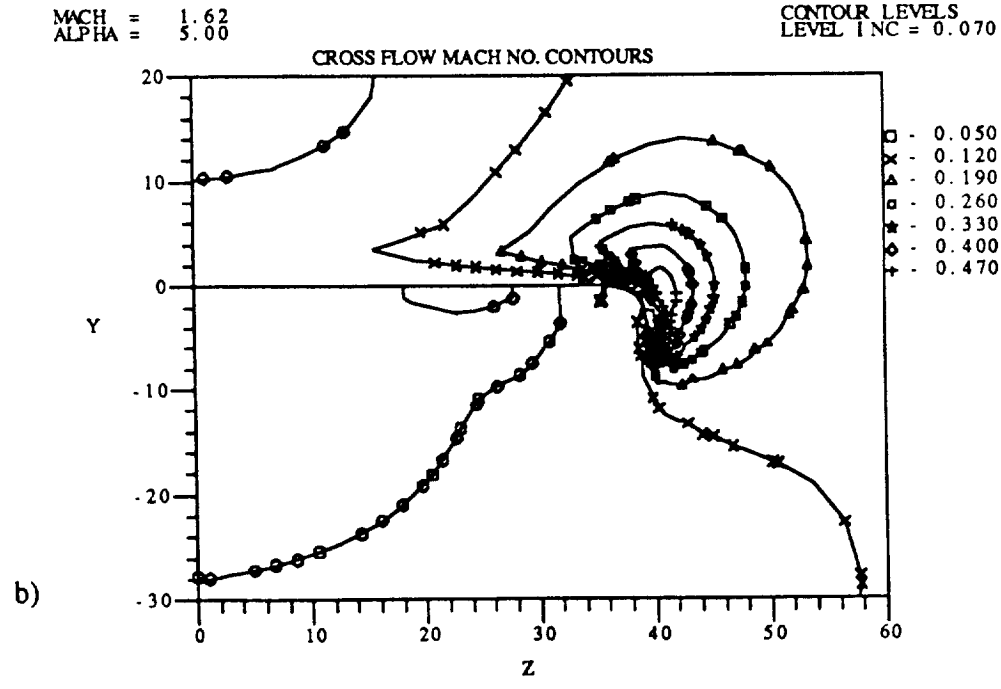

b)

Figure 4.14.9: NACA 1402 base wing-winglet at axial location 99.6 units and a 5° angle of attack, M=1.62, a) surface pressure coefficient; b) crossflow Mach number contours; c) static pressure ratio contours and d) enlarged scale static pressure ratio contours.

c)

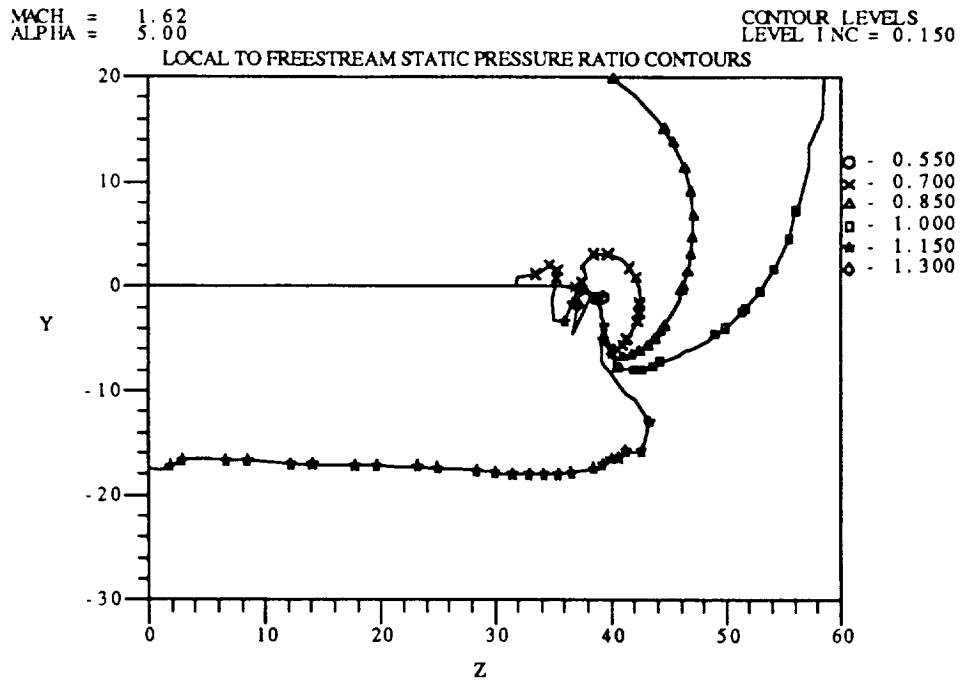

d)

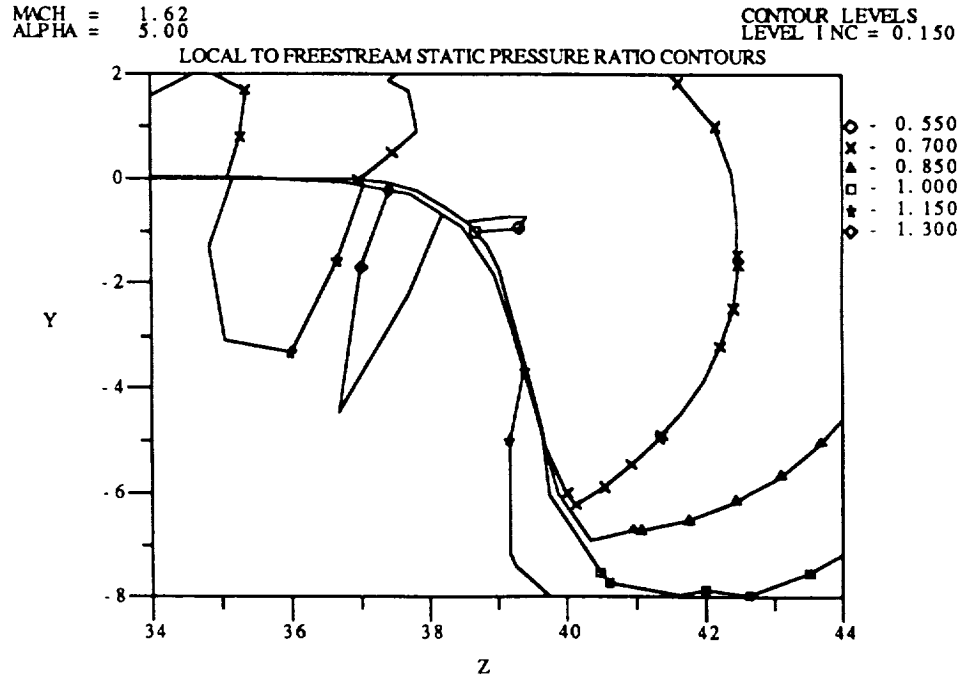

Figure 4.14.9: Continued.

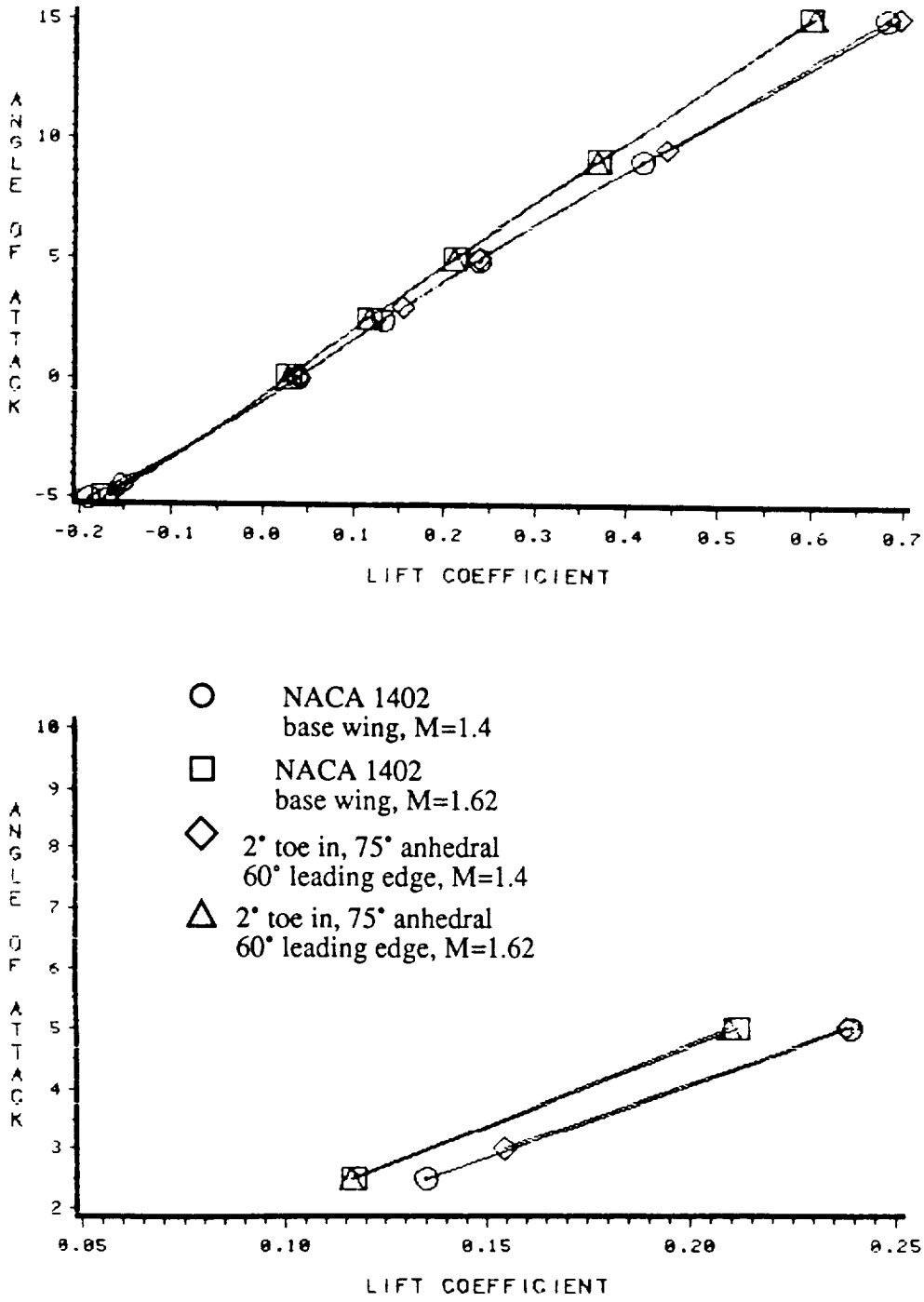

Figure 4.14.10: Predicted performance comparison between the NACA 1402 base wing with extension and the base wing with a 4% thick, 2° toe in, uncambered, 60° leading edge sweep, 75° anhedral winglet for various Mach numbers; M=1.40, 1.62; angle of attack versus lift coefficient.

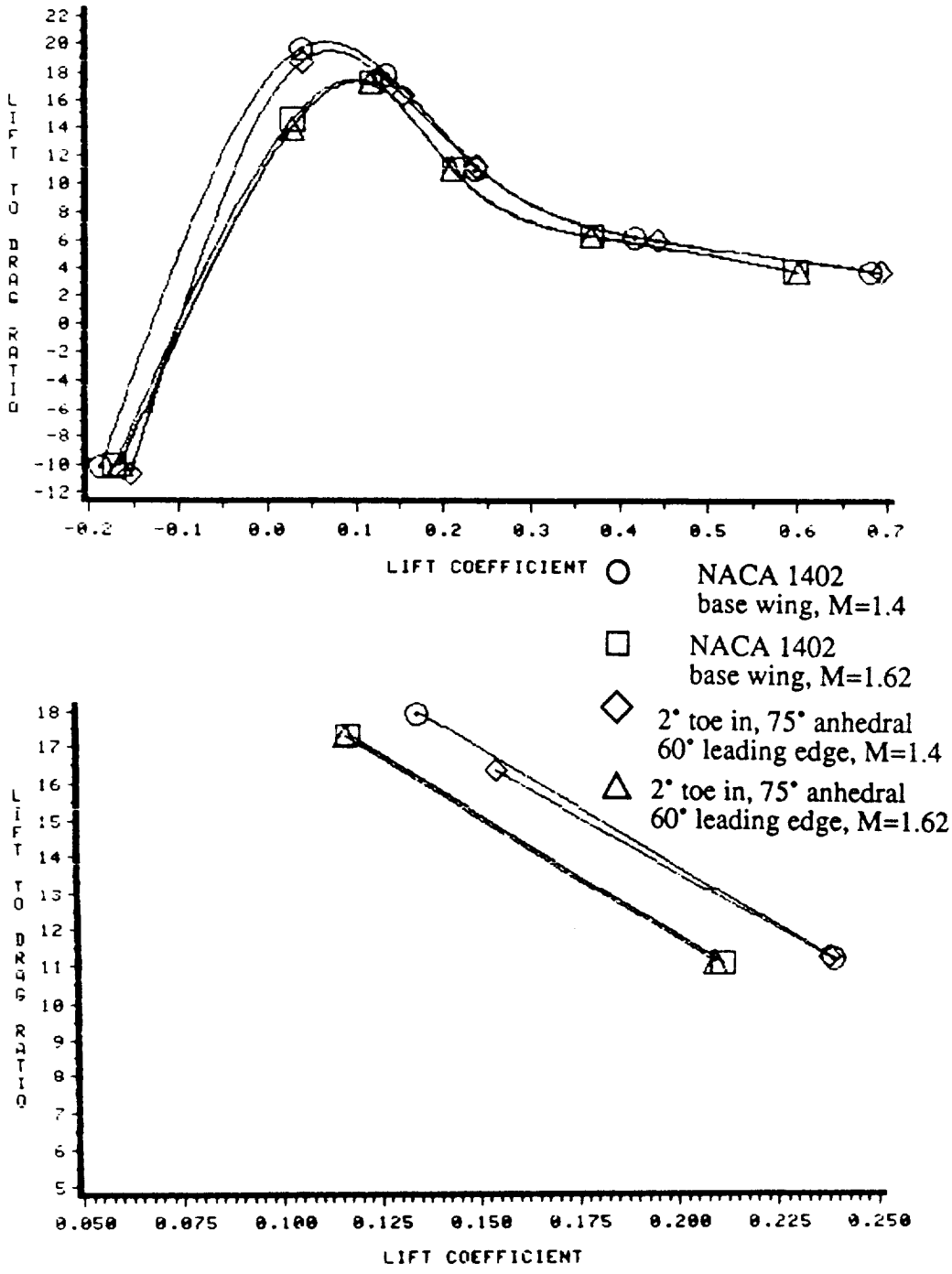

Figure 4.14.11: Predicted performance comparison between the NACA 1402 base wing with extension and the base wing with a 4% thick, 2° toe in, uncambered, 60° leading edge sweep, 75° anhedral winglet for various Mach numbers; M=1.40, 1.62; lift-to-pressure drag ratio versus lift coefficient.

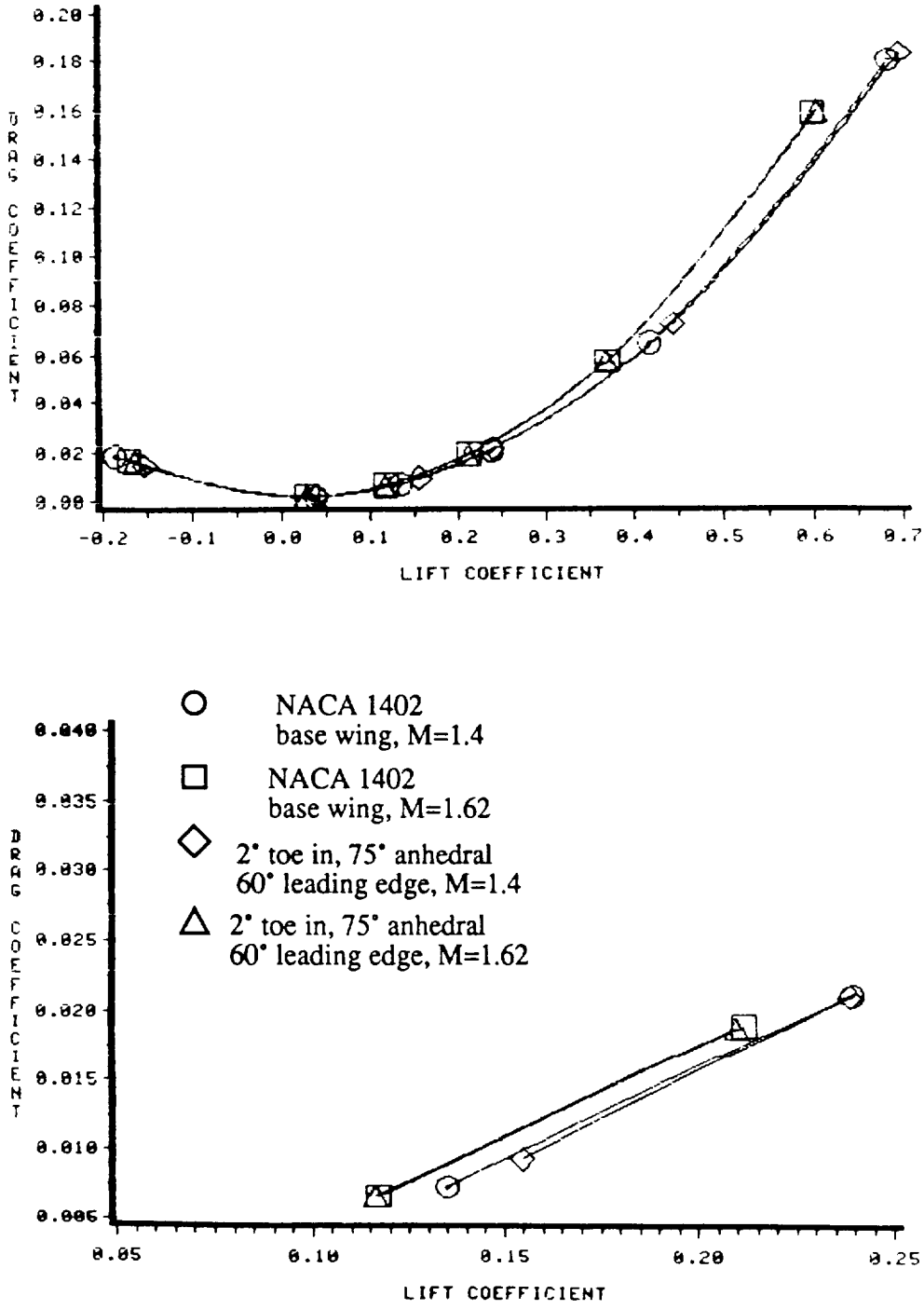

Figure 4.14.12: Predicted performance comparison between the NACA 1402 base wing with extension and the base wing with a 4% thick, 2° toe in, uncambered, 60° leading edge sweep, 75° anhedral winglet for various Mach numbers; M=1.40, 1.62; pressure drag coefficient versus lift coefficient.

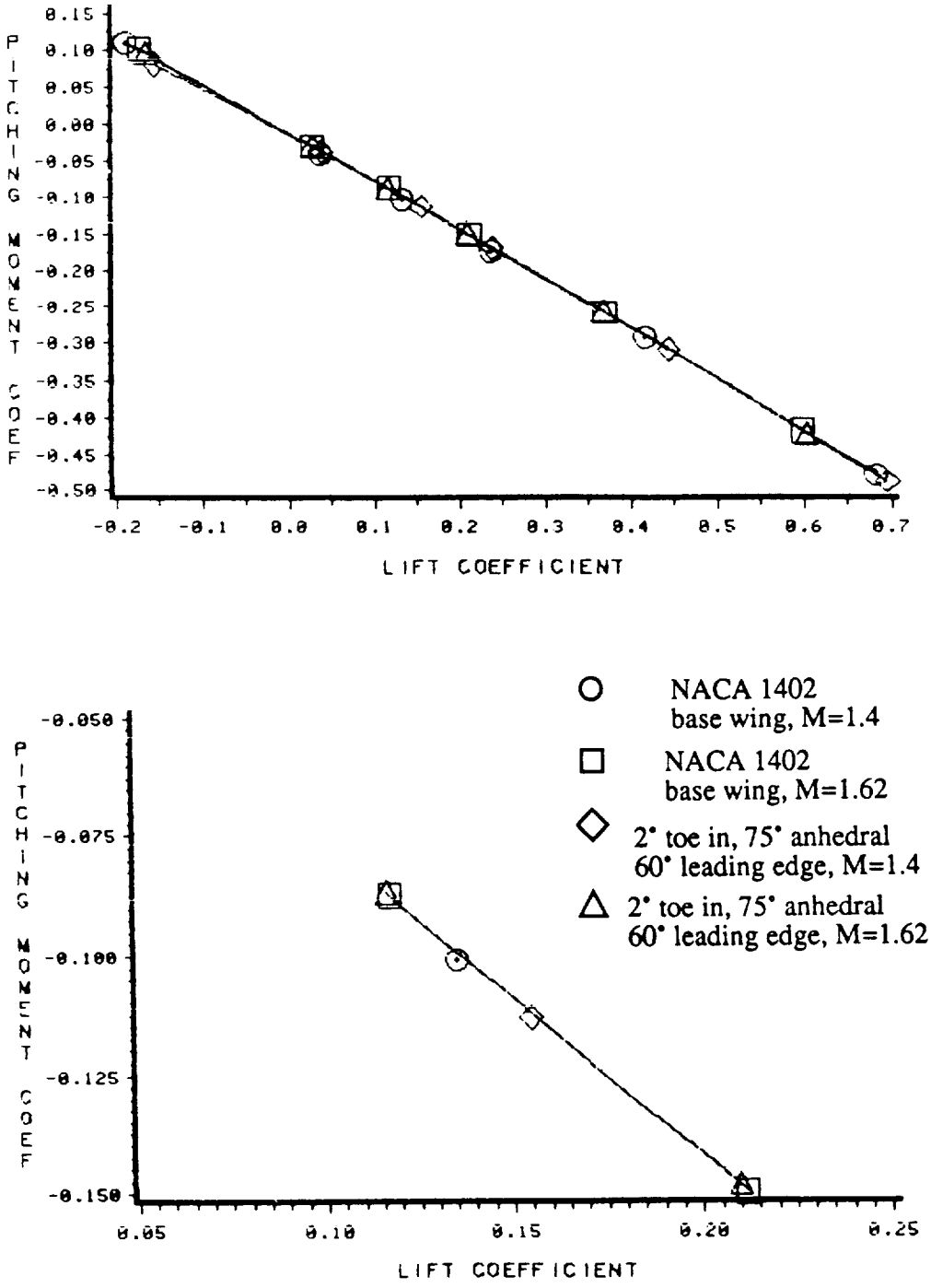

Figure 4.14.13: Predicted performance comparison between the NACA 1402 base wing with extension and the base wing with a 4% thick, 2° toe in, uncambered, 60° leading edge sweep, 75° anhedral winglet for various Mach numbers; M=1.40, 1.62; pitching moment coefficient versus lift coefficient.

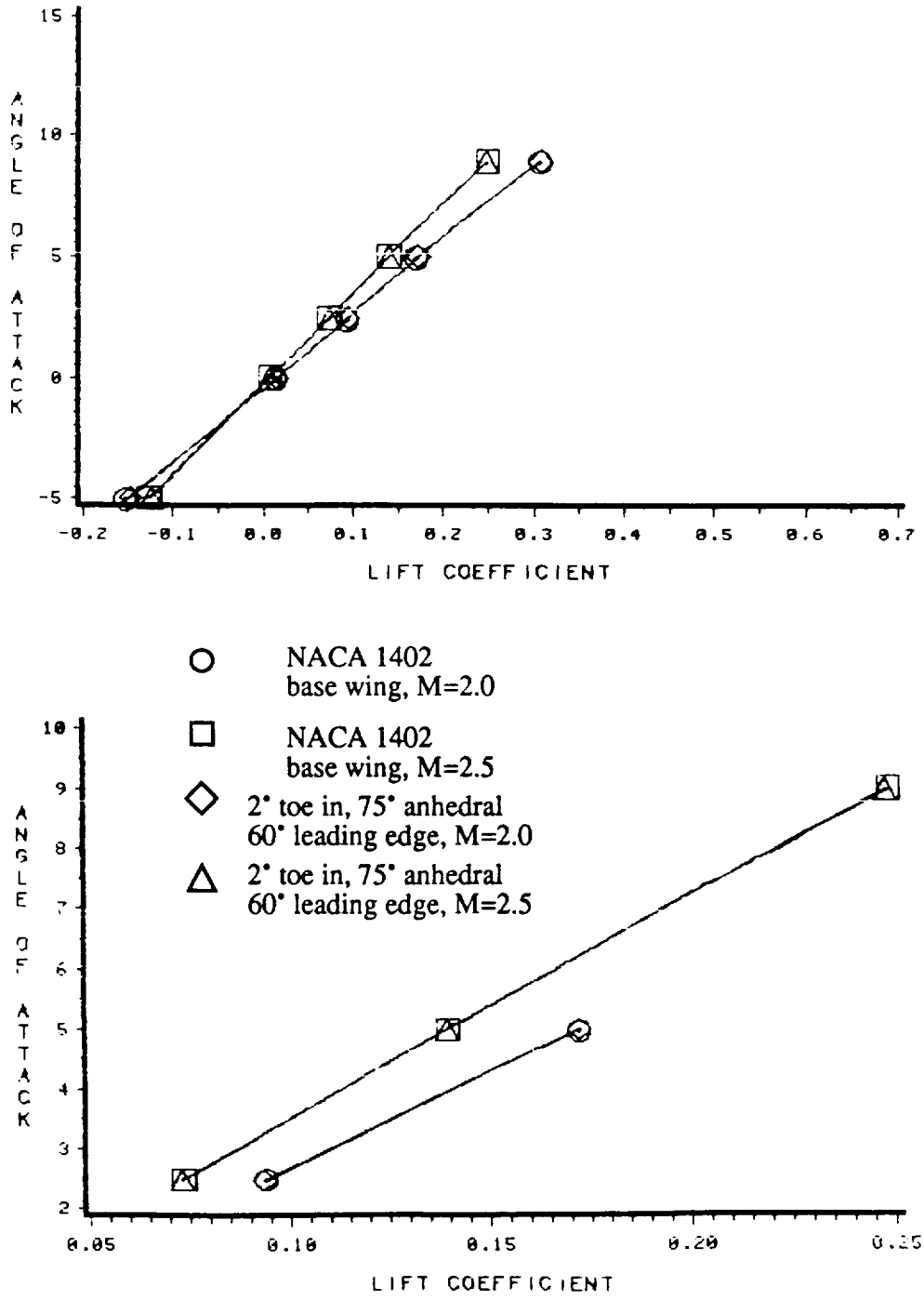

Figure 4.14.14: Predicted performance comparison between the NACA 1402 base wing with extension and the base wing with a 4% thick, 2° toe in, uncambered, 60° leading edge sweep, 75° anhedral winglet for various Mach numbers; M=2.0, 2.5; angle of attack versus lift coefficient.

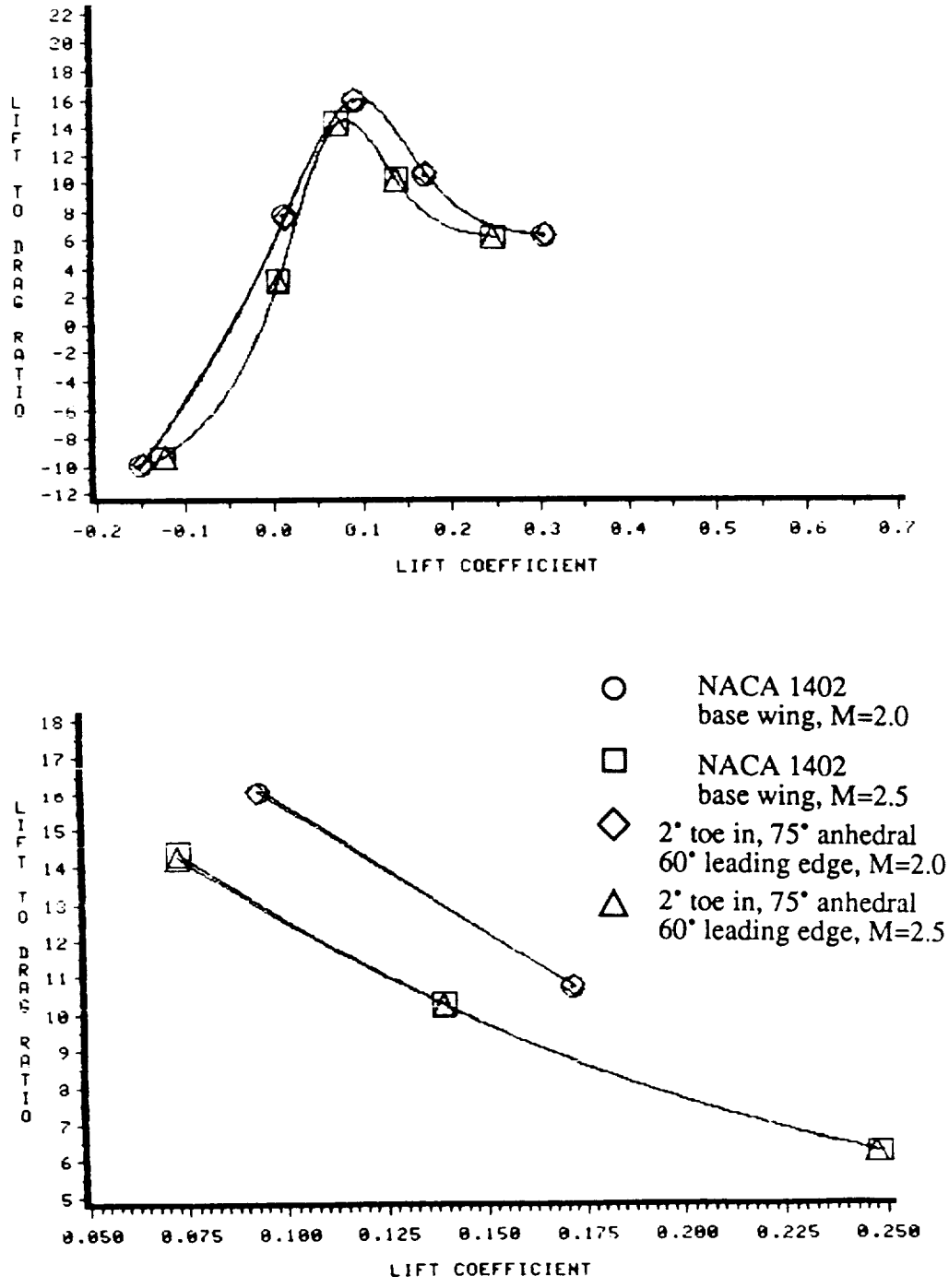

Figure 4.14.15: Predicted performance comparison between the NACA 1402 base wing with extension and the base wing with a 4% thick, 2° toe in, uncambered, 60° leading edge sweep, 75° anhedral winglet for various Mach numbers; M=2.0, 2.5; lift-to-pressure drag ratio versus lift coefficient.

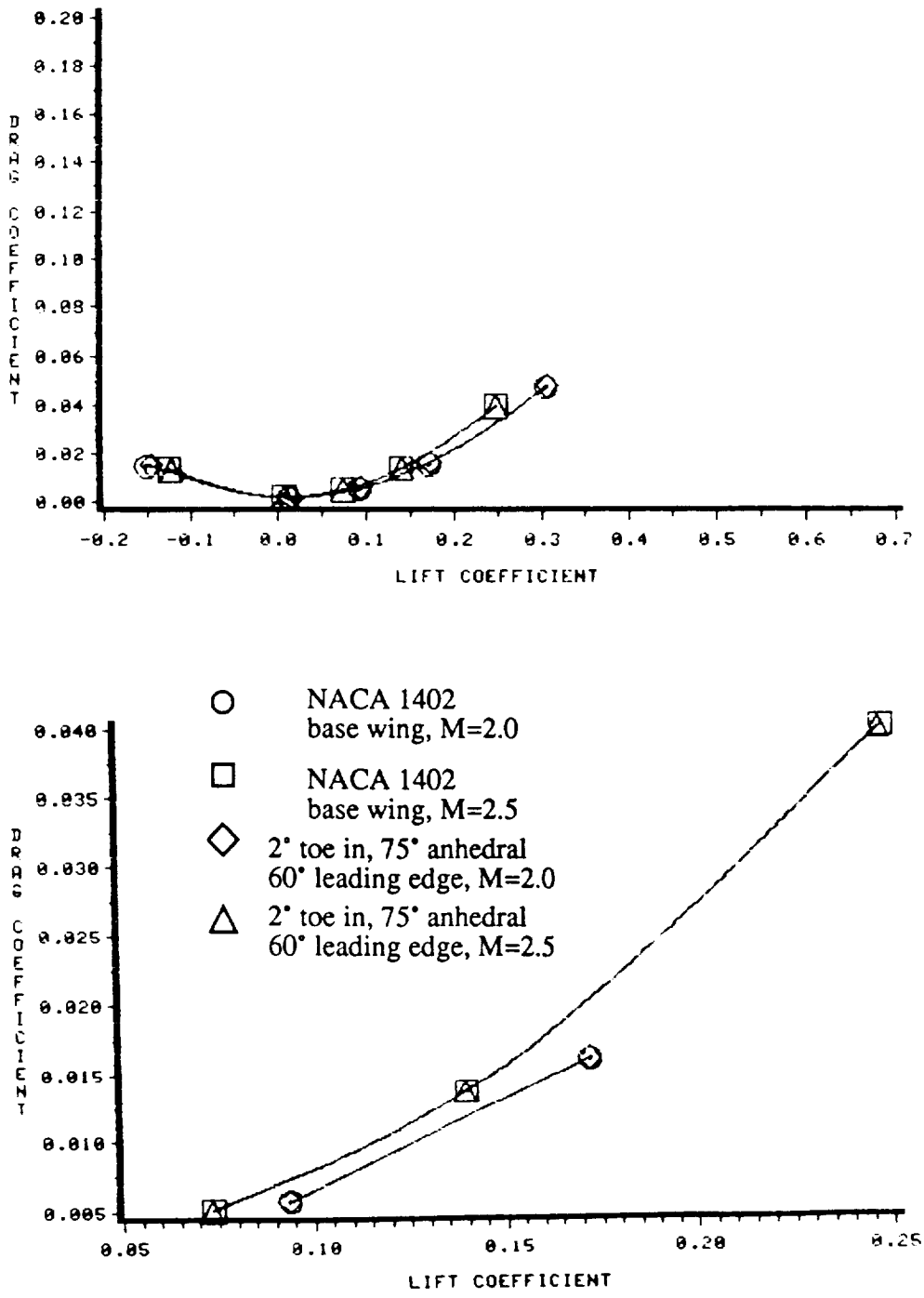

Figure 4.14.16: Predicted performance comparison between the NACA 1402 base wing with extension and the base wing with a 4% thick, 2° toe in, uncambered, 60° leading edge sweep, 75° anhedral winglet for various Mach numbers; M=2.0, 2.5; pressure drag coefficient versus lift coefficient.

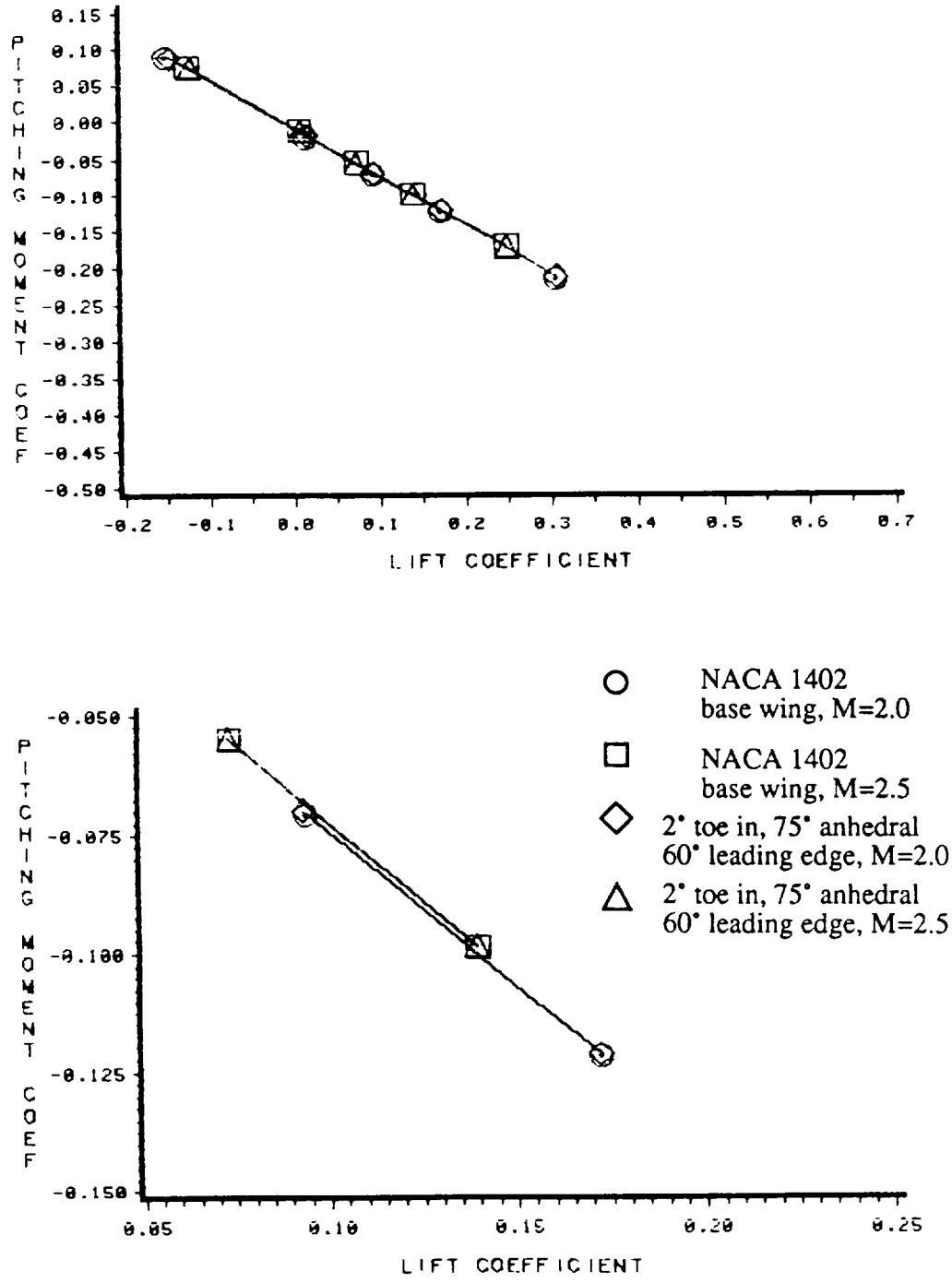

Figure 4.14.17: Predicted performance comparison between the NACA 1402 base wing with extension and the base wing with a 4% thick, 2° toe in, uncambered, 60° leading edge sweep, 75° anhedral winglet for various Mach numbers; M=2.0, 2.5; pitching moment coefficient versus lift coefficient.

C-3

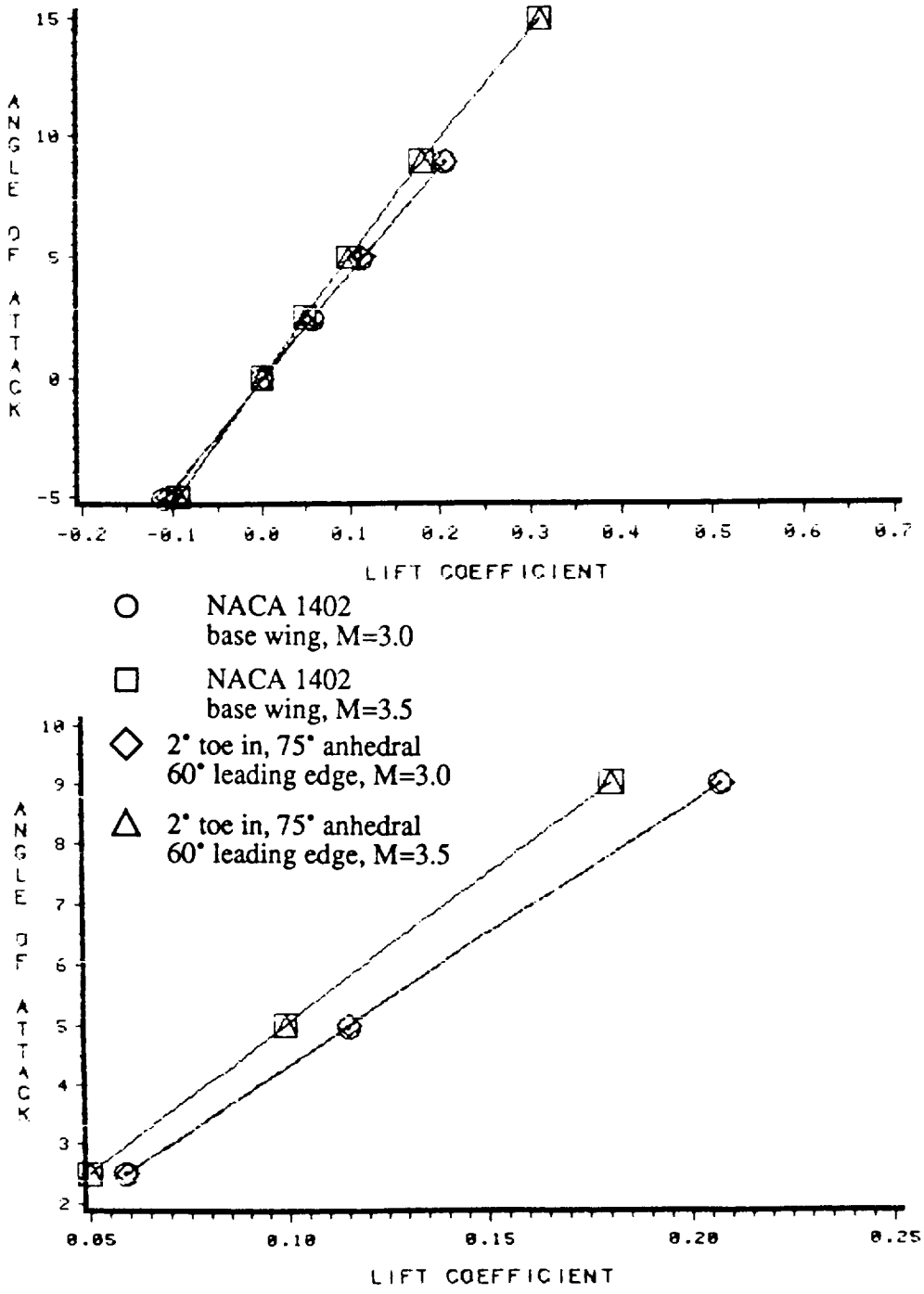

Figure 4.14.18: Predicted performance comparison between the NACA 1402 base wing with extension and the base wing with a 4% thick, 2° toe in, uncambered, 60° leading edge sweep, 75° anhedral winglet for various Mach numbers; M=3.0, 3.5; angle of attack versus lift coefficient.

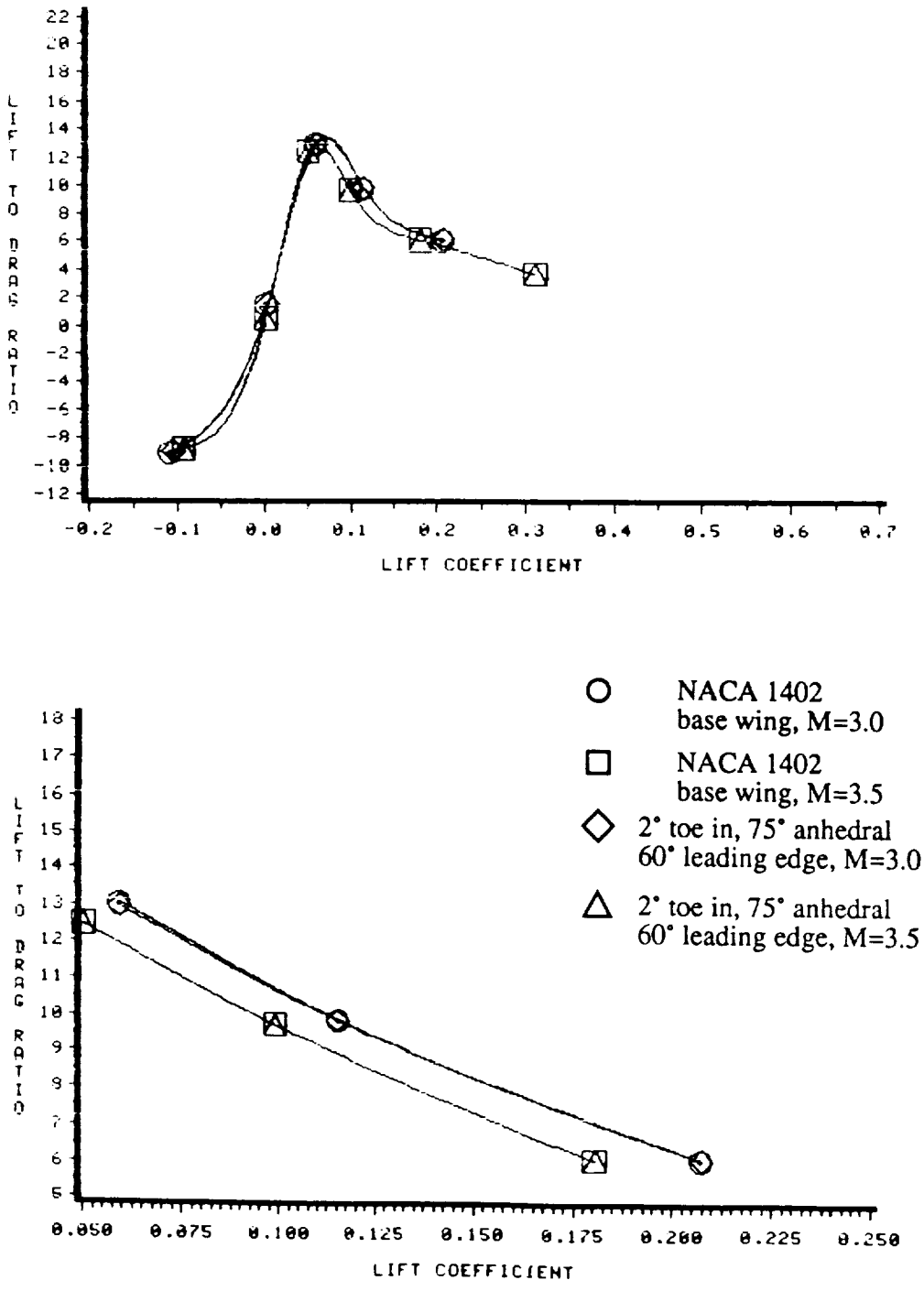

Figure 4.14.19: Predicted performance comparison between the NACA 1402 base wing with extension and the base wing with a 4% thick, 2° toe in, uncambered, 60° leading edge sweep, 75° anhedral winglet for various Mach numbers; M=3.0, 3.5; lift-to-pressure drag ratio versus lift coefficient.

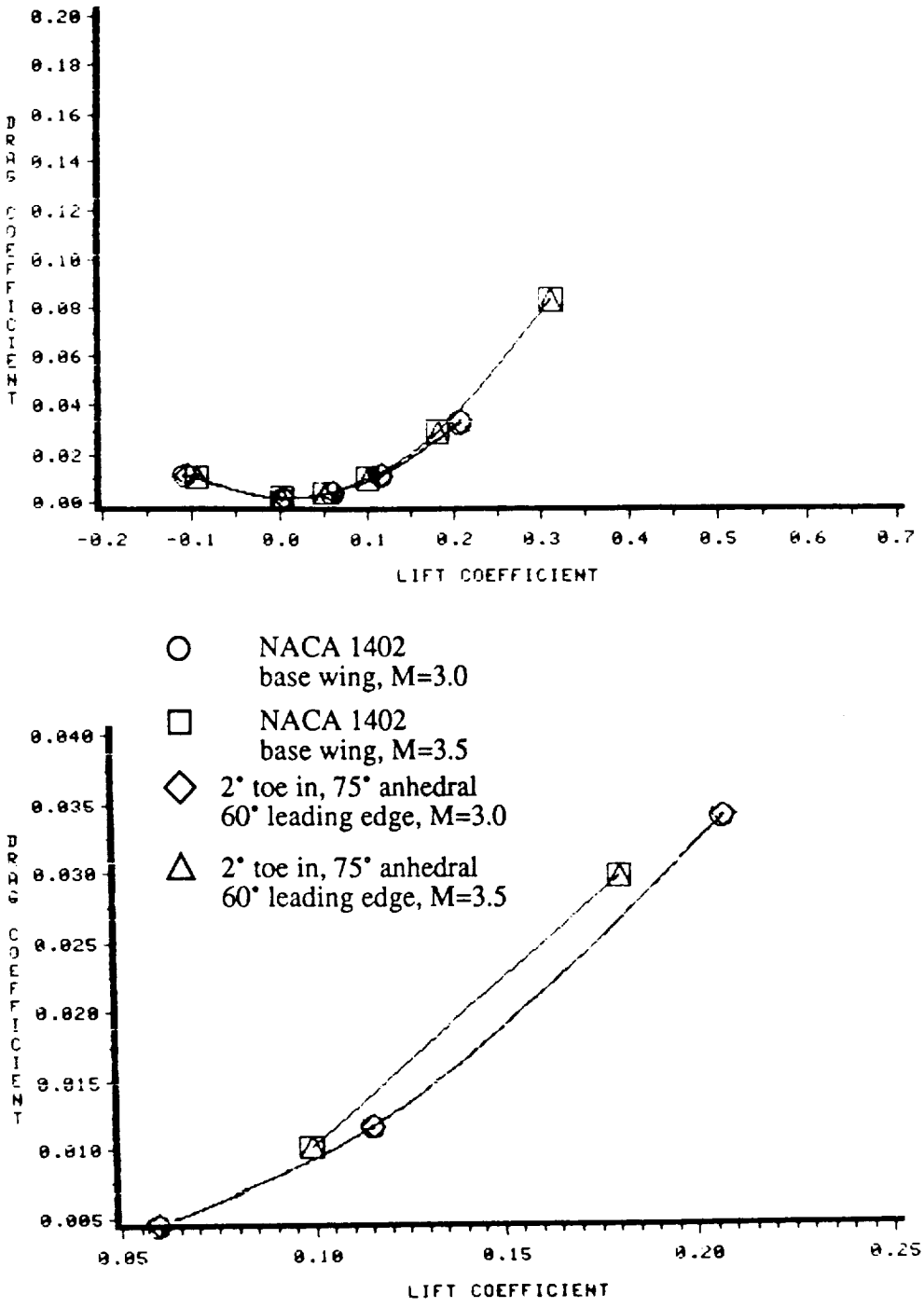

Figure 4.14.20: Predicted performance comparison between the NACA 1402 base wing with extension and the base wing with a 4% thick, 2° toe in, uncambered, 60° leading edge sweep, 75° anhedral winglet for various Mach numbers; M=3.0, 3.5; pressure drag coeffient versus lift coefficient.

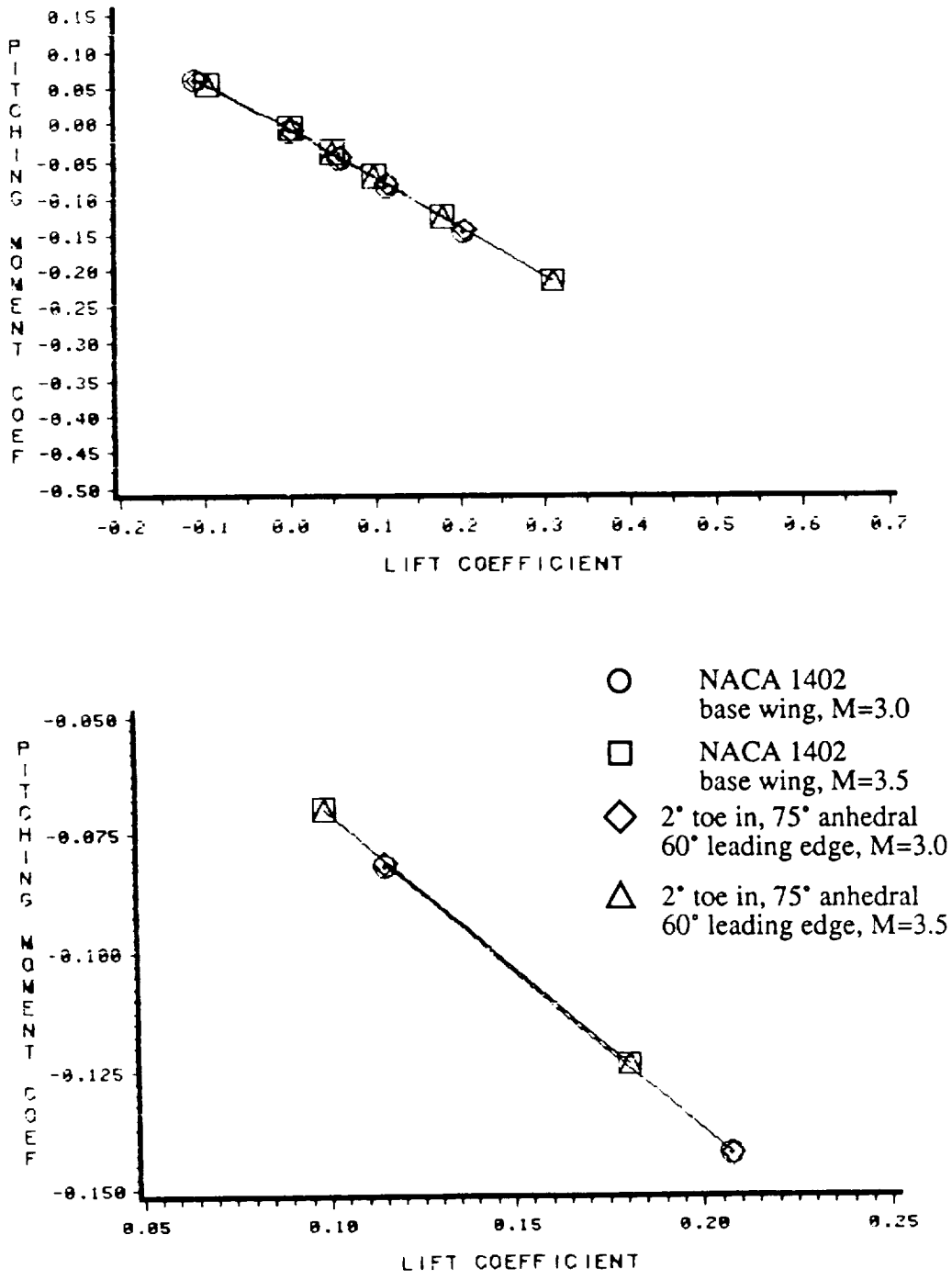

Figure 4.14.21: Predicted performance comparison between the NACA 1402 base wing with extension and the base wing with a 4% thick, 2° toe in, uncambered, 60° leading edge sweep, 75° anhedral winglet for various Mach numbers; M=3.0, 3.5; pitching moment coefficient versus lift coefficient.

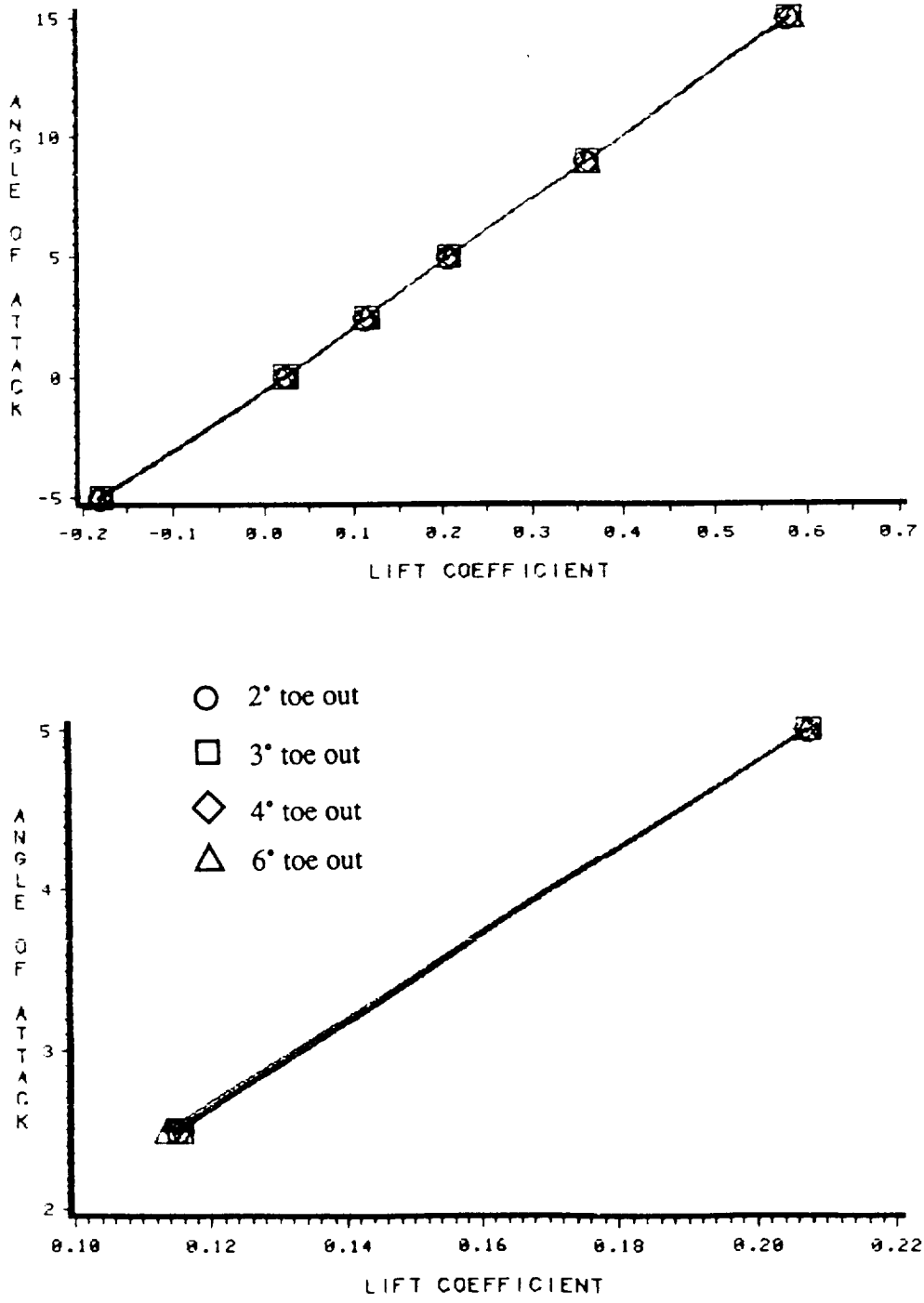

Figure 4.15.1: Predicted performance of the NACA 1402 base wing with 75° dihedral, full tip winglets; M=1.62; angle of attack versus lift coefficient.

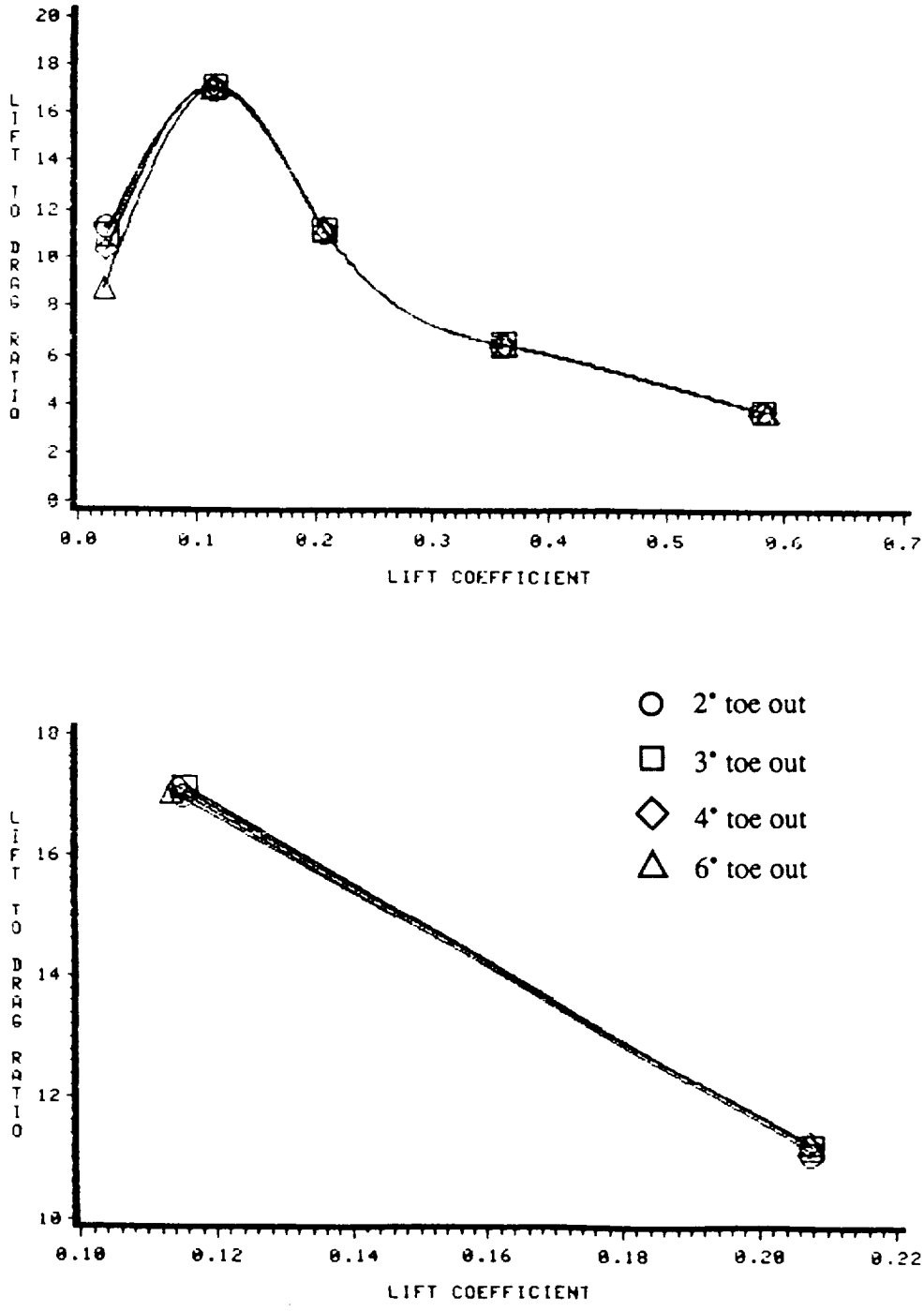

Figure 4.15.2: Predicted performance of the NACA 1402 base wing with 75° dihedral, full tip winglets; M=1.62; lift-to-pressure drag ratio versus lift coefficient.

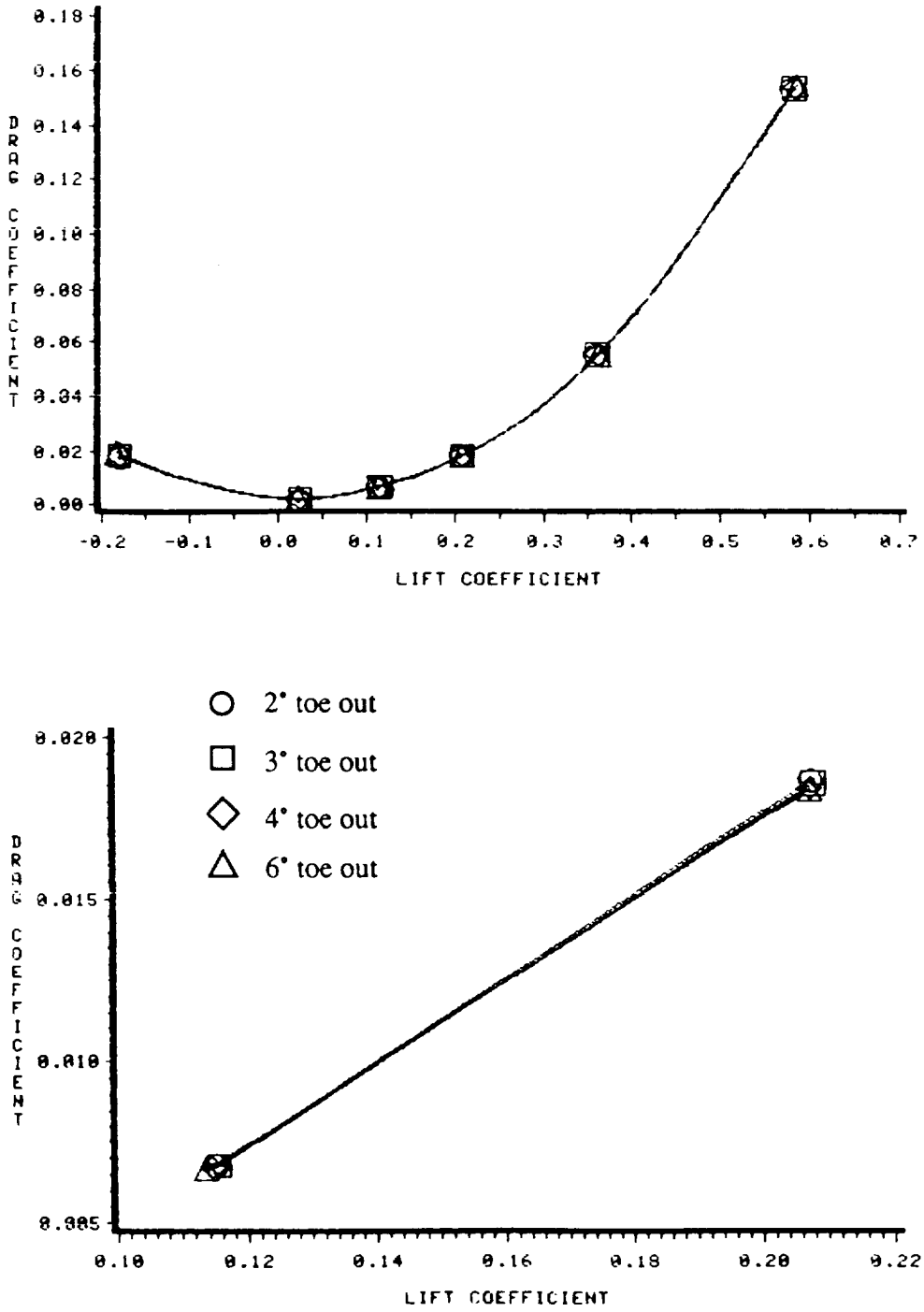

Figure 4.15.3: Predicted performance of the NACA 1402 base wing with 75° dihedral, full tip winglets; M=1.62; pressure drag coefficient versus lift coefficient.

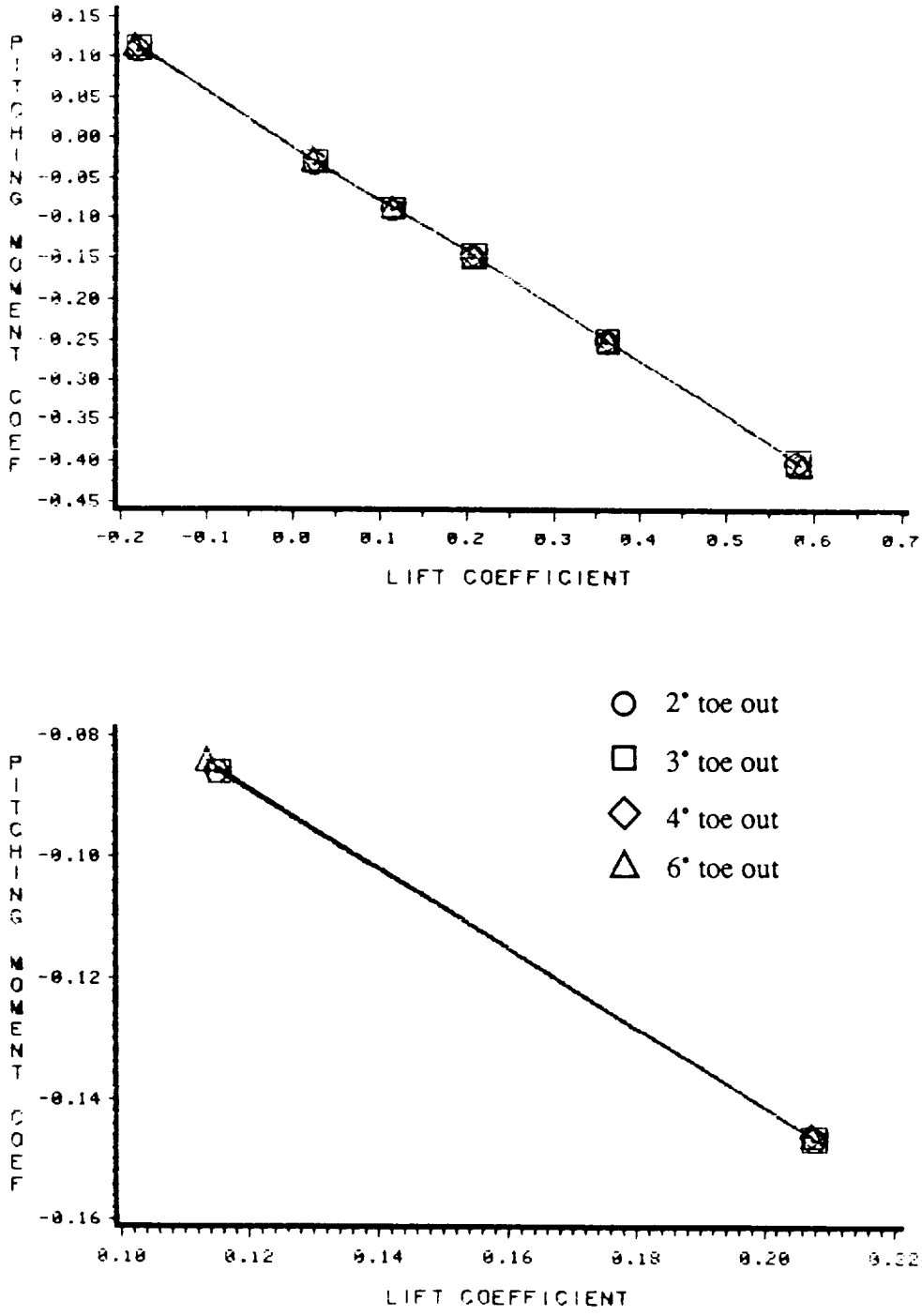

Figure 4.15.4: Predicted performance of the NACA 1402 base wing with 75° dihedral, full tip winglets; M=1.62; pitching moment coefficient versus lift coefficient.

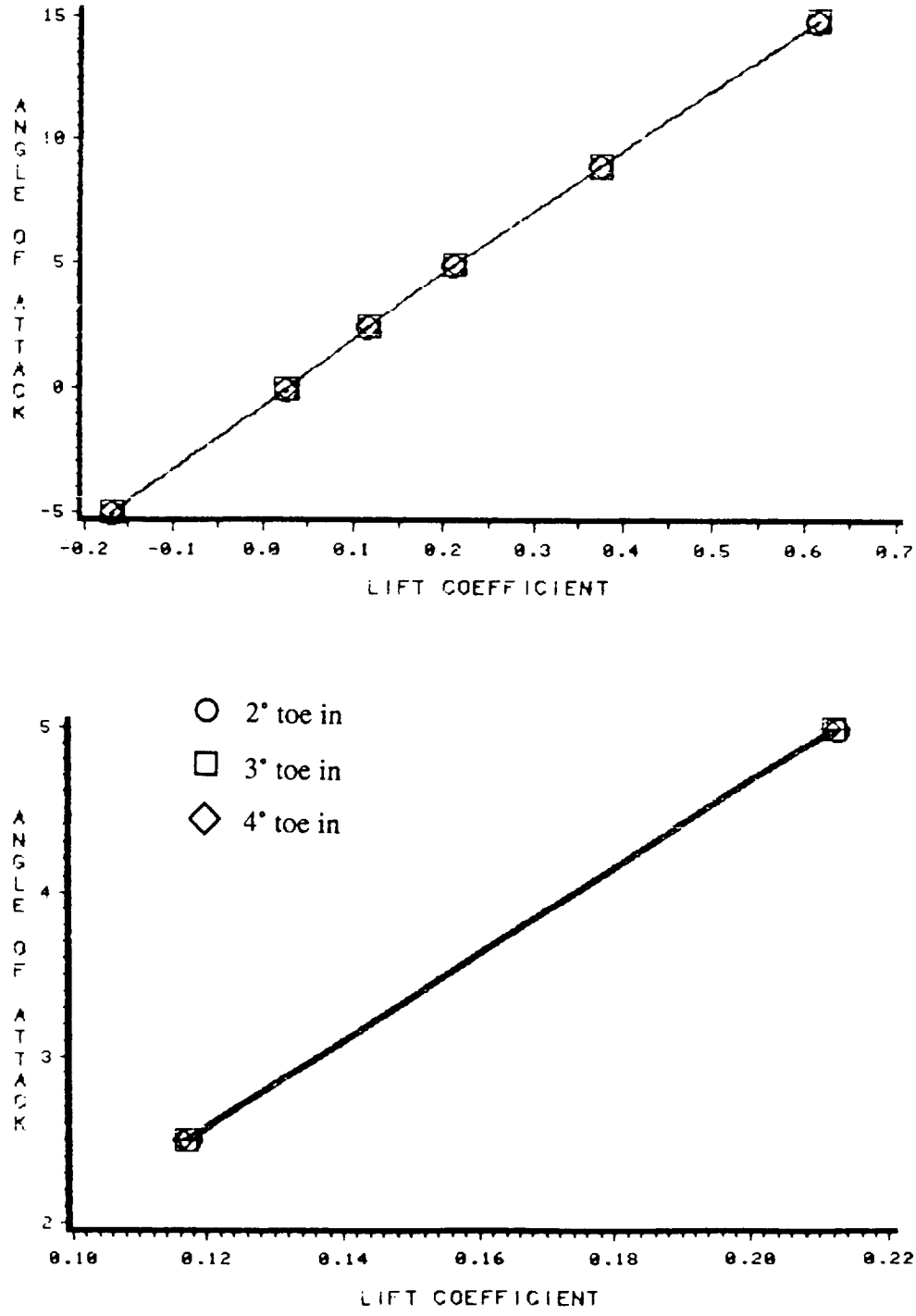

Figure 4.15.5: Predicted performance of the NACA 1402 base wing with 75° anhedral, full tip winglets; M=1.62; angle of attack versus lift coefficient.

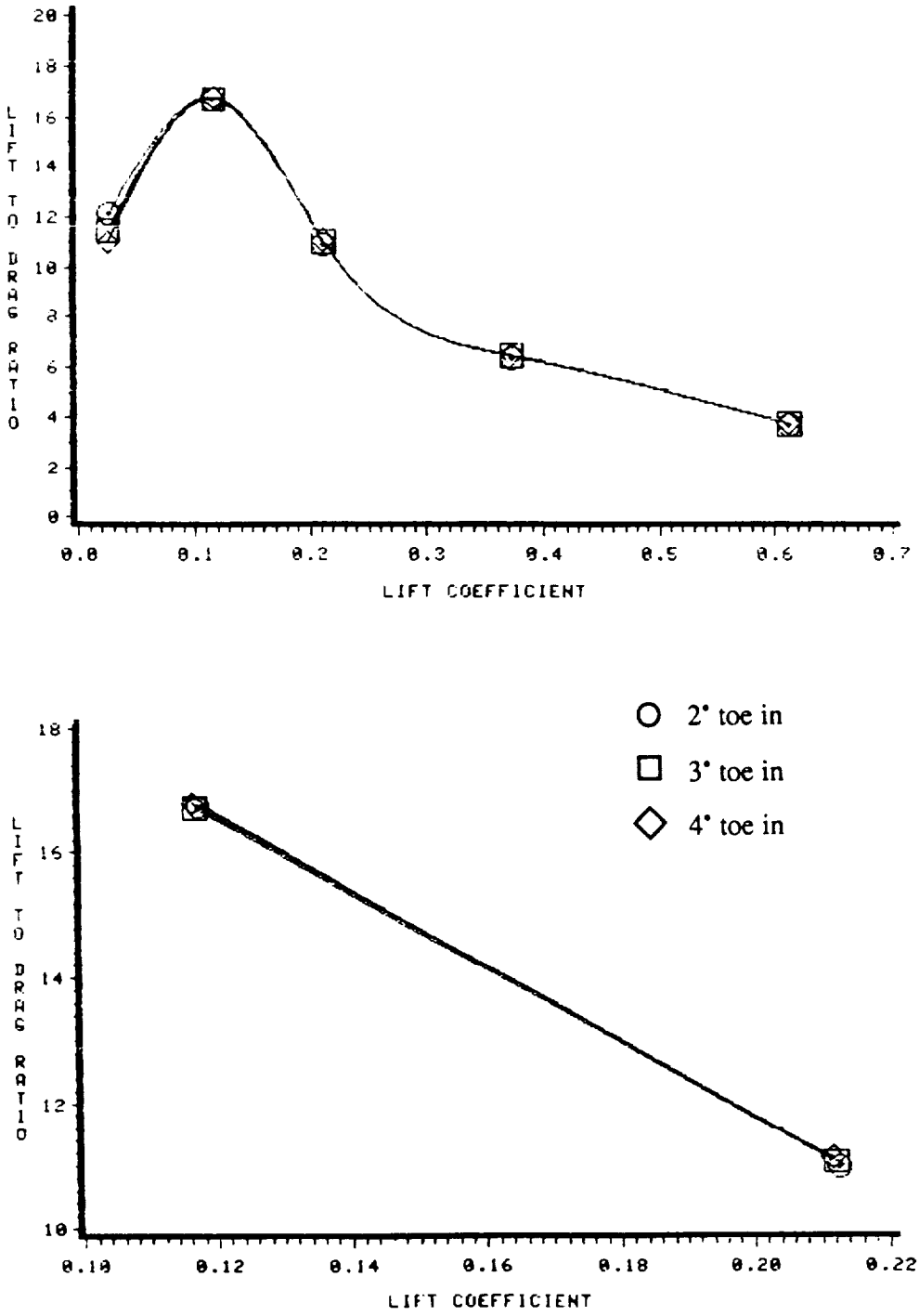

Figure 4.15.6: Predicted performance of the NACA 1402 base wing with 75° anhedral, full tip winglets; M=1.62; lift-to-pressure drag ratio versus lift coefficient.

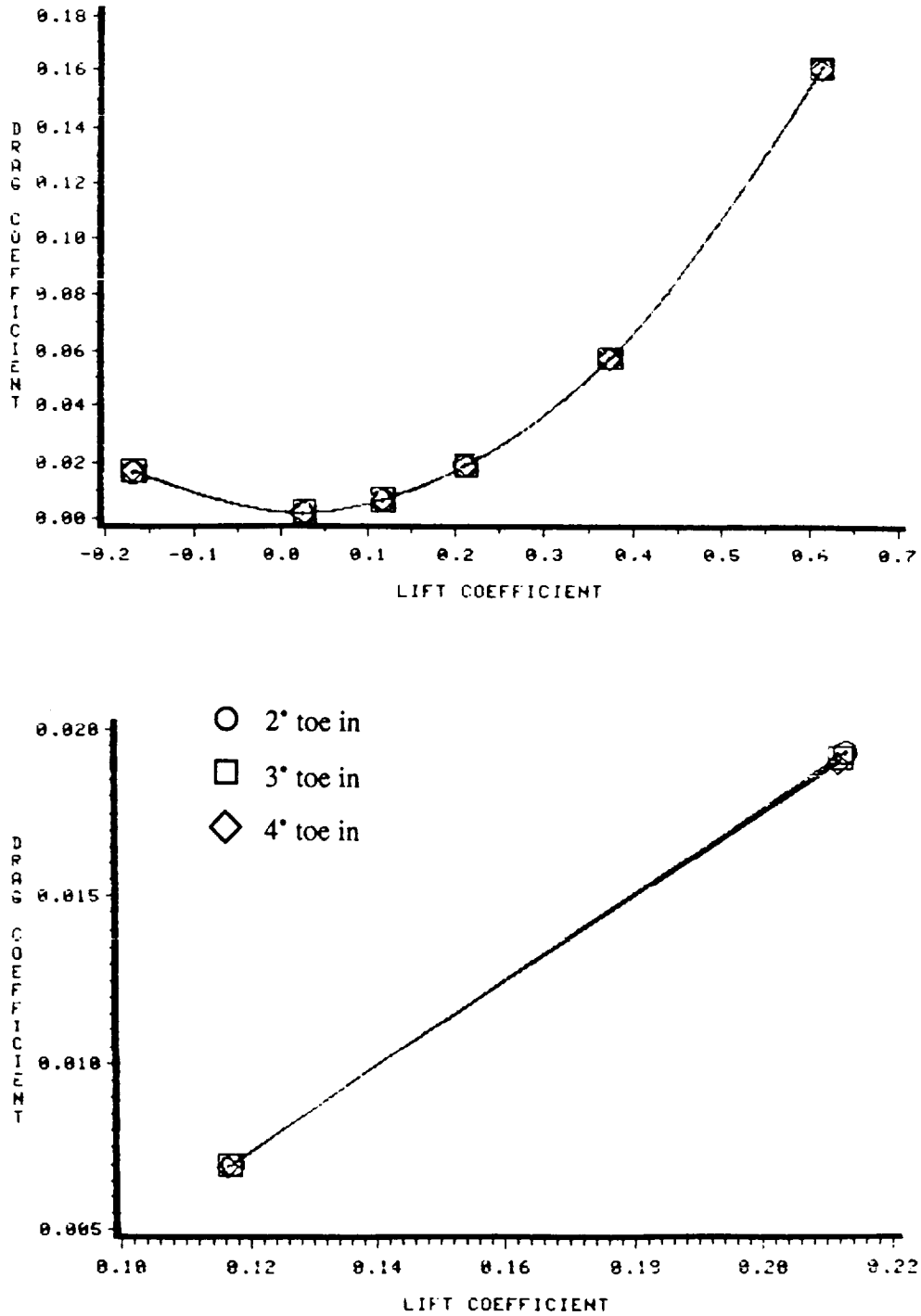

Figure 4.15.7: Predicted performance of the NACA 1402 base wing with 75° anhedral, full tip winglets; M=1.62; pressure drag coefficient versus lift coefficient.

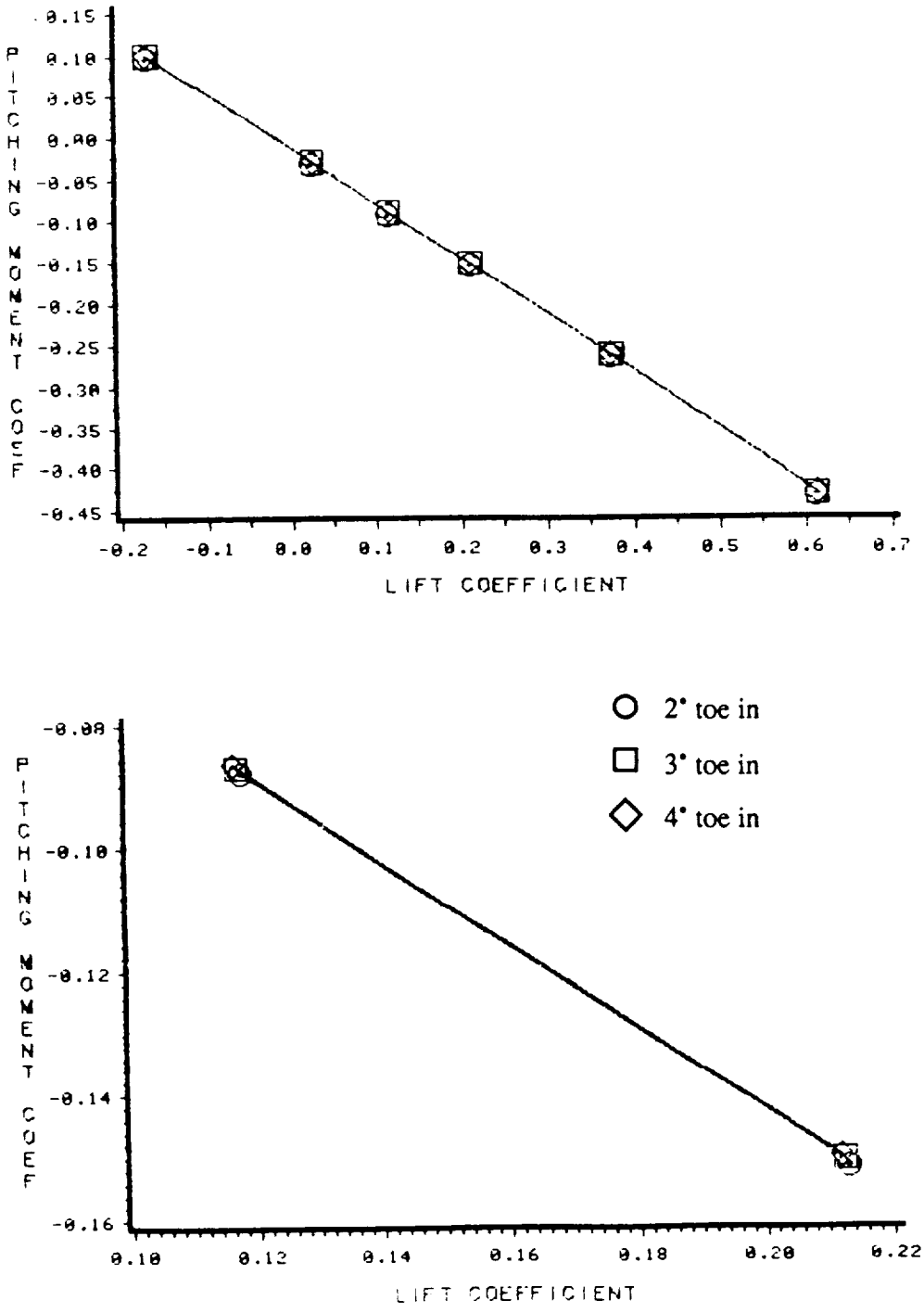

Figure 4.15.8: Predicted performance of the NACA 1402 base wing with 75° anhedral, full tip winglets; M=1.62; pitching moment coefficient versus lift coefficient.

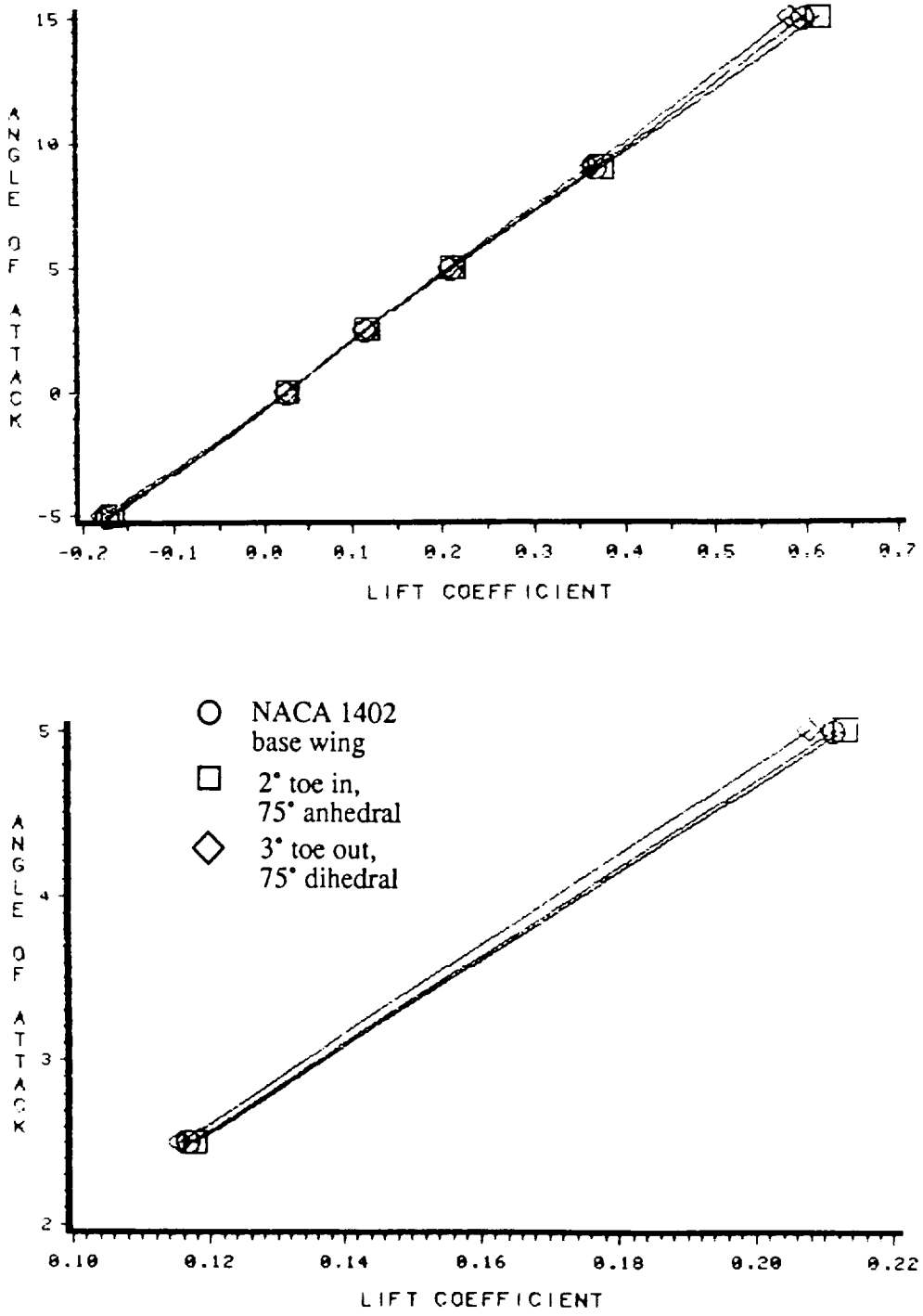

Figure 4.15.9: Comparison of the predicted performance of the NACA 1402 base wing, the 3° toe out, 75° dihedral, full tip winglet, and the 2° toe in, 75° anhedral, full tip winglet; M=1.62; angle of attack versus lift coefficient.

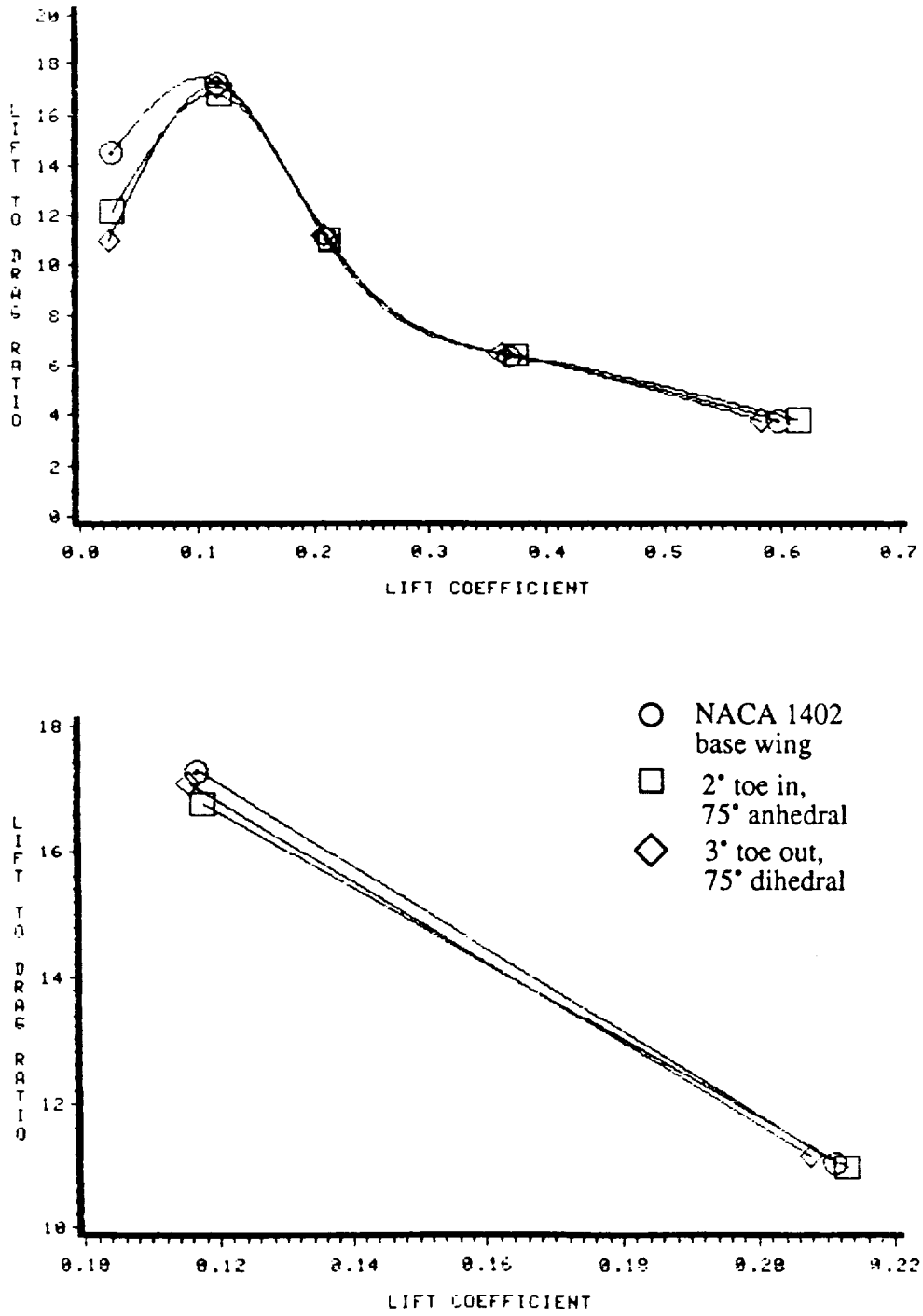

Figure 4.15.10: Comparison of the predicted performance of the NACA 1402 base wing, the 3° toe out, 75° dihedral, full tip winglet, and the 2° toe in, 75° anhedral,full tip winglet; M=1.62; lift-to-pressure drag ratio versus lift coefficient.

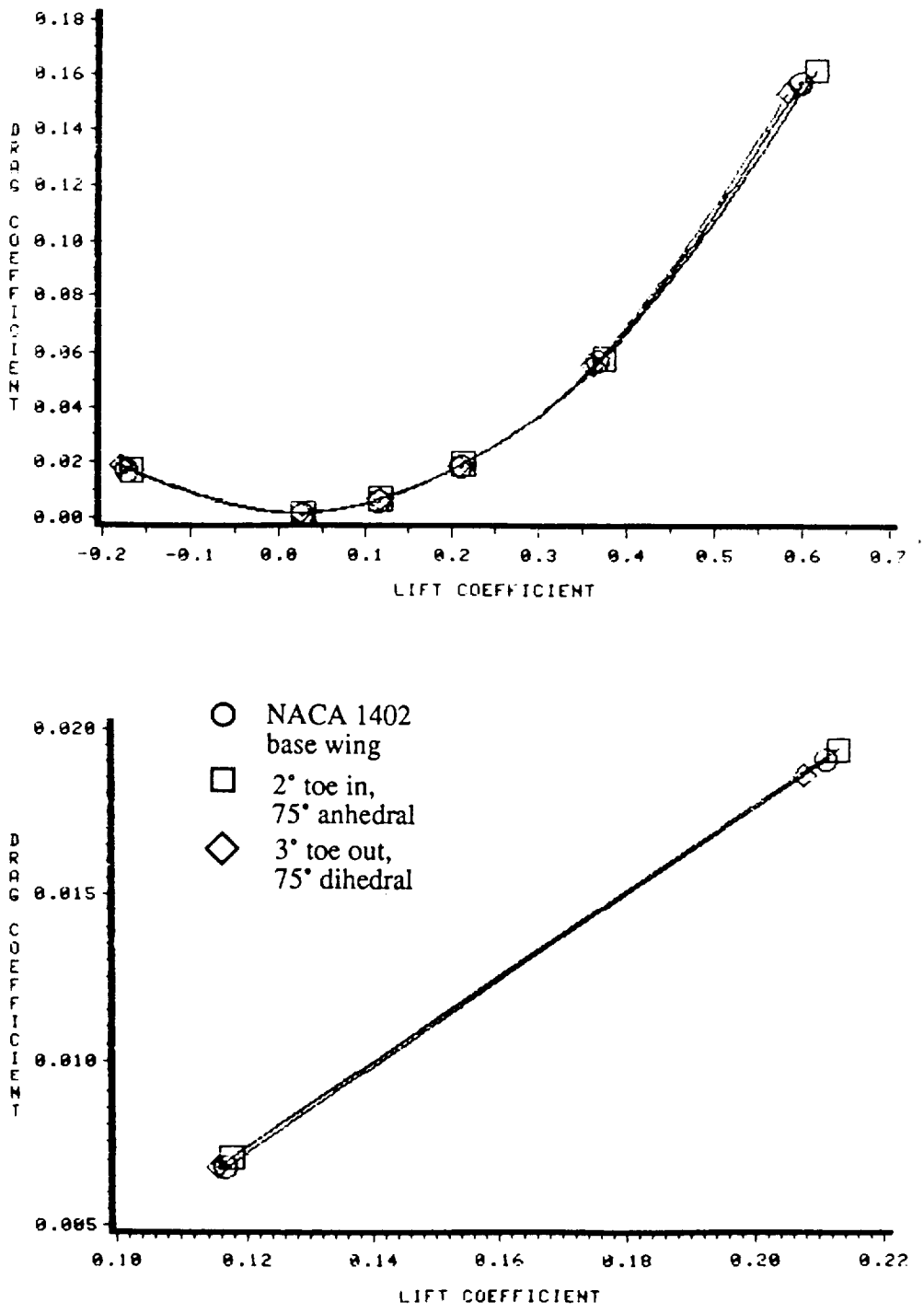

Figure 4.15.11: Comparison of the predicted performance of the NACA 1402 base wing, the 3° toe out, 75° dihedral, full tip winglet, and the 2° toe in, 75° anhedral, full tip winglet; M=1.62; pressure drag coefficient versus lift coefficient.

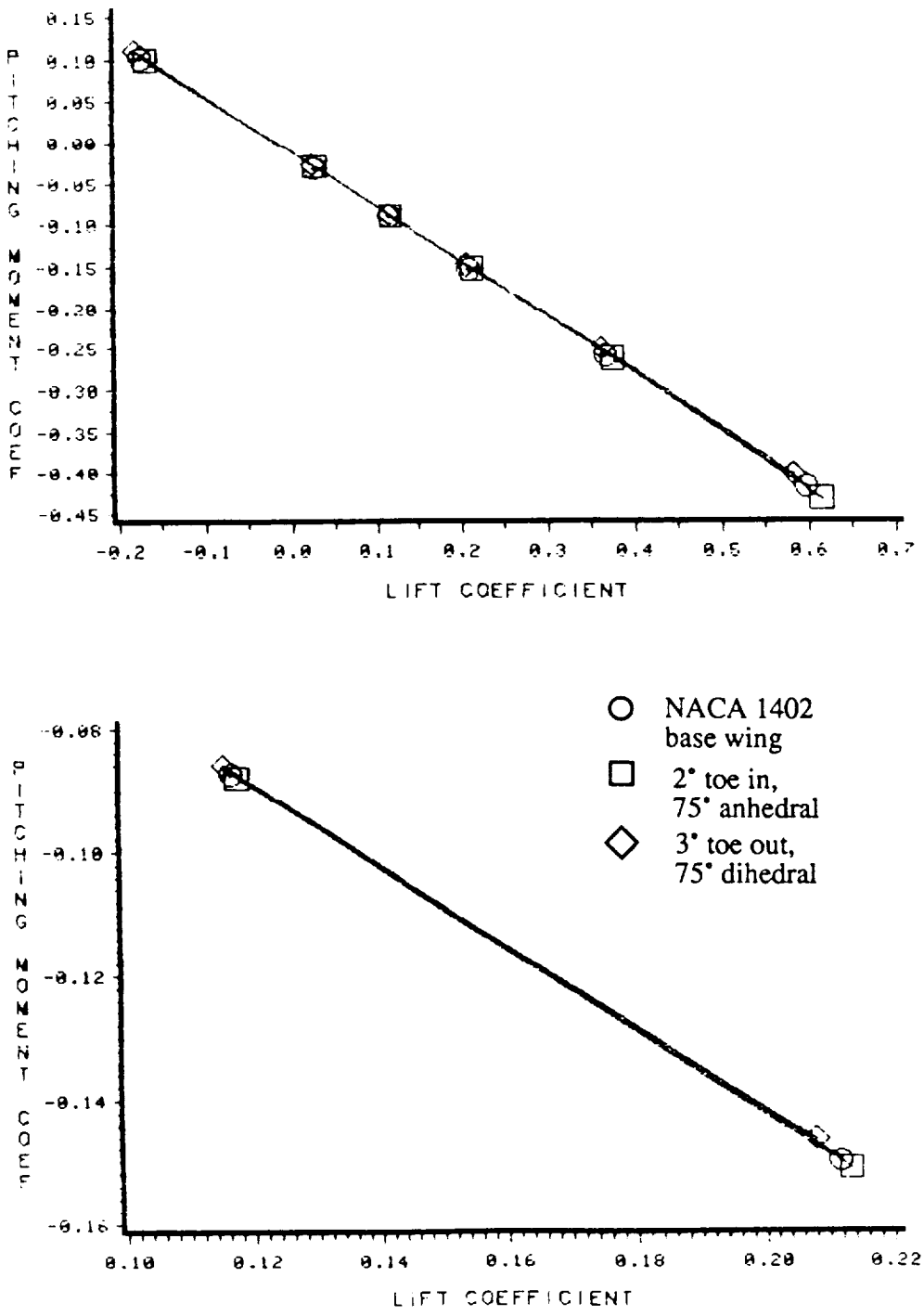

Figure 4.15.12: Comparison of the predicted performance of the NACA 1402 base wing, the 3° toe out, 75° dihedral, full tip winglet, and the 2° toe in, 75° anhedral, full tip winglet; M=1.62; pitching moment coefficient versus lift coefficient.

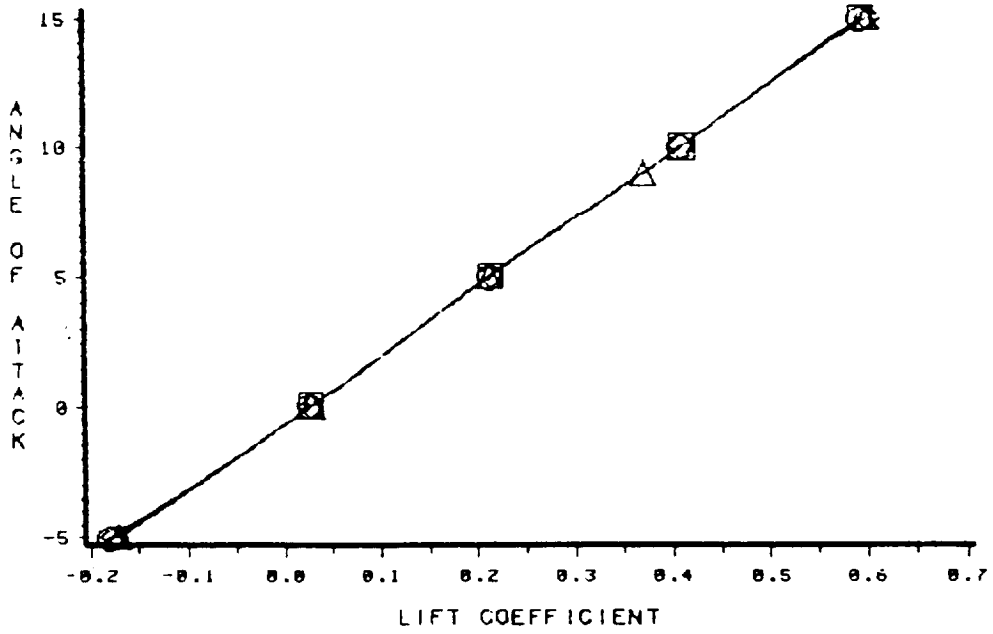

Figure 4.15.13: Comparison of the predicted performance of the NACA 1402 base wing and wing-winglets with 75° dihedral, full tip winglets having various maximum camber locations; M=1.62; angle of attack versus lift coefficient.

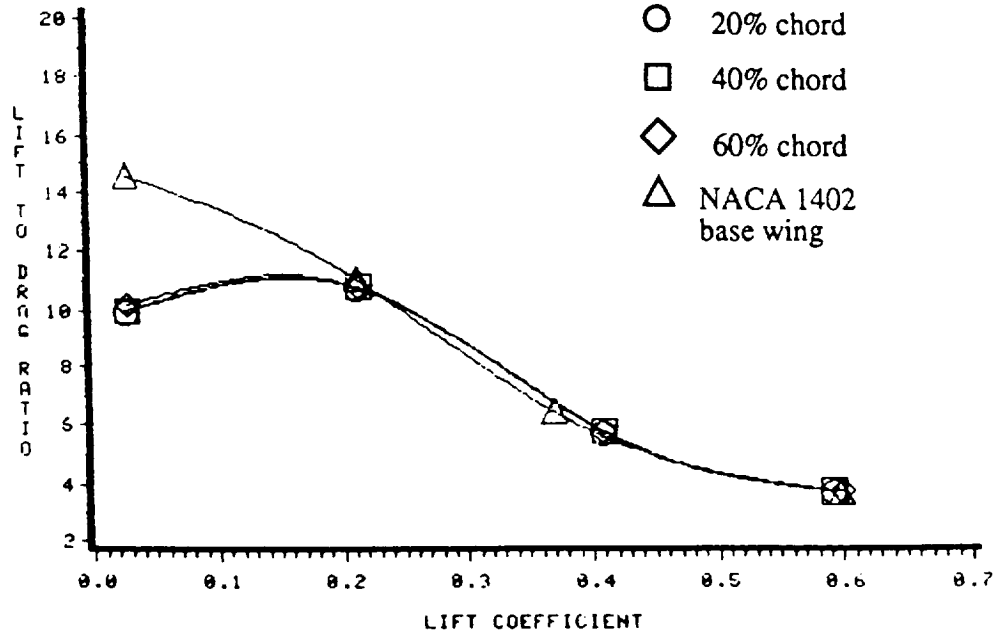

Figure 4.15.14: Comparison of the predicted performance of the NACA 1402 base wing and wing-winglets with 75° dihedral, full tip winglets having various maximum camber locations; M=1.62; lift-to-pressure drag ratio versus lift coefficient.

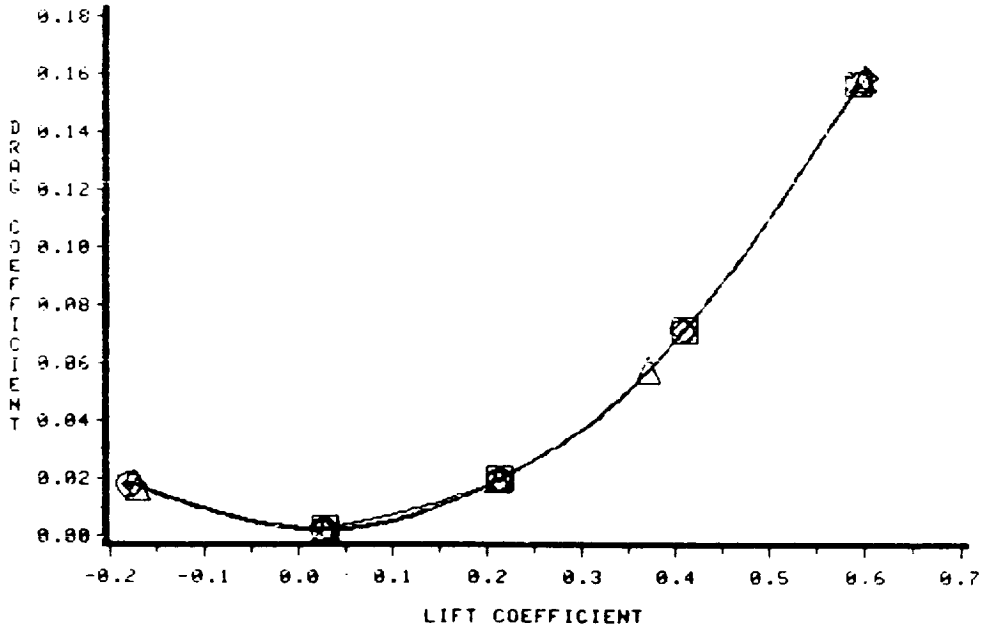

Figure 4.15.15: Comparison of the predicted performance of the NACA 1402 base wing and wing-winglets with 75° dihedral, full tip winglets having various maximum camber locations; M=1.62; pressure drag coefficient versus lift coefficient.

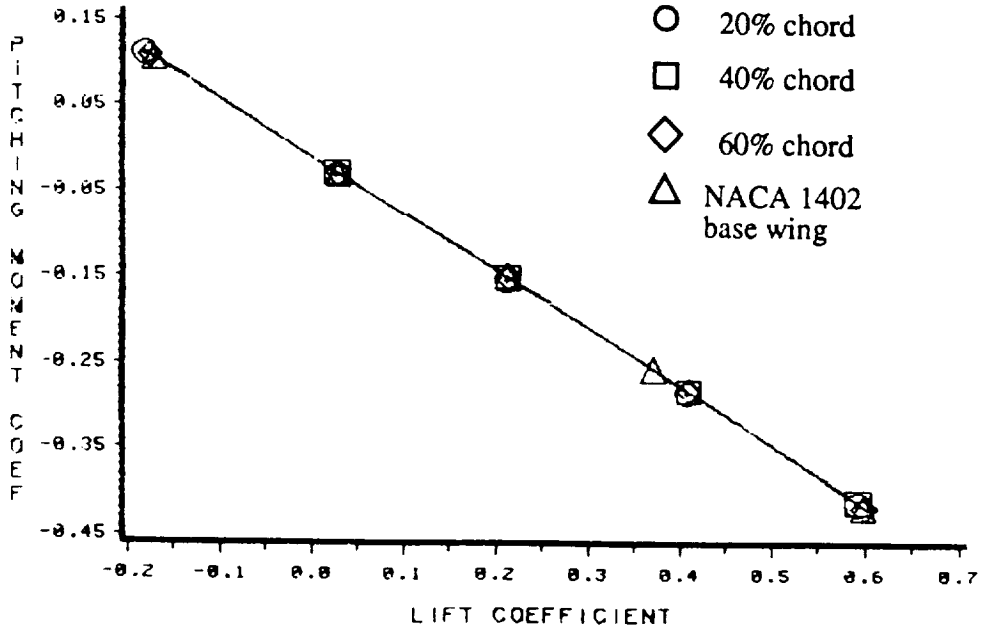

Figure 4.15.16: Comparison of the predicted performance of the NACA 1402 base wing and wing-winglets with 75° dihedral, full tip winglets having various maximum camber locations; M=1.62; pitching moment coefficient versus lift coefficient.

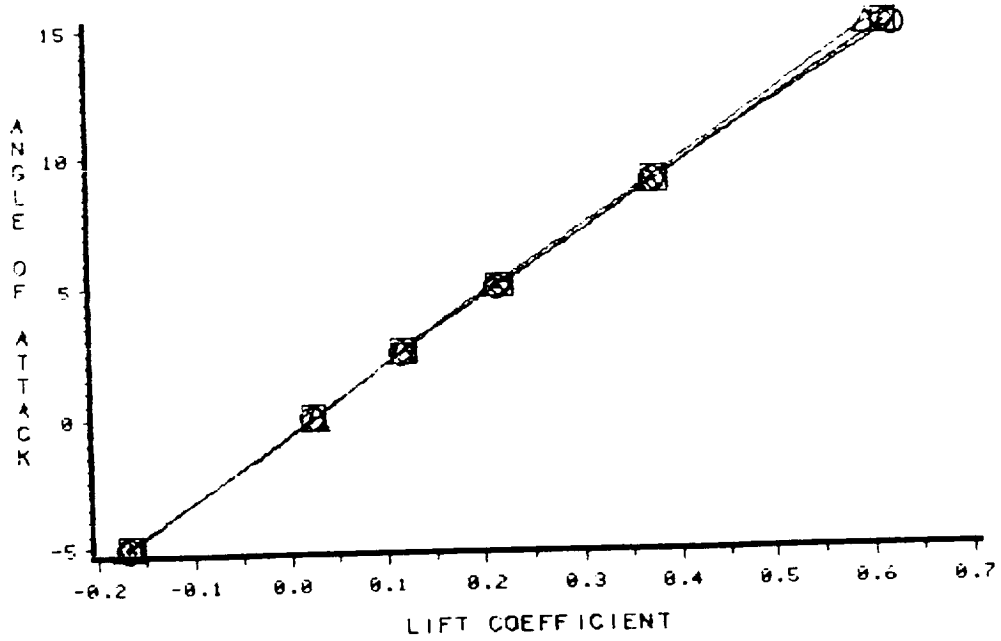

Figure 4.15.17: Comparison of the predicted performance of the NACA 1402 base wing and wing-winglets with 75° anhedral, full tip winglets having various maximum camber locations; M=1.62; angle of attack versus lift coefficient.

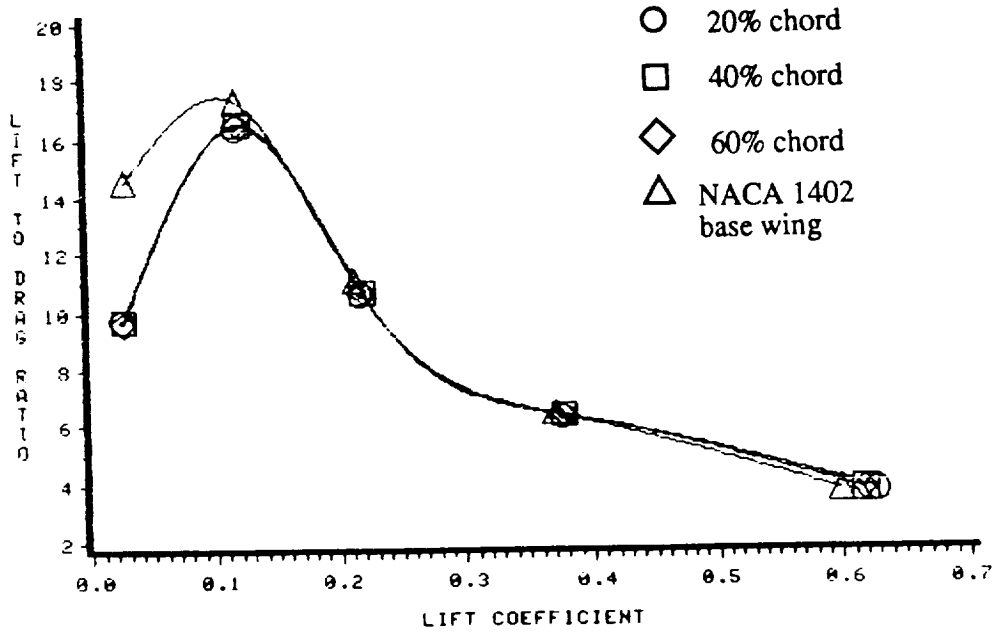

Figure 4.15.18: Comparison of the predicted performance of the NACA 1402 base wing and wing-winglets with 75° anhedral, full tip winglets having various maximum camber locations; M=1.62; lift-to-pressure drag ratio versus lift coefficient.

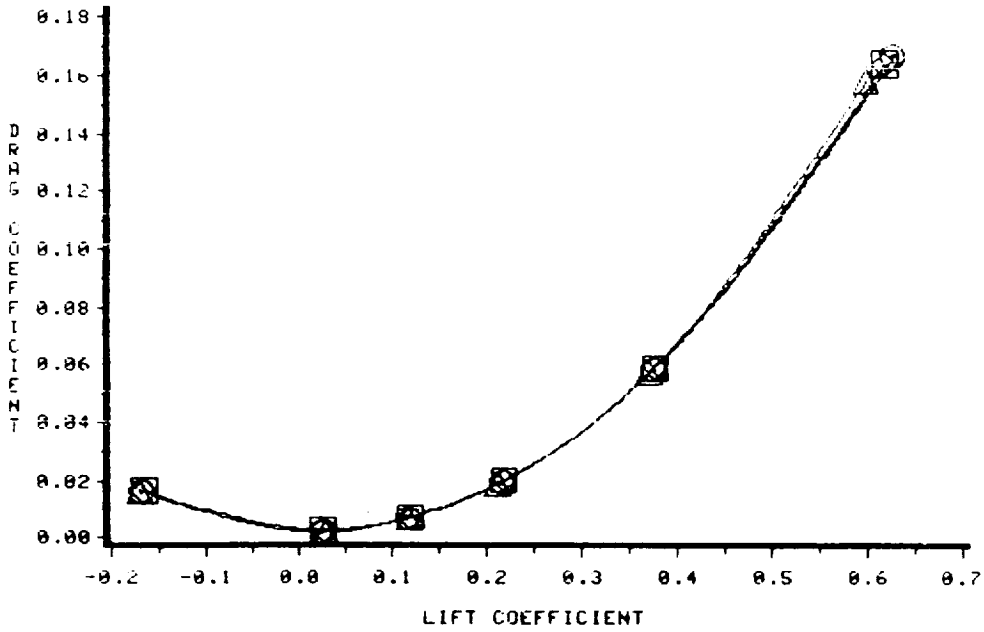

Figure 4.15.19: Comparison of the predicted performance of the NACA 1402 base wing and wing-winglets with 75° anhedral, full tip winglets having various maximum camber locations; M=1.62; pressure drag coefficient versus lift coefficient.

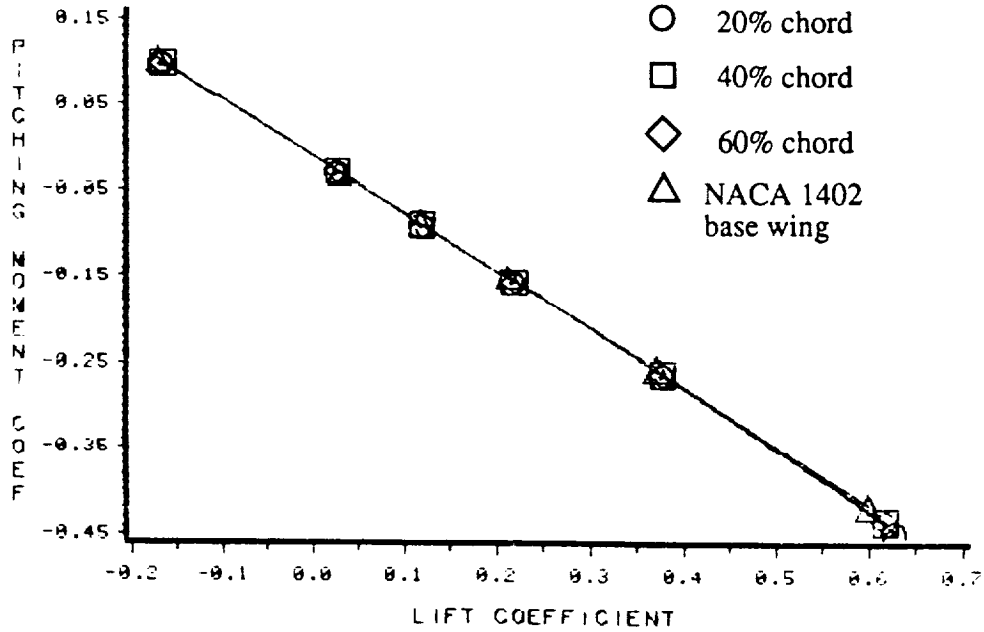

Figure 4.15.20: Comparison of the predicted performance of the NACA 1402 base wing and wing-winglets with 75° anhedral, full tip winglets having various maximum camber locations; M=1.62; pitching moment coefficient versus lift coefficient.

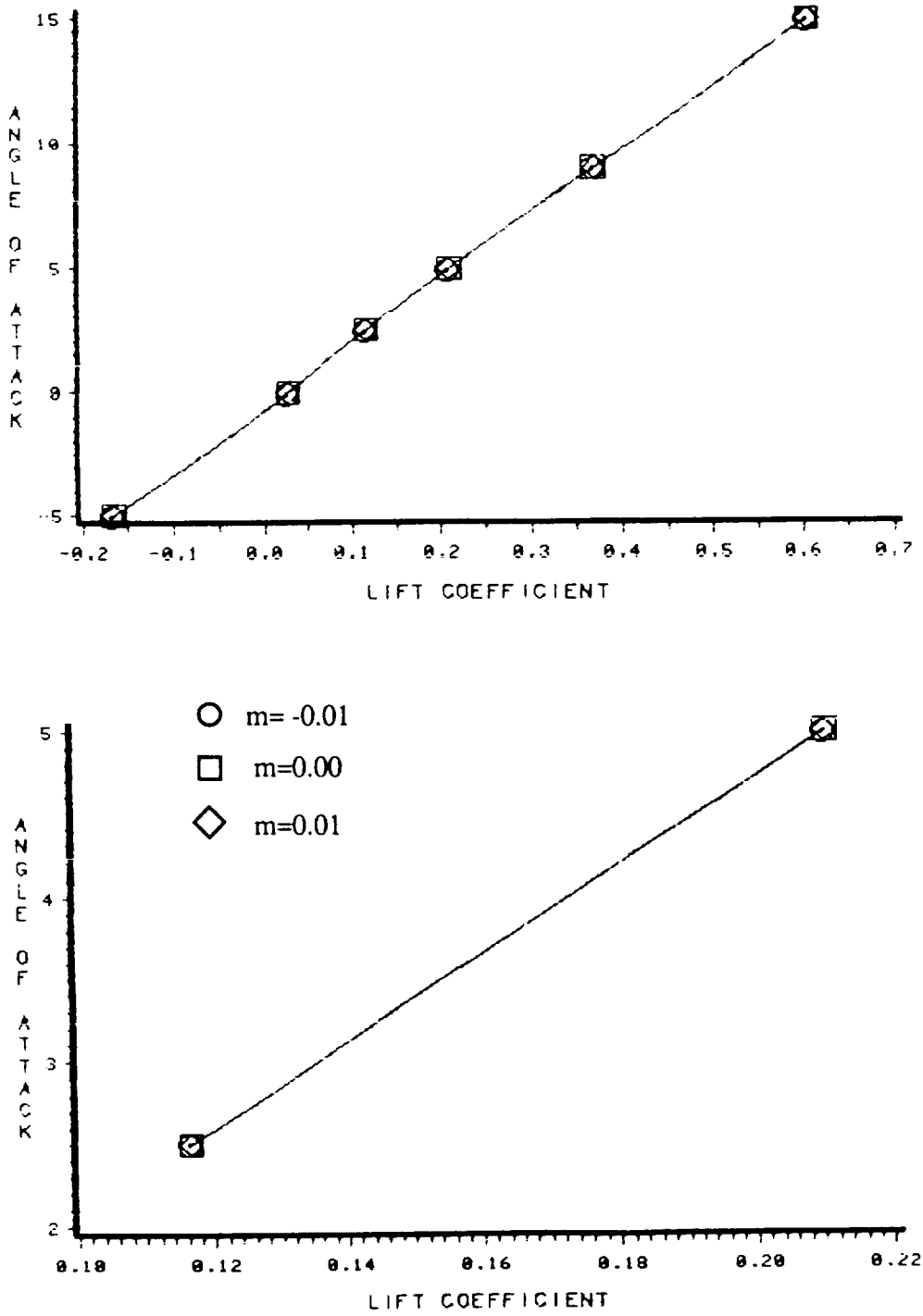

Figure 4.15.21: Predicted performance of the NACA 1402 base wing with 2% thick, 75° anhedral winglets with various cambers; M=1.62; angle of attack versus lift coefficient.

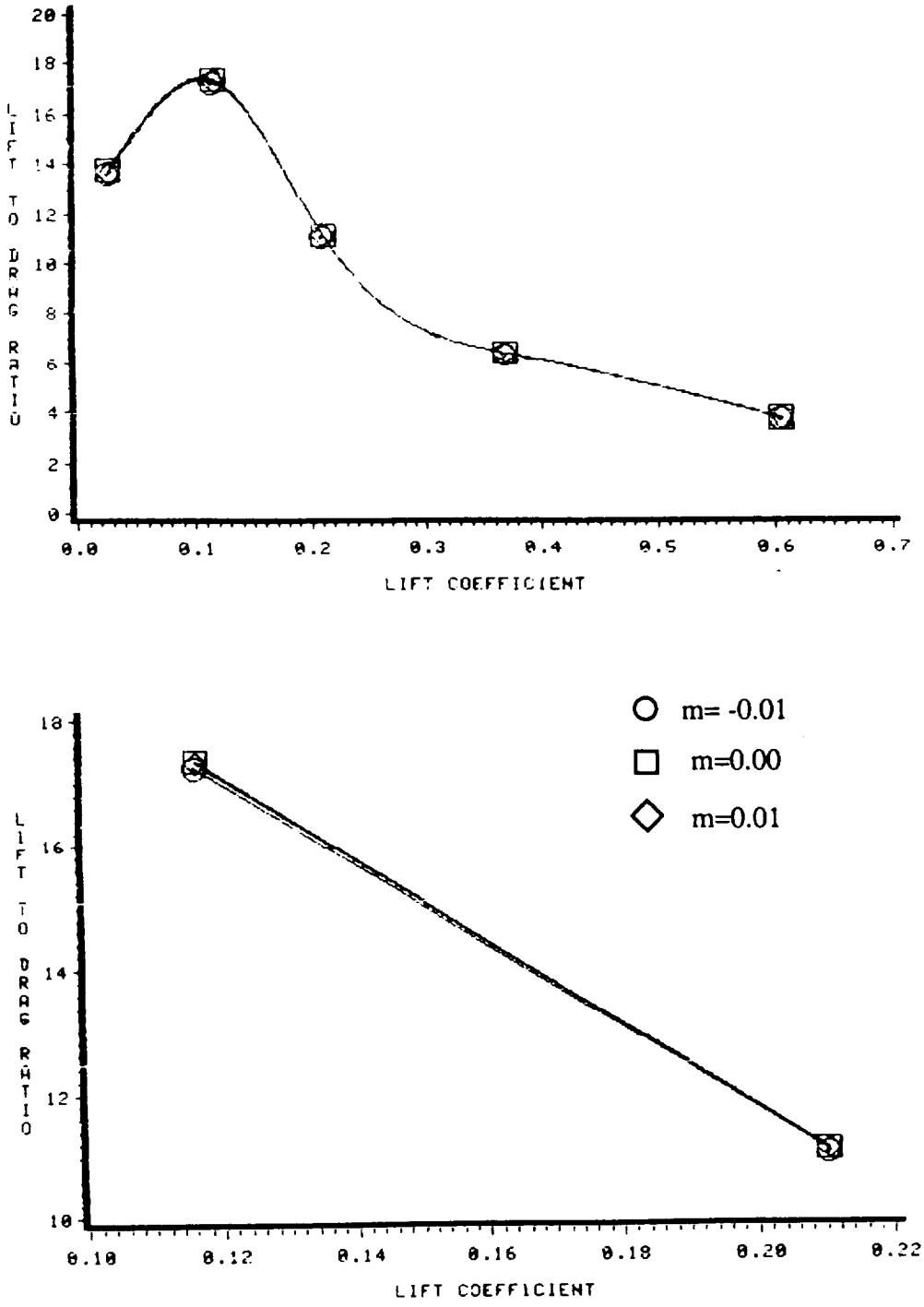

Figure 4.15.22: Predicted performance of the NACA 1402 base wing with 2% thick, 75° anhedral winglets with various cambers; M=1.62; lift-to-pressure drag ratio versus lift coefficient.

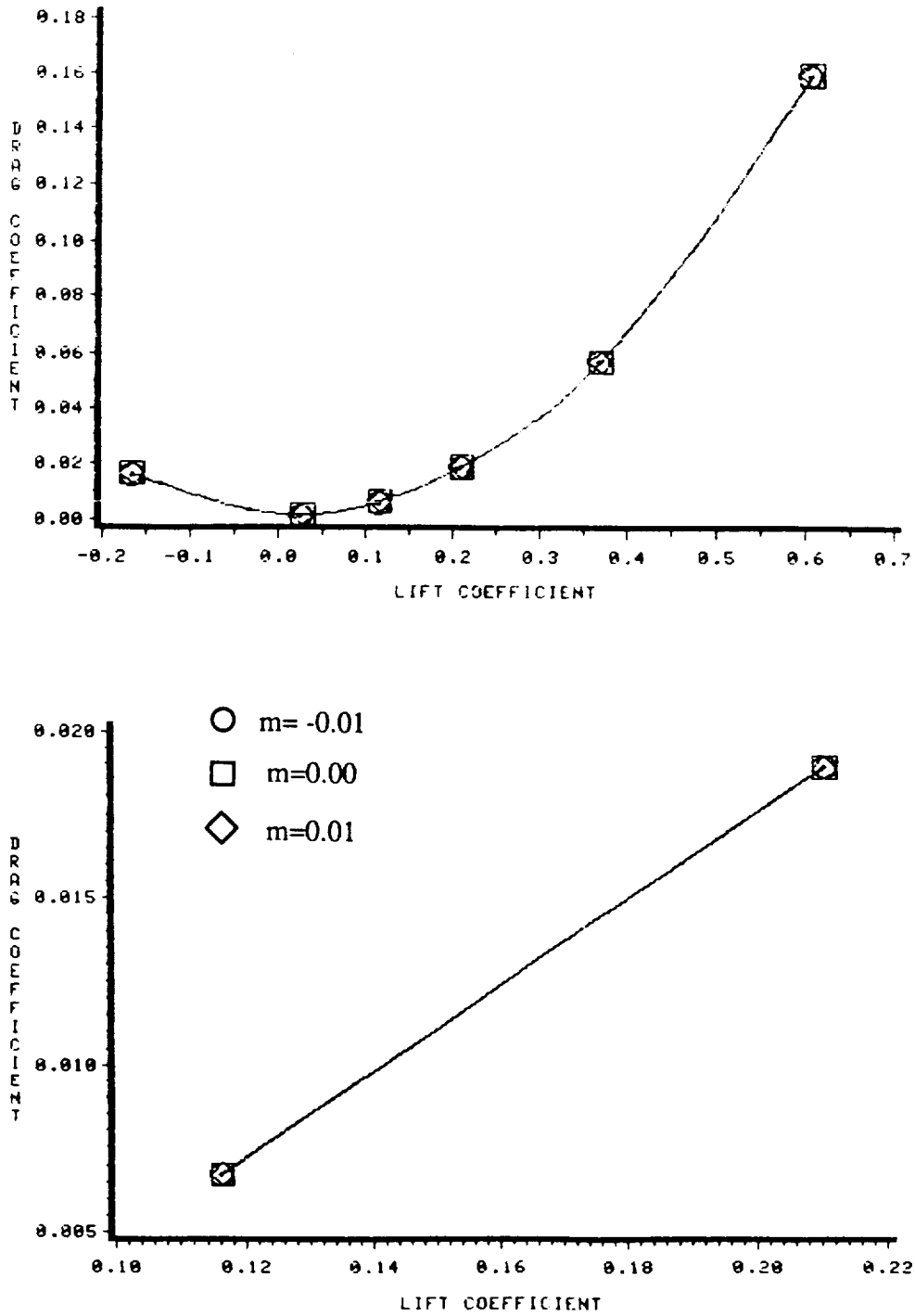

Figure 4.15.23: Predicted performance of the NACA 1402 base wing with 2% thick, 75° anhedral winglets with various cambers; M=1.62; pressure drag coefficient versus lift coefficient.

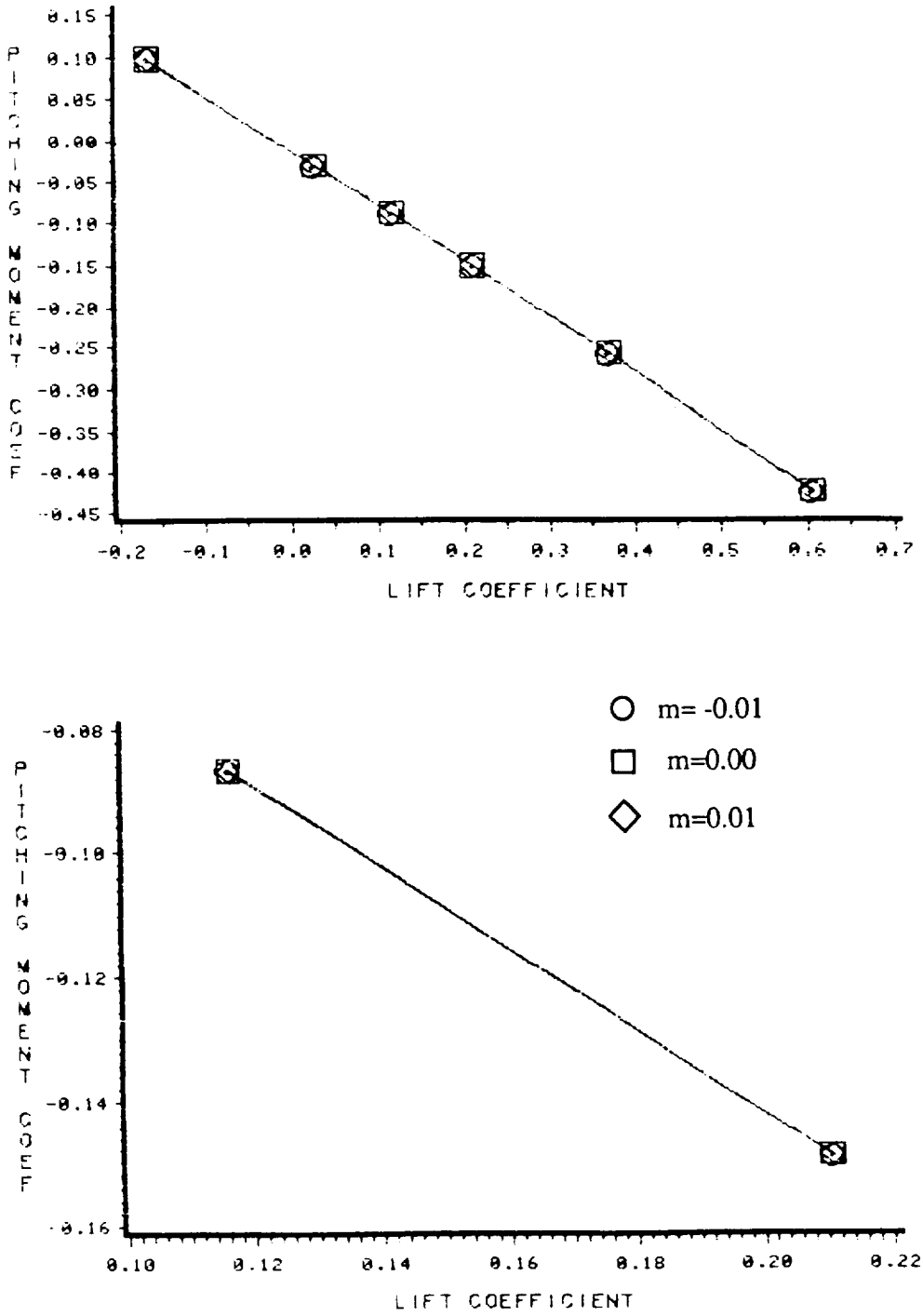

Figure 4.15.24: Predicted performance of the NACA 1402 base wing with 2% thick, 75° anhedral winglets with various cambers; M=1.62; pitching moment coefficient versus lift coefficient.

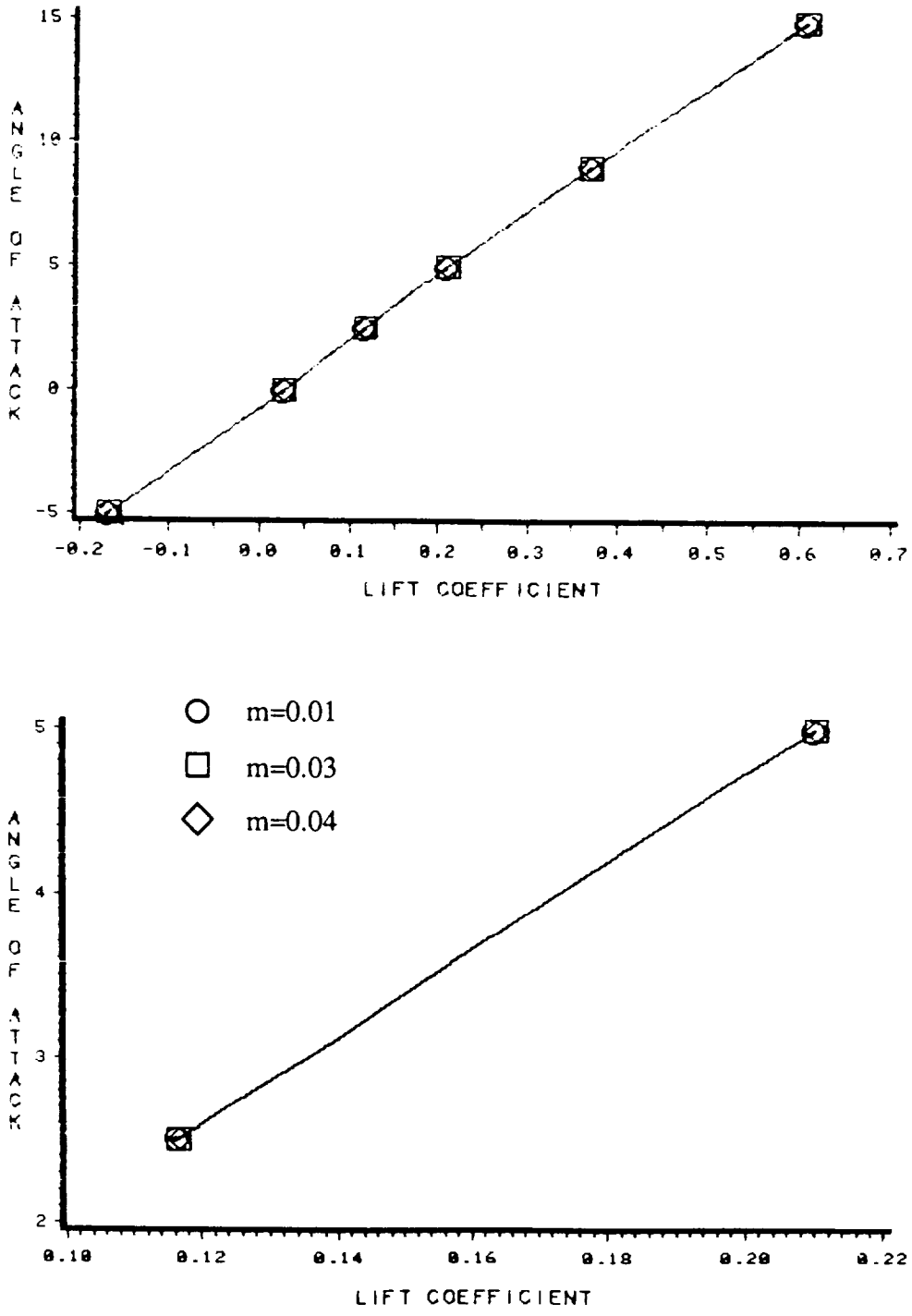

Figure 4.15.25: Predicted performance of the NACA 1402 base wing with 2% thick, 75° anhedral winglets with various cambers; M=1.62; angle of attack versus lift coefficient.

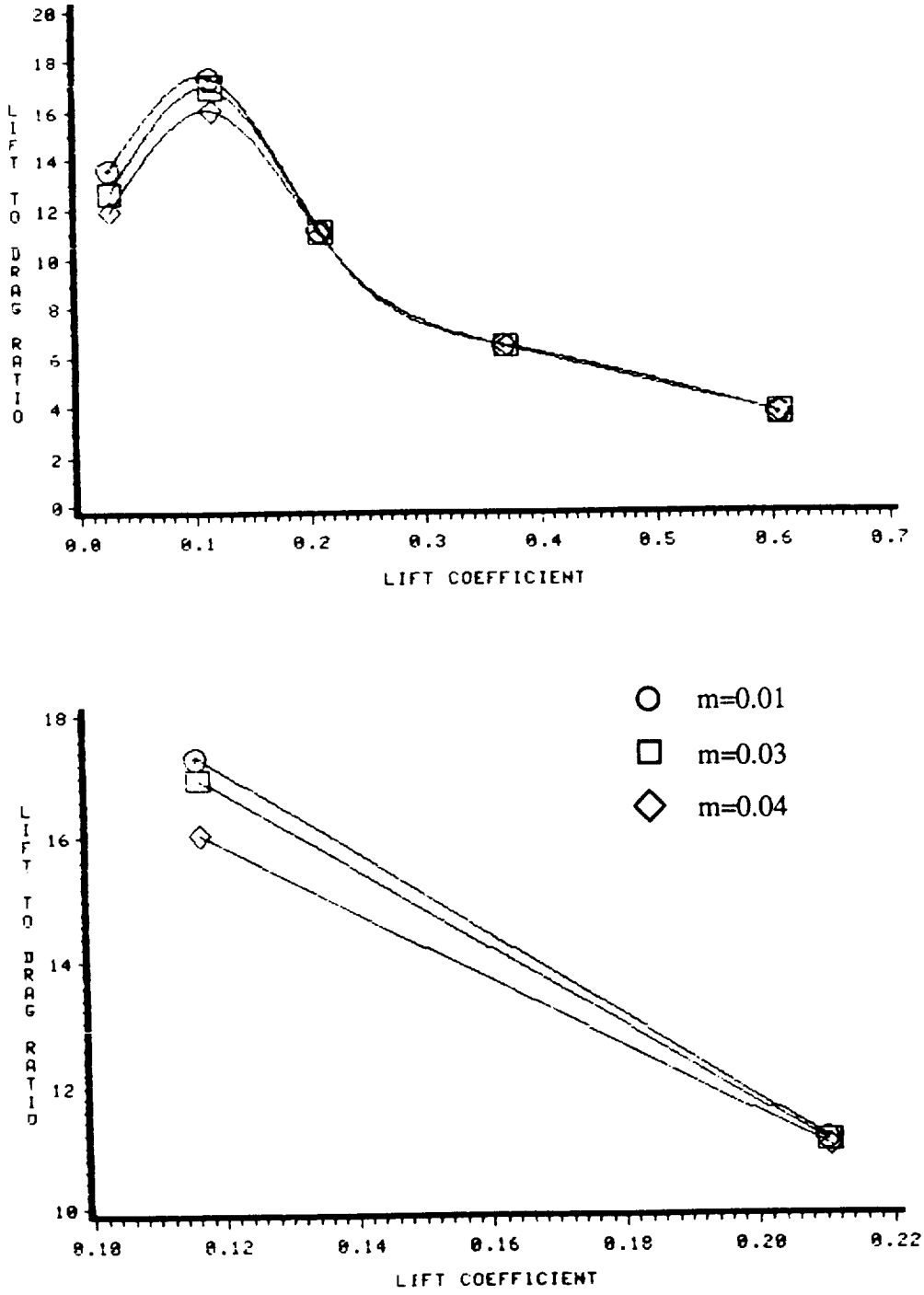

Figure 4.15.26: Predicted performance of the NACA 1402 base wing with 2% thick, 75° anhedral winglets with various cambers; M=1.62; lift-to-pressure drag ratio versus lift coefficient.

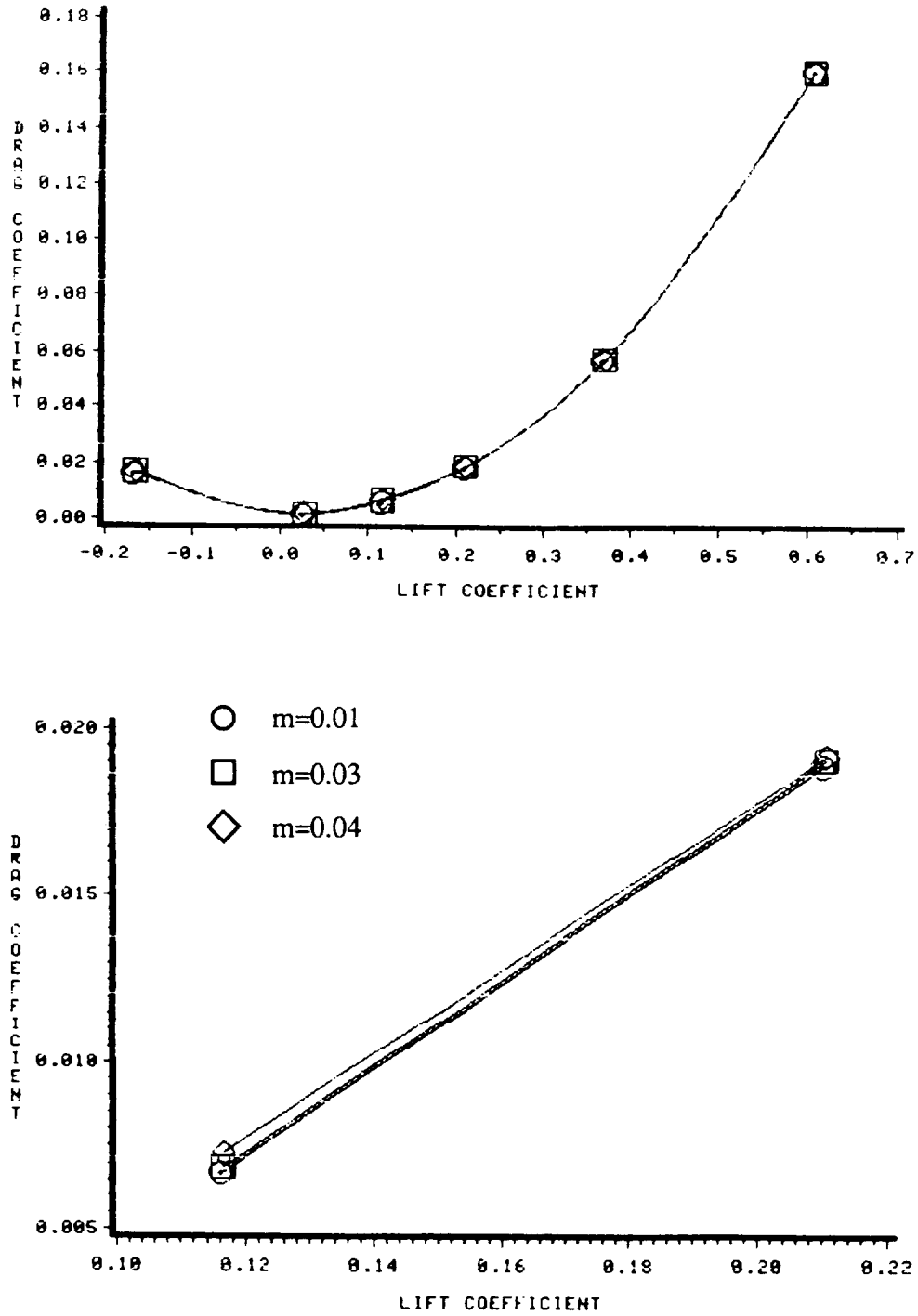

Figure 4.15.27: Predicted performance of the NACA 1402 base wing with 2% thick, 75° anhedral winglets with various cambers; M=1.62; pressure drag coefficient versus lift coefficient.

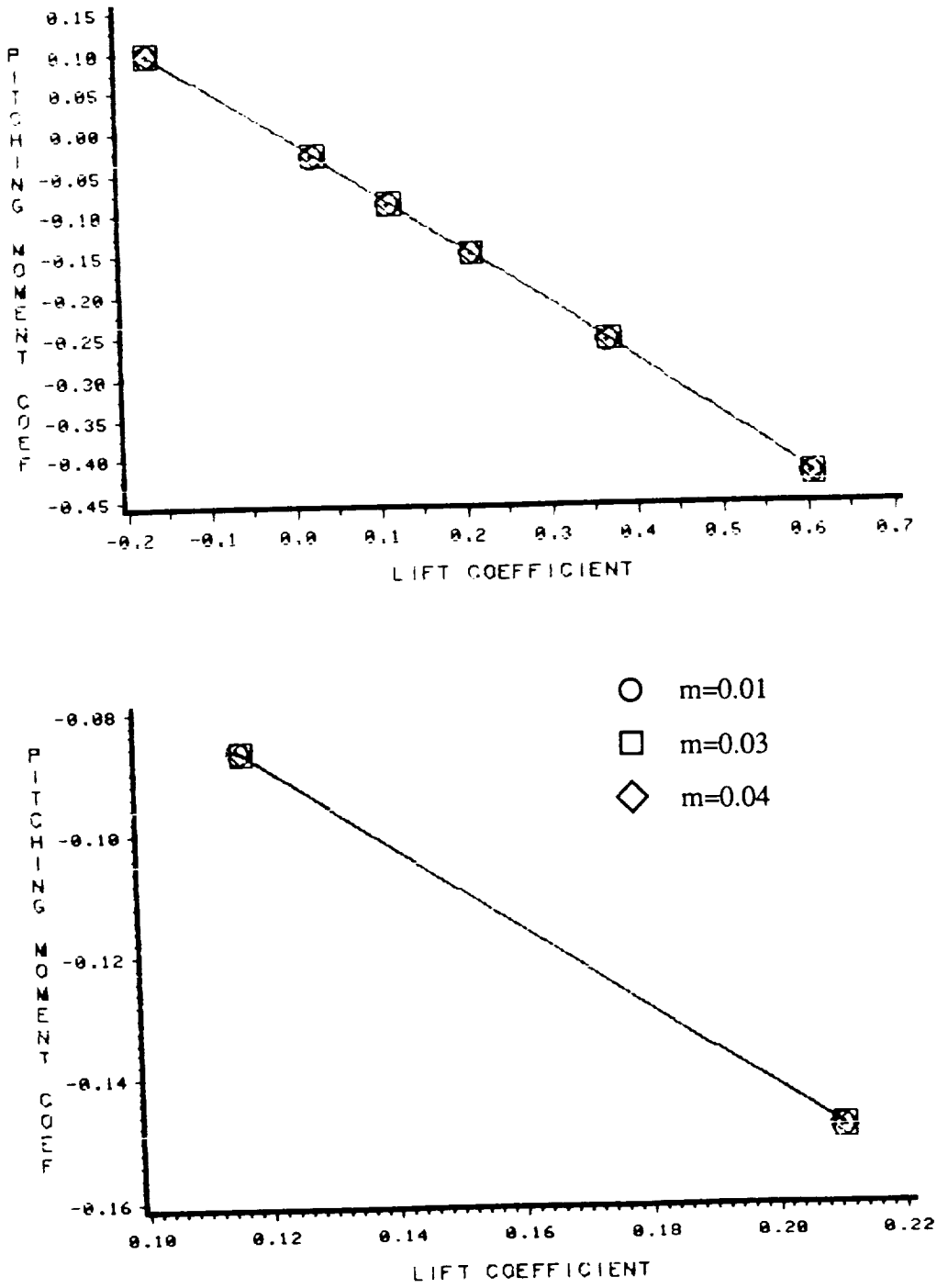

Figure 4.15.28: Predicted performance of the NACA 1402 base wing with 2% thick, 75° anhedral winglets with various cambers; M=1.62; pitching moment coefficient versus lift coefficient.

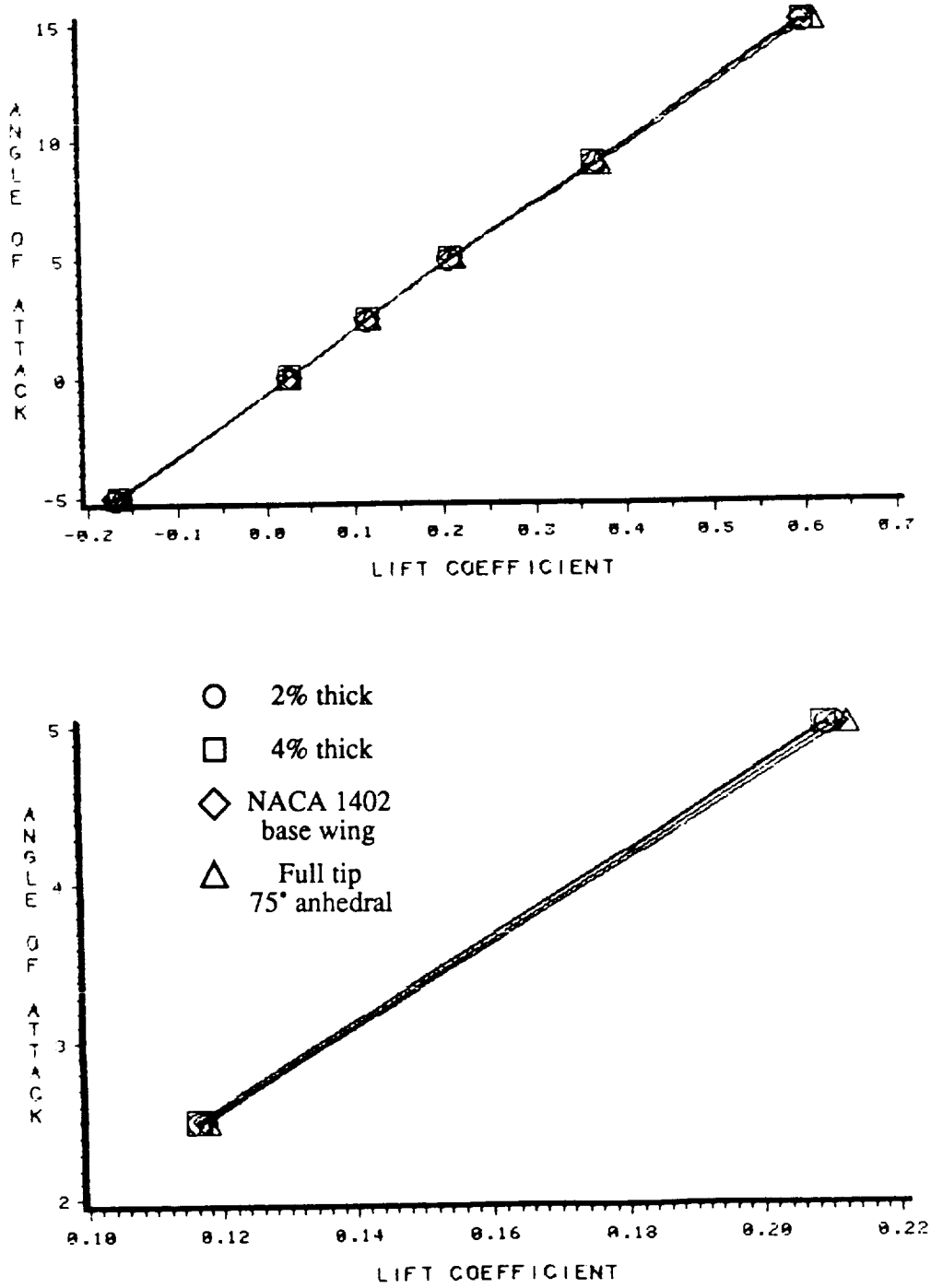

Figure 4.15.29: Comparison of the predicted performance of the NACA 1402 base wing with extension and three wing-winglets where the winglets were: 2% thick, 4% thick, and full tip at 75° anhedral; M=1.62; angle of attack versus lift coefficient.

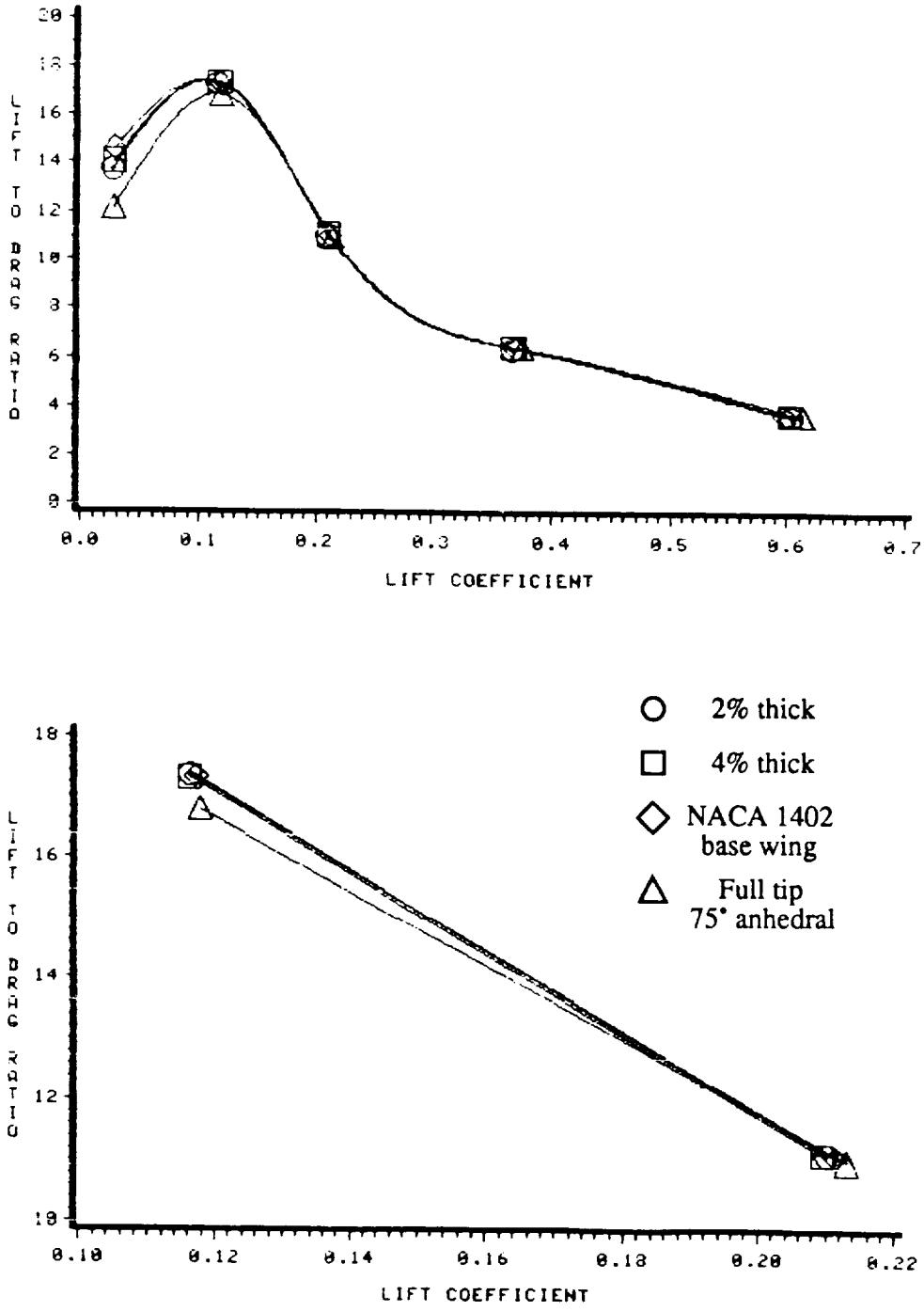

Figure 4.15.30: Comparison of the predicted performance of the NACA 1402 base wing with extension and three wing-winglets where the winglets were: 2% thick, 4% thick, and full tip at 75° anhedral; M=1.62; lift-to-pressure drag ratio versus lift coefficient.

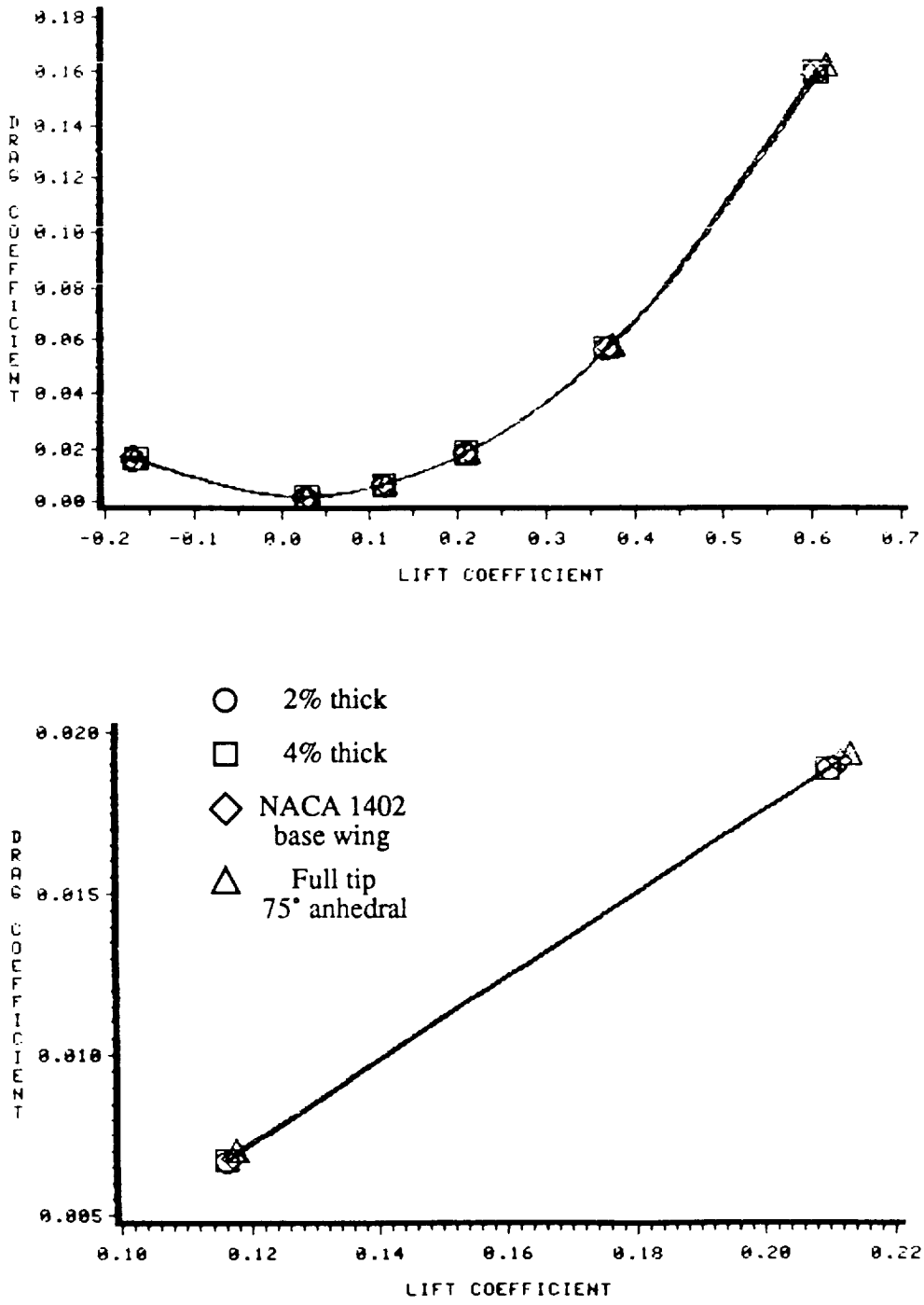

Figure 4.15.31: Comparison of the predicted performance of the NACA 1402 base wing with extension and three wing-winglets where the winglets were: 2% thick, 4% thick, and full tip at 75° anhedral; M=1.62; pressure drag coefficient versus lift coefficient.

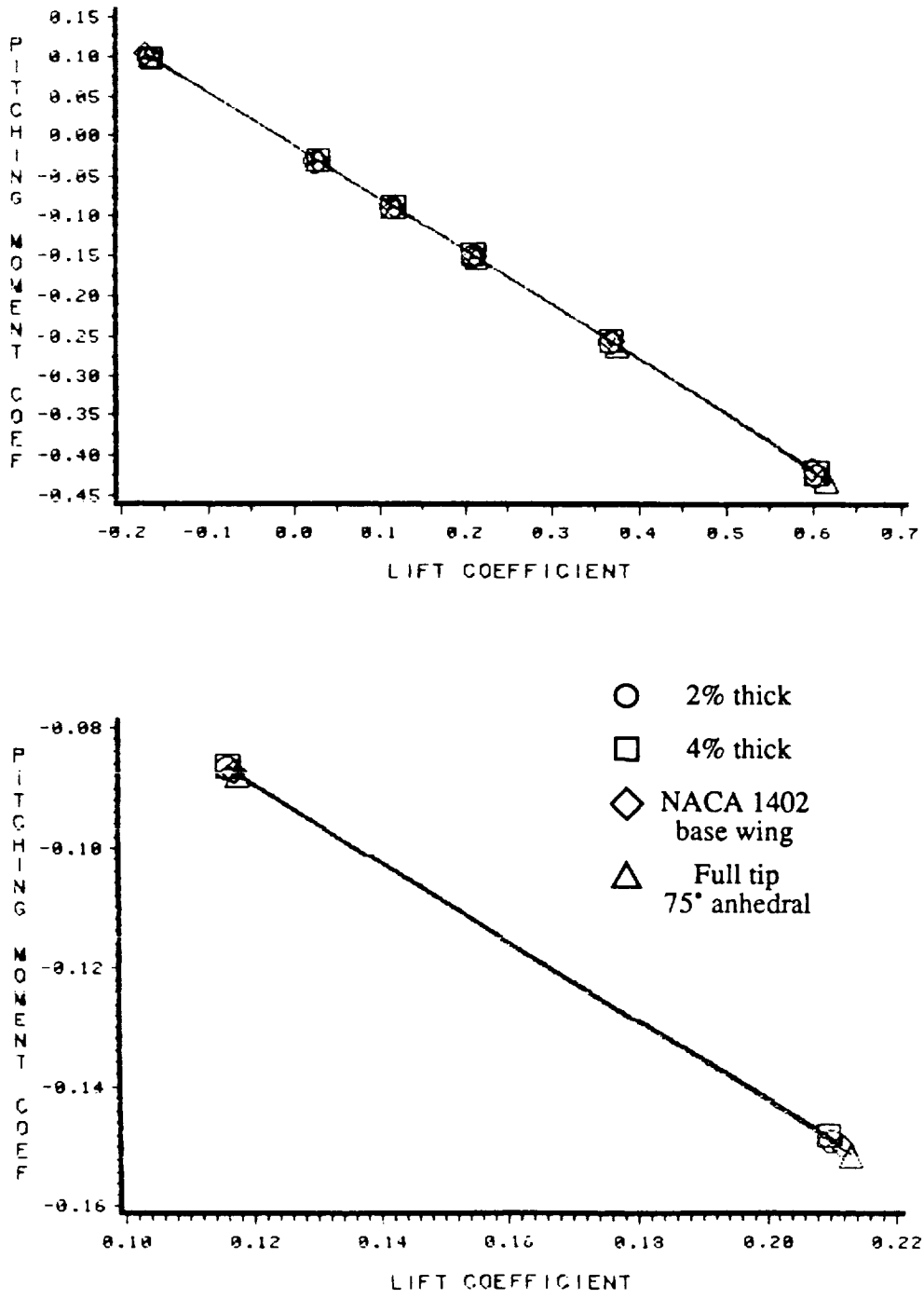

Figure 4.15.32: Comparison of the predicted performance of the NACA 1402 base wing with extension and three wing-winglets where the winglets were: 2% thick, 4% thick, and full tip at 75° anhedral; M=1.62; pitching moment coefficient versus lift coefficient.

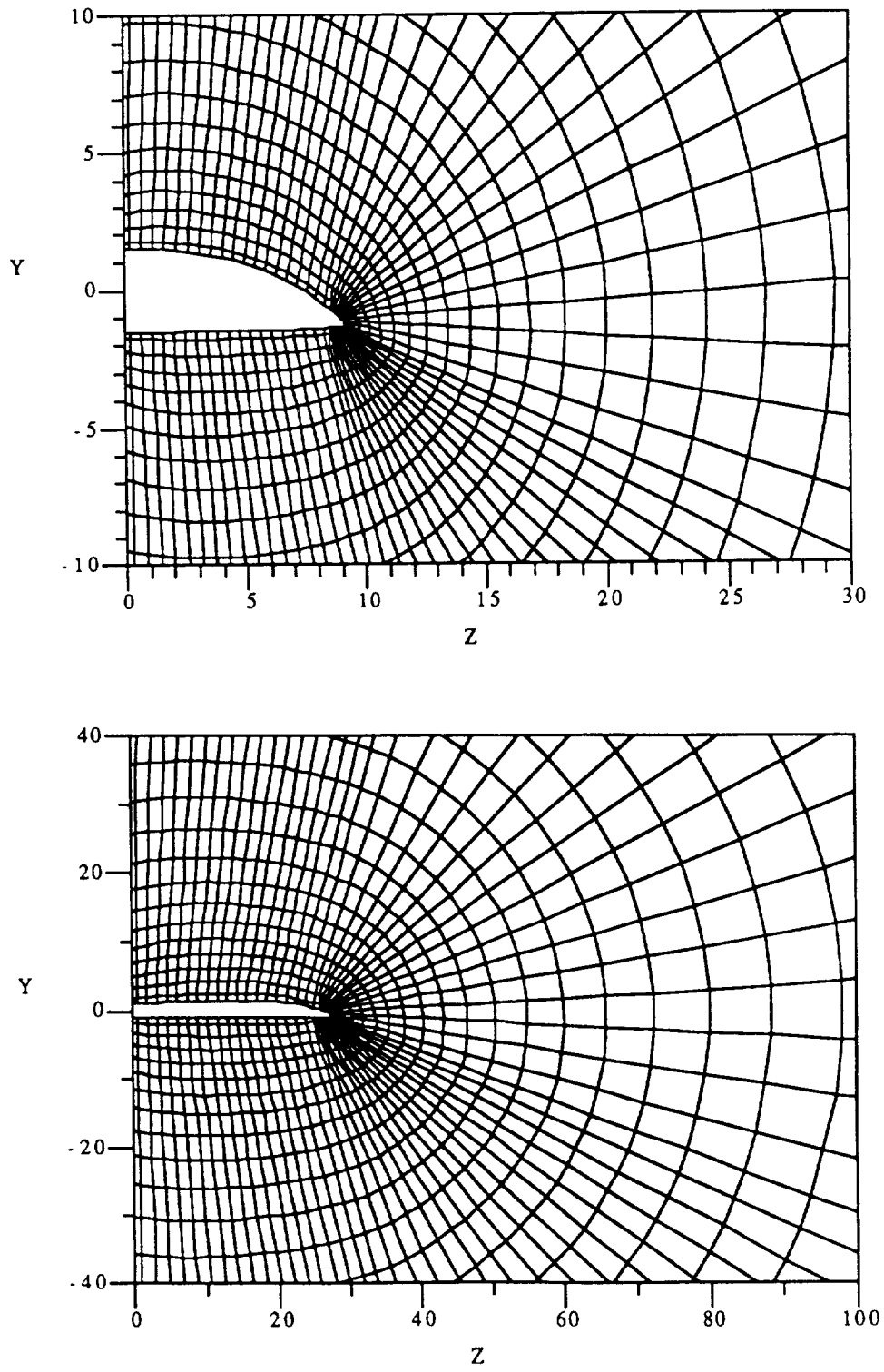

Figure 4.16.1: Computational grids for the "natural" flow wing at x= 19.7, 59.7, 92.8, 99.6.

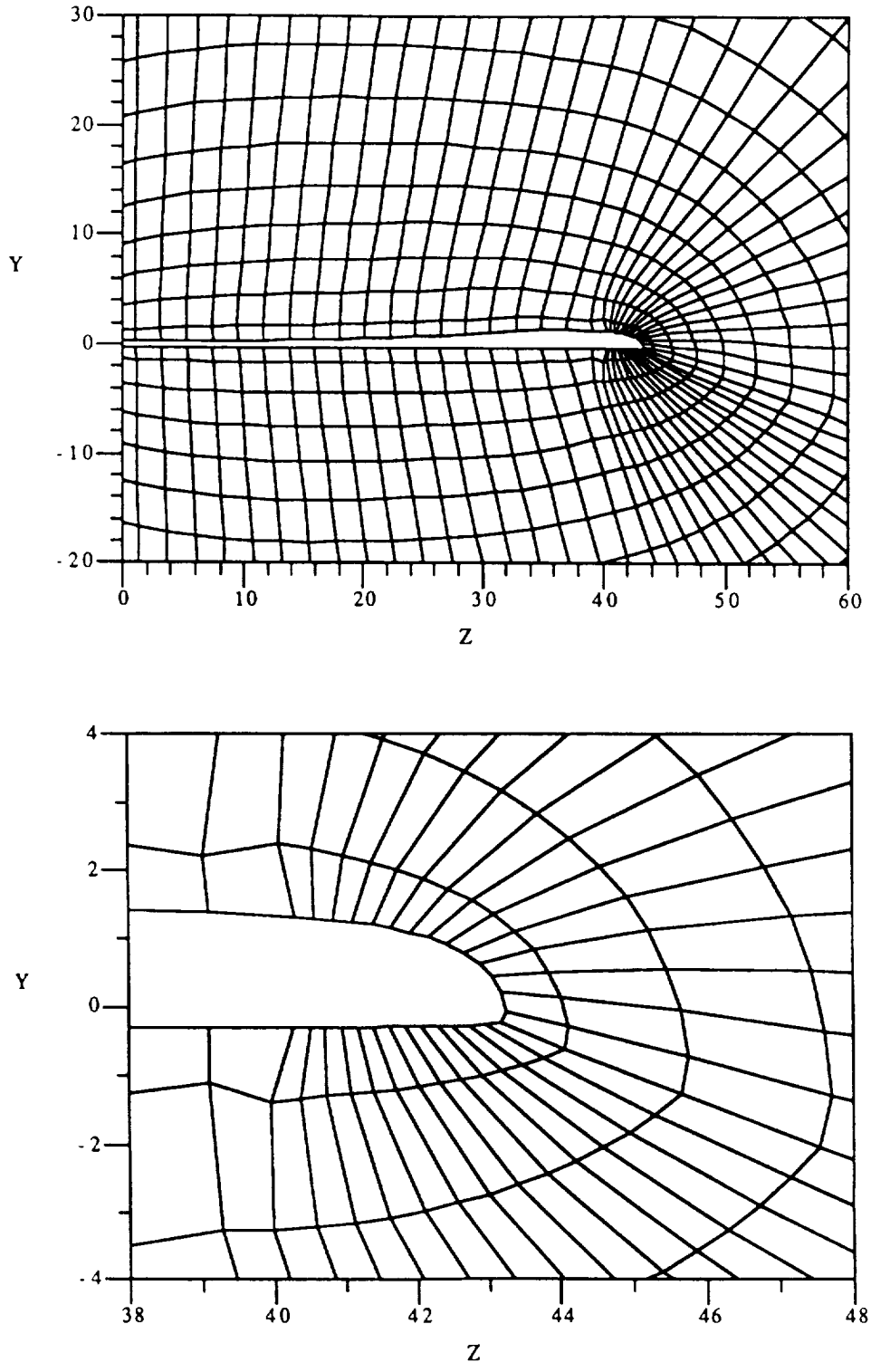

Figure 4.16.1: Continued, x=92.8.

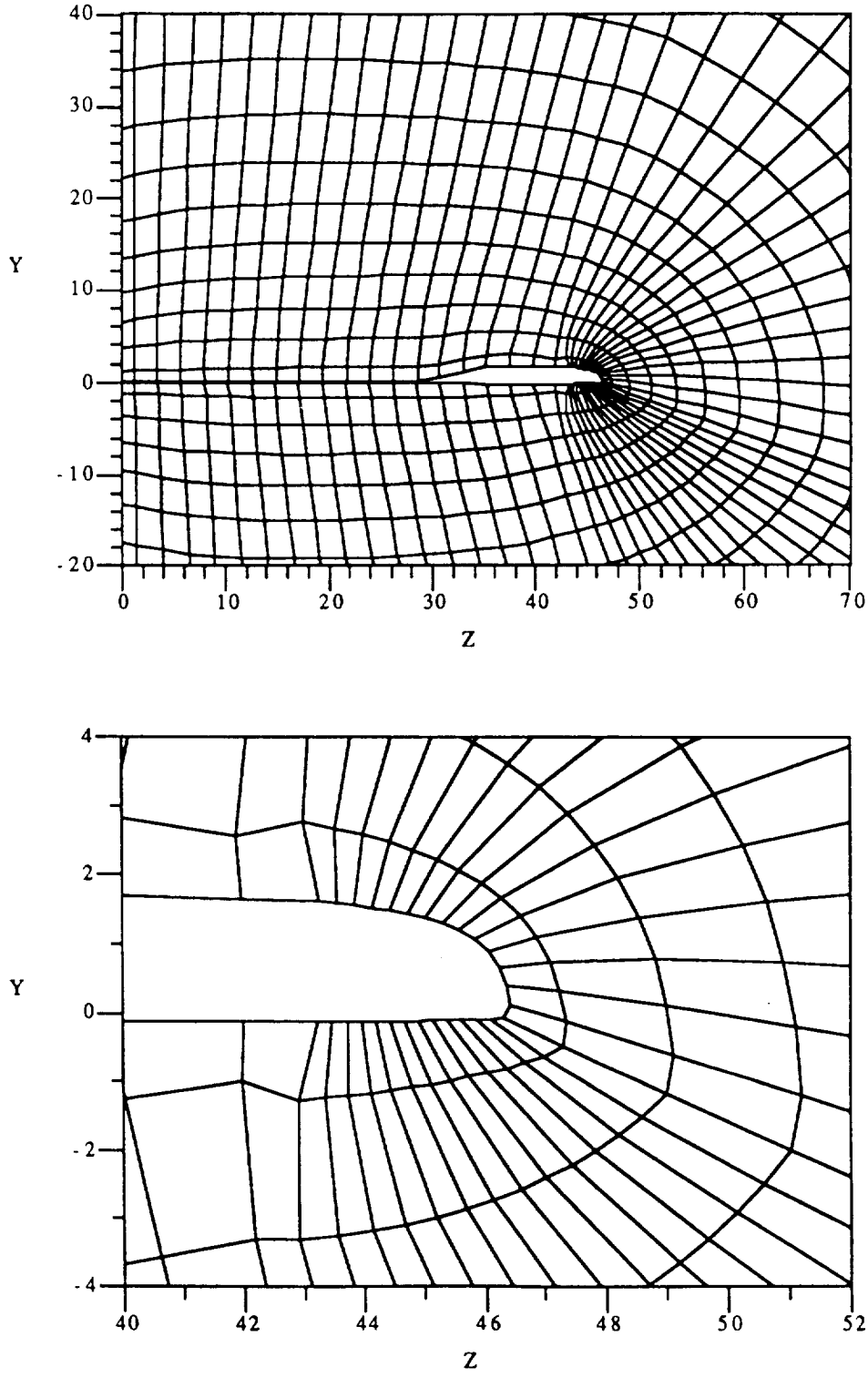

Figure 4.16.1: Continued, x=99.6.

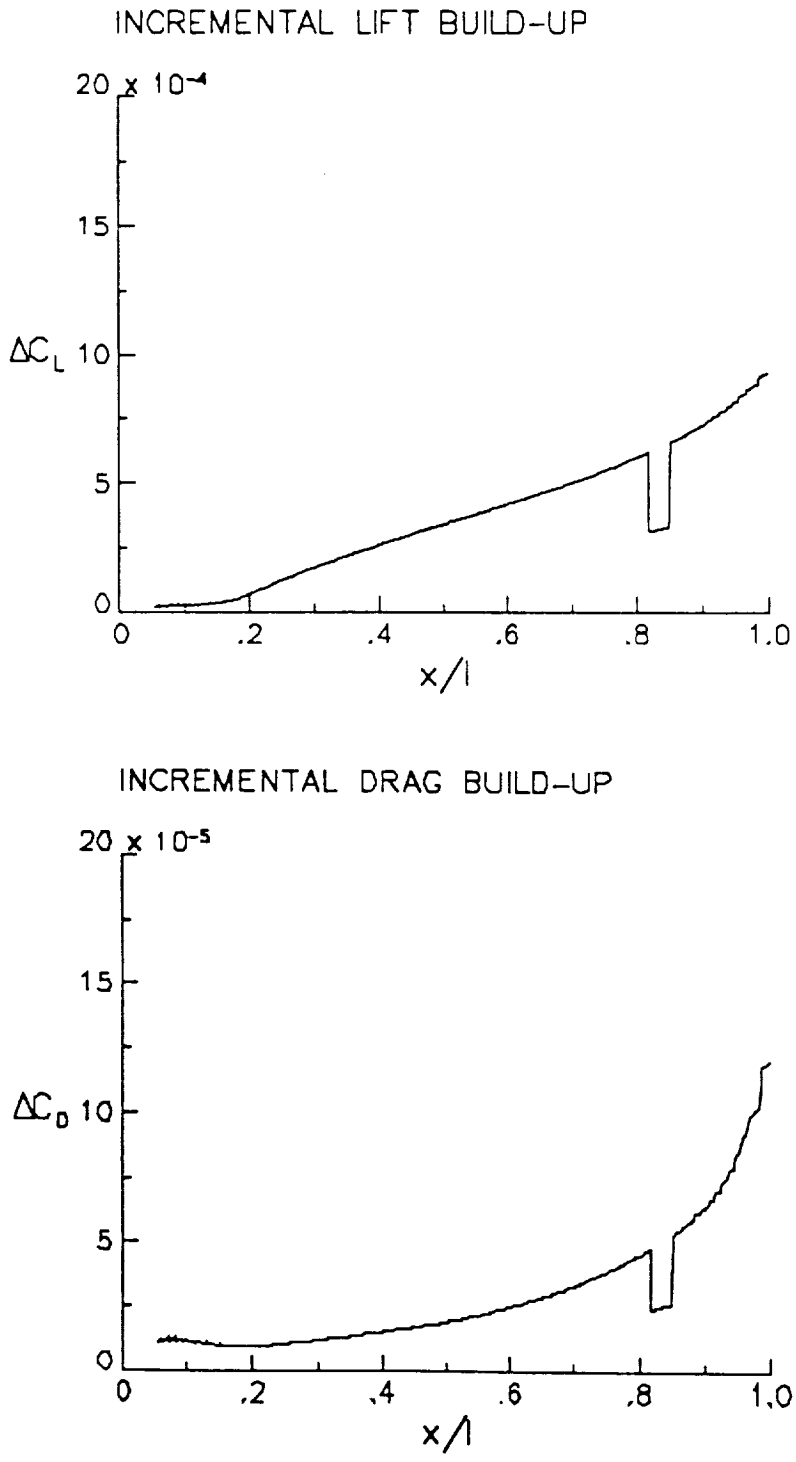

Figure 4.16.2: Incremental lift and pressure drag build up for the "natural" flow wing at 5° angle of attack, M=1.62.

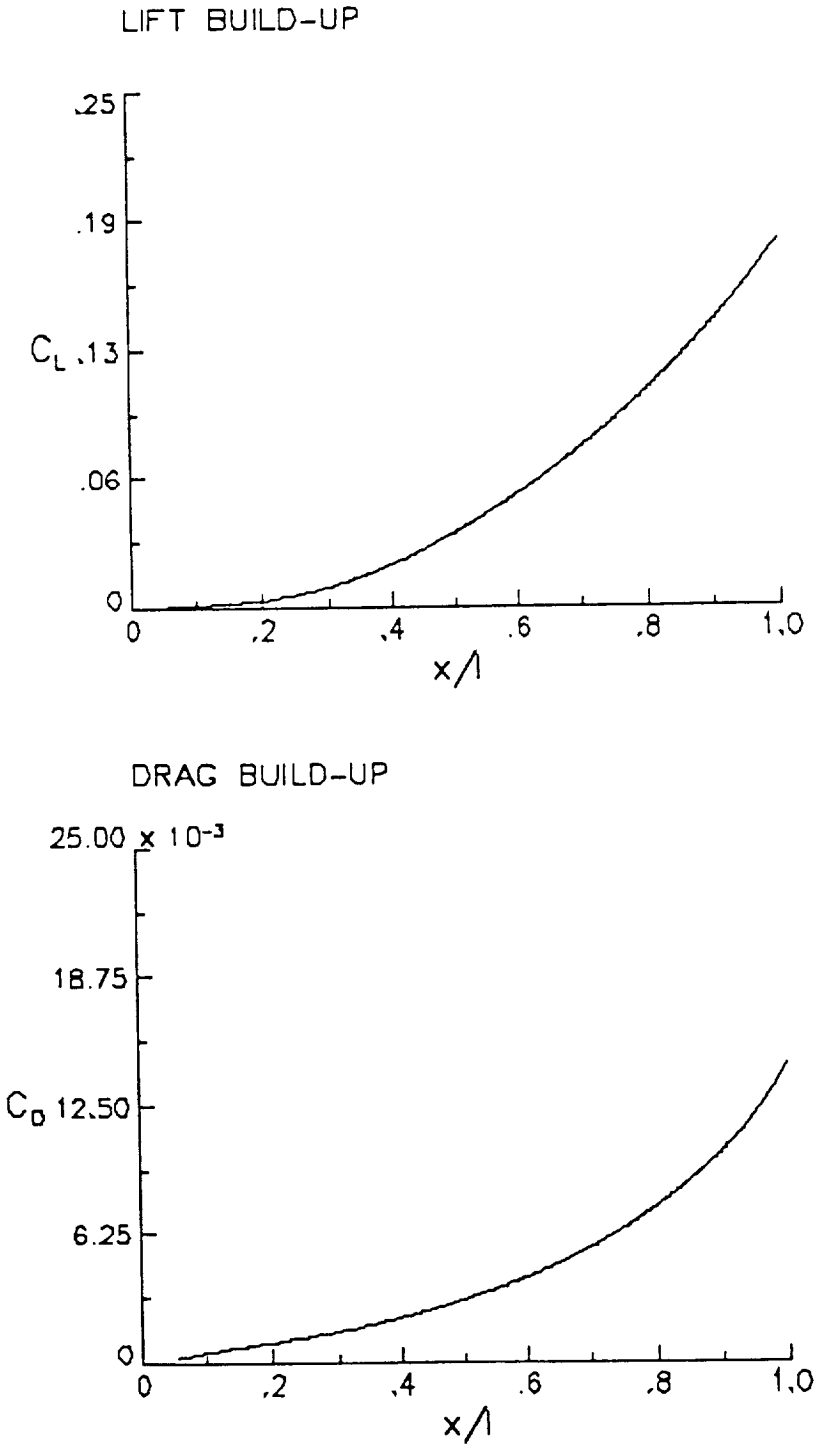

Figure 4.16.3: Total lift and pressure drag build up for the "natural" flow wing at 5° angle of attack, M=1.62.

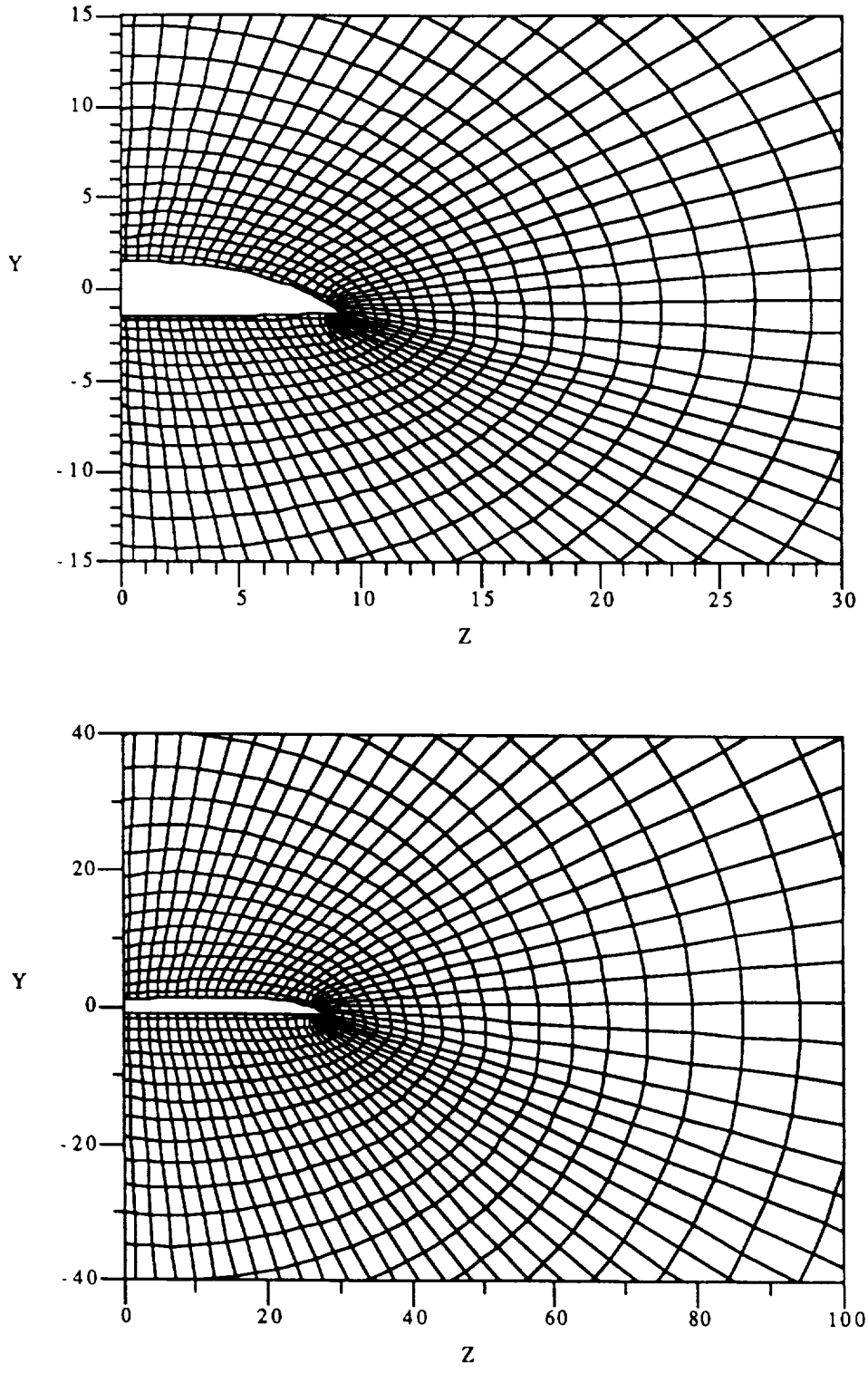

Figure 4.16.4: Computational grids for the "natural" flow wing with a 2° toe out, 65° dihedral at x= 19.7, 59.7, 92.8, 99.6.

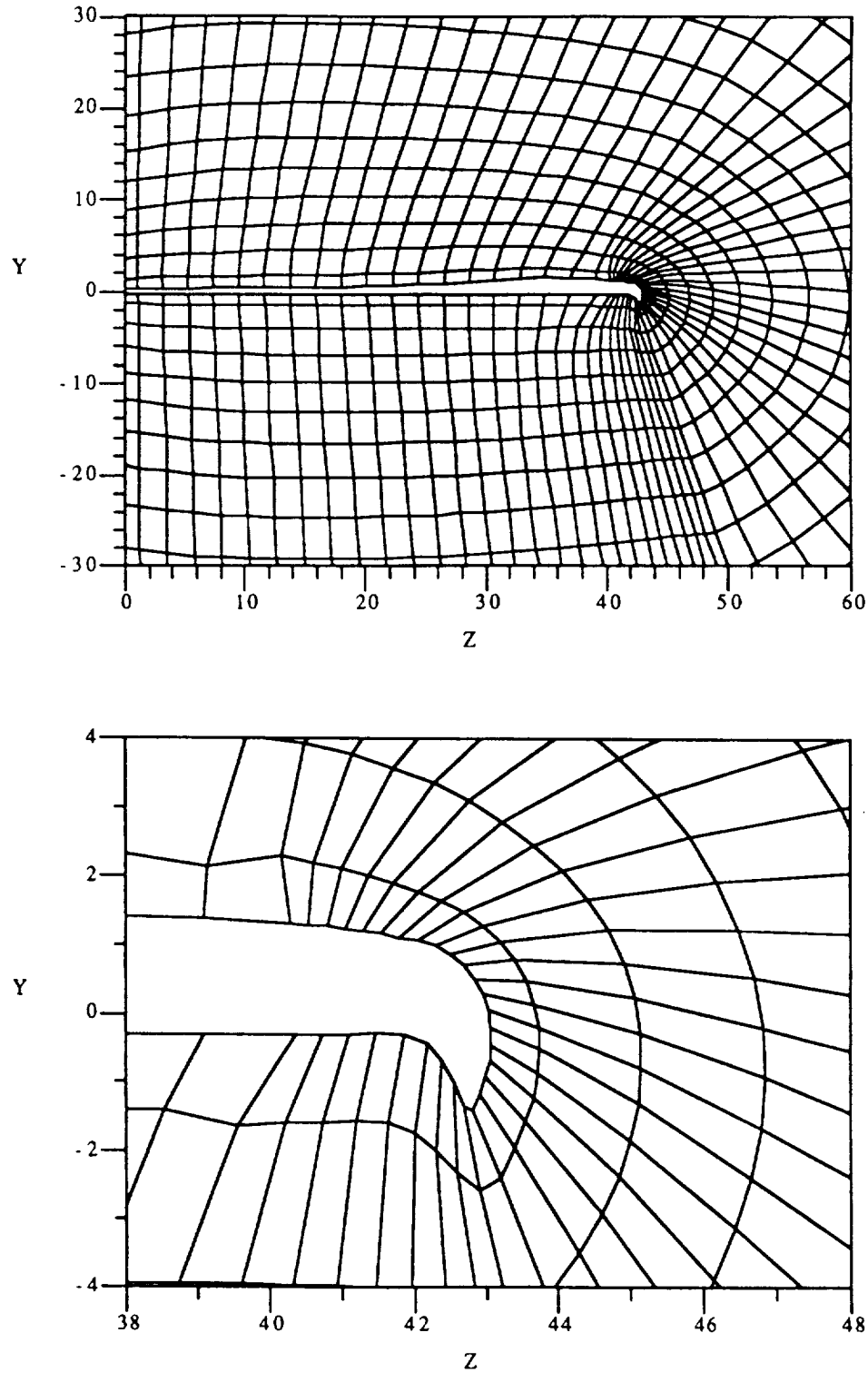

Figure 4.16.4: Continued, x=92.8.

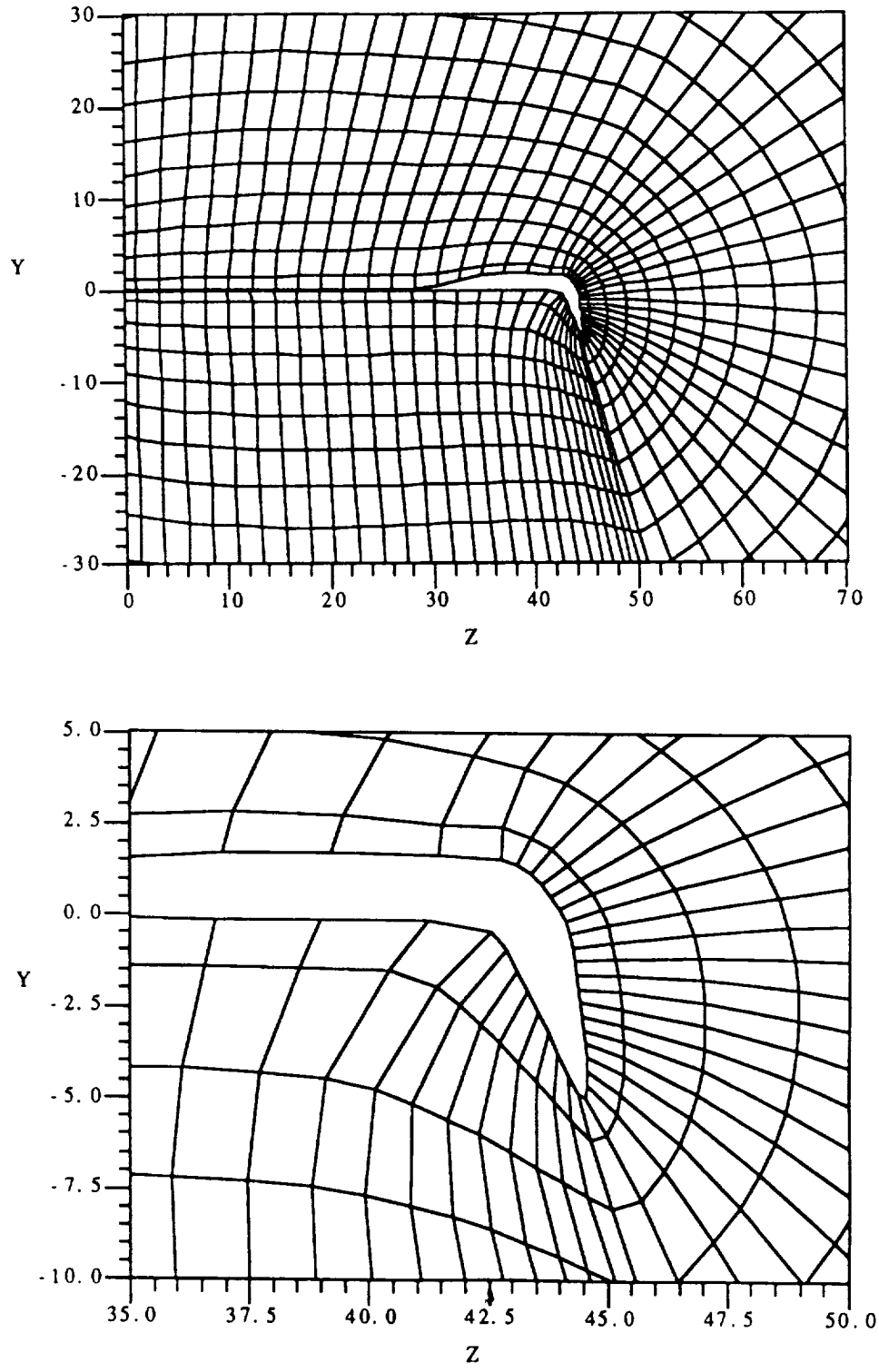

Figure 4.16.4: Continued, x=99.6.

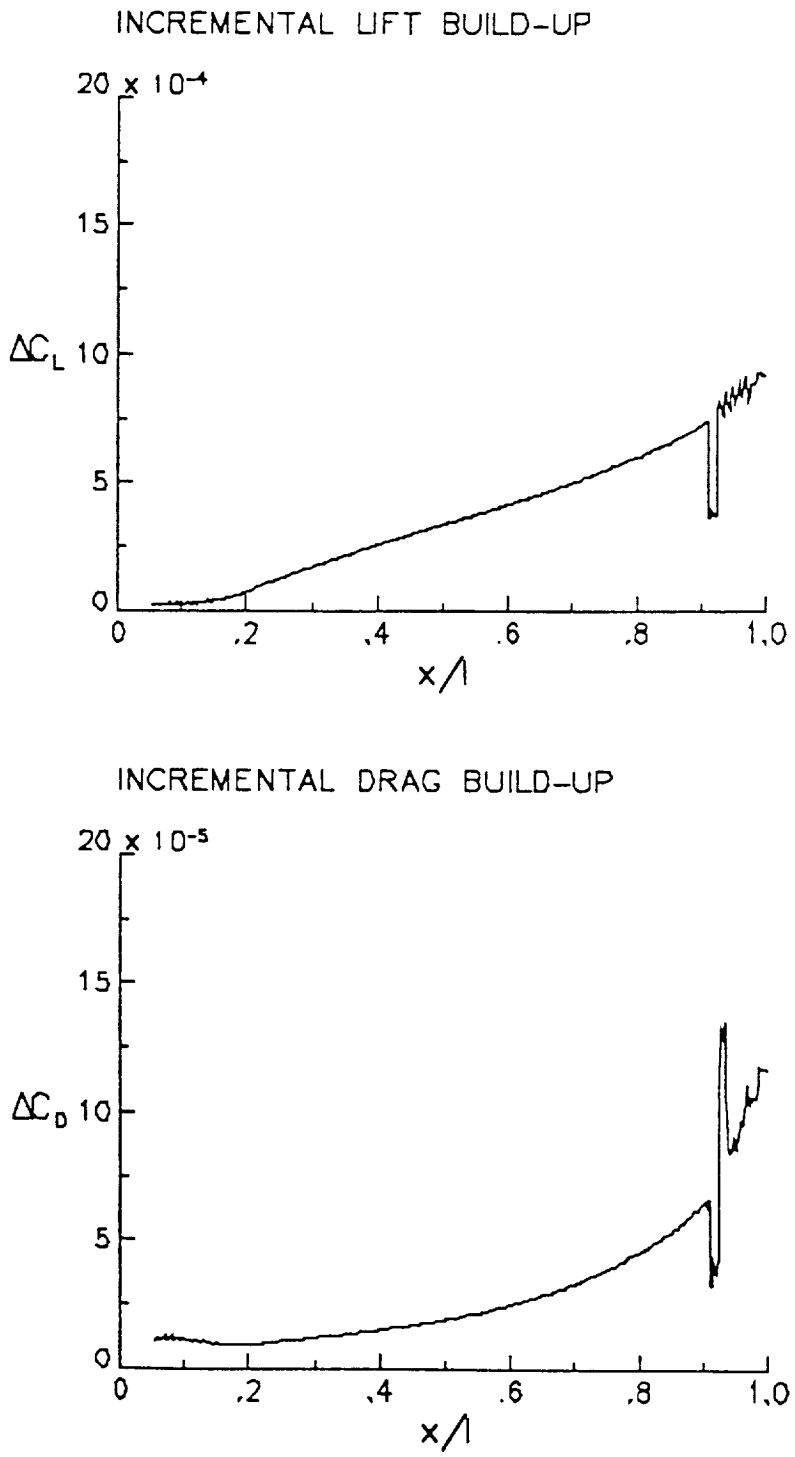

Figure 4.16.5: Incremental lift and pressure drag build up for the "natural" flow wing with a 2° toe out, 65° anhedral winglet at 5° angle of attack, M=1.62.

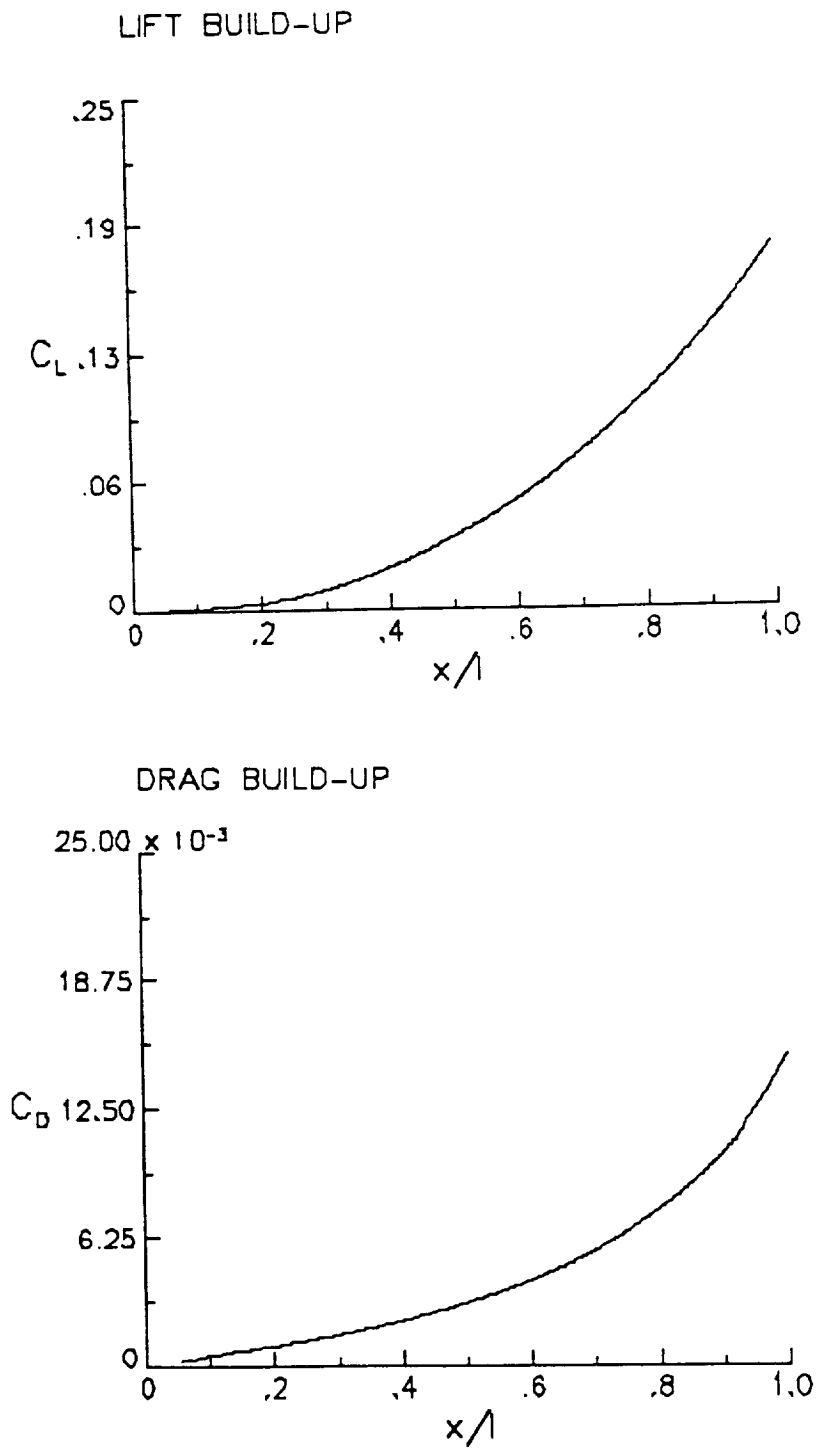

Figure 4.16.6: Total lift and pressure drag build up for the "natural" flow wing with a 2° toe out, 65° anhedral winglet at 5° angle of attack, M=1.62.

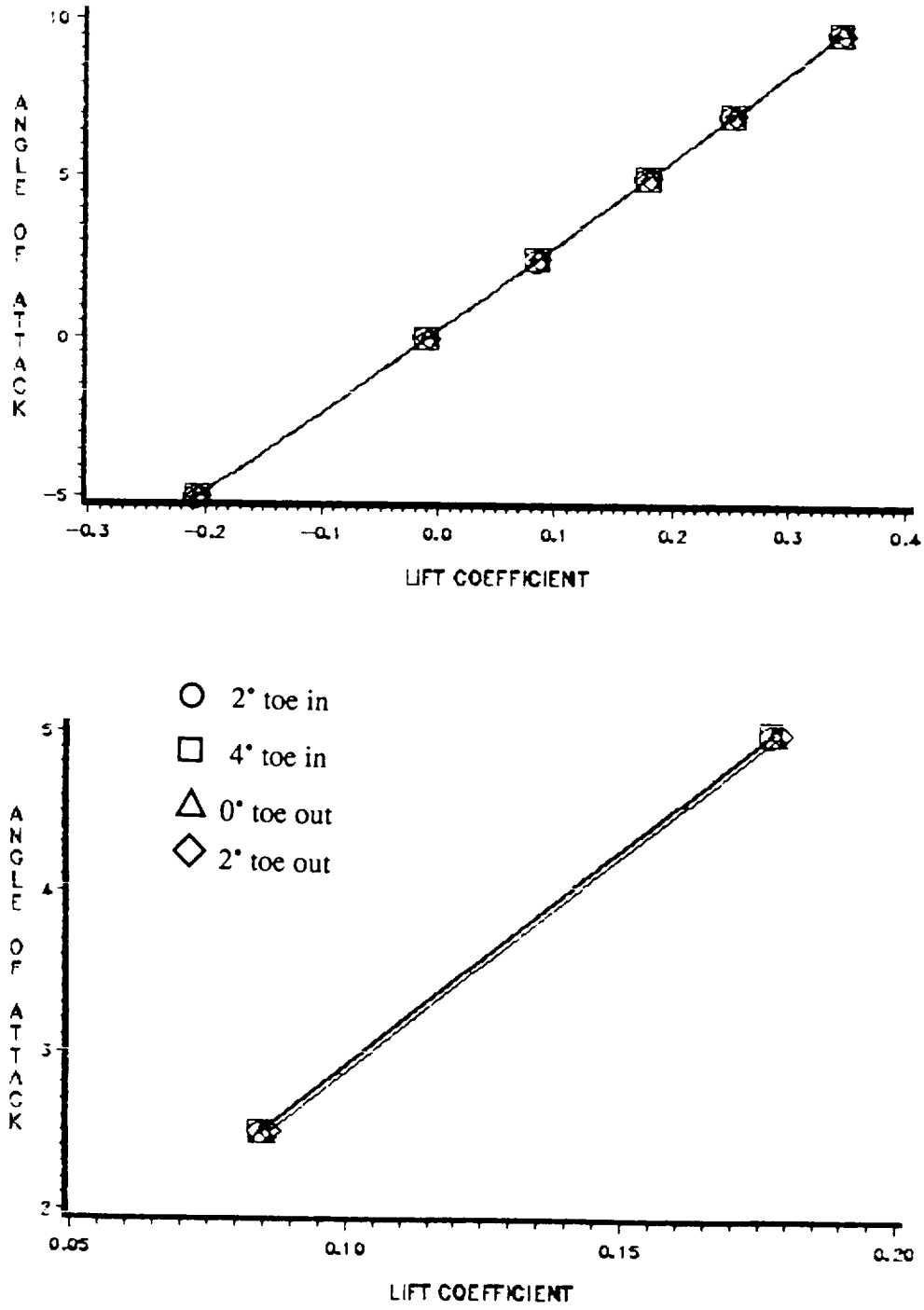

Figure 4.16.7: Predicted performance of the "natural" flow wing with 65° anhedral winglets at various toe angles; M=1.62; angle of attack versus lift coefficient.

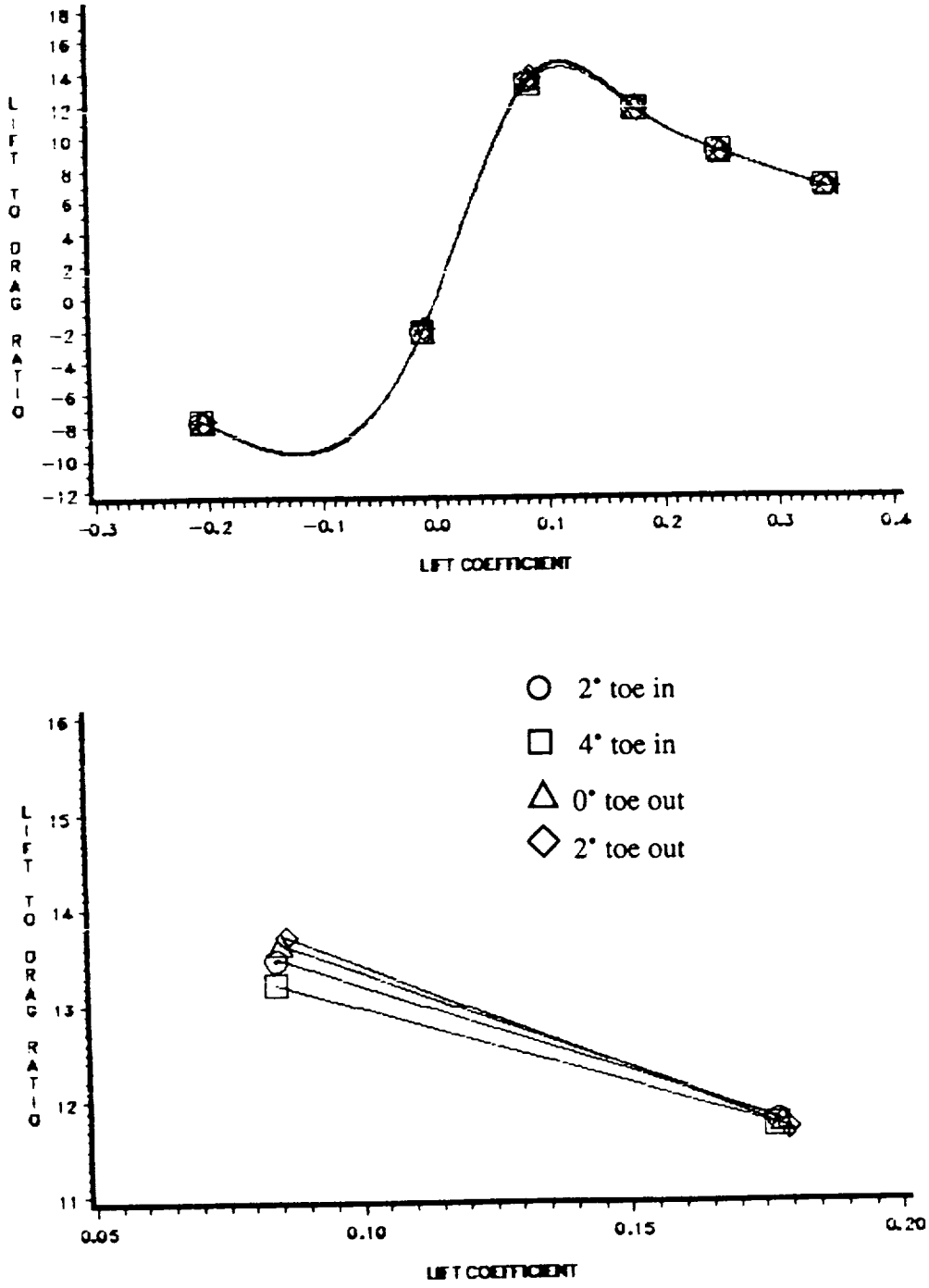

Figure 4.16.8: Predicted performance of the "natural" flow wing with 65° anhedral winglets at various toe angles; M=1.62; lift-to-drag ratio versus lift coefficient.

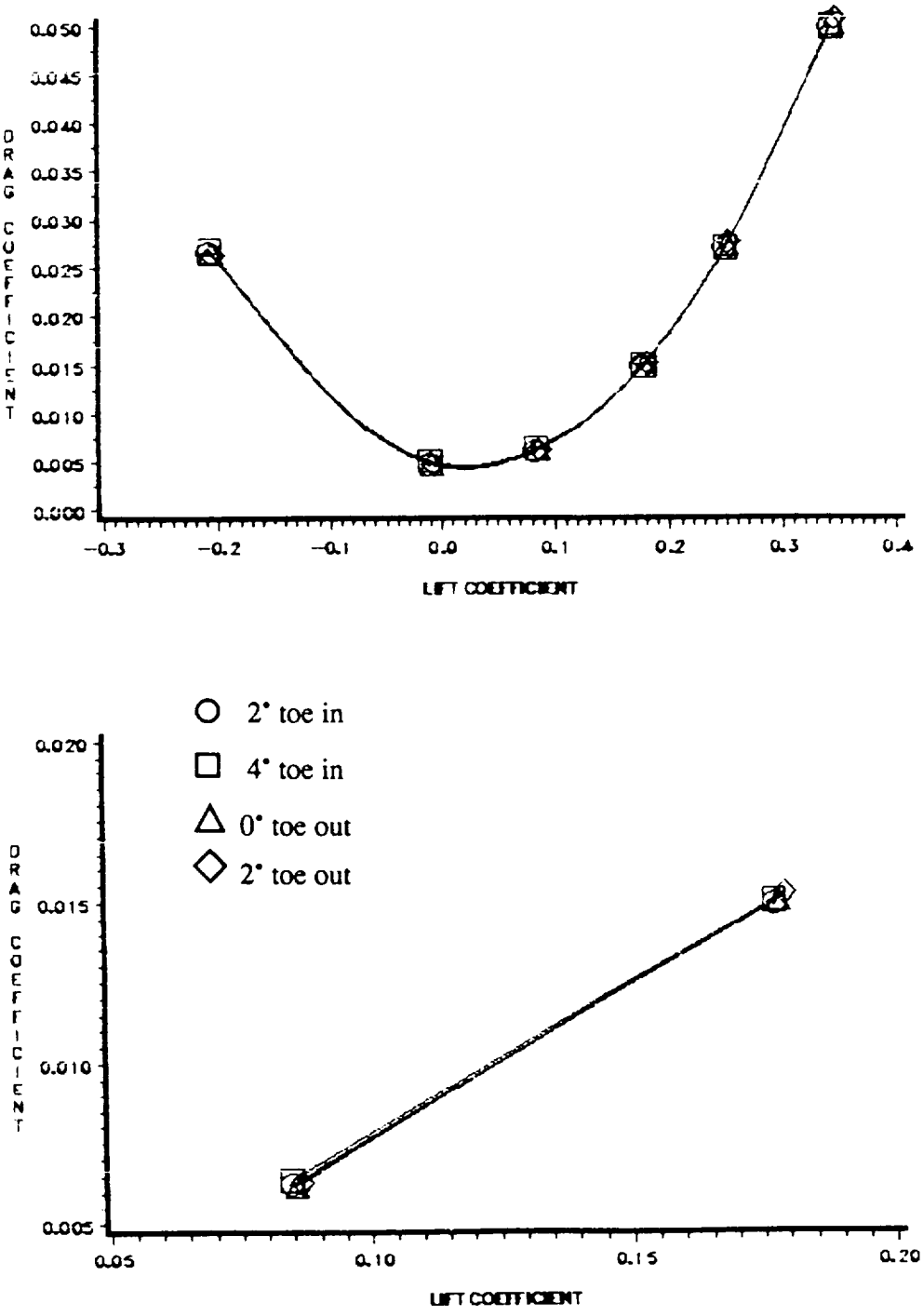

Figure 4.16.9: Predicted performance of the "natural" flow wing with 65° anhedral winglets at various toe angles; M=1.62; pressure drag coefficient versus lift coefficient.

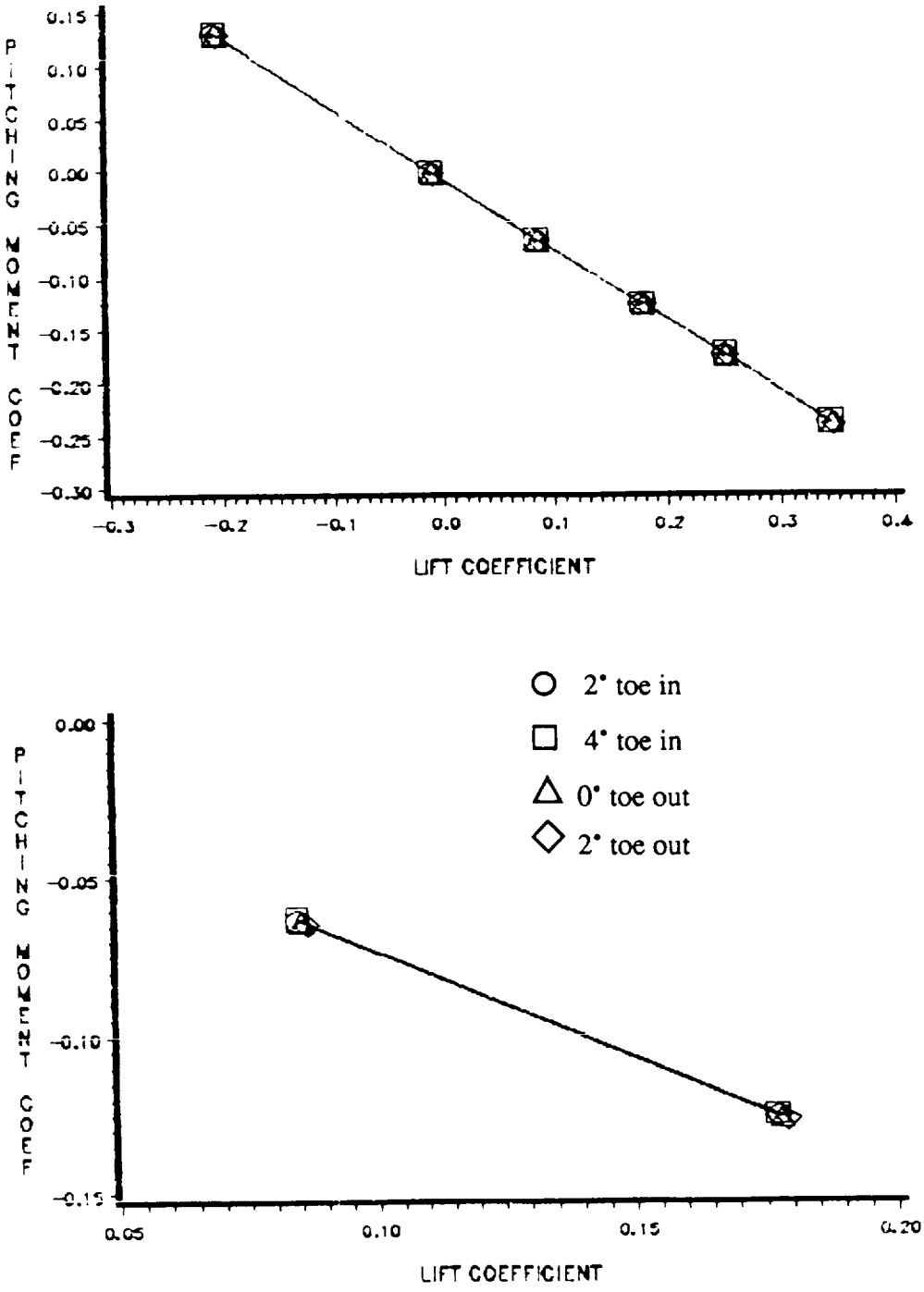

Figure 4.16.10: Predicted performance of the "natural" flow wing with 65° anhedral winglets at various toe angles; M=1.62; pitching moment coefficient versus lift coefficient.

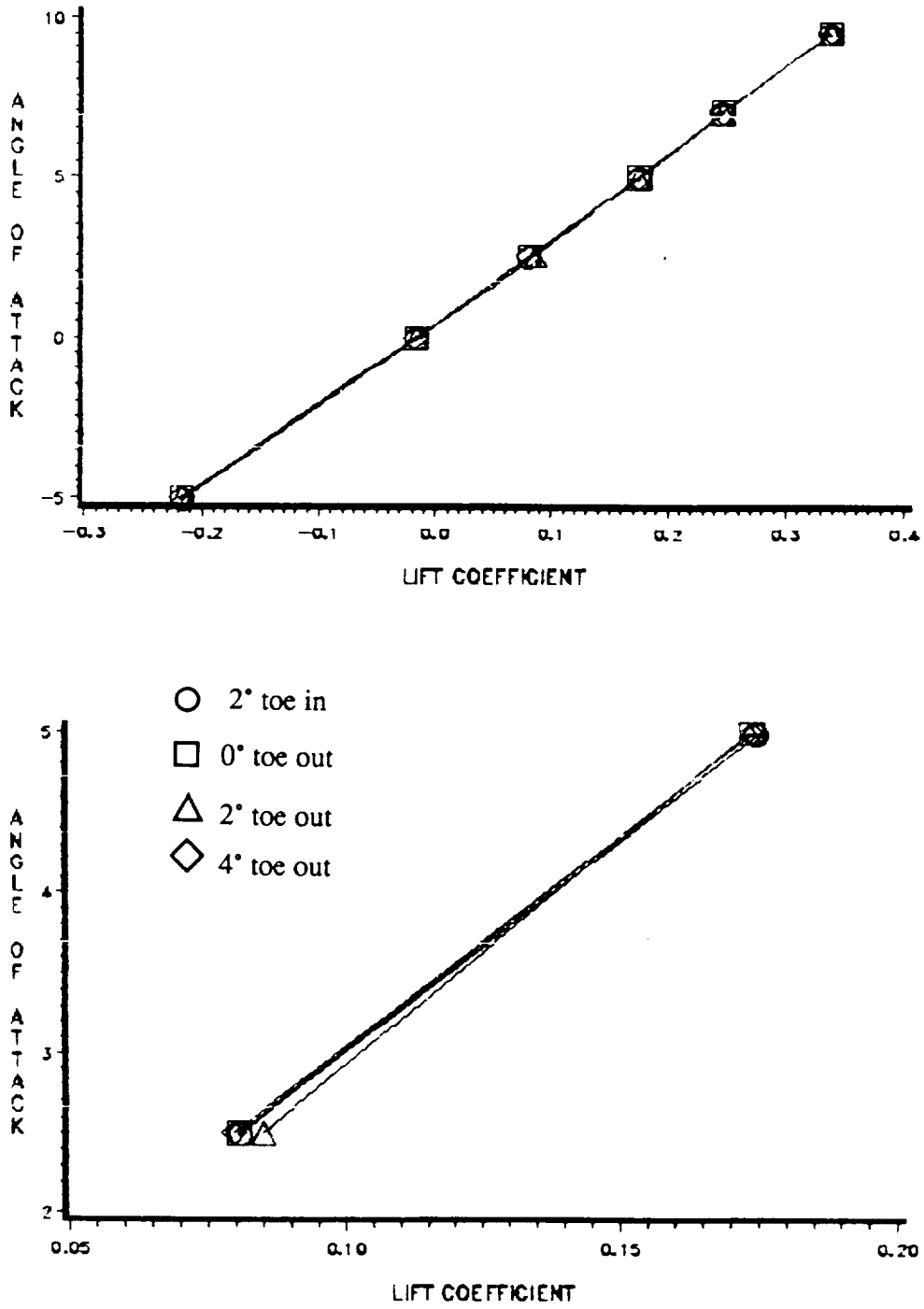

Figure 4.16.11: Predicted performance of the "natural" flow wing with 65° dihedral winglets at various toe angles; M=1.62; angle of attack versus lift coefficient.

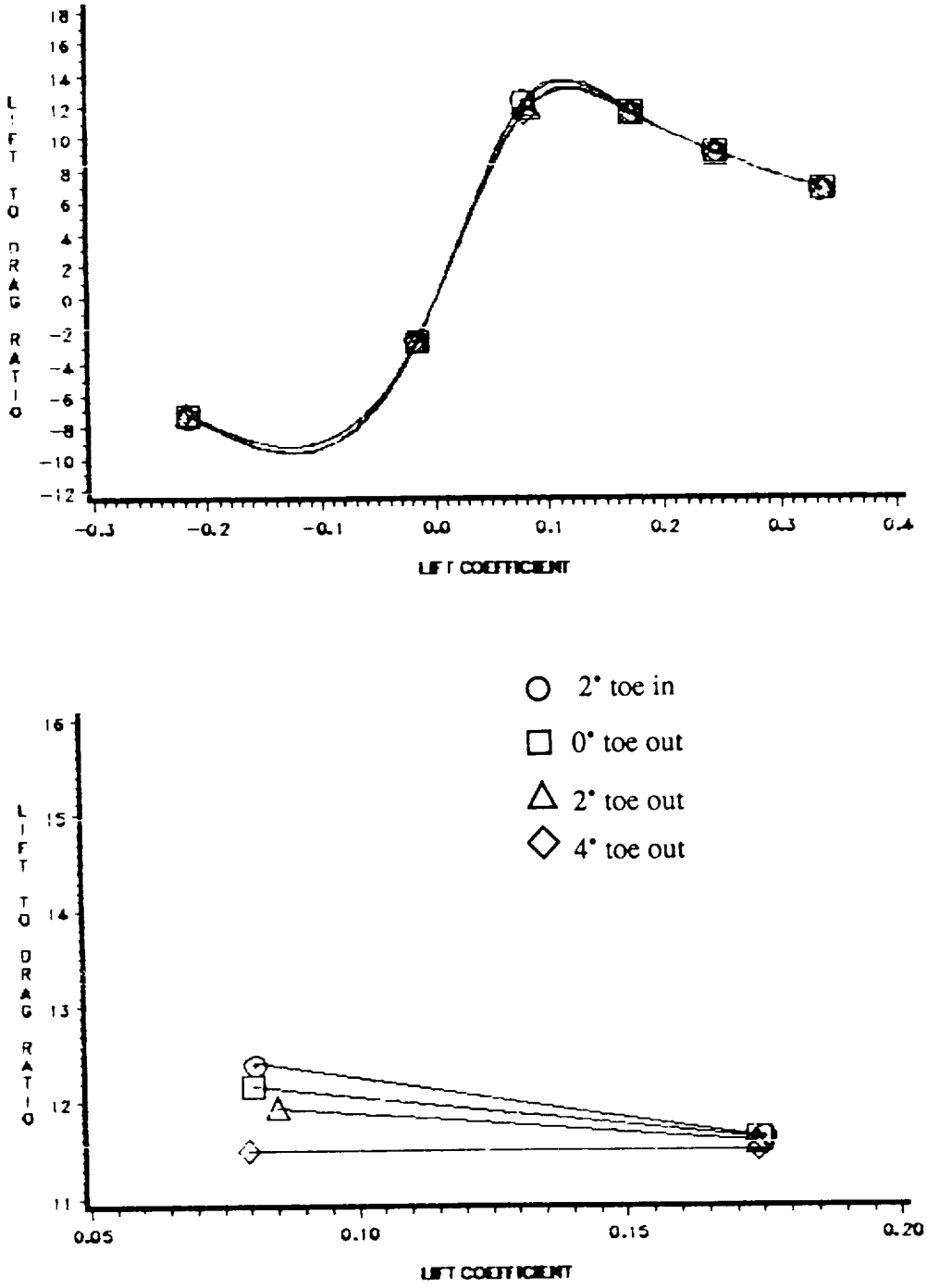

Figure 4.16.12: Predicted performance of the "natural" flow wing with 65° dihedral winglets at various toe angles; M=1.62; lift-to-pressure drag ratio versus lift coefficient.

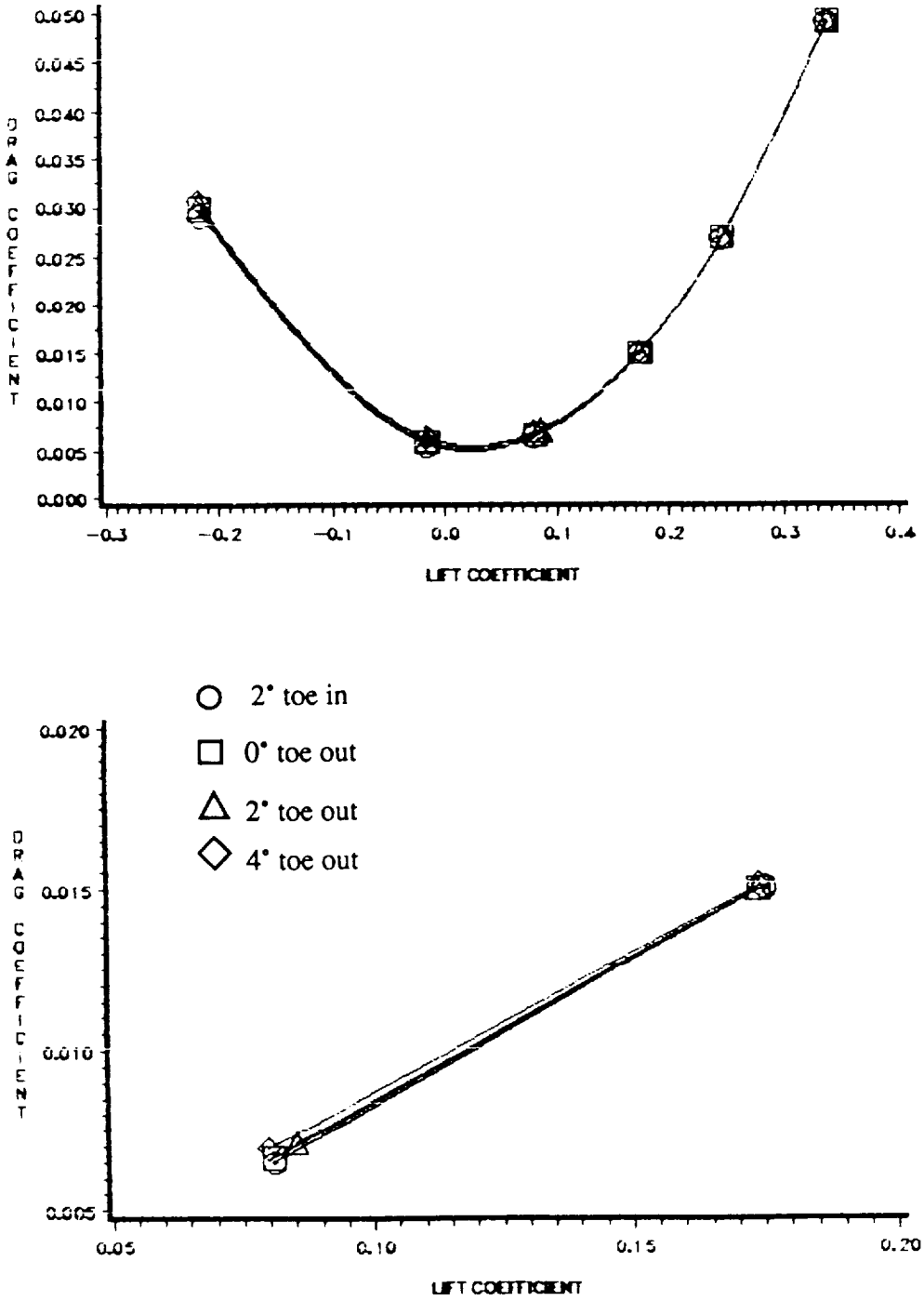

Figure 4.16.13: Predicted performance of the "natural" flow wing with 65° dihedral winglets at various toe angles; M=1.62; pressure drag coefficient versus lift coefficient.

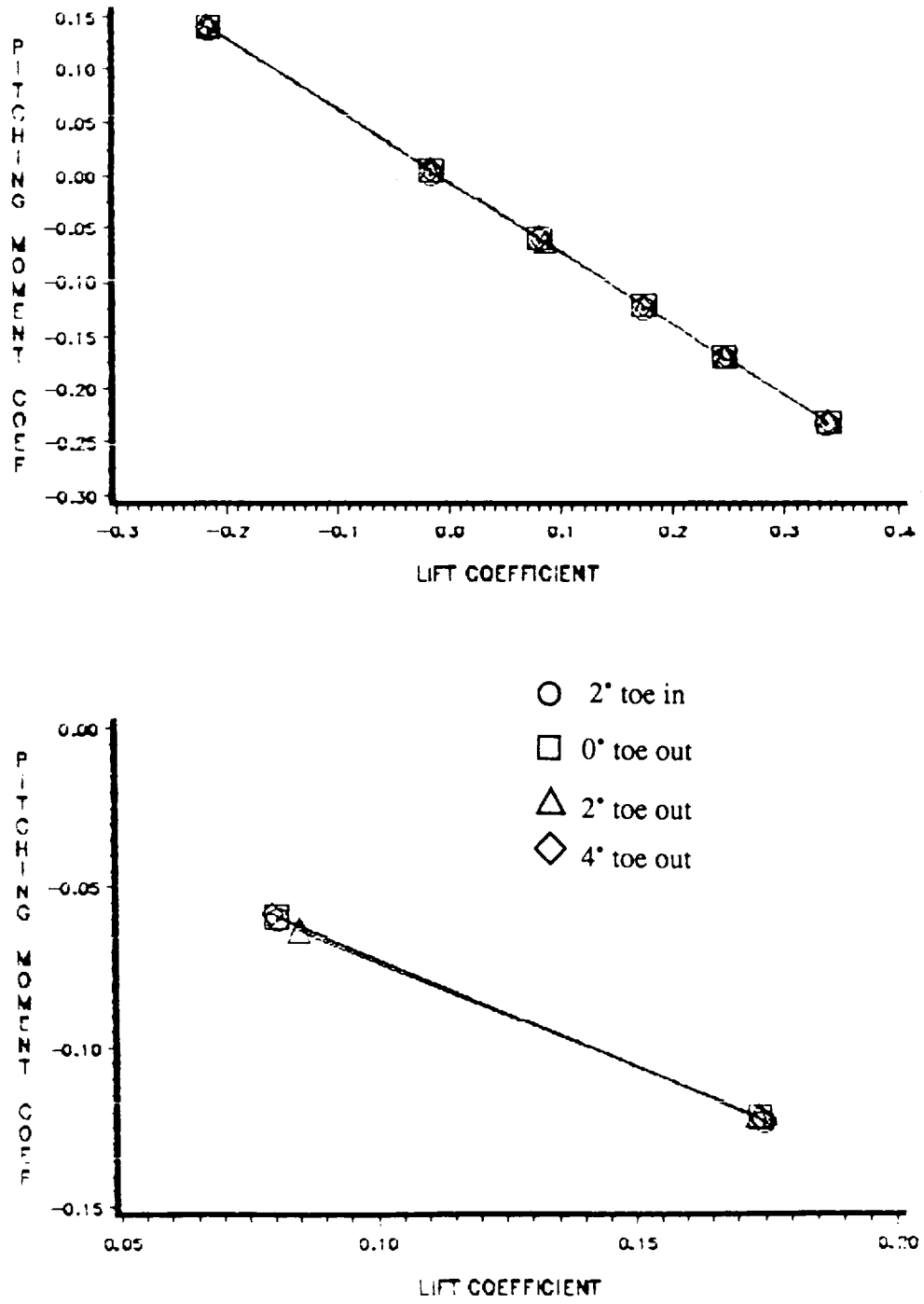

Figure 4.16.14: Predicted performance of the "natural" flow wing with 65° dihedral winglets at various toe angles; M=1.62; pitching moment coefficient versus lift coefficient.

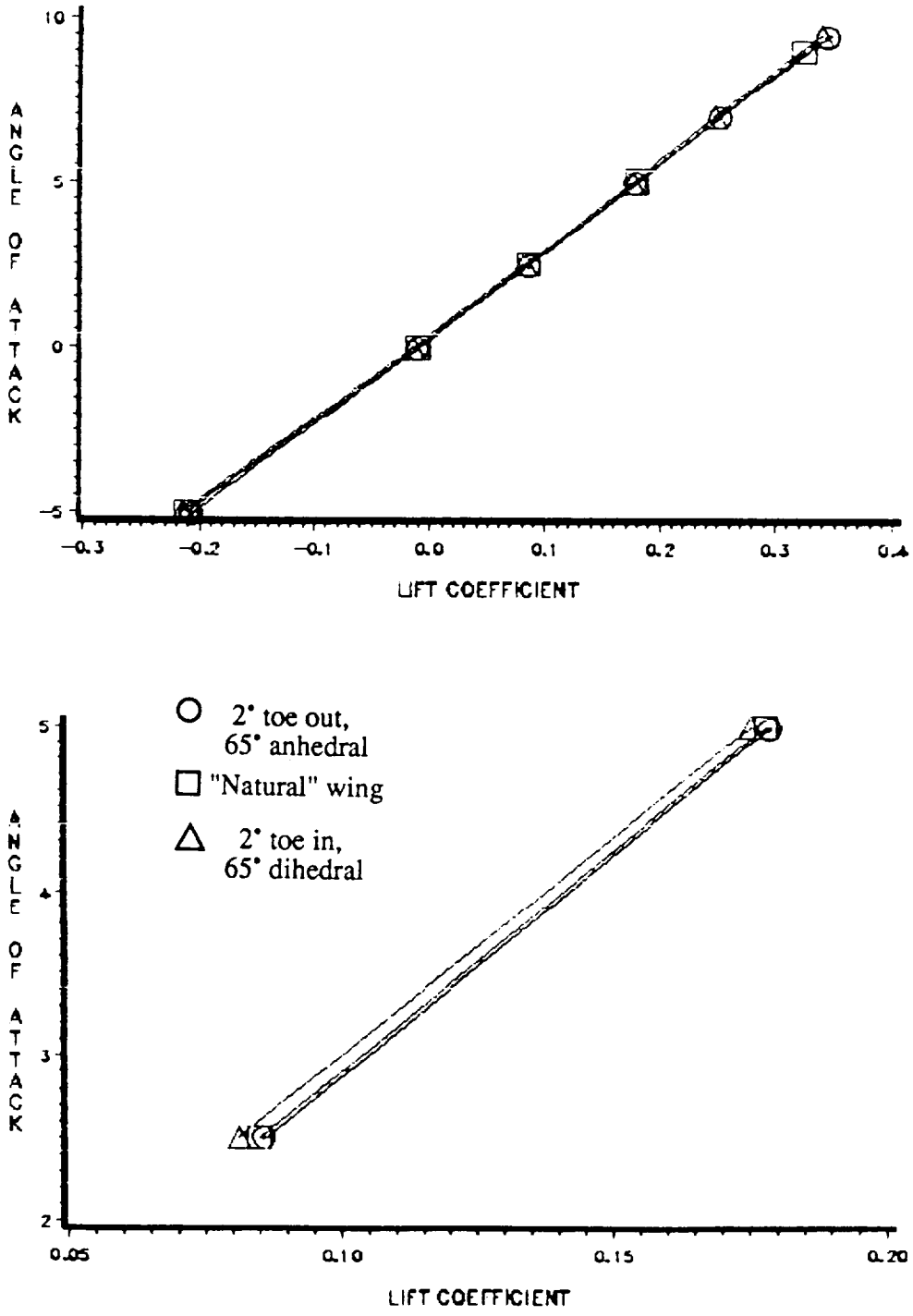

Figure 4.16.15: Comparison of the predicted performance of the "natural" flow wing; the 2° toe out, 65° anhedral winglet; and the 2° toe in, 65° dihedral winglet; M=1.62; angle of attack versus lift coefficient.

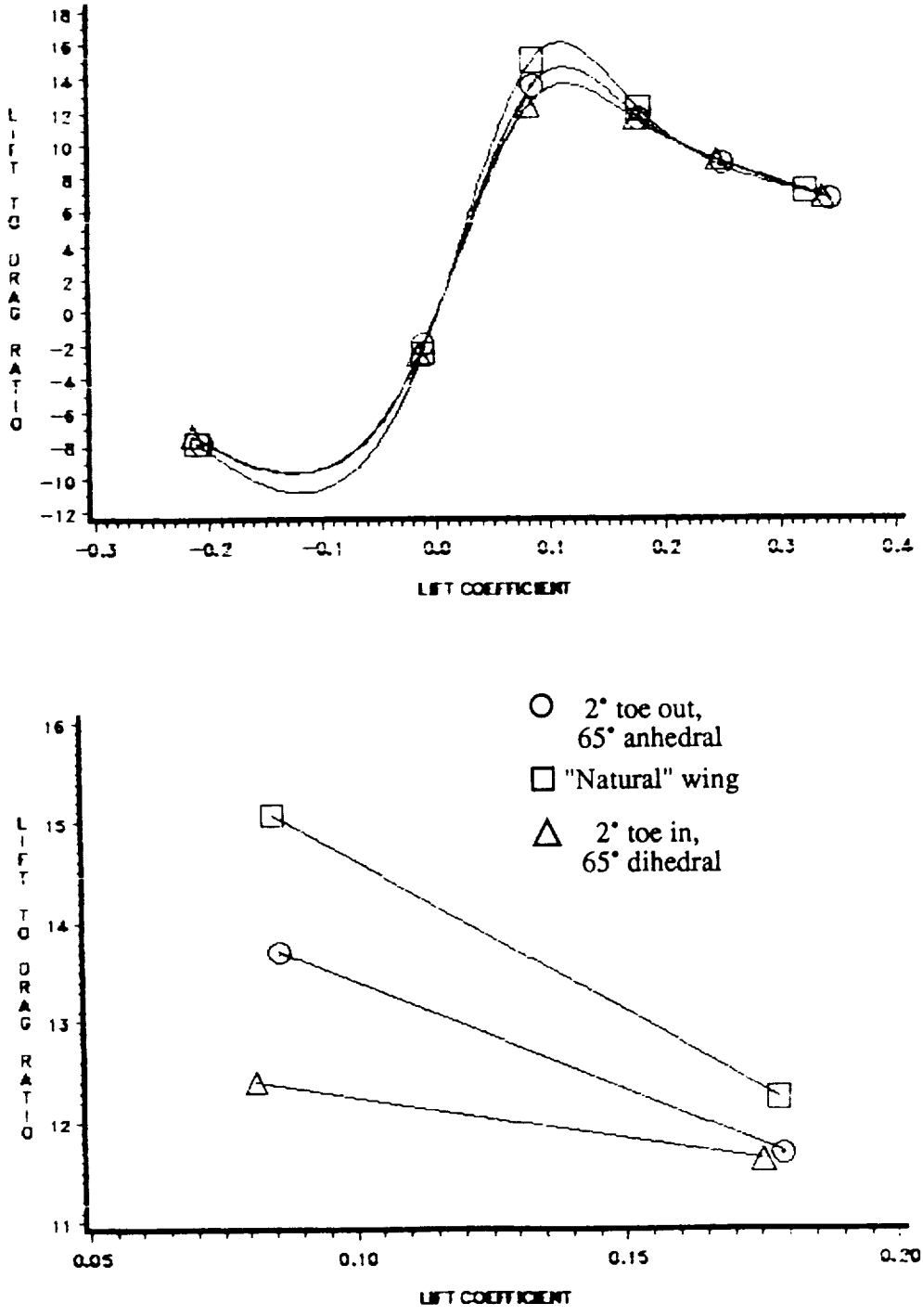

Figure 4.16.16: Comparison of the predicted performance of the "natural" flow wing; the 2° toe out, 65° anhedral winglet; and the 2° toe in, 65° dihedral winglet; M=1.62; lift-to-pressure drag ratio versus lift coefficient.

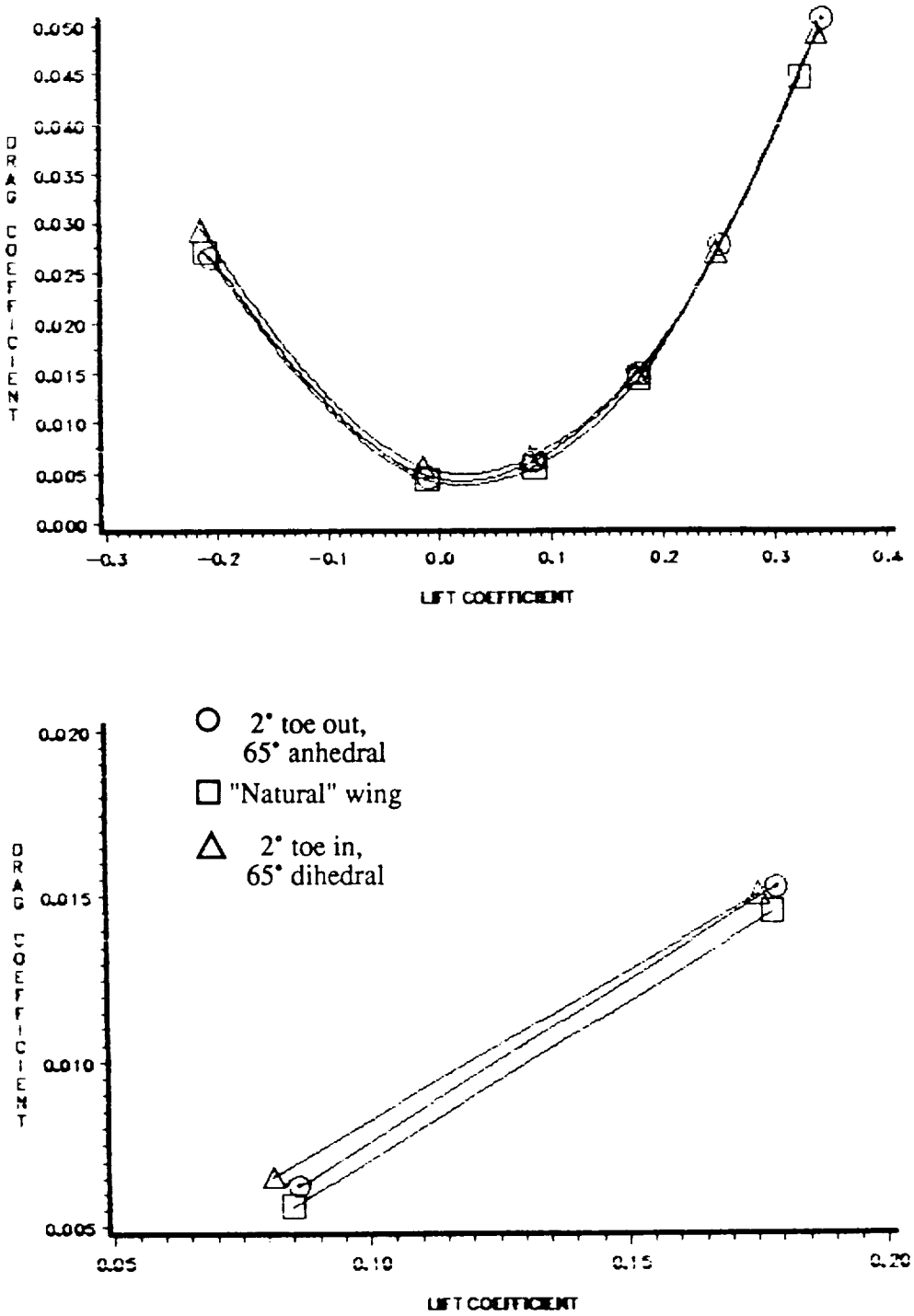

Figure 4.16.17: Comparison of the predicted performance of the "natural" flow wing; the 2° toe out, 65° anhedral winglet; and the 2° toe in, 65° dihedral winglet; M=1.62; pressure drag coefficient versus lift coefficient.

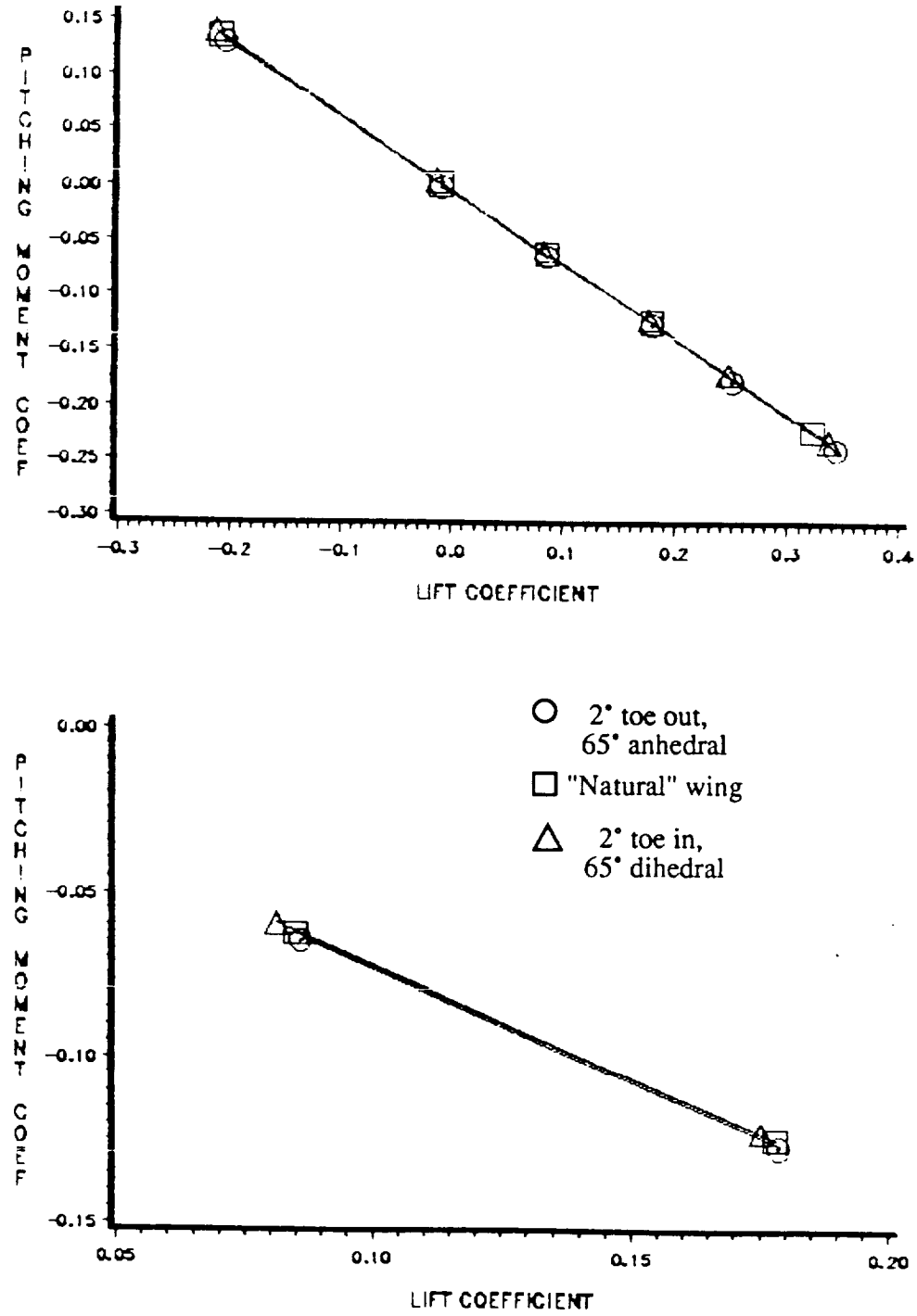

Figure 4.16.18: Comparison of the predicted performance of the "natural" flow wing; the 2° toe out, 65° anhedral winglet; and the 2° toe in, 65° dihedral winglet; M=1.62; pitching moment coefficient versus lift coefficient.

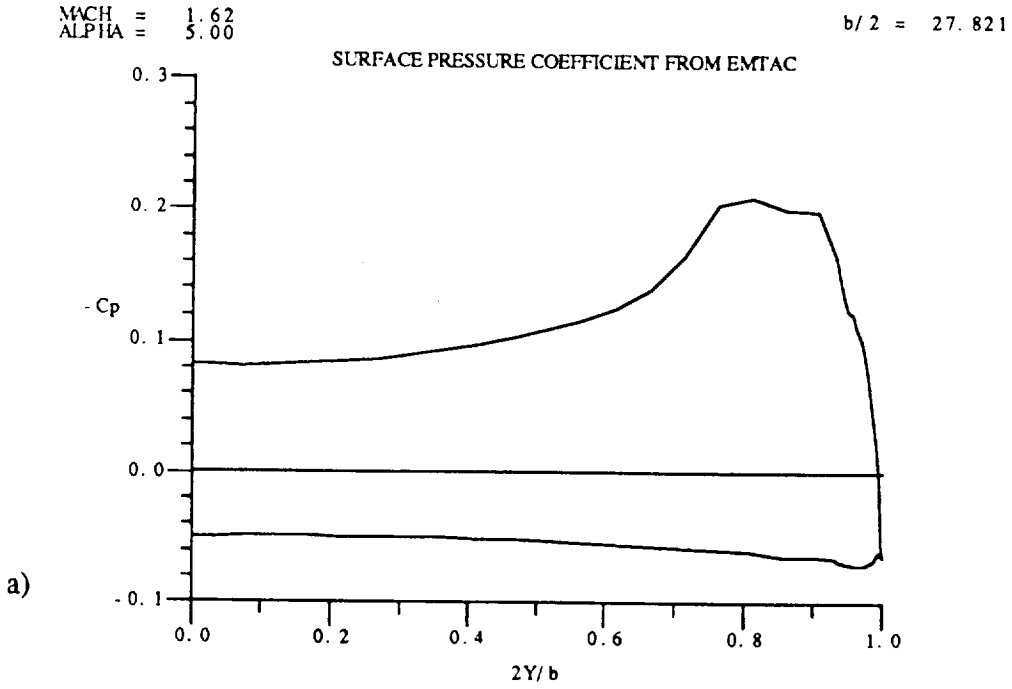

a)

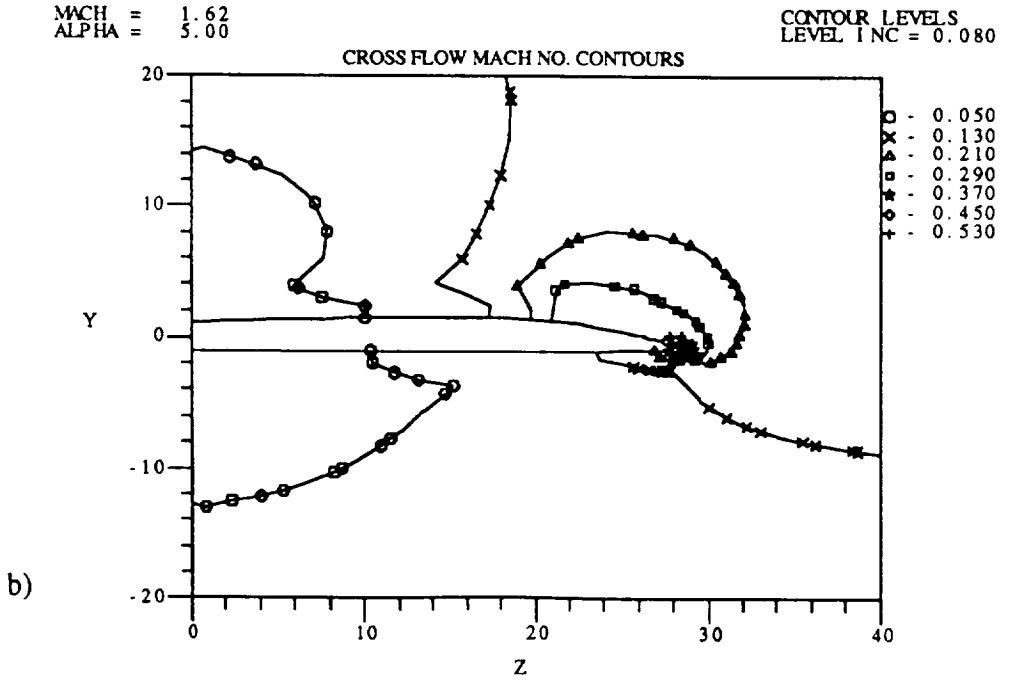

b)

Figure 4.16.19: "Natural" flow wing at axial location 59.7 units and a 5° angle of attack, M=1.62, a) surface pressure coefficient; b) crossflow Mach number contours; c) static pressure ratio contours and d) enlarged scale static pressure ratio contours.

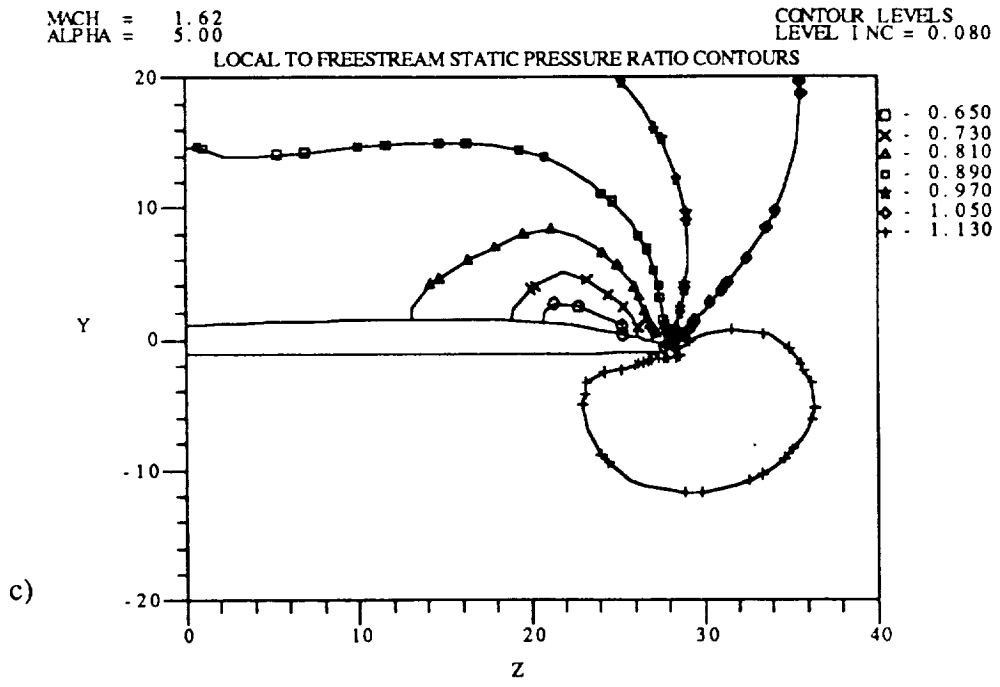

c)

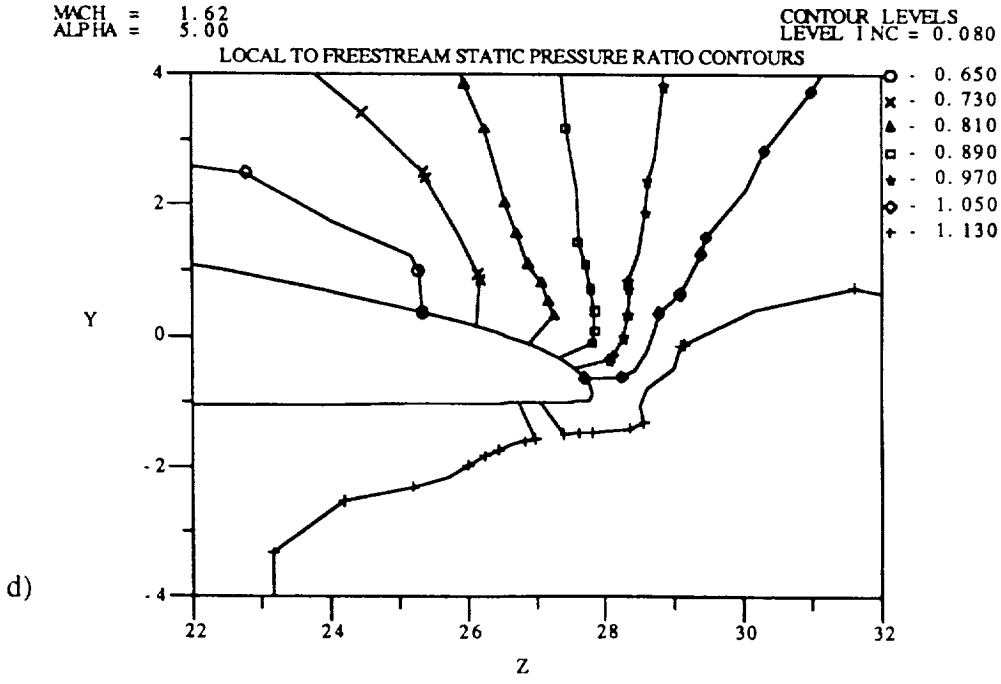

d)

Figure 4.16.19: Continued.

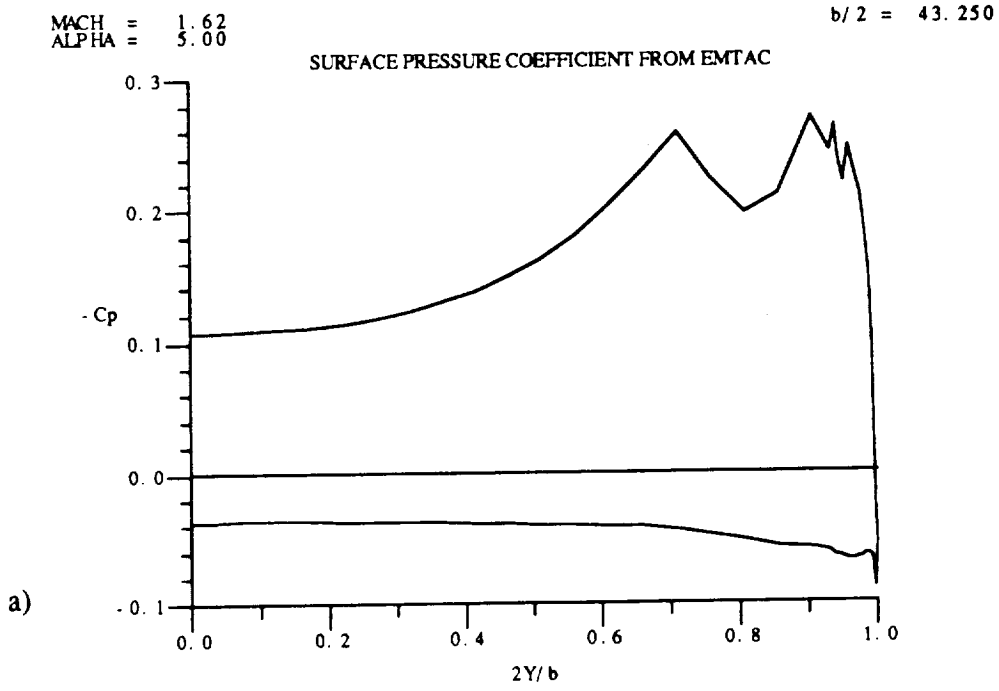

a)

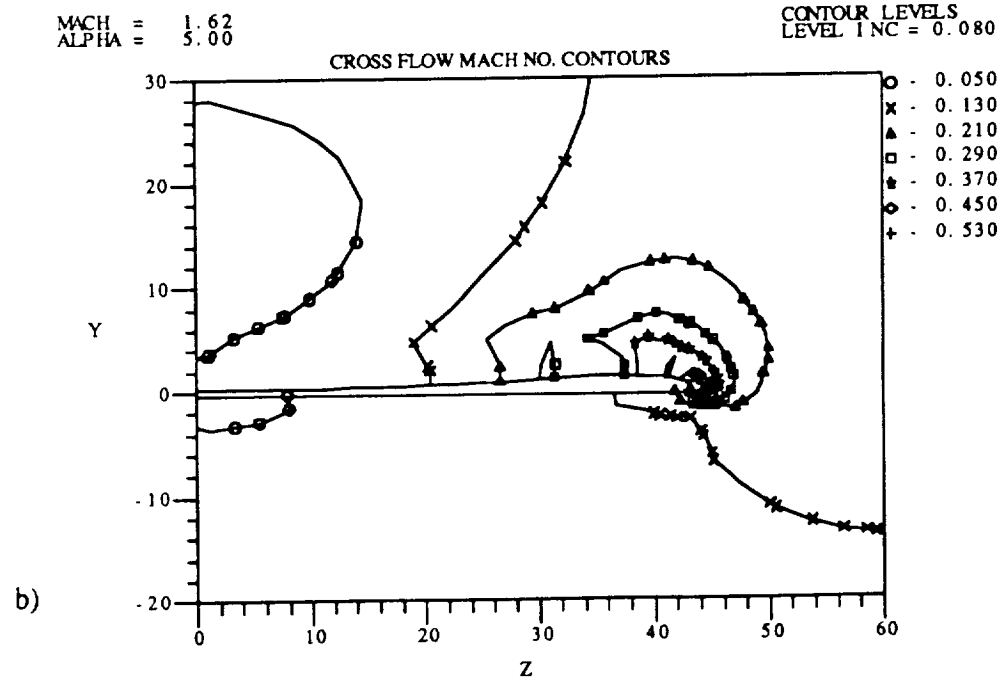

b)

Figure 4.16.20: "Natural" flow wing at axial location 92.8 units and a 5° angle of attack, M=1.62, a) surface pressure coefficient; b) crossflow Mach number contours; c) static pressure ratio contours and d) enlarged scale static pressure ratio contours.

c)

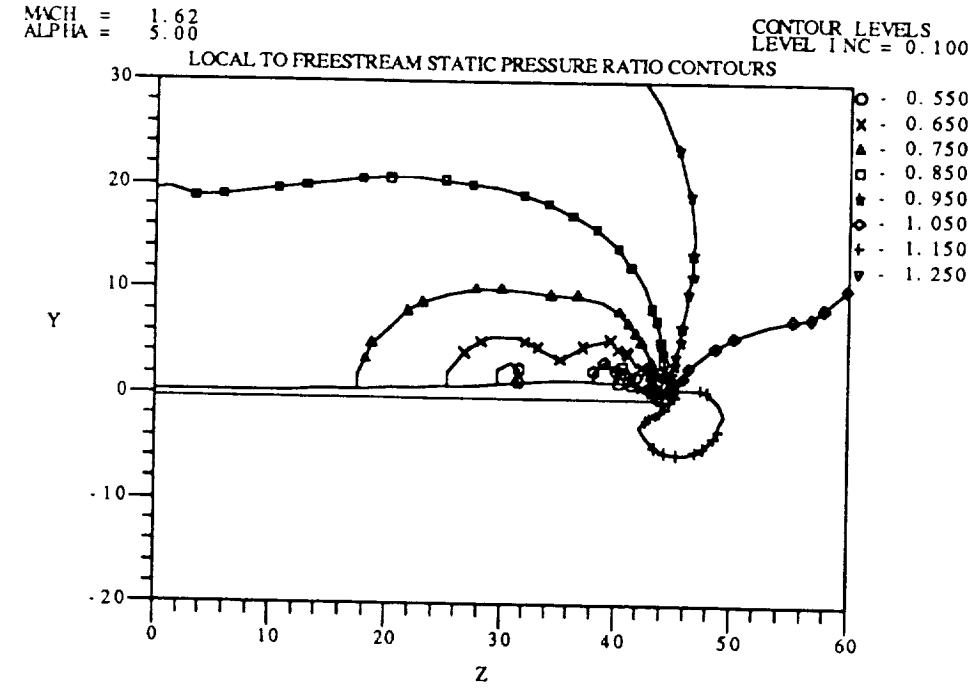

d)

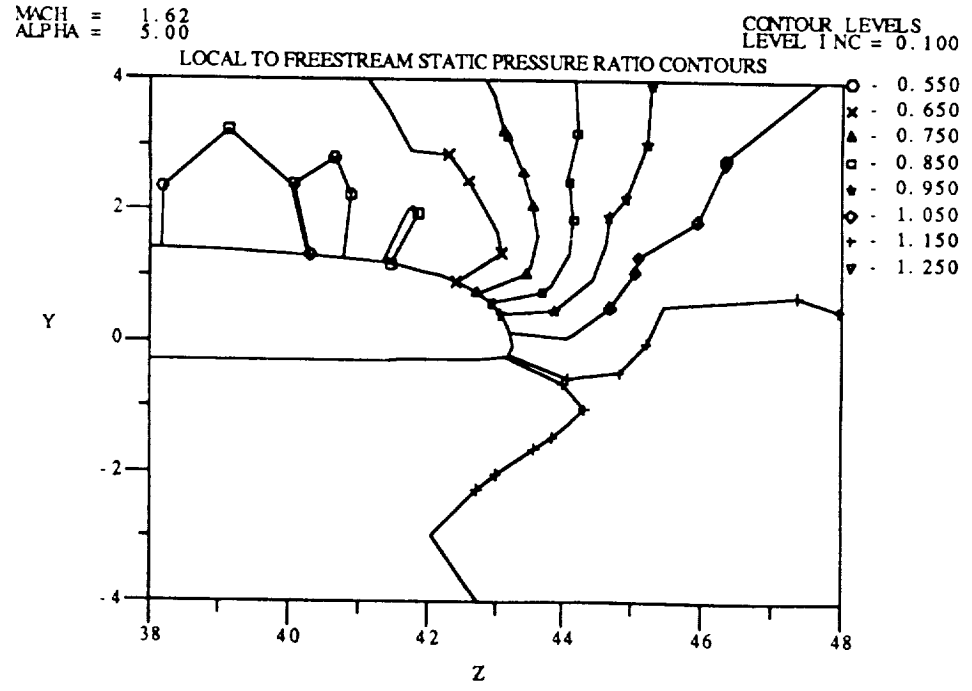

Figure 4.16.20: Continued.

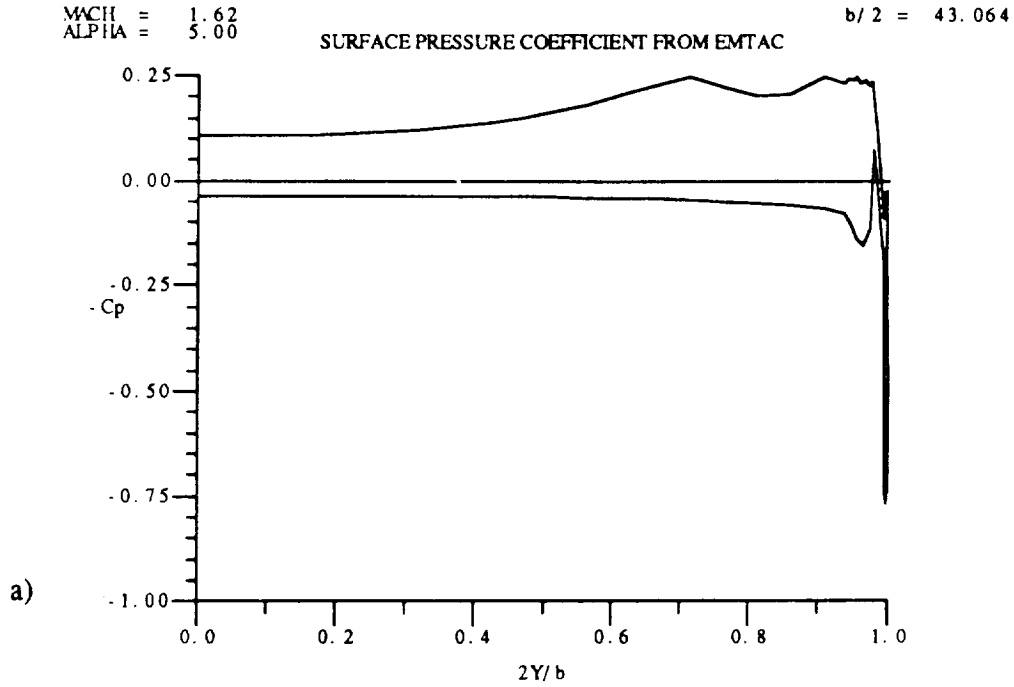

a)

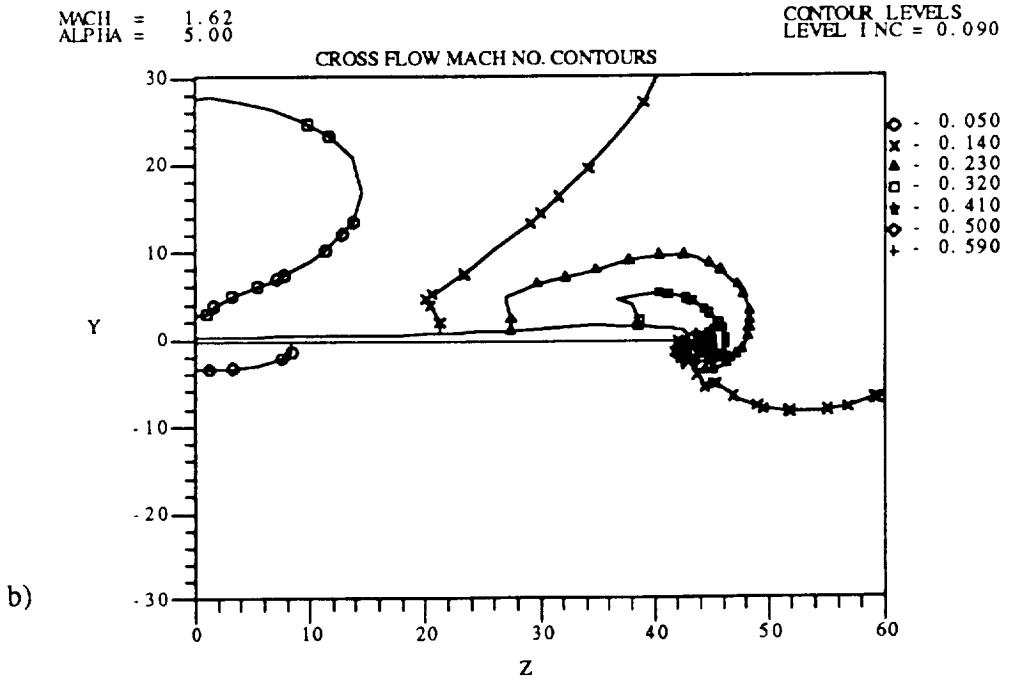

b)

Figure 4.16.21: "Natural" flow wing-winglet at axial location 92.8 units and a 5° angle of attack, M=1.62, a) surface pressure coefficient; b) crossflow Mach number contours; c) static pressure ratio contours and d) enlarged scale static pressure ratio contours.

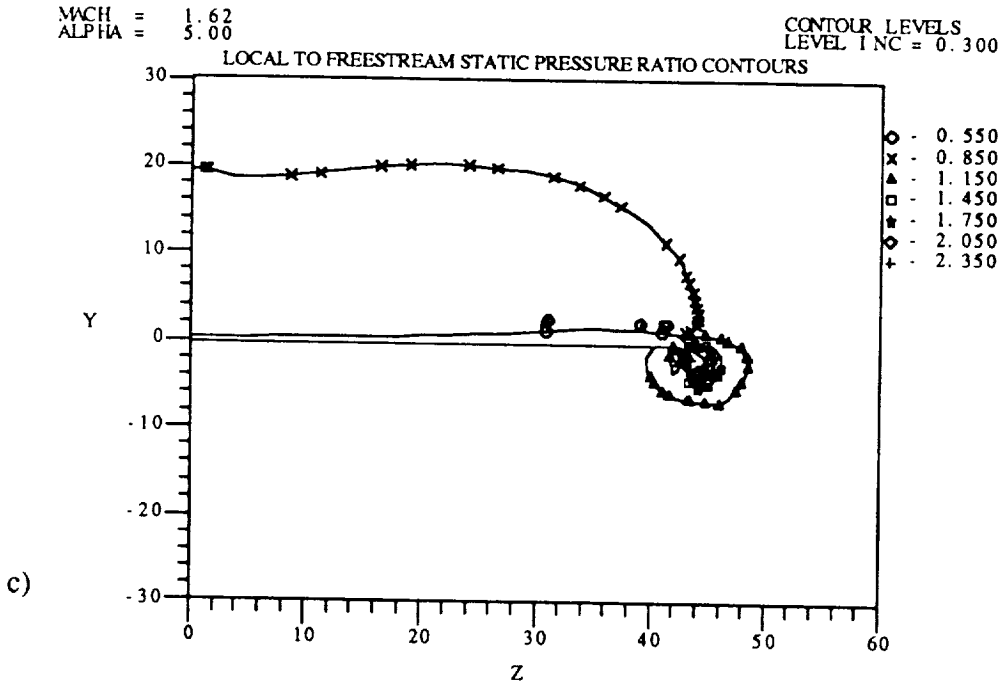

c)

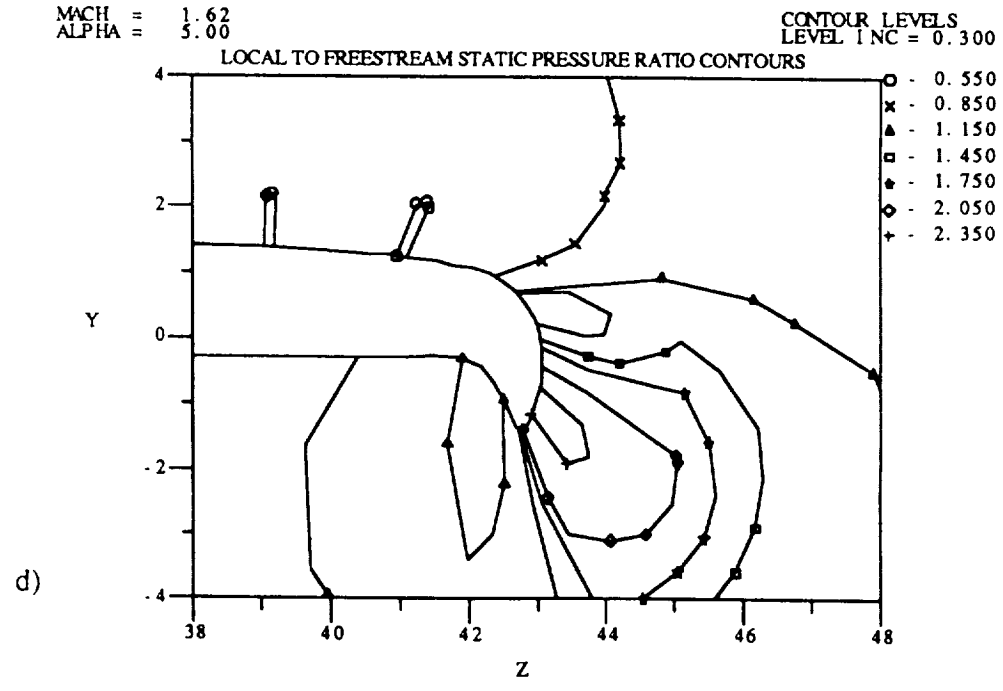

d)

Figre 4.16.21: Continued.

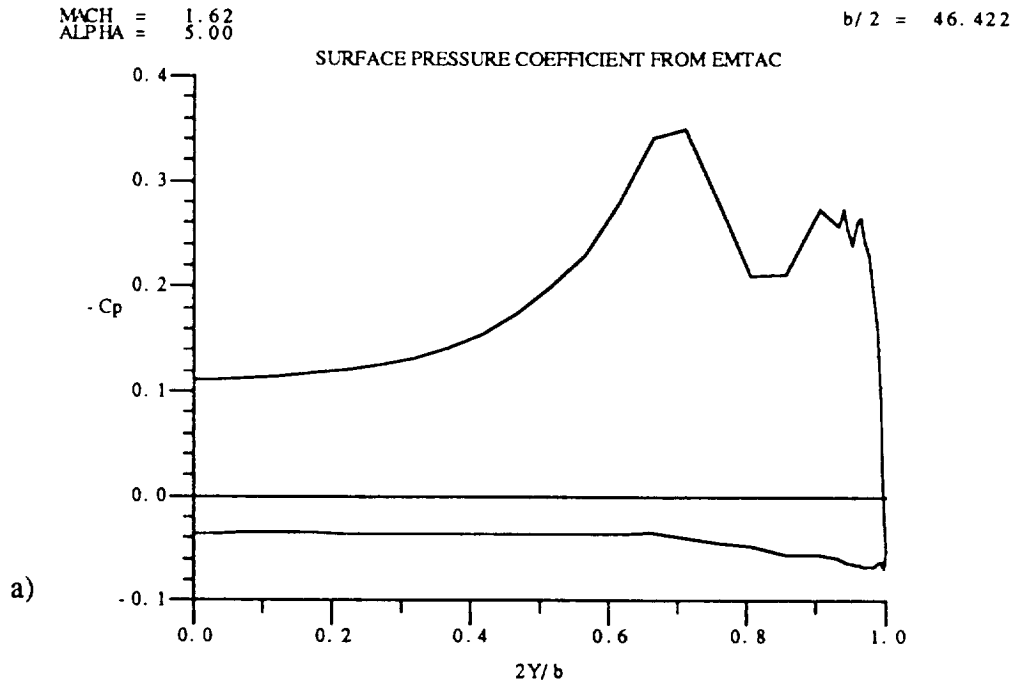

a)

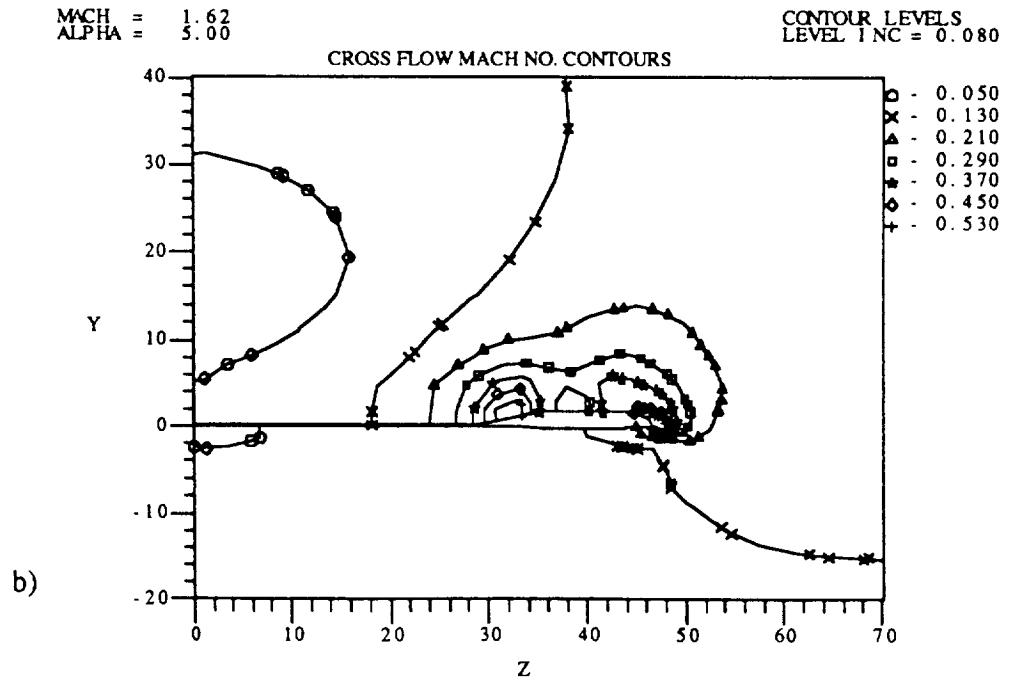

b)

Figure 4.16.22: "Natural" flow wing at axial location 99.6 units and a 5° angle of attack, M=1.62, a) surface pressure coefficient; b) crossflow Mach number contours; c) static pressure ratio contours and d) enlarged scale static pressure ratio contours.

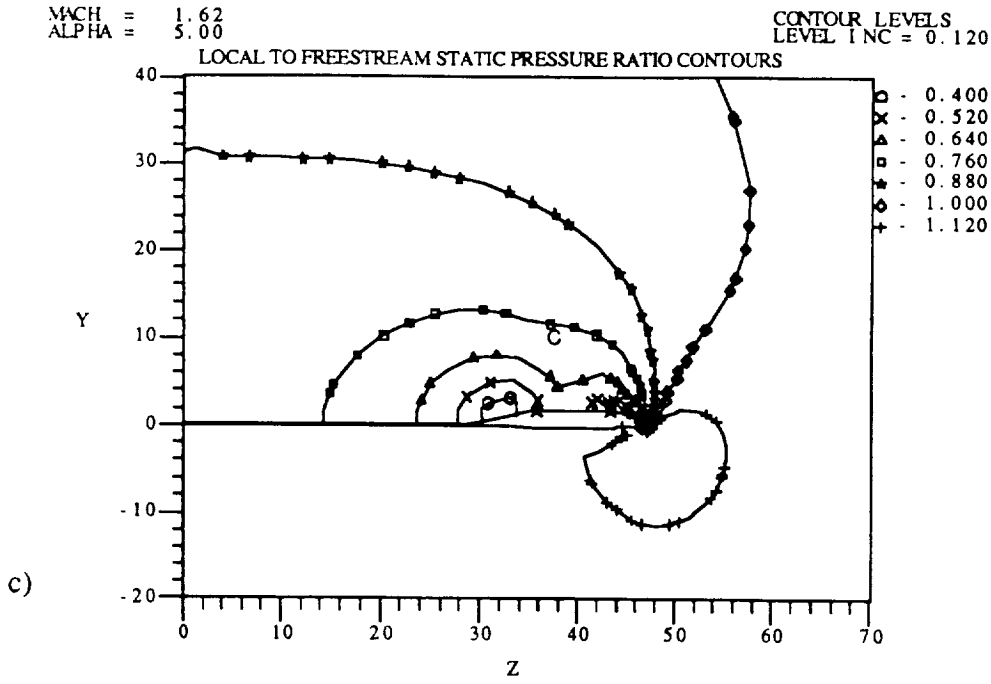

c)

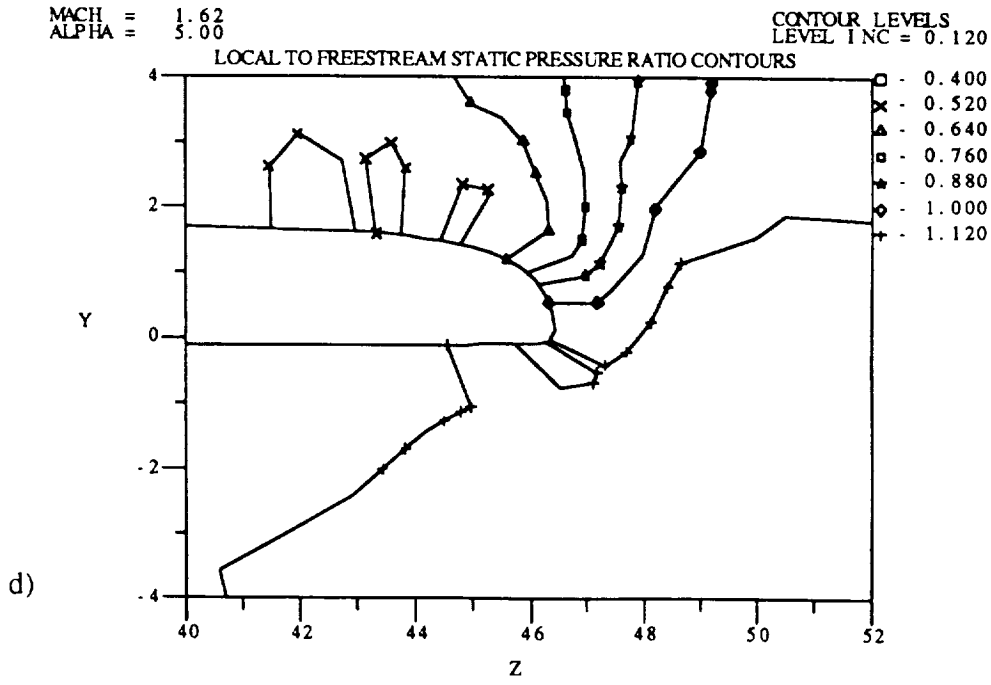

d)

Figure 4.16.22: Continued.

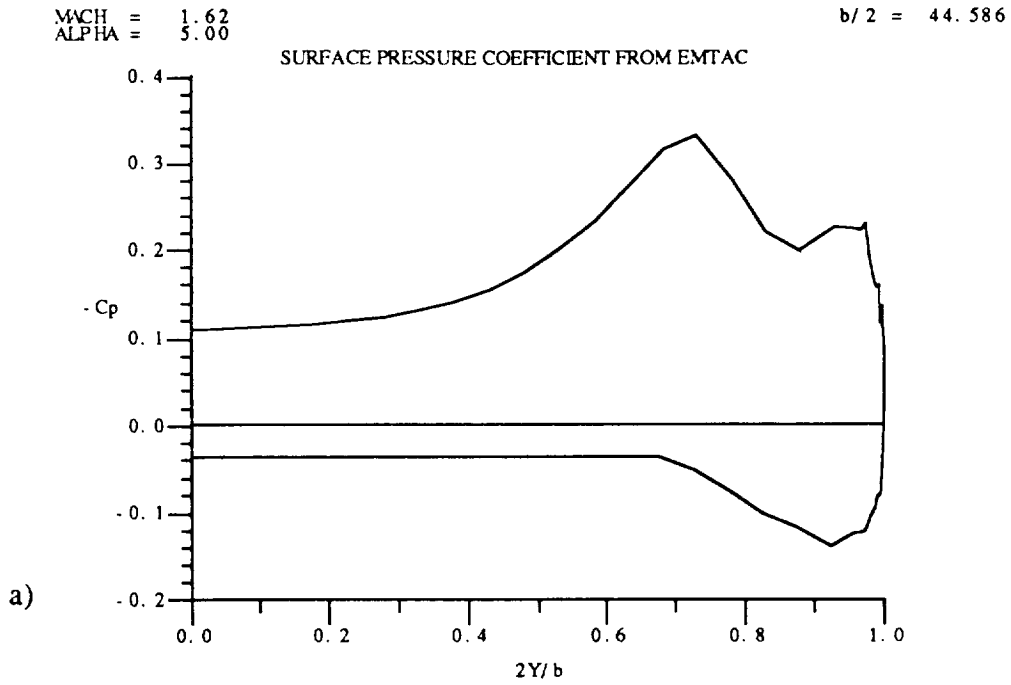

a)

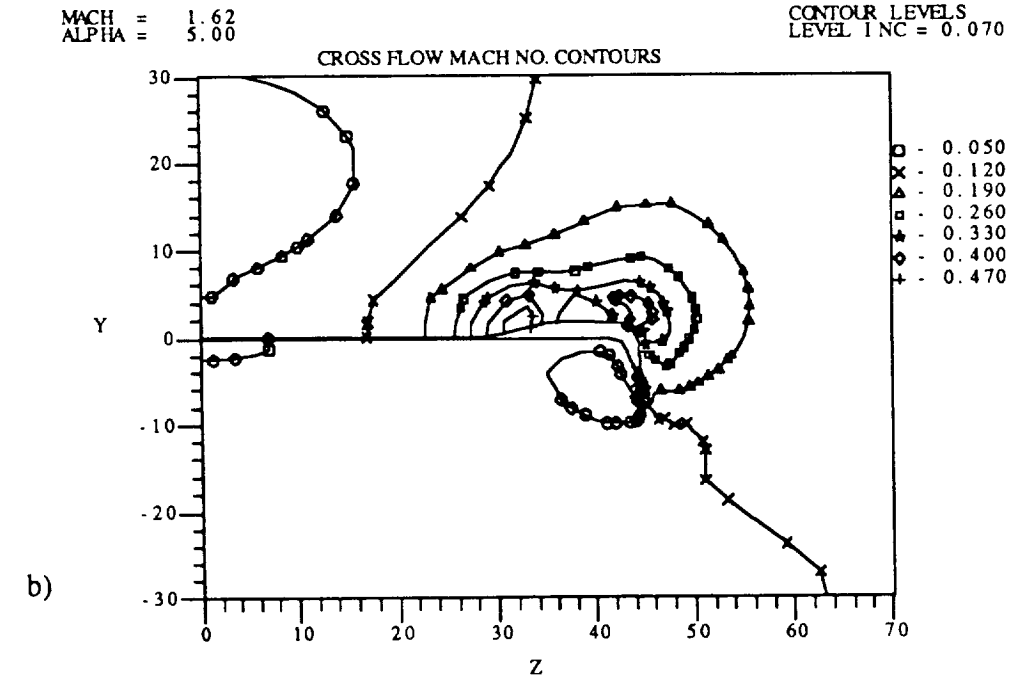

b)

Figure 4.16.23: "Natural" flow wing-winglet at axial location 99.6 units and a 5° angle of attack, M=1.62, a) surface pressure coefficient; b) crossflow Mach number contours; c) static pressure ratio contours and d) enlarged scale static pressure ratio contours.

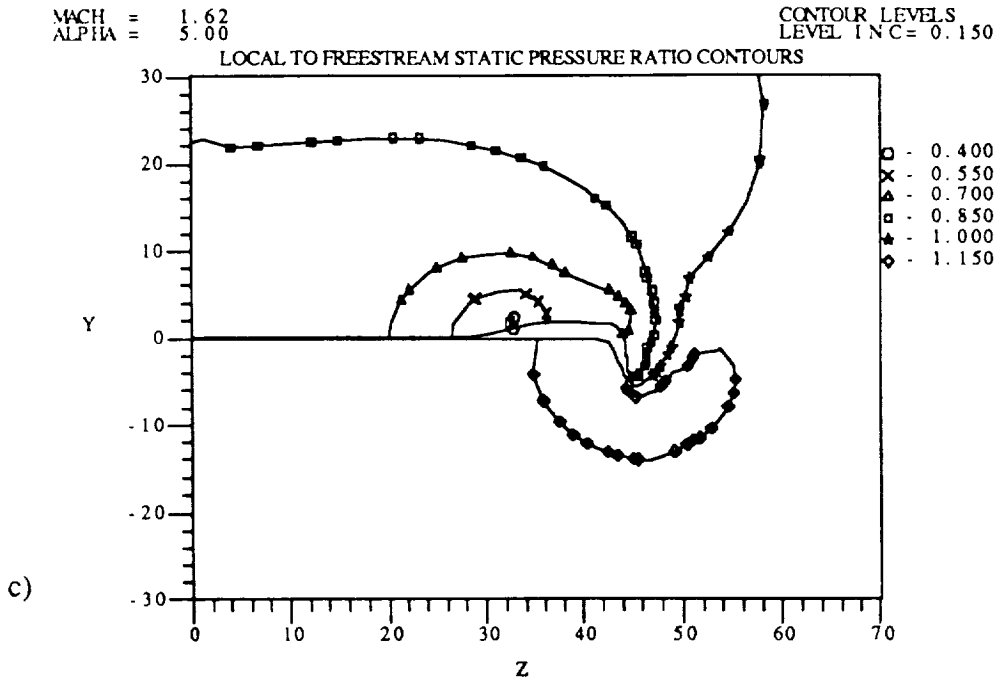

c)

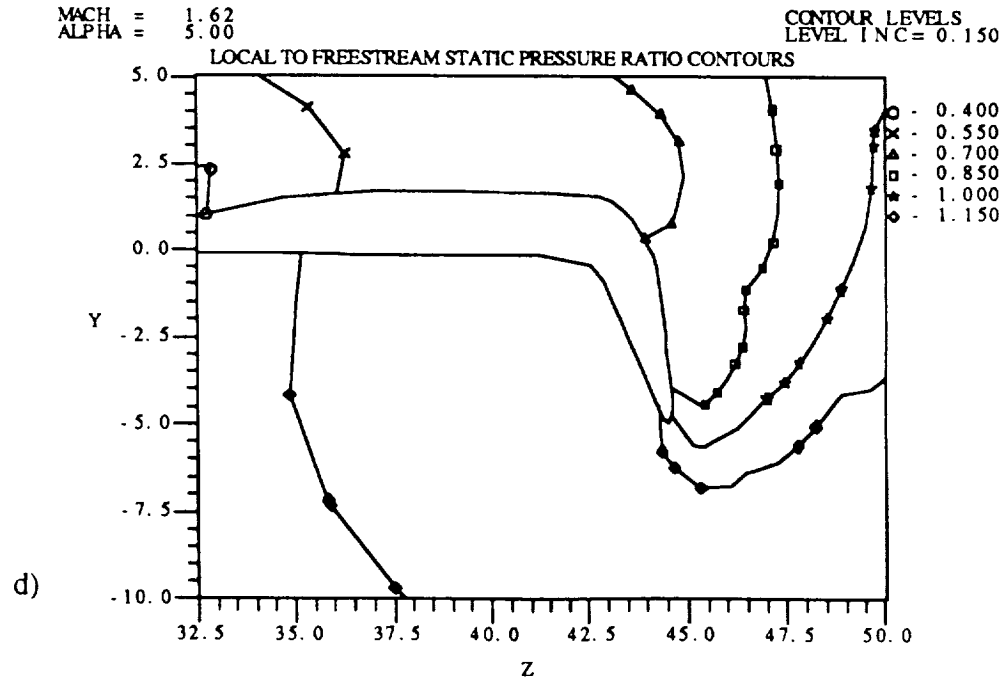

d)

Figure 4.16.23: Continued.

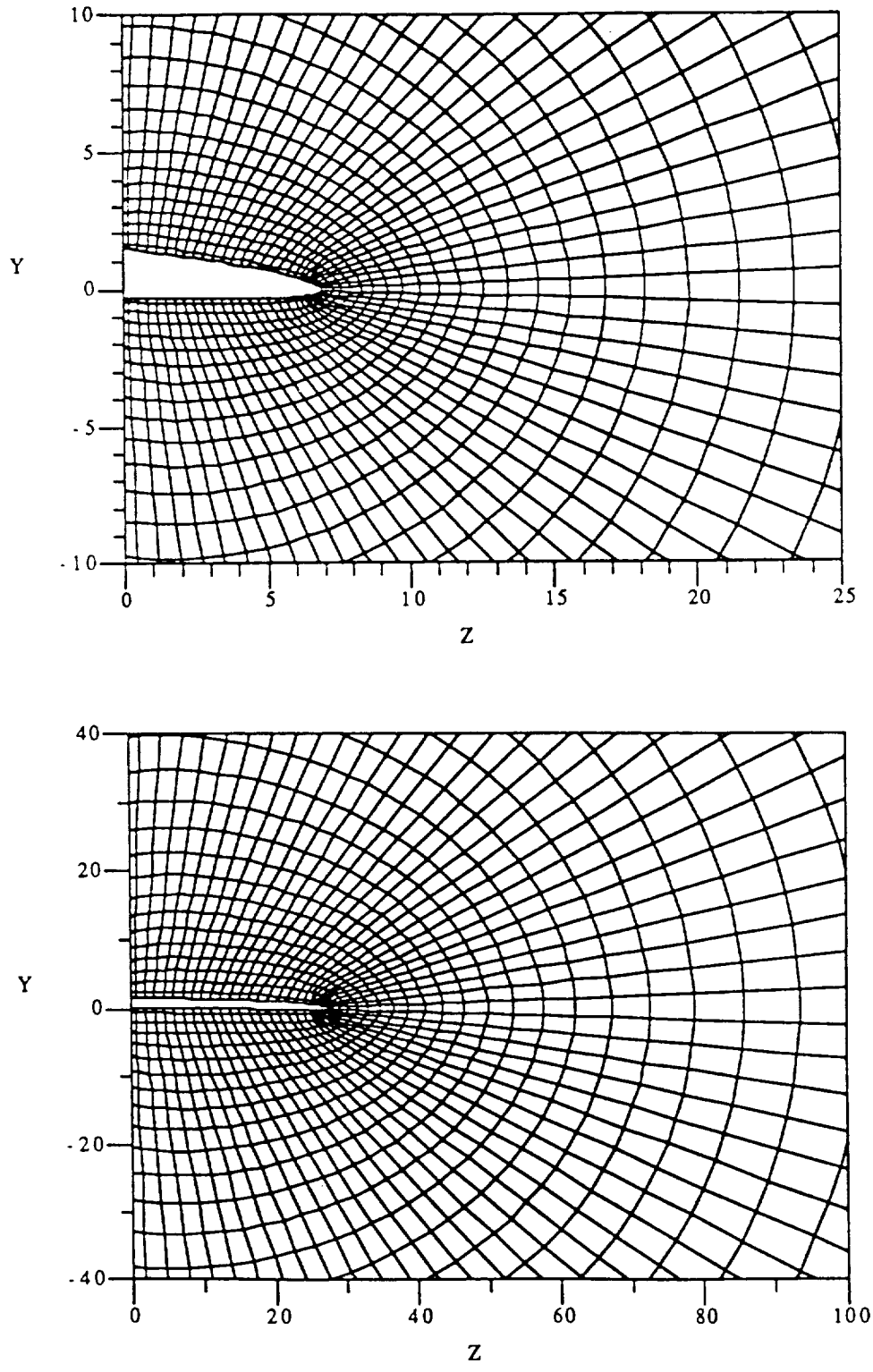

Figure A.3.1: Typical grid for the NACA 1402 base wing.

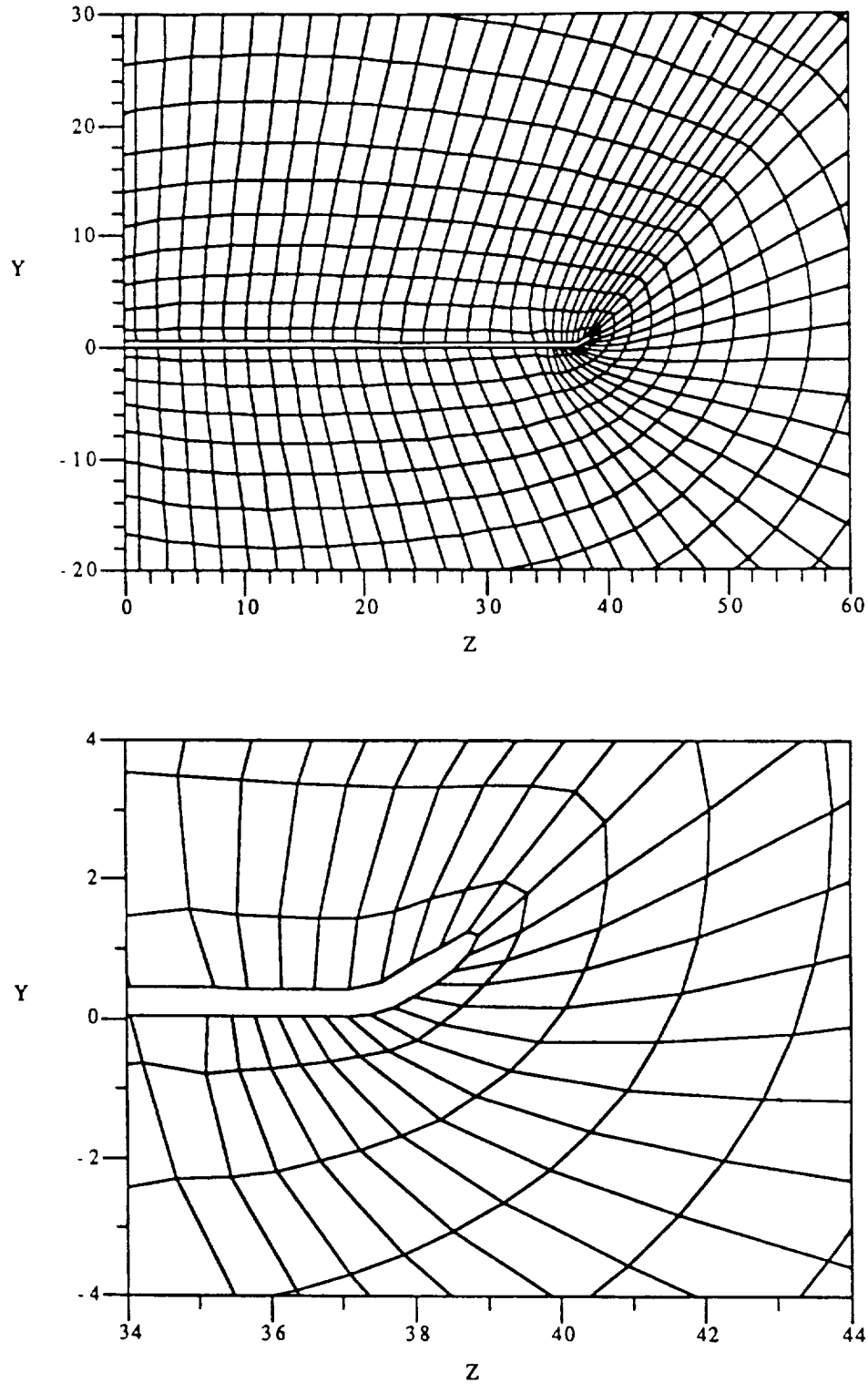

Figure A.3.2: Typical grid for the NACA 1402 base wing with a dihedral winglet beginning to form.

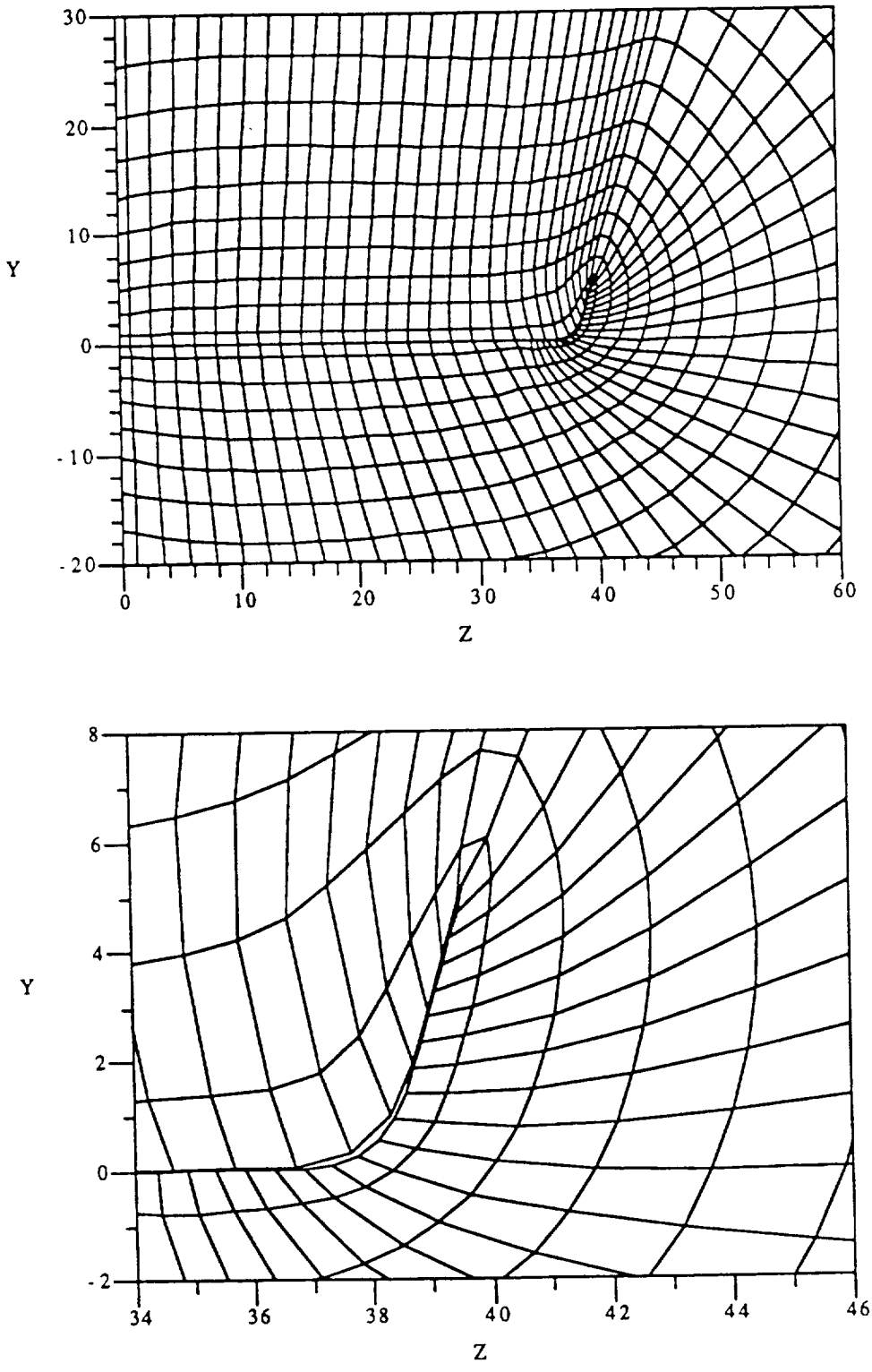

Figure A.3.3: Typical grid for the NACA 1402 base wing with a dihedral winglet.

Table 4.2.1: Grid input parameters for the NACA 1402 base wing.

Geometry	XSTART	XEND	NPT	INU	THTU	Δx
NACA	3.0	81.2	20-10-10-20	30	0°	0.2
1402, base	81.2	83.0	20-10-10-20	30	0°	0.1
wing	83.0	84.4	20-10-10-20	30	0°	0.1
	84.4	99.8	20-10-10-20	30	0°	0.2

Table 4.2.2: Predicted performance coefficients for the NACA 1402 base wing.

Geometry	α (deg)	C_L	C_{DP}	C_M
NACA 1402 base wing	-5.0	-.17190	.01696	.1029
	0.0	.02796	.00192	-.0294
	2.5	.11710	.00677	-.0873
	5.0	.21150	.01912	-.1497
	9.0	.36970	.05756	-.2561
	15.0	.59840	.15900	-.4160

Table 4.3.1: Grid input parameters for the NACA 1402 base wing with 0% thick winglets.

Geometry	XSTART	XEND	NPT	INU	THTU	Δx
75° dihedral	3.0	83.0	20-10-10-20	30	0°	0.2
	83.0	87.0	20-10-15-20	30 45	30° -65°	0.1
	87.0	90.0	20-10-15-20	30 45	60° -65°	0.1
	90.0	99.8	20-10-20-20	30 50	75° -65°	0.2
75° anhedral	3.0	81.0	20-10-10-20	30	0°	0.2
	81.0	84.0	20-15-10-20	20 35	65° -30°	0.1
	84.0	87.0	20-15-10-20	20 35	65° -60°	0.1
	87.0	99.8	20-20-10-20	20 40	65° -80°	0.2

Table 4.3.2: Predicted performance coefficients for the NACA 1402 base wing with 0% thick, 75° dihedral winglets.

Geometry	α (deg)	C_L	C_{DP}	C_M
0° toe out	-5.0	-.17090	.01682	.1021
	0.0	.02720	.00191	-.0286
	2.5	.11470	.00667	-.0852
	5.0	.20500	.01857	-.1438
	9.0	.35800	.05571	-.2453
	15.0	.58100	.15430	-.3994
2° toe out	-5.0	-.17180	.01699	.1030
	0.0	.02677	.00189	-.0282
	2.5	.11450	.00659	-.0849
	5.0	.20500	.01847	-.1438
	9.0	.35830	.05567	-.2456
	15.0	.58130	.15440	-.3998
4° toe out	-5.0	-.17370	.01735	.1048
	0.0	.02596	.00193	-.0275
	2.5	.11430	.00654	-.0847
	5.0	.20530	.01841	-.1441
	9.0	.35900	.05573	-.2463
	15.0	.58230	.15470	-.4007
6° toe out	-5.0	-.17530	.01777	.1066
	0.0	.02511	.00202	-.0266
	2.5	.11400	.00653	-.0844
	5.0	.20570	.01841	-.1444
	9.0	.36080	.05594	-.2478
	15.0	.58400	.15520	-.4022
2° toe in	-5.0	-.17030	.01671	.1016
	0.0	.02769	.00197	-.0291
	2.5	.11510	.00679	-.0856
	5.0	.20530	.01873	-.1442
	9.0	.35830	.05587	-.2457
	15.0	.58130	.15440	-.3998
4° toe in	-5.0	-.16990	.01666	.1012
	0.0	.02810	.00210	-.0295
	2.5	.11560	.00702	-.0860
	5.0	.20590	.01900	-.1447
	9.0	.35900	.05617	-.2464
	15.0	.58210	.15460	-.4005
6° toe in	-5.0	-.16950	.01674	.1008
	0.0	.02866	.00241	-.0300
	2.5	.11630	.00744	-.0866
	5.0	.20660	.01948	-.1454
	9.0	.35980	.05670	-.2472
	15.0	.58320	.15510	-.4016

Table 4.4.1: Predicted performance coefficients for the NACA 1402 base wing with 0% thick, 75° anhedral winglets.

Geometry	α (deg)	C_L	C_{DP}	C_M
0° toe out	-5.0	-.16470	.01633	.0964
	0.0	.02791	.00193	-.0293
	2.5	.11640	.00677	-.0867
	5.0	.20950	.01903	-.1481
	9.0	.36750	.05736	-.2544
	15.0	.60160	.16000	-.4195
2° toe in	-5.0	-.16520	.01640	.0968
	0.0	.02737	.00193	-.0288
	2.5	.11580	.00667	-.0861
	5.0	.20890	.01882	-.1475
	9.0	.36670	.05698	-.2536
	15.0	.60020	.15930	-.4180
4° toe in	-5.0	-.16580	.01651	.0974
	0.0	.02675	.00197	-.0282
	2.5	.11510	.00660	-.0855
	5.0	.20820	.01862	-.1468
	9.0	.36580	.05659	-.2527
	15.0	.59880	.15860	-.4166
6° toe in	-5.0	-.16640	.01663	.0980
	0.0	.02618	.00205	-.0276
	2.5	.11460	.00660	-.0850
	5.0	.20760	.01851	-.1462
	9.0	.36510	.05631	-.2520
	15.0	.59780	.15800	-.4155
2° toe out	-5.0	-.16480	.01635	.0965
	0.0	.02866	.00200	-.0300
	2.5	.11750	.00696	-.0878
	5.0	.21100	.01939	-.1496
	9.0	.36960	.05804	-.2565
	15.0	.60450	.16130	-.4226
4° toe out	-5.0	-.16440	.01638	.0960
	0.0	.02989	.00218	-.0312
	2.5	.11920	.00736	-.0894
	5.0	.21310	.02004	-.1516
	9.0	.37220	.05908	-.2591
	15.0	.60790	.16300	-.4261
6° toe out	-5.0	-.16430	.01653	.0958
	0.0	.03149	.00255	-.0327
	2.5	.12180	.00805	-.0919
	5.0	.21600	.02094	-.1543
	9.0	.37730	.06091	-.2642
	15.0	.61310	.16550	-.4314

Table 4.5.1: Predicted performance coefficients for the NACA 1402 base wing with 0% thick, 2° toe in, 75° anhedral winglets with various cambers.

Geometry	α (deg)	C_L	C_{DP}	C_M
m = -0.02	-5.0	-.16500	.01641	.0967
	0.0	.02746	.00195	-.0288
	2.5	.11600	.00672	-.0863
	5.0	.20920	.01890	-.1478
	9.0	.36710	.05712	-.2540
	15.0	.60060	.15950	-.4184
m = -0.01	-5.0	-.16510	.01640	.0968
	0.0	.02743	.00193	-.0288
	2.5	.11600	.00669	-.0863
	5.0	.20920	.01886	-.1477
	9.0	.36700	.05707	-.2539
	15.0	.60090	.15950	-.4187
m = 0.00	-5.0	-.16520	.01640	.0968
	0.0	.02737	.00193	-.0288
	2.5	.11580	.00667	-.0861
	5.0	.20890	.01882	-.1475
	9.0	.36670	.05698	-.2536
	15.0	.60020	.15930	-.4180
m = 0.01	-5.0	-.16520	.01641	.0969
	0.0	.02733	.00194	-.0287
	2.5	.11580	.00668	-.0862
	5.0	.20890	.01882	-.1475
	9.0	.36670	.05697	-.2536
	15.0	.60020	.15930	-.4181
m = 0.02	-5.0	-.16530	.01642	.0969
	0.0	.02730	.00197	-.0287
	2.5	.11580	.00670	-.0862
	5.0	.20890	.01884	-.1475
	9.0	.36660	.05698	-.2536
	15.0	.60120	.15950	-.4190

Table 4.6.1: Predicted performance coefficients for the NACA 1402 base wing with 0% thick, 2° toe in, 75° anhedral, uncambered winglets with various leading edge sweeps.

Geometry	α (deg)	C_L	C_{DP}	C_M
22° leading edge	-5.0	-.16750	.01687	.0990
	0.0	.02815	.00203	-.0295
	2.5	.11480	.00727	-.0853
	5.0	.21090	.01915	-.1493
	9.0	.37730	.05871	-.2634
	15.0	.60760	.16110	-.4250
44° leading edge	-5.0	-.16650	.01663	.0981
	0.0	.02702	.00196	-.0284
	2.5	.11660	.00669	-.0867
	5.0	.21080	.01892	-.1492
	9.0	.37020	.05738	-.2568
	15.0	.60630	.16080	-.4238
65° leading edge	-5.0	-.16520	.01640	.0968
	0.0	.02737	.00193	-.0288
	2.5	.11580	.00667	-.0861
	5.0	.20890	.01882	-.1475
	9.0	.36670	.05698	-.2536
	15.0	.60020	.15930	-.4180

Table 4.7.1: Predicted performance coefficients for the NACA 1402 base wing with 0% thick, 2° toe in, 75° anhedral, uncambered winglets at various lengths.

Geometry	α (deg)	C_L	C_{DP}	C_M
10% b/2 winglet length	-5.0	-.16520	.01639	.0968
	0.0	.02721	.00191	-.0286
	2.5	.11550	.00665	-.0858
	5.0	.20850	.01878	-.1471
	9.0	.36610	.05689	-.2530
	15.0	.59920	.15900	-.4170
12.5% b/2 winglet length	-5.0	-.16530	.01641	.0969
	0.0	.02720	.00192	-.0286
	2.5	.11560	.00665	-.0859
	5.0	.20860	.01879	-.1472
	9.0	.36640	.05692	-.2533
	15.0	.59970	.15910	-.4175
15% b/2 winglet length	-5.0	-.16520	.01640	.0968
	0.0	.02737	.00193	-.0288
	2.5	.11580	.00667	-.0861
	5.0	.20890	.01882	-.1475
	9.0	.36670	.05698	-.2536
	15.0	.60020	.15930	-.4180

Table 4.8.1: Grid input parameters for the NACA 1402 base wing with 4% thick winglets.

Geometry	XSTART	XEND	NPT	INU	THTU	Δx
75° dihedral	3.0	83.0	20-10-10-20	30	0°	0.2
with 50° LE	83.0	88.0	20-10-15-20	30 45	30° -65°	0.1
sweep	88.0	89.6	20-10-15-20	30 45	50° -65°	0.1
	89.6	99.8	20-10-15-20	30 50	75° -65°	0.2
75° anhedral	3.0	81.0	20-10-10-20	30	0°	0.2
with 50° LE	81.0	84.0	20-15-10-20	20 35	65° -30°	0.1
sweep	84.0	87.0	20-15-10-20	20 35	65° -60°	0.1
	87.0	99.8	20-20-10-20	20 40	65° -80°	0.2

Table 4.8.2: Predicted performance coefficients for the NACA 1402 base wing with 4% thick, 75° dihedral winglets.

Geometry	α (deg)	C_L	C_{DP}	C_M
0° toe out	-5.0	-.17290	.01729	.1040
	0.0	.02684	.00213	-.0283
	2.5	.11500	.00686	-.0855
	5.0	.20550	.01872	-.1444
	9.0	.35850	.05580	-.2458
	15.0	.58050	.15420	-.3989
2° toe out	-5.0	-.17420	.01757	.1052
	0.0	.02588	.00213	-.0274
	2.5	.11450	.00674	-.0850
	5.0	.20560	.01856	-.1444
	9.0	.35920	.05574	-.2465
	15.0	.58010	.15360	-.3987
3° toe out	-5.0	-.17520	.01777	.1062
	0.0	.02532	.00215	-.0269
	2.5	.11430	.00669	-.0847
	5.0	.20560	.01849	-.1444
	9.0	.35960	.05572	-.2467
	15.0	.58150	.15450	-.3999
4° toe out	-5.0	-.17640	.01798	.1073
	0.0	.02492	.00217	-.0265
	2.5	.11410	.00666	-.0845
	5.0	.20570	.01845	-.1445
	9.0	.36120	.05587	-.2482
	15.0	.58220	.15470	-.4005

Table 4.9.1: Predicted performance coefficients for the NACA 1402 base wing with 4% thick, 75° anhedral winglets.

Geometry	α (deg)	C_L	C_{DP}	C_M
1° toe out	-5.0	-.16530	.01650	.0970
	0.0	.02850	.00215	-.0298
	2.5	.11780	.00709	-.0880
	5.0	.21180	.01951	-.1502
	9.0	.37110	.05825	-.2575
	15.0	.60810	.16210	-.4259
0° toe out	-5.0	-.16530	.01652	.0970
	0.0	.02820	.00213	-.0296
	2.5	.11740	.00701	-.0876
	5.0	.21130	.01935	-.1498
	9.0	.37040	.05800	-.2572
	15.0	.60740	.16160	-.4251
1° toe in	-5.0	-.16570	.01658	.0973
	0.0	.02782	.00212	-.0292
	2.5	.11700	.00693	-.0872
	5.0	.21090	.01920	-.1494
	9.0	.37010	.05777	-.2568
	15.0	.60670	.16140	-.4244
2° toe in	-5.0	-.16610	.01666	.0977
	0.0	.02740	.00213	-.0288
	2.5	.11660	.00687	-.0868
	5.0	.21050	.01907	-.1489
	9.0	.36950	.05745	-.2562
	15.0	.60560	.16060	-.4232
3° toe in	-5.0	-.16660	.01677	.0982
	0.0	.02696	.00215	-.0284
	2.5	.11610	.00682	-.0864
	5.0	.21010	.01894	-.1485
	9.0	.36910	.05720	-.2558
	15.0	.60500	.16020	-.4225
4° toe in	-5.0	-.16700	.01687	.0986
	0.0	.02654	.00218	-.0279
	2.5	.11570	.00678	-.0860
	5.0	.20960	.01882	-.1481
	9.0	.36860	.05696	-.2553
	15.0	.60390	.15960	-.4214

Table 4.10.1: Predicted performance coefficients for the NACA 1402 base wing with 4% thick, 2° toe in, 75° anhedral winglets at various cambers.

Geometry	α (deg)	C_L	C_{DP}	C_M
m = -0.01	-5.0	-.16580	.01658	.0975
	0.0	.02734	.00206	-.0287
	2.5	.11660	.00683	-.0868
	5.0	.21050	.01906	-.1489
	9.0	.36940	.05747	-.2561
	15.0	.60500	.16060	-.4225
m = 0.00	-5.0	-.16590	.01658	.0975
	0.0	.02735	.00204	-.0287
	2.5	.11660	.00680	-.0868
	5.0	.21050	.01903	-.1489
	9.0	.36960	.05747	-.2563
	15.0	.60554	.16060	-.4229
m = 0.01	-5.0	-.16600	.01661	.0977
	0.0	.02736	.00207	-.0287
	2.5	.11650	.00681	-.0868
	5.0	.21050	.01903	-.1489
	9.0	.36960	.05745	-.2563
	15.0	.60510	.16050	-.4226
m = 0.02	-5.0	-.16610	.01666	.0977
	0.0	.02740	.00213	-.0288
	2.5	.11660	.00687	-.0868
	5.0	.21050	.01907	-.1489
	9.0	.36950	.05745	-.2562
	15.0	.60560	.16060	-.4232
m = 0.03	-5.0	-.16620	.01674	.0978
	0.0	.02747	.00222	-.0289
	2.5	.11670	.00696	-.0870
	5.0	.21060	.01915	-.1491
	9.0	.36960	.05751	-.2564
	15.0	.60540	.16060	-.4230

Table 4.11.1: Predicted performance coefficients for the NACA 1402 base wing with 4% thick, 75° anhedral, uncambered winglets at various lengths.

Geometry	α (deg)	C_L	C_{DP}	C_M
7.5% b/2	-5.0	-.16520	.01638	.0968
winglet length	0.0	.02740	.00194	-.0288
	2.5	.11570	.00670	-.0860
	5.0	.20870	.01886	-.1473
	9.0	.36620	.05698	-.2531
	15.0	.59950	.15920	-.4172
10% b/2	-5.0	-.16530	.01641	.0970
winglet length	0.0	.02737	.00195	-.0288
	2.5	.11590	.00671	-.0862
	5.0	.20910	.01887	-.1476
	9.0	.36690	.05704	-.2538
	15.0	.60060	.15940	-.4183
12.5% b/2	-5.0	-.16650	.01646	.0971
winglet length	0.0	.02735	.00197	-.0287
	2.5	.11600	.00672	-.0863
	5.0	.20930	.01889	-.1479
	9.0	.36740	.05710	-.2543
	15.0	.60130	.15960	-.4191
15% b/2	-5.0	-.16540	.01646	.0971
winglet length	0.0	.02748	.00197	-.0289
	2.5	.11620	.00673	-.0865
	5.0	.20960	.01891	-.1481
	9.0	.36780	.05714	-.2546
	15.0	.60210	.15980	-.4198

Table 4.12.1: Predicted performance coefficients for the NACA 1402 base wing with 4% thick, 75° anhedral, uncambered winglets having various leading edge sweeps.

Geometry	α (deg)	C_L	C_{DP}	C_M
50° leading edge	-5.0	-.16590	.01658	.0975
	0.0	.02735	.00204	-.0287
	2.5	.11660	.00680	-.0868
	5.0	.21050	.01903	-.1489
	9.0	.36960	.05747	-.2563
	15.0	.60554	.16060	-.4229
60° leading edge	-5.0	-.16540	.01646	.0971
	0.0	.02748	.00197	-.0289
	2.5	.11620	.00673	-.0865
	5.0	.20960	.01891	-.1481
	9.0	.36780	.05714	-.2546
	15.0	.60210	.15980	-.4198
65° leading edge	-5.0	-.16510	.01641	.0968
	0.0	.02754	.00197	-.0289
	2.5	.11590	.00671	-.0862
	5.0	.20900	.01885	-.1475
	9.0	.36670	.05699	-.2536
	15.0	.60030	.15930	-.4181
68° leading edge	-5.0	-.16490	.01636	.0966
	0.0	.02753	.00194	-.0289
	2.5	.11570	.00669	-.0860
	5.0	.20850	.01882	-.1471
	9.0	.36580	.05688	-.2528
	15.0	.59890	.15900	-.4167

Table 4.14.1: Grid input parameters for the NACA 1402 base wing with extension and the base wing with an uncambered, 2° toe in, 60° leading edge sweep, 75° anhedral winglet.

Geometry	XSTART	XEND	NPT	INU	THTU	Δx
NACA 1402	3.0	81.2	20-10-10-20	30	0°	0.2
base wing	81.2	83.0	20-10-10-20	30	0°	0.1
	83.0	84.4	20-10-10-20	30	0°	0.1
	84.4	99.8	20-10-10-20	30	0°	0.2
75° anhedral	3.0	81.0	20-10-10-20	30	0°	0.2
with 2° toe	81.0	84.0	20-15-10-20	20 35	65° -30°	0.1
out	84.0	87.0	20-18-10-20	20 38	65° -65°	0.1
	84.4	99.8	20-21-10-20	20 40	65° -80°	0.2

Table 4.14.2: Predicted performance coefficients for the NACA 1402 base wing with extension and the base wing with an uncambered, 2° toe in, 60° leading edge sweep, 75° anhedral winglet.

Geometry	α (deg)	C_L	C_{DP}	C_M
NACA	-5.0	-.17190	.01696	.1029
1402 base	0.0	.02796	.00192	-.0294
wing	2.2	.10640	.00584	-.0803
	2.5	.11710	.00677	-.0873
	4.8	.20310	.01778	-.1440
	5.0	.21150	.01912	-.1497
	9.0	.36970	.05756	-.2561
	15.0	.59840	.15900	-.4160
2° toe in,	-5.0	-.16520	.01643	.0968
60° leading edge,	0.0	.02767	.00197	-.0290
75° anhedral winglet	2.2	.10590	.00584	-.0799
	2.5	.11620	.00672	-.0865
	4.8	.20240	.01768	-.1435
	5.0	.20960	.01890	-.1481
	9.0	.36790	.05716	-.2547
	15.0	.60290	.16000	-.4206

Table 4.14.3: Numerical comparison between the NACA 1402 base wing and and the base wing with an uncambered, 2° toe in, 60° leading edge sweep, 75° anhedral winglet

Geometry	C_L	C_{DP}	C_D	L/D	% diff in L/D	% diff in C_D
NACA 1402	0.1064	0.005838	0.012633	8.4223	0.3586	-0.1108
wing	0.2031	0.01778	0.024576	8.2642	0.1355	-0.4801
75° dihedral	0.1059	0.005841	0.012619	8.3921	0.3586	-0.1108
wing-winglet	0.2024	0.01768	0.024458	8.2754	0.1355	-0.4801

Table 4.14.4: Predicted performance coefficients for the NACA 1402 base wing and the base wing with an uncambered, 2° toe in, 60° leading edge sweep, 75° anhedral winglet at various Mach numbers.

Geometry	α (deg)	C_L	C_{DP}	C_M	M
NACA 1402 base wing	-5.0	-.18640	.01851	.1112	1.4
	0.0	.03936	.00199	-.0382	
	2.5	.13530	.00754	-.1005	
	5.0	.23950	.02143	-.1697	
	9.0	.41860	.06547	-.2908	
	15.0	.68320	.18120	-.4755	
	-5.0	-.17190	.01696	.1029	1.62
	0.0	.02796	.00192	-.0294	
	2.5	.11710	.00677	-.0873	
	5.0	.21150	.01912	-.1497	
	9.0	.36970	.05756	-.2561	
	15.0	.59840	.15900	-.4160	
	-5.0	-.14980	.01522	.0894	2.0
	0.0	.01524	.00197	-.0191	
	2.5	.09407	.00585	-.0704	
	5.0	.17230	.01613	-.1215	
	9.0	.30660	.04846	-.2117	
	-5.0	-.12600	.01342	.0755	2.5
	0.0	.00679	.00213	-.0116	
	2.5	.07338	.00512	-.0551	
	5.0	.13950	.01366	-.0984	
	9.0	.24790	.04001	-.1710	
	-5.0	-.10750	.01189	.0643	3.0
	0.0	.00339	.00216	-.0082	
	2.5	.05940	.00456	-.0446	
	5.0	.11550	.01172	-.0813	
	9.0	.20750	.03394	-.1426	
	-5.0	-.09458	.01072	.0565	3.5
	0.0	.00111	.00203	-.0056	
	2.5	.04994	.00401	-.0375	
	5.0	.09909	.01022	-.0697	
	9.0	.18050	.02968	-.1237	
	15.0	.31100	.08393	-.2150	

Table 4.14.4: Continued.

Geometry	α (deg)	C_L	C_{DP}	C_M	M
2° toe in, 60° leading edge, 75° anhedral winglet	-4.5	-.15440	.01440	.0819	1.4
	0.0	.03854	.00205	-.0374	
	3.0	.15460	.00947	-.1131	
	5.0	.23820	.02123	-.1687	
	9.5	.44300	.07297	-.3080	
	15.0	.69440	.18390	-.4865	
	-5.0	-.16540	.01646	.0971	1.62
	0.0	.02748	.00197	-.0289	
	2.5	.11620	.00673	-.0865	
	5.0	.20960	.01891	-.1481	
	9.0	.36780	.05714	-.2546	
	15.0	.60210	.15980	-.4198	
	-5.0	-.14710	.01507	.0870	2.0
	0.0	.01507	.00200	-.0189	
	2.5	.09333	.00583	-.0697	
	5.0	.17190	.01606	-.1213	
	9.0	.30610	.04834	-.2114	
	-5.0	-.12380	.01328	.0735	2.5
	0.0	.00669	.00217	-.0115	
	2.5	.07289	.00512	-.0546	
	5.0	.13910	.01363	-.0981	
	9.0	.24700	.03985	-.1702	
	-5.0	-.10550	.01176	.0625	3.0
	0.0	.00349	.00220	-.0082	
	2.5	.05919	.00458	-.0444	
	5.0	.11520	.01171	-.0811	
	9.0	.20770	.03397	-.1428	
	-5.0	-.09458	.01072	.0565	3.5
	0.0	.00111	.00203	-.0058	
	2.5	.04994	.00401	-.0375	
	5.0	.09909	.01022	-.0697	
	9.0	.18050	.02968	-.1237	
	15.0	.31100	.08393	-.2150	

Table 4.15.1: Grid input parameters fo the NACA 1402 base wing with full tip chord winglets.

Geometry	XSTART	XEND	NPT	INU	THTU	Δx
75° dihedral	3.0	81.2	20-10-10-20	30	30°	0.2
	81.2	83.0	20-10-15-20	30 45	30° -75°	0.1
	83.0	84.4	20-10-15-20	30 45	60° -75°	0.1
	84.4	99.8	20-10-20-20	30 50	75° -75°	0.2
75° anhedral	3.0	80.4	20-10-10-20	30	0°	0.2
	80.4	81.4	20-15-10-20	20 35	75° -30°	0.1
	81.4	82.2	20-15-10-20	20 35	75° -55°	0.1
	82.2	99.8	20-20-10-20	20 40	75° -80°	0.2

Table 4.15.2: Predicted performance coefficients for the NACA 1402 base wing with full tip, 75° dihedral winglets.

Geometry	α (deg)	C_L	C_{DP}	C_M
2° toe out	-5.0	-.17820	.01811	.1087
	0.0	.02522	.00223	-.0269
	2.5	.11530	.00680	-.0857
	5.0	.20780	.01872	-.1464
	9.0	.36130	.05589	-.2483
	15.0	.58080	.15430	-.3995
3° toe out	-5.0	-.17960	.01841	.1100
	0.0	.02432	.00222	-.0261
	2.5	.11550	.00676	-.0859
	5.0	.20770	.01859	-.1463
	9.0	.36170	.05579	-.2486
	15.0	.58190	.15450	-.4005
4° toe out	-5.0	-.18090	.01875	.1113
	0.0	.02343	.00227	-.0252
	2.5	.11450	.00670	-.8490
	5.0	.20720	.01847	-.1458
	9.0	.36160	.05565	-.2484
	15.0	.58290	.15470	-.4011
6° toe out	-5.0	-.18420	.01960	.1143
	0.0	.02134	.00245	-.0233
	2.5	.11350	.00668	-.0839
	5.0	.20730	.01842	-.1458
	9.0	.36280	.05569	-.2495
	15.0	.58560	.15550	-.4035

Table 4.15.3: Predicted performance coefficients for the NACA 1402 base wing with full tip, 75° anhedral winglets.

Geometry	α (deg)	C_L	C_{DP}	C_M
2° toe in	-5.0	-.16750	.01692	.0990
	0.0	.02709	.00223	-.0286
	2.5	.11770	.00702	-.0879
	5.0	.21300	.01937	-.1512
	9.0	.37460	.05826	-.2608
	15.0	.61430	.16280	-.4311
3° toe in	-5.0	-.16850	.01714	.0999
	0.0	.02621	.00229	-.0277
	2.5	.11690	.00699	-.0871
	5.0	.21210	.01918	-.1503
	9.0	.37340	.05782	-.2596
	15.0	.61300	.16210	-.4297
4° toe in	-5.0	-.16930	.01730	.1006
	0.0	.02567	.00233	-.0272
	2.5	.11640	.00693	-.0866
	5.0	.21160	.01902	-.1498
	9.0	.37300	.05754	-.2591
	15.0	.61240	.16150	-.4290

Table 4.15.4: Predicted performance coefficients for the NACA 1402 base wing with full tip, 75° anhedral winglets having variable maximum camber location.

Geometry	α (deg)	C_L	C_{DP}	C_M
20% chord upward winglet	-5.0	-.17990	.01857	.1095
	0.0	.02740	.00275	-.0292
	5.0	.21370	.01988	-.1520
	10.0	.40940	.07119	-.2829
	15.0	.59320	.15770	-.4107
40% chord upward winglet	0.0	.02728	.00273	-.0291
	5.0	.21340	.01979	-.1517
	10.0	.40920	.07116	-.2827
	15.0	.59260	.15750	-.4101
60% chord upward winglet	-5.0	-.17590	.01812	.1055
	0.0	.02762	.00271	-.0294
	5.0	.21280	.01969	-.1511
	10.0	.40830	.07099	-.2819
	15.0	.59950	.15950	-.4173
20% chord downward winglet	-5.0	-.16640	.01669	.0979
	0.0	.02600	.00266	-.0287
	2.5	.11960	.00727	-.0897
	5.0	.21830	.02053	-.1553
	9.0	.37660	.05920	-.2628
	15.0	.62850	.16770	-.4455
40% chord downward winglet	-5.0	-.16660	.01673	.0981
	0.0	.02567	.00264	-.0284
	2.5	.11940	.00723	-.0895
	5.0	.21860	.02053	-.1553
	9.0	.37650	.05912	-.2627
	15.0	.61750	.16450	-.4345
60% chord downward winglet	-5.0	-.16660	.01670	.0981
	0.0	.02556	.00266	-.0283
	2.5	.11920	.00722	-.0893
	5.0	.21870	.02052	-.1557
	9.0	.37650	.05908	-.2627
	15.0	.61650	.16430	-.4335

Table 4.15.5: Grid input parameters fo the NACA 1402 base wing with 2% thick, 75° anhedral winglets.

Geometry	XSTART	XEND	NPT	INU	THTU	Δx
75° anhedral	3.0	81.0	20-10-10-20	30	0°	0.2
	81.0	84.0	20-15-10-20	20 35	65° -30°	0.1
	84.0	87.0	20-15-10-20	20 35	65° -60°	0.1
	87.0	99.8	20-20-10-20	20 40	65° -80°	0.2

Table 4.15.6: Predicted performance coefficients for the NACA 1402 base wing with 2% thick, 75° anhedral winglets having variable camber.

Geometry	α (deg)	C_L	C_{DP}	C_M
m = -0.01	-5.0	-.16590	.01656	.0976
	0.0	.02720	.00199	-.0286
	2.5	.11640	.00675	-.0867
	5.0	.21040	.01898	-.1488
	9.0	.36970	.05746	-.2563
	15.0	.60530	.16060	-.4228
m = 0.00	-5.0	-.16610	.01656	.0977
	0.0	.02718	.00197	-.0286
	2.5	.11640	.00671	-.0866
	5.0	.21030	.01893	-.1488
	9.0	.36930	.05734	-.2560
	15.0	.60530	.16060	-.4228
m = 0.01	-5.0	-.16610	.01659	.0977
	0.0	.02726	.00200	-.0287
	2.5	.11640	.00672	-.0867
	5.0	.21030	.01892	-.1488
	9.0	.36960	.05735	-.2563
	15.0	.60570	.16060	-.4233
m = 0.03	-5.0	-.16630	.01671	.0978
	0.0	.02730	.00216	-.0287
	2.5	.11660	.00688	-.0869
	5.0	.21050	.01905	-.1490
	9.0	.36950	.05741	-.2563
	15.0	.60640	.16070	-.4240
m = 0.04	-5.0	-.16630	.01681	.0979
	0.0	.02736	.00230	-.0288
	2.5	.11670	.00728	-.0870
	5.0	.21060	.01920	-.1491
	9.0	.36970	.05756	-.2565
	15.0	.60540	.16060	-.4231

Table 4.16.1: Grid input parameters for the "natural" flow wing and the "natural" flow wing with 65° anhedral and dihedral winglets.

Geometry	XSTART	XEND	NPT	INU	THTU	Δx
"Natural"	5.0	81.2	20-15-15-20	20 35 50	75° -20° -75°	0.2
wing	81.2	83.0	20-15-15-20	20 35 50	75° -20° -75°	0.1
	83.0	84.4	20-15-15-20	20 35 50	75° -20° -75°	0.1
	84.4	99.8	20-15-15-20	20 35 50	75° -20° -75°	0.2
65° dihedral	5.0	90.8	20-10-10-20	30	-15°	0.2
	90.8	91.4	20-10-15-20	30 45	5° -65°	0.1
	91.4	94.0	20-10-18-20	30 48	35° -65°	0.1
	94.0	99.8	20-10-21-20	30 51	60° -65°	0.2
65° anhedral	5.0	90.4	20-10-10-20	30	-15°	0.2
	90.4	91.2	20-15-10-20	20 35	65° -35°	0.1
	91.2	91.8	20-18-10-20	20 38	65° -60°	0.1
	91.8	99.8	20-21-10-20	30 41	65° -75°	0.2

Table 4.16.2: Predicted performance coefficients for the "natural" flow wing; M=1.62.

Geometry	α (deg)	C_L	C_{DP}	C_M
"Natural" flow	-5.0	-.21100	.02705	.1340
	0.0	-.01080	.00438	.0006
wing	2.5	.08486	.00563	-.0629
	5.0	.17820	.01454	-.1252
	9.0	.32280	.04475	-.2233

Table 4.16.3: Predicted performance coefficients for the "natural" flow wing with 65° anhedral winglets with various toe angles; M=1.62.

Geometry	α (deg)	C_L	C_{DP}	C_M
2° toe out	-5.0	-.20470	.02651	.1287
	0.0	-.00879	.00476	-.0017
	2.5	.08623	.00629	-.0647
	5.0	.17920	.01532	-.1267
	7.0	.25220	.02794	-.1762
	9.5	.34490	.05095	-.2397
0° toe out	-5.0	-.20590	.02672	.1299
	0.0	-.00983	.00484	-.0007
	2.5	.08511	.00624	-.0636
	5.0	.17790	.01510	-.1255
	7.0	.25090	.02761	-.1749
	9.5	.34330	.05043	-.2380
2° toe in	-5.0	-.20640	.02689	.1304
	0.0	-.01029	.00496	-.0003
	2.5	.08464	.00628	-.0631
	5.0	.17750	.01505	-.1250
	7.0	.25030	.02745	-.1742
	9.5	.34260	.05018	-.2373
4° toe in	-5.0	-.20660	.02703	.1305
	0.0	-.01075	.00512	.0001
	2.5	.08430	.00638	-.0628
	5.0	.17710	.01509	-.1246
	7.0	.25000	.02740	-.1739
	9.5	.34240	.05005	-.2370

Table 4.16.4: Predicted performance coefficients for the "natural" flow wing with 65° dihedral winglets with various toe angles; M=1.62.

Geometry	α (deg)	C_L	C_{DP}	C_M
2° toe in	-5.0	-.21510	.02932	.1389
	0.0	-.01453	.00569	.0037
	2.5	.08114	.00654	-.0598
	5.0	.17530	.01509	-.1229
	7.0	.24650	.02709	-.1707
	9.5	.33770	.04940	-.2325
0° toe out	-5.0	-.21640	.0298	.1402
	0.0	-.01570	.00591	.0059
	2.5	.08058	.00663	-.0593
	5.0	.17400	.01500	-.1217
	7.0	.24640	.02705	-.1705
	9.5	.33760	.04932	-.2324
2° toe out	-5.0	-.21720	.03025	.1410
	0.0	-.01654	.00613	.0057
	2.5	.08487	.00711	-.0633
	5.0	.17360	.01500	-.1213
	7.0	.24610	.02705	-.1703
	9.5	.33750	.04930	-.2323
4° toe out	-5.0	-.21820	.03065	.1420
	0.0	-.01707	.00640	.0062
	2.5	.07956	.00692	-.0583
	5.0	.17400	.01513	-.1217
	7.0	.24610	.02713	-.1702
	9.5	.33750	.04938	-.2324

APPENDIX A

EMTAC CODE DESCRIPTION

A.1 Conservation Equations

The fortran program EMTAC, Euler Marching Technique for Accurate Computation, is a marching algorithm designed for computing supersonic flows over realistic configurations, particularly fighter-like configurations. To gain an understanding of the code, several areas had to be addressed. Among these areas were the governing equations, the solution process, the information necessary for the program to operate, the gridding technique, and the geometric input format. With the approach to be described, the code was able to solve the unsteady Euler equations and take into account supersonic speeds while allowing subsonic pockets to exist. With the use of the Euler equations, a wider range of flows could be computed, including flows with strong shocks as well as weak shocks in the flow, relative to those which could be calculated using a full potential method.

Since the code of interest was an Euler based program, the primary starting point was converting the exact Euler conservation equations into a discretized conservation law form. The conservation law form of the unsteady Euler equations in cartesion coordinates and time, t, was given by:

$$\frac{\partial(\rho u)}{\partial x} + \frac{\partial(\rho v)}{\partial y} + \frac{\partial(\rho w)}{\partial z} = 0 \qquad \text{(A.1.1)}$$

$$\rho \frac{\partial u_i}{\partial t} + \rho\, u_j \frac{\partial u_i}{\partial x_j} = \frac{\partial p}{\partial x_j} \qquad \text{(A.1.2)}$$

$$\frac{\partial e}{\partial t} + \nabla\cdot(e\,\vec{\nabla}) = \nabla\cdot(-p\,\delta_{ij}) \qquad \text{(A.1.3)}$$

Equations A.1.1 through A.1.3 were then written into vector columns by assigning particular variables into groups of

$$Q=\begin{bmatrix} e \\ \rho \\ \rho u \\ \rho v \\ \rho w \end{bmatrix}, E=\begin{bmatrix} (e+p)u \\ \rho u \\ \rho u^2+p \\ \rho vu \\ \rho wu \end{bmatrix}, F=\begin{bmatrix} (e+p)v \\ \rho v \\ \rho uv \\ \rho v^2+p \\ \rho wv \end{bmatrix}, G=\begin{bmatrix} (e+p)w \\ \rho w \\ \rho uw \\ \rho vw \\ \rho w^2+p \end{bmatrix}$$

where Q, E, F, and G were used in the conservation equations.The new form of the equations became the following:

$$Q_t + E_x + F_y + G_z = 0 \qquad \text{(A.1.4)}$$

For this code, energy was given the definition of

$$e=\frac{p}{(\gamma-1)}+\frac{\rho(u^2+v^2+w^2)}{2} \qquad \text{(A.1.5)}$$

The next steps were to convert equation A.1.4 to form a numerical approximation through use of a finite volume technique. The developers of the code accomplished this conversion by assuming a time invariant grid and using the transformation of coordinates with

$$\tau = t \qquad \text{(A.1.6)}$$
$$\xi = \xi(x,y,z) \qquad \text{(A.1.7)}$$
$$\eta = \eta(x,y,z) \qquad \text{(A.1.8)}$$
$$\zeta = \zeta(x,y,z) \qquad \text{(A.1.9).}$$

With this set of transformation equations, the Jacobian of the transformation became

$$J=\frac{\partial(\xi,\eta,\zeta)}{\partial(x,y,z)} \qquad \text{(A.1.10)}$$

Using the Jacobian of the transformation, the quantities Q, E, F, and G were transformed into the following:

$$\underline{Q} = Q / J \qquad \text{(A..1.11)}$$
$$\underline{E} = (\xi_x/J)\,E + (\xi_y/J)\,F + (\xi_z/J)\,G \qquad \text{(A.1.12)}$$
$$\underline{F} = (\eta_x/J)\,E + (\eta_y/J)\,F + (\eta_z/J)\,G \qquad \text{(A.1.13)}$$
$$\underline{G} = (\zeta_x/J)\,E + (\zeta_y/J)\,F + (\zeta_z/J)\,G \qquad \text{(A.1.14)}$$

Equations A.1.11 through A.1.14 were used in conjunction with A.1.6 through A.1.9 and substituted into A.1.4 to yield.

$$\underline{Q}\,\tau + \underline{E}\,\xi + \underline{F}\,\eta + \underline{G}\,\zeta = 0 \qquad \text{(A.1.15)}$$

Finally, associating the ξ, η, and ζ directions with the subscripts j, k, and l, respectively, the numerical approximation in semidiscrete conservation law form was given as

$$(Q'_{j,k,l})_\tau + (E'_{j+1/2,k,l} - E'_{j-1/2,k,l}) + (F'_{j,k+1/2,l} - F'_{j,k-1/2,l}) + (G'_{j,k,l+1/2} - G'_{j,k,l-1/2}) = 0 \qquad \text{(A.1.16)}$$

In equation A.1.16, the values of E', F', and G' were numerical fluxes at the boundary sides of the cell for which discrete conservation was considered. $Q'_{j,k,l}$ was the representative conserved quantity considered conveniently to be the cell average value. The integer subscripts denote the cell or centroid of the cell while the half-integer subscripts denote cell sides. Once the semidiscrete conservation form was established, the next area of concern was the solution process.

A.2 The Solution Process

To obtain solutions for the equation A.1.16, several factors must be dealt with. Two such factors were the normals or metrics of a cell and the volume of each cell. These cell parameters were important since A.1.16 could be regarded as a finite volume discretization if the following associations were made:

$$Q'_{j,k,l} = Q\,V_{j,k,l} \qquad \text{(A.2.1)}$$

where "V" is the cell volume under consideration. Also, the cell normals were to be found. However, the four "corners" used in defining the normal vectors of the cell surface did not necessarily lie in one plane. Thus the normal vector was actually a representative normal. With the geometric details completed, the next step of the solution process was a discretization scheme for total variation diminishing, TVD. For more information on TVD schemes consult references 23, 24, and 25.

In determining the numerical flux, Q_m and Q_{m+1} were taken as neighboring states. A Riemann solver was employed since the solver can divide the flux between neighboring states into component parts associated with each wave field. In turn, these components can be again divided into positive and negative wave speeds. The actual fluxes, E, F, and G, when evaluated with the metrics equated to cell face normals can be written in the same functional form:

$$\underline{E},\ \underline{F},\ \underline{G} = f(Q, n_x, n_y, n_z) = f(Q,N) \qquad (A.2.2)$$

From the Riemann solvers, an underlying upwind scheme was based on Roe's approximate Riemann solver. With this approach, cell interface values of density, velocities, and enthalpy were computed using a special averaging procedure where

$$\rho_{m+1/2} = \sqrt{\rho_m}\ \sqrt{\rho_{m+1}} \qquad (A.2.3)$$

$$(u,v,w)_{m+1/2} = \frac{(u,v,w)_{m+1}\sqrt{\rho_{m+1}} + (u,v,w)_m\sqrt{\rho_m}}{\sqrt{\rho_{m+1}} + \sqrt{\rho_m}} \qquad (A.2.4)$$

$$h_{m+1/2} = \frac{h_{m+1}\sqrt{\rho_{m+1}} + h_m\sqrt{\rho_m}}{\sqrt{\rho_{m+1}} + \sqrt{\rho_m}} \qquad (A.2.5)$$

and m could equal j, k, or l.

From the last three equations, the speed of sound was calculated to be

$$c_{m+1/2} = \sqrt{\left\{h - (u^2 + v^2 + w^2)/2\right\}(\gamma - 1)} \qquad (A.2.6)$$

Finally, a contravariant velocity was defined:

$$\underline{U} = n_x u + n_y v + n_z w \qquad (A.2.7).$$

As for the eigennvalues, the following were given:

$$\lambda^1 = \underline{U} - c\sqrt{n_x^2 + n_y^2 + n_z^2} \qquad (A.2.8)$$

$$\lambda^{2,3,4} = \underline{U} \qquad (A.2.9)$$

$$\lambda^5 = \underline{U} + c\sqrt{n_x^2 + n_y^2 + n_z^2} \qquad (A.2.10).$$

Also defined were the following:

$$n = n_{x,y,z} / \sqrt{n_x^2 + n_y^2 + n_z^2} \qquad \text{(A.2.11)},$$

$$\theta = \frac{u^2 + v^2 + w^2}{2} \qquad \text{(A.2.12)}.$$

These equations, A.2.3 through A.2.12, were the main emphasis of the Riemann solver. For upwind biased schemes, various accuracies can be obtained. In this case, a high accuracy TVD scheme was used (see references 23,24,25).

A.3 Code Information, Grids, and Geometric Format

The information for utilizing the EMTAC code was given in the "header" section of the code input. The following example (page 264) was for a wing-alone and the final three examples of header data (pp. 265-267) were for wing-winglet geometries once the winglet section was encountered.

To place the grid around the wing, the code only needed two crossflow regions. Between these regions, the header allowed for controlling of the grid line between the two, such as the radial line angle with the horizontal. For wing-winglet geometries, more effort was needed for the grid and in controlling key radial lines. If care was not taken, the grid tended to overlap itself at the winglet. With an overlapped grid, erroneous results would be obtained. Figures A.3.1 through A.3.3 give typical grid examples.

Finally, for the code to place a grid around the geometry, a specified format was needed. The geometry listing given on pages 268 through 271 was that typically used. The first numbers listed gave the geometric axial location and how many patches the cross sectional cut had. Next, the line of integers gave the patch number and the number of points per patch. Each cut was given in this manner with the header instructing the EMTAC code at which axial location to stop.

```
 1000       NMARCH          NO. OF STREAMWISE STEP.
   25       KMAX (JMAX)     NO. OF POINT IN NORMAL DIR.
   69       LMAX (KMAX)     NO. OF POINT IN CIRCUM. DIR.
    2       NRM             NO. OF GRIDN SECTION.
   20       NDISK           RESTART SOL.FOR EVERY # STEP.
   40       NPRNT           OUTPUT FOR EVERY NP STEPS.
    1       MRCHAC          MARCH ACCURACY. ( 1:1ST ORDER; 2:2ND ORDER )
    2       CROSAC          CROSS SECTION ACCURACY.(1:1ST ORDER; 2:2ND ORDER)
    5       GLOBIT          INTERNAL ITERATION IN X STEP.
  300       NCON            INITIAL CONICAL DATA ITERATIONS,
   30       NITER           NO. OF ITERATION FOR GRID.
    6       NSPTI           NO. OF ZTA LOCATIONS FOR DETAILED FLOWFIELD OUTPUT (MAX
OF 25 LOCATIONS)
    0       BCONAC          ORDER OF B.C. EXTRAPOLATION.
   50       LWKSU           WAKE STARTING POINT ON THE UPPER SURFACE.
   50       LWKEL           WAKE ENDING POINT ON THE LOWER SURFACE.
    1       ITERGS          NUMBER OF STARTING GLOB ITERATION.
    1       ITERGE          NUMBER OF  END GLOB ITERATION.
  5.0       CFLIN  F10.5    ** NOT USED **
   .20      DZTAIN          INPUT STEP SIZE.
   .20      DZMAX           MAX. STEP SIZE.
   .20      DZMIN           MIN. STEP SIZE.A DIR.
  1.62      FSMACH          FREE STREAM MACH NO.
 15.00      ALFA            ANGLE OF ATTACK.
  70.       THTO            OUTER BOUNDARY. (DEGREE)
  1.4       GAM             RATIO OF SPECIFIC HEAT.
 -1.00      SCHEME          TVD SCHEME. (S)
  2.0       CMPRES          COMPRESSION FACTOR FOR CLIPPING. (3-S)/(1-S)
0.0001      GLOBER          CONVERGENCE CRITERION. ** NOT USED **
  0.1       DETA            ** NOT USED **
  0.1       DXI             ** NOT USED **
  0.1       DZTA            ** NOT USED **
  8.0       XSTART          STARTING X LOCATION.
 81.00      XEND            ENDING X LOCATION.
 0.010      DTINOW          INVERSE OF THE TIME STEP.
10.050      DTISUB          INVERSE OF THE TIME STEP FOR SUB SONIC. ** NOT USED **
 0.010      DTISUP          INVERSE OF THE TIME STEP FOR SUP SONIC. ** NOT USED **
   0.       XXX1            ** NOT USED **
 100.00     XWAKE           WAKE START LOCATION.(X)
   0.0      ZWAKE           WAKE START LOCATION.(Z)  ** NOT USED **
   1.0      CHL             GEOMETRIC SCALE FACTOR
   0.0      PTNOSE          AXIAL COORDINATE SHIFT.
  0.000     YSHIFT          Y-AXIS COORDINATE SHIFT.
  00.00     XM0             REF. X FOR MOMENT REFERENCE CENTER
 000.0      YM0             REF. Y FOR MOMENT REFERENCE CENTER
4476.5540   AAA             REF. AREA.
   100.00   ALL             REF. LENGTH FOR PITCH MOMENT.
  1.00      OMEGA           RELAXIATION FACTOR.
   T        OPRNT    L3     T:BOUNDARY OUTPUT ONLY; F:FULL OUTPUT.
   T        NUGRID          NUMERICAL GRID GENERATION?
   T        IREAD           T:INPUT BODY GEOM;F:ANALYTIC GEOM.
   F        RPLANE          ** NOT USED **
   F        DISKIN          RESTART DATA FROM TAPE?
   T        TAPEW           WRITE  RESTART DATA ON UNIT 2 AND 4
   F        TAPE8W          WRITE  DATA ON UNIT 8 FOR SUBSONIC FLOW.
   T        FORCE           DO FORCE CALCULATION
  30   00   00   00   00     INU 5I5 GRID SECTION LINE.
   0.0      00.0     00.0      00.0      00.0                        THTU ANGLE
  10.00   20.00   30.00   40.00   60.00   79.00   00.00
  04       ISC             NO. OF PATCH. (GEOMETRY)
  20   10   10   20   00   00   00   00   00                        NPT
  00   00   00   00   00   00   00   00   00                        ND
*****   end of emtac header   *****
```

```
1000       NMARCH          NO. OF STREAMWISE STEP.
  25       KMAX (JMAX)     NO. OF POINT IN NORMAL DIR.
  74       LMAX (KMAX)     NO. OF POINT IN CIRCUM. DIR.
   3       NRM             NO. OF GRIDN SECTION.
   1       NDISK           RESTART SOL.FOR EVERY # STEP.
  40       NPRNT           OUTPUT FOR EVERY NP STEPS.
   1       MRCHAC          MARCH ACCURACY. ( 1:1ST ORDER; 2:2ND ORDER )
   2       CROSAC          CROSS SECTION ACCURACY.(1:1ST ORDER; 2:2ND ORDER)
   5       GLOBIT          INTERNAL ITERATION IN X STEP.
  50       NCON            INITIAL CONICAL DATA ITERATIONS,
  30       NITER           NO. OF ITERATION FOR GRID.
   3       NSPTI           NO. OF ZTA LOCATIONS FOR DETAILED FLOWFIELD OUTPUT (MAX
OF 25 LOCATIONS)
   0       BCONAC          ORDER OF B.C. EXTRAPOLATION.
  50       LWKSU           WAKE STARTING POINT ON THE UPPER SURFACE.
  50       LWKEL           WAKE ENDING POINT ON THE LOWER SURFACE.
   1       ITERGS          NUMBER OF STARTING GLOB ITERATION.
   1       ITERGE          NUMBER OF  END GLOB ITERATION.
 5.0       CFLIN  F10.5    ** NOT USED **
  .20      DZTAIN          INPUT STEP SIZE.
  .20      DZMAX           MAX. STEP SIZE.
  .20      DZMIN           MIN. STEP SIZE.A DIR.
 1.62      FSMACH          FREE STREAM MACH NO.
15.00      ALFA            ANGLE OF ATTACK.
  70.      THTO            OUTER BOUNDARY. (DEGREE)
 1.4       GAM             RATIO OF SPECIFIC HEAT.
-1.00      SCHEME          TVD SCHEME. (S)
 2.0       CMPRES          COMPRESSION FACTOR FOR CLIPPING. (3-S)/(1-S)
0.0001     GLOBER          CONVERGENCE CRITERION. ** NOT USED **
 0.1       DETA            ** NOT USED **
 0.1       DXI             ** NOT USED **
 0.1       DZTA            ** NOT USED **
 81.0      XSTART          STARTING X LOCATION.
84.00      XEND            ENDING X LOCATION.
0.010      DTINOW          INVERSE OF THE TIME STEP.
10.050     DTISUB          INVERSE OF THE TIME STEP FOR SUB SONIC. ** NOT USED **
0.010      DTISUP          INVERSE OF THE TIME STEP FOR SUP SONIC. ** NOT USED **
  0.       XXX1            ** NOT USED **
 100.00    XWAKE           WAKE START LOCATION.(X)
   0.0     ZWAKE           WAKE START LOCATION.(Z)  ** NOT USED **
   1.0     CHL             GEOMETRIC SCALE FACTOR
   0.0     PTNOSE          AXIAL COORDINATE SHIFT.
  0.000    YSHIFT          Y-AXIS COORDINATE SHIFT.
  00.00    XM0             REF. X FOR MOMENT REFERENCE CENTER
 000.0     YM0             REF. Y FOR MOMENT REFERENCE CENTER
4476.5540  AAA             REF. AREA.
  100.00   ALL             REF. LENGTH FOR PITCH MOMENT.
  1.00     OMEGA           RELAXIATION FACTOR.
   T       OPRNT     L3    T:BOUNDARY OUTPUT ONLY; F:FULL OUTPUT.
   T       NUGRID          NUMERICAL GRID GENERATION?
   T       IREAD           T:INPUT BODY GEOM;F:ANALYTIC GEOM.
   F       RPLANE          ** NOT USED **
   T       DISKIN          RESTART DATA FROM TAPE?
   T       TAPEW           WRITE  RESTART DATA ON UNIT 2 AND 4
   F       TAPE8W          WRITE  DATA ON UNIT 8 FOR SUBSONIC FLOW.
   T       FORCE           DO FORCE CALCULATION
   20   35   00   00   00      INU 5I5 GRID SECTION LINE.
   65.0     -30.0      00.0       00.0       00.0                    THTU ANGLE
   81.40   82.50   83.60   00.00   00.00   00.00   00.00
   04      ISC             NO. OF PATCH. (GEOMETRY)
   20   15   10   20   00   00   00   00   00                        NPT
   00   00   00   00   00   00   00   00   00                        ND
*****   end of emtac header   *****
```

```
  1000       NMARCH          NO. OF STREAMWISE STEP.
    25       KMAX (JMAX)     NO. OF POINT IN NORMAL DIR.
    74       LMAX (KMAX)     NO. OF POINT IN CIRCUM. DIR.
     3       NRM             NO. OF GRIDN SECTION.
     1       NDISK           RESTART SOL.FOR EVERY # STEP.
    40       NPRNT           OUTPUT FOR EVERY NP STEPS.
     1       MRCHAC          MARCH ACCURACY. ( 1:1ST ORDER; 2:2ND ORDER )
     2       CROSAC          CROSS SECTION ACCURACY.(1:1ST ORDER; 2:2ND ORDER)
     5       GLOBIT          INTERNAL ITERATION IN X STEP.
    50       NCON            INITIAL CONICAL DATA ITERATIONS,
    30       NITER           NO. OF ITERATION FOR GRID.
     3       NSPTI           NO. OF ZTA LOCATIONS FOR DETAILED FLOWFIELD OUTPUT (MAX
 OF 25 LOCATIONS)
     0       BCONAC          ORDER OF B.C. EXTRAPOLATION.
    50       LWKSU           WAKE STARTING POINT ON THE UPPER SURFACE.
    50       LWKEL           WAKE ENDING POINT ON THE LOWER SURFACE.
     1       ITERGS          NUMBER OF STARTING GLOB ITERATION.
     1       ITERGE          NUMBER OF  END GLOB ITERATION.
   5.0       CFLIN  F10.5    ** NOT USED **
    .20      DZTAIN          INPUT STEP SIZE.
    .20      DZMAX           MAX. STEP SIZE.
    .20      DZMIN           MIN. STEP SIZE.A DIR.
   1.62      FSMACH          FREE STREAM MACH NO.
  15.00      ALFA            ANGLE OF ATTACK.
    70.      THTO            OUTER BOUNDARY. (DEGREE)
   1.4       GAM             RATIO OF SPECIFIC HEAT.
 -1.00       SCHEME          TVD SCHEME. (S)
   2.0       CMPRES          COMPRESSION FACTOR FOR CLIPPING. (3-S)/(1-S)
 0.0001      GLOBER          CONVERGENCE CRITERION. ** NOT USED **
   0.1       DETA            ** NOT USED **
   0.1       DXI             ** NOT USED **
   0.1       DZTA            ** NOT USED **
   84.0      XSTART          STARTING X LOCATION.
  87.00      XEND            ENDING X LOCATION.
  0.010      DTINOW          INVERSE OF THE TIME STEP.
 10.050      DTISUB          INVERSE OF THE TIME STEP FOR SUB SONIC. ** NOT USED **
  0.010      DTISUP          INVERSE OF THE TIME STEP FOR SUP SONIC. ** NOT USED **
     0.      XXX1            ** NOT USED **
   100.00    XWAKE           WAKE START LOCATION.(X)
     0.0     ZWAKE           WAKE START LOCATION.(Z)  ** NOT USED **
     1.0     CHL             GEOMETRIC SCALE FACTOR
     0.0     PTNOSE          AXIAL COORDINATE SHIFT.
    0.000    YSHIFT          Y-AXIS COORDINATE SHIFT.
    00.00    XM0             REF. X FOR MOMENT REFERENCE CENTER
   000.0     YM0             REF. Y FOR MOMENT REFERENCE CENTER
 4476.5540   AAA             REF. AREA.
    100.00   ALL             REF. LENGTH FOR PITCH MOMENT.
    1.00     OMEGA           RELAXIATION FACTOR.
     T       OPRNT     L3    T:BOUNDARY OUTPUT ONLY; F:FULL OUTPUT.
     T       NUGRID          NUMERICAL GRID GENERATION?
     T       IREAD           T:INPUT BODY GEOM;F:ANALYTIC GEOM.
     F       RPLANE          ** NOT USED **
     T       DISKIN          RESTART DATA FROM TAPE?
     T       TAPEW           WRITE  RESTART DATA ON UNIT 2 AND 4
     F       TAPE8W          WRITE  DATA ON UNIT 8 FOR SUBSONIC FLOW.
     T       FORCE           DO FORCE CALCULATION
    20   38   00   00   00      INU 5I5 GRID SECTION LINE.
    65.0      -60.0      00.0       00.0       00.0                    THTU ANGLE
    84.40   85.50   86.60   00.00   00.00   00.00   00.00
    04       ISC             NO. OF PATCH. (GEOMETRY)
    20   18   10   20   00   00   00   00   00                         NPT
    00   00   00   00   00   00   00   00   00                         ND
*****   end of emtac header   *****
```

```
1000       NMARCH          NO. OF STREAMWISE STEP.
  25       KMAX (JMAX)     NO. OF POINT IN NORMAL DIR.
  79       LMAX (KMAX)     NO. OF POINT IN CIRCUM. DIR.
   3       NRM             NO. OF GRIDN SECTION.
  20       NDISK           RESTART SOL.FOR EVERY # STEP.
  80       NPRNT           OUTPUT FOR EVERY NP STEPS.
   1       MRCHAC          MARCH ACCURACY. ( 1:1ST ORDER; 2:2ND ORDER )
   2       CROSAC          CROSS SECTION ACCURACY.(1:1ST ORDER; 2:2ND ORDER)
   5       GLOBIT          INTERNAL ITERATION IN X STEP.
  50       NCON            INITIAL CONICAL DATA ITERATIONS,
  30       NITER           NO. OF ITERATION FOR GRID.
   5       NSPTI           NO. OF ZTA LOCATIONS FOR DETAILED FLOWFIELD OUTPUT (MAX
OF 25 LOCATIONS)
   0       BCONAC          ORDER OF B.C. EXTRAPOLATION.
  50       LWKSU           WAKE STARTING POINT ON THE UPPER SURFACE.
  50       LWKEL           WAKE ENDING POINT ON THE LOWER SURFACE.
   1       ITERGS          NUMBER OF STARTING GLOB ITERATION.
   1       ITERGE          NUMBER OF  END GLOB ITERATION.
 5.0       CFLIN  F10.5    ** NOT USED **
  .20      DZTAIN          INPUT STEP SIZE.
  .20      DZMAX           MAX. STEP SIZE.
  .20      DZMIN           MIN. STEP SIZE.A DIR.
 1.62      FSMACH          FREE STREAM MACH NO.
15.00      ALFA            ANGLE OF ATTACK.
  70.      THTO            OUTER BOUNDARY. (DEGREE)
 1.4       GAM             RATIO OF SPECIFIC HEAT.
-1.00      SCHEME          TVD SCHEME. (S)
 2.0       CMPRES          COMPRESSION FACTOR FOR CLIPPING. (3-S)/(1-S)
0.0001     GLOBER          CONVERGENCE CRITERION. ** NOT USED **
 0.1       DETA            ** NOT USED **
 0.1       DXI             ** NOT USED **
 0.1       DZTA            ** NOT USED **
 87.0      XSTART          STARTING X LOCATION.
99.80      XEND            ENDING X LOCATION.
0.010      DTINOW          INVERSE OF THE TIME STEP.
10.050     DTISUB          INVERSE OF THE TIME STEP FOR SUB SONIC. ** NOT USED **
0.010      DTISUP          INVERSE OF THE TIME STEP FOR SUP SONIC. ** NOT USED **
  0.       XXX1            ** NOT USED **
 100.0     XWAKE           WAKE START LOCATION.(X)
   0.0     ZWAKE           WAKE START LOCATION.(Z)  ** NOT USED **
   1.0     CHL             GEOMETRIC SCALE FACTOR
   0.0     PTNOSE          AXIAL COORDINATE SHIFT.
  0.000    YSHIFT          Y-AXIS COORDINATE SHIFT.
  00.00    XM0             REF. X FOR MOMENT REFERENCE CENTER
 000.0     YM0             REF. Y FOR MOMENT REFERENCE CENTER
4476.5540  AAA             REF. AREA.
   100.00  ALL             REF. LENGTH FOR PITCH MOMENT.
  1.00     OMEGA           RELAXIATION FACTOR.
   T       OPRNT     L3    T:BOUNDARY OUTPUT ONLY; F:FULL OUTPUT.
   T       NUGRID          NUMERICAL GRID GENERATION?
   T       IREAD           T:INPUT BODY GEOM;F:ANALYTIC GEOM.
   F       RPLANE          ** NOT USED **
   T       DISKIN          RESTART DATA FROM TAPE?
   T       TAPEW           WRITE  RESTART DATA ON UNIT 2 AND 4
   F       TAPE8W          WRITE  DATA ON UNIT 8 FOR SUBSONIC FLOW.
   T       FORCE           DO FORCE CALCULATION
  20   41   00   00   00      INU 5I5 GRID SECTION LINE.
  65.0      -80.0          00.0        00.0          00.0                    THTU ANGLE
  88.40   91.50   94.00   96.00   99.60   00.00   00.00
  04       ISC             NO. OF PATCH. (GEOMETRY)
  20   21   10   20   00   00   00   00   00                                 NPT
  00   00   00   00   00   00   00   00   00                                 ND
*****   end of emtac header   *****
```


C-4

```
    1.000000     4
1    30    0
     .305776          .000000
     .300579          .012889
     .295382          .025779
     .290185          .038668
     .284988          .051558
     .279791          .064447
     .274594          .077337
     .269398          .090226
     .264201          .103116
     .259004          .116005
     .253807          .128894
     .248610          .141784
     .243413          .154673
     .238216          .167563
     .233019          .180452
     .227822          .193342
     .222625          .206231
     .217428          .219121
     .212231          .232010
     .207034          .244900
     .201837          .257789
     .196640          .270678
     .191443          .283568
     .186246          .296457
     .181049          .309347
     .175852          .322236
     .168339          .335126
     .159279          .348015
     .150219          .360905
     .141159          .373794
2    30    0
     .141159          .373794
     .138227          .376984
     .135295          .380174
     .132363          .383364
     .129431          .386555
     .126499          .389745
     .123568          .392935
     .120636          .396125
     .117704          .399315
     .114772          .402505
     .111840          .405695
     .108908          .408886
     .105976          .412076
     .103044          .415266
     .100112          .418456
     .095299          .421646
     .088492          .424836
     .081685          .428026
     .074877          .431216
     .068070          .434407
     .061263          .437597
     .054456          .440787
     .047649          .443977
     .040842          .447167
     .034035          .450357
     .027228          .453547
     .020421          .456738
     .013614          .459928
     .006807          .463118
     .000000          .466308
3    30    0
     .000000          .466308
    -.005726          .463118
```

```
   -.011452          .459928
   -.017178          .456738
   -.022904          .453547
   -.028631          .450357
   -.034357          .447167
   -.040083          .443977
   -.045809          .440787
   -.051535          .437597
   -.057261          .434407
   -.062987          .431216
   -.068713          .428026
   -.074439          .424836
   -.080166          .421646
   -.084155          .418456
   -.086505          .415266
   -.088855          .412076
   -.091205          .408886
   -.093555          .405695
   -.095905          .402505
   -.098254          .399315
   -.100604          .396125
   -.102954          .392935
   -.105304          .389745
   -.107654          .386555
   -.110004          .383364
   -.112354          .380174
   -.114704          .376984
   -.117054          .373794
4    30     0
   -.117054          .373794
   -.123652          .360905
   -.130250          .348015
   -.136848          .335126
   -.141806          .322236
   -.144308          .309347
   -.146809          .296457
   -.149311          .283568
   -.151813          .270678
   -.154314          .257789
   -.156816          .244900
   -.159318          .232010
   -.161819          .219121
   -.164321          .206231
   -.166823          .193342
   -.169324          .180452
   -.171826          .167563
   -.174328          .154673
   -.176829          .141784
   -.179331          .128894
   -.181833          .116005
   -.184334          .103116
   -.186836          .090226
   -.189337          .077337
   -.191839          .064447
   -.194341          .051558
   -.196842          .038668
   -.199344          .025779
   -.201845          .012889
   -.204347          .000000
   2.000000     4
 1    30     0
    .492600          .000000
    .481545          .027418
    .470491          .054835
    .459436          .082253
    .448382          .109670
```

```
      .437327         .137088
      .426273         .164505
      .415218         .191923
      .404163         .219340
      .393108         .246758
      .382054         .274175
      .370999         .301593
      .359944         .329010
      .348890         .356428
      .337835         .383845
      .326781         .411263
      .315726         .438680
      .304671         .466098
      .293617         .493515
      .282562         .520933
      .271507         .548350
      .260453         .575768
      .249398         .603185
      .238344         .630603
      .227289         .658020
      .216234         .685438
      .205180         .712855
      .194125         .740273
      .183071         .767690
      .172016         .795108
2     30     0
      .172016         .795108
      .168683         .799850
      .165350         .804591
      .162017         .809333
      .158684         .814074
      .155351         .818816
      .152019         .823558
      .148686         .828299
      .145353         .833041
      .142020         .837783
      .138365         .842524
      .134007         .847266
      .129650         .852007
      .125292         .856749
      .120934         .861491
      .116576         .866232
      .112218         .870974
      .107860         .875716
      .103503         .880457
      .099145         .885199
      .091059         .889940
      .080941         .894682
      .070823         .899424
      .060706         .904165
      .050588         .908907
      .040470         .913649
      .030353         .918390
      .020235         .923132
      .010118         .927873
      .000000         .932615
3     30     0
      .000000         .932615
     -.008511         .927873
     -.017022         .923132
     -.025533         .918390
     -.034044         .913649
     -.042555         .908907
     -.051066         .904165
     -.059577         .899424
     -.068088         .894682
```

```
   -.076599          .889940
   -.083340          .885199
   -.086833          .880457
   -.090326          .875716
   -.093818          .870974
   -.097311          .866232
   -.100804          .861491
   -.104297          .856749
   -.107790          .852007
   -.111283          .847266
   -.114776          .842524
   -.117537          .837783
   -.119965          .833041
   -.122392          .828299
   -.124819          .823558
   -.127246          .818816
   -.129673          .814074
   -.132100          .809333
   -.134528          .804591
   -.136955          .799850
   -.139382          .795108
4   30    0
   -.139382          .795108
   -.144703          .767690
   -.150025          .740273
   -.155346          .712855
   -.160667          .685438
   -.165989          .658020
   -.171310          .630603
   -.176631          .603185
   -.181953          .575768
   -.187274          .548350
   -.192595          .520933
   -.197917          .493515
   -.203238          .466098
   -.208559          .438680
   -.213880          .411263
   -.219202          .383845
   -.224523          .356428
   -.229844          .329010
   -.235166          .301593
   -.240487          .274175
   -.245808          .246758
   -.251130          .219340
   -.256451          .191923
   -.261773          .164505
   -.267094          .137088
   -.272415          .109670
   -.277736          .082253
   -.283058          .054835
   -.288379          .027418
   -.293700          .000000
```

APPENDIX B

NACA FOUR DIGIT AIRFOIL SERIES DESCRIPTION

B.1 Naming Convention and Equations

In studying the effects of winglets on wings at supersonic Mach numbers, a systematic approach was needed to geometrically describe both the wing and winglet. The approach chosen was to use a series of airfoil shapes. Since no family of airfoil shapes was obviously better than another, the NACA four digit series of wing sections was selected due to their ease in being analytically defined.

The four digit series had a precise naming convention and limited number of equations to define the airfoil. An example of the NACA series was a NACA 1402 airfoil. In this example, the first number indicated that the airfoil had a maximum camber of 1% which was the vertical maximum camber divided by the chord length. The second number, four, gave the location of the maximum camber as four tenths of chord from the leading edge and similarly, the remaining two digits gave the thickness of the airfoil as 2 percent of chord. To numerically describe the shape at all points on the airfoil, equations B.1.1 through B.1.5 were used. These equations were the following:

$$\left.\begin{aligned} x_u &= x - y_t \sin\theta \\ x_l &= x + y_t \sin\theta \\ y_u &= y_c + y_t \cos\theta \\ y_l &= y_c - y_t \cos\theta \end{aligned}\right\} \quad \text{(B.1.1)}$$

$$y_t = \frac{t}{0.2}\left(0.269\sqrt{x} - 0.126\,x - 0.3516\,x^2 + 0.2843\,x^3 - 0.1015\,x^4\right) \quad \text{(B.1.2)}$$

$$r_t = 1.109\,t^2 \quad \text{(B.1.3)}$$

$$y_c = \frac{m}{p^2}\left(2\,p\,x - x^2\right) \quad \text{(B.1.4)}$$

$$y_c = \frac{m}{(1-p)^2}\left((1-2p) + 2px - x^2\right) \quad \text{(B.1.5)}$$

where equation B.1.4 was used forward of the maximum mean line ordinate and B.1.5 was for aft of the maximum ordinate. In these equations, "m" was the maximum

ordinate of the mean line expressed as a fraction of chord and "p" was the chordwise position of the maximum ordinate. Also, the angle, θ, was defined as:

$$\theta = \tan^{-1}\left(\frac{dy_c}{dx_c}\right) \qquad \text{(B.1.6)}$$

In the present study, the airfoils of the base wing remained unchanged while those airfoils describing the winglets were altered. The basic wing had an airfoil section of a NACA 1402. Also, the wing tip extension had the same airfoil shape.

B.2 Program to Represent the Four Digit Airfoils

To obtain a number of discrete points for the program in Appendix C, the following program written by Dr. J. M. Kuhlman was used. This program was based on equations B.1.1 through B.1.6 and generated output in three different formats. These formats would allow various other codes to graphically display the individual airfoils generated, and to write output files of these airfoils in WIBCO[26,27] and Hess formats. This program is listed on the following pages.

```
      PROGRAM FOURDIG(OUTPUT,TAPE6=OUTPUT,TAPE7,TAPE9,TAPE11)
      DIMENSION XOC(60),XUP(60),ZUP(60,1),XLO(60),ZLO(60,1)
      DIMENSION ZUPT(60),ZLOT(60)
      DIMENSION ZUPTT(1),ZLOTT(1)
      REAL M,T,P,RT
      NXOC=51
      NXOCM=NXOC-1
      DXOC=1./FLOAT(NXOCM)
      WRITE(6,110) DXOC
      XOC(1)=0.
      IORDER=1
      IPT=-1
      DO 11 I=2,NXOC
   11 XOC(I)=XOC(I-1)+DXOC
      WRITE(6,110) (XOC(I),I=1,NXOC)
      NXOC=NXOC+3
      NXOCM=NXOC-1
      DO 2 I=NXOC,4,-1
    2 XOC(I)=XOC(I-3)
      XOC(2)=0.001
      XOC(3)=0.002
      XOC(4)=0.003
      WRITE(6,110) (XOC(I),I=1,NXOC)
  110 FORMAT(6E11.4)
C
C     NOW HAVE 54 XOC CHORD STATIONS: 51 EQUALLY SPACED EVERY 2%
C     AND 3 AT 0.1,0.2,0.3 %
C
C     NACA 4-DIGIT AIRFOIL FAMILY; SEE PP 113-115, ABBOTT AND VON
C     DOENHOFF
C
C     M = MAX ORDINATE OF CAMBER LINE
C     P = PERCENT CHORD POSITION OF MAX ORDINATE
C
C     T = MAX SEMI-THICKNESS
C     RT = NOSE RADIUS = 1.1019*T*T
C
      M=0.02
      T=0.00
      P=0.4
      RT=1.1019*T*T
      DO 4 I=1,NXOC
      CALL YCS(XOC(I),YC,P,M)
      CALL DYCDX(XOC(I),DYDX,P,M)
      CALL YTH(XOC(I),YT,T)
      THETA=ATAN(DYDX)
      ST=SIN(THETA)
      CT=COS(THETA)
C
C     USE NOSE RADIUS FOR SMALL XOC
C
      IF(I.GE.5.OR.YT.GT.RT) GOTO 3
      IF(XOC(I).GE.RT*CT) GOTO 3
      XMCL=XOC(I)/COS(THETA)
      PHI=ACOS(1.-XMCL/RT)
      YTN=RT*SIN(PHI)
      IF(YT.LT.YTN) YT=YTN
    3 CONTINUE
      XUP(I)=XOC(I)-YT*ST
      ZUP(I,1)=YC+YT*CT
      XLO(I)=XOC(I)+YT*ST
      ZLO(I,1)=YC-YT*CT
    4 CONTINUE
C
C     CHECK EXACT, ORIGINAL DATA
C
```

```
      WRITE(6,111)
  111 FORMAT(/5X,18HEND OF EXACT CALCS)
      WRITE(6,110) (XUP(I),I=1,NXOC)
      WRITE(6,110) (ZUP(I,1),I=1,NXOC)
      WRITE(6,110) (XLO(I),I=1,NXOC)
      WRITE(6,110) (ZLO(I,1),I=1,NXOC)
C
C     NOW INTERPOLATE TO EQUAL XOC LOCATIONS FOR UPPER AND LOWER SURF
C
      ZUPT(1)=0.
      ZLOT(1)=0.
      ZUPT(NXOC)=ZUP(NXOC,1)
      ZLOT(NXOC)=ZLO(NXOC,1)
      DO 5 I=2,NXOCM
      XTER=XOC(I)
      CALL IUNI(60,NXOC,XUP,1,ZUP,IORDER,XTER,ZUPTT,IPT,IER)
      IF (IER.NE.0) GOTO 999
      IPT=-1
      CALL IUNI(60,NXOC,XLO,1,ZLO,IORDER,XTER,ZLOTT,IPT,IER)
      IF(IER.NE.0) GOTO 999
      IPT=-1
      ZUPT(I)=ZUPTT(1)
      ZLOT(I)=ZLOTT(1)
    5 CONTINUE
   10 FORMAT(7F10.6)
      WRITE(7,10) (XOC(I),I=1,NXOC)
      WRITE(7,10) (ZUPT(I),I=1,NXOC)
      WRITE(7,10) (ZLOT(I),I=1,NXOC)
C
C     HESS FORMAT OUTPUT FILE, SPAN=1
C
      Y=0.
      DO 77 I=1,NXOC
      NC=0
      IF(I.EQ.1) NC=2
   77 WRITE(9,81) XOC(I),Y,ZUPT(I),NC,0
      NC=0
      DO 78 I=NXOC,1,-1
   78 WRITE(9,81) XOC(I),Y,ZLOT(I),NC,0
      Y=1.
      DO 79 I=1,NXOC
      NC=0
      IF(I.EQ.1) NC=1
   79 WRITE(9,81) XOC(I),Y,ZUPT(I),NC,0
      NC=0
      DO 80 I=NXOC,1,-1
   80 WRITE(9,81) XOC(I),Y,ZLOT(I),NC,0
   81 FORMAT(3F10.5,2I1)
C
C     WRITE SAS FILE OF AIRFOIL COORDS, TO FTP TO WVU VAX CLUSTER
C
   82 FORMAT(1X,3F10.6)
      DO 83 I=1,NXOC
   83 WRITE(11,82) XOC(I),ZUPT(I)
      DO 84 I=NXOC,1,-1
   84 WRITE(11,82) XOC(I),ZLOT(I)
      GOTO 1000
  998 FORMAT(/5X,30HERROR IN SUBROUTINE IUNI-IERR=,2I5,F10.6/)
  999 WRITE(6,998) IER,I,XTER
 1000 CONTINUE
      END
      SUBROUTINE YCS(X,Y,P,VM)
      Y=VM*(2.*P*X-X*X)/P/P
      IF(X.LE.P) GOTO 1
      Y=VM*((1.-2.*P)+2.*P*X-X*X)/(1.-P)/(1.-P)
    1 CONTINUE
```

```
      RETURN
      END
      SUBROUTINE DYCDX(X,SLP,P,VM)
      SLP=2.*VM*(P-X)/P/P
      IF(X.LE.P) GOTO 1
      SLP=2.*VM*(P-X)/(1.-P)/(1.-P)
    1 CONTINUE
      RETURN
      END
      SUBROUTINE YTH(X,Y,T)
      C0=0.29690
      C1=0.1260
      C2=0.35160
      C3=0.28430
      C4=0.10150
      Y=C0*SQRT(X)-C1*X-C2*X*X+C3*X**3-C4*X**4
      Y=Y*T/0.2
      RETURN
      END
```

APPENDIX C

PROGRAM FOR CROSS SECTIONAL CUTS

C.1 The Input File and Description

The fortran program, KEENANB, was the primary code used to establish geometries with cross sectional cuts perpendicular to the axial direction, as required by the EMTAC program. The input for this code consisted of a series of airfoils described by a specified number of discrete points. A description of the input file format is given below, while a sample input is given on pages 281-283. A listing of the program appears on pages 284-295.

The first three lines of the input file were remnants from the input geometry files used in the WIBCO-PPW[26,27] code and transonic winglet studies. The fourth line gave the number of airfoils on the base wing while the next number to the right gave the number of points used to describe each airfoil. After the fourth line, the data for the first airfoil, in this case the root airfoil, was given. The information of the fifth line was the leading edge location, the span location of the airfoil, the trailing edge location, the geometric twist of the airfoil in degrees and whether the airfoil shape was the same as the last airfoil. Here, a zero indicated that the airfoil shape would be the same as the last airfoil shape read by the program. A number one indicated that a new shape was to be read into the program. In the event of a new airfoil description, the next eight lines would give the chord position of the upper airfoil and lower airfoil points in terms of fraction of chord, x/c. The next two blocks of eight lines gave the upper airfoil position in fraction of chord and the lower airfoil position in fraction of chord. This was the input format used for the base wing.

For the description of the juncture between the wing and winglet, an integer was specified after the last base wing airfoil. This integer gave the number of airfoils used in forming the juncture. A format similar to that used for the base wing was used to describe these juncture airfoils. A typical block of data to describe a juncture airfoil gave a series of

four real numbers that told the program that the airfoil was part of the juncture, the number of points per airfoil, an unused value, and the dihedral of the airfoil as rotated about the axis through the base wing's span location and averaged trailing edge location. Once again, the next three blocks of data were the fractional chord locations, upper airfoil points, and the lower airfoil points in terms of fraction of chord.

After the juncture was defined, the winglets were typically defined as listed in the input file. Three lines were used, where one was a comment line, the next was a space line, and the last line gave relevant winglet information. This information was the number of airfoils used to define the winglet, the number of points per airfoil, an unused number, and the dihedral of the winglet to be studied. The file then listed the leading edge of the airfoil, the span location of the airfoil before being rotated to the dihedral angle, the trailing edge location, the geometric twist to be applied, and whether the airfoil was a new shape or not. Again, the coordinates of the airfoil were given in terms of chord fractions. This file was typical of the input used for the NACA 1402 base wing with a winglet.

C.2 Cross Sectional Cut Program

Program KEENANB was the program used to generate the cross sectional cuts perpendicular to the axial direction of the wing. The fortran code began by initializing relevant variables and then proceeded by beginning to read the input file. In this program, one airfoil geometry was read at a time. The coordinates of the wing were found from the twist and the chord fractions, x/c and z/c. The actual location of the leading and trailing edges were also necessary to determine the actual chord length. All computed coordinates were saved in arrays as each airfoil was transformed to dimensional values. Another section of the program calculated the coordinates for the winglet as being in the plane of the wing. Once these coordinates were found, they were rotated

about an axis passing through the base wing span location and the averaged trailing edge of the span airfoil.

After transforming the wing and winglet into actual coordinates, the program began dealing with winglet geometries and geometrical shifts. A geometrical shift was used to minimize the effect of the winglet and the juncture coming inboard when rotated upwards. This prevented the winglet geometries from having a "hooked" shape in the cross flow planes. The shift was enforced by using the dihedral angles between airfoils after they had rotated out of the wing plane. This shift was performed by moving the outboard airfoil further outboard. To determine where to shift the airfoil to, either the leading or trailing edge points of the airfoils were used to form the dihedral angle with the horizontal. Also, the geometric twist was considered in the geometric shift. If the twist would cause the winglet to be moved inboard, then the dihedral angle would be used at the leading edge to shift the outer airfoils.

Upon calculating the wing or wing-winglet geometric coordinates, the process of creating cross sectional cuts began. The program had previously found the maximum distance in the axial direction which was taken in the direction from the leading edge to the body's trailing edge. With this maximum distance and a number of cuts specified in the program, KEENANB then made the cuts at a uniform incremental distance by using the maximum distance divided by the number of cuts as the incremental distance. At each cross sectional cut, a first order interpolation was used to calculate the points on the cut. The interpolation began on the inner most airfoil's upper surface and then proceeded to calculate points between that airfoil and the next outboard airfoil, due to the swept constant x/c lines crossing the cut. When the interpolation was completed between these airfoils, the next outboard airfoil was interpolated on. This process continued outboard until encountering the leading edge, the wing tip, or the winglet tip. After the upper surface of the cut was determined, a similar process of moving from airfoil, between airfoils and to the next airfoil was used on the lower surface. However, the span

marching proceeded by moving from the outboard section of the geometry towards the base wing root chord. As each cut was calculated, the resulting coordinates were used to create a file that was to be used by the programs listed in Appendices D or F. The present program's execution was completed when the trailing edge cross sectional cut was produced.

C.3 The Output File of the Program

The format of the output file generated consisted of the axial location for the cut, the spanwise locations of the points, and the vertical locations of the wing surface coordinates calculated. A typical example of an output file has been given on page 296. This particular file was the output for the input file listed previously.

```
WING 64-204,CHORDROOT=100.,SWEEP=65DEG,CHORDT=20.,
3.          0.8          1.0        3.80        150.        150.        3.          1.
0.          1.0          0.0
16.         54.          1.          0.          0.        4476.554    0.8
  0.000000   0.000000100.000000   0.000000   1.000000
   .000000    .001000    .002000    .003000    .020000    .040000    .060000
   .080000    .100000    .120000    .140000    .160000    .180000    .200000
   .220000    .240000    .260000    .280000    .300000    .320000    .340000
   .360000    .380000    .400000    .420000    .440000    .460000    .480000
   .500000    .520000    .540000    .560000    .580000    .600000    .620000
   .640000    .660000    .680000    .700000    .720000    .740000    .760000
   .780000    .800000    .820000    .840000    .860000    .880000    .900000
   .920000    .940000    .960000    .980000   1.000000
   .000000    .000995    .001423    .001750    .004926    .007297    .009187
   .010793    .012192    .013424    .014514    .015477    .016325    .017067
   .017710    .018258    .018716    .019089    .019378    .019588    .019720
   .019777    .019760    .019672    .019527    .019340    .019114    .018849
   .018546    .018207    .017831    .017420    .016975    .016496    .015984
   .015438    .014860    .014251    .013609    .012936    .012231    .011495
   .010728    .009930    .009101    .008241    .007349    .006426    .005471
   .004484    .003465    .002413    .001328    .000210
   .000000   -.000837   -.001180   -.001418   -.002937   -.003468   -.003613
  -.003574   -.003426   -.003212   -.002954   -.002669   -.002370   -.002063
  -.001757   -.001456   -.001165   -.000889   -.000629   -.000389   -.000171
   .000022    .000189    .000328    .000451    .000571    .000687    .000796
   .000899    .000995    .001081    .001159    .001227    .001284    .001330
   .001364    .001387    .001397    .001394    .001379    .001350    .001308
   .001253    .001184    .001102    .001007    .000899    .000777    .000643
   .000496    .000337    .000166   -.000016   -.000210
  0.268063   0.125000100.000000   0.000000   0.000000
  0.536127   0.250000100.000000   0.000000   0.000000
  1.072253   0.500000100.000000   0.000000   0.000000
  2.144507   1.000000100.000000   0.000000   0.000000
  3.216760   1.500000100.000000   0.000000   0.000000
  8.000000   3.730461100.000000   0.000000   0.000000
 16.000000   7.460923100.000000   0.000000   0.000000
 24.000000  11.191384100.000000   0.000000   0.000000
 32.000000  14.921845100.000000   0.000000   0.000000
 40.000000  18.652307100.000000   0.000000   0.000000
 48.000000  22.382768100.000000   0.000000   0.000000
 56.000000  26.113229100.000000   0.000000   0.000000
 64.000000  29.843690100.000000   0.000000   0.000000
 72.000000  33.574152100.000000   0.000000   0.000000
 80.000000  37.304613100.000000   0.000000   0.000000
 4
1.          54.          1.         -15.
 81.884601  37.584398100.000000    .000000   1.000000
   .000000    .001000    .002000    .003000    .020000    .040000    .060000
   .080000    .100000    .120000    .140000    .160000    .180000    .200000
   .220000    .240000    .260000    .280000    .300000    .320000    .340000
   .360000    .380000    .400000    .420000    .440000    .460000    .480000
   .500000    .520000    .540000    .560000    .580000    .600000    .620000
   .640000    .660000    .680000    .700000    .720000    .740000    .760000
   .780000    .800000    .820000    .840000    .860000    .880000    .900000
   .920000    .940000    .960000    .980000   1.000000
   .000000    .001095    .001561    .001917    .005269    .007701    .009608
   .011209    .012591    .013798    .014858    .015788    .016601    .017307
   .017915    .018428    .018852    .019192    .019451    .019633    .019740
   .019774    .019738    .019634    .019474    .019273    .019034    .018756
   .018441    .018091    .017705    .017285    .016832    .016346    .015829
   .015279    .014698    .014088    .013446    .012775    .012073    .011342
   .010581    .009792    .008972    .008123    .007244    .006335    .005396
   .004426    .003425    .002393    .001330    .000235
   .000000   -.000956   -.001346   -.001623   -.003513   -.004319   -.004685
  -.004833   -.004849   -.004779   -.004648   -.004475   -.004276   -.004055
  -.003824   -.003588   -.003350   -.003118   -.002892   -.002676   -.002474
```

```
  -.002287  -.002118  -.001969  -.001829  -.001687  -.001545  -.001405
  -.001267  -.001131  -.001001  -.000875  -.000755  -.000642  -.000536
  -.000439  -.000348  -.000267  -.000195  -.000131  -.000078  -.000034
   .000000   .000025   .000040   .000045   .000041   .000027   .000004
  -.000027  -.000067  -.000116  -.000171  -.000235
1.        54.       1.       -30.
 83.769202 37.864182100.000000   .000000  1.000000
   .000000   .001000   .002000   .003000   .020000   .040000   .060000
   .080000   .100000   .120000   .140000   .160000   .180000   .200000
   .220000   .240000   .260000   .280000   .300000   .320000   .340000
   .360000   .380000   .400000   .420000   .440000   .460000   .480000
   .500000   .520000   .540000   .560000   .580000   .600000   .620000
   .640000   .660000   .680000   .700000   .720000   .740000   .760000
   .780000   .800000   .820000   .840000   .860000   .880000   .900000
   .920000   .940000   .960000   .980000  1.000000
   .000000   .001218   .001731   .002122   .005692   .008199   .010127
   .011722   .013083   .014259   .015282   .016171   .016941   .017603
   .018167   .018636   .019019   .019320   .019542   .019689   .019765
   .019771   .019711   .019586   .019409   .019191   .018935   .018642
   .018312   .017948   .017549   .017118   .016655   .016161   .015637
   .015082   .014498   .013886   .013245   .012576   .011879   .011154
   .010401   .009621   .008813   .007978   .007114   .006223   .005303
   .004354   .003377   .002369   .001332   .000265
   .000000  -.001102  -.001551  -.001876  -.004222  -.005369  -.006006
  -.006385  -.006602  -.006709  -.006735  -.006701  -.006624  -.006510
  -.006372  -.006214  -.006043  -.005864  -.005680  -.005495  -.005311
  -.005133  -.004962  -.004800  -.004639  -.004470  -.004295  -.004117
  -.003935  -.003751  -.003567  -.003382  -.003198  -.003016  -.002836
  -.002660  -.002486  -.002317  -.002153  -.001992  -.001838  -.001688
  -.001543  -.001404  -.001270  -.001140  -.001016  -.000897  -.000783
  -.000672  -.000566  -.000463  -.000362  -.000265
1.        54.       1.       -45.
 85.653804 38.143967100.000000   .000000  1.000000
   .000000   .001000   .002000   .003000   .020000   .040000   .060000
   .080000   .100000   .120000   .140000   .160000   .180000   .200000
   .220000   .240000   .260000   .280000   .300000   .320000   .340000
   .360000   .380000   .400000   .420000   .440000   .460000   .480000
   .500000   .520000   .540000   .560000   .580000   .600000   .620000
   .640000   .660000   .680000   .700000   .720000   .740000   .760000
   .780000   .800000   .820000   .840000   .860000   .880000   .900000
   .920000   .940000   .960000   .980000  1.000000
   .000000   .001374   .001946   .002381   .006227   .008828   .010782
   .012370   .013704   .014841   .015817   .016655   .017371   .017977
   .018485   .018900   .019230   .019481   .019656   .019760   .019796
   .019767   .019676   .019526   .019327   .019087   .018810   .018497
   .018148   .017767   .017352   .016907   .016432   .015928   .015395
   .014834   .014246   .013632   .012991   .012325   .011633   .010916
   .010173   .009405   .008612   .007794   .006950   .006081   .005186
   .004264   .003315   .002339   .001335   .000303
   .000000  -.001286  -.001810  -.002196  -.005117  -.006693  -.007673
  -.008344  -.008815  -.009146  -.009371  -.009512  -.009589  -.009611
  -.009589  -.009531  -.009443  -.009332  -.009201  -.009054  -.008894
  -.008726  -.008552  -.008374  -.008187  -.007984  -.007768  -.007542
  -.007305  -.007059  -.006806  -.006547  -.006282  -.006013  -.005740
  -.005465  -.005186  -.004906  -.004625  -.004342  -.004060  -.003776
  -.003492  -.003208  -.002923  -.002637  -.002351  -.002064  -.001776
  -.001487  -.001195  -.000901  -.000603  -.000303
 1.        54.       1.       -60.
  87.538405 38.423751100.000000   .000000  1.000000
    .000000   .001000   .002000   .003000   .020000   .040000   .060000
    .080000   .100000   .120000   .140000   .160000   .180000   .200000
    .220000   .240000   .260000   .280000   .300000   .320000   .340000
    .360000   .380000   .400000   .420000   .440000   .460000   .480000
    .500000   .520000   .540000   .560000   .580000   .600000   .620000
    .640000   .660000   .680000   .700000   .720000   .740000   .760000
    .780000   .800000   .820000   .840000   .860000   .880000   .900000
```

```
    .920000    .940000    .960000    .980000   1.000000
    .000000    .001577    .002226    .002718    .006922    .009648    .011635
    .013213    .014512    .015599    .016514    .017285    .017930    .018464
    .018900    .019244    .019506    .019691    .019804    .019851    .019836
    .019761    .019632    .019449    .019220    .018952    .018648    .018309
    .017936    .017531    .017096    .016633    .016142    .015623    .015080
    .014511    .013918    .013301    .012661    .011998    .011313    .010605
    .009876    .009125    .008351    .007555    .006737    .005896    .005033
    .004146    .003235    .002300    .001339    .000353
    .000000   -.001526   -.002148   -.002612   -.006284   -.008419   -.009846
   -.010896   -.011698   -.012321   -.012804   -.013173   -.013451   -.013648
   -.013779   -.013851   -.013872   -.013849   -.013786   -.013689   -.013561
   -.013406   -.013228   -.013029   -.012807   -.012561   -.012292   -.012003
   -.011694   -.011368   -.011026   -.010669   -.010299   -.009916   -.009523
   -.009118   -.008702   -.008278   -.007845   -.007403   -.006954   -.006496
   -.006030   -.005557   -.005076   -.004587   -.004090   -.003584   -.003071
   -.002547   -.002014   -.001472   -.000918   -.000353
WINGLET LEADING EDGE SWEEP 60 DEG HIGHSWEEP,TR=.31275
DUMMY LINE
 4.        54.        1.       -75.
 89.423006 38.703536100.000000 -2.000000  1.000000
    .000000    .001000    .002000    .003000    .020000    .040000    .060000
    .080000    .100000    .120000    .140000    .160000    .180000    .200000
    .220000    .240000    .260000    .280000    .300000    .320000    .340000
    .360000    .380000    .400000    .420000    .440000    .460000    .480000
    .500000    .520000    .540000    .560000    .580000    .600000    .620000
    .640000    .660000    .680000    .700000    .720000    .740000    .760000
    .780000    .800000    .820000    .840000    .860000    .880000    .900000
    .920000    .940000    .960000    .980000   1.000000
    .000000    .001852    .002605    .003176    .007866    .010759    .012792
    .014357    .015609    .016627    .017460    .018139    .018689    .019125
    .019462    .019710    .019879    .019975    .020006    .019976    .019891
    .019754    .019571    .019343    .019075    .018769    .018427    .018053
    .017647    .017212    .016749    .016261    .015748    .015211    .014653
    .014073    .013472    .012852    .012213    .011555    .010879    .010185
    .009473    .008744    .007996    .007231    .006448    .005646    .004826
    .003986    .003126    .002246    .001344    .000420
    .000000   -.001852   -.002605   -.003176   -.007866   -.010759   -.012792
   -.014357   -.015609   -.016627   -.017460   -.018139   -.018689   -.019125
   -.019462   -.019710   -.019879   -.019975   -.020006   -.019976   -.019891
   -.019754   -.019571   -.019343   -.019075   -.018769   -.018427   -.018053
   -.017647   -.017212   -.016749   -.016261   -.015748   -.015211   -.014653
   -.014073   -.013472   -.012852   -.012213   -.011555   -.010879   -.010185
   -.009473   -.008744   -.007996   -.007231   -.006448   -.005646   -.004826
   -.003986   -.003126   -.002246   -.001344   -.000420
 91.846011 40.102459100.000000 -2.000000  0.000000
 94.269017 41.501382100.000000 -2.000000  0.000000
 96.692023 42.900305100.000000 -2.000000  0.000000
```

```
      PROGRM KEENNB(OUTPUT,TPE5,TPE6=OUTPUT)
C       ************************************
C       CHANGING FORM BOPPE STRUCTURE TO CROSS-
C       SECTIONAL GEOMETRIC CUTS PERPENDICULAR
C       TO THE FREESTREAM VECTOR
C       ************************************
       REAL RU,RL,BS,TU,TL,TWU,TWL,ALFA,DI,ZMAX
       REAL Y1,Y2,X1,XO,DX,XMAX,CUTS
       REAL SPANIN,WWLTR,SLOPE,ASPAN,WLENGTH
       INTEGER NTAB,IERR,IPT,IORDER,IZMAX
       INTEGER WAF,TF,MD,MDD,K1,K2
      DIMENSION D(20),DH(50),M(100),AL(50)
      DIMENSION YDUMU(100),YDUML(100)
      DIMENSION ZDUMU(100),ZDUML(100)
      DIMENSION ZDUMMU(100),ZDUMML(100),XDUMM(100)
      DIMENSION XDUMU(100),XDUML(100)
       DIMENSION XU(60,60),XL(60,60),YU(60,60)
       DIMENSION YL(60,60),ZU(60,60),ZL(60,60)
       DIMENSION XX(60),YY(60,1),ZO(1),YO(1),ZZ(60,1)
       PI=4.*ATAN(1.)
   20 FORMAT(7F10.6)
   30 FORMAT(3F10.5,2I1)
31      FORMAT(3F15.6)
39      FORMAT(I2)
   40 FORMAT(/)
      SPAN=0.0
       DI=0.0
       NUM=0
       IZMAX=0
       XAV1=0.0
       XAV2=0.0
       YAV1=0.0
       YAV2=0.0
       ZAV1=0.0
       ZAV2=0.0
       NWWJF=0
       Y2=0.0
      K=0
       ASPAN=0.0
       WLENGTH=0.0
       WWLTR=0.0
       SPANIN=0.0
C       ***********************
C       READING IN THE NUMBERS
C       ***********************
      READ(5,40)
      READ(5,20)(D(J),J=1,3)
      READ(5,20)(D(J),J=4,10)
      D2=D(2)
       WAF=IFIX(D(4))
      LOOP=IFIX(D(5))
      D(7)=0.0
    75 READ(5,20)(D(J),J=11,15)
      D15=IFIX(D(15))
   80  READ(5,20)(XDUMM(J),J=1,LOOP)
      READ(5,20)(ZDUMMU(J),J=1,LOOP)
      READ(5,20)(ZDUMML(J),J=1,LOOP)
    60 K=K+1
       DH(K)=D(7)*PI/180.
       AL(K)=D(14)*PI/180.0
      CHORD=D(13)-D(11)
      DO 10 I=1,LOOP
      M(I)=0
    10 CONTINUE
      M(1)=1
      IF(K.EQ.1) M(1)=2
```

```
C       *************************
C       COMPUTING COORDS FOR WING
C       *************************
      ALFA=D(14)*PI/180.0
      IF(D2.EQ.1.AND.K.GT.WAF)GO TO 110
      DO 50 I=1,LOOP
      YDUMU(I)=D(12)
      YDUML(I)=D(12)
       BS=(CHORD)-CHORD*XDUMM(I)
       IF(BS.LE.0.)THEN
       XDUMU(I)=D(13)
       XDUML(I)=D(13)
       ZDUMU(I)=ZDUMMU(I)*CHORD
       ZDUML(I)=ZDUMML(I)*CHORD
       GO TO 50
       ENDIF
       RU=(BS**2.+(CHORD*ZDUMMU(I))**2.)**0.5
       RL=(BS**2.+(CHORD*ZDUMML(I))**2.)**0.5
       TU=ATAN(CHORD*ZDUMMU(I)/BS)
       TL=ATAN(CHORD*ZDUMML(I)/BS)
       ZDUMU(I)=RU*SIN(ALFA+TU)
       ZDUML(I)=RL*SIN(ALFA+TL)
       XDUMU(I)=D(11)+CHORD-RU*COS(ALFA+TU)
       XDUML(I)=D(11)+CHORD-RL*COS(ALFA+TL)
50     CONTINUE
       IF(K.EQ.WAF) THEN
       ZAVE=(ZDUMU(LOOP)+ZDUML(LOOP))/2.0
       ENDIF
      GO TO 125
C       ****************************
C       COMPUTING COORDS FOR WINGLET
C       ****************************
110    DI=D(7)*PI/180.
       DO 120 I=1,LOOP
       BS=(CHORD)-CHORD*XDUMM(I)
       IF(BS.LE.0.)THEN
       XDUMU(I)=D(13)
       XDUML(I)=D(13)
       ZDUMU(I)=ZDUMMU(I)*CHORD
       ZDUML(I)=ZDUMML(I)*CHORD
       GO TO 250
       ENDIF
       RU=(BS**2.+(CHORD*ZDUMMU(I))**2.)**0.5
       RL=(BS**2.+(CHORD*ZDUMML(I))**2.)**0.5
       TU=ATAN(CHORD*ZDUMMU(I)/BS)
       TL=ATAN(CHORD*ZDUMML(I)/BS)
       ZDUMU(I)=RU*SIN(ALFA+TU)
       ZDUML(I)=RL*SIN(ALFA+TL)
       XDUMU(I)=D(11)+CHORD-RU*COS(ALFA+TU)
       XDUML(I)=D(11)+CHORD-RL*COS(ALFA+TL)
C      ***********************************************
C      BECAUSE OF USE OF THE SINE FUNCTION CARE MUST
C      BE TAKEN TO SEE IF  RESULTS GIVE THE CORRECT
C      QUADRANT OR SIGN FOR THE WINGLET ROTATION
C      ***********************************************
250    IF(SPAN.EQ.D(12)) THEN
       IF(ZDUMU(I).LT.0.0) THEN
       TWU=-PI/2.
       ELSE
       TWU=PI/2.
       ENDIF
       IF(ZDUML(I).LT.0.) THEN
       TWL=-PI/2.
       ELSE
       TWL=PI/2.
       ENDIF
```

```
      GO TO 115
      ENDIF
      TWU=ATAN((ZDUMU(I)-ZAVE)/(D(12)-SPAN))
      TWL=ATAN((ZDUML(I)-ZAVE)/(D(12)-SPAN))
115   RU=((ZDUMU(I)-ZAVE)**2.+(D(12)-SPAN)**2.)**0.5
      RL=((ZDUML(I)-ZAVE)**2.+(D(12)-SPAN)**2.)**0.5
      ZDUMU(I)=RU*SIN(DI+TWU)+ZAVE
      ZDUML(I)=RL*SIN(DI+TWL)+ZAVE
      YDUMU(I)=SPAN+RU*COS(DI+TWU)
      YDUML(I)=SPAN+RL*COS(DI+TWL)
120   CONTINUE
125   CONTINUE
C     ***************************
C     COORDS FOR WING AND WINGLET
C     ***************************
      DO 5 I=1,LOOP
      XU(K,I)=XDUMU(I)
      XL(K,I)=XDUML(I)
      YU(K,I)=YDUMU(I)
      YL(K,I)=YDUML(I)
      ZU(K,I)=ZDUMU(I)
      ZL(K,I)=ZDUML(I)
C     WRITE(6,20) XU(K,I),YU(K,I),ZU(K,I),XL(K,I),YL(K,I),ZL(K,I)
5     CONTINUE
      DY=0.0
      IF(DI.EQ.0.0.OR.K.LE.WAF) GOTO 1011
      XAV1=0.5*(XU(K,LOOP)+XL(K,LOOP))
      ZAV1=0.5*(ZU(K,LOOP)+ZL(K,LOOP))
      ZAV2=0.5*(ZU(K-1,LOOP)+ZL(K-1,LOOP))
      YAV1=0.5*(YU(K,LOOP)+YL(K,LOOP))
      YAV2=0.5*(YU(K-1,LOOP)+YL(K-1,LOOP))
      AL(K)=ATAN(YAV1-YU(K,1))/(XAV1-XU(K,1))
      IF(AL(K).LE.0.0.AND.DH(K).GE.0.0) THEN
      IF(ZAV1.GT.ZAV2) THEN
      Y2=(ZAV1-ZAV2)/TAN(DI)+YAV2
      ELSE
      Y2=(ZAV2-ZAV1)/TAN(DI)+YAV2
      ENDIF
      DY=Y2-YAV1
      GOTO 1009
      ENDIF
      IF(AL(K).GE.0.0.AND.DH(K).GE.0.0) THEN
      IF(ZU(K,1).GT.ZU(K-1,1)) THEN
      Y2=(ZU(K,1)-ZU(K-1,1))/TAN(DI)+YU(K-1,1)
      ELSE
      Y2=(ZU(K-1,1)-ZU(K,1))/TAN(DI)+YU(K-1,1)
      ENDIF
      DY=Y2-YU(K,1)
      GOTO 1009
      ENDIF
      IF(AL(K).LE.0.0.AND.DH(K).LT.0.0) THEN
      IF(ZAV1.LT.ZAV2) THEN
      Y2=(ZAV1-ZAV2)/TAN(DI)+YAV2
      ELSE
      Y2=(ZAV2-ZAV1)/TAN(DI)+YAV2
      ENDIF
      DY=Y2-YAV1
      ELSE
      IF(ZU(K,1).LT.ZU(K-1,1)) THEN
      Y2=(ZU(K,1)-ZU(K-1,1))/TAN(DI)+YU(K-1,1)
      ELSE
      Y2=(ZU(K-1,1)-ZU(K,1))/TAN(DI)+YU(K-1,1)
      ENDIF
      DY=Y2-YU(K,1)
      ENDIF
1009  DO 1010 I=1,LOOP
```

```
      ZU(K,J)=ZU(K,J)-RU*SIN(ALFA+TU)
1040  ZL(K,J)=ZL(K,J)-RL*SIN(ALFA+TL)
      ENDIF
      Y1=YU(K+1,1)+(ZU(K,1)-ZU(K+1,1))/(TAN(DH(K)))
      RU=((XU(K,1)-XAV1)**2.+(YU(K,1)-YAV1)**2.)**.5
      X1=XAV1-(RU*RU-(Y1-YAV1)**2.)**.5
      ALFA=ATAN((Y1-YAV1)/(XAV1-X1))
      DO 1030 J=1,LOOP-1
      TU=ATAN((YU(K,J)-YAV1)/(XAV1-XU(K,J)))
      TL=ATAN((YL(K,J)-YAV1)/(XAV1-XL(K,J)))
      RU=((YU(K,J)-YAV1)**2.+(XU(K,J)-XAV1)**2.)**0.5
      RL=((YL(K,J)-YAV1)**2.+(XL(K,J)-XAV1)**2.)**0.5
      YU(K,J)=YAV1+RU*SIN(ALFA+TU)
      XU(K,J)=XAV1-RU*COS(ALFA+TU)
      YL(K,J)=YAV1+RL*SIN(ALFA+TL)
1030  XL(K,J)=XAV1-RL*COS(ALFA+TL)
      ELSE
      DI=ATAN((ZAV2-ZAV1)/(YAV2-YAV1))
C     IF(DI.GE.DH(K)) GOTO 1020
      Y1=YAV2+(ZAV1-ZAV2)/(TAN(DH(K)))
      RU=((XU(K,1)-XAV1)**2.+(YU(K,1)-YAV1)**2.)**.5
      X1=XU(K,1)+(RU*RU-(Y1-YU(K,1))**2.)**.5
      DX=XAV1-X1
      ALFA=ATAN((Y1-YU(K,1))/(X1-XU(K,1)))
      DO 3020 J=LOOP,2,-1
      TU=ATAN((YU(K,J)-YU(K,1))/(XU(K,J)-XU(K,1)))
      TL=ATAN((YL(K,J)-YL(K,1))/(XL(K,J)-XL(K,1)))
      RU=((YU(K,J)-YU(K,1))**2.+(XU(K,J)-XU(K,1))**2.)**0.5
      RL=((YL(K,J)-YL(K,1))**2.+(XL(K,J)-XL(K,1))**2.)**0.5
      YU(K,J)=YU(K,1)+RU*SIN(ALFA+TU)
      IF(J.EQ.LOOP) GOTO 3021
      XU(K,J)=XU(K,1)+RU*COS(ALFA+TU)+DX
      XL(K,J)=XL(K,1)+RL*COS(ALFA+TL)+DX
3021  CONTINUE
3020  YL(K,J)=YL(K,1)+RL*SIN(ALFA+TL)
      ENDIF
      ELSE
      IF(AL(WAF+NWWJF+1).LT.0.0) THEN
      DI=ATAN((ZU(K+1,1)-ZU(K,1))/(YU(K+1,1)-YU(K,1)))
C     IF(DI.LE.DH(K)) GOTO 1020
      IF(ZU(K,1).LT.ZU(K+1,1))THEN
      DZ=ZU(K,1)-ZU(K+1,1)
      DZ=1.05*DZ
      UL=((XAV1-XU(K,1))**2.0+(ZAV1-ZU(K,1))**2.)**0.5
      ALFA=ATAN(DZ/UL)
      DO 4040 J=1,LOOP-1
      RU=((XAV1-XU(K,J))**2.+(ZAV1-ZU(K,J))**2.)**.5
      RL=((XAV1-XL(K,J))**2.+(ZAV1-ZL(K,J))**2.)**.5
      TU=ATAN((ZAV1-ZU(K,J))/(XAV1-XU(K,J)))
      TL=ATAN((ZAV1-ZL(K,J))/(XAV1-XL(K,J)))
      XU(K,J)=XAV1-RU*COS(ALFA+TU)
      XL(K,J)=XAV1-RL*COS(ALFA+TL)
      ZU(K,J)=ZU(K,J)-RU*SIN(ALFA+TU)
4040  ZL(K,J)=ZL(K,J)-RL*SIN(ALFA+TL)
      ENDIF
      Y1=YU(K+1,1)+(ZU(K,1)-ZU(K+1,1))/(TAN(DH(K)))
      RU=((XU(K,1)-XAV1)**2.+(YU(K,1)-YAV1)**2.)**.5
      X1=XAV1-(RU*RU-(Y1-YAV1)**2.)**.5
      ALFA=ATAN((Y1-YAV1)/(XAV1-X1))
      DO 4030 J=1,LOOP-1
      TU=ATAN((YU(K,J)-YAV1)/(XAV1-XU(K,J)))
      TL=ATAN((YL(K,J)-YAV1)/(XAV1-XL(K,J)))
      RU=((YU(K,J)-YAV1)**2.+(XU(K,J)-XAV1)**2.)**0.5
      RL=((YL(K,J)-YAV1)**2.+(XL(K,J)-XAV1)**2.)**0.5
      YU(K,J)=YAV1+RU*SIN(ALFA+TU)
      XU(K,J)=XAV1-RU*COS(ALFA+TU)
```

```
      YU(K,I)=YU(K,I)+DY
      YL(K,I)=YL(K,I)+DY
      WRITE(6,20) XU(K,I),YU(K,I),ZU(K,I),XL(K,I),YL(K,I),ZL(K,I)
1010  CONTINUE
C      ****************************
C      LOGICAL THINKING STATEMENTS
C      ****************************
1011  IF(D2.EQ.0.0) THEN
      IF(K.GE.WAF) GOTO 325
      READ(5,20) (D(J),J=11,15)
      IF(D(15).EQ.1.0) GOTO 80
      GOTO 60
      ELSE
      IF(K.LT.WAF) THEN
      READ(5,20) (D(J),J=11,15)
      IF(D(15).EQ.1.0) GOTO 80
      GOTO 60
      ENDIF
      IF(NWWJF.EQ.0) THEN
      SPAN=D(12)
      READ(5,39) NWWJF
      ENDIF
      IF(K.LT.WAF+NWWJF) THEN
      READ(5,20) (D(J),J=4,7)
      READ(5,20) (D(J),J=11,15)
      IF(D(15).EQ.1.0) GOTO 80
      GOTO 60
      ENDIF
      IF(K.EQ.WAF+NWWJF) THEN
      READ(5,40)
      READ(5,20) (D(J),J=4,7)
      NUM=IFIX(D(4))
      ENDIF
      IF(K.GE.WAF+NUM+NWWJF) GOTO 325
      READ(5,20) (D(J),J=11,15)
      IF(D(15).EQ.1.0) GOTO 80
      GOTO 60
      ENDIF
C     ********************************************
C     SHIFTING AIFOILS IN JUNCTURE AND ON WINGLET
C     ********************************************
325   IF(D2.EQ.0) THEN
      NUM=0
      ELSE
      DO 1020 K=WAF+NWWJF,WAF+1,-1
      XAV1=0.5*(XU(K,LOOP)+XL(K,LOOP))
      YAV1=0.5*(YU(K,LOOP)+YL(K,LOOP))
      ZAV1=0.5*(ZU(K,LOOP)+ZL(K,LOOP))
      YAV2=0.5*(YU(K+1,LOOP)+YL(K+1,LOOP))
      ZAV2=0.5*(ZU(K+1,LOOP)+ZL(K+1,LOOP))
      IF(DH(WAF+NWWJF).GE.0.0) THEN
      IF(AL(WAF+NWWJF+1).LT.0.0) THEN
      DI=ATAN((ZU(K+1,1)-ZU(K,1))/(YU(K+1,1)-YU(K,1)))
C     IF(DI.GE.DH(K)) GOTO 1020
      IF(ZU(K,1).GT.ZU(K+1,1))THEN
      DZ=ZU(K,1)-ZU(K+1,1)
      DZ=1.05*DZ
      UL=((XAV1-XU(K,1))**2.0+(ZAV1-ZU(K,1))**2.)**0.5
      ALFA=ATAN(DZ/UL)
      DO 1040 J=1,LOOP-1
      RU=((XAV1-XU(K,J))**2.+(ZAV1-ZU(K,J))**2.)**.5
      RL=((XAV1-XL(K,J))**2.+(ZAV1-ZL(K,J))**2.)**.5
      TU=ATAN((ZAV1-ZU(K,J))/(XAV1-XU(K,J)))
      TL=ATAN((ZAV1-ZL(K,J))/(XAV1-XL(K,J)))
      XU(K,J)=XAV1-RU*COS(ALFA+TU)
      XL(K,J)=XAV1-RL*COS(ALFA+TL)
```

```
      YL(K,J)=YAV1+RL*SIN(ALFA+TL)
4030  XL(K,J)=XAV1-RL*COS(ALFA+TL)
      ELSE
      DI=ATAN((ZAV2-ZAV1)/(YAV2-YAV1))
C     IF(DI.LE.DH(K)) GOTO 1020
      Y1=YAV2+(ZAV1-ZAV2)/(TAN(DH(K)))
      RU=((XU(K,1)-XAV1)**2.+(YU(K,1)-YAV1)**2.)**.5
      X1=XU(K,1)+(RU*RU-(Y1-YU(K,1))**2.)**.5
      DX=XAV1-X1
      ALFA=ATAN((Y1-YU(K,1))/(X1-XU(K,1)))
      DO 4020 J=LOOP,2,-1
      TU=ATAN((YU(K,J)-YU(K,1))/(XU(K,J)-XU(K,1)))
      TL=ATAN((YL(K,J)-YL(K,1))/(XL(K,J)-XL(K,1)))
      RU=((YU(K,J)-YU(K,1))**2.+(XU(K,J)-XU(K,1))**2.)**0.5
      RL=((YL(K,J)-YL(K,1))**2.+(XL(K,J)-XL(K,1))**2.)**0.5
      YU(K,J)=YU(K,1)+RU*SIN(ALFA+TU)
      IF(J.EQ.LOOP) GOTO 4021
      XU(K,J)=XU(K,1)+RU*COS(ALFA+TU)+DX
      XL(K,J)=XL(K,1)+RL*COS(ALFA+TL)+DX
4021  CONTINUE
4020  YL(K,J)=YL(K,1)+RL*SIN(ALFA+TL)
      ENDIF
      ENDIF
1020  CONTINUE
      ENDIF
      IF(NUM.EQ.0) GOTO 1050
C     ********************************************************
C     FINDING THE SPAN OF THE WING AND LENGTH OF THE WINGLET
C     ********************************************************
      TF=WAF+NUM+NWWJF
      YAV1=0.5*(YU(TF,LOOP)+YL(TF,LOOP))
      YAV2=0.5*(YU(TF-1,LOOP)+YL(TF-1,LOOP))
      ZAV1=0.5*(ZU(TF,LOOP)+ZL(TF,LOOP))
      ZAV2=0.5*(ZU(TF-1,LOOP)+ZL(TF-1,LOOP))
      SLOPE=(YAV1-YAV2)/(ZAV1-ZAV2)
      ASPAN=YAV1-SLOPE*ZAV1
      WLENGTH=((ASPAN-YAV1)**2.+(ZAV1)**2.)**.5
      WWLTR=(WLENGTH/SPAN)*100.0
      SPANIN=((YAV1-SPAN)/SPAN)*100.0
1050  WRITE(6,20) ASPAN,WLENGTH,WWLTR,SPANIN
C     ************************************************
C     DETERMINATION OF THE MAXIMUM DOWNSTREAM DISTANCE
C     ************************************************
      XMAX=0.0
      XMAXU=0.0
      XMAXL=0.0
      DO 140 K=1,WAF+NUM+NWWJF
      DO 140 J=1,LOOP
      IF(XU(K,J).GT.XMAXU) XMAXU=XU(K,J)
      IF(XL(K,J).GT.XMAXL) XMAXL=XL(K,J)
140   XMAX=0.5*(XMAXL+XMAXU)
C     ****************************************
C     CREATING CROSS-SECTIONAL CUTS IN GEOMETRY
C     ****************************************
C     * INTERPOLATION IS PERFORMED ON UPPER    *
C     * SURFACE POINTS FROM INBOARD TO OUT-    *
C     * BOARD THEN ON THE LOWER SURFACE FROM   *
C     * OUTBOARD POINTS TO INBOARD POINTS      *
C     ****************************************
      IF(NUM.EQ.0) THEN
      WRITE(6,31) YU(WAF,1),0.0,ZU(WAF,1)
      ELSE
      I=WAF+NWWJF/2
C     I=WAF+1
C     I=WAF
      WRITE(6,31) YU(WAF,1),YU(I,1),ZU(WAF+NUM+NWWJF,1)
```

```
      ENDIF
      CUTS=100.0
      DX=XMAX/CUTS
C     DX=1.0
C     XMAX=100.0
      XO=0.0
      NTAB=1
425   XO=XO+DX
C     ********************************
C     INTERPOLATION ON UPPER AIRFOILS
C     ********************************
      DO 400 K=1,WAF+NUM+NWWJF
      IF(XO.LT.XU(1,1)) GOTO 425
      JU=0
      DO 410 J=1,LOOP
      XX(J)=XU(K,J)
      YY(J,1)=YU(K,J)
      IF(J.EQ.1) GOTO 410
      IF(XX(J-1).GT.XU(K,J)) JU=J
410   ZZ(J,NTAB)=ZU(K,J)
      J=1
      IF(XU(K,1).GT.XO) GOTO 430
      L=LOOP
      IORDER=1
      IF(XU(K,LOOP).LT.XO) GOTO 550
      IF(JU.EQ.0) GOTO 553
      IF(XO.GT.XU(K,JU).AND.XO.LT.XU(K,1)) THEN
      DO 551 N=1,JU
      XX(N)=XU(K,N)
      YY(N,1)=YU(K,N)
 551  ZZ(N,1)=ZU(K,N)
      IPT=-1
      IORDER=1
      L=JU
      CALL IUNI(L,L,XX,NTAB,ZZ,IORDER,XO,ZO,IPT,IERR)
      IF(IERR.NE.0) THEN
      WRITE(6,*) 'IERR=',IERR
      ENDIF
      IF(K.GT.WAF) THEN
      IF(XO.GT.XU(K,LOOP-1)) IORDER=1
      IPT=-1
      CALL IUNI(L,L,XX,NTAB,YY,IORDER,XO,YO,IPT,IERR)
      IF(IERR.NE.0) THEN
      WRITE(6,*)'IERR=',IERR
      ENDIF
      WRITE(6,31) XO,YO(1),ZO(1)
      ELSE
      WRITE(6,31) XO,YU(K,J),ZO(1)
      ENDIF
      DO 552 N=JU,LOOP
      XX(N-JU+1)=XU(K,N)
      YY(N-JU+1,1)=YU(K,N)
552   ZZ(N-JU+1,1)=ZU(K,N)
      L=LOOP-JU+1
      IPT=-1
      IORDER=1
      IF(XO.GT.XU(K,LOOP-1)) IORDER=1
      CALL IUNI(L,L,XX,NTAB,ZZ,IORDER,XO,ZO,IPT,IERR)
      IF(IERR.NE.0) THEN
      WRITE(6,*) 'IERR=',IERR
      ENDIF
      IF(K.GT.WAF) THEN
      IF(XO.GT.XU(K,LOOP-1)) IORDER=1
      IPT=-1
      CALL IUNI(L,L,XX,NTAB,YY,IORDER,XO,YO,IPT,IERR)
      IF(IERR.NE.0) THEN
```

```
      WRITE(6,*)'IERR=',IERR
      ENDIF
      WRITE(6,31) XO,YO(1),ZO(1)
      ELSE
      WRITE(6,31) XO,YU(K,J),ZO(1)
      ENDIF
      GOTO 550
      ELSE
      DO 555 N=JU,LOOP
      XX(N-JU+1)=XU(K,N)
      YY(N-JU+1,1)=YU(K,N)
555   ZZ(N-JU+1,1)=ZU(K,N)
      L=LOOP-JU+1
      IPT=-1
      IORDER=1
      IF(XO.GT.XU(K,LOOP-1)) IORDER=1
      CALL IUNI(L,L,XX,NTAB,ZZ,IORDER,XO,ZO,IPT,IERR)
      IF(IERR.NE.0) THEN
      WRITE(6,*) 'IERR=',IERR
      ENDIF
      IF(K.GT.WAF) THEN
      IF(XO.GT.XU(K,LOOP-1)) IORDER=1
      IPT=-1
      CALL IUNI(L,L,XX,NTAB,ZZ,IORDER,XO,ZO,IPT,IERR)
      IF(IERR.NE.0) THEN
      WRITE(6,*)'IERR=',IERR
      ENDIF
      WRITE(6,31) XO,YO(1),ZO(1)
      ELSE
      WRITE(6,31) XO,YU(K,J),ZO(1)
      ENDIF
      GOTO 550
      ENDIF
553   IF(XO.GT.XU(K,LOOP-1)) IORDER=1
      IPT=-1
      CALL IUNI(L,L,XX,NTAB,ZZ,IORDER,XO,ZO,IPT,IERR)
      IF(IERR.NE.0) THEN
      WRITE(6,*)'IERR=',IERR
      ENDIF
      IF(K.GT.WAF) THEN
      IF(XO.GT.XU(K,LOOP-1)) IORDER=1
      IPT=-1
      CALL IUNI(L,L,XX,NTAB,YY,IORDER,XO,YO,IPT,IERR)
      IF(IERR.NE.0) THEN
      WRITE(6,*)'IERR=',IERR
      ENDIF
      WRITE(6,31) XO,YO(1),ZO(1)
      ELSE
      WRITE(6,31) XO,YU(K,J),ZO(1)
      ENDIF
C      **************************************************
C      INTERPOLATION IN BETWEEN AIRFOILS ON UPPER SURFACE
C      **************************************************
550   L=LOOP
705   L=L-1
      IF(L.EQ.0) GOTO 700
      IF(K.EQ.WAF+NUM+NWWJF) GOTO 700
      IF(XU(K+1,LOOP).LT.XO) GOTO 700
      IF(K.LE.WAF-2.OR.K.GE.WAF+2) THEN
      IF(K.GE.WAF+NUM-2) GOTO 715
      DO 707 N=1,2
      XX(N)=XU(K+N-1,L)
      YY(N,1)=YU(K+N-1,L)
707   ZZ(N,1)=ZU(K+N-1,L)
C     IF(XU(K,2).GT.XO.AND.XU(K,1).LT.XO) GOTO 2001
      IF(XX(1).GE.XO-0.05*DX) GOTO 705
```

```
      IF(XX(2).LE.XO+0.05*DX) GOTO 700
2001  IORDER=1
      IPT=-1
      N=2
      CALL IUNI(N,N,XX,NTAB,ZZ,IORDER,XO,ZO,IPT,IERR)
      IF(IERR.NE.0) THEN
      WRITE(6,*) 'IERR=',IERR
      ENDIF
      IPT=-1
      CALL IUNI(N,N,XX,NTAB,YY,IORDER,XO,YO,IPT,IERR)
      IF(IERR.NE.0) THEN
      WRITE(6,*)'IERR=',IERR
      ENDIF
      WRITE(6,31) XO,YO(1),ZO(1)
      GOTO 705
      ELSE
      GOTO 715
      ENDIF
715   L=LOOP
720   L=L-1
      IF(L.EQ.0) GOTO 700
      IF(K.EQ.WAF+NUM) GOTO 700
      IF(XU(K+1,LOOP).LT.XO) GOTO 700
      DO 725 N=1,2
      XX(N)=XU(K+N-1,L)
      YY(N,1)=YU(K+N-1,L)
725   ZZ(N,1)=ZU(K+N-1,L)
C     IF(XU(K,2).GT.XO.AND.XU(K,1).LT.XO) GOTO 2002
      IF(XX(1).GE.XO-0.05*DX) GOTO 720
      IF(XX(2).LE.XO+0.05*DX) GOTO 700
2002  IORDER=1
      IPT=-1
      N=2
      CALL IUNI(N,N,XX,NTAB,ZZ,IORDER,XO,ZO,IPT,IERR)
      IF(IERR.NE.0) THEN
      WRITE(6,*)'IERR=',IERR
      ENDIF
      IPT=-1
      CALL IUNI(N,N,XX,NTAB,YY,IORDER,XO,YO,IPT,IERR)
      IF(IERR.NE.0) THEN
      WRITE(6,*)'IERR=',IERR
      ENDIF
      WRITE(6,31) XO,YO(1),ZO(1)
      GOTO 720
700   CONTINUE
400   CONTINUE
C      ************************************************************
C      INTERPOLATION IN BETWEEN THE AIRFOILS ON LOWER SURFACE
C      ************************************************************
430   DO 600 K=WAF+NUM+NWWJF,1,-1
      L=0
805   L=L+1
      IF(L.GT.LOOP) GOTO 800
      IF(K.EQ.WAF+NUM+NWWJF) GOTO 800
      IF(XL(K+1,LOOP).LT.XO) GOTO 800
      IF(K.LE.WAF-1.OR.K.GE.WAF+3) THEN
      IF(K.LT.2) GOTO 815
      DO 808 N=1,2
      XX(N)=XL(K+2-N,L)
      YY(N,1)=YL(K+2-N,L)
808   ZZ(N,1)=ZL(K+2-N,L)
C     IF(XL(K,2).GT.XO.AND.XL(K,1).LT.XO) GOTO 2003
      IF(XX(2).GE.XO-0.05*DX) GOTO 800
      IF(XX(1).LE.XO+0.05*DX) GOTO 805
2003  IORDER=1
      IPT=-1
```

```
      N=2
      CALL IUNI(N,N,XX,NTAB,ZZ,IORDER,XO,ZO,IPT,IERR)
      IF(IERR.NE.0) THEN
      WRITE(6,*)'IERR=',IERR
      ENDIF
      IPT=-1
      CALL IUNI(N,N,XX,NTAB,YY,IORDER,XO,YO,IPT,IERR)
      IF(IERR.NE.0) THEN
      WRITE(6,*)'IERR=',IERR
      ENDIF
      WRITE(6,31) XO,YO(1),ZO(1)
      GOTO 805
      ELSE
      GOTO 815
      ENDIF
815   L=0
820   L=L+1
      IF(L.GT.LOOP) GOTO 800
      IF(XL(K+1,LOOP).LT.XO) GOTO 800
      DO 825 N=1,2
      XX(N)=XL(K+2-N,L)
      YY(N,1)=YL(K+2-N,L)
825   ZZ(N,1)=ZL(K+2-N,L)
C     IF(XL(K,2).GT.XO.AND.XL(K,1).LT.XO) GOTO 2004
      IF(XX(2).GE.XO-0.05*DX) GOTO 800
      IF(XX(1).LE.XO+0.05*DX) GOTO 820
2004  IORDER=1
      IPT=-1
      N=2
      CALL IUNI(N,N,XX,NTAB,ZZ,IORDER,XO,ZO,IPT,IERR)
      IF(IERR.NE.0) THEN
      WRITE(6,*)'IERR=',IERR
      ENDIF
      IPT=-1
      CALL IUNI(N,N,XX,NTAB,YY,IORDER,XO,YO,IPT,IERR)
      IF(IERR.NE.0) THEN
      WRITE(6,*)'IERR=',IERR
      ENDIF
      WRITE(6,31) XO,YO(1),ZO(1)
      GOTO 820
800   CONTINUE
C      *********************************
C      INTERPOLATION ON LOWER AIRFOILS
C      *********************************
      IF(XL(K,1).GT.XO) GOTO 600
      JL=0
      DO 408 J=1,LOOP
      XX(J)=XL(K,J)
      YY(J,1)=YL(K,J)
      IF(J.EQ.1) GOTO 408
      IF(XX(J-1).GT.XL(K,J)) JL=J
408   ZZ(J,NTAB)=ZL(K,J)
      J=1
      L=LOOP
      IORDER=1
      IF(XL(K,LOOP).LT.XO) GOTO 600
      IF(JL.EQ.0) GOTO 443
      IF(XO.GT.XL(K,JL).AND.XO.LT.XL(K,1)) THEN
      DO 441 N=1,JL
      XX(N)=XL(K,N)
      YY(N,1)=YL(K,N)
441   ZZ(N,1)=ZL(K,N)
      IPT=-1
      IORDER=1
      L=JL
      CALL IUNI(L,L,XX,NTAB,ZZ,IORDER,XO,ZO,IPT,IERR)
```

```
      IF(IERR.NE.0) THEN
      WRITE(6,*) 'IERR=',IERR
      ENDIF
      IF(K.GT.WAF) THEN
      IF(XO.GT.XL(K,LOOP-1)) IORDER=1
      IPT=-1
      CALL IUNI(L,L,XX,NTAB,YY,IORDER,XO,YO,IPT,IERR)
      IF(IERR.NE.0) THEN
      WRITE(6,*)'IERR=',IERR
      ENDIF
      WRITE(6,31) XO,YO(1),ZO(1)
      ELSE
      WRITE(6,31) XO,YL(K,J),ZO(1)
      ENDIF
      DO 442 N=JL,LOOP
      XX(N-JL+1)=XL(K,N)
      YY(N-JL+1,1)=YL(K,N)
442   ZZ(N-JL+1,1)=ZL(K,N)
      L=LOOP-JL+1
      IPT=-1
      IORDER=1
      IF(XO.GT.XL(K,LOOP-1)) IORDER=1
      CALL IUNI(L,L,XX,NTAB,ZZ,IORDER,XO,ZO,IPT,IERR)
      IF(IERR.NE.0) THEN
      WRITE(6,*) 'IERR=',IERR
      ENDIF
      IF(K.GT.WAF) THEN
      IF(XO.GT.XL(K,LOOP-1)) IORDER=1
      IPT=-1
      CALL IUNI(L,L,XX,NTAB,YY,IORDER,XO,YO,IPT,IERR)
      IF(IERR.NE.0) THEN
      WRITE(6,*)'IERR=',IERR
      ENDIF
      WRITE(6,31) XO,YO(1),ZO(1)
      ELSE
      WRITE(6,31) XO,YL(K,J),ZO(1)
      ENDIF
      GOTO 600
      ELSE
      DO 444 N=JL,LOOP
      XX(N-JL+1)=XL(K,N)
      YY(N-JL+1,1)=YL(K,N)
444   ZZ(N-JL+1,1)=ZL(K,N)
      L=LOOP-JL+1
      IPT=-1
      IORDER=1
      IF(XO.GT.XL(K,LOOP-1)) IORDER=1
      CALL IUNI(L,L,XX,NTAB,ZZ,IORDER,XO,ZO,IPT,IERR)
      IF(IERR.NE.0) THEN
      WRITE(6,*) 'IERR=',IERR
      ENDIF
      IF(K.GT.WAF) THEN
      IF(XO.GT.XL(K,LOOP-1)) IORDER=1
      IPT=-1
      CALL IUNI(L,L,XX,NTAB,YY,IORDER,XO,YO,IPT,IERR)
      IF(IERR.NE.0) THEN
      WRITE(6,*)'IERR=',IERR
      ENDIF
      WRITE(6,31) XO,YO(1),ZO(1)
      ELSE
      WRITE(6,31) XO,YL(K,J),ZO(1)
      ENDIF
      GOTO 600
      ENDIF
443   IF(XO.GT.XL(K,LOOP-1)) IORDER=1
      IPT=-1
```

```
      CALL IUNI(L,L,XX,NTAB,ZZ,IORDER,XO,ZO,IPT,IERR)
      IF(IERR.NE.0) THEN
      WRITE(6,*)'IERR=',IERR
      ENDIF
      IF(K.GT.WAF) THEN
      IF(XO.GT.XL(K,LOOP-1)) IORDER=1
      IPT=-1
      CALL IUNI(L,L,XX,NTAB,YY,IORDER,XO,YO,IPT,IERR)
      IF(IERR.NE.0) THEN
      WRITE(6,*)'IERR=',IERR
      ENDIF
      WRITE(6,31) XO,YO(1),ZO(1)
      ELSE
      WRITE(6,31) XO,YL(K,J),ZO(1)
      ENDIF
600   CONTINUE
      IF(XMAX.GT.XO) GOTO 425
      WRITE(6,31) 666.
      STOP
      END
```

```
38.674675  5.515441 14.784876  6.616219
     37.304613       37.934041       -5.434903
      1.000000         .000000         .305776
      1.000000         .125000         .255377
      1.000000         .250000         .204978
      1.000000         .327398         .173771
      1.000000         .373794         .141159
      1.000000         .420097         .098604
      1.000000         .466308         .000000
      1.000000         .466308         .000000
      1.000000         .420097        -.082946
      1.000000         .373794        -.117054
      1.000000         .327398        -.140804
      1.000000         .250000        -.155826
      1.000000         .125000        -.180087
      1.000000         .000000        -.204347
      2.000000         .000000         .492600
      2.000000         .125000         .442201
      2.000000         .250000         .391801
      2.000000         .500000         .291002
      2.000000         .795108         .172016
      2.000000         .841036         .139733
      2.000000         .886871         .097608
      2.000000         .932615         .000000
      2.000000         .932615         .000000
      2.000000         .886871        -.082108
      2.000000         .841036        -.115872
      2.000000         .795108        -.139382
      2.000000         .500000        -.196658
      2.000000         .250000        -.245179
      2.000000         .125000        -.269440
      2.000000         .000000        -.293700
      3.000000         .000000         .611150
      3.000000         .125000         .578686
      3.000000         .250000         .546222
      3.000000         .475824         .487573
      3.000000         .500000         .477826
      3.000000        1.000000         .276228
      3.000000        1.262819         .170261
      3.000000        1.308278         .138308
      3.000000        1.353646         .096612
      3.000000        1.398923         .000000
      3.000000        1.398923         .000000
      3.000000        1.353646        -.081270
      3.000000        1.308278        -.114689
      3.000000        1.262819        -.137960
      3.000000        1.000000        -.188969
      3.000000         .500000        -.286011
      3.000000         .475824        -.290703
      3.000000         .250000        -.304726
      3.000000         .125000        -.312488
      3.000000         .000000        -.320250
      4.000000         .000000         .729700
      4.000000         .125000         .697236
      4.000000         .250000         .664772
      4.000000         .500000         .599845
      4.000000         .951648         .482547
      4.000000        1.000000         .463052
      4.000000        1.500000         .261454
      4.000000        1.730530         .168506
      4.000000        1.775520         .136882
      4.000000        1.820420         .095616
      4.000000        1.865231         .000000
      4.000000        1.865231         .000000
      4.000000        1.820420        -.080432
      4.000000        1.775520        -.113507
```

APPENDIX D

DESCRIPTION OF PROGRAM EXPCONX

D.1 Input File Description

The input file for the program, EXPCONX, was the output file generated by the program KEENANB, described in Appendix C. This file began with two lines of information where the second line was used by EXPCONX for decision purposes. For an example of the input file to EXPCONX, refer to Appendix C, Section 3. This example showed that the first column gave the axial location of the cross sectional cut while the second column gave the span location of the points and the last column was for the vertical location of points. The last line of the input file gave a "flag" number that would not be encountered in any of the geometries studied. This "flag" number indicated to EXPCONX that the end of the file had been reached.

D.2 Description of EXPCONX

The purpose of EXPCONX was to take the cross sectional cuts generated by KEENANB (Appendix C) and convert them into a usable form for either the EMTAC or SIMP codes. The program began by initializing variables. In particular, a variable was defined that would determine at what percent of the local span the patches would start and stop. EXPCONX would then read the first two lines of the input file. The first line was read by dummy variables and was not used. However, the second line gave information that was necessary to determine where patches began and ended. The first variable gave the span of the base wing while the second variable gave either a span location in a wing-winglet juncture or was set to zero. The third value in line two was the vertical location of the leading edge of the last airfoil. The fourth value was not used.

After reading the first two lines, the program then proceeded by reading one cut of input data at a time. However, the values of line two determined how the cut was read. The first two values indicated whether the geometry was a wing alone or a wing-

winglet geometry. For wing alone geometries, the cross sectional cut was read until the coordinates had reached a local span maximum and began to return inboard. Once the maximum local span was found, the program interpolated thirty surface points per patch with two patches used to define the upper surface. Lengths of the two patches were determined by the percentage of the span value previously specified. This possibly uneven division of span allowed better geometric definition where needed. After the upper surface linear interpolation was completed, the program wrote the calculated values to an output file in the required format for the EMTAC or SIMP codes. Upon completing the upper surface calculations, the program interpolated the two lower surface patches for wing alone geometries where each patch had 30 points per patch. This procedure repeated for each cross section until the numerical "flag" was read.

The program operated differently for wing-winglet geometries. Since the majority of the geometry still consisted of the wing, the program would read one cross sectional cut at a time until the local span maximum was read and interpolated as before. As for the output, the format remained the same. However, if the program encountered a cross section that had span values larger than the second value of line two, which was the wing semispan, the search was no longer for the maximum span value. The program began using the third value listed in line two of the input file. This value indicated if the winglet and juncture were above or below the plane of the wing. For winglets with dihedral, the program would find the maximum vertical distance of the cut after the specified span location. This vertical location was the ending point for the outer upper surface patch and the beginning point for the lower outer surface patch. Once the patch locations were known, the program interpolated and reformatted the upper surface of the cut for use by EMTAC. Winglets that had anhedral required that EXPCONX look for a minimum vertical location beyond the indicated wing span. As before, the upper surface was manipulated into EMTAC or SIMP format. For the lower surface of the configuration, the program would read from the input file until the next cut began. The lower points

were divided, used for interpolation, and the new points were written in EMTAC format. This interpolation process was essentially identical for winglets rotated above or below the plane of the wing. With the interpolation completed by EXPCONX, the geometry was ready to be used in the EMTAC or SIMP codes. A listing of program EXPCONX is given on pages 300-306.

D.3 Output File Description

The output file from EXPCONX was generated for use in either the EMTAC or SIMP codes. In particular, this program generated cross sectional cuts with 30 points per patch and had four patches per cross sectional cut. A typical section of the output file is given on pages 307-308.

```
      PROGRAM EXPCONX(OUTPUT,TAPE5,TAPE6=OUTPUT)
C     ****************************************
C     PROGRAM TO WRITE CONSTANT "X"-CUT INPUT
C     INTO SIMP OR EMTAC FORMAT
C     (PRESENTLY SET FOR FOUR PATCHES)
C     ****************************************
      REAL SPAN,SWLT,NEND,ZAVE,YO,YAVE,ZWLT
      INTEGER I,J,K,L,M,N,J2,ITRIG,ISC,IORDER
      INTEGER IPT,J1,IERR,IFLAG,UFU,UFFU
      DIMENSION XO(200),Y(200),Z(200),YY(100),ZZ(100,1)
      DIMENSION ZO(1),YF(200),ZF(200),FYY(100),FZZ(100,1)
      DIMENSION FY(100),FZ(100)
10    FORMAT(F15.6,I5)
11    FORMAT(3I5)
12    FORMAT(2F15.6)
14    FORMAT(3F15.6)
15    FORMAT(4F10.6)
16    FORMAT(4F15.6)
      PI=4.*ATAN(1.)
      ITRIG=0
      IERR=0
      LFU=0
      LFFU=0
      I=0
      ISC=4
      PERSPAN=.90
      J=0
      THT1=0.0
      THT2=0.0
      READ(5,15) DUM1,DUM2,DUM3,DUM4
      READ(5,16) SPAN,SWLT,ZWLT,XWLT
      IF(SWLT.EQ.0.0) THEN
      NEND=SPAN
      ELSE
      NEND=SWLT
      ENDIF
C     ****************************************
C     READING IN ONE GEOMETRIC CUT AT A TIME
C     ****************************************
100   NEOP=0
      I=I+1
      READ(5,14) XO(I),Y(I),Z(I)
      IF(I.EQ.1) GOTO 100
      IF(Y(I-1).EQ.Y(I).AND.Y(I).NE.0.0) THEN
      ZAVE=(Z(I-1)+Z(I))/2.
      Z(I-1)=ZAVE
      I=I-1
      GOTO 100
      ENDIF
      IF(XO(I).NE.XO(I-1))THEN
      J2=I-1
      XO(1)=XO(I)
      Y(1)=Y(I)
      Z(1)=Z(I)
      ITRIG=0
      GOTO 200
      ENDIF
      IF(ITRIG.EQ.1) GOTO 100
      IF(ZWLT.GE.0.0) THEN
      IF(Y(I-1).GT.Y(I)) THEN
      ITRIG=1
      GOTO 105
      ENDIF
      IF(Y(I-1).GE.NEND.AND.Z(I-1).GT.Z(I)) THEN
      ITRIG=1
C     YAVE=(Y(I)+Y(I-1))/2.
```

```
C       Y(I-1)=YAVE
C       ZAVE=(Z(I)+Z(I-1))/2.
C       Z(I-1)=ZAVE
C       I=I-1
        GOTO 105
        ENDIF
        ELSE
        IF(Y(I-1).GT.NEND) GOTO 5
        IF(Y(I-1).GT.Y(I)) THEN
        ITRIG=1
        GOTO 105
        ENDIF
5       IF(Y(I-1).GE.NEND.AND.Z(I-1).LT.Z(I)) THEN
        ITRIG=1
C       YAVE=(Y(I)+Y(I-1))/2.
C       Y(I-1)=YAVE
C       ZAVE=(Z(I)+Z(I-1))/2.
C       Z(I-1)=ZAVE
C       I=I-1
        GOTO 105
        ENDIF
        ENDIF
        GOTO 100
C       ****************************************
C       UPPER SURFACE INTERPOLATION TO CREATE
C       THE SAME NUMBER OF POINTS PER PATCH
C       ****************************************
105     J=I-1
106     YM=0.0
        YMAX=0.0
        K=1
        N=1
        UFU=0
        UFFU=0
        NEOP=0
        IF(J.LE.3) THEN
         WRITE(6,*)'MORE POINTS NEED TO BE ADDED AT LOCATION', XO(I)
        GOTO 999
        ENDIF
        DO 110 L=1,J
        YY(L)=Y(J-(L-1))
        IF(YMAX.LT.YY(L)) YMAX=YY(L)
        IF(L.EQ.1) GOTO 110
        IF(YY(L).LT.YY(L-1).AND.UFU.EQ.0) UFFU=L
        IF(YY(L).GT.YY(L-1)) UFU=L
110     ZZ(L,1)=Z(J-(L-1))
C       IF(NEOP.EQ.0.OR.NEOP.LE.2.OR.XO(I).LT.XWLT) THEN
        YM=(YMAX-YY(J))*PERSPAN+YY(J)
        DO 111 L=1,J
        IF(YM.LT.YY(L)) THEN
        GOTO 111
        ELSE
        NEOP=L
        GOTO 112
        ENDIF
111     CONTINUE
C       ENDIF
112     IORDER=1
        DO 500 L=NEOP,J
        FYY(L-NEOP+1)=YY(L)
500     FZZ(L-NEOP+1,1)=ZZ(L,1)
        IPT=-1
        DO 115 L=1,28
        YF(L)=YY(NEOP)-REAL(L)*(YY(NEOP)-YY(J))/(28.+1.)
        YO=YF(L)
        IF(YO.LE.YY(J-1)) IORDER=1
```

```
      M=J-NEOP+1
      CALL KIUNI(M,M,FYY,1,FZZ,IORDER,YO,ZO,IPT,IERR)
      IF(IERR.NE.0) THEN
      WRITE(6,*)'IERR=',IERR
      ENDIF
115   ZF(L)=ZO(1)
C     ****************************************
C     WRITING THE INTERPOLATED UPPER SURFACE
C     IN SIMP OR EMTAC FORMAT
C     ****************************************
      WRITE(6,10) XO(I),ISC
      WRITE(6,11) 1,30,0
      WRITE(6,12) ZZ(J,1),YY(J)
      DO 120 L=28,1,-1
120   WRITE(6,12) ZF(L),YF(L)
      WRITE(6,12) ZZ(NEOP,1),YY(NEOP)
      IORDER=1
      IF(UFU.EQ.0.OR.UFFU.EQ.J) THEN
      IPT=-1
C     ****************************************
C     INTERPOLATION ON OUTBOARD UPPER SURFACE
C     ****************************************
      DO 2150 L=1,28
      YF(L)=YMAX-(YMAX-YY(NEOP))*(REAL(L)/(28.+1.))
      YO=YF(L)
      IF(YO.LE.YY(NEOP-1)) IORDER=1
      CALL KIUNI(J,J,YY,1,ZZ,IORDER,YO,ZO,IPT,IERR)
      IF(IERR.NE.0) THEN
      WRITE(6,*)'IERR=',IERR
      ENDIF
2150  ZF(L)=ZO(1)
      ELSE
      IF(UFFU.NE.0) THEN
      WRITE(6,*) UFFU
      WRITE(6,*) 'IERR, PROBLEMS AT CUT  ',XO(I)
      ENDIF
      IF(UFU.GT.NEOP.OR.UFFU.GT.NEOP) GOTO 2600
      IF(UFFU.EQ.0) THEN
      K=0
      GOTO 3200
      ENDIF
      DO 3000 L=1,UFFU
      FYY(L)=Y(J-(L-1))
3000  FZZ(L,1)=Z(J-(L-1))
      IPT=-1
      IORDER=1
      DO 3150 L=1,28
      YF(L)=YMAX-(YMAX-YY(NEOP))*(REAL(L)/(28.+1.))
      IF(YF(L).LT.FYY(UFFU).OR.YF(L).GT.FYY(1))THEN
      N=L
      GOTO 3200
      ENDIF
      YO=YF(L)
      CALL KIUNI(UFFU,UFFU,FYY,1,FZZ,IORDER,YO,ZO,IPT,IERR)
      IF(IERR.NE.0) THEN
      WRITE(6,*)'IERR=',IERR
      ENDIF
3150  ZF(L)=ZO(1)
3200  DO 2350 L=1,UFU-UFFU+K
      FYY(L)=Y(J-(UFFU+L)+1+K)
2350  FZZ(L,1)=Z(J-(UFFU+L)+1+K)
      IPT=-1
      IORDER=1
      DO 2400 L=1,28
      FY(L)=YMAX-(YMAX-YY(NEOP))*(REAL(L)/(28.+1.))
      IF(FY(L).LT.FYY(1).OR.FY(L).GT.YMAX) THEN
```

```
      N=L
      GOTO 2450
      ENDIF
      YO=FY(L)
      IF(YO.LE.YY(NEOP-1)) IORDER=1
      IF(YO.LE.FYY(UFU-1)) IORDER=1
      M=UFU-UFFU+K
      CALL KIUNI(M,M,FYY,1,FZZ,IORDER,YO,ZO,IPT,IERR)
      IF(IERR.NE.0) THEN
      WRITE(6,*)'IERR=',IERR
      ENDIF
2400   FZ(L)=ZO(1)
2450  IORDER=1
      DO 2500 L=1,J-UFU+1
      FYY(L)=Y(J-(UFU+L)+2)
2500  FZZ(L,1)=Z(J-(UFU+L)+2)
      IPT=-1
      DO 2550 L=1,28-(N-1)
      YF(L)=YMAX-(YMAX-YY(NEOP))*(REAL(L)/(28.+2.-REAL(N)))
      YO=YF(L)
      IF(YO.LE.YY(NEOP-1)) IORDER=1
      M=J-UFU+1
      CALL KIUNI(M,M,FYY,1,FZZ,IORDER,YO,ZO,IPT,IERR)
      IF(IERR.NE.0) THEN
      WRITE(6,*)'IERR=',IERR
      ENDIF
2550  ZF(L)=ZO(1)
      ENDIF
2600  CONTINUE
C     ************************************************
C     WRITING THE INTERPOLATED OUTBOARD UPPER SURACE
C     INTO SIMP OR EMTAC GEOMETRIC FORMAT
C     ************************************************
      WRITE(6,11) 2,30,0
      WRITE(6,12) ZZ(NEOP,1),YY(NEOP)
      IF(ZWLT.GE.0.0.OR.N.EQ.1) THEN
      DO 130 L=28,1,-1
130   WRITE(6,12) ZF(L),YF(L)
      ELSE
      DO 135 L=28-(N-1),1,-1
135   WRITE(6,12) ZF(L),YF(L)
      DO 136 L=1,N-1
136   WRITE(6,12) FZ(L),FY(L)
      ENDIF
      WRITE(6,12) ZZ(1,1),YY(1)
      GOTO 100
C     ****************************************
C     LOWER SURFACE INTERPOLATIONS TO CREATE
C     SAME NUMBER OF POINTS PER PATCH
C     ****************************************
200   J1=J2-J+1
      K=1
      N=1
      THT1=0.0
       YM=0.0
      NEOP=0
      YMAX=0.0
      LFFU=0
      LFU=0
      J=J-1
      IF(J1.LE.3) THEN
       WRITE(6,*)'MORE POINTS NEED TO BE ADDED AT LOCATION', XO(J2)
      GOTO 999
      ENDIF
      DO 210 L=1,J1
      YY(L)=Y(J+L)
```

```
      ZZ(L,1)=Z(J+L)
      IF(YMAX.LT.YY(L)) YMAX=YY(L)
      IF(L.EQ.1) GOTO 210
      IF(YY(L).LT.YY(L-1).AND.LFU.EQ.0) LFFU=L
      IF(YY(L).GT.YY(L-1)) LFU=L
      IF(NEOP.NE.0) GOTO 210
      THT1= ATAN((ZZ(L,1)-ZZ(L-1,1))/(YY(L)-YY(L-1)))
      IF(L.LE.J1/4) GOTO 210
      IF(THT1.LT.(THT2-.1745)) NEOP=L-1
210   THT2=THT1
C     IF(NEOP.EQ.0.OR.NEOP.LE.3) THEN
      YM=(YMAX-YY(J1))*PERSPAN+YY(J1)
      DO 211 L=1,J1
      IF(YM.LT.YY(L)) THEN
      GOTO 211
      ELSE
      NEOP=L
      GOTO 212
      ENDIF
211   CONTINUE
C     ENDIF
212   IORDER=1
      IF(LFU.EQ.0.OR.LFFU.EQ.J1) THEN
      IPT=-1
      DO 215 L=1,28
      YF(L)=YMAX-(YMAX-YY(NEOP))*(REAL(L)/(28.+1.))
      YO=YF(L)
      IF(YO.LE.YY(NEOP-1)) IORDER=1
      CALL KIUNI(J1,J1,YY,1,ZZ,IORDER,YO,ZO,IPT,IERR)
      IF(IERR.NE.0) THEN
      WRITE(6,*)'IERR=',IERR
      ENDIF
215   ZF(L)=ZO(1)
      ELSE
      IF(LFU.GT.NEOP.OR.LFFU.GT.NEOP) GOTO 260
      IF(LFFU.EQ.0) THEN
      K=0
      GOTO 320
      ENDIF
      DO 300 L=1,LFFU
      FYY(L)=Y(J+L)
300   FZZ(L,1)=Z(J+L)
      IPT=-1
      IORDER=1
      DO 315 L=1,28
      YF(L)=YMAX-(YMAX-YY(NEOP))*(REAL(L)/(28.+1.))
      IF(YF(L).LT.FYY(LFFU).OR.YF(L).GT.FYY(1))THEN
      N=L
      GOTO 320
      ENDIF
      YO=YF(L)
      CALL KIUNI(LFFU,LFFU,FYY,1,FZZ,IORDER,YO,ZO,IPT,IERR)
      IF(IERR.NE.0) THEN
      WRITE(6,*)'IERR=',IERR
      ENDIF
315   ZF(L)=ZO(1)
320   DO 235 L=1,LFU-LFFU+K
      FYY(L)=Y(J+L+LFFU-K)
235   FZZ(L,1)=Z(J+L+LFFU-K)
      IPT=-1
      IORDER=1
      DO 240 L=1,28
      FY(L)=YMAX-(YMAX-YY(NEOP))*(REAL(L)/(28.+1.))
      IF(FY(L).LT.FYY(1).OR.FY(L).GT.YMAX) THEN
      N=L
      GOTO 245
```

```
      ENDIF
      YO=FY(L)
      IF(YO.LE.YY(NEOP-1)) IORDER=1
      IF(YO.LE.FYY(LFU-1)) IORDER=1
      M=LFU-LFFU+K
      CALL KIUNI(M,M,FYY,1,FZZ,IORDER,YO,ZO,IPT,IERR)
      IF(IERR.NE.0) THEN
      WRITE(6,*)'IERR=',IERR
      ENDIF
240   FZ(L)=ZO(1)
245   IORDER=1
      DO 250 L=1,J1-LFU+1
      FYY(L)=Y(J+L+LFU-1)
250   FZZ(L,1)=Z(J+L+LFU-1)
      IPT=-1
      DO 255 L=1,28-(N-1)
      YF(L)=YMAX-(YMAX-YY(NEOP))*(REAL(L)/(28.+2.-REAL(N)))
      YO=YF(L)
      IF(YO.LE.YY(NEOP-1)) IORDER=1
      M=J1-LFU+1
      CALL KIUNI(M,M,FYY,1,FZZ,IORDER,YO,ZO,IPT,IERR)
      IF(IERR.NE.0) THEN
      WRITE(6,*)'IERR=',IERR
      ENDIF
255   ZF(L)=ZO(1)
      ENDIF
260   CONTINUE
C     ****************************************
C     WRITING THE INTERPOLATE LOWER SURFACE
C     IN SIMP OR EMTAC FORMAT
C     ****************************************
      WRITE(6,11) 3,30,0
      WRITE(6,12) ZZ(1,1),YY(1)
      IF(ZWLT.GE.0.0.OR.N.NE.1) THEN
      DO 350 L=N-1,1,-1
350   WRITE(6,12) FZ(L),FY(L)
      DO 355 L=1,28-(N-1)
355   WRITE(6,12) ZF(L),YF(L)
      ELSE
      DO 220 L=1,28
220   WRITE(6,12) ZF(L),YF(L)
      ENDIF
      WRITE(6,12) ZZ(NEOP,1),YY(NEOP)
      IORDER=1
      DO 340 L=1,J1-NEOP+1
      YY(L)=Y(J+L+NEOP-1)
 340  ZZ(L,1)=Z(J+L+NEOP-1)
      IPT=-1
      DO 225 L=1,28
      YF(L)=YY(1)-REAL(L)*(YY(1)-YY(J1-NEOP+1))/(28.+1.)
      YO=YF(L)
      IF(YO.LE.YY((J1-NEOP+1)-1)) IORDER=1
      CALL KIUNI(J1-NEOP+1,J1-NEOP+1,YY,1,ZZ,IORDER,YO,ZO,IPT,IERR)
      IF(IERR.NE.0) THEN
      WRITE(6,*) 'IERR=',IERR
      ENDIF
225   ZF(L)=ZO(1)
C     ************************************************
C     WRITING THE INTERPOLATED INBOARD LOWER SURFACE
C     INTO SIMP OR EMTAC GEOMETRIC FORMAT
C     ************************************************
      WRITE(6,11) 4,30,0
      WRITE(6,12) ZZ(1,1),YY(1)
      DO 230 L=1,28
230   WRITE(6,12) ZF(L),YF(L)
      WRITE(6,12) ZZ(J1-NEOP+1,1),YY(J1-NEOP+1)
```

```
      IF(XO(1).EQ.666.) GOTO 999
      I=1
      IFLAG=0
      LFU=0
      LFFU=0
      GOTO 100
999   STOP
      END
      SUBROUTINE KIUNI(MM,NN,X,KTAB,Y,IORDER,XO,YO,IPT,IERR)
      INTEGER IORDER,MM,NN,IERR,KTAB,IPT,KN,KOLD
      REAL X(NN),Y(MM,KTAB),XO,YO,SLOPE
      IF(IPT.EQ.-1) THEN
      KN=1
      KOLD=1
      ELSE
      KN=KOLD
      ENDIF
      IF(XO.LT.X(KN)) GOTO 9001
9002  IF(KN.GE.NN) GOTO 9000
      IF(XO.GT.X(KN+1)) THEN
      KN=KN+1
      GOTO 9002
      ELSE
      KOLD=KN
      IF(XO.LT.X(KN+1).AND.XO.GT.X(KN)) THEN
      SLOPE=((Y(KN+1,KTAB)-Y(KN,KTAB))*(XO-X(KN)))/(X(KN+1)-X(KN))
      YO=Y(KN,KTAB)+SLOPE
      ENDIF
      ENDIF
9001  IF(XO.LT.X(NN)) GOTO 9000
      IF(KOLD.EQ.1) KN=2
9003  IF(KN.GT.NN) GOTO 9000
      IF(XO.LT.X(KN)) THEN
      KN=KN+1
      GOTO 9003
      ELSE
      KOLD=KN
      IF(XO.GT.X(KN).AND.XO.LT.X(KN-1)) THEN
      SLOPE=((Y(KN,KTAB)-Y(KN-1,KTAB))*(XO-X(KN-1)))/(X(KN)-X(KN-1))
      YO=Y(KN-1,KTAB)+SLOPE
      ENDIF
      ENDIF
9000  CONTINUE
      END
```

```
   1.000000     4
1    30     0
     .305776          .000000
     .300579          .012889
     .295382          .025779
     .290185          .038668
     .284988          .051558
     .279791          .064447
     .274594          .077337
     .269398          .090226
     .264201          .103116
     .259004          .116005
     .253807          .128894
     .248610          .141784
     .243413          .154673
     .238216          .167563
     .233019          .180452
     .227822          .193342
     .222625          .206231
     .217428          .219121
     .212231          .232010
     .207034          .244900
     .201837          .257789
     .196640          .270678
     .191443          .283568
     .186246          .296457
     .181049          .309347
     .175852          .322236
     .168339          .335126
     .159279          .348015
     .150219          .360905
     .141159          .373794
2    30     0
     .141159          .373794
     .138227          .376984
     .135295          .380174
     .132363          .383364
     .129431          .386555
     .126499          .389745
     .123568          .392935
     .120636          .396125
     .117704          .399315
     .114772          .402505
     .111840          .405695
     .108908          .408886
     .105976          .412076
     .103044          .415266
     .100112          .418456
     .095299          .421646
     .088492          .424836
     .081685          .428026
     .074877          .431216
     .068070          .434407
     .061263          .437597
     .054456          .440787
     .047649          .443977
     .040842          .447167
     .034035          .450357
     .027228          .453547
     .020421          .456738
     .013614          .459928
     .006807          .463118
     .000000          .466308
3    30     0
     .000000          .466308
    -.005726          .463118
```

```
    -.011452          .459928
    -.017178          .456738
    -.022904          .453547
    -.028631          .450357
    -.034357          .447167
    -.040083          .443977
    -.045809          .440787
    -.051535          .437597
    -.057261          .434407
    -.062987          .431216
    -.068713          .428026
    -.074439          .424836
    -.080166          .421646
    -.084155          .418456
    -.086505          .415266
    -.088855          .412076
    -.091205          .408886
    -.093555          .405695
    -.095905          .402505
    -.098254          .399315
    -.100604          .396125
    -.102954          .392935
    -.105304          .389745
    -.107654          .386555
    -.110004          .383364
    -.112354          .380174
    -.114704          .376984
    -.117054          .373794
4    30     0
    -.117054          .373794
    -.123652          .360905
    -.130250          .348015
    -.136848          .335126
    -.141806          .322236
    -.144308          .309347
    -.146809          .296457
    -.149311          .283568
    -.151813          .270678
    -.154314          .257789
    -.156816          .244900
    -.159318          .232010
    -.161819          .219121
    -.164321          .206231
    -.166823          .193342
    -.169324          .180452
    -.171826          .167563
    -.174328          .154673
    -.176829          .141784
    -.179331          .128894
    -.181833          .116005
    -.184334          .103116
    -.186836          .090226
    -.189337          .077337
    -.191839          .064447
    -.194341          .051558
    -.196842          .038668
    -.199344          .025779
    -.201845          .012889
    -.204347          .000000
    2.000000     4
1    30     0
     .492600          .000000
     .481545          .027418
     .470491          .054835
     .459436          .082253
     .448382          .109670
```

APPENDIX E

PROGRAM FOR JUNCTURE AIRFOILS

To define the juncture between a wing and winglet, a series of airfoils were needed. The following program was written by C.K. Brown and was designed to generate a series of four airfoils to be used in the juncture of a wing-winglet geometry. These juncture airfoils were linearly interpolated from the base wing tip airfoil and the root airfoil of the winglet. The input file and output file were similar to the input file discussed in Appendix C and were written in what was generally referred to as the WIBCO-PPW[26,27] format.

```
      PROGRAM TWOAIRT(OUTPUT,TAPE5,TAPE6=OUTPUT)
C
C THIS PROGRAM READS 2 AIRFOILS IN WIBCO-PPW FORMAT AND
C INTERPOLATES A SPECIFIED NUMBER OF NEW AIRFOILS
C BETWEEN THEM USING FIRST ORDER LINEAR EQUATION.
C
C NUMAF = THE NUMBER OF NEW AIRFOILS
C
      DIMENSION XOC1(60),XOC2(60),ZTU1(60),ZTU2(60),ZTL1(60),ZTL2(60)
      DIMENSION ZU(60,60),ZL(60,60),ZUC(60,60),ZLC(60,60)
      DIMENSION XPL(60),XPT(60),Y(60),CHORD(60),SLOPE(60)
      DIMENSION ZTUC1(60),ZTUC2(60),ZTLC1(60),ZTLC2(60)
20    FORMAT(7F10.6)
30    FORMAT(/)
C
C READ  WIBCO-PPW FORMATTED GEOMETRY, 2 AIRFOILS ONLY
C
      READ(5,30)
      READ(5,20) PY,VER,POD
      READ(5,20) ASPECT,ANIN,ANOSW,XMOM,ZWING,REFAR,WS
      NXOC=IFIX(ANIN)
      READ(5,20) XPL1,YP1,XPT1,TWIST1,AKODE1
      READ(5,20) (XOC1(J),J=1,NXOC)
      READ(5,20) (ZTU1(J),J=1,NXOC)
      READ(5,20) (ZTL1(J),J=1,NXOC)
      READ(5,20) XPL2,YP2,XPT2,TWIST2,AKODE2
      READ(5,20) (XOC2(J),J=1,NXOC)
      READ(5,20) (ZTU2(J),J=1,NXOC)
      READ(5,20) (ZTL2(J),J=1,NXOC)
      NUMAF=4
      SSPAN=YP2-YP1
      YINCR=SSPAN/(FLOAT(NUMAF)+1.)
      NUMT=NUMAF+2
C
C INTERPOLATION MODULE
C
      DO 50 K=1,NUMT
       Y(K)=YP1+YINCR*FLOAT(K-1)
       XPL(K)=XPL1+(XPL2-XPL1)*(Y(K)-YP1)/(YP2-YP1)
       XPT(K)=XPT1+(XPT2-XPT1)*(Y(K)-YP1)/(YP2-YP1)
       CHORD(K)=XPT(K)-XPL(K)
       CHORD1=XPT1-XPL1
       CHORD2=XPT2-XPL2
       SLOPE(K)=(Y(K)-YP1)/(YP2-YP1)
       DO 55 J=1,NXOC
        ZTUC1(J)=ZTU1(J)*CHORD1
        ZTUC2(J)=ZTU2(J)*CHORD2
        ZUC(K,J)=ZTUC1(J)+(ZTUC2(J)-ZTUC1(J))*SLOPE(K)
        ZU(K,J)=ZUC(K,J)/CHORD(K)
        ZTLC1(J)=ZTL1(J)*CHORD1
        ZTLC2(J)=ZTL2(J)*CHORD2
        ZLC(K,J)=ZTLC1(J)+(ZTLC2(J)-ZTLC1(J))*SLOPE(K)
        ZL(K,J)=ZLC(K,J)/CHORD(K)
55     CONTINUE
       WRITE(6,20) XPL(K),Y(K),XPT(K),TWIST1,AKODE1
       WRITE(6,20) (XOC1(J),J=1,NXOC)
       WRITE(6,20) (ZU(K,J),J=1,NXOC)
       WRITE(6,20) (ZL(K,J),J=1,NXOC)
50    CONTINUE
      END
```

APPENDIX F

PROGRAM FOR PATCH ALTERATION AND GEOMETRIC SPLICING

The fortran program, CHANGE, was used for two purposes involving the "natural" flow wing [15,16]. The first purpose was to convert the EMTAC format as given by researchers from NASA-Langley. To describe wing-winglet geometries, at least four patches per cross section were found to be necessary on the wing and winglet. However, the original "natural" wing had an EMTAC description consisting of only three patches per cross sectional cut. Because of the three patch format, CHANGE was used to split the second patch into two patches if the winglet was not yet present at a particular cross section. When the winglet was present at a cross section, the code would alter only the points on the outboard part of the wing such that the winglet and juncture could be attached to the wing. This involved eliminating the original "natural" wing points beyond a specified span location and interpolating the necessary points per patch for the winglet. In this study, the specified span location was fixed at 90% of the trailing edge semispan The integrated wing and winglet coordinates were written to an output file in EMTAC format consisting of four patches per cross sectional cut. A listing of the CHANGE program follows.

```
      PROGRAM CHANGE(OUTPUT,TAPE5,TAPE7,TAPE6=OUTPUT)
C     ****************************************
C     PROGRAM TO CHANGE NATURAL 3 PATCH WING INTO
C     A 4 PATCH WING OR WING-WINGLET COMBINATION
C     ****************************************
      REAL SPAN,SWLT,NEND,ZAVE,YO,YAVE,ZWLT,XWLT,YMAX,YPER,XO
      REAL DUM1,DUM2,DUM3,DUM4,XJ,YJ
      INTEGER I,J,K,L,M,N,J2,ITRIG,ISC,IORDER,NPT,ND
      INTEGER IPTT,IERR,IFLAG,UFU,UFFU
      DIMENSION Y(5,30),Z(5,30),YY(200),ZZ(200,1),ITH(5)
      DIMENSION ZO(1),YF(200),ZF(200),FYY(100),FZZ(100,1),IPT(5)
      DIMENSION FY(100),FZ(100),YM(150),ZM(150),KPER(5,5)
10     FORMAT(F15.6,I5)
15     FORMAT(3I5)
20     FORMAT(2F15.6)
25     FORMAT(3F15.6)
30     FORMAT(4F10.6)
35     FORMAT(4F15.6)
C     ****************************************
C     READING IN THE THREE PATCH FORMAT
C     ONE PATCH AT A TIME
C     ****************************************
      YPER=41.97
C     YPER=43.70
      READ(7,30) DUM1,DUM2,DUM3,DUM4
      READ(7,35) SPAN,SWLT,ZWLT,XWLT
      IF(SWLT.EQ.0.0) THEN
      NEND=SPAN
      ELSE
      NEND=SWLT
      ENDIF
50     READ(5,10) XO,ISC
      IF(XO.EQ.999) GOTO 999
      YMAX=0.0
      L=0
      ITRIG=0
      J=0
1000   J=J+1
      READ(5,15) ITH(J),IPT(J),ND
      L=0
      DO 1005 N=1,2
1005   KPER(J,N)=0
      DO 1100 K=1,IPT(J)
      READ(5,20) Z(J,K),Y(J,K)
      IF(Y(J,K).GT.YPER.AND.ITRIG.EQ.0)THEN
      L=L+1
```

```
      ITRIG=1
      KPER(J,L)=K-1
      ENDIF
      IF(Y(J,K).LT.YPER.AND.ITRIG.EQ.1) THEN
      L=L+1
      ITRIG=0
      KPER(J,L)=K
      ENDIF
1100  IF(Y(J,K).GT.YMAX) YMAX=Y(J,K)
      IF(ITH(J).LT.ISC) GOTO 1000
      WRITE(6,10) XO,ISC+1
      IPT(ISC+1)=IPT(ISC)
      NPT=(IPT(ISC-1)+1)/2
      IPT(ISC-1)=NPT
      IPT(ISC)=NPT
      IF(YMAX.LE.YPER) THEN
      WRITE(6,15) 1,IPT(1),ND
      DO 1200 K=1,IPT(1)
1200  WRITE(6,20) Z(1,K),Y(1,K)
      WRITE(6,15) 2,IPT(ISC-1),ND
      DO 1220 K=1,IPT(2)
1220  WRITE(6,20) Z(2,K),Y(2,K)
      WRITE(6,15) 3,IPT(ISC),ND
      DO 1240 K=IPT(2),IPT(2)+NPT-1
1240  WRITE(6,20) Z(2,K),Y(2,K)
      WRITE(6,15) 4,IPT(ISC+1),ND
      DO 400 K=1,IPT(ISC+1)
400   WRITE(6,20) Z(3,K),Y(3,K)
      GOTO 50
      ELSE
1300  READ(7,25) XJ,YJ,ZJ
      IF(XJ.LT.XO) GOTO 1300
1500  READ(7,25) XJ,YJ,ZJ
      IF(YJ.LT.YPER) GOTO 1500
      L=1
      YM(L)=YJ
      ZM(L)=ZJ
1600  L=L+1
      READ(7,25) XJ,YM(L),ZM(L)
      IF(L.LT.2) GOTO 1600
      IF(YM(L).EQ.YM(L-1)) THEN
      L=L-1
      GOTO 1600
      ENDIF
      IF(ZWLT.GE.0.0) THEN
      IF(YM(L-1).GT.YM(L)) GOTO 1700
```

```
      IF(YM(L-1).GE.NEND.AND.ZM(L-1).GT.ZM(L)) GOTO 1700
      GOTO 1600
      ELSE
      IF(YM(L-1).GT.NEND) GOTO 5
      IF(YM(L-1).GT.YM(L)) GOTO 1700
      ENDIF
5     IF(YM(L-1).GE.NEND.AND.ZM(L-1).LT.ZM(L)) GOTO 1700
      GOTO 1600
1700  YMAX=0.0
      IF(KPER(1,1).EQ.0) THEN
      I=KPER(2,1)+L-1
      CUTS=23.
      NCUTS=23
      ELSE
      I=L-1
      CUTS=REAL(IPT(1)-KPER(1,1))+23.
      NCUTS=IPT(1)-KPER(1,1)+23
      ENDIF
      K=1
      N=1
      UFU=0
      UFFU=0
      IORDER=1
      DO 175 K=1,L-1,1
      YY(K)=YM(L-K)
175   ZZ(K,1)=ZM(L-K)
      IF(KPER(1,1).NE.0) GOTO 181
      DO 180 K=1,KPER(2,1)
      YY(L-1+K)=Y(2,KPER(2,1)+1-K)
180   ZZ(L-1+K,1)=Z(2,KPER(2,1)+1-K)
181   DO 185 K=1,I
      IF(YMAX.LT.YY(K)) YMAX=YY(K)
      IF(K.EQ.1) GOTO 185
      IF(YY(K).LT.YY(K-1).AND.UFU.EQ.0) UFFU=K
      IF(YY(K).GT.YY(K-1)) UFU=K
185   CONTINUE
      K=1
      YM(1)=YM(L-1)
      ZM(1)=ZM(L-1)
      YM(2)=YM(L)
      ZM(2)=ZM(L)
      IF(UFU.EQ.0.OR.UFFU.EQ.I) THEN
      IPTT=-1
      DO 2150 L=1,NCUTS
      YF(L)=YMAX-(YMAX-YY(I))*(REAL(L)/(CUTS+1.))
      YO=YF(L)
```

```
      IERR=0
      IF(YO.LE.YY(I-1)) IORDER=1
      CALL KIUNI(I,I,YY,1,ZZ,IORDER,YO,ZO,IPTT,IERR)
      IF(IERR.NE.0) THEN
      WRITE(6,*)'IERR=',IERR
      ENDIF
2150  ZF(L)=ZO(1)
      ELSE
      IF(UFFU.NE.0) THEN
      WRITE(6,*) UFFU
      WRITE(6,*) 'IERR, PROBLEMS AT CUT  ',XO
      ENDIF
      IF(UFFU.EQ.0) THEN
      K=0
      GOTO 3200
      ENDIF
      DO 3000 L=1,UFFU
      FYY(L)=YY(I-(L-1))
3000  FZZ(L,1)=ZZ(I-(L-1),1)
      IPTT=-1
      IORDER=1
      DO 3150 L=1,NCUTS
      YF(L)=YMAX-(YMAX-YY(I))*(REAL(L)/(CUTS+1.))
      IF(YF(L).LT.FYY(UFFU).OR.YF(L).GT.FYY(1))THEN
      N=L
      GOTO 3200
      ENDIF
      YO=YF(L)
      IERR=0
      CALL KIUNI(UFFU,UFFU,FYY,1,FZZ,IORDER,YO,ZO,IPTT,IERR)
      IF(IERR.NE.0) THEN
      WRITE(6,*)'IERR=',IERR
      ENDIF
3150  ZF(L)=ZO(1)
3200  DO 2350 L=1,UFU-UFFU+K
      FYY(L)=YY(L-UFFU+K)
2350  FZZ(L,1)=ZZ(L-UFFU+K,1)
      IPTT=-1
      IORDER=1
      DO 2400 L=1,NCUTS
      FY(L)=YMAX-(YMAX-YY(I))*(REAL(L)/(CUTS+1.))
      IF(FY(L).LT.FYY(1).OR.FY(L).GT.YMAX) THEN
      N=L
      GOTO 2450
      ENDIF
      YO=FY(L)
```

```
      IF(YO.LE.FYY(UFU-1)) IORDER=1
      M=UFU-UFFU+K
      IERR=0
      CALL KIUNI(M,M,FYY,1,FZZ,IORDER,YO,ZO,IPTT,IERR)
      IF(IERR.NE.0) THEN
      WRITE(6,*)'IERR=',IERR
      ENDIF
2400    FZ(L)=ZO(1)
2450   IORDER=1
      DO 2500 L=1,I-UFU+1
      FYY(L)=YY(UFU+L-1)
2500   FZZ(L,1)=ZZ(UFU+L-1,1)
      IPTT=-1
      DO 2550 L=1,NCUTS-(N-1)
      YF(L)=YMAX-(YMAX-YY(I))*(REAL(L)/(CUTS+2.-REAL(N)))
      YO=YF(L)
      M=I-UFU+1
      IERR=0
      CALL KIUNI(M,M,FYY,1,FZZ,IORDER,YO,ZO,IPTT,IERR)
      IF(IERR.NE.0) THEN
      WRITE(6,*)'IERR=',IERR
      ENDIF
2550   ZF(L)=ZO(1)
      ENDIF
      IF(KPER(1,1).EQ.0) THEN
      WRITE(6,15) 1,IPT(1),0
      DO 1710 L=1,IPT(1)
1710   WRITE(6,20) Z(1,L),Y(1,L)
      WRITE(6,15) 2,25,0
      WRITE(6,20) ZZ(I,1),YY(I)
      IF(ZWLT.GE.0.0.OR.N.EQ.1) THEN
      DO 130 L=NCUTS,1,-1
130    WRITE(6,20) ZF(L),YF(L)
      ELSE
      DO 135 L=23-(N-1),1,-1
135    WRITE(6,20) ZF(L),YF(L)
      DO 136 L=1,N-1
136    WRITE(6,20) FZ(L),FY(L)
      ENDIF
      WRITE(6,20) ZZ(1,1),YY(1)
      ELSE
      WRITE(6,15) 1,IPT(1),ND
      DO 1750 K=1,KPER(1,1)
1750   WRITE(6,20) Z(1,K),Y(1,K)
      M=NCUTS-IPT(1)+KPER(1,1)
      DO 1775 K=NCUTS-(N-1),M-(N-1)+1,-1
```

```
1775  WRITE(6,20) ZF(K),YF(K)
      WRITE(6,15) 2,25,0
      WRITE(6,20) ZF(M-(N-1)+1),YF(M-(N-1)+1)
      IF(ZWLT.GE.0.0.OR.N.EQ.1) THEN
      DO 13010 L=M,1,-1
13010 WRITE(6,20) ZF(L),YF(L)
      ELSE
      DO 13015 L=M-(N-1),1,-1
13015 WRITE(6,20) ZF(L),YF(L)
      DO 13016 L=1,N-1
13016 WRITE(6,20) FZ(L),FY(L)
      ENDIF
      WRITE(6,20) ZZ(1,1),YY(1)
      ENDIF
      L=2
500   L=L+1
      READ(7,25) XJ,YM(L),ZM(L)
      IF(YM(L).EQ.YM(L-1)) THEN
      L=L-1
      GOTO 500
      ENDIF
      IF(YM(L).GT.YPER) GOTO 500
      IF(KPER(3,1).EQ.0) THEN
      I=(L-1)+IPT(2)+NPT-KPER(2,2)
      NCUTS=23
      CUTS=23.
      ELSE
      I=L-1
      CUTS=REAL(KPER(3,1)-1)+23.
      NCUTS=23+KPER(3,1)-1
      ENDIF
      N=1
      YMAX=0.0
      LFFU=0
      LFU=0
      DO 505 K=1,L-1
      YY(K)=YM(K)
505   ZZ(K,1)=ZM(K)
      IF(KPER(3,1).NE.0) GOTO 511
      DO 510 K=KPER(2,2),IPT(2)+NPT
      YY(K+L-KPER(2,2))=Y(2,K)
510   ZZ(K+L-KPER(2,2),1)=Z(2,K)
511   DO 515 K=1,I
      IF(YY(K).GT.YMAX) YMAX=YY(K)
      IF(K.EQ.1) GOTO 515
      IF(YY(K).LT.YY(K-1).AND.LFU.EQ.0) LFFU=K
```

```
      IF(YY(K).GT.YY(K-1)) LFU=K
515    CONTINUE
      K=1
      IF(LFU.EQ.0.OR.LFFU.EQ.I) THEN
      IPTT=-1
      DO 215 L=1,NCUTS
      YF(L)=YMAX-(YMAX-YY(I))*(REAL(L)/(CUTS+1.))
      YO=YF(L)
      IERR=0
      CALL KIUNI(I,I,YY,1,ZZ,IORDER,YO,ZO,IPTT,IERR)
      IF(IERR.NE.0) THEN
      WRITE(6,*)'IERR=',IERR
      ENDIF
215    ZF(L)=ZO(1)
      ELSE
      IF(LFFU.EQ.0) THEN
      K=0
      GOTO 320
      ENDIF
      DO 300 L=1,LFFU
      FYY(L)=YY(L)
300    FZZ(L,1)=ZZ(L,1)
      IPTT=-1
      IORDER=1
      DO 315 L=1,NCUTS
      YF(L)=YMAX-(YMAX-YY(I))*(REAL(L)/(CUTS+1.))
      IF(YF(L).LT.FYY(LFFU).OR.YF(L).GT.FYY(1))THEN
      N=L
      GOTO 320
      ENDIF
      YO=YF(L)
      IERR=0
      CALL KIUNI(LFFU,LFFU,FYY,1,FZZ,IORDER,YO,ZO,IPTT,IERR)
      IF(IERR.NE.0) THEN
      WRITE(6,*)'IERR=',IERR
      ENDIF
315    ZF(L)=ZO(1)
320    DO 235 L=1,LFU-LFFU+K
      FYY(L)=YY(L+LFFU-K)
235    FZZ(L,1)=ZZ(L+LFFU-K,1)
      IPTT=-1
      IORDER=1
      DO 240 L=1,NCUTS
      FY(L)=YMAX-(YMAX-YY(I))*(REAL(L)/(CUTS+1.))
      IF(FY(L).LT.FYY(1).OR.FY(L).GT.YMAX) THEN
      N=L
```

```
      GOTO 245
      ENDIF
      YO=FY(L)
      IF(YO.LE.FYY(LFU-1)) IORDER=1
      M=LFU-LFFU+K
      IERR=0
      CALL KIUNI(M,M,FYY,1,FZZ,IORDER,YO,ZO,IPTT,IERR)
      IF(IERR.NE.0) THEN
      WRITE(6,*)'IERR=',IERR
      ENDIF
240    FZ(L)=ZO(1)
245    IORDER=1
      DO 250 L=1,I-LFU+1
      FYY(L)=YY(L+LFU-1)
250    FZZ(L,1)=ZZ(L+LFU-1,1)
      IPTT=-1
      DO 255 L=1,NCUTS-(N-1)
      YF(L)=YMAX-(YMAX-YY(I))*(REAL(L)/(CUTS+2.-REAL(N)))
      YO=YF(L)
      M=I-LFU+1
      IERR=0
      CALL KIUNI(M,M,FYY,1,FZZ,IORDER,YO,ZO,IPTT,IERR)
      IF(IERR.NE.0) THEN
      WRITE(6,*)'IERR=',IERR
      ENDIF
255    ZF(L)=ZO(1)
      ENDIF
C     ***************************************
C     WRITING THE INTERPOLATE LOWER SURFACE
C     IN SIMP OR EMTAC FORMAT
C     ***************************************
      IF(KPER(3,1).EQ.0) THEN
      WRITE(6,15) 3,25,0
      WRITE(6,20) ZZ(1,1),YY(1)
      IF(ZWLT.GE.0.0.OR.N.NE.1) THEN
      DO 350 L=N-1,1,-1
350    WRITE(6,20) FZ(L),FY(L)
      DO 355 L=1,NCUTS-(N-1)
355    WRITE(6,20) ZF(L),YF(L)
      ELSE
      DO 220 L=1,NCUTS
220    WRITE(6,20) ZF(L),YF(L)
      ENDIF
      WRITE(6,20) ZZ(I,1),YY(I)
      WRITE(6,15) 4,IPT(ISC+1),0
      DO 3050 L=1,IPT(ISC+1)
```

```
3050   WRITE(6,20) Z(3,L),Y(3,L)
       ELSE
       M=NCUTS-KPER(3,1)-1
       WRITE(6,15) 3,25,0
       WRITE(6,20) ZZ(1,1),YY(1)
       IF(ZWLT.GE.0.0.OR.N.NE.1) THEN
       DO 3500 L=N-1,1,-1
3500   WRITE(6,20) FZ(L),FY(L)
       DO 3550 L=1,M-(N-1)
3550   WRITE(6,20) ZF(L),YF(L)
       ELSE
       DO 2200 L=1,M
2200   WRITE(6,20) ZF(L),YF(L)
       ENDIF
       WRITE(6,20) ZF(M+1),YF(M+1)
       WRITE(6,15) 4,IPT(4),0
       DO 3555 L=M+1,NCUTS
3555   WRITE(6,20) ZF(L),YF(L)
       DO 3560 L=KPER(3,1),IPT(4)
3560   WRITE(6,20) Z(3,L),Y(3,L)
       ENDIF
       ENDIF
       GOTO 50
999    STOP
       END
       SUBROUTINE KIUNI(MM,NN,X,KTAB,Y,IORDER,XO,YO,IPTT,IERR)
       INTEGER IORDER,MM,NN,IERR,KTAB,IPTT,KN,KOLD
       REAL X(NN),Y(MM,KTAB),XO,YO,SLOPE
       IF(IPTT.EQ.-1) THEN
       KN=1
       KOLD=1
       ELSE
       KN=KOLD
       ENDIF
       IF(XO.LT.X(KN)) GOTO 9001
9002   IF(KN.GE.NN) GOTO 9000
       IF(XO.GT.X(KN+1)) THEN
       KN=KN+1
       GOTO 9002
       ELSE
       KOLD=KN
       IF(XO.LT.X(KN+1).AND.XO.GT.X(KN)) THEN
       SLOPE=((Y(KN+1,KTAB)-Y(KN,KTAB))*(XO-X(KN)))/(X(KN+1)-X(KN))
       YO=Y(KN,KTAB)+SLOPE
       ENDIF
       ENDIF
```

```
9001   IF(XO.LT.X(NN)) GOTO 9000
       IF(KOLD.EQ.1) KN=2
9003   IF(KN.GT.NN) GOTO 9000
       IF(XO.LT.X(KN)) THEN
       KN=KN+1
       GOTO 9003
       ELSE
       KOLD=KN
       IF(XO.GT.X(KN).AND.XO.LT.X(KN-1)) THEN
       SLOPE=((Y(KN,KTAB)-Y(KN-1,KTAB))*(XO-X(KN-1)))/(X(KN)-X(KN-1))
       YO=Y(KN-1,KTAB)+SLOPE
       ENDIF
       ENDIF
9000   CONTINUE
       END
```

NASA
National Aeronautics and Space Administration

Report Documentation Page

1. Report No.	2. Government Accession No.	3. Recipient's Catalog No.
NASA CR-4407		

4. Title and Subtitle	5. Report Date
The Effects of Winglets on Low Aspect Ratio Wings at Supersonic Mach Numbers	November 1991
	6. Performing Organization Code

7. Author(s)	8. Performing Organization Report No.
James A. Keenan John M. Kuhlman	10. Work Unit No. 505-59-30-01

9. Performing Organization Name and Address	11. Contract or Grant No.
West Virginia University Department of Mechanical and Aerospace Engineering Morgantown, WV 26506-6101	NAG 1-951

12. Sponsoring Agency Name and Address	13. Type of Report and Period Covered
National Aeronautics and Space Administration Langley Research Center Hampton, Virginia 23665-5225	Contractor Report 2/89 - 4/91
	14. Sponsoring Agency Code

15. Supplementary Notes

Langley Technical Monitor: Steven X. S. Bauer and Peter F. Covell

16. Abstract

A computational study has been conducted on two wings, of aspect ratios 1.244 and 1.865, each having 65° leading edge sweep angles, to determine the effects of nonplanar winglets at supersonic Mach numbers. A Mach number of 1.62 was selected as the design value. The winglets studied were parametrically varied in alignment, length, sweep, camber, thickness, and dihedral angle to determine which geometry had the best predicted performance. For the computational analysis, an available Euler marching technique was used.

The results indicated that the possibility existed for wing-winglet geometries to equal the performance of wing-alone bodies in supersonic flows with both bodies having the same semispan. The first wing with winglet used NACA 1402 airfoils for the base wing and was shown to have lift-to-pressure drag ratios within 0.136 percent to 0.360 percent of the NACA 1402 wing-alone. The other base wing was a "natural" flow wing which was previously designed specifically for a Mach number of 1.62. The results obtained showed that the "natural" wing-alone had a slightly higher lift-to-pressure drag than the "natural" wing with winglets.

17. Key Words (Suggested by Author(s))	18. Distribution Statement
Supersonic Flow Winglet Design Drag Reduction	Unclassified - Unlimited Subject Category 02

19. Security Classif. (of this report)	20. Security Classif. (of this page)	21. No. of pages	22. Price
Unclassified	Unclassified	348	A15

NASA FORM 1626 OCT 86

For sale by the National Technical Information Service, Springfield, Virginia 22161-2171

NASA-Langley, 1991

National Aeronautics and
Space Administration
Code NTT

Washington, D.C.
20546-0001

Official Business
Penalty for Private Use, $300

NASA

National Aeronautics and
Space Administration

Washington, D.C.
20546

SPECIAL FOURTH CLASS MAIL
BOOK

Postage an Fees Paid
National Aeronautics and
Space Administration
NASA-451

Official Business
Penalty for Private Use $300

U.S. MAIL

L2 001 CR-4374 911113S090569A
NASA
CENTER FOR AEROSPACE INFORMATION
ACCESSIONING DEPT
P O BOX 8757 BWI ARPRT
BALTIMORE MD 21240